Heteroleptic light-emitting copper(I) complexes with possible applications in light-emitting electrochemical cells

Inauguraldissertation

zur

Erlangung der Würde eines Doktors der Philosophie

vorgelegt der

Philosophisch-Naturwissenschaftlichen Fakultät

der Universität Basel

von

Sarah Keller

aus Deutschland

Basel, 2018

Genehmigt von der Philosophisch-Naturwissenschaftlichen Fakultät

auf Antrag von:

Prof. Dr. C. E. Housecroft und Prof. Dr. J.-F. Nierengarten

Basel, den 12.12.2017

Dekan Prof. Dr. Martin Spiess

"*So much universe, and so little time.*" – Terry Pratchett

Image of the Butterfly Nebula, NGC 6302. Distance: 4000 light years, Constellation: Scorpius.
Photo credit: NASA, ESA and the Hubble SM4 ERO Team. Picture used with permission from ESA/Hubble.
https://www.spacetelescope.org/images/heic0910h (17.11.2017).

Table of contents

List of abbreviations

°	degree
°C	degree celcius
2-MeTHF	2-methyl-tetrahydrofuran
Ø	average
a, b, c	unit cell axes
A	ampere
Å	Ångström (0.1 nanometres)
α, β, γ	unit cell angles
au	atomic units
a.u.	arbitrary units
BIPHEP	2,2'-Bis(diphenylphosphino)-1,1'-biphenyl
bp	boiling point
bpy	2,2'-bipyridine
br	broad
BuLi	*n*-butyllithium
calc.	calculated
cd	candela
CIE	Commission internationale de l'éclairage
cm	centimetre
COSY	correlated spectroscopy
CT	charge transfer
d	doublet (NMR)
dd	doublet of doublets of doublets (NMR)
ddd	doublet of doublets of doublets of doublets (NMR)
DFT	density functional theory
dm	decimetre
dppa	bis(diphenylphosphino)acetylene, IUPAC: bis(diphenylphosphino)ethyne
dppb	1,2-bis(diphenylphosphino)benzene
dppe	1,2-bis(diphenylphosphino)ethane
dppf	1,1'-bis(diphenylphosphino)ferrocene
dppm	1,2-bis(diphenylphosphino)methane
dppp	1,2-bis(diphenylphosphino)propane
dt	doublet of triplets
δ	chemical shift
E	half-cell potential; energy
E_{pa}	anodic peak potential
E_{pc}	cathodic peak potential
e.g.	for example
ε	extinction coefficient
EDG	electron-donating group
EL	electroluminescence
[EMIM][PF_6]	1-ethyl-3-methylimidazolium hexafluorophosphate
eq.	equivalent
EQE	external quantum efficiency
ESI MS	electron spray ionization mass spectrometry
Et	ethyl, -C_2H_5
EtLi	ethyllitium
et al.	and others
eV	electronvolt
EWG	electron-withdrawing group
EXSY	exchange spectroscopy
Fc	ferrocene
FWHM	full width at half maximum

g	gram
G	Gibbs energy
GS	ground state
h	hour
HOMO	highest occupied molecular orbital
HMBC	heteronuclear multiple bond correlation
HMQC	heteronuclear multiple quantum coherence
Hz	Hertz
IL	ionic liquid
*i*Pr	isopropyl
ir	irreversible
IR	infrared
ISC	intersystem crossing
iTMC	ionic transition metal complex
ITO	indium tin oxide
J	coupling constant (NMR)
K	Kelvin
kHz	kilohertz
kJ	kilojoule
k_{nr}	non-radiative decay rate constant
k_r	radiative decay rate constant
λ	wavelength
λ_{exc}	excitation wavelength
$\lambda^{em}{}_{max}$	wavelength of emission maximum
$\lambda^{EL}{}_{max}$	wavelength of electroluminescence maximum
L	litre
LC	ligand-centred; liquid chromatography
LEC	light emitting electrochemical cell
LED	light emitting diode
LLCT	ligand-to-ligand charge transfer
lm	lumen
Lum_{max}	maximum luminance
LUMO	lowest unoccupied molecular orbital
m	metre; multiplet (NMR)
M	molarity
MALDI-TOF	matrix-assisted laser desorption ionization – time of flight
MC	metal-centred
Me	methyl
MeLi	methyllithium
Mes	mesityl, 1,3,5-trimethylphenyl, -$C_6H_2Me_3$
mg	milligram
µg	microgram
MHz	Megahertz
min	minute
mL	millilitre
µL	microlitre
MLCT	metal-to-ligand charge transfer
mmol	millimole
µmol	micromole
mol	mole
m.p.	melting point
MS	mass spectrometry
µs	microsecond
MW	microwave
m/z	mass to charge ratio
ν	frequency
$\tilde{\nu}$	wavenumber
nm	nanometre
NMR	nuclear magnetic resonance

NOESY	nuclear Overhauser effect spectroscopy
ns	nanosecond
OLED	organic light-emitting diode
PEDOT:PSS	poly(3,4-ethylenedioxythiophene):poly(styrenesulfonate)
Ph	phenyl, -C_6H_5
Phen	1,10-phenanthroline
PLQY	photoluminescence quantum yield
PMMA	poly(methyl methacrylate)
POP	bis(2-(diphenyl-phosphino)phenyl)ether
ppm	parts per million
qr	quasi-reversible
quant.	quantitative
RT	room temperature
σp	Hammett parameter (para)
s	second; singlet (NMR)
S_0	ground state
S_1	lowest-lying singlet excited state
sept	septet (NMR)
sh	shoulder
τ	excited state lifetime
t	triplet
T	temperature
T_1	lowest-lying triplet excited state
$t_{1/2}$	half lifetime (time to reach half of the maximum luminance)
*t*Bu	tertbutyl
*t*Bu-xantphos	9,9-dimethyl-4,5-bis(di-*tert*-butylphosphino)xanthene
td	triplet of doublets
TD	time-dependent
TGA	thermogravimetric analysis
THF	tetrahydrofuran
t_{on}	turn-on time (time to reach the maximum luminance)
tpy	2,2':6',2"-terpyridine
UV	ultraviolet
V	Volt
Vis	visible
W	Watt
xantphos	4,5-bis(diphenylphosphino)-9,9-dimethylxanthene
Z	number of formula units in the unit cell

List of publications

Parts of this thesis are based on the publications and manuscripts listed below and are referred to in the text by the employment of square brackets.

[1] S. Keller, E. C. Constable, C. E. Housecroft, M. Neuburger, A. Prescimone, G. Longo, A. Pertegás, M. Sessolo and H. J. Bolink, "$[Cu(bpy)(P\text{^}P)]^+$ containing light-emitting electrochemical cells: improving performance through simple substitution", *Dalton Trans.*, 2014, **43**, 16593.

[2] S. Keller, A. Pertegás, G. Longo, L. Martinez, J. Cerdá, J. M. Junquera-Hernández, A. Prescimone, E. C. Constable, C. E. Housecroft, E. Ortí and H. J. Bolink, "Shine bright or live long: substituent effects in $[Cu(N\text{^}N)(P\text{^}P)]^+$-based light-emitting electrochemical cells where N^N is a 6-substituted 2,2'-bipyridine", *J. Mater. Chem. C.*, 2016, **4**, 3857.

[3] S. Keller, A. Prescimone, H. Bolink, A. Pertegás, G. Longo, E. C. Constable and C. E. Housecroft, "Luminescent Cu(I) complexes with bisphosphanes and halogen-substituted 2,2'-bipyridine ligands, submission planned for January 2018.

[4] S. Keller, F. Brunner, J. M. Junquera-Hernández, A. Pertegás, M.-G. La-Placa, A. Prescimone, E. C. Constable, H. J. Bolink, E. Ortí and C. E. Housecroft, "CF_3 substitution of $[Cu(P\text{^}P)(bpy)][PF_6]$ complexes: Effects on photophysical properties and light-emitting electrochemical cell performance", *ChemPlusChem*, submitted 20.11.2017.

[5] S. Keller, F. Brunner, A. Prescimone, E. C. Constable, C. E. Housecroft, "Hexafluoridophosphate partial hydrolysis leading to the one-dimensional coordination polymer $[\{Cu(xantphos)(\mu\text{-}PO_2F_2)\}_n]$, *Inorg. Chem. Comm.*, 2015, **58**, 64.

[6] S. Keller, A. Prescimone, E. C. Constable and C. E. Housecroft, "Copper(I) and silver(I) complexes of 9,9-dimethyl-4,5-bis(di-*tert*-butylphosphino)xanthene: photophysical properties and structural perturbation under pressure", *Photochem. Photobiol. Sci.*, submitted 23.11.2017.

[7] S. Keller, T. N. Camenzind, J. Abraham, A. Prescimone, D. Häussinger, E. C. Constable and C. E. Housecroft, "Self-Assembly of heteroleptic dinuclear silver(I) complexes bridged by bis(diphenylphosphino)ethyne", *Dalton Trans.*, 2018, accepted 13.12.2017, DOI: 10.1039/c7dt03923a.

All papers that were published before the printing of this thesis were included with permission from the publisher.

Abstract

The overall aim of this project was the design, synthesis and characterization of copper(I) complexes that, upon excitation, emit light in the region of the electromagnetic spectrum that is visible to the human eye. The complexes are incorporated into light-emitting devices and their electroluminescent behaviour was studied and the results used to further optimize the compounds in an iterative manner. The main focus was on complexes of the general formula [Cu(P^P)(N^N)][PF_6], where P^P is a chelating bisphosphane and N^N is a 2,2'-bipyridine (bpy), phenanthroline or moiety of similar structure. The commercially available bisphosphanes, bis(2-(diphenylphosphino)phenyl)ether (POP) and 4,5-bis(diphenylphosphino)-9,9-dimethylxanthene (xantphos) were chosen as our standard P^P chelating ligands in order to investigate the role of the N^N chelating ligand and study the effects of modifications on the bpy or its derivatives on the copper complexes. Detailed structural, photophysical and electrochemical characterizations, as well as quantum chemical calculations of the synthesized complexes were carried out and the most promising compounds were evaluated in light-emitting electrochemical cells (LECs). In order to make the reader familiar with the topic, we start with the motivation for this project and continue with an introduction about general properties of copper and its emissive complexes. The principle of thermally activated delayed fluorescence (TADF) is explained and the characteristics of LECs are described. In Chapter I, a series of complexes with alkyl substituents in different positions in the bpy and phen ligands are compared. In Chapter II, the results of the investigation of complexes with chloro-and bromo-substituted bpy ligands are shown. The effect of CF_3 substitution in the bpy on complex and device properties is exposed in Chapter III. The subject of Chapter IV is the fortuitous formation of an inorganic coordination polymer. The potential of an alkyl phosphane as a ligand for emissive copper(I) complexes was evaluated and the resulting complexes are shown in Chapter V. A side project with dimeric silver(I) complexes and their self-assembling properties is presented in Chapter VI. The thesis is concluded with an outlook about projects for the near future and the potential of copper(I) based light-emitting electrochemical cells as an illumination technique is discussed.

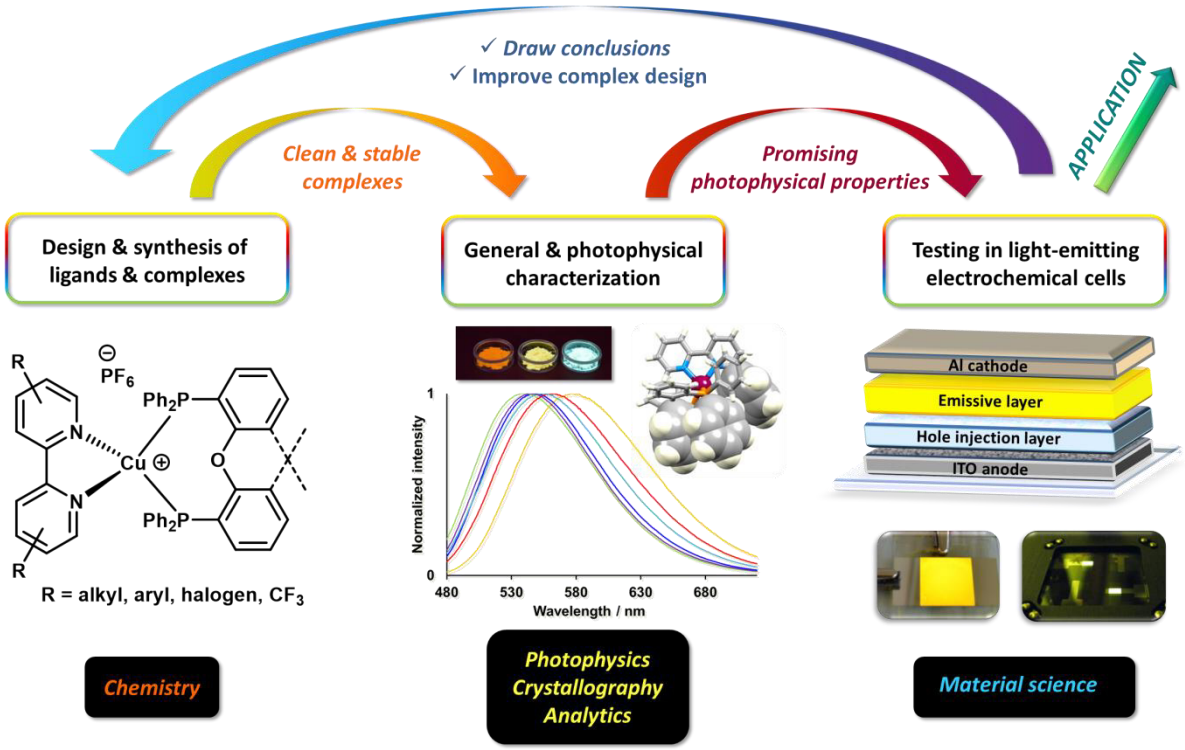

Introduction

Motivation and significance for society

Humanity faces enormous challenges for the current and future decades. With global warming on our doorstep, increasing population and aggravated pollution, our challenges are difficult. A depressing image unfolds when we look at the so-called Earth overshoot day, which marks the day on which we have consumed more from nature than our planet can renew within the whole year. In 2017, this was already the case on the 2nd of August, and while we consumed the equivalent of one Earth in 1969, it is now 1.7 Earths in one year.[1] While it would without doubt be helpful if the worldwide human population were static, a worldwide drop of birth rates is not in sight.[2,3] Therefore, efforts to reduce our consumption of energy and reliance on non-renewable resources have the utmost importance. As scientists, we are obliged to draw from our knowledge, skills and creativity to develop solutions to make our daily life more environmentally friendly. The resources at our disposal must be used more wisely and efficiently and to do so, we have to develop new technologies with these goals in mind.

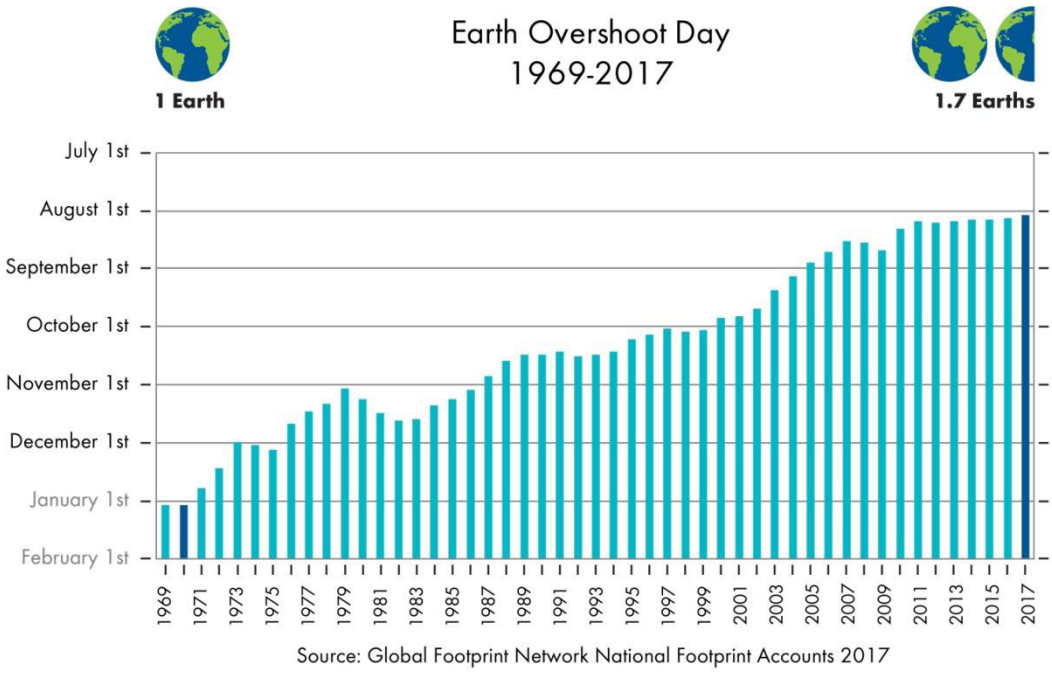

Fig. 1. Annual dates of the Earth Overshoot Day from 1969-2007.[4]

The good news is that some positive changes are already happening: Instead of wasting fossil fuels on transportation or for the production of electricity, a switch to renewable energies has not only become possible from a technology point of view, but is often also economically favourable. From wind turbines, hydroelectric power plants and geothermic energy to a variety of solar cell systems (from classic silicon based devices to dye-sensitized solar cells and perovskites), regenerative energy systems are on the rise. Ideally, these systems would be combined with improved methods to store the produced energy which is not immediately used, for example with large-scale battery systems for each household. Another very elegant method would be to use the excess energy which is generated in peak periods for splitting of water into O_2 and H_2. Dihydrogen is a high-energy molecule and upon combustion only gives clean H_2O. With the help of solar-driven water-splitting devices, sunlight could even directly be used to generate solar fuels.[5,6,7]

Despite the development of more sustainable ways to produce energy, it is still vital to reduce our energy consumption. Realistically, this is only implementable if consumers and industry do not have to reduce their level of comfort and if the additional costs are bearable. And it is of course even better when additional advantages of the new technologies make the shift in energy production attractive for all consumers. Many countries have taken action in forms of mandatory energy efficiency policies, for example to enforce the use of more energy efficient heating and cooling systems or household items such as refrigerators, washing machines and illuminating devices.[8]

In Switzerland in 2015, about 12% of the total consumed electricity was used for illumination. In the combined sectors of service and agriculture, it summed up to almost 24%.[9] The demand for more efficient and sustainable

lighting technologies drew our attention to light-emitting electrochemical cells (LECs). The working principle of both LECs and organic light-emitting diodes (OLEDs) is electroluminescence, which allows the direct conversion of electrical energy into light and is therefore more efficient than incandescent lighting, where large amounts of the invested energy are wasted as heat. The benefit of LECs is that their setup is significantly easier than that of OLEDs and, as a result, their production is ecologically as well as economically favourable.[10] We decided to apply our experience in inorganic complex chemistry to create light-emitting copper(I) complexes and collaborate with material scientists at the University of Valencia,[11] who employ the compounds as luminophores in LECs. While the majority of metallic-based emitters employ iridium due to its high efficiency and relative ease of tunability,[12] the use of copper(I) is coming to the fore. It has a much higher natural abundance (27 ppm vs. 3.7×10^{-5} for iridium, Earth's crust)[13], lower price and possesses the ability to exhibit thermally activated delayed fluorescence (TADF), allowing photoluminescence quantum yields (PLQYs) up to 100%.[14,15]
To understand the process of effective light-emission in copper(I) complexes and to make use of that knowledge to design the best materials and employ them in promising devices is an immensely fascinating challenge. The usefulness of such a project is obvious, and even a scientifically indifferent person can agree that versatile lighting systems based on abundant materials is worth the investment of a doctoral research project. It is my hope that this research has a positive impact on the environment and society and might bring us closer to the noble goal of a World with sustainable lighting.

Electroluminescence and Devices

Background

The famous chemist Albert Hofmann stated that we are "beings of light",[16] and it is indeed very apparent that light – both emanating from the sun and artificially generated – is one of the most elemental human needs. For many decades, incandescent lighting illuminated our lives at times or in places that the sun does not reach. Copper has been connected to illumination since the very beginning of electricity powered illumination. In fact, almost 80 years before Thomas Alva Edison, among others in the same time frame, developed the incandescent light bulb in 1879, Alessandro Giuseppe Antonio Anastasio Volta invented the "Volta lamp" – a device which employed a glowing copper wire.[17] The credit and exact date of the invention of the incandescent light bulb is not entirely clear[18], but the very practical version that Thomas Edison presented to the public was filed for a US patent on the 4th of November 1879. Incandescent light bulbs were the first devices in which light was generated with the help of electricity. What they still have in common with far more primitive systems such as torches or oil lamps is that in all these cases, the respective material is heated up and we profit from the occurring incandescence as illumination. It is therefore no surprise that the efficiency of these systems is far from optimal, because a large amount of energy is wasted as heat. Luminescence is the light produced by mechanisms other than incandescence, and because it does not come with elevated temperature it is also called "cold light". In chemiluminescence and bioluminescence, light emission is generated through chemical reactions, and photoluminescence is the light emission triggered by excitation with light. The working principle behind solid state lighting (SSL) devices such as light-emitting diodes (LEDs), OLEDs and LECs is electroluminescence, light emission upon electrical excitation. Due to the higher efficiency of these devices in comparison to incandescent lighting, the use of energy for illumination already dropped with the increasing distribution of SSL technologies.[19] Another advantage of these systems is that the majority of the used materials are non-toxic, as opposed to the mercury containing energy-saving light bulbs or halogen lamps. Furthermore, the possibility to fabricate them into panels of various sizes makes them extremely versatile in their application.[20] Smartphones, and modern computer and television screens employ solid state lighting and the large impact that this technology has on our society is indisputable.

Light-emitting electrochemical cells – Setup

Technically, as with the development of the precursor to the incandescent light bulb,[17] Alessandro Volta can again be named as the inventor of the electrochemical cell (also known as a battery). However, it is Heeger *et al.* who are credited for the invention of the first light-emitting electrochemical cell.[21] It was based on an electroactive polymer together with added electrolyte. Two main categories of LECs are being investigated, with the emissive layer based on conjugated polymers or ionic transition metal complexes (iTMCs). LECs require ionic materials in order to function. This necessitates the addition of salts and ion-conducting polymers in the former type of LECs, whereas the iTMCs in the latter are inherently composed of mobile ions, although sometimes ionic liquids are added to further assist the ion transport. In contrast, for OLEDs most of the materials are non-charged, which is due to the required sublimability for vacuum deposition used in their fabrication. In general, the setup of LECs is very simple

and only consists of four layers, which is also one of the main advantages over OLEDs, which have additional electron transport and injection layers and thus require complicated multi-layer evaporation processes (Fig. 2).

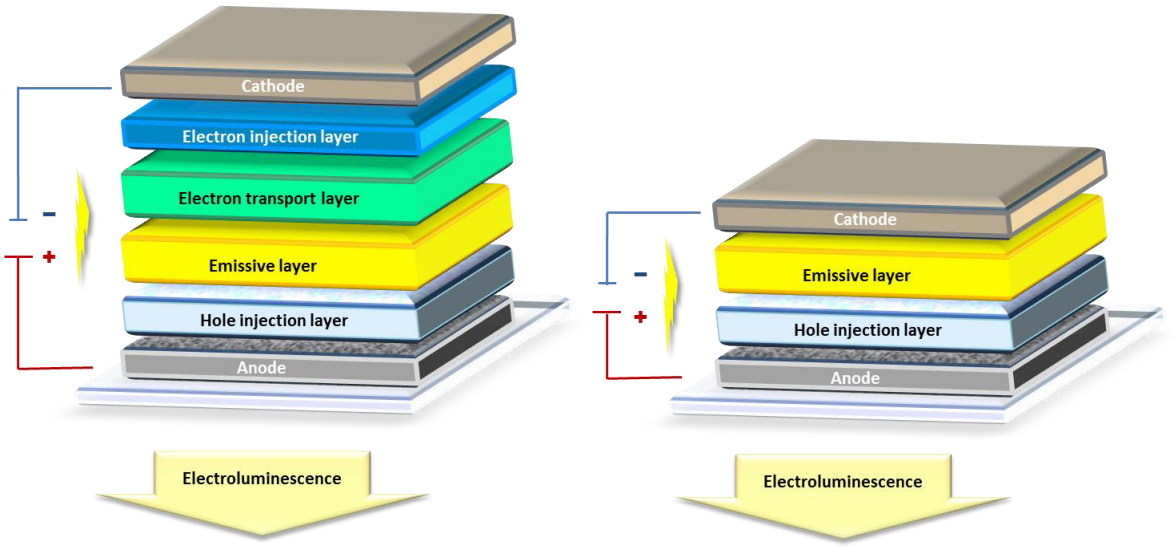

Fig. 2. Left: Device architechture of an organic light-emitting diode (OLED); right: schematic setup of a light-emitting electrochemical cell (LEC).

Furthermore, OLEDs are very sensitive to air and moisture, and require extremely pure materials and rigorous sealing. Due to the employed materials in LECs (such as aluminium instead of calcium (as in an OLED) as cathode, for example), these devices have a more robust nature. An additional cost and effort factor is the fabrication of OLEDs, which are usually almost entirely based on vacuum deposition, a process that requires significantly more energy than, for example, solution casting such as spin-coating, which is the preferred technique for LECs.[22,23]
In general, the fabrication of the LECs that are used for the compounds in this project is as follows.: The anode is the first layer on top of the substrate plate, which is usually made of glass, but can also be a flexible plastic sheet. The anode is usually composed of indium tin oxide (ITO) is widely used, including for the LECs tested in this project, but also other materials have successfully been employed, such as for example carbon nanotubes.[20] In this project, commercially available patterned ITO coated glass substrates were used (Fig. 3 (left)). Usually a hole injection layer is added by spin-coating on top of the anode, in our case PEDOT:PSS which is a mixture of the polymers poly(3,4-ethylenedioxythiophene) and polystyrene sulfonate. Next comes the active layer composed of a mixture of the emissive ionic transition metal complex (iTMC) and an ionic liquid (IL), which assists the ion transport. In this project, the iTMC is always a cationic copper(I) complex with $[PF_6]^-$ as counterion and 1-ethyl-3-methylimidazolium hexafluoridophosphate ([EMIM][PF_6]) is used as the ionic liquid. While for this layer spin-coating is also the preferred method, the metal cathode, here aluminium, which makes the final layer is added by vacuum deposition. In Fig. 3 (middle), a LEC ready for testing is illustrated, without encapsulation, Fig. 3 (right) shows a LEC in test mode.

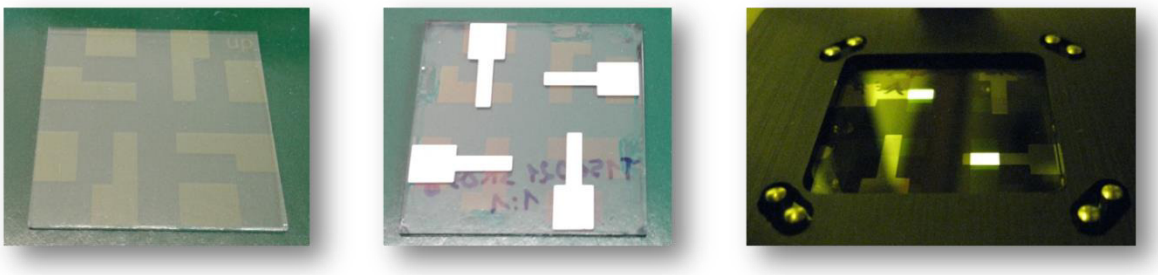

Fig. 3. Left: Glass substrate with patterned ITO coating; middle: finished LEC incuding all layers; right: a LEC device being tested.

Electroluminescence and the processes inside the LEC

Electroluminescence is a process that describes the non-thermal generation of light when an electrical field is applied. In an electroluminescent device, electrons and holes are injected into the emissive layer via the cathode and anode, respectively. Electrostatic interactions result in the recombination of the electrons and holes, thus generating excitons. The term exciton describes a state where an electron and a hole are bound by attraction of electrostatic Coulomb forces. Energy is generated by the formation of excitons, which is passed on to the emitter molecules, where an electron is excited from the ground state to the excited state. The relaxation process back to the ground state is in the best case a radiative process and induces the light-emission of the electroluminescent material. Under operation of the device, this process is constantly repeated, leading to a steady generation of light.[24] Which processes exactly take place and how, during the operation of the LEC, is still subject to investigation and discussion. Two main theories about the operational mechanisms of LECs have been postulated, the Electrochemical Doping (ECD) Model and the Electrodynamic (ED) Model.

In the former, electrochemical doping of the active layer leads to the in situ formation of a p-i-n structure (p = positively doped, n = negatively doped, i = intrinsic). Oxidation and reduction of the semiconductor takes place by injection of electrons and holes via the electrodes. Electrostatic compensation by anions and cations leads to p-type and n-type doped regions, with the region in between remaining intrinsic; this is where charge recombination happens and the largest electric field is present. The Preferential Electrochemical Doping Model (PECDM) is similar to the ECD Model, with the main difference that there is only either n- or p-doping in the active layer. According to the ED Model, the second theory about LEC device physics, electric double layers at the interfaces are formed by mobile. In an operation mode, these ions drift towards these interfaces, thus creating large electric fields located at the electrodes until the middle of the active layer is field free. Due these fields at the interface between electrodes and active layer, charge injection is promoted, with the injected charge carriers diffusing to until electron and holes recombine. In contrast to the ECD Model, the electric fields are located close to the electrodes instead of in the middle of the active layer.[12]

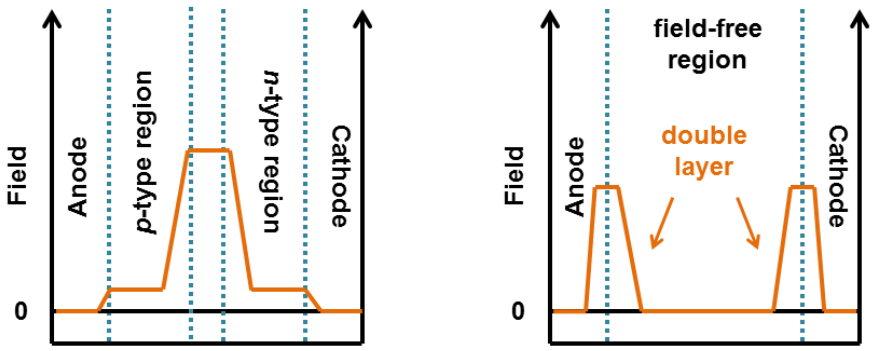

Fig. 4. Left: Spatial distribution of the electric field according to the ECD Model; right: Spatial distribution of the electric field as described in the ED Model.

Absorption, emission and perception of light

In the solution absorption spectra there are usually intense high-energy absorptions, which arise from ligand-based $\pi^*\leftarrow\pi$ transitions, but we are mostly interested in the metal to ligand charge transfer (MLCT) bands.. For the yellow to red [Cu(P^P)(N^N)][PF_6] complexes that are described in this thesis, MLCT bands are usually broad bands in the region between 340 and 430 nm, giving rise to the visible colour of the compounds. The wavelengths of the MLCT bands correspond to the required energy to allow a charge transfer from the metal to the ligand in the ground state. In reality, this is not just a single LUMO←HOMO transition, but a number of different transfer processes with orbitals of similar energies (e.g. also LUMO+1 and HOMO–1) involved.[25] In order to see the emission that is connected with this charge transfer, excitation wavelengths in the area of the MLCT band are chosen. Thus the electrons are promoted from the ground state to the excited state and upon relaxation emit light. An important parameter to measure the efficiency of this process is the photoluminescence quantum yield PLQY. It is defined as the number of emitted photons with respect of the number of absorbed photons and is usually given in %.

$$\boldsymbol{PLQY}\ \phi = \frac{\boldsymbol{\#\ photons\ emitted}}{\boldsymbol{\#\ photons\ absorbed}}$$

It is obvious that the higher the PLQY ϕ of a compound, the better an emitter it is. Once the electron is in the excited state, there are radiative and non-radiative pathways, with the rate constants k_r and k_{nr} ($k_r + k_{nr} = 1$) for it to

relax back to the ground state. In order to have a high PLQY, the probability for non-radiative decay must be reduced and the radiative decay rate constant k_r as high as possible.
The lifetime of the excited state is also an important parameter for emissive compounds. It is connected to the PLQY via the radiative decay rate constant k_r. For application as emitters the, excited state lifetime should be relatively short, with high PLQY and k_r. Short lifetimes are desired in order to minimize non-radiative quenching processes and avoid chemical reactions that can take place in the excited state.[26]

$$\boldsymbol{Lifetime\ \tau = \frac{PLQY\ \phi}{k_r}}$$

However, sometimes an emission is perceived to be brighter than the measured PLQY suggests, or vice versa. This is due to the sensitivity of the human eye to different wavelengths. The receptors in our eyes are most sensitive at a wavelength of 555 nm under daylight conditions. As a result, green light at this wavelength produces the impression of highest "brightness" when compared to light at other wavelengths. For example, at 490 nm the photopic sensitivity of the human eye only makes 20%, which means that in order to produce light of the same perceived brightness as at 555 nm, the light source needs to emit five times as much.[27]
In order to better describe and compare the colour that a light source emits, a system was introduced that is based on the perception of the human eye. The CIE chromaticity diagram (CIE – Commission internationale de l'éclairage) is a two-dimensional plot, that includes monochromatic light of wavelengths between 380 and 700 nm and colours are described by two xy coordinates (Fig. 5). Also further colour models exist that are based on three dimensions.

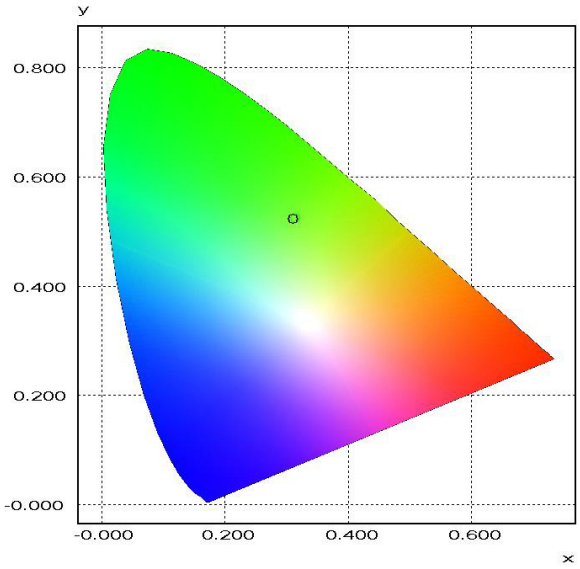

Fig. 5. CIE colour space used by the Hamamatsu absolute photoluminescence (PL) quantum yield spectrometer C11347 Quantaurus-QY.

Copper

General information

Group 11 by IUPAC numbering is also known as the copper group or, due to their former usage, the elements copper, silver and gold are also called coinage metals. The heaviest analogue is roentgenium, a radioactive synthetic element. Since copper, silver and gold can also occur as elements in their natural form, it is likely that they were among the first elements to be discovered.[28] The element copper is named after the island of Cyprus, which is "cuprum" in Latin. There is evidence that copper was used in tools as early as 5000–4000 BC.[29] Much later, when in addition to the high thermal conductivity, the electrical conducting properties of copper were also discovered, the doors were opened to many applications, and copper still plays an important role in the electronics industry. With 27 ppm of copper in the Earth's crust[13] it is one of the more abundant elements and rooves, train tracks and even monuments consist of copper. The most famous example is probably the Statue of Liberty, which is covered in 90,800 kilograms of copper sheets.[30] While the statue originally had the typical reddish copper colour, oxidation of

the copper sheets resulted in the formation of Verdigris (copper salts, especially of acetate, carbonate, chloride and hydroxide), which covers the statue in the typical green patina as we know it today.

Fig. 6. Left: Image of copper wire;[31] right: Close-up photograph of the Statue of Liberty.[31]

Together with vanadium, chromium, manganese, iron, cobalt, zinc, molybdenum and the non-metals selenium, fluorine and iodine, copper is one of the trace elements in the human body, with around 80 mg in the adult body. It is a constituent of a number of enzymes, especially oxidases, and is required for the development of for example bones and nerve coverings. Both Cu deficiency and toxicity are rare in humans.[32] While mammals use the iron containing haemoglobin for the oxygen transport in the body, proteins with copper complexes are responsible for this process in some crustaceans.[33]

General properties of copper(I)

The electron configuration of elemental copper is [Ar] $3d^{10}4s^{1}$ and the most common oxidation states are 0, +I and +II. While Cu(II) is more common and more stable, the stabilization of Cu(I) is achievable with the right combination of ligands. Cu^{+} is in d^{10} configuration and prefers a tetrahedral complex geometry, as in the cation $[Cu(MeCN)_4]^{+}$, whereas the optimal coordination geometry for Cu^{2+} (d^{9}) is square planar, as the example of $[Cu(NH_3)_4]^{2+}$ shows (Fig.7).

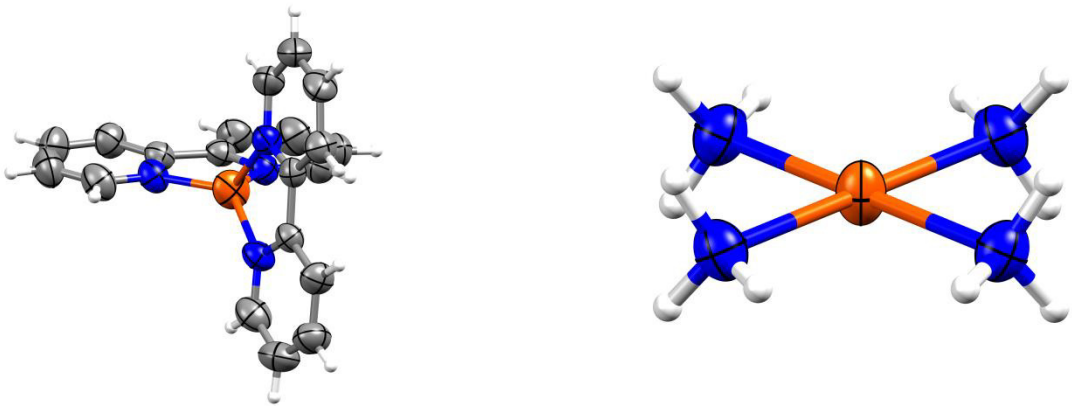

Fig. 7. Left: Structure of the cation $[Cu(bpy)_2]^{+}$ in $[Cu(bpy)_2][CF_3SO_3]$, ellipsoids plotted at 50% probability level, CCDC 601277;[34] right: structure of the cation $[Cu(NH_3)_4]^{2+}$ in $[Cu(NH_3)_4][C_5H_3N_2O_2]_2$, ellipsoids plotted at 50% probability level, CCDC 643038.[35]

The strategy to prevent oxidation of Cu(I) and stabilize this oxidation state is to employ ligands that promote the tetrahedral geometry and that are too sterically hindered to allow a flattening of the complex to square planar. This is especially important because the orbitals of copper(I) complexes in the excited state resemble those of copper(II), but since we want to avoid permanent oxidation but instead radiative relaxation back to the tetrahedral ground state, the tetrahedral geometry needs to be stable. The rigidification of the complex geometry has the additional benefit of reducing quenching mechanisms, which is described later.

Copper(I) based luminescent materials

At the start of this project in 2013, the majority of efficient emitter materials for OLEDs and LECs that are ionic transition metal complexes (iTMCs) employ iridium. Although these compounds show high PLQYs, good device performance and tuning of the emissive colour is relatively systematic, the metals low abundance obstructs large scale application of iridium-based emitters. Looking for a more sustainable and low-priced alternative, our interest turned to emissive copper(I) complexes with N^N and P^P chelating ligands. The precursor $[Cu(MeCN)_4][PF_6]$ is almost ten times cheaper than that of iridium complexes, $IrCl_3{\cdot}H_2O$. Furthermore, the synthesis of $[Cu(P^P)(N^N)][PF_6]$ complexes is very straightforward in comparison to iridium compounds,[36] since it only requires stirring of the starting material and appropriate ligands at room temperature and eventually layer crystallization and a washing process. An earlier Master's project in our group had already shown promising potential of with P^P = POP or dppb and N^N = bpy or phen in LECs[37] and we decided to dedicate this PhD project to the design of optimized copper(I) emitters and their employment in sustainable LECs.

Depending on the ligands, copper(I) complexes exhibit excellent photoluminescence and electroluminescence. Starting from the late 1970s, copper(I) complexes with two chelating diimine ligands have been investigated more intensely in terms of their photophysical properties and excited state behaviour, and especially the work of McMillin and coworkers was pioneering.[38] The emissive properties of these $[Cu(N^N)_2]^+$ complexes where N^N = 2,9-dimethyl-1,10-phenanthroline, 2,9-dimethyl-4,7-diphenyl-1,10-phenanthroline and 4,4',6,6'-tetramethyl-2,2'-bipyridine were studied at lower temperature and the existence of two excited states that are thermally equilibrated was postulated.[39] Another later study of $[Cu(phen)_2]^+$ complexes with phenanthroline ligands of increasing steric demand gave deeper insight into the photophysical characteristics and processes. Low temperature studies in a rigid matrix were carried out and the positive effect of bulkiness and alkyl chains at the ligands on the photophysical properties are described.[40]

It is known today that in general, the emissive properties of heteroleptic copper(I) complexes with phosphanes and N^N chelating ligands are superior in comparison to homoleptic $[Cu(N^N)_2]^+$ complexes. This was already observed in early examples of heteroleptic $[Cu(PR_3)_2(N^N)]^+$ complexes with PR_3 = PPh_3 or PPh_2CH_3. The complexes $[Cu(PPh_3)_2(phen)]^+$, $[Cu(PPh_3)_2(dmp)]^+$ and $[Cu(PPh_2CH_3)_2(dmp)]^+$ (dmp = 2,9-dimethylphenanthroline) exhibit an intense yellow-green emission at room temperature; whereas $[Cu(PPh_3)_2(bpy)]^+$ and $[Cu(PPh_3)_2(biq)]^+$ (biq = 2,2'-biquinoline) weakly emit in the yellow and orange. In comparison, the $[Cu(dmp)_2]^+$ complex showed only a very weak red emission, which is attributed to a large stokes shift. Also here a low temperature study of the heteroleptic complexes revealed that the excited state lifetimes at 77 K are significantly elongated with respect to the lifetime values recorded at room temperature.[41]

In the next generation of heteroleptic copper(I) complexes, the two PPh_3 ligands were exchanged for chelating bisphosphanes. The goal was to supress ligand dissociation, and in addition it was also found that less solvent-induced quenching occurs for example for $[Cu(P^P)(N^N)]^+$ systems where P^P = POP than for similar complexes with two PPh_3 ligands attached.[42] This might be due to the lower flexibility of a P^P chelating ligand, where the bite angle stays in a certain range, as opposed to two PR_3 ligands that can move independently. An additional advantage of a bisphosphane is the entropic gain when a $[Cu(MeCN)_4]^+$ salt is used as starting material, because upon coordination of two chelating ligands to the copper, four acetonitrile molecules are released into solution.

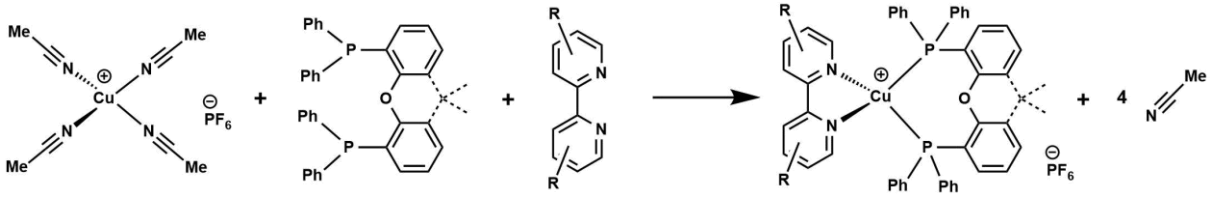

Scheme 1. Synthestic route to heteroleptic $[Cu(P^P)(N^N)][PF_6]$ complexes starting from $[Cu(MeCN)_4][PF_6]$.

Solvent-induced quenching is often a problem in copper(I) complexes. Aggregation or the formation of exciplex molecules induce or enhance non-radiative decay and thus lead to quenching of the emission. Rigidification of the tetrahedral complex geometry is beneficial in order to avoid flattening and Franck-Condon processes. This can be realized by the employment of bulky ligands, which also function as protection of the copper centre.[15,43]

Although copper(I) complexes have long been known, it was only recently that they were in the spotlight in connection with the Nobel Prize in Chemistry 2016. It was awarded jointly to Jean-Pierre Sauvage, Sir J. Fraser Stoddart and Bernard L. Feringa "for the design and synthesis of molecular machines". Copper(I) played a crucial role in the development of these systems, because it is used to assemble the ligands, for example modified phenanthrolines. The ligands coordinate to the metal centre and the resulting dihedral angle between the ligands is relatively fixed as a result of this coordination. Then the two ligands can easily be entwined by attaching macrocyclic moieties, and as a final step removal of the metal yields the desired [2]catenane. This strategy

developed by Sauvage marked a huge step forward in the synthesis of interlocked ring systems and the development of molecular machines.[44,45]

In addition to the huge potential of these systems in general, the approach to sterically constrain specifically copper(I) complexes is also interesting for potential emitter materials. In 2012, a series of heteroleptic copper(I) pseudo-rotaxanes [Cu(P^P)(phen)][BF_4] was synthesized, where the bisphosphanes dppe, dppp, POP or dppf were combined with a macrocyclic phenanthroline based ligand, which has a ring size of 37 atoms and is therefore abbreviated as phen37 (see Fig. 8). In the complexes, all the phosphanes were found to be nicely surrounded by the macrocyclic ligand. Intense yellow-orange emission in both solid state and solution was reported for the complexes [Cu(POP)(phen37)][BF_4], [Cu(dppe)(phen37)][BF_4] and [Cu(dppp)(phen37)][BF_4].[46] In a further study, a smaller macrocyclic phenanthroline based ligand phen30 (30 atom ring system) was investigated together with the bisphosphanes dppp and POP. In the obtained Cu(I) complex with POP, the phosphane was found to be only partially threaded through the macrocycle (Fig. 8) and the complex was not very stable. The phosphane dppp on the other hand acts as a bridging ligand to form the dimer [Cu_2(μ-dppp)(m30)$_2$][BF_4], which exhibits weak yellow-green luminescence in solid state and solution.[47]

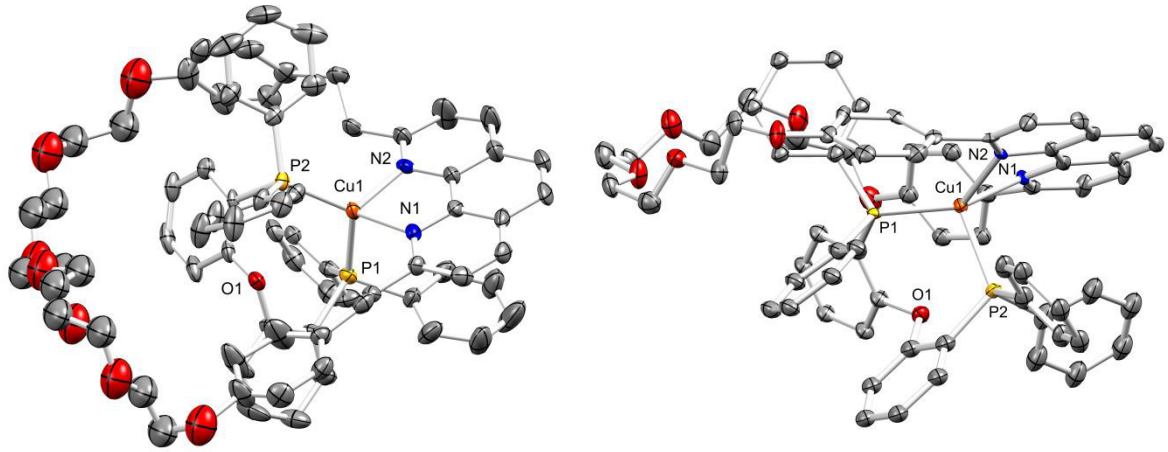

Fig. 8. Left: Structure of the cation [Cu(POP)(phen37)]$^+$ in [Cu(POP)(phen37)][BF_4]. Ellipsoids plotted at 30% probability level due to large thermal ellipsoids of the macrocyclic chain, H atoms omitted. CCCD 877890;[46] right: Structure of the cation [Cu(POP)(phen30)]$^+$ in [Cu(POP)(phen30)][BF_4]. Ellipsoids plotted at 50% probability level, H atoms omitted. CCCD 970019.[47]

To our knowledge, these complexes with pseudo-rotaxanes were never tested as emitters in a light-emitting device. Copper complexes are often relatively labile in solution and subjected to ligand exchange. However, these topologically and sterically constrained complexes might have a higher stability as a result of their interlocked geometry, which might be helpful to prevent possible dissociation or degradation in the device. In the future, eventually also the employment of a macrocyclic phosphane ligand might be worth investigating or a covalent chain that connects the bisphosphane to the N^N chelating ligand.

Another approach to avoid the competition between the formation of heteroleptic [Cu(P^P)(N^N)]$^+$ and homoleptic [Cu(P^P)$_2$]$^+$ and [Cu(N^N)$_2$]$^+$ complexes[48] is to employ mixed-type ligands of the motif N^P, N^P^N or P^N^N (Scheme 2). Examples with the phosphane being bound directly to the hereroaryl ring or an aliphatic group are known, as well as 1,2-phenyl bridged N^P, N^P^N and P^N^N ligands.[49] It is also for these type of complexes that an interesting synthetic approach to synthesize luminescent copper(I) compounds was described. Grinding the solid starting materials together, with only a drop of acetonitrile necessary to promote the complex formation, yielded pure and luminescent materials. This mechanochemical technique was successfully applied to synthesize for example dinuclear [Cu_2X_2(dpypp)$_2$] complexes with X = Cl, Br, I and dpypp = 2,2′-(phenylphosphinediyl)dipyridine[50] and [(2-(2-(Diphenylphosphanyl)phenyl)pyridine)$_2$$Cu_2I_2$] as well as mononuclear [(2-(2-(Diphenylphosphanyl)-phenyl)pyridine)(PPh_3)CuI].[49] It is a very environmentally friendly approach that is worth testing for our compounds as well. Especially also for the synthesis of copper(I) complexes for dye-sensitized solar cells, where the anchoring groups at the ligands often impede their solubility, this technique might prove beneficial.

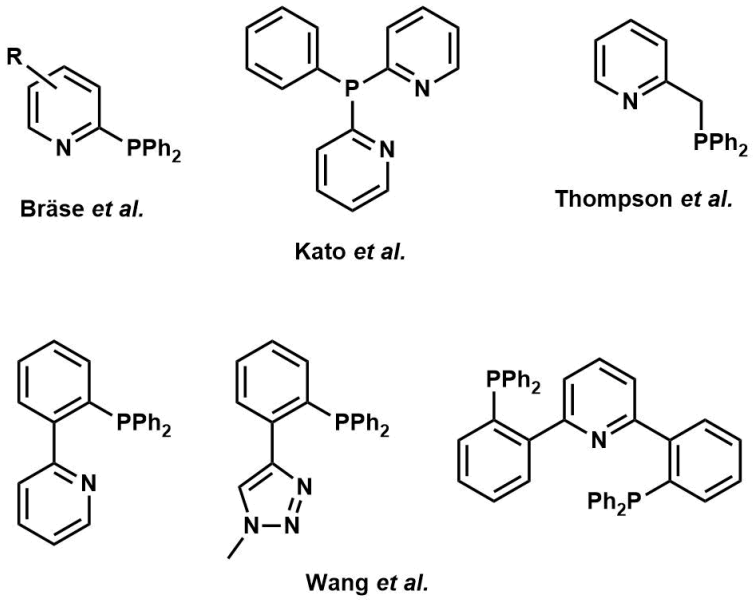

Scheme 2. Examples of N^N and N^P^N chelating ligands that used in emissive copper(I) complexes by Bräse *et al.*,[51] Thompson *et al.*[52] and Wang *et al.*.[49]

Thermally activated delayed fluorescence (TADF)

Although low temperature lifetime and emission measurements to investigate the emissive states and processes of copper complexes were carried out already over 30 years ago, this characteristic feature has only moved into the spotlight in the last few years. The term thermally activated delayed fluorescence (TADF) is now used to classify emitter compounds that exhibit this type of emissive behaviour. While TADF has also been observed in purely organic compounds, copper(I) complexes are the largest class of TADF emitters.[15] Upon photoexcitation to the singlet excited state S_1, a very effective and fast (3 to 30 ps) inter system crossing (ISC) process to the T_1 excited state ($S_1 \rightarrow T_1$) takes place, prompt fluorescence from the S_1 to the ground state is not detected. Depending on the energy separation between the triplet and singlet excited state, $\Delta E(S_1 - T_1)$ and the available thermal energy, the S_1 state can be repopulated according to the Boltzmann distribution. The energy separation $\Delta E(S_1 - T_1)$ up to which this repopulation, and thus TADF, is expected to have a significant contribution is proposed to be 0.37 eV (3000 cm^{-1}). The reverse ISC (RISC) or up-ISC is faster than all emissive processes. The resulting fluorescence from S_1, called TADF, is long-lived, because it is fed from the long-living triplet reservoir. Although it is called "delayed", this emission is still faster than the direct phosphorescence from the T_1 state. [15]

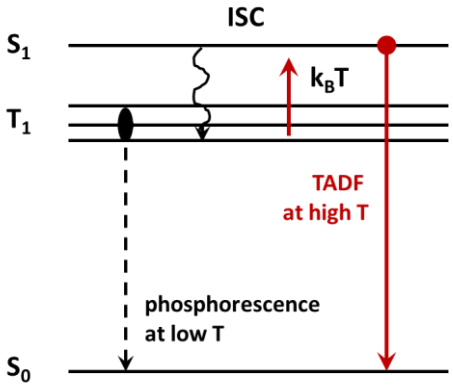

Fig. 9. Schematic diagram to illustrate the molecular mechanism of thermally activated delayed fluorescence (TADF). Figure reproduced and adapted.[15]

At room temperature, the measured emission is however a combination of phosphorescence and TADF. In order to supress the $T_1 \rightarrow S_1$ RISC, the available thermal energy is reduced by cooling the sample down. The obtained emission at lower temperature is more or even entirely composed of long-lived phosphorescence, which can be directly observed by significantly elongated excited state lifetime values τ and a redshift of the emission maximum

due to the lower energy of the excited triplet state. Due to the TADF process, luminescent materials are able to exhibit PLQY values up to 100%. In the electroluminescent devices, this process is also called singlet harvesting, because it allows the recombination of electrons and holes via triplet and singlet pathways, thus making the devices more efficient. Molecules that exhibit TADF are therefore a promising class of emitters and a dinuclear copper(I) TADF complex has been employed in an OLED that shows one of the highest efficiencies (23% EQE) reported so far for a copper-based device (see also Outlook, page 165)[53]

Silver(I) compounds – alternative emitters?

Although the noble metal silver is one of the more expensive elements on the market, with 5.5×10^{-2} ppm in the Earth's crust, it is still significantly more abundant than iridium[13] and therefore silver(I) compounds are still worth being considered as emitter materials.

Heteroleptic silver(I) complexes with different phenanthrolines and the bisphosphane ligands dppm, dppe, dppp and POP have been investigated by Nierengarten *et al.*. Their study shows that silver is more versatile in its coordination modes than copper and more prone to tolerate trigonal coordination, which lead to the formation of mono- and dinuclear species. [Ag(POP)(phen)][BF_4] was isolated as pure mononuclear complex, whereas in the case of dppm and dppe and dppp, mono- and dibridged dinuclear silver dications were obtained.[54]

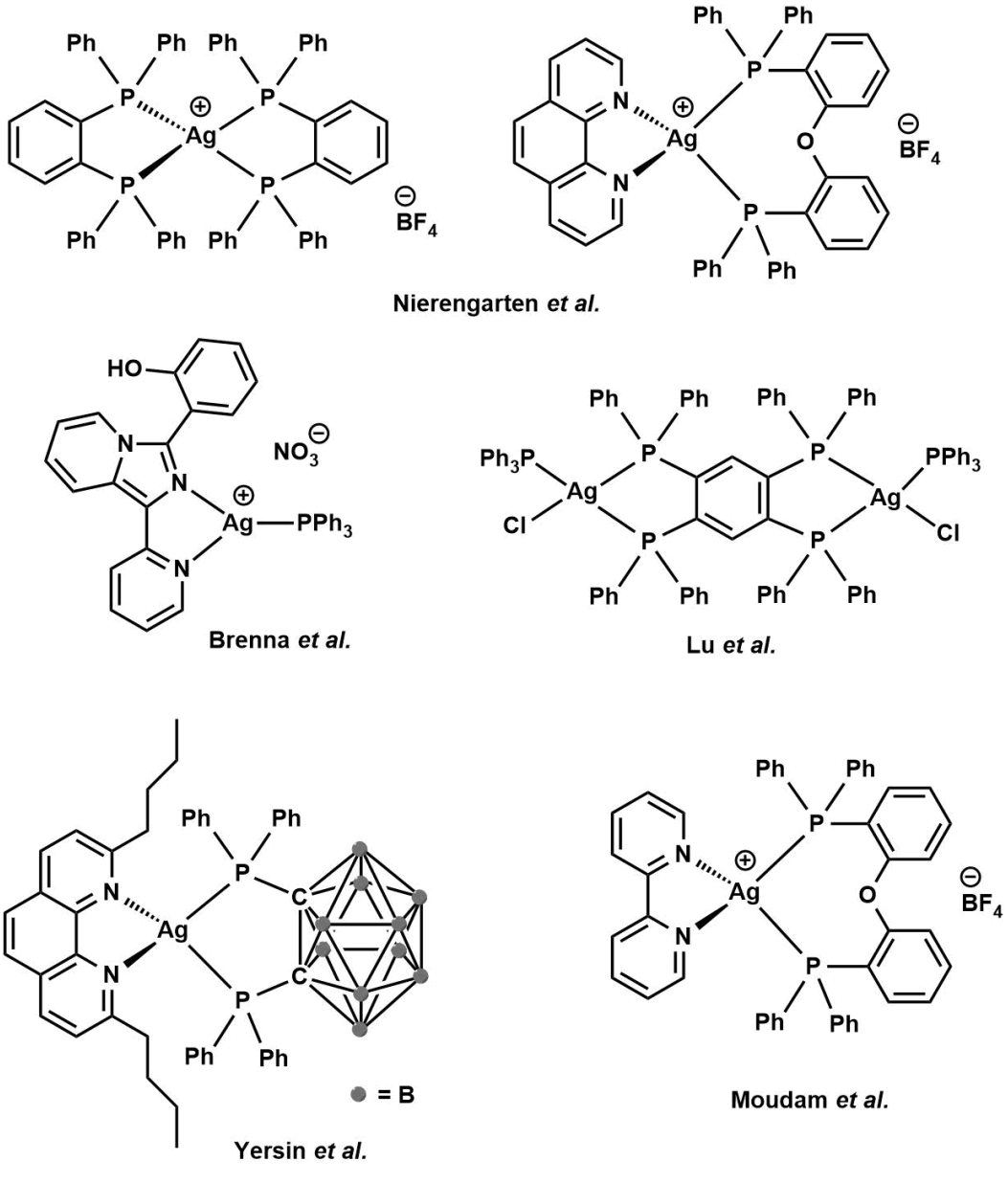

Scheme 3. Examples of emissive mono- and dinuclear Ag(I) complexes published by Nierengarten *et al.*,[54,57] Brenna *et al.*,[55] Lu *et al.*,[56] Yersin *et al.*[60] and Moudam *et al.*.[58]

The ability of silver to tolerate frustrated coordination is nicely illustrated by the isolation of trigonal planar $[Ag(N^N)(PR_3)][NO_3]$ complexes (N^N = 2-(1-(pyridin-2-yl)imidazo[1,5-a]pyridin-3-yl)phenol; PR_3 = PPh_3, PMe_2Ph, $PMePh_2$, P(*p*-tolyl)$_3$, P(*n*Bu)$_3$, P(OPh)$_3$ and P(OEt)$_3$. The complexes are all emissive in solution and in solid state, with the highest PLQY values of 68% in solid state and 52% in solution for $[Ag(N^N)(PPh_3)][NO_3]$.[55] A series of neutral dinuclear silver complexes $[Ag(PPh_3)(X)]_2$(tpbz) with tpbz = 1,2,4,5-tetrakis(diphenylphosphanyl)benzene as bridging ligand and X = the halogens chlorine, bromine or iodine showed intense white-blue (λ_{max} = 475 nm for X = chlorine and 471 nm for X = bromine) and green (λ_{max} = 495 nm for X = iodine) photoluminescence in the solid state with quantum yields of up to 98% for $[Ag(PPh_3)(Cl)]_2$(tpbz). Elongated emission lifetimes of the powder at lower temperature (3.0 µs at 298 K to 638 µs at 77 K) identify this compound as TADF emitter.[56] Homoleptic $[Ag(P^P)_2][BF_4]$ complexes with P^P = dppb or POP were synthesized. $[Ag(dppb)_2][BF_4]$ exhibits a PLQY of 22 % in solid state and a significantly elongated lifetime on going from solid state (6.8 µs) to a frozen matrix of THF at 77 K (3.4 ms). A light-emitting device with $[Ag(dppb)_2][BF_4]$ and poly(vinyl carbazole as host material produced almost white light with a maximum brightness of 365 cdm^{-2} at 20 V, however no information about stability and lifetime of the device were published.[57] In analogy to the copper(I) complexes with the established combination of a P^P and an N^N chelating ligand, $[Ag(POP)(bpy)][BF_4]$ was synthesized and tested successfully in LECs. The complex had a PLQY of 14% in solid and the device showed a maximum brightness of 395 cd m^{-2} at 5.5 V with warm white light. However, the maximum efficacy of 0.45 cd A^{-1} is less than a tenth than what was obtained for the best copper complex of our series and the device was not tested in terms of its lifetime and stability.[58] Recently, a series of promising neutral Ag(phen)(P_2-nCB) complexes with P_2-nCB = *nido*-carborane-bis(diphenylphosphine) and phenanthrolines of increasing steric demand was investigated by Yersin *et al.*.[59] A breakthrough in terms of TADF efficiency was achieved with the complex with the most sterically demanding phen ligand, 2,9-di-*n*butyl-1,10-phenanthroline: The shortest so far reported TADF lifetime τ(TADF) of 1.4 µs and a PLQY of 100% make this compound an excellent candidate as an electroluminophore in a light-emitting device.[60]

The above presented examples show that Ag(I) compounds have an enormous potential as emitters. Whereas neutral complexes are more beneficial for OLED applications because of the option of vacuum deposition, charged complexes are ideal as emitters for LECs. The high PLQY of some silver complexes compensate the lower abundance of silver in comparison to copper. The employment of silver in small scale devices, where only small amounts of material are needed, is very plausible, especially if recycling of the devices can be realized. However, especially for illumination at a larger scale, copper is still the preferred material in terms of sustainability.

References

1 In order to calculate the date, our Ecological Footprint (humanity's total yearly consumption) is compared with the capacity of the Earth to regenerate renewable natural resources in that year (biocapacity). The date of Earth Overshoot Day is calculated by comparing humanity's total yearly consumption (Ecological Footprint) with Earth's capacity to regenerate renewable natural resources in that year (biocapacity). www.overshootday.org/why-past-earth-overshoot-day-dates-keep-changing (08.09.2017).

2 P. Gerland, A. E. Raftery, H. Ševčíková, N. Li, D. Gu, T. Spoorenberg, L. Alkema, B. K. Fosdick, J. Chunn, N. Lalic, G. Bay, T. Buettner, G. K. Heilig and J. Wilmoth, *Science*, 2014, **346**, 234.

3 S. KC and W. Lutz, *Global Environmental Change*, 2017, **42**, 181.

4 Image taken with permission from www.overshootday.org/why-past-earth-overshoot-day-dates-keep-changing (08.09.2017).

5 J. R. McKone, N. S. Lewis and H. B. Gray, *Chem. Mater.*, 2014, **26**, 407.

6 T. Jafari, E. Moharreri, A. S. Amin, R. Miao, W. Song and S. L. Suib, *Molecules*, 2016, **21**, 900.

7 C. Acar, I. Dincer and G. F. Naterer, *Int. J. Energy Res.*, 2016, **40**, 1449.

8 Energy Efficiency Market Report 2016, International Energy Agency (IEA).

9 https://tinyurl.com/y97zdxkc (08.09.2017), Bundesamt für Energie BFE.

10 E. Fresta and R. D. Costa, *J. Mater. Chem. C*, 2017, **5**, 5643.

11 Thanks to H. J. Bolink and E. Ortí including their group members, Instituto de Ciencia Molecular (ICMol), Universidad de Valencia.

12 *Light-Emitting Electrochemical Cells*, ed. R. D. Costa, Springer International Publishing AG, Cham, Switzerland, 1st edn, 2017.

13 http://www.rsc.org/periodic-table (08.11.2017).

14 C. E. Housecroft and E. C. Constable, *Chem. Soc. Rev.*, 2015, **44**, 8386.

15 R. Czerwieniec, M. J. Leitl, H. H.H. Homeier and H. Yersin, *Coord. Chem. Rev.*, 2016, **325**, 2.

16 *Tun und Lassen – Essays, Gedanken und Gedichte*, A. Hofmann, Nachtschatten Verlag AG, Solothurn, 2011.

17 *The European Edisons: Volta, Tesla, and Tigerstedt*, A. K. Sethi, Springer, 2016.

18 *Edison's electric light: biography of an invention*, F. Israel, R. Israel and P. Israel, Rutgers University press, New Brunswick, New Jersey, 1986, 115.

19 Solid-State Lighting 2016 R&D Plan, Prepared for: Solid-State Lighting Program, Building Technologies Office, Office of Energy Efficiency and Renewable Energy, U.S. Department of Energy, DOE/EE-1418
20 L. Martínez-Sarti, A. Pertegás, M. Monrabal-Capilla, E. Gilshteyn, I. Varjos, E. I. Kauppinen, A. G. Nasibulin, M. Sessolo, H. J. Bolink, *Organic Electronics*, 2016, **30**, 36.
21 Q. Pei, G. Yu, C. Zhang, Y. Yang and A. J. Heeger, *Science*, 1995, **269**, 1086.
22 *Applied Photochemistry – When Light Meets Molecules*, ed. G. Bergamini, S. Silvi, Springer International Publishing AG, Cham, Switzerland, 1st edn, 2016.
23 N. Armaroli, G. Accorsi, M. Holler, O. Moudam, J.-F. Nierengarten, Z. Zhou, R. T. Wegh and R. Welter, *Adv. Mater.*, 2006, **18**, 1313.
24 F. Dumur, in *Luminescence in Electrochemistry*, ed. F. Miomandre and P. Audebert, Springer International Publishing AG, Cham, Switzerland, 1st edn, 2017, pp. 327–364.
25 B. Bozic-Weber, V. Chaurin, E. C. Constable, C. E. Housecroft, M. Meuwly, M. Neuburger, J. A. Rudd, E. Schönhofer and L. Siegfried, *Dalton Trans.*, 2012, **41**, 14157.
26 R. Czerwieniec, H. Yersin, M. Z. Shafikov and A. F. Suleymanova, *ChemPhysChem*, 10.1002/cphc.201700872.
27 https://light-measurement.com/spectral-sensitivity-of-eye (05.11.2017)
28 *Chemistry of the Elements*, N. N. Greenwood and A. Earnshaw, Butterworth-Heinemann, 2nd edition 1997, p. 1173.
29 *Inorganic Chemistry*, C. E. Housecroft and A. G. Sharpe, Pearson Education Limited, Edinburgh, 4th edition 2012, p. 764.
30 *The Statue of Liberty*, C. A. Sutherland, Barnes & Noble Books, New York City, 2003.
31 Creative Commons Zero (CC0) license and therefore free for personal and even commercial use. Picture taken from pexels.com or pixabay.com.
32 C. G. Fraga, *Molecular Aspects of Medicine*, 2005, **26**, 235.
33 http://www.rsc.org/periodic-table/element/29/copper (04.11.2017)
34 P. Tomislav, *Acta Crystallogr., Sect. E: Struct. Rep. Online*, 1995, **51**, 623.
35 S.-W. Peng, Y.-L. Miao and W.-D. Song, *Acta Crystallogr., Sect. E: Struct. Rep. Online*, 2006, **62**, m620.
36 F. Zhang, Y Guan, X. Chen, S. Wang, D. Liang, Y. Feng, S. Chen, S. Li, Z. Li, F. Zhang, C. Lu, G. Cao and B. Zhai, *Inorg. Chem.*, 2017, **56**, 3742
37 R. D. Costa, D. Tordera, E. Ortí, H. J. Bolink, J. Schönle, S. Graber, C. E. Housecroft, E. C. Constable and J. A. Zampese, *J. Mater. Chem.,* 2011, **21**, 16108.
38 D. R. McMillin, M. T. Buckner, and B. T. Ahn, *Inorg. Chem.*, 1977, **16**, 943.
39 J. R. Kirchhoff, R. E. Gamache, M. W. Blaskie, A. A. del Paggio, R. K. Lengel and D. R. McMillin, *Inorg. Chem.*, 1983, **22**, 2380.
40 D. Felder, J.-F. Nierengarten, F. Barigelletti, B. Ventura and N. Armaroli, *J. Am. Chem. Soc.*, 2001, **123**, 6291.
41 P. A. Breddels, P. A. M. Berdowski, G. Blasse and D. R. McMillin, *J. Chem. Soc., Faraday Trans. 2*, 1982, **78**, 595.
42 D. G. Cuttell, S.-M. Kuang, P. E. Fanwick, D. R. McMillin and R. A. Walton, J. Am. Chem. Soc., 2002, 24, 6.
43 T. J. Penfold, S. Karlsson, G. Capano, F. A. Lima, J. Rittmann, M. Reinhard, M. H. Rittmann-Frank, O. Braem, E. Baranoff, R. Abela, I. Tavernelli, U. Rothlisberger, C. J. Milne and M. Chergui, *J. Phys. Chem. A*, 2013, **117**, 4591.
44 *The Nobel Prize in Chemistry 2016 - Advanced Information*, Nobel Media AB, 2014, www.nobelprize.org/nobel_prizes/chemistry/laureates/2016/advanced.html (10.11.2017).
45 J.-P. Sauvage, *Angew. Chem. Int. Ed.*, 2017, **56**, 11080.
46 M. Mohankumar, M. Holler, J.-F. Nierengarten and J.-P. Sauvage, *Chem. Eur. J.*, 2012, **18**, 12192
47 M. Mohankumar, F. Monti, M. Holler, F. Niess, B. Delavaux-Nicot, N. Armaroli, J.-P. Sauvage and J.-F. Nierengarten, *Chem. Eur. J.,* 2014, **20**, 12083.
48 A. Kaeser, M. Mohankumar, J. Mohanraj, F. Monti, M. Holler, J.-J. Cid, O. Moudam, I.Nierengarten, L. Karmazin-Brelot, C. Duhayon, B. Delavaux-Nicot, N. Armaroli, J.-F. Nierengarten, *Inorg. Chem.*, 2013, **52**, 12140.
49 C. Zeng, N. Wang, T. Peng and S. Wang, *Inorg. Chem.*, 2017, **56**, 1616.
50 A. Kobayashi, T. Hasegawa, M. Yoshida and M. Kato, *Inorg. Chem.*, 2016, **55**, 1978.
51 D. Volz, D. M. Zink, T. Bocksrocker, J. Friedrichs, M. Nieger, T. Baumann, U. Lemmer, S. Bräse, *Chem. Mater.*, 2013, **25**, 3414.
52 Z. Liu, P. I. Djurovich, M. T. Whited and M. E. Thompson, *Inorg. Chem.*, 2012, **51**, 230.
53 M. J. Leitl, D. M. Zink, A. Schinabeck, T. Baumann, D. Volz and H. Yersin, *Top. Curr. Chem. (Z)*, 2016, **374**, 25.
54 A. Kaeser, B. Delavaux-Nicot, C. Duhayon, Y. Coppel and J.-F. Nierengarten, *Inorg. Chem.*, 2013, **52**, 14343.
55 S. Durini, G. A. Ardizzoia, B. Therrien and S. Brenna, *New J.Chem.*, 2017, **41**, 3006.
56 J. Chen, T. Teng, L. Kang, X.-L. Chen, X.-Y. Wu, R. Yu and C.-Z. Lu, *Inorg. Chem.*, 2016, **55**, 9528.
57 A. Kaeser, O. Moudam, G. Accorsi, I. Séguy, J. Navarro, A. Belbakra, C. Duhayon, N. Armaroli, B. Delavaux-Nicot and J.-F. Nierengarten, *Eur. J. Inorg. Chem.*, 2014, **8**, 1345.
58 O. Moudam, A. C. Tsipis, S. Kommanaboyina, P. N. Horton and S. J. Coles, *RSC Adv.* 2015, **5**, 95047.
59 M. Z. Shafikov, A. F. Suleymanova, R. Czerwieniec and H. Yersin, *Inorg. Chem.*, 2017, **56**, 13274.
60 M. Z. Shafikov, A. F. Suleymanova, R. Czerwieniec and H. Yersin, *Chem. Mater.*, 2017, **29**, 1708.

Chapter I: [Cu(P^P)(N^N)][PF_6] complexes with alkyl or phenyl substituted bipyridines and 2-ethyl-phenanthroline

Summary

The modification of bpys with alkyl and aryl substituents was the first project of my PhD, with two papers about these types of complexes already published and the project still ongoing. In 2013, few heteroleptic $[Cu(P^P)(N^N)]^+$ complexes were known, and even fewer were tested for their photophysical properties. Our group already had experience with copper(I) emitters and some of these compounds had been tested in light-emitting electrochemical cells (LECs) by the group of H. Bolink and E. Ortí at the University of Valencia.[1] We decided to continue the work on emissive copper(I) complexes with bis(2-(diphenylphosphino)phenyl)ether (POP) as P^P chelating ligand, and we chose 4,5-bis(diphenylphosphino)-9,9-dimethylxanthene (xantphos) as a less flexible, more rigid analogue. We were interested in the effect of alkyl and aryl substituents 6-, 5- and 4-positions at the N^N chelating ligand on the complex properties, especially concerning the photophysics and their behaviour in LECs. The complexes [Cu(POP)(N^N)][PF_6] and [Cu(xantphos)(N^N)][PF_6] complexes with N^N = 6-Mebpy, 6,6'-Me_2bpy, 6-Etbpy, 6-Phbpy are published in the papers **[1]** and **[2]** (see below). They are compared to the not yet published complexes of the same type, where the N^N chelating ligand is either 4,4'-*t*Bu_2bpy, 5,5'-Me_2bpy, 6-*t*Bubpy or 2-Etphen. The effects of the different substitution patterns on the complexes are discussed and the photophysical, electrochemical and device properties are described and conclusions for the design of future copper(I) emitters are drawn.

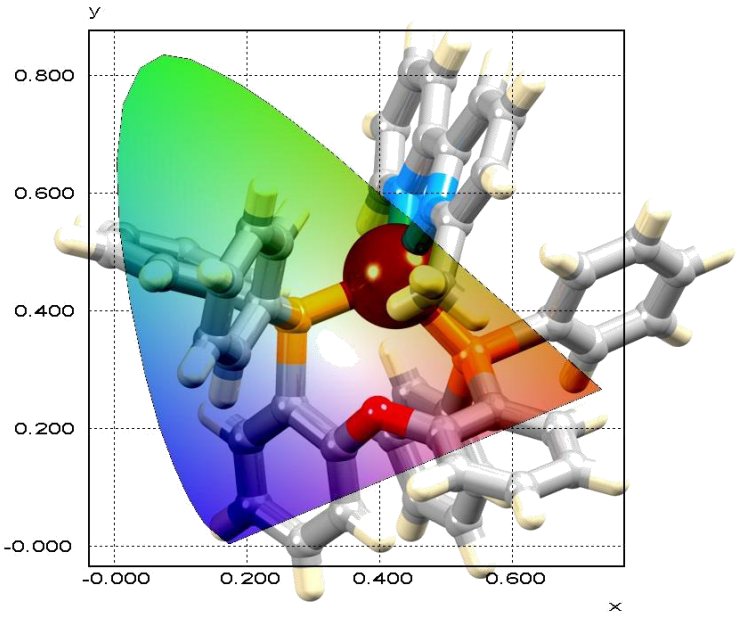

This chapter is a summary of the following papers:

[1] S. Keller, E. C. Constable, C. E. Housecroft, M. Neuburger, A. Prescimone, G. Longo, A. Pertegás, M. Sessolo, H. J. Bolink, *Dalton Trans.*, 2014, **43**, 16593.

[2] S. Keller, A. Pertegás, G. Longo, L. Martinez, J. Cerdá, J. M. Junquera-Hernández, A. Prescimone, E. C. Constable, C. E. Housecroft, E. Ortí, H. J. Bolink, *J. Mater. Chem. C.*, 2016, **4**, 3857.

The complexes [Cu(POP)(bpy)][PF_6] and [Cu(xantphos)(bpy)][PF_6] are also discussed/published in the paper/chapter about complexes with CF_3-modified bpy ligands (**[4]**, S. Keller, F. Brunner, J. M. Junquera-Hernández, A. Pertegás, M.-G. La-Placa, A. Prescimone, E. C. Constable, H. J. Bolink, E. Ortí and C. E. Housecroft, *ChemPlusChem*, submitted 21.11.2017), but shall be used here as base compounds to evaluate the effect of alkyl- and aryl substitution.

Contribution of Sarah Keller: Idea of the project and selection of ligands ❖ Synthesis of starting materials, ligands and complexes ❖ Analytical characterization (electrospray mass spectroscopy, NMR spectroscopy) ❖ Photophysical and electrochemical characterization ❖ Writing of the manuscript.

Results

In this chapter, a series of [Cu(P^P)(N^N)][PF_6] complexes is described, where P^P is either bis(2-(diphenylphosphino)phenyl)ether (POP) or 4,5-bis(diphenylphosphino)-9,9-dimethylxanthene (xantphos) and N^N is an alkyl- or phenyl-substituted 2,2'-bipyridine or 2-ethyl-1,10-phenanthroline. Structures of the complexes and the investigated ligands including atom labelling for NMR spectroscopic assignments are illustrated in Scheme 1.

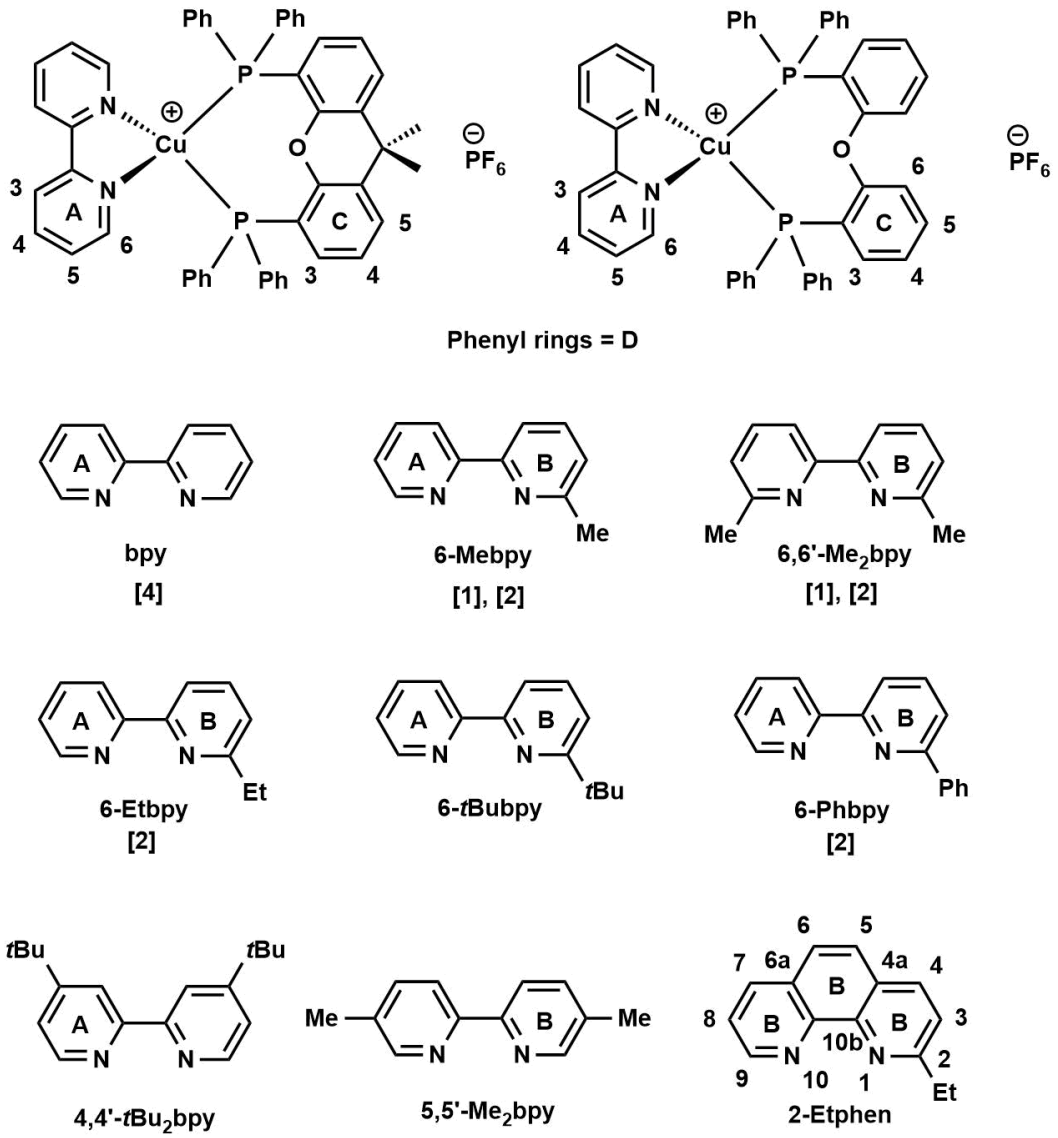

Scheme 1. Complex structures and ligands, including atom labelling for NMR spectroscopic assignments. References for the ligands where the respective complexes are published are given in square brackets.

Synthesis and steric behaviour

General

[$Cu(MeCN)_4$][PF_6] is a low-cost and convenient starting material, which is synthesized directly from Cu_2O and HPF_6 in high yield[2] and shows good stability when stored under nitrogen in the fridge. For the synthesis of the heteroleptic copper(I) complexes, two different approaches were used. The POP-containing complexes [Cu(POP)(N^N)][PF_6] were prepared by sequential addition of the POP first and N^N ligands after a 2h stirring period to [$Cu(MeCN)_4$][PF_6] in CH_2Cl_2, whereas in the case of xantphos a concerted addition of the two ligands to [$Cu(MeCN)_4$][PF_6] has been shown to be a good method.[15,16] For 6,6'-Me_2bpy, a slight excess of POP was used to push the equilibrium towards the exclusive formation of the heteroleptic [Cu(P^P)(6,6'-Me_2bpy)][PF_6]. The excess amount of bisphosphane was removed by washing the crude material with Et_2O/hexane and recrystallization (Et_2O

over complex solution in CH_2Cl_2). (For details see experimental section). The complexes were obtained as yellow solids in moderate to excellent yields (59 to 98%).

The electrospray mass spectrum of each [Cu(POP)(N^N)][PF_6] and [Cu(xantphos)(N^N)][PF_6] complex exhibited a base peak corresponding to the $[Cu(P^P)(N^N)]^+$ ion, with an isotope pattern that agreed with that calculated. Purity of the compounds was assured using elemental analysis. The formation of the heteroleptic complexes was further confirmed using NMR spectroscopic measurements (^1H, ^{13}C, ^{31}P respectively $^{31}P\{1H\}$, ^{31}P–^1H HMBC, COSY, NOESY, HMQC, HMBC) in $(CD_3)_2CO$ or CD_2Cl_2, which allow the assignment of all signals. In addition to the septet signal of $[PF_6]^-$ with J_{PF} = 710 Hz at around δ −144 ppm, for the heteroleptic [Cu(P^P)(N^N)][PF_6] complexes, the ^{31}P respectively $^{31}P\{^1H\}$ NMR spectra typically show only one broad signal in the region of δ −12 ppm, both for complexes with symmetrically and unsymmetrically substituted N^N chelating ligands.

NMR spectroscopy with focus on the structures with unsymmetrical bpy ligands

The solution ^1H and ^{13}C NMR spectra of [Cu(xantphos)(6,6'-Me_2bpy)][PF_6] were in accord with an apparent C_{2v} symmetry on the NMR timescale (due to the structure being dynamic in solution), showing only one pyridine environment (ring B, Scheme 2 (left)), and one ring C and one ring D environment (Scheme 2 (left)).

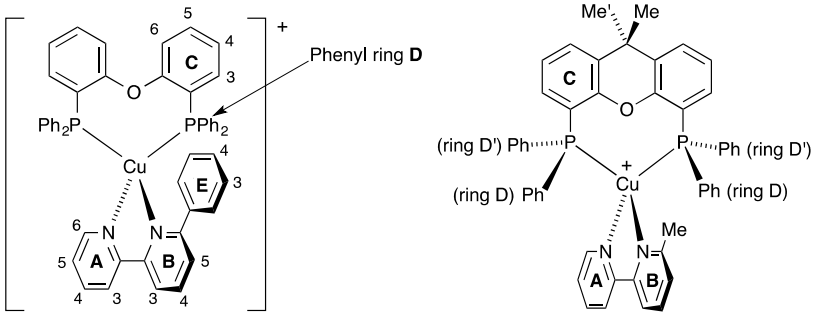

Scheme 2. Left: Atom labelling in $[Cu(POP)(6\text{-Phbpy})]^+$ for NMR spectroscopic assignments; right: Structure of $[Cu(xantphos)(6\text{-Mebpy})]^+$ showing inequivalence of phenyl rings in each PPh_2 unit, and inequivalence of the methyl groups in the xantphos ligand.

However, on going to [Cu(xantphos)(6-Mebpy)][PF_6], the symmetry is reduced (Scheme 2 (right)); Fig. 1 (left) compares the ^1H NMR spectra of [Cu(xantphos)(6,6'-Me_2bpy)][PF_6] and [Cu(xantphos)(6-Mebpy)][PF_6]. The assignments of the ^1H and the corresponding ^{13}C NMR spectra were made using COSY, HMQC and HMBC methods. Fig. 1 (right) shows part of the NOESY spectrum of [Cu(xantphos)(6-Mebpy)][PF_6]; the D and D' phenyl rings can be distinguished from the bpy-Me/H^{D2} cross peak. Analogous cross peaks in the NOESY spectrum of [Cu(xantphos)(6-Etbpy)][PF_6] between the phenyl ring H^{D2} and ethyl CH_2 protons were observed, and these in addition to HMQC and HMBC spectra allowed the complete assignments of the ^1H and ^{13}C NMR spectra of [Cu(xantphos)(6-Etbpy)][PF_6] (see experimental section and Fig. 2).

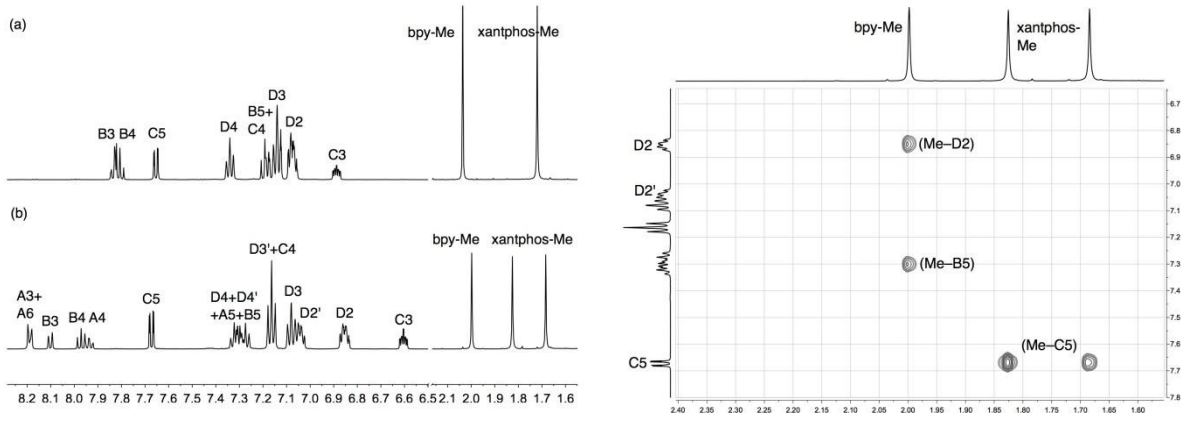

Figure 1. Left: 500 MHz ^1H NMR spectra of CD_2Cl_2 solutions of (a) [Cu(xantphos)(6,6'-Me_2bpy)][PF_6] and (b) [Cu(xantphos)(6-Mebpy)][PF_6]. See Schemes 1 and 2 for atom numbering. Chemical shifts in δ/ppm; right: Part of the NOESY spectrum of [Cu(xantphos)(6-Mebpy)][PF_6] (500 MHz, CD_2Cl_2); the bpy-Me/D2 cross peak distinguishes D2 from D2' (see Scheme 2, right).

A change in the P^P ligand on going from [Cu(xantphos)(6-Etbpy)][PF_6] to [Cu(POP)(6-Etbpy)][PF_6] is accompanied by a shift to lower frequency (δ 7.68 to 7.31 ppm) for the signal for H^{C5} (the ring CH adjacent to the bridging CMe_2 unit in xantphos), and the appearance of a signal for H^{C6} (see Scheme 2). The bpy domain is little affected (Fig. 2, top versus bottom). The chemical shift separation between signals for phenyl ring protons H^{D2} and $H^{D2'}$ becomes less on going from [Cu(xantphos)(6-Etbpy)][PF_6] to [Cu(POP)(6-Etbpy)][PF_6] (Fig. 2, top versus bottom) and this is also true if one compares the ^{1}H NMR spectra of [Cu(xantphos)(6-Mebpy)][PF_6] (Fig. 1 (left), b) and [Cu(POP)(6-Mebpy)][PF_6] (δ 7.07 and 6.96 ppm for H^{D2} and $H^{D2'}$).[16]

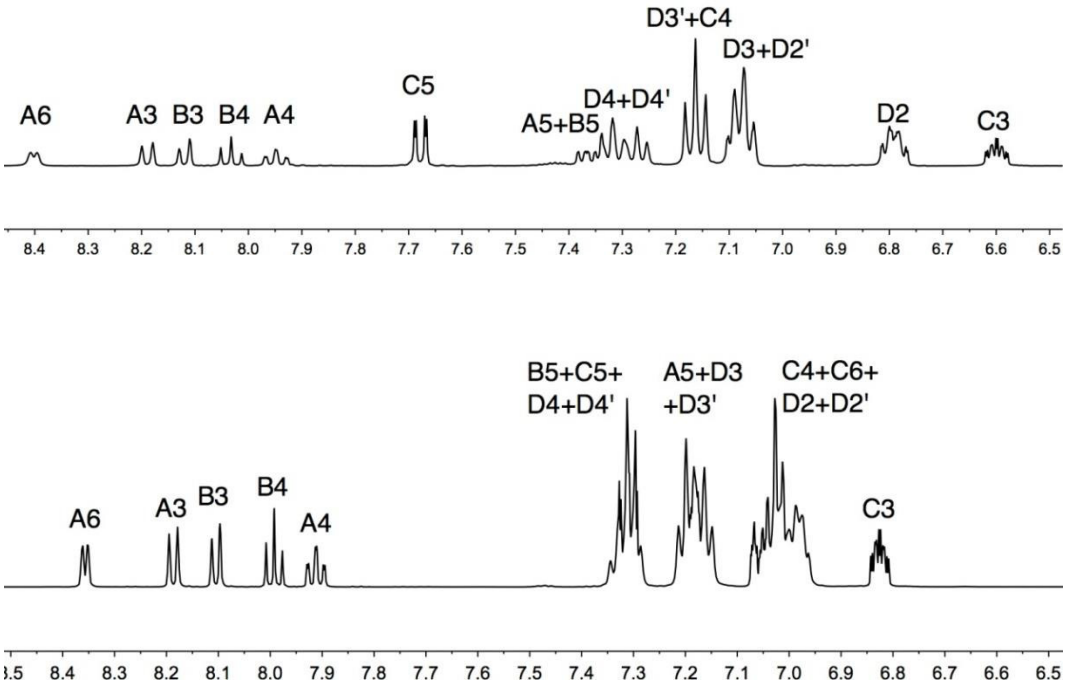

Figure 2. Top: Aromatic region of the 500 MHz ^{1}H NMR spectrum of [Cu(xantphos)(6-Etbpy)][PF_6] (CD_2Cl_2), see Scheme 2 for atom labelling; bottom: Aromatic region of the 500 MHz ^{1}H NMR spectrum of [Cu(POP)(6-Etbpy)][PF_6] (CD_2Cl_2), see Scheme 2 for atom labelling.

The room temperature solution ^{1}H and ^{13}C NMR spectra of [Cu(POP)(6-Phbpy)][PF_6] were assigned by 2D methods and are consistent with the inequivalence of the two pyridine rings in the N^N ligand and the inequivalence of the two phenyl rings in each PPh_2 unit (Fig. 3a). A change from POP to xantphos leads to the expected shift in the signal for H^{C5} (see above) and the loss of the signal for H^{C6} (Fig. 3). Most notably, no signal for H^{A6} is observed at 295 K in the 1D ^{1}H NMR spectrum of [Cu(xantphos)(6-Phbpy)][PF_6], although an HMBC cross peak between C^{A6} and H^{A4} is visible; signals for phenyl protons H^{E3} and H^{E4} are broad (Fig. 3b). The doublet for H^{E2} (Fig. 3b) was assigned on the basis of NOESY cross peaks to H^{B5} and to H^{D2}; the latter is consistent with the phenyl substituent of the N^N domain being close to phenyl D rings of the PPh_2 units (see structural discussion).

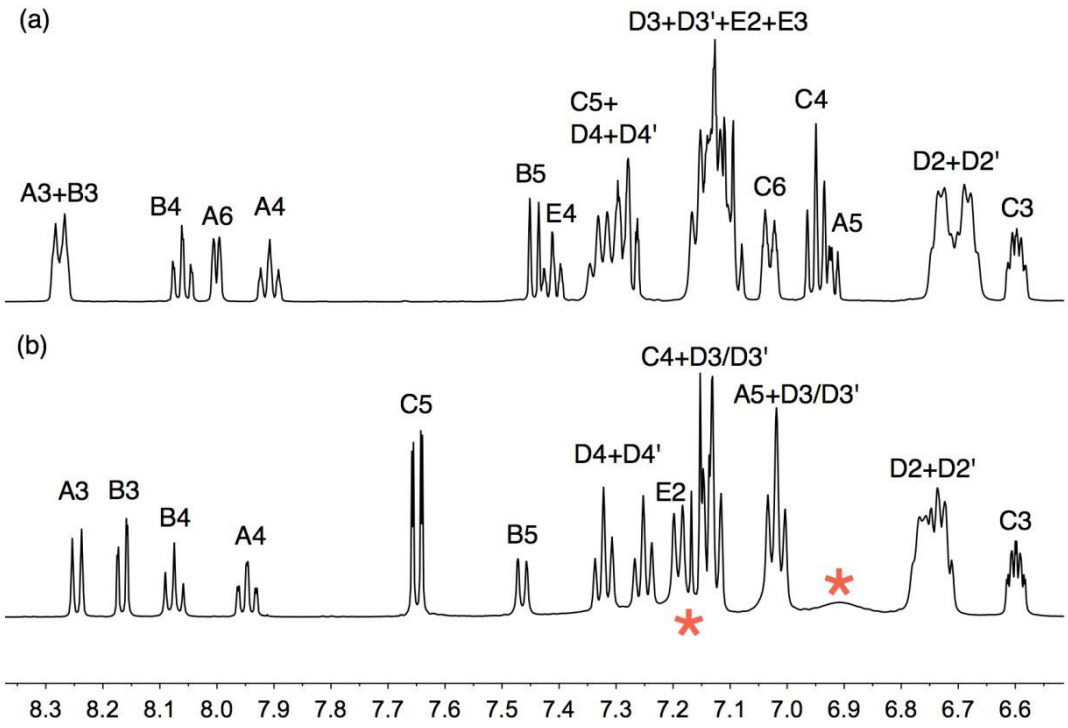

Figure 3. Aromatic region of the 500 MHz ^{1}H NMR spectra of CD_2Cl_2 solutions of (a) [Cu(POP)(6-Phbpy)][PF_6] and (b) [Cu(xantphos)(6-Phbpy)][PF_6] at 295 K. See Scheme 2 for atom numbering. Chemical shifts in δ/ppm. In (b), broad signals are marked by asterisks (see text).

The room temperature NMR spectroscopic signature of [Cu(xantphos)(6-Phbpy)][PF_6] prompted a variable temperature study. On cooling, all signals collapse and split, leading to two sets of signals at 205 K (Fig. 4) which are assigned to two conformers. The signals in Fig. 4 were assigned using COSY and HMQC spectra recorded at 205 K, and the EXSY spectrum (at 205 K, Fig. 5 (left)) was consistent with the assignments. NOESY cross peaks between H^{B5} and H^{E2} were used to confirm the bpy-to-phenyl connections in each conformer. Signal integrals at 205 K indicate that the populations of the two conformers are similar (ratio ~ 1.0:0.8). The greatest difference in chemical shifts for analogous protons in the two conformers is observed for bpy H^{A6}, and pendant phenyl H^{E3} and H^{E4} (Fig. 5 (left)). The disparate values of δ 8.42 and 6.35 ppm, respectively, for H^{A6} in the two conformers are especially noteworthy. The ^{31}P{^{1}H} NMR spectra are also consistent with the presence of two conformers. At 295 K, the ^{31}P{^{1}H} NMR spectrum shows a broad signal at δ –12.8 ppm (in addition to a septet for [PF_6]$^-$), and at 205 K, two singlets at δ –11.2 and –14.4 ppm with relative integrals of ~1.0:0.9 are observed. The cross peaks in a ^{31}P–^{1}H HMBC spectrum (Fig. 6 (left)) at 205 K are consistent with the assignments of the H^{D3}, H^{C3} and H^{C4} protons shown in Fig. 1a. Samples kept in CD_2Cl_2 solution were prone to ligand dissociation,[32] and a ^{31}P{^{1}H} NMR signal at δ –18.1 ppm was assigned to free xantphos.

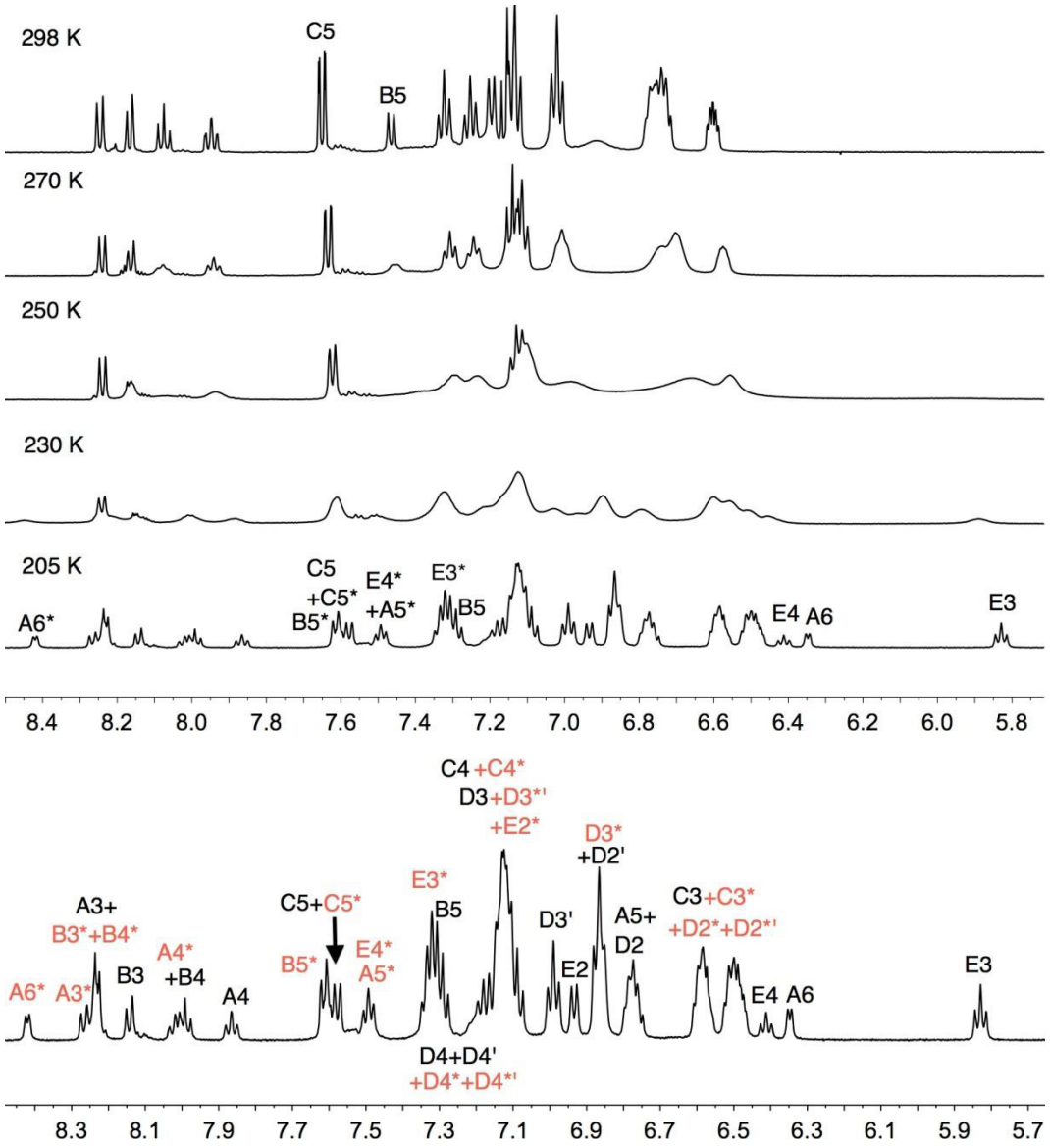

Figure 4. Top: Variable temperature ^{1}H NMR spectra of [Cu(xantphos)(6-Phbpy)][PF_6] (500 MHz, CD_2Cl_2). Complete assignments at 205 K are given in Fig. 1; bottom: Aromatic region of the 500 MHz ^{1}H NMR spectrum of [Cu(xantphos)(6-Phbpy)][PF_6] (CD_2Cl_2) at 205 K; signals marked with (red) and without (black) an asterisk arise from two different conformers.

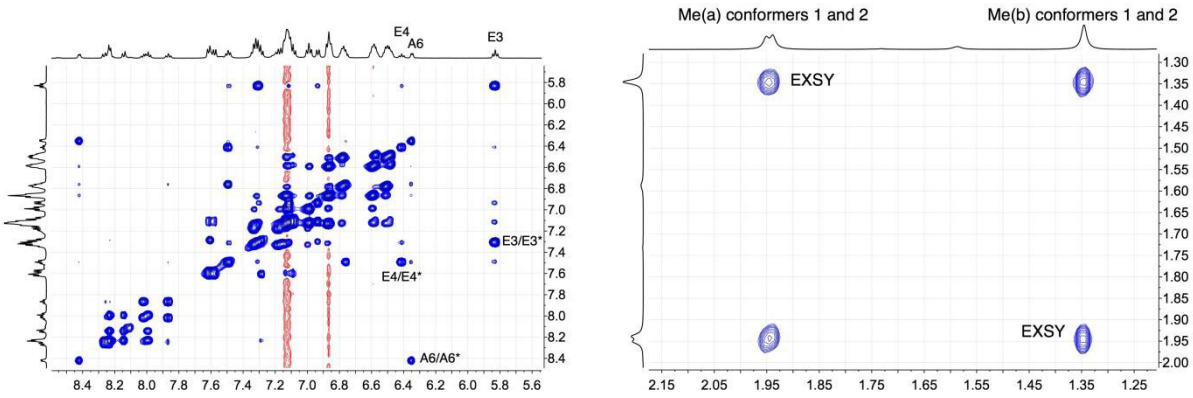

Figure 5. Left: Aromatic region of the EXSY spectrum of [Cu(xantphos)(6-Phbpy)][PF_6] (500 MHz, CD_2Cl_2) at 205 K; exchange peaks are the most intense cross peaks; weaker cross peaks are NOESY signals; right: Methyl region in the EXSY spectrum at 205 K; see Scheme 3.

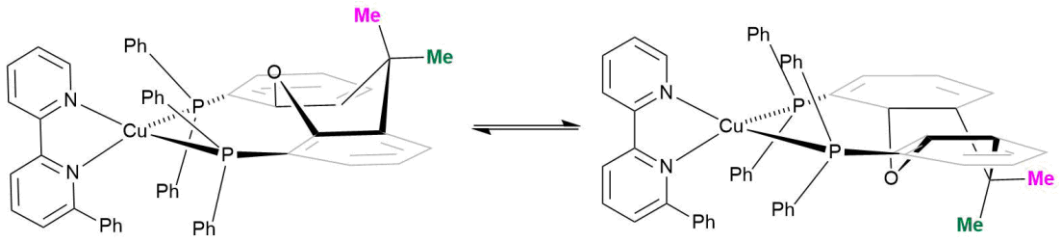

Scheme 3. Proposed conformers of [Cu(xantphos)(6-Phbpy)]$^+$ observed at 205 K in CD_2Cl_2 solution, and interconversion pathway through inversion of the xanthene unit. See also Fig. 6 (right).

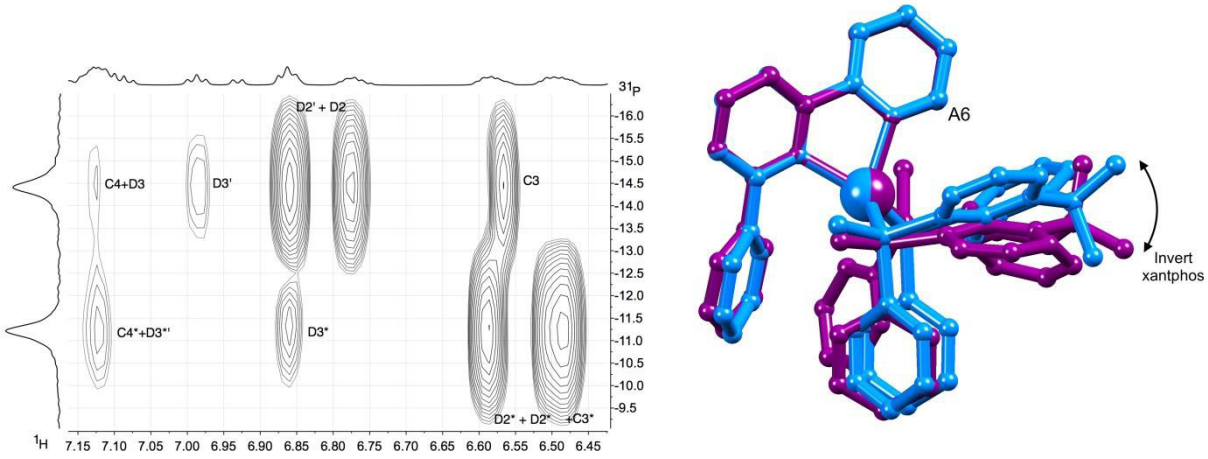

Figure 6. Left: ^{31}P–^{1}H HMBC spectrum (600 MHz, CD_2Cl_2) of [Cu(xantphos)(6-Phbpy)][PF_6] at 205 K; right: Overlay of the DFT geometry-optimized structures of two conformers of [Cu(xantphos)(6-Phbpy)]$^+$ which are related by inversion of the xanthene unit; for clarity, H atoms are omitted and only the *ipso*-C atoms of PPh_2 phenyl rings in front and behind the Cu atoms are shown. The Cu atoms and pairs of corresponding N atoms were overlaid. The position of the bpy H^{A6} protons is marked as "A6".

One possible explanation for the presence of two conformers of [Cu(xantphos)(6-Phbpy)]$^+$ is different orientations of the asymmetric N^N ligand with respect to xantphos, as we shall later consider for solid-state structures. However, a 180° rotation of the bpy unit would involve dissociation of a Cu–N bond, as discussed for the interconversion of rotational isomers of [Cu(Mepypm)(POP)]$^+$ and [Cu(Mepypm)(dppp)]$^+$ (Mepypm = 4-methyl-2-(2'-pyridyl)pyrimidine, dppp = 1,3-bis(diphenylphosphino)propane)[3] and for the interconversion of enantiomers of [Cu(N^N')$_2$]$^+$ complexes in which N^N' is an asymmetrical chelate.[4] The most important clue as to the origin of the conformer interconversion comes from the behaviour of the signals for the xantphos CMe_2 group on going from room temperature to 205 K, and the exchange peaks in the low temperature EXSY spectrum that support a change in conformation through inversion of the bowl-like conformation of the xantphos unit.[5] Signals for the two xantphos methyl groups appear at δ 1.80 and 1.61 ppm (relative integrals 1:1) at 298 K; on cooling, these collapse and then give rise to three signals at δ 1.95, 1.94 and 1.34 ppm at 205 K (relative integrals 1:1:2). The EXSY peaks shown in Fig. 5 (right) confirm exchange of the outer and inner pointing methyl groups which can only occur if the xanthene unit inverts as shown in Scheme 3.

The structures of the two conformers of the [Cu(xantphos)(6-Phbpy)]$^+$ cation depicted in Scheme 3 were optimized using B3LYP-D3/(6-31G**+LANL2DZ) calculations; this was carried out in the group of Enrique Ortí in Valencia. The xanthene units of the two structures adopt boat conformations (folded up along the O···C_{sp^3} axis) as is typical for xantphos.[6] An overlay of the geometry-optimized structures is shown in Fig. 6 (right) and confirms that protons H^{A6} experience very different environments in the two conformers. Whereas in the blue conformer in Fig. 6, proton H^{A6} is directed to the cavity of the xantphos unit and is mainly interacting with the π-system of the benzene rings, in the purple conformer it lies only 2.35 Å away from the oxygen atom. The calculated energies of the conformers differ by 3.57 kcal mol^{-1}, with the structure shown in blue in Fig. 6 (right) being the more stable.

The same dynamic behaviour was also observed for [Cu(xantphos)(bpy)]$^+$ complexes with larger aromatic substituents than phenyl (namely 1-naphthyl, 2-naphthyl or 1-pyrenyl) in 6-position at the bpy ligand.[7] Whereas for [Cu(xantphos)(6-Phbpy)]$^+$ the ratio of conformers is almost equal, with increasing steric hindrance at 6-position of the bpy one conformation becomes more preferred, with the ratio for [Cu(xantphos)(1-Pyrbpy)][PF_6] coming to

~0.05 : 1.0. In the crystal structure of [Cu(xantphos)(1-Pyrbpy)][PF_6], the pyrenyl substituent points away from the bowl-shaped xanthene-backbone, which is the same conformation as found in the solid state structure of [Cu(xantphos)(6-Phbpy)][PF_6]. For the complexes with the unsymmetrical bipyridines 6-*t*Bubpy and 2-Etphen, only one signal for H^{A6} was found in the ^{1}H NMR spectra, which leads us to the conclusion that mainly one conformer is present in solution. However, the ethyl group at the bpy ligand in [Cu(xantphos)(2-Etphen)]$^+$ faces towards the xanthene bowl, which is the opposite conformation as in the solid state structures with aromatic substituents in 6-posiiton of the bipyridine.

Meeting steric limitation

The formation of [Cu(P^P)(N^N)][PF_6] complexes by treatment of [Cu(MeCN)$_4$][PF_6] with the N^N and P^P ligands[8] can be complicated by the formation of homoleptic [Cu(N^N)$_2$][PF_6] and [Cu(P^P)$_2$][PF_6], or formation of [Cu(P^P)]$^+$.[32] While pure heteroleptic [Cu(P^P)(N^N)][PF_6] complexes were obtained for all N^N chelating ligands described above, the sterically more challenging ligands 6,6-Et_2bpy and 6,6-Ph_2bpy caused problems. Attempts to prepare [Cu(POP)(Et_2bpy)][PF_6] and [Cu(POP)(Ph_2bpy)][PF_6] led to mixtures of products which proved difficult to separate and purify. The steric repulsion of two ethyl respectively phenyl groups in both 6-positions of the bipyridine inhibits the (exclusive) formation of the heteroleptic complexes for these ligands.

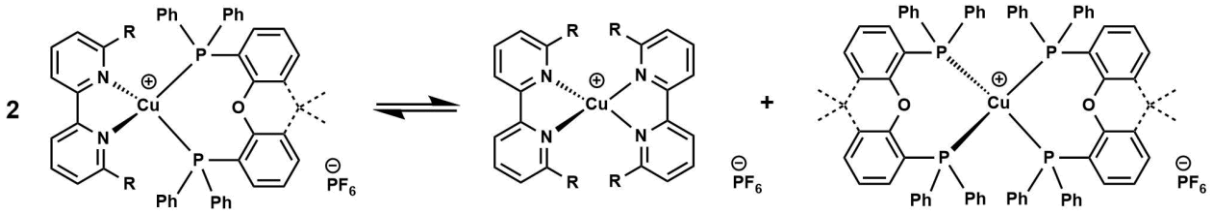

Scheme 4. Equilibrium between heteroleptic [Cu(P^P)(N^N)][PF_6] and homoleptic [Cu(N^N)$_2$][PF_6] and [Cu(P^P)$_2$][PF_6] complexes, here illustrated with P^P = POP or xantphos and modified bipyridine, with the substituents in 6,6'-positions at the bpy being sterically demanding.

The ^{31}P NMR spectrum of the solid product of the attempted preparation of [Cu(POP)(Et_2bpy)][PF_6] dissolved in CD_2Cl_2 shows two broad signals, with the one at δ −16.8 ppm being assigned to [Cu(POP)$_2$]$^+$. Recrystallization by layer diffusion of Et_2O into a solution of the material in CH_2Cl_2 resulted in the formation of colourless, red and yellow crystals that could be manually separated. Electrospray mass spectra of the red crystals show that they mainly consist of homoleptic [Cu(Et_2bpy)$_2$][PF_6], the yellow crystals were identified as heteroleptic [Cu(POP)(Et_2bpy)][PF_6]. However, the ^{31}P NMR spectra of the dissolved yellow crystals show again the same result as of the crude material, confirming the lability of the complexes and equilibrium between the heteroleptic and homoleptic species. The attempted preparation of [Cu(POP)(Ph_2bpy)][PF_6] resulted in the isolation of a red solid, which was identified to mainly consist of homoleptic [Cu(Ph_2bpy)$_2$][PF_6] and [Cu(POP)$_2$][PF_6], the electrospray mass spectra show the two heteroleptic cations as major species and a minor peak assigned to the heteroleptic [Cu(POP)(Ph_2bpy)]$^+$ cation. The same type of equilibrium was also observed in the attempted preparation of heteroleptic [Cu(P^P)(N^N)][PF_6] with 6,6'-(CF_3)$_2$bpy (see Chapter III).

Electrochemistry

The electrochemical behaviour of the heteroleptic complexes was investigated using cyclic voltammetry (CV). The cyclic voltammogram of [Cu(xantphos)(6-Mebpy)][PF_6] is illustrated in Fig.7 as example and the oxidation potentials $E_{1/2}^{ox}$ are summarized in Table 1. The first oxidation peak in the voltammogram (Fig. 7, left) is assigned to the Cu^+/Cu^{2+} process, whereas the second oxidation peak, which was also found for all the complexes, is attributed to oxidation of the phosphane ligand. The additional peak in the back scan is also associated to the oxidation of the phosphane ligand and is missing when the scan is only recorded up to the potential of the oxidation process Cu^+/Cu^{2+} (Fig. 7, right).

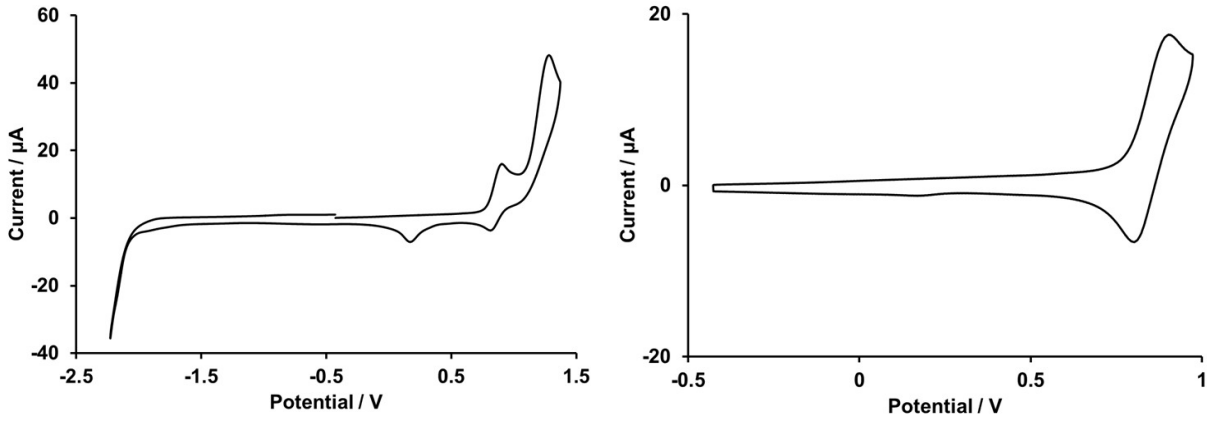

Figure 7. Cyclic voltammogram of a CH_2Cl_2 solution of [Cu(xantphos)(6-Mebpy)][PF_6] (vs. Fc^+/Fc, [$n$$Bu_4N$][$PF_6$] supporting electrolyte, scan rate = 0.1 V s^{-1}). Left: Complete scan; right: scan until oxidation peak of Cu^+/Cu^{2+}.

The oxidation potentials for the copper(I) complexes with alkyl substituents at bpy in 6-position are higher (+0.90 to +0.98 V) than for the complexes with unmodified bpy (0.72 V for [Cu(POP)(bpy)][PF_6] and 0.76 V for [Cu(xantphos)(bpy)][PF_6]). ([Cu(POP)(6-Mebpy)]$^+$ is here an exception). This is an indication for impeded Cu^+/Cu^{2+} oxidation. The alkyl groups in the 6- and 6,6'-position of the bpy stabilize the tetrahedral complex geometry preferred by Cu^+ cations and thus the oxidation state +I, as a consequence higher voltages are required for the oxidation to Cu(II) for these complexes. The oxidation processes are quasi-reversible and no reduction processes were visible for any of the complexes.

Table 1. Cyclic voltammetric data for [Cu(xantphos)(bpy)][PF_6] complexes referenced to internal Fc/Fc^+ = 0.V; CH_2Cl_2 (freshly distilled) solutions with [$n$$Bu_4N$][$PF_6$] as supporting electrolyte and scan rate of 0.1 V s^{-1}.

Complex cation	$E_{1/2}^{ox}$ / V	($E_{pc} - E_{pa}$ / mV)
[Cu(POP)(bpy)]$^+$ **[4]**	+0.71	91
[Cu(xantphos)(bpy)]$^+$ **[4]**	+0.76	110
[Cu(POP)(6-Mebpy)]$^+$ **[1]**	+0.69	125
[Cu(xantphos)(6-Mebpy)]$^+$ **[2]**	+0.85	100
[Cu(POP)(6,6'-Me_2bpy)]$^+$ **[1]**	+0.92	183
[Cu(xantphos)(6,6'-Me_2bpy)]$^+$ **[2]**	+0.89	145
[Cu(POP)(6-Etbpy)]$^+$ **[2]**	+0.80	86
[Cu(xantphos)(6-Etbpy)]$^+$ **[2]**	+0.86	80
[Cu(POP)(6-*t*Bubpy)]$^+$	+0.83	136
[Cu(xantphos)(6-*t*Bubpy)]$^+$	+0.87	99
[Cu(POP)(5,5'-Me_2bpy)]$^+$	+0.70	127
[Cu(xantphos)(5,5'-Me_2bpy)]$^+$	+0.75	131
[Cu(POP)(4,4'-*t*Bu_2bpy)]$^+$	+0.70	124
[Cu(xantphos)(4,4'-*t*Bu_2bpy)]$^+$	+0.73	112
[Cu(POP)(2-Etphen)]$^+$	+0.80	92
[Cu(xantphos)(2-Etphen)]$^+$	+0.86	91

See summary of this chapter (page 18) for references **[1]**, **[2]** and **[4]**.

Photophysics

Absorption in solution

The solution absorption spectra of the [Cu(P^P)(N^N)][PF_6] complexes are shown in Fig. 8. The intense, high energy bands arise from ligand-based π*←π and π*←*n* transitions. Lower intensity metal-to-ligand charge transfer (MLCT) bands have relatively similar values of λ_{max} (355 to 390 nm) for the complexes (Fig. 9) in CH_2Cl_2.

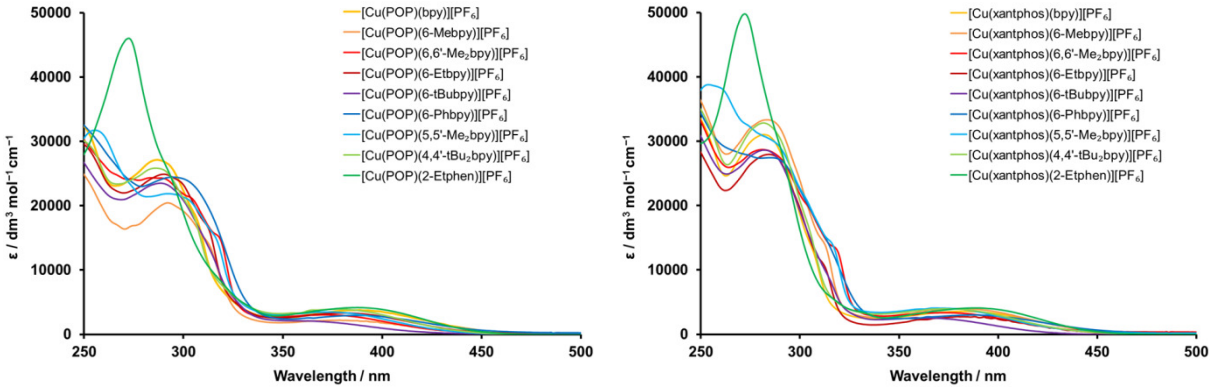

Figure 8. Solution absorption spectra of the [Cu(P^P)(N^N)][PF_6] complexes (CH_2Cl_2, 2.5×10^{-5} mol dm^{-3}). Left: Complexes with POP; right: complexes with xantphos.

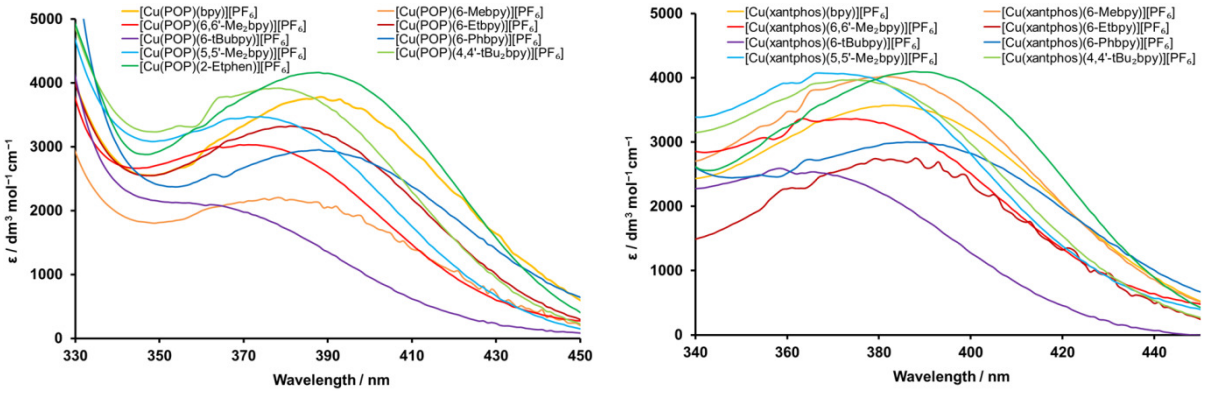

Figure 9. Expansion of the lowest-energy MLCT region of the solution absorption spectra of the [Cu(P^P)(N^N)][PF_6] complexes (CH_2Cl_2, 2.5×10^{-5} mol dm^{-3}). Left: Complexes with POP; right: complexes with xantphos.

To confirm this assignment, the lower-lying singlet excited states ($S_{n>1}$) of the complexes [Cu(xantphos)(6,6'-Me_2bpy)][PF_6], [Cu(P^P)(6-Mebpy)][PF_6], [Cu(P^P)(6-Etbpy)][PF_6] and [Cu(P^P)(6-Phbpy)][PF_6] were computed using the TD-DFT approach; this work was carried out by the group of Enrique Ortí in Valencia. Intense electronic transitions are predicted below 300 nm corresponding to S_n states with mainly ligand-centred (LC) character and some MLCT contribution, both involving the xantphos or POP ligands and the bpy moiety. A lower intensity band of MLCT nature is found in the 405–415 nm range, slightly overestimating the experimental values. It is assumed that the remaining complexes show similar results, calculations are planned for the publication of these compounds in the near future. The positions of the MLCT maxima (λ_{max}) are very similar for all the here investigated POP and xantphos complexes and are therefore mostly determined by the N^N chelating ligand. The most blueshifted absorption was recorded for the complexes with 6-*t*Bubpy, then for 6,6'-Me_2bpy, 5,5'-Me_2bpy and 4,4'-*t*Bu_2bpy. This can be explained by the +*I* effect of alkyl groups, which destabilizes the LUMO (which is mainly located on the N^N chelating ligand), thus leading to a larger HOMO-LUMO gap and the absorption of shorter wavelengths (Fig. 9). The phenyl group in 6-Phbpy on the other hand appears to be responsible for the most pronounced redshift of the MLCT band of the complexes (Fig. 9), which can be attributed to the extension of the aromatic π system. It is a common strategy in the design of dyes (copper(I) based and others) for the application in dye-sensitized solar cells to extend the aromatic π system in order to design darker dyes and allow for more light absorption.[9]

Emissive properties

Dichloromethane solutions of the [Cu(P^P)(N^N)][PF_6] complexes are all weak yellow emitters when excited at 372–400 nm (Table 2), and exhibit broad, slightly structured emission bands (Fig. 10). As observed for the absorption spectra, the solution emission maxima λ_{em}^{max} are also very similar for the complexes with POP and xantphos in combination with the same bpy ligand, the complexes with 6,6'-Me_2bpy and 2-Etphen being the only exceptions. For the [Cu(POP)(N^N)][PF_6] complexes, 6,6'-Me_2bpy leads to the shortest emission wavelengths (564, 645 nm), followed by 2-Etphen (597, 629 nm). The emission bands for the complexes with 6-Mebpy and 6-Etbpy are in the medium range of this series and very similar to each other. The complex with unsubstituted bpy exhibits the most pronounced bathochromic shift. Comparison with the emission spectra of the respective xantphos complexes identifies the complex [Cu(xantphos)(2-Etphen)][PF_6] as the most blueshifted, followed by the complexes with 6-Mebpy, 6,6'-Me_2bpy and 6-Etbpy, whose emission bands strongly resemble each other. Same as for the analogue POP complex, [Cu(xantphos)(bpy)][PF_6] has the emission with the strongest redshift. The redshift of the complexes with unsubstituted bipyridine is easily explained. Since there are no substituents in 6-position, the flattening of the tetrahedral complex geometry is facilitated leading to attack by oxygen or solvent-induced quenching mechanisms.[10,11] The general lack of substituents in the bpy which could destabilize the LUMO and lead to a larger HOMO-LUMO gap, is another reason and explains the additional (slight) redshift in comparison to complexes with bpys bearing electron-donating groups in 4- or 5-position, such as 5,5'-Me_2bpy and 4,4'-*t*Bu_2bpy. While the strongest blueshift in the POP series was expected for [Cu(POP)(6,6'-Me_2bpy)][PF_6] for the same reasons of rigidity of the complex geometry, protection of the copper centre and inductive +*I* effect of two alkyl groups, it was surprising to find that [Cu(xantphos)(2-Etphen)][PF_6] is emitting at higher energy than [Cu(xantphos)(6,6'-Me_2bpy)][PF_6]. It is also interesting to see, that the emission of [Cu(POP)(6,6'-Me_2bpy)][PF_6] is blueshifted in comparison to its xantphos analogue, whereas the situation is inverted for 2-Etphen, where the complex with POP emits further in the red than the one with xantphos. Although xantphos has been shown to undergo conformational changes in solution as evaluated earlier in this chapter, the different emissive behaviour in these cases might be linked to a more hindered flattening motion of the copper complex due to the more rigid nature of xantphos in comparison to POP. We currently have no explanation for this phenomenon, but excited state DFT calculations are planned for the future. Further insights might also be gained by energy dispersive X-ray absorption spectroscopy (ED-XAS), a method that allows the observation of photoinduced excited states in solution. We already established a collaboration with G. Smolentsev who has previously investigated the MLCT states of $[Cu(dmp)_2]^+$ (dmp =2,9-dimethyl-1,10-phenanthroline) and $[Cu(dbtmp)_2]^+$ (dbtmp =2,9-di-n-butyl-3,4,7,8-tetramethyl-1,10-phenanthroline)[12] and will hopefully find out more about the excited state behaviour of our heteroleptic copper complexes in the near future. However, the huge differences in the behaviour of POP and xantphos for only some of the complexes confirm our observation that the emissive properties of the complexes are difficult to predict, and systematic tuning is challenging.

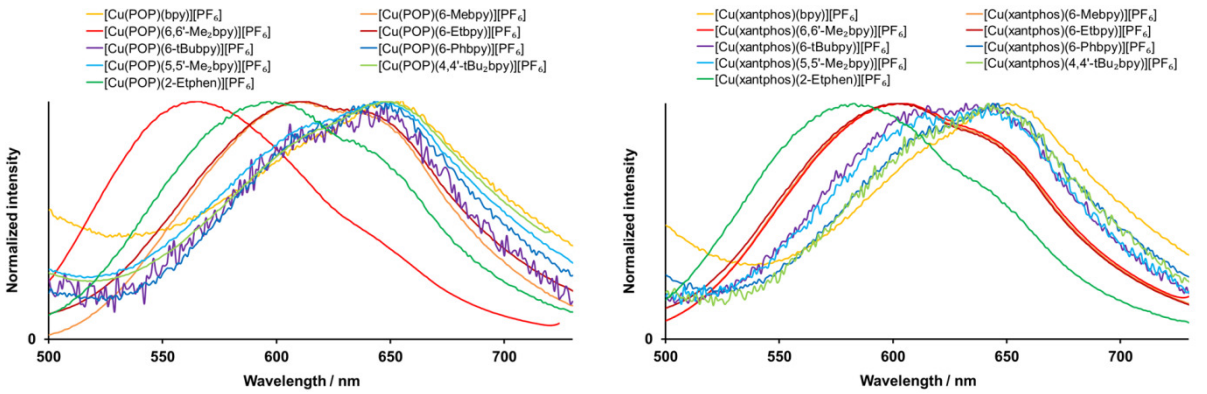

Figure 10. Normalized solution emission spectra of [Cu(P^P)(bpy)][PF_6] complexes (CH_2Cl_2, 2.5×10^{-5} mol dm^{-3}). For λ_{exc} see Table 2. Left: Complexes with POP; right: complexes with xantphos.

Reduction of the amount of dissolved O_2 by applying an argon gas flow through the solution for 20 min leads to noteworthy improved PLQY values for the complexes with the bpy ligands 6-Mebpy, 6,6'-Me_2bpy, 6-Etbpy and 2-Etphen. This effect has previously been reported for $[Cu(P^P)(N^N)]^+$ complexes[13] and is most pronounced for the complexes with 6,6'-Me_2bpy and 2-Etphen, where the quantum yields are about 10 times higher upon deaeration, for example increasing from 1.3% to 13.8 % for [Cu(POP)(6,6'-Me_2bpy)][PF_6]. Minor improvements are shown for the complexes with 6-Mebpy and 6-Etbpy, for the remaining compounds the PLQY values stay below 1%. Upon elimination of the dissolved oxygen, the remaining possible quenching mechanisms are either due to the flattening

motion of the complex (Franck-Condon principle) or solvent induced, due to exciplex formation.[14] These are the factors that are likely to be responsible for quenching the emission of the complexes where the bpy is unsubstituted in 6-position, namely bpy, 5,5'-Me_2bpy and 4,4'-*t*Bu_2bpy. The lack of improvement of the PLQY upon deaeration for the complexes with 6-*t*Bubpy and 6-Phbpy, is somewhat surprising, because for those with the other unsymmetrically substituted ligands 6-Mebyp, 6-Etpy and 2-Etphen the values were increased. Therefore, in the case of 6-*t*Bubpy and 6-Phbpy, additional quenching processes must be taking place. A possible explanation is that vibrational quenching via the additional C–H bonds offers additional non-radiative decay pathways. C–H stretching modes are some of the vibrations with the highest frequency, with C_{sp2}–H vibrations between 3100 and 3010 cm^{-1} and C_{sp3}–H vibrations between 2950 and 2850 cm^{-1}.[15] The more vibrations that are present and the higher the energy of these vibrations, the easier it is to match an electronic gap with vibrational energy.[16] On going from 6-Mebpy to 6-tBubpy, six C–H bonds more are present, for 6-Phbpy two more at slightly higher energy because of the sp^2 nature. In the case of 6-Phbpy, the extended aromatic system might also play a role in the quenching process.

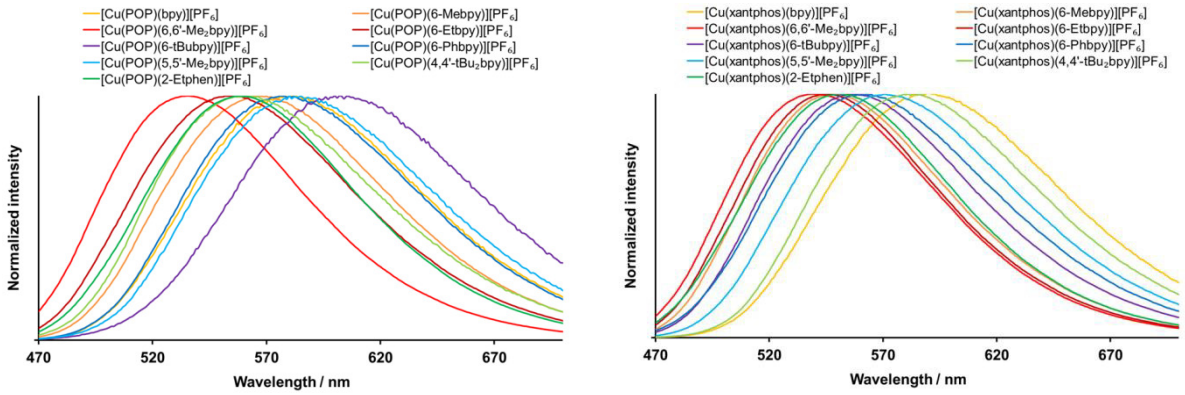

Figure 11. Normalized emission spectra of solid [Cu(P^P)(bpy)][PF_6] complexes. For λ_{exc} see Table 2. Left: Complexes with POP; right: complexes with xantphos.

Powder samples of the complexes exhibit enhanced emission behaviour.[13,17] The emission bands for the powders are broad and unstructured (Fig. 11), and are blueshifted with respect to the solution emissions, but the solids remain yellow emitters. Similar blueshifts from solution to powder are observed for [Cu(POP)(pypz)]$^+$ and [Cu(POP)(3-Mepypz)]$^+$ (pypz = 2-pyridylpyrazole, 3-Mepypz = 3-methyl-2-pyridylpyrazole).[18] The values of λ_{em}^{max} range from 535 to 602 nm (Table 2) and PLQYs from 1.1 to 43.2% were measured. The lifetimes $\tau_{1/2}$ are in the microsecond area between 0.4 and 11.4 µs. While rough trends can be found in the emission maxima and intensity for the different bpy ligands, they are not entirely systematic. For the same bpy, sometimes the respective POP complex is emitting at shorter wavelengths, sometimes the one with POP. The same holds true for the PLQY and lifetime values. This indicates that in solid state, packing interactions might have an enhanced influence on the photophysical properties of the complexes. Nevertheless, some of the observations are very conclusive as detailed below.

The most blueshifted emission was found for both the POP and the xantphos complex with 6,6'-Me_2bpy (535 and 539 nm, respectively). These are also the complexes with the highest PLQY values (43.2 for [Cu(POP)(6,6'-Me_2bpy)][PF_6] and 37.3 for [Cu(POP)(6,6'-Me_2bpy)][PF_6]) and long excited state lifetimes (10.5 and 11.4 µs). This can be attributed to the additive +*I* effect of the two alkyl groups in combination with rigidification. The second most blueshifted complexes in both the POP and xantphos series are those with 6-Etbpy, which also show good PLQYs (23.6 and 36.7%). The most redshifted complex in the POP series is [Cu(POP)(6-*t*Bubpy)][PF_6] with λ_{em}^{max} = 602 nm and the lowest quantum yield of 1.1%. This is surprising, because the tBu group should have an even more pronounced +*I* effect than Me or Et, and a destabilization of the LUMO was found in the shorter wavelength of the MLCT band in the absorption spectrum (Fig. 9). For the complexes with xantphos, [Cu(POP)(6-*t*Bubpy)][PF_6] has the most bathochromic shift with λ_{em}^{max} = 587 nm and the lowest PLQY of 1.7%. If we just compare the complexes with mono-substitution in 6-position, an interesting trend is noticeable. For both the complexes in the POP and the xantphos series, the PLQY and lifetime values increase on going from 6-Mebpy to 6-Etbpy, decrease again on going to 6-Phbpy and the lowest values are found for the complexes with 6-*t*Bubpy (see Table 2 for values). The increase upon exchange of the methyl for an ethyl group might be explained with the additional rigidification of the tetrahedral complex geometry, a benefit that might exceed possible vibrational quenching by the additional two C–H bonds of the ethyl group. For the complexes with 6-Phbpy, the opposite effects of tetrahedral stabilization and vibrational quenching leads to lower PLQY values than for those with 6-Mebpy. However it should be pointed out that the photophysical properties are still enhanced in comparison to the

complexes with unsubstituted bpy. Furthermore, the emissive properties are significantly better than for a family of [Cu(POP)(tpy)][PF_6] complexes (tpy = 2,2':2',6"-terpyridine or a 4'-derivative of tpy), where the PLQY values of the powder samples were no higher than 1%.[19] In a project with my former Master's student Fabian Brunner,[20] we found that phenyl groups in 4-positions at 6,6'-Me_2bpy lead to a redshift of the solid state emission maxima (λ_{em}^{max} = 550 and 562 nm for the complex with POP respectively xanthphos). This redshift is accompanied with a significantly decreased PLQY and lifetime in the case of the complex with xantphos (21% and 5.7 µs), however for [Cu(POP)(6,6'-Me_2-4,4'-Ph_2bpy)][PF_6] the values are almost unaffected by the phenyl substitution (44% and 10.2 µs). In the case of 6-*t*Bubpy, the drop in the PLQY and lifetime values with respect to the 6-Mebpy and 6-Etbpy complexes and even compared to [Cu(POP)(bpy)][PF_6] is likely attributed to the non-radiative decay offered by C–H bond vibrations (see above and discussion for the solution emission). The emission is extremely impaired for [Cu(POP)(6-tBubpy)][PF6], whereas for the xantphos analogue the PLQY of 9.6%, although worse than for the complex with 6-Mebpy, is still acceptable. This is another prominent example where the complex with xantphos behaves very differently than the corresponding complex with POP.

A comparison between the complexes with 6-Etbpy and those with 2-Etphen shows that the emission maxima $\lambda_{em}^{max}$of the respective POP and xantphos complexes are in a very similar range (557 and 558 nm for POP and 545 and 550 nm for xantphos). The same is true for the lifetime values $\tau_{1/2}$, which are 7.2 and 8.7 µs for the POP and 11.1 and 10.2 µs for the xantphos complexes. The only noticeable outlier is found in the PLQY of [Cu(xantphos)(2-Etphen)][PF_6], which is significantly lower than for the other complexes (9.8% in comparison to 23.6 to 36.7%). The effect of alkyl substitution in 4-and 5-position on the solid state emissive properties is noticeable, but marginal. The emission bands for the complexes with 5,5'-Me_2bpy and 4,4'-*t*Bu_2bpy are blueshifted with respect to the complexes with unsubstituted bpy, except for [Cu(POP)(5,5'-Me_2bpy)][PF_6]. The lifetime values are elongated for all these complexes and the PLQY values are higher, again with the exception of [Cu(POP)(5,5'-Me_2bpy)][PF_6]. The better values can be attributed to the *+I* effect of the alkyl groups, whereas the unexpected behavior of [Cu(POP)(5,5'-Me_2bpy)][PF_6] remains obscure.

Table 2. Emission maxima, photoluminescence quantum yields (PLQY) and lifetimes ($\tau_{1/2}$) for [Cu(P^P)(N^N)][PF_6] complexes. Solution concentration (CH_2Cl_2, 2.5×10^{-5} mol dm^{-3}) except where labelled with an asterisk (CH_2Cl_2, 5.0×10^{-5} mol dm^{-3}).

Complex cation	CH_2Cl_2 solution				Powder		
	λ_{exc}/ nm	λ_{em}^{max}/ nm	PLQY (non-deaerated / deaerated) / %	$\tau_{1/2}$ (non-deaerated / deaerated) / ns	λ_{em}^{max} / nm	PLQY / %	$\tau_{1/2}$ / µs
[Cu(POP)(bpy)]$^+$ **[4]**	388	618, 649	0.4/0.5	43/46[b]	580	3.0	1.5
[Cu(xantphos)(bpy)]$^+$ **[4]**	390	620, 650	0.5/0.5	75/104[b]	587	1.7	1.3
[Cu(POP)(6-Mebpy)]$^+$ **[1]**	378	610, 639	0.6/1.2	126/172	567	9.5	2.6
[Cu(xantphos)(6-Mebpy)]$^+$ **[2]**	379	605, 635	1.0/1.8	272/784	547	33.8	9.7
[Cu(POP)(6,6'-Me_2bpy)]$^+$ **[1]**	372	564, 645	1.3/13.8	310/4032	535	43.2	10.5
[Cu(xantphos)(6,6'-Me_2bpy)]$^+$ **[2]**	379	606, 635	1.6/10.0	451/3406	539	37.3	11.4
[Cu(POP)(6-Etbpy)]$^+$ **[2]**	390	611, 635	0.6/1.1	187/331	557	23.6	7.2
[Cu(xantphos)(6-Etbpy)]$^+$ **[2]**	390	603, 635	0.8/1.9	282/833	545	36.7	11.1
[Cu(POP)(6-*t*Bubpy)]$^+$	390*	614, 648*	0.5/0.5	39/45	602	1.1	0.4
[Cu(xantphos)(6-*t*Bubpy)]$^+$	390*	615, 632*	0.4/0.5	76/93	556	9.6	3.3
[Cu(POP)(6-Phbpy)]$^+$ **[2]**	400	620, 643	0.7/0.7	102/150	576	5.2	4.0
[Cu(xantphos)(6-Phbpy)]$^+$ **[2]**	390	620, 644	0.6/0.7	143/221	563	10.4	5.8
[Cu(POP)(5,5'-Me_2bpy)]$^+$	390	622, 643	0.5/0.7	57/108	585	2.7	2.3
[Cu(xantphos)(5,5'-Me_2bpy)]$^+$	390	616, 642	0.4/0.9	153/338	571	6.3	5.1
[Cu(POP)(4,4'-*t*Bu_2bpy)]$^+$	377	619, 647	0.5/0.6	55/65	561	3.7	3.3
[Cu(xantphos)(4,4'-*t*Bu_2bpy)]$^+$	390	627, 642	0.5/0.7	98/151	581	3.9	1.9
[Cu(POP)(2-Etphen)]$^+$	390	597, 629	0.8/6.0	240/2401	558	27.5	8.7
[Cu(xantphos)(2-Etphen)]$^+$	390	583, 626	0.9/9.6	262/4987	550	9.8	10.2

See summary of this chapter (page 18) for references **[1]**, **[2]** and **[4]**.

This extended study of the photophysical properties of the complexes revealed some important trends and showed that, in general, most substitutions at the bpy ligand lead to improved photophysical properties. However, the effect of a given ligand in combination with POP can be different from that with xantphos, so the investigation of both compounds is advisable and deductions about the effect of a certain bpy or phenanthroline have to be regarded with caution. In order to reach even higher PLQY values and further blueshifts of the emission, a combined alkyl substitution at different positions of the N^N chelating ligand might be promising. The most promising compounds were evaluated in light-emitting electrochemical cells and the results are discussed below.

Evaluation of the complexes in LECs

Operation and complex to ionic liquid ratio

In order to evaluate the electroluminescence (EL) properties of the complexes, LEC devices were prepared using a two-layer architecture, which consisted on a PEDOT:PSS layer and the [Cu(P^P)(N^N)][PF_6] complex mixed with the ionic liquid (IL) [Emim][PF_6]. The ratio of iTMC:IL has a large effect on the turn-on-time and lifetime of the LECs. Previously,[16] for [Cu(POP)(Me_2bpy)][PF_6] and [Cu(POP)(Mebpy)][PF_6], an iTMC:IL ratio of 1:1 was used. The devices were operated under a pulsed current driving (average current density 50 A m^{-2}, 1 kHz, 50% duty cycle and block wave). This driving method was previously demonstrated to lead to better lifetimes[21] than constant current (DC). The LECs prepared showed the typical behaviour of LEC operation under this driving, where the luminance rises whereas the voltage drops due to the decrease of the resistance during the p- and n-doped regions growing in the active layer.[22,23]

The majority of the LECs prepared with an iTMC:IL ratio of 1:1 composition showed a fast decrease in luminance accompanied by an increase of the operating voltage. This implies that permanent degradation occurs. For LECs using the same complexes but with a lower amount of ionic liquid (iTMC:IL ratio of 4:1), the increase in voltage was not observed and the luminance decay was slower. For this reason, the new complexes were evaluated in LECs using this iTMC:IL composition.

Device performances

The most promising complexes with acceptable solid state PLQY values were used for the fabrication of light-emitting electrochemical cells (LECs). In order to evaluate the electroluminescence (EL) properties for the complexes LEC devices were prepared using a two-layer architecture, which consisted on a PEDOT:PSS layer and the [Cu(P^P)(N^N)][PF_6] complex mixed with the ionic liquid (IL) [Emim][PF_6]. [Emim][PF_6] was selected as the IL in order to enhance the LEC response due to its higher ionic mobility compared with other commonly used ILs such as 1-butyl-3-methylimidazolium hexafluoridophosphate [Bmim][PF_6].[24] The device data for all evaluated complexes of this series are summarized in Table 3. All the devices (except the one with [Cu(POP)(bpy)][PF_6] which was investigated in an earlier project by J. Schönle[1]) were operated under a pulsed current driving, which has been demonstrated to provide better lifetimes and device performances[25] than the constant current (DC) driving method. Yellow to orange electroluminescence was produced by the devices and the electroluminescence (EL) spectra which were recorded during the device operation are illustrated in Fig. 12. For better comparability, only the results of devices with an iTMC:IL ratio of 4:1 at average current density of 50 A m^{-2} are illustrated in Figures 12 to 14, but all the tested devices are included in the discussion. The EL maxima λ_{EL}^{max} are blueshifted for all complexes with respect to [Cu(POP)(bpy)][PF_6] (597 nm). The LEC emission is similar for all these complexes (580–586 nm), except for [Cu(POP)(6,6'-Me_2bpy)][PF_6] and [Cu(xantphos)(6,6'-Me_2bpy)][PF_6], for which the EL emission maxima λ_{EL}^{max} are even more blueshifted (577 and 567 nm) with respect to the other complexes. In the solid-state emission spectra, the complexes with 6,6'-Me_2bpy are also the most hypsochromically shifted of the complexes (Table 2 and Fig. 11).

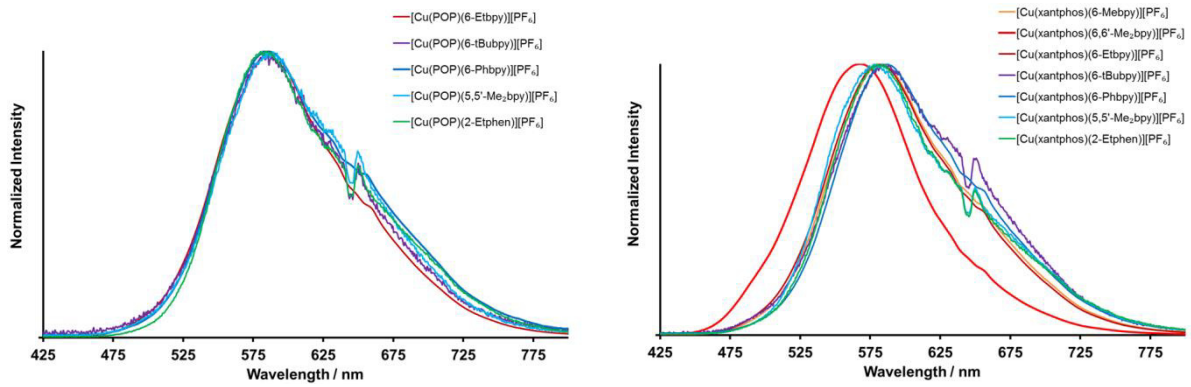

Figure 12. Electroluminescence (EL) spectra for ITO/PEDOT:PSS/[Cu(P^P)(bpy)][PF_6]:[Emim][PF_6] 4:1/Al LECs. Left: Complexes with POP; right: complexes with xantphos.

The majority of the LECs prepared showed the typical behaviour of LEC operation under pulsed current driving. Initially, the luminance rises whereas the voltage drops due to the decrease of the resistance during the p- and n-doped regions growing in the active layer (illustrated for selected complexes in Figures 13 and 14).[26,27] The time

that the device needs to reach its maximum luminance is given as the turn-on time t_{on} and values between 2 and 348 minutes are found for devices with the evaluated copper complexes. In order to be suitable for application, devices with short turn-on times, or at least with high initial luminances are desired. Extremely short turn on times (<12 seconds) were found in devices with [Cu(N^N)(6,6'-Cl_2bpy)][PF_6] (see Chapter II).

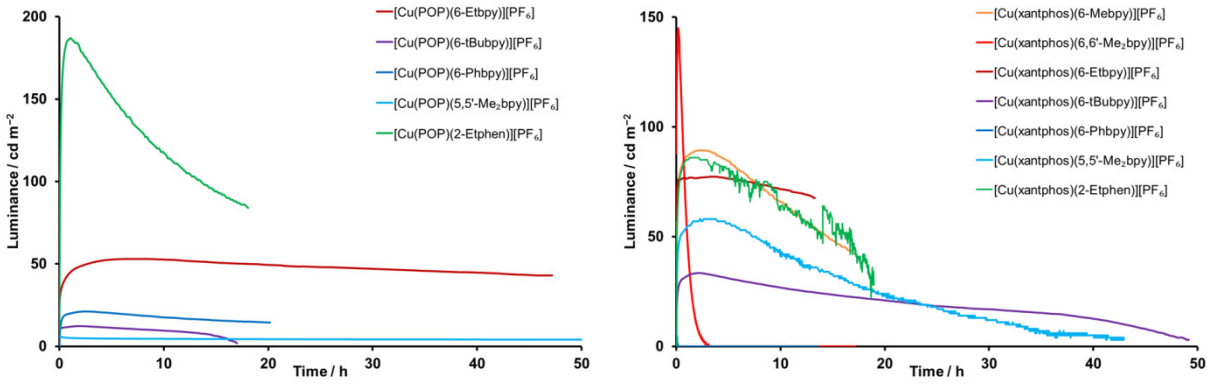

Figure 13. Luminance versus time characteristics for ITO/PEDOT:PSS/[Cu(P^P)(bpy)][PF_6]:[Emim][PF_6] 4:1/Al LECs operated at pulsed current (average current density 50 A m^{-2}, 1 kHz, 50% duty cycle, block wave). Left: Complexes with POP; right: complexes with xantphos.

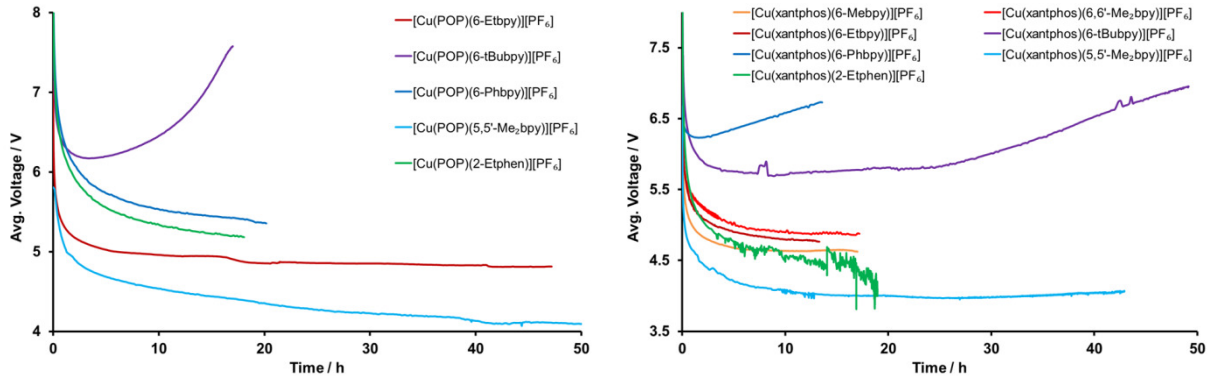

Figure 14. Average voltage versus time characteristics for ITO/PEDOT:PSS/[Cu(P^P)(bpy)][PF_6]:[Emim][PF_6] 4:1/Al LECs operated at pulsed current (average current density 50 A m^{-2}, 1 kHz, 50% duty cycle, block wave). Left: Complexes with POP; right: complexes with xantphos.

However, the turn on time is just one of the important device parameters, the maximum luminance Lum_{max} and the device lifetime $t_{1/2}$ (time until the device has lost half of the maximum luminance) are even more important when it comes to the desired properties for application.

The brightest devices (at operation of 50 A m^{-2} average current density) were built with [Cu(POP)(2-Etphen)][PF_6] and [Cu(xantphos)(6,6'-Me_2bpy)][PF_6] (Lum_{max} = 186 and 145 cd m^{-2}). For the former, operation at 100 A m^{-2} average current density even lead to 430 cd m^{-2}, which makes it one of the brightest copper(I) based LECs reported so far.[28] The EQE of this device is 2.0% and the efficacy comes to 4.3 cd A^{-1}. A comparable complex with [Cu(POP)(2,9-*n*Bu_2phen)][BF_4] gave an EQE of 16% in a LEC, one of the highest reported for a copper-based LEC, however the device lifetime was below 1.3 hours.[29,30] However, the lifetime of our devices with [Cu(POP)(2-Etphen)][PF_6] is significantly better, with 6.4 and 4.8 hours for operation at 100 respectively 50 A m^{-2}. This is also a significant improvement with respect to the second brightest devices of our series with 6,6'-Me_2bpy, where the device lifetimes are shorter than two hours, even for operation at only 10 A m^{-2}. The longest device lifetimes (with acceptable luminance values) were obtained for the ethyl-substituted complexes [Cu(POP)(6-Etbpy)][PF_6] (82 hours) and [Cu(xantphos)(6-Etbpy)][PF_6] (51 hours). [Cu(POP)(6-Etbpy)][PF_6] achieves an efficiency of 0.6 cd A^{-1} and [Cu(xantphos)(6-Etbpy)][PF_6] reaches 1.7 cd A^{-1}; both are comparable with the efficiencies of LECs containing [Cu(POP)(6-Mebpy)][PF_6] (0.6 cd A^{-1}) and [Cu(xantphos)(6-Mebpy)][PF_6] (1.9 cd A^{-1}). Relatively long lifetimes were also found for devices with [Cu(POP)(5,5'-Me_2bpy)][PF_6] (53.5 h), [Cu(POP)(6-Phbpy)][PF_6] (36 h) and [Cu(xantphos)(6-*t*Bubpy)][PF_6] (30.5 h), however the devices were not very efficient, with EQE values at 0.3%

or lower and Lum_{max} values of 33 cd m^{-2} or lower, which is in accordance with the low PLQY for these complexes (Table 2). While the Lum_{max} values usually follow the trends of the solid state PLQY, finding a ligand combination that gives stable devices has been challenging and the long device lifetimes for the complexes with mono-ethyl (and mono-methyl) substituted bpy ligands were surprising. Degradation of the devices is usually accompanied by an increase of the steady-state voltage in the devices which happens relatively fast in the devices with [Cu(POP)(6-*t*Bubpy)][PF_6] and [Cu(xantphos)(6-Phbpy)][PF_6] (Fig. 14). How and why exactly the degradation of the devices and the loss of luminance occur is a topic that deserves significantly more attention. For this series of complexes, the device lifetimes cover a range from 0.1 to 82 hours, which is an enormous difference. Finding out not only which copper complexes give elongated lifetimes with respect to others, but also why would be extremely valuable for the design of better emitter materials and could help boosting light-emitting electrochemical cells towards commercial application.

Table 3. Performance of LEC devices of the architecture ITO/PEDOT:PSS/iTMC:[Emim][PF_6]/Al measured using a pulsed current driving (average current density 10, 50 or 100 A m^{-2}, 1 kHz, 50% duty cycle, block wave). LECs in publication **[1]** were built with a 1:1 molar ratio of copper(I) complexe : IL, while LECs in publication **[2]** have a 4:1 molar ratio. In earlier LECs by Schönle *et al.* used a 1:1 molar ratio of comples:IL and the devices were tested at applied bias of 5 V (marked with an asterisk). All used iTMCs are $[PF_6]^-$ salts.

iTMC	Avg. current density / A m^{-2}	t_{on} [a] / min	Lum_0 [b] / cd m^{-2}	Lum_{max} [c] / cd m^{-2}	$t_{1/2}$ [d] / h	EQE_{max} [e] / %	PCE_{max} [f] / lm W^{-1}	$Efficacy_{max}$ / cd A^{-1}	λ_{EL}^{max} / nm
[Cu(POP)(bpy)]$^+$	*	2	–	25.8	0.07	–	–	1.25	597
[Cu(POP)(6-Mebpy)]$^+$ **[1]**	10	65	–	6.7	11.5	–	–	0.6	574
[Cu(xantphos)(6-Mebpy)]$^+$ **[2]**	50	102	41	90	15	0.7	0.6	1.9	583
[Cu(POP)(6,6'-Me_2bpy)]$^+$ **[1]**	10	23	–	53	1.5	–	–	5.2	577
[Cu(xantphos)(6,6'-Me_2bpy)]$^+$ **[2]**	50	10	88	145	0.8	1.0	0.8	3.0	567
[Cu(POP)(6-Etbpy)]$^+$ **[2]**	50	260	25	53	82	0.2	0.2	0.6	582
[Cu(xantphos)(6-Etbpy)]$^+$ **[2]**	50	42	57	77	51	0.7	0.5	1.7	581
[Cu(POP)(6-*t*Bubpy)]$^+$	100	72	–	12	14.7	<0.1	<0.1	0.1	582
[Cu(xantphos)(6-*t*Bubpy)]$^+$	100	109	–	33	30.5	<0.1	<0.1	0.3	586
[Cu(POP)(6-Phbpy)]$^+$ **[2]**	50	156	0	21	36	0.1	0.1	0.4	584
[Cu(xantphos)(6-Phbpy)]$^+$ **[2]**	50	2	1	5	0.1	<0.1	<0.1	<0.1	586
[Cu(POP)(5,5'-Me_2bpy)]$^+$	50	348	–	33	53.5	0.3	0.2	0.7	584
[Cu(POP)(5,5'-Me_2bpy)]$^+$	100	9	–	82	7.6	0.4	0.3	0.8	584
[Cu(xantphos)(5,5'-Me_2bpy)]$^+$	50	168	–	58	16.7	0.5	0.4	1.2	578
[Cu(xantphos)(5,5'-Me_2bpy)]$^+$	100	5	–	86	3.3	0.4	0.3	0.9	578
[Cu(POP)(2-Etphen)]$^+$	50	53	–	186	6.4	1.7	0.5	3.7	583
[Cu(POP)(2-Etphen)]$^+$	100	10	–	430	4.8	2.0	1.1	4.3	583
[Cu(xantphos)(2-Etphen)]$^+$	50	88	–	86	15.5	0.7	0.5	1.7	580
[Cu(xantphos)(2-Etphen)]$^+$	100	26	–	176	10.4	0.8	0.5	1.8	580

See summary of this chapter (page 18) for references **[1]**, **[2]** and **[4]**.

Conclusions and Outlook

Project summary

We have described the synthesis and characterization of a series of [Cu(POP)(N^N)][PF_6] and [Cu(xantphos)(N^N)][PF_6] complexes with N^N being either naked bpy, mono-substituted 6-Mebpy, 6-Etbpy, 6-*t*Bubpy, 6-Phbpy and 2-Etphen or disubstituted 6,6'-Me_2bpy, 5,5'-Me_2bpy and 4,4'-Me_2bpy. In these distorted tetrahedral copper(I) complexes, the asymmetrical N^N ligands can be oriented so that the 6-substituent lies over either two PPh_2 units of the P^P ligand, or the $O(C_6H_4)_2$ unit or the xanthene 'bowl' of the P^P domain. Both conformers are represented among the crystallographically determined structures of the complexes. For the xantphos-containing complexes with 6-Mebpy, 6-Etbpy and 6-Phbpy, the energy difference between conformers was calculated and found to be very small (0.25–0.54 kcal mol^{-1}). In solution, VT-NMR spectroscopic data for [Cu(xantphos)(Phbpy)][PF_6] in CD_2Cl_2 evidence the presence of two conformers which are related by inversion of the xanthene 'bowl'. In the solid-state, the conformation of the xanthene unit is constant and provides a 'bowl' to accommodate one end of the N^N ligand. Cyclovoltammetry revealed that the oxidation potentials for the investigated copper(I) complexes with alkyl substituents at bpy in 6-position (with exception of ([Cu(POP)(6-Mebpy)][PF_6]) are significantly higher (+0.90 to +0.98 V) than for the complexes with unmodified bpy (0.72 V for [Cu(POP)(bpy)][PF_6] and 0.76 V for [Cu(xantphos)(bpy)][PF_6]), which indicates impeded Cu^+/Cu^{2+} oxidation and stabilization of the oxidation state +I by rigidification of its preferred tetrahedral complex geometry. The [Cu(P^P)(N^N)][PF_6] complexes exhibit MLCT absorption bands in the range 355 to 390 nm, and are yellow to orange emitters when excited into the MLCT band. The PLQYs increase from solution to powder samples. Especially in solid state, the PLQY and lifetime values cover a wide range, depending on the nature and position of the substituent. The highest PLQY values was measured for [Cu(POP)(6,6'-Me_2bpy)][PF_6] (43.2%), which also shows one of the longest lifetimes (10.5 µs) and the most blueshifted emission (535 nm). The most bathochromic emission was recorded for [Cu(POP)(6-*t*Bubpy)][PF_6] (602 nm), which also has the lowest PLQY (1.1%) and shortest lifetime (0.4 µs). However, with the exception of [Cu(POP)(6-*t*Bubpy)][PF_6], the introduction of alkyl-or aryl substituents leads to improved photophysical properties with respect to the complexes with unsubstituted bpy, [Cu(POP)(bpy)][PF_6] and [Cu(xantphos)(bpy)][PF_6]. The complexes were tested in LEC configuration devices which exhibit relatively rapid turn-on times. The LEC using [Cu(POP)(2-Etphen)][PF_6] as the electroluminescent material achieves the highest luminances Lum_{max} of 430 and 180 cd m^{-2} with 6.4 and 4.8 hours lifetime for operation at 100 respectively 50 A m^{-2}. The efficacy of these devices comes to 3.7 cd A^{-1} respectively 4.3 cd A^{-1} for operation at 50 and 100 A m^{-2}. The highest efficacy was obtained for the device with [Cu(POP)(6,6'-Me_2bpy)][PF_6] (5.2 cd A^{-1}), however this device was operated at lower current density (10 A m^{-2}) and only reached a maximum luminance Lum_{max} of 53 cd m^{-2} and a device lifetime of 1.5 hours. Efficiency and PLQY were found to follow similar trends for this series of complexes. Long-lived LECs were realized with [Cu(xantphos)(6-Etbpy)][PF_6] and [Cu(POP)(6-Etbpy)][PF_6] in the active layer ($t_{1/2}$ > 40 and 80 h, respectively), however with lower luminances (53 and 77 cd m^{-2}) and thus a loss in efficiency (0.6 and 1.7 cd A^{-1}). This trade-off between brightness and lifetime is one of the main challenges to be addressed in the future. The number of possible bpy ligands with alkyl or aryl substituents is large and the effects of the changes in substituents are not always predictable. However, we made promising discoveries and were able to identify and explain trends and patterns, that will be invaluable for the development of future copper(I) emitters and already were implemented in our strategies to design the next generation of complexes.

In progress

We found out that for [Cu(P^P)(N^N)][PF_6] complexes, one methyl or respectively one ethyl group in 6-position of the bpy ligand leads to significantly prolonged device lifetimes. One *tert*-butyl or phenyl group on the other hand is detrimental to the photoluminescent properties as well as the device performance, both in terms of luminance and efficiency. In the next step, we would like to investigate the effect of alkyl groups in 4-position further. In Scheme 5 the bpy ligands with alkyl modifications that we are currently investigating are illustrated.

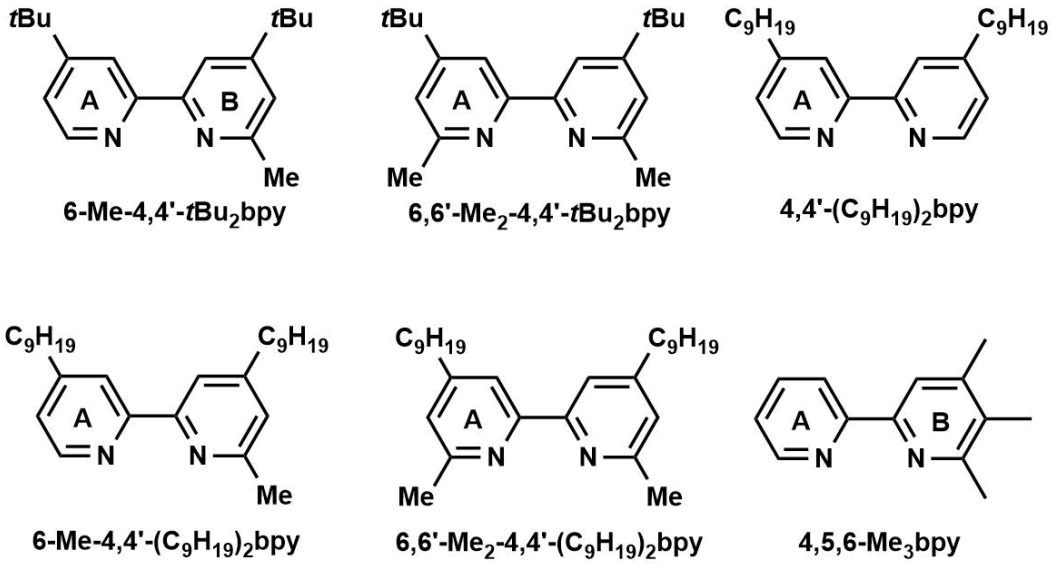

Scheme 5. Alkyl-modified 2,2'-bipyridines that are under investigation or planned to be evaluated as ligands for light-emissive [Cu(P^P)(N^N)][PF_6] complexes. 4,4'-(C_9H_{19})$_2$bpy is commercially available. 4,5,6-Me_3bpy is synthesized by coupling 2-Cl-4,5,6-Me_3-pyridine[31] with 2-pyridyl zinc bromide.[32] The other ligands are synthesized by methylation with MeLi of the commercially available 4,4'-disubstituted bpy.

Costa *et al.*[33] reported, that substituents at the bpy in 4-position can have considerable influence on the photophysical properties of [Cu(P^P)(bpy)][PF_6] complexes, both on the quantum yield and performance of the devices. They systematically studied the effect of electron donating and electron withdrawing substituents in this position and found that the more negative the σ-Hammett parameter σp, which describes the σ-donation ability of a given substituent, the more enhanced is the performance of the LEC which employs the respective compound, within a given series of complexes. However, in this study only bpy ligands without substituents in the 6-position were investigated, whereas we would like to combine 4- and 6-substitution in order to further optimize the emissive properties of the complexes and their behaviour in the devices.

The solid state PLQY of the complexes on going from unsubstituted bpy to 4,4'-*t*Bubpy is improved (although not drastically) and the emission is blueshifted. Compounds with an emission in the blue are desirable because there is still a relative shortage of efficient and sustainable blue emitters. In addition, the *t*Bu or nonyl groups might be beneficial for the performance in the LECs by reducing intermolecular interaction.[34,35] 4,5,6-Me_3bpy is an interesting ligand candidate because it is very unsymmetrical, and the employment of the unsymmetrical monosubsituted bpys was very beneficial for the device lifetime. Furthermore, the LUMO-destabilizing effect of three methyl groups is expected to be additive, which should then lead to a very blueshifted emission. Last but not least we were interested to see if our hypothesis would be confirmed, that emission quenching by C–H bond vibrations only occurs when these C–H bonds are in the vicinity of the copper centre, as for example in complexes with 6-*t*Bubpy or the bisphosphane *t*Bu-xantphos (see also Chapter V).

However, also a move from 2,2'-bipyridine to 1,10-phenanthroline ligands has to be considered, since some of the device properties of the complexes with 2-Etphen are superior to those with bpy ligands. While we can already see trends and patterns in the effects of alkyl-substitution at the bpy, the results of the completed study presented in this chapter in combination with the ongoing projects should lead to a full understanding of the effect of different alkyl groups in different positions at the bpy on the complex properties. The results will be incorporated in the design of new luminescent copper(I) complexes, where alkyl groups can be combined with other substituents at the ligands in order to further optimize and tune the emissive properties.

Experimental of the alkyl chapter

"The language of experiment is more authoritative than any reasoning; facts can destroy our ratiocination—not vice versa." – Alessandro Volta

General

^{1}H, ^{13}C and ^{31}P NMR spectra were recorded at room temperature using a Bruker Avance III-600, III-500 or III-400 NMR spectrometer. ^{1}H and ^{13}C NMR chemical shifts were referenced to residual solvent peaks with respect to δ(TMS) = 0 ppm and ^{31}P NMR chemical shifts with respect to δ(85% aqueous H_3PO_4) = 0 ppm. Solution absorption and emission spectra were measured using an Agilent 8453 spectrophotometer and a Shimadzu RF-5301PC spectrofluorometer, respectively. Electrospray ionization (ESI) mass spectra were recorded on a Bruker esquire 3000plus instrument. Quantum yields in CH_2Cl_2 solution and powder were measured using a Hamamatsu absolute photoluminescence (PL) quantum yield spectrometer C11347 Quantaurus-QY. Emission lifetimes and powder emission spectra were measured with a Hamamatsu Compact Fluorescence lifetime Spectrometer C11367 Quantaurus-Tau, using an LED light source with λ_{exc} = 365 nm. Quantum yields and PL emission spectra in thin films were recorded using a Hamamatsu absolute quantum yield C9920. The preparation of the thin film samples consisted of deposition on a quartz plate (1 cm^2) of the complex with addition of the ionic liquid 1-ethyl-3-methylimidazolium hexafluoridophosphate [Emim][PF_6]. These samples were excited using a light source with λ_{exc} = 365 nm at room temperature under ambient conditions.

Crystallography

Data were collected on a Bruker Kappa Apex2 diffractometer with data reduction, solution and refinement using the programs APEX[36] and CRYSTALS.[37] Structural analysis was carried out using Mercury v. 3.5.1.[38,39]

Computational details (carried out by E. Ortí and coworkers in Valencia)

Dispersion-corrected density functional calculations (DFT-D) were carried out with the D.01 revision of the Gaussian 09 program package[40] using Becke's three-parameter B3LYP exchange-correlation functional[41,42] together with the 6-31G** basis set for C, H, and N,[43] and the "double-ζ" quality LANL2DZ basis set for the Cu element[44] in which an effective core potential (ECP) replaces the inner core electrons. The D3 Grimme's dispersion term with Becke-Johnson damping was added to the B3LYP functional (B3LYP-D3) to get a better description of the intramolecular non-covalent interactions that are expected to play a relevant role in determining the molecular geometry of the studied systems.[45,46] The geometries of both the singlet ground electronic state (S_0) and the lowest-energy triplet state (T_1) were fully optimized without imposing any symmetry restriction. The geometry of T_1 was calculated at the spin-unrestricted UB3LYP-D3 level using a spin multiplicity of three. Phosphorescence emission energies were estimated as the vertical energy difference between the energy of the minimum of the lowest-energy triplet state and the energy of S_0 at the T_1 optimized geometry. All the calculations were performed in the presence of the solvent (CH_2Cl_2). Solvent effects were considered within the self-consistent reaction field (SCRF) theory using the polarized continuum model (PCM) approach.[47,48,49] The calculation of the energy of S_0 at the T_1 geometry was performed as an equilibrium single-point calculation with respect to the solvent reaction field/solute electronic density polarization process. Time-dependent DFT (TD-DFT)[50,51,52] calculations of the lowest-lying 30 singlet excited states and the lowest-lying 30 triplets of all the complexes were performed in the presence of the solvent at the minimum-energy geometry optimized for the ground state.

Device preparation (carried out by H. Bolink and coworkers in Valencia)

LECs were prepared on top of a patterned indium tin oxide (ITO, 15 Ω $\square^{-1}$) coated glass substrate (www.naranjosubstrates.com) previously cleaned as follows: a) sonication with soap, b) deionized water, c) isopropanol and d) UV-O_3 lamp for 20 min. The thickness of the films was determined with an Ambios XP-1 profilometer. Prior to the deposition of the emitting layer, 80 nm of poly(3,4-ethylenedioxythiophene):poly(styrenesulfonate) (PEDOT:PSS) (CLEVIOS™ P VP AI 4083, aqueous dispersion, 1.3–1.7% solid content, Heraeus) was coated in order to increase the reproducibility of the cells. The emitting layer (130 nm) was prepared by spin-coating of an MeCN solution consisting of the emitting compound with the addition of an ionic liquid 1-ethyl-3-methylimidazolium hexafluoridophosphate [Emim][PF_6] (> 98.5%, Sigma-Aldrich) in a 4 to 1 molar ratio. The devices were then transferred to an inert atmosphere glovebox (< 0.1 ppm O_2 and H_2O, MBraun), where a layer (70 nm) of aluminium (the top electrode) was thermally evaporated onto the devices using an Edwards Auto500 evaporator integrated in the inert atmosphere glovebox. The area of the device was 6.5 mm^2. The devices were not encapsulated and were characterized inside the glovebox at room temperature.

Device characterization

The device lifetime was measured by applying a pulsed current and monitoring the voltage and luminance versus time by a True Colour Sensor MAZeT (MTCSiCT Sensor) with a Botest OLT OLED Lifetime-Test System. The average current density is determined by multiplying the peak current density by the time-on time and dividing by the total cycle time. The average luminance is directly obtained by taking the average of the obtained photodiode results and correlating it to the value of a luminance meter. The current efficiency is obtained by dividing the average luminance by the average current density. The electroluminescent (EL) spectra were measured using an Avantes AvaSpec-2048 Fiber Optic Spectrometer during device lifetime measurement.

Ligands

The following ligands were obtained from commercial sources: POP (Acros), xantphos (Fluorochem), bpy (TCI chemicals), 4,4'-*t*Bu$_2$bpy (Sigma-Alrich), 6,6'-Me$_2$bpy (Fluochem), 5,5'-Me$_2$bpy (Sigma-Aldrich), phen (Sigma-Aldrich).

The compounds 6-Mebpy, 6-Etbpy, 2-Etphen and 6-Phbpy were prepared following literature methods[53,54] and the NMR spectroscopic data matched those reported.[35,55] The ligand 6-*t*Bubpy was synthesized from 2-chloro-6-methyl-pyridine[56] adapting previously reported methods (Negishi coupling with 2-pyridylzinc bromide)[31].

2-Etphen

In anology to the synthesis of 6-Mebpy and 6-Etbpy.[32,33] The batch size was 11 mmol and the title compound was obtained as colourless oil (121 mg, 0.6 mmol, 5%). ^{1}H NMR (500 MHz, $CDCl_3$, 298 K) δ /ppm 9.21 (dd, J = 4.3, 1.8 Hz, 1H, H^{B9}), 8.22 (dd, J = 8.1, 1.8 Hz, 1H, H^{B7}), 8.17 (d, J = 8.2 Hz, 1H, H^{B4}), 7.76 (d, J = 8.8 Hz, 1H, H^{B5}), 7.72 (d, J = 8.8 Hz, 1H, H^{B6}), 7.60 (dd, J = 8.0, 4.3 Hz, 1H, H^{B8}), 7.56 (d, J = 8.2 Hz, 1H, H^{B3}), 3.26 (q, J = 7.7 Hz, 2H, $H^{Et\text{-}CH2}$), 1.46 (t, J = 7.7 Hz, 3H, $H^{Et\text{-}CH3}$). ^{13}C NMR (126 MHz, $CDCl_3$, 298 K) δ /ppm 164.8 (C^{B2}), 150.4 (C^{B9}), 146.3 (C^{B10a}), 145.8 (C^{B10b}), 136.5 (C^{B4}), 136.1 (C^{B7}), 128.9 (C^{B6a}), 127.0 (C^{B4a}), 126.6 (C^{B5}), 125.6 (C^{B3}), 122.8 (C^{B8}), 122.4 (C^{B3}), 32.7 ($C^{Et\text{-}CH2}$), 14.7 ($C^{Et\text{-}CH3}$).

Complex synthesis

[Cu(MeCN)$_4$][PF$_6$] was prepared from Cu$_2$O and HPF$_6$ in MeCN by the published method.[57] Unless stated otherwise, the following procedures were applied for the synthesis of the heteroleptic [Cu(P^P)(N^N)][PF$_6$] complexes with a standard batch size of 0.25 mmol.

Standard procedure for POP:

A colourless solution of POP (1.0 eq) and [Cu(MeCN)$_4$][PF$_6$] (1.0 eq) in CH_2Cl_2 was stirred for 2h. The N^N chelating ligand (1.0 eq) was added and the colour of the solution changed to yellow or orange. After stirring for an additional 2h, the solution was filtered, the solvent was removed *in vacuo* and the crude material was washed with Et_2O/hexane. Unless otherwise stated, the solid was redissolved in CH_2Cl_2 and layered with Et_2O to give the title compound as pure crystalline material.

Standard procedure for xantphos:

The compounds xantphos (1.0 eq) and the respective N^N chelating ligand (1.0 eq) were dissolved in CH_2Cl_2. The colourless solution was added to a colourless solution of [Cu(MeCN)$_4$][PF$_6$] (1.0 eq) in CH_2Cl_2 and the then yellow to orange solution was stirred for 2 h. The solution was filtered, the solvent was removed *in vacuo* and the crude material was washed with Et_2O/hexane. Unless otherwise stated, the solid was redissolved in CH_2Cl_2 and layered with Et_2O to give the title compound as pure crystalline material.

[Cu(POP)(bpy)][PF$_6$]. (SK002)

Batch size: 0.25 mmol. The title compound was obtained as yellow crystals in good yield (210 mg, 0.22 mmol, 87%) and the signals in the ^{1}H, ^{13}C and ^{31}P NMR spectra matched those reported.[1]

[Cu(xantphos)(bpy)][PF$_6$]. (SK178)

The title compound [Cu(xantphos)(bpy)][PF$_6$] was obtained as yellow crystals in good yield (225 mg, 0.24 mmol, 96%). ^{1}H NMR (500 MHz, $(CD_3)_2CO$, 298 K) δ/ppm 8.64 (d, J = 8.2 Hz, 2H, H^{B3}), 8.35 – 8.33 (m, 2H, H^{B6}), 8.17 (td, J = 7.9, 1.6 Hz, 2H, H^{B4}), 7.87 (dd, J = 7.8, 1.4 Hz, 2H, H^{C5}), 7.47 (ddd, J = 7.6, 5.1, 1.0 Hz, 2H, H^{B5}), 7.34 (t, J = 7.5 Hz, 4H, H^{D4}), 7.28 (t, J = 7.7 Hz, 2H, H^{C4}), 7.20 (t, J = 7.8 Hz, 8H, H^{D3}), 7.06 – 7.02 (m, 8H, H^{D2}), 6.60 (dtd, J = 7.7, 3.9, 1.4 Hz, 2H, H^{C3}), 1.80 (s, 6H, $H^{xantphos\text{-}Me}$). ^{13}C NMR (126 MHz, $(CD_3)_2CO$, 298 K) δ/ppm 155.7 (t, J = 6.5 Hz, C^{C1}), 152.8 (t, J = 2.4 Hz, C^{B2}), 150.1 (C^{B6}), 140.0 (C^{B4}), 135.1 (t, J = 1.8 Hz, C^{C6}), 133.7 (t, J = 8.2 Hz, C^{D2}), 132.4 (t, J = 17.4 Hz, C^{D1}), 131.9 (C^{C3}), 130.9 (C^{D4}), 129.7 (t, J = 5.0 Hz, C^{D3}), 128.6 (C^{C5}), 127.3 (C^{B5}), 126.2 (t, J = 2.6 Hz, C^{C4}), 123.8 (C^{B3}), 120.6 (t, J = 13.8 Hz, C^{C2}), 37.0 ($C^{xantphos\text{-}bridge}$), 28.4 ($C^{xantphos\text{-}Me}$). ^{31}P{^{1}H} NMR (202 MHz, $(CD_3)_2CO$, 298 K) δ/ppm −12.7 (broad, FWHM = 345 Hz, xantphos), −144.2 (septet, J_{PF} = 708 Hz, $[PF_6]^-$). ESI MS: *m/z* 797.4 $[M–PF_6]^+$ (base peak, calc. 797.2). Found C 62.11, H 4.44, N 3.37; [Cu(xantphos)(bpy)][PF$_6$] requires C 62.39, H 4.27, N 2.97.

[Cu(POP)(6-Mebpy)][PF6]. (SK003, SK024)

The title compound [Cu(POP)(6-Mebpy)][PF_6] was obtained as yellow crystals in good yield (220 mg, 0.24 mmol, 96 %). ^{1}H NMR (500 MHz, CD_2Cl_2, 298 K) δ/ppm 8.31 (d, J = 5.1 Hz, 1H, H^{A6}), 8.17 (d, J = 8.2 Hz, 1H, H^{A3}), 8.07 (d, J = 7.9 Hz, 1H, H^{B3}), 7.91 (overlapping m, 2H, H^{A4+B4}), 7.36 – 7.28 (m, 6H, $H^{C5+D4+D4'}$), 7.25 (d, J = 7.7 Hz, 1H, H^{B5}), 7.21 (t, J = 7.5 Hz, 4H, $H^{D3/D3'}$), 7.17 (m, 5H, $H^{A5+D3/D3'}$), 7.07 (m, 4H, $H^{D2/D2'}$), 7.05 (m, 4H, H^{C6+C4}), 6.96 (m, 4H, $H^{D2/D2'}$), 6.87 (m, 2H, H^{C3}), 2.35 (s, 3H, H^{Me}).^{13}C{^{1}H} NMR (126 MHz, CD_2Cl_2) ∂/ppm 159.5 (C^{B6}), 158.4 (m, $C^{C1+C1'}$), 152.9 (C^{A2}), 152.0 (C^{B2}), 149.5 (C^{A6}), 139.3 (C^{B4}), 138.9 (C^{A4}), 134.7 (C^{C3}), 133.6 (t, J_{PC} = 7.9 Hz, $C^{D2/D2'}$), 133.4 (t, J_{PC} = 7.9 Hz, $C^{D2/D2'}$), 132.6 (C^{C5}), 131.5 (t, J = 17.1 Hz, $C^{D1+D1'}$), 130.7 ($C^{D4/D4'}$), 130.5 ($C^{D4/D4'}$), 129.3 (t, J = 4.6 Hz, $C^{D3/D3'}$), 129.2 (t, J = 4.6 Hz, $C^{D3/D3'}$), 126.5 (C^{B5}), 126.0 (C^{A5}), 125.7 (t, J = 2.0 Hz, C^{C4}), 124.7 (t, J = 14.5 Hz, C^{C2}), 122.8 (C^{A3}), 120.7 (C^{C6}), 120.1 (C^{B3}), 26.7 (C^{Me}). ^{31}P{^{1}H} NMR (162 MHz, CD_2Cl_2). ∂ / ppm −12.4 (broad, FWHM = 500 Hz, POP), −144.5 (septet, J_{PF} = 710 Hz, $[PF_6]^-$). ESI MS: m/z 771.5 $[M–PF_6]^+$ (base peak, calc. 771.2). Found C 60.95, H 4.55, N 3.33; [Cu(POP)(6-Mebpy)][PF_6]·0.5 H_2O requires C 60.94, H 4.24, N 3.02.

[Cu(xantphos)(6-Mebpy)][PF6]. (SK038)

The title compound [Cu(xantphos)(6-Mebpy)][PF_6] was obtained as a yellow powder (274 mg, 0.29 mmol, 81%). ^{1}H NMR (500 MHz, CD_2Cl_2) δ/ppm 8.19 (m, 2H, H^{A6+A3}), 8.10 (d, J = 7.9 Hz, 1H, H^{B3}), 7.97 (m, 1H, H^{B4}), 7.94 (m, 1H, H^{A4}), 7.67 (dd, J = 7.8, 1.4 Hz, 2H, H^{C5}), 7.35–7.24 (m, 6H, $H^{A5+B5+D4+D4'}$), 7.16 (m, 6H, $H^{D3'+C4}$), 7.08 (m, 4H, H^{D3}), 7.04 (m, 4H, $H^{D2'}$), 6.85 (m, 4H, H^{D2}), 6.61 (m, 2H, H^{C3}), 2.00 (s, 3H, $H^{bpy\text{-}Me}$), 1.83 (s, 3H, $H^{xantphos\text{-}Me}$), 1.68 (s, 3H, $H^{xantphos\text{-}Me}$). ^{13}C NMR (126 MHz, CD_2Cl_2) δ/ppm 159.1 (C^{B6}), 155.5 (m, $C^{C1+C1'}$), 152.7 (t, J_{PC} = 2.5 Hz, C^{A2}), 151.7 (t, J_{PC} = 2.1 Hz, C^{B2}), 149.2 (C^{A6}), 139.5 (C^{B4}), 139.1 (C^{A4}), 134.4 (C^{C6}), 133.5 (t, J_{PC} = 8.2 Hz, C^{D2}), 133.1 (t, J_{PC} = 8.0 Hz, $C^{D2'}$), 132.2 (t, J_{PC} = 16.4 Hz, $C^{D1/D1'}$), 131.9 (t, J_{PC} = 17.9 Hz, $C^{D1/D1'}$), 131.3 (C^{C3}), 130.6 ($C^{D4/D4'}$), 130.5 ($C^{D4/D4'}$), 129.4 (t, J_{PC} = 4.7 Hz, $C^{D3/D3'}$), 129.3 (t, J_{PC} = 4.7 Hz, $C^{D3/D3'}$), 127.8 (C^{C5}), 126.6 ($H^{A5/B5}$), 126.3 ($H^{A5/B5}$), 125.7 (t, J_{PC} = 2.6 Hz, C^{C4}), 123.1 (C^{A3}), 120.9 (t, J_{PC} = 14.0 Hz, C^{C2}), 120.3 (C^{B3}), 36.7 ($C^{xantphos\text{-}bridge}$), 30.1 ($C^{xantphos\text{-}Me}$), 26.8 ($C^{xantphos\text{-}Me}$), 26.5 ($C^{bpy\text{-}Me}$). ^{31}P{^{1}H} NMR (202 MHz, CD_2Cl_2) δ/ppm −12.4 (br, FWHM = 240 Hz, xantphos), −144.5 (septet, J_{PF} = 710 Hz, $[PF_6]^-$). ESI MS: m/z 811.6 $[M–PF_6]^+$ (base peak, calc. 811.2). Found C 63.24, H 4.86, N 3.33; $C_{50}H_{42}CuF_6N_2OP_3$ requires C 62.73, H 4.42, N 2.93%.

[Cu(POP)(6,6'-Me2bpy)][PF6]. (SK037)

A slight excess of POP (1.1 to 1.2 eq) was used for the synthesis of [Cu(POP)(6,6'-Me_2bpy)][PF_6]. The title compound was obtained as pale yellow powder (320 mg, 0.34 mmol, 98%). ^{1}H NMR (500 MHz, CD_2Cl_2) ∂ /ppm 7.89 (d, J = 7.3 Hz, 2H, H^{A3}), 7.85 (t, J = 7.8 Hz, 2H, H^{A4}), 7.32 (m, 2H, H^{B5}), 7.28 (m, 4H, H^{C4}), 7.23 (dd, J = 7.4, 0.8 Hz, 2H, H^{A5}), 7.21–7.16 (overlapping m, 4H, H^{B3+B4}), 7.12 (m, 8H, H^{C3}), 7.01 (m, 8H, H^{C2}), 6.93 (m, 2H, H^{B6}), 2.22 (s, 6H, H^{Me}). ^{13}C{^{1}H} NMR (126 MHz, CD_2Cl_2, 298 K) δ/ppm 159.3 (C^{A6}), 158.7 (m, C^{B1}), 152.9 (C^{A2}), 139.2 (C^{A4}), 134.3 (C^{B3}), 133.5 (t, J_{PC} = 8.1 Hz, C^{C2}), 132.7 (C^{B5}), 132.2 (t, J = 16.5 Hz, C^{C1}), 130.4 (C^{C4}), 129.2 (t, J = 5.1 Hz, C^{C3}), 126.6 (C^{A5}), 125.7 (C^{B4}), 120.6 (t, J = 2.0 Hz, C^{B6}), 120.2 (C^{A3}), 26.9 (C^{Me}). ^{31}P{^{1}H} NMR (202 MHz, CD_2Cl_2). ∂ / ppm −13.5 (broad, FWHM = 380 Hz, POP), −144.5 (septet, J_{PF} = 710 Hz, $[PF_6]^-$). ESI MS: m/z 785.5 $[M–PF_6]^+$ (base peak, calc. 785.2). Found C 63.07, H 4.71, N 3.05; [Cu(POP)(6,6'-Me_2bpy)][PF_6]·0.5hexane requires C 62.86, H 4.86, N 2.87

[Cu(xantphos)(6,6'-Me2bpy)][PF6]. (SK039)

The title compound [Cu(6,6'-Me_2bpy)(xantphos)][PF_6] was isolated as yellow powder (220 mg, 0.23 mmol, 85%). ^{1}H NMR (500 MHz, CD_2Cl_2) δ/ppm 7.84 (dd, J = 8.0, 1.4 Hz, 2H, H^{B3}), 7.81 (t, J = 8.0 Hz, 2H, H^{B4}), 7.65 (dd, J = 7.8, 1.4 Hz, 2H, H^{C5}), 7.34 (m, 4H, H^{D4}), 7.21–7.17 (m, 4H, H^{B5+C4}), 7.16–7.12 (m, 8H, H^{D3}), 7.08 (m, 8H, H^{D2}), 6.89 (m, 2H, H^{C3}), 2.04 (s, 6H, $H^{bpy\text{-}Me}$), 1.72 (s, 6H, $H^{xantphos\text{-}Me}$). ^{13}C NMR (126 MHz, CD_2Cl_2) δ/ppm 158.8 (C^{B6}), 155.5 (t, J_{PC} = 6.5 Hz, C^{C1}), 152.5 (t, J_{PC} = 1.8 Hz, C^{B2}), 139.1 (C^{B4}), 134.3 (t, J_{PC} = 1.7 Hz, C^{C6}), 133.7 (t, J_{PC} = 7.7 Hz, C^{D2}), 131.9 (t, J_{PC} = 16.3 Hz, C^{D1}), 130.9 (C^{C3}), 130.6 (C^{D4}), 129.3 (t, J_{PC} = 4.5 Hz, C^{D3}), 128.0 (C^{C5}), 126.2 (C^{B5}), 125.8 (t, J_{PC} = 2.3 Hz, C^{C4}), 122.2 (t, J_{PC} = 13.0 Hz, C^{C2}), 120.3 (C^{B3}), 36.6 ($C^{xantphos\text{-}bridge}$), 28.7 ($C^{xantphos\text{-}Me}$), 27.1 ($C^{bpy\text{-}Me}$). ^{31}P NMR (202 MHz, CD_2Cl_2) δ/ppm −13.3 (br, FWHM = 240 Hz, xantphos), −144.5 (sept, J_{PF} = 710 Hz, $[PF_6]^-$). ESI MS: m/z 825.6 $[M–PF_6]^+$ (base peak, calc. 825.2). Found C 63.29, H 4.95, N 3.27; $C_{51}H_{44}CuF_6N_2OP_3$ requires C 63.06, H 4.57, N 2.88%.

[Cu(POP)(6-Etbpy)][PF6]. (SK066)

The title compound [Cu(POP)(6-Etbpy)][PF_6] was isolated as yellow powder (190 mg, 0.20 mmol, 80%). ^{1}H NMR (500 MHz, CD_2Cl_2) δ/ppm 8.36 (d, J = 5.1 Hz, 1H, H^{A6}), 8.19 (d, J = 8.2 Hz, 1H, H^{A3}), 8.10 (d, J = 7.7 Hz, 1H, H^{B3}), 7.99 (t, J = 7.8 Hz, 1H, H^{B4}), 7.91 (td, J = 8.1, 1.6 Hz, 1H, H^{A4}), 7.34–7.29 (overlapping m, 7H, $H^{B5+C5+D4+D4'}$), 7.21–7.15 (overlapping m, 9H, $H^{A5+D3+D3'}$), 7.07–6.96 (overlapping m, 12H, $H^{C4+C6+D2+D2'}$), 6.83 (m, 2H, H^{C3}), 2.78 (q, J = 7.6 Hz, 2H, $H^{Et\text{-}CH2}$), 0.69 (t, J = 7.6 H, 3H, $H^{Et\text{-}CH3}$). ^{13}C NMR (126 MHz, CD_2Cl_2) δ/ppm 164.7 (C^{B6}), 158.4 (m, $C^{C1+C1'}$), 153.1 (C^{A2}), 151.8 (m, C^{B2}), 149.5 (C^{A6}), 139.5 (C^{B4}), 138.9 (C^{A4}), 134.8 (C^{C3}), 133.6 (overlapping t, J_{PC} = 7.8 Hz, $C^{D2+D2'}$), 132.6 (C^{C5}), 131.5 (m, $C^{D1+D1'}$), 130.6 ($C^{D4+D4'}$), 129.3 (overlapping t, J = 5.0 Hz, $C^{D3+D3'}$),

126.1 (C^{A5}), 125.7 (m, C^{C4}), 124.6 (t, J_{PC} = 14.3 Hz, C^{C2}), 124.5 (C^{B5}), 122.8 (C^{A3}), 120.7 (C^{C6}), 120.4 (C^{B3}), 34.2 ($C^{Et\text{-}CH_2}$), 12.9 ($C^{Et\text{-}CH_3}$). ^{31}P NMR (162 MHz, CD_2Cl_2) δ/ppm −12.4 (br, FWHM = 245 Hz, POP), −144.5 (sept, J_{PF} = 710 Hz, $[PF_6]^-$). UV-Vis (CH_2Cl_2, 2.5 × 10^{-5} mol dm^{-3}): λ/nm (ε/dm^3 mol^{-1} cm^{-1}) 247sh (30100), 290 (24900), 312sh (30000), 381 (3300). ESI MS: *m/z* 785.5 $[M–PF_6]^+$ (base peak, calc. 785.2). Found C 61.91, H 4.42, N 3.37; $C_{48}H_{40}CuF_6N_2OP_3$ requires C 61.90, H 4.33, N 3.01%.

[Cu(xantphos)(6-Etbpy)][PF$_6$]. (SK080)

The title compound [Cu(xantphos)(6-Etbpy)][PF_6] was isolated as a yellow powder (203 mg, 0.21 mmol, 84%). ^{1}H NMR (500 MHz, CD_2Cl_2) δ/ppm 8.40 (d, J = 5.1 Hz, 1H, H^{A6}), 8.19 (d, J = 8.2 Hz, 1H, H^{A3}), 8.12 (d, J = 7.9 Hz, 1H, H^{B3}), 8.03 (d, J = 7.8 Hz, 1H, H^{B4}), 7.95 (td, J = 7.9, 1.6 Hz, 1H, H^{A4}), 7.68 (dd, J = 7.8, 1.4 Hz, 2H, H^{C5}), 7.37 (overlapping m, 2H, H^{A5+B5}), 7.32 (m, 2H, $H^{D4/D4'}$), 7.27 (m, 2H, $H^{D4/D4'}$), 7.16 (m, 8H, $H^{D3/D3'+C4}$), 7.11–7.04 (m, 8H, $H^{D2/D2'+D3/D3'}$), 6.79 (m, 4H, $H^{D2/D2'}$), 6.60 (m, 2H, H^{C3}), 2.29 (q, J = 7.6 Hz, 2H, $H^{Et\text{-}CH_2}$), 1.89 (s, 3H, $H^{Me\text{-}xantphos}$), 1.64 (s, 3H, $H^{Me\text{-}xantphos}$), 0.44 (t, J = 7.6 Hz, 3H, $H^{Et\text{-}CH_3}$). ^{13}C NMR (126 MHz, CD_2Cl_2) δ/ppm 164.3 (C^{B6}), 155.5 (m, $C^{C1+C1'}$), 149.3 (C^{A6}), 139.8 (C^{B4}), 139.1 (C^{A4}), 134.4 (C^{C6}), 133.7 (t, J_{PC} = 8.1 Hz, C^{D2}), 133.0 (t, J = 7.6 Hz, $C^{D2'}$), 132.3 (m, $C^{D1/D1'}$), 131.9 (m, $C^{D1/D1'}$), 131.4 (C^{C3}), 130.7 ($C^{D4/D4'}$), 130.5 ($C^{D4/D4'}$), 129.4 (overlapping m, $C^{D3+D3'}$), 127.8 (C^{C5}), 126.4 ($C^{A5/B5}$), 125.8 (C^{C4}), 124.5 ($C^{A5/B5}$), 123.1 (C^{A3}), 121.0 (t, J_{PC} = 13.6 Hz, C^{C2}), 120.6 (C^{B3}), 36.7 ($C^{xantphos\text{-}bridge}$), 34.3 ($C^{Et\text{-}CH_2}$), 31.0 ($C^{Me\text{-}xantphos}$), 25.9 ($C^{Me\text{-}xantphos}$), 12.6 ($C^{Et\text{-}CH_3}$). ^{31}P NMR (162 MHz, CD_2Cl_2, 297) δ/ppm −12.2 (br, FWHM = 240 Hz, xantphos), −144.5 (sept, J_{PF} = 710 Hz, $[PF_6]^-$). ESI MS: *m/z* 825.2 $[M–PF_6]^+$ (base peak, calc. 825.2). Found C 63.13, H 4.95, N 3.22; $C_{51}H_{44}CuF_6N_2OP_3$ requires C 63.06, H 4.57, N 2.88%.

[Cu(POP)(6-*t*Bubpy)][PF$_6$]. (SK149)

The title compound [Cu(POP)(6-*t*Bubpy)][PF_6] was isolated as pale yellow powder (220 mg, 0.23 mmol, 92%). ^{1}H NMR (500 MHz, $(CD_3)_2CO$, 298 K) δ/ppm 8.42 (d, J = 8.1 Hz, 1H, H^{A3}), 8.39 (d, J = 4.8 Hz, 1H, H^{A6}), 8.26 (dd, J = 7.9, 0.7 Hz, 1H, H^{B3}), 8.05 (t, J = 7.9 Hz, 1H, H^{B4}), 8.04 (td, J = 7.9, 1.7 Hz, 1H, H^{A4}), 7.63 (dd, J = 7.9, 0.6 Hz, 1H, H^{B5}), 7.45 (ddd, J = 8.2, 7.5, 1.7 Hz, 2H, H^{C5}), 7.41 (t, J = 7.4 Hz, 4H, H^{D4}), 7.30 (t, J = 7.1 Hz, 8H, H^{D3}), 7.23 (m, 3H, H^{A5+C6}), 7.15 (td, J = 7.5, 1.1 Hz, 2H, H^{C4}), 7.10 (broad signal, 8H, H^{D2}), 6.93 (dtd, J = 7.8, 4.0, 1.7 Hz, 2H, H^{C3}), 1.27 (s, 9H, H^{tBu}). ^{13}C NMR (126 MHz, $(CD_3)_2CO$, 298 K) δ/ppm 170.9 (C^{B6}), 158.3 (t, J = 6.3 Hz, C^{C1}), 154.9 (C^{A2}), 154.3 (C^{B2}), 150.0 (C^{A6}), 139.9 (C^{B4}), 139.6 (C^{A4}), 135.2 (C^{C3}), 134.1 (t, J = 8.2Hz, C^{D2}), 133.3 (C^{C5}), 131.5 (t, J = 16.1 Hz, C^{D1}), 131.1 (C^{D4}), 129.8 (t, J = 4.8 Hz, C^{D3}), 126.1 (t, J = 2.4 Hz, C^{C4}), 125.9 (C^{A5}), 124.6 (t, J = 14.6 Hz, C^{C2}), 124.2 (C^{A3}), 123.2 (C^{B5}), 121.7 (C^{B3}), 120.7 (C^{C6}), 37.9 ($C(CH_3)_3$), 31.0 ($C(CH_3)_3$). ^{31}P NMR (162 MHz, $(CD_3)_2CO$, 295 K) δ/ppm −15.1 (br, FWHM = 125 Hz, POP), −144.2 (sept, J_{PF} = 708 Hz, $[PF_6]^-$). ESI MS: *m/z* 813.3 $[M–PF_6]^+$ (base peak, calc. 813.2). Found C 61.82, H 5.23, N 3.29; $C_{50}H_{44}CuF_6N_2OP_3$·0.5MeCN requires C 62.51, H 4.68, N 3.57%.

[Cu(xantphos)(6-*t*Bubpy)][PF$_6$]. (SK150)

The title compound [Cu(POP)(6-*t*Bubpy)][PF_6] was isolated as a light yellow powder (225 mg, 0.23 mmol, 92%). ^{1}H NMR (500 MHz, $(CD_3)_2CO$, 298 K) δ/ppm 8.47 (dt, J = 8.2, 1.0 Hz, 1H, H^{A3}), 8.29 (dd, J = 7.9, 1.0 Hz, 1H, H^{B3}), 8.24 (broad signal, 1H, H^{A6}), 8.16 (t, J = 7.9 Hz, 1H, H^{B4}), 8.11 (td, J = 8.0, 1.5 Hz, 1H, H^{A4}), 7.86 (dd, J = 7.8, 1.4 Hz, 2H, H^{C5}), 7.79 (d, J = 7.9 Hz, 1H, H^{B5}), 7.43 (m, 1H, H^{A5}), 7.38 (t, J = 7.0 Hz, 4H, H^{D4}), 7.28 (t, J = 7.7 Hz, 2H, H^{C4}), 7.21 (t, J = 7.7 Hz, 8H, H^{D3}), 7.07 (q, J = 5.5 Hz, 8H, H^{D2}), 6.72 (dtd, J = 7.6, 3.8, 1.4 Hz, 2H, H^{C3}), 1.81 (s, 6H, $Me^{xantphos}$), 1.13 (s, 9H, H^{tBu}). ^{13}C NMR (126 MHz, $(CD_3)_2CO$, 298 K) δ/ppm 171.4 (C^{B6}), 155.4 (t, J = 6.2 Hz, C^{C1}), 154.3 (C^{B2}), 149.4 (C^{A2}), 140.2 (C^{B4}), 140.0 (C^{A4}), 134.6 (t, J = 1.8 Hz, C^{C6}), 134.1 (broad signal, C^{D1}), 131.7 (C^{C3}), 131.1 (broad signal, C^{D1+D4}), 129.8 (t, J = 4.9 Hz, C^{D3}), 128.6 (C^{C5}), 126.4 (C^{A5}), 126.2 (t, J = 2.7 Hz, C^{C4}), 124.8 (C^{A3}), 123.9 (C^{B5}), 122.4 (C^{B3}), 121.1 (t, J = 13.5 Hz, C^{C2}), 37.9 ($C(CH_3)_3$), 36.82 ($C^{xantphos\text{-}bridge}$), 36.80($Me^{xantphos}$, 31.1 ($C(CH_3)_3$). ^{31}P NMR (162 MHz, $(CD_3)_2CO$, 295 K) δ/ppm −13.0 (br, FWHM = 133 Hz, xantphos), −144.2 (sept, J_{PF} = 709 Hz, $[PF_6]^-$). ESI MS: *m/z* 853.4 $[M–PF_6]^+$ (base peak, calc. 853.3). Found C 63.30, H 5.37, N 3.17; $C_{53}H_{48}CuF_6N_2OP_3$ requires C 63.69, H 4.84, N 2.80%.

[Cu(POP)(6-Phbpy)][PF$_6$]. (SK007)

The title compound [Cu(POP)(6-Phbpy)][PF_6] was obtained as yellow powder (230 mg, 0.22 mmol, 88%). ^{1}H NMR (500 MHz, CD_2Cl_2) δ/ppm 8.27 (overlapping m, 2H, H^{A3+B3}), 8.06 (t, J = 7.8 Hz, 1H, H^{B4}), 8.00 (d, J = 5.1 Hz, 1H, H^{A6}), 7.91 (t, J = 7.8 Hz, 1H, H^{A4}), 7.44 (d, J = 7.7 Hz, 1H, H^{B5}), 7.41 (t, J = 7.3 Hz, 1H, H^{E4}), 7.36–7.25 (overlapping m, 6H, $H^{D4+D4'+C5}$), 7.19−7.07 (overlapping m, 12H, $H^{D3+D3'+E2+E3}$), 7.03 (m, 2H, H^{C6}), 6.95 (t, J = 7.5 Hz, 2H, H^{C4}), 6.92 (m, 1H, H^{A5}), 6.73 (m, 4H, $H^{D2/D2'}$), 6.68 (m, 4H, $H^{D2/D2'}$), 6.60 (m, 2H, H^{C3}). ^{13}C NMR (126 MHz, CD_2Cl_2) δ/ppm 161.5 (C^{B6}), 157.7 (m, $C^{C1+C1'}$), 153.4 ($C^{A2/B2}$), 153.1 ($C^{A2/B2}$), 149.4 (C^{A6}), 141.3 (C^{E1}), 139.2 (C^{B4}), 138.9 (C^{A4}), 135.1 (C^{C3}), 134.7 (t, J_{PC} = 7.4 Hz, $C^{D2/D2'}$), 133.0 (t, J_{PC} = 7.4 Hz, $C^{D2/D2'}$), 132.5 (C^{C5}), 131.5

(m, $C^{D1+D1'}$), 130.8 ($C^{D4/D4'}$), 130.3 ($C^{D4/D4'}$), 130.0 (C^{E4}), 129.8 ($C^{E2/E3}$), 129.1 (overlapping m, ($C^{D3+D3'}$), 128.9 ($C^{E2/E3}$), 127.3 (C^{B5}), 126.0 (C^{A5}), 125.6 (t, J_{PC} = 2.3 Hz, C^{C4}), 124.5 (t, J_{PC} =14.1 Hz, C^{C2}), 123.0 ($C^{A3/B3}$), 122.0 ($C^{A3/B3}$), 120.2 (t, J_{PC} = 1.8 Hz, C^{C6}). ^{31}P NMR (162 MHz, CD_2Cl_2) δ/ppm −12.6 (br, FWHM = 260 Hz, POP), −144.5 (sept, J_{PF} = 710 Hz, $[PF_6]^-$). ESI MS: *m/z* 873.6 $[M-PF_6]^+$ (base peak, calc. 873.2). Found C 63.40, H 4.67, N 3.19; $C_{52}H_{40}CuF_6N_2OP_3$ requires C 63.77, H 4.12, N 2.86%.

[Cu(xantphos)(6-Phbpy)][PF$_6$]. (SK042)

The title compound [Cu(xantphos)(6-Phbpy)][PF_6] was isolated as a yellow solid (180 mg, 0.18 mmol, 71%). ^{1}H NMR (500 MHz, CD_2Cl_2) δ/ppm 8.25 (d, J = 8.2 Hz, 1H, H^{A3}), 8.17 (dd, J = 8.0 Hz, 1H, H^{B3}), 8.07 (t, J = 7.8 Hz, 1H, H^{B4}), 7.95 (td, J = 8.0, 1.6 Hz, 1H, H^{A4}), 7.65 (dd, J = 7.8 Hz, 2H, H^{C5}), 7.46 (d, J = 7.4 Hz 1H, H^{B5}), 7.32 (t, J = 7.5 Hz, 2H, $H^{D4/D4'}$), 7.25 (t, J = 7.5 Hz, 2H, $H^{D4/D4'}$), 7.19 (d, J = 7.5 Hz, 2H, H^{E2}), 7.17–7.11 (overlapping m, 6H, $H^{C4+D3/D3'}$), 7.02 (m, 5H, $H^{A5+D3/D3'}$), 6.91 (br, see text), 6.78–6.71 (m, 8H, $H^{D2+D2'}$), 6.60 (m, 2H, H^{C3}), 1.80 (s, 3H, $H^{xantphos\text{-}Me}$), 1.61 (s, 3H, $H^{xantphos\text{-}Me}$), (for signals for H^{A6}, H^{E3} and H^{E4}, see text). ^{13}C NMR (126 MHz) δ/ppm 161.5 (C^{B6}), 155.2 ($C^{C1+C1'}$), 153.7 ($C^{A2/B2}$), 153.4 ($C^{A2/B2}$), 148.9 (C^{A6}), 139.5 (C^{B4}), 139.3 (C^{A4}), 134.5 (C^{C6}), 133.9 (t, J_{PC} = 7.4 Hz, $C^{D2/D2'}$), 133.4 (t, J_{PC} = 7.4 Hz, $C^{D2/D2'}$), 131.3 (C^{C3}), 130.5 ($C^{D4/D4'}$), 130.45 ($C^{D4/D4'}$), 129.8 (C^{E1}), 129.3 (t, J_{PC} = 4.6 Hz, $C^{D3/D3'}$), 128.9 (t, J_{PC} = 4.8 Hz, $C^{D3/D3'}$) 128.2 (C^{E2}), 127.7 (C^{C5}), 127.1 (C^{B5}), 125.9 (C^{A5}), 125.6 (t, J_{PC} = 2.5 Hz, C^{C4}), 123.5 (C^{A3}), 122.3 (C^{B3}), 36.6 ($C^{xantphos\text{-}bridge}$), 29.5 ($C^{xantphos\text{-}Me}$), 26.9 ($C^{xantphos\text{-}Me}$). ^{31}P NMR (202 MHz, CD_2Cl_2) δ/ppm −12.8 (br, FWHM = 420 Hz, xantphos), −144.5 (sept, J_{PF} = 710 Hz, $[PF_6]^-$). ESI MS: *m/z* 873.6 $[M-PF_6]^+$ (base peak, calc. 873.2). Found C 63.84, H 4.70, N 3.07; $C_{55}H_{44}CuF_6N_2OP_3 \cdot H_2O$ requires C 63.68, H 4.47, N 2.70%.

[Cu(POP)(5,5'-Me$_2$bpy)][PF$_6$]. (SK025, SK202)

The title compound [Cu(POP)(5,5'-Me_2bpy)][PF_6] was isolated as yellow crystals in good yield (160 mg, 0.17 mmol, 69 %). ^{1}H NMR (500 MHz, $(CD_3)_2CO$, 298 K) δ/ppm 8.41 (d, J = 8.4 Hz, 2H, H^{B3}), 8.40 – 8.38 (m, 2H, H^{B6}), 7.91 (m, 2H, H^{B4}),7.45 – 7.41 (m, 2H, H^{C5}), 7.38 (t, J = 7.4 Hz, 4H, H^{D4}), 7.27 (t, J = 7.6 Hz, 8H, H^{D3}), 7.22 (dtd, J = 5.8, 3.1, 1.0 Hz, 2H, H^{C6}), 7.16 – 7.12 (m, 8H, H^{D2}), 7.09 (td, J = 7.5, 0.6 Hz, 2H, H^{C4}), 6.78 (dtd, J = 7.8, 4.3, 1.6 Hz, 2H, H^{C3}), 2.15 (s, 6H, $H^{bpy\text{-}Me}$). ^{13}C NMR (126 MHz, $(CD_3)_2CO$, 298 K) δ/ppm 159.2 (C^{C1}), 150.7 (C^{B6}), 150.5 (C^{B2}), 139.8 (C^{B4}), 137.0 (C^{B5}), 135.0 (C^{C3}), 134.1 (t, J = 8.2 Hz, C^{D2}), 133.1 (C^{C5}), 131.9 (t, J = 17.1 Hz, C^{D1}), 131.0 (C^{D4}), 129.6 (t, J = 4.8 Hz, C^{D3}), 126.1 (t, J = 2.2 Hz, C^{C4}), 124.8 (t, J = 14.7 Hz, C^{C2}), 122.6 (C^{B3}), 121.5 (C^{C6}), 18.1 (CH_3). ^{31}P{^{1}H} NMR (202 MHz, $(CD_3)_2CO$, 298 K) δ/ppm −11.1 (broad, FWHM = 305 Hz, POP), −144.2 (septet, J_{PF} = 708 Hz, $[PF_6]^-$). ESI MS: *m/z* 785.5 $[M-PF_6]^+$ (base peak, calc. 785.2). Found C 60.63, H 4.49, N 3.19; [Cu(POP)(5,5'-Me_2bpy)][PF_6]·H_2O requires C 60.73, H 4.46, N 2.95.

[Cu(xantphos)(5,5'-Me$_2$bpy)][PF$_6$]. (SK173)

The title compound [Cu(xantphos)(5,5'-Me_2bpy)][PF_6] was isolated as yellow crystals in good yield (215 mg, 0.22 mmol, 88 %). ^{1}H NMR (500 MHz, $(CD_3)_2CO$, 298 K) δ /ppm 8.48 (d, J = 9.0 Hz, 2H, H^{B3}), 7.95 (m, 2H, H), 7.94 (m, 2H, H^{B4}), 7.89 (dd, J = 7.8, 1.4 Hz, 2H, H^{C5}), 7.35 – 7.31 (m, 4H, H^{D4}), 7.28 (t, J = 7.7 Hz, 2H, H^{C4}), 7.22 – 7.18 (m, 8H, H^{D3}), 7.07 – 7.02 (m, 8H, H^{D2}), 6.55 – 6.51 (m, 2H, H^{C3}), 2.10 (s, 6H, $H^{bpy\text{-}Me}$), 1.83 (s, 6H, $H^{xantphos\text{-}Me}$). ^{13}C NMR (126 MHz, $(CD_3)_2CO$, 298 K) δ /ppm 155.9 (t, J = 6.2 Hz, C^{C1}), 150.5 (t, J = 2.1 Hz, C^{B2}), 150.2 (C^{B6}), 140.1 (C^{B4}), 137.2 (C^{B5}), 135.1 (t, J = 1.5 Hz, C^{C6}), 133.8 (t, J = 8.1 Hz, C^{D2}), 132.4 (t, J = 17.2 Hz, C^{D1}), 132.0 (C^{C3}), 130.9 (C^{D4}), 129.7 (t, J = 4.8 Hz, C^{D3}), 128.4 (C^{C5}), 126.2 (t, J = 2.4 Hz, C^{C4}), 122.9 (C^{B3}), 120.8 (t, J = 13.7 Hz, C^{C2}), 37.0 (t, J = 1.5 Hz, $C^{xantphos\text{-}bridge}$), 28.3 ($C^{xantphos\text{-}Me}$), 18.0 ($C^{bpy\text{-}Me}$). ^{31}P NMR (162 MHz, $(CD_3)_2CO$, 294 K) δ / ppm −11.6 (broad, FWHM = 230 Hz, xantphos), −144.2 (septet, J_{PF} = 708 Hz, $[PF_6]^-$). Found C 62.87, H 4.77, N 3.26; $C_{51}H_{44}CuF_6N_2OP_3$ requires C 63.06, H 4.57, N 2.88.

[Cu(POP)(4,4'-*t*Bu$_2$bpy)][PF$_6$]. (SK005, SK203)

The title compound [Cu(POP)(4,4'-*t*Bu_2bpy)][PF_6] was isolated as yellow powder in moderate yield (150 mg, 0.15 mmol, 59 %) ^{1}H NMR (500 MHz, CD_2Cl_2) δ /ppm 8.37 (dd, J = 5.6, 0.7 Hz, 2H, H^{A6}), 8.08 (d, J = 1.1 Hz, 2H, H^{A3}), 7.31 – 7.29 (m, 6H, H^{C5+D4}), 7.23 (dd, J = 5.5, 1.8 Hz, 2H, H^{A5}), 7.17 (t, J = 7.8 Hz, 8H, H^{D3}), 7.06 (dtd, J = 8.2, 2.6, 1.0 Hz, 2H, H^{C6}), 7.01 (m, 8H, H^{D2}), 6.99 (d, J = 1.0 Hz, 2H, H^{C4}), 6.77 (dtd, J = 7.9, 4.1, 1.6 Hz, 2H, H^{C3}), 1.39 (s, 18H, $C(Me)_3$). ^{13}C{^{1}H} NMR (126 MHz, CD_2Cl_2) δ /ppm 163.5 (C^{A4}), 158.9 (t, J = 6.2 Hz, C^{C1}), 152.5 (C^{A2}), 149.7 (C^{A6}), 134.8 (C^{C3}), 133.6 (t, J = 8.2 Hz, C^{D2}), 132.5 (C^{C5}), 131.5 (t, J = 17.1 Hz, C^{D1}), 130.5 (C^{D4}), 129.2 (t, J = 4.8 Hz, C^{D3}), 125.6 (t, J = 2.1 Hz, C^{C4}), 124.4 (t, J = 14.7 Hz, C^{C2}), 123.6 (CA5), 121.0 (t, J = 1.7 Hz, C^{C6}), 35.8 ($C^{C(CH3)3,\ Cq}$), 30.7 (C^{Me}). ^{31}P{^{1}H} NMR (162 MHz, CD_2Cl_2). δ / ppm −11.7 (FWHM = 200 Hz, coordinated POP), −144.6 (septet, J_{PF} = 706 Hz, $[PF_6]^-$). UV-Vis (CH_2Cl_2, 2.5 × 10^{-5} mol dm^{-3}): λ / nm (ε / dm^3 mol^{-1} cm^{-1}) 250sh (23060), 287 (19590), 303sh (15000), 377 (2800). ESI MS: *m/z* 869.6 $[M-PF_6]^+$ (base peak, calc. 869.28). Found C 56.00, H 4.69, N 2.71; [Cu(POP)(4,4'-*t*Bu_2bpy)][PF_6]·$3CH_2Cl_2$ requires C 55.87, H 5.21, N 2.07.

[Cu(xantphos)(4,4'-*t*Bu$_2$bpy)][PF$_6$]. (SK174)

The title compound [Cu(xantphos)(4,4'-(*t*Bu$_2$)bpy)][PF$_6$] was isolated as yellow crystals in good yield (201 mg, 19.0 mmol, 76%). ^{1}H NMR (500 MHz, (CD$_3$)$_2$CO, 298 K) δ /ppm 8.61 (d, J = 1.4 Hz, 2H, H^{B3}), 8.24 (d, J = 5.5 Hz, 2H, H^{B6}), 7.86 (dd, J = 7.8, 1.4 Hz, 2H, H^{C5}), 7.47 (dd, J = 5.5, 1.8 Hz, 2H, H^{B5}), 7.34 (t, J = 7.4 Hz, 4H, H^{D4}), 7.28 (t, J = 7.7 Hz, 2H, H^{C4}), 7.20 (t, J = 7.8 Hz, 8H, H^{D3}), 7.06 – 7.02 (m, 8H, H^{D2}), 6.67 – 6.64 (m, 2H, H^{C3}), 1.79 (s, 6H, H$^{xantphos-Me}$), 1.39 (s, 18H, H^{tBu}). ^{13}C NMR (126 MHz, (CD$_3$)$_2$CO, 298 K) δ /ppm 164.3 (C^{B4}), 155.7 (t, J = 6.5 Hz, C^{C1}), 153.2 (t, J = 2.0 Hz, C^{B2}), 149.8 (C^{B6}), 135.0 (t, J = 1.6 Hz, C^{C6}), 133.7 (t, J = 8.0 Hz, C^{D2}), 132.5 (t, J = 17.0 Hz, C^{D1}), 131.9 (C^{C3}), 130.8 (C^{D4}), 129.6 (t, J = 4.7 Hz, C^{D3}), 128.6 (C^{C5}), 126.1 (t, J = 2.3 Hz, C^{C4}), 124.0 (C^{B5}), 120.72 (C^{B3}), 120.69 (t, J = 13.6 Hz, C^{C2}), 36.9 (t, J = 1.5 Hz, C$^{xantphos-bridge}$), 36.1 (C$^{quarternery\ tBu}$, 30.5 (C^{tBu}), 28.5 (C$^{xantphos-Me}$). ^{31}P NMR (162 MHz, (CD$_3$)$_2$CO, 300 K) δ / ppm −13.0 (broad, FWHM = 155 Hz, xantphos), −144.2 (septet, J_{PF} = 708 Hz, [PF$_6$]$^-$). ESI MS: *m/z* 909.4 [M–PF$_6$]$^+$ (base peak, calc. 909.3). Found C 64.71, H 5.61, N 3.03; C$_{57}$H$_{56}$CuF$_6$N$_2$OP$_3$ requires C 64.86, H 5.35, N 2.65.

[Cu(POP)(2-Etphen)][PF$_6$]. (SK154)

Batch size: 0.29 mmol. The title compound [Cu(POP)(2-Etphen)][PF$_6$] was obtained as yellow crystals in good yield (247 mg, 0.26 mmol, 90%). ^{1}H NMR (500 MHz, (CD$_3$)$_2$CO, 298 K) δ /ppm 9.12 (m, 1H, H^{B9}), 8.75 (d, J = 8.4 Hz, 1H, H^{B4}), 8.67 (dd, J = 8.2, 1.2 Hz, 1H, H^{B7}), 8.21 (d, J = 8.8 Hz, 1H, H^{B5}), 8.14 (d, J = 8.9 Hz, 1H, H^{B6}), 7.90 (d, J = 8.4 Hz, 1H, H^{B3}), 7.79 (dd, J = 8.2, 4.7 Hz, 1H, H^{B8}), 7.47 (ddd, J = 8.2, 7.5, 1.7 Hz, 2H, H^{C5}), 7.33 (q, J = 7.5 Hz, 4H, H$^{D4/D4'}$), 7.26 (m, 2H, H^{C6}), 7.23 (m, 4H, H$^{D3/D3'}$), 7.19 (m, 4H, H$^{D3/D3'}$), 7.16 (m, 4H, H$^{D2/D2'}$), 7.14 (td, J = 7.6, 1.0 Hz, 2H, H^{C4}), 7.01 (q, J = 6.1 Hz, 4H, H$^{D2/D2'}$), 6.86 (dtd, J = 7.8, 4.1, 1.6 Hz, 2H, H^{C3}), 2.99 (q, J = 7.7 Hz, 2H, H^{Et-CH2}), 0.75 (t, J = 7.7 Hz, 3H, H^{Et-CH3}). ^{13}C NMR (126 MHz, (CD$_3$)$_2$CO, 298 K) δ /ppm 165.8 (C^{B2}), 159.0 (t, J = 6.0 Hz, C^{C1}), 150.7 (C^{B9}), 144.5 (C^{B10a}), 143.6 (C^{B10b}), 139.4 (C^{B4}), 138.7 (C^{B7}), 135.0 (C^{C3}), 134.2 (t, J = 7.6 Hz, C$^{D2/D2'}$), 133.7 (t, J = 7.4 Hz, C$^{D2/D2'}$), 133.2 (C^{C5}), 132.2 (t, J = 16.7 Hz, C$^{D1/D1'}$), 131.0 (d, J = 12.3 Hz, C$^{D4/D4'}$), 130.7 (C^{B6a}), 129.7 (m, C$^{D3/D3'}$), 129.1 (C^{B4a}), 128.1 (C^{B5}), 127.2 (C^{B6}), 126.1 (t, J = 2.2 Hz, C^{C4}), 125.6 (C^{B8}), 125.0 (d, J = 14.0 Hz, C^{C2}), 124.9 (C^{B3}), 121.3 (t, J = 1.8 Hz, C^{C6}), 34.8 (C^{Et-CH2}), 13.2 (C^{Et-CH3}). ^{31}P NMR (162 MHz, (CD$_3$)$_2$CO, 294 K) δ / ppm −12.7 (broad, FWHM = 375 Hz, xantphos), −144.2 (septet, J_{PF} = 708 Hz, [PF$_6$]$^-$). ESI MS: *m/z* 809.4 [M–PF$_6$]$^+$ (base peak, calc. 809.2). Found C 62.76, H 4.52, N 3.30; C$_{50}$H$_{40}$CuF$_6$N$_2$OP$_3$ requires C 62.86, H 4.22, N 2.93.

[Cu(xantphos)(2-Etphen)][PF$_6$]. (SK155)

Batch size: 0.29 mmol. The title compound [Cu(xantphos)(2-Etphen)][PF$_6$] was obtained as yellow crystals in good yield (259 mg, 0.26 mmol, 90%). ^{1}H NMR (500 MHz, (CD$_3$)$_2$CO, 298 K) δ/ppm 9.10 (d, J = 4.3 Hz, 1H, H^{B9}), 8.76 (d, J = 8.4 Hz, 1H, H^{B4}), 8.68 (dd, J = 8.1, 1.1 Hz, 1H, H^{B7}), 8.20 (d, J = 8.9 Hz, 1H, H^{B5}), 8.12 (d, J = 8.9 Hz, 1H, H^{B6}), 7.90 (d, J = 5.8 Hz, 1H, H^{B3}), 7.89 (dd, J = 6.5, 1.3 Hz, 2H, H^{C5}), 7.88 (dd, J = 8.2, 4.7 Hz, 1H, H^{B8}), 7.41 – 7.36 (m, 2H, H$^{D4/D4'}$), 7.30 (m, 2H, H^{C5}), 7.29 – 7.24 (m, 8H, H$^{D2/D2'+D3/D3'}$), 7.20 – 7.16 (m, 2H, H$^{D4/D4'}$), 7.00 – 6.94 (m, 4H, H$^{D3/D3'}$), 6.79 (ddd, J = 8.3, 6.6, 3.2 Hz, 4H, H$^{D2/D2'}$), 6.71 (ddd, J = 7.5, 5.5, 2.4 Hz, 2H, H^{C3}), 2.59 (q, J = 7.7 Hz, 2H, H^{Et-CH2}), 1.99 (s, 3H, H$^{xantphos-CH3}$), 1.66 (s, 3H, H$^{xantphos-CH3}$), 0.57 (t, J = 7.7 Hz, 3H, H^{Et-CH3}). ^{13}C NMR (126 MHz, (CD$_3$)$_2$CO, 298 K) δ/ppm 165.2 (C^{B2}), 155.9 (t, J = 6.3 Hz, C^{C1}), 150.4 (C^{B9}), 144.5 (C^{B10a}), 143.5 (C^{B10b}), 139.4 (C^{B4}), 138.7 (C^{B7}), 135.0 (t, J = 1.6 Hz, C^{C6}), 133.8 (t, J = 8.1 Hz, C$^{D2/D2'}$), 133.5 (t, J = 7.8 Hz, C$^{D2/D2'}$), 132.7 (t, J = 16.2 Hz, C$^{D1/D1'}$), 132.5 (t, J = 17.9 Hz, C$^{D1/D1'}$), 131.7 (C^{C3}), 130.9 (C$^{D4/D4'}$), 130.8 (C^{B6a}), 129.9 (t, J = 4.8 Hz, C$^{D3/D3'}$), 129.5 (t, J = 4.6 Hz, C$^{D3/D3'}$), 129.3 (C^{B4a}), 128.6 (C^{C5}), 128.1 (C^{B5}), 127.3 (C^{B6}), 126.2 (t, J = 2.4 Hz, C^{C4}), 125.9 (C^{B8}), 124.9 (C^{B3}), 121.4 (m, C^{C2}), 37.0 (t, J = 1.4 Hz, C$^{xantphos-bridge}$), 35.0 (C^{Et-CH2}), 31.4 (C$^{xantphos-Me}$), 25.7 (C$^{xantphos-Me}$), 13.1 (C^{Et-CH3}). ^{31}P NMR (162 MHz, (CD$_3$)$_2$CO, 300 K) δ/ppm −12.7 (broad, FWHM = 340 Hz, xantphos), −144.5 (septet, J_{PF} = 708 Hz, [PF$_6$]$^-$). ESI MS: *m/z* 849.4 [M–PF$_6$]$^+$ (base peak, calc. 849.2). Found C 63.51, H 4.71, N 3.14; C$_{53}$H$_{44}$CuF$_6$N$_2$OP$_3$ requires C 63.95, H 4.46, N 2.81.

Single crystal structures determined for the alkyl chapter

[Cu(POP)(bpy)][PF_6]·$CHCl_3$ was already published.[1]

[Cu(xantphos)(bpy)][PF_6].

$C_{49}H_{40}CuF_6N_2OP_3$, M = 943.32, yellow block, monoclinic, space group $P2_1/n$, a = 10.4166(10), b = 21.747(2), c = 19.1754(18) Å, β = 95.873(3), U = 4320.9(7) Å^3, Z = 4, D_c = 1.450 Mg m^{-3}, μ(Cu-Kα) = 2.331 mm^{-1}, T = 123 K. Total 27920 reflections, 7723 unique, R_{int} = 0.028. Refinement of 7596 reflections (559 parameters) with $I > 2\sigma(I)$ converged at final R_1 = 0.0302 (R_1 all data = 0.0306), wR_2 = 0.0753 (wR_2 all data = 0.0753), gof = 1.0277. CCDC 1581158.

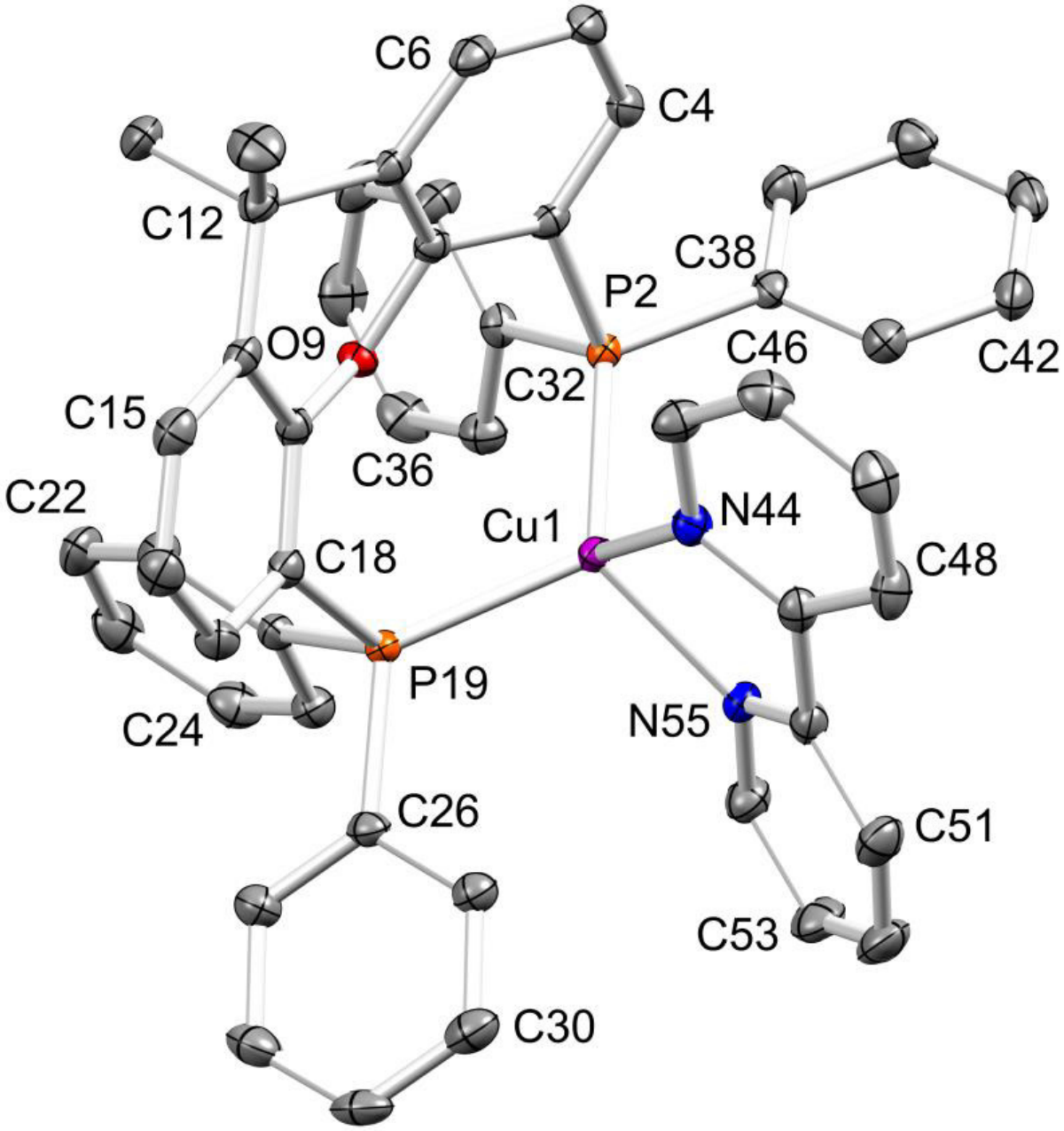

Structure of the [Cu(xantphos)(bpy)]$^+$ cation in [Cu(xantphos)(bpy)[PF_6] with ellipsoids plotted at 50% probability level; H atoms are omitted. Selected bond parameters: Cu1–P2 = 2.2539(4), Cu1–P19 = 2.2830(4), Cu1–N44 = 2.1210(12), Cu1–N55 = 2.0583(12) Å; P2–Cu1–P19 = 113.816(14), P2–Cu1–N44 = 105.59(3), P19–Cu1–N44 = 116.58(3), P2–Cu–N55 = 125.38(3), P19–Cu1–N55 = 111.24(3), N44–Cu1–N55 = 79.32(5)°.

[Cu(POP)(6-Mebpy)][PF_6].

After SQUEEZE: $C_{49}H_{60}ClCuF_6N_2OP_3$, M = 917.29, yellow needle, monoclinic, space group $P2_1/n$, a = 9.7056(4), b = 16.3421(7), c = 29.3522(14) Å, β = 96.439(2)°, U = 4626.2(4) Å^3, Z = 4, D_c = 1.317 Mg m^{-3}, μ(Cu-Kα) = 2.161 mm^{-1}, T = 123 K. Total 51874 reflections, 8423 unique, R_{int} = 0.028. Refinement of 8278 reflections (659 parameters) with $I > 3\sigma(I)$ converged at final R_1 = 0.0394 (R_1 all data = 0.0398), wR_2 = 0.0392 (wR_2 all data = 0.0396), gof = 1.0728. CCDC 996509.

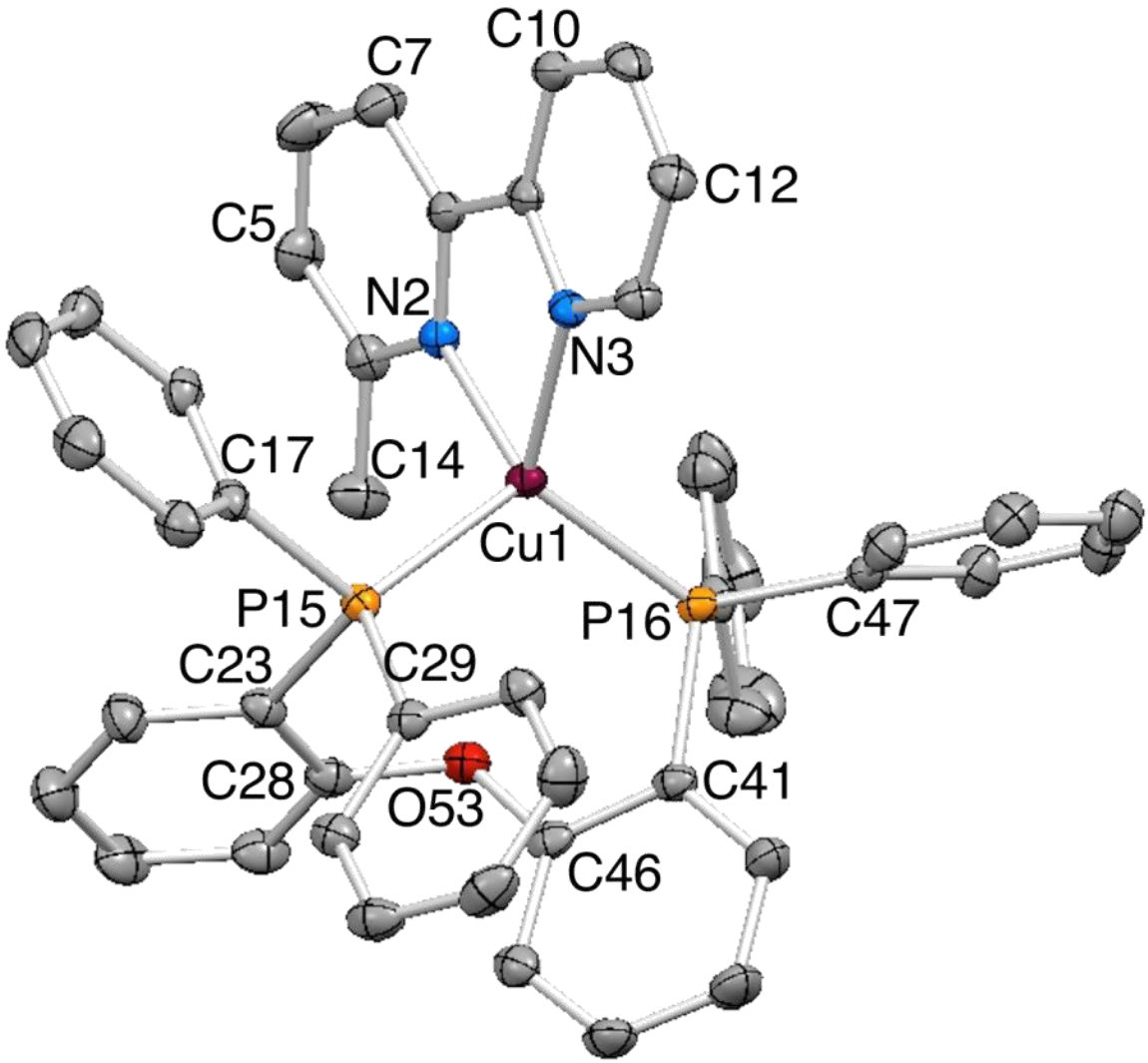

Structure of the [Cu(POP)(6-Mebpy)]$^+$ cation (ellipsoids plotted at 40% probability level, H atoms omitted; major occupancy site of 6-Mebpy is shown. Selected bond metrics: Cu1–P15 = 2.2694(4), Cu1–P16 = 2.2514(4), Cu1–N2 = 2.1164(10), Cu1–N3 = 2.0466(10) Å; P15–Cu1–P16 = 112.952(16), P15–Cu1–N2 = 108.81(4), P16–Cu1–N2 = 119.58(4), P15–Cu1–N3 = 113.06(4), P16–Cu1–N3 = 118.09(4), N2–Cu1–N3 = 80.39(4), C28–O53–C46 = 118.79(12)°.

[Cu(xantphos)(6-Mebpy)][PF_6]·CH_2Cl_2·0.4Et_2O.

$C_{52.60}H_{48}Cl_2CuF_6N_2O_{1.40}P_3$, M = 1071.93, yellow block, triclinic, space group $P\bar{1}$, a = 11.0240(10), b = 15.0242(13), c = 18.1498(16) Å, α = 109.274(4), β = 96.649(3), γ = 109.556(3)°, U = 2586.0(2) Å^3, Z = 2, D_c = 1.377 Mg m^{-3}, μ(Cu-Kα) = 2.947 mm^{-1}, T = 123 K. Total 31667 reflections, 8960 unique, R_{int} = 0.028. Refinement of 8640 reflections (615 parameters) with $I > 2\sigma(I)$ converged at final R_1 = 0.0660 (R_1 all data = 0.0673), wR_2 = 0.1763 (wR_2 all data = 0.1770), gof = 1.0065. CCDC 1422372.

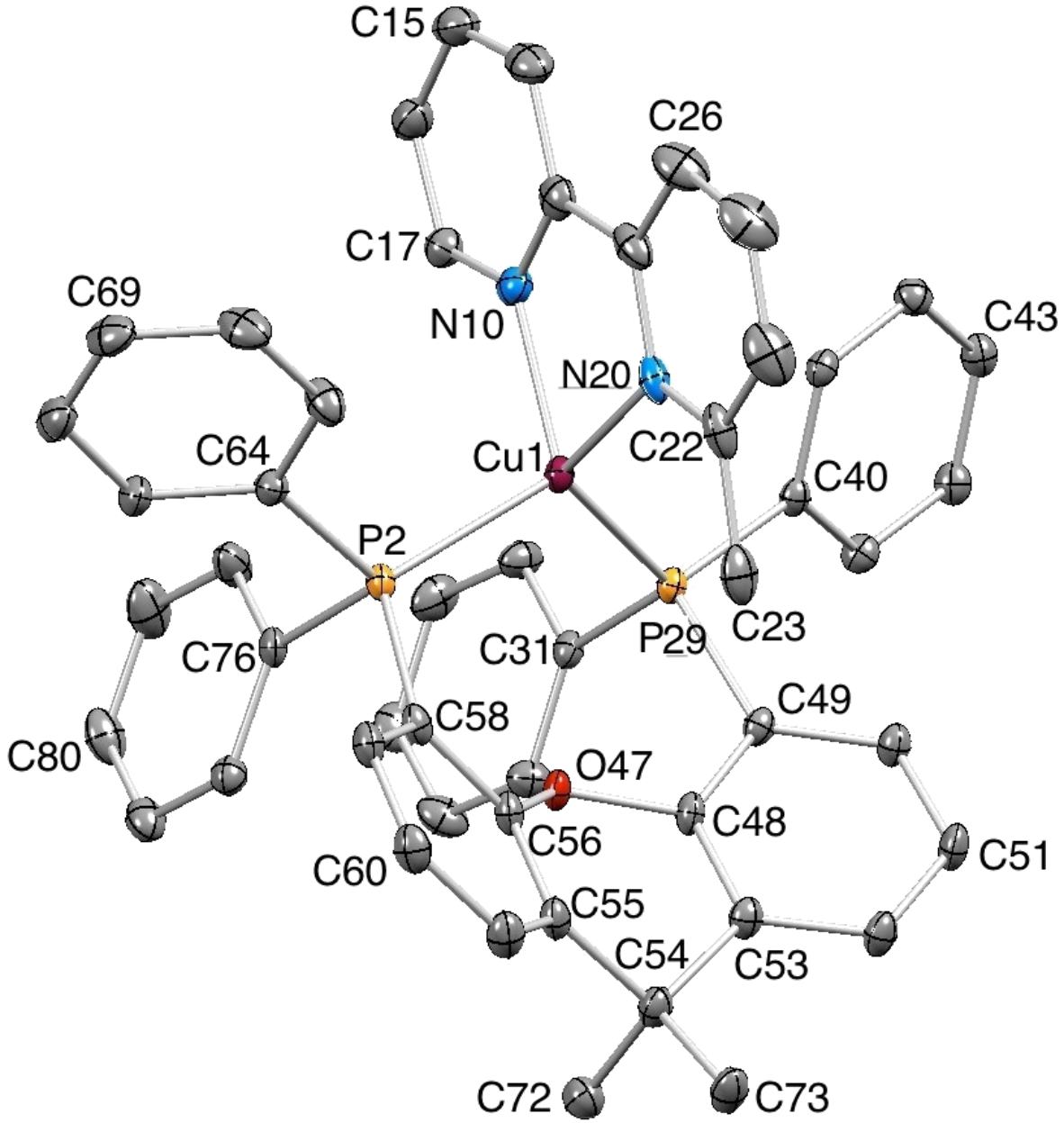

Structure of the [Cu(xantphos)(6-Mebpy)]$^+$ cation in [Cu(xantphos)(6-Mebpy)[PF_6]·CH_2Cl_2·0.4Et_2O with ellipsoids plotted at 30% probability level; H atoms are omitted. Selected bond parameters: Cu1–P2 = 2.2662(9), Cu1–N10 = 2.042(3), Cu1–N20 = 2.073(3), Cu1–P29 = 2.2489(9) Å; P2–Cu1–N10 = 110.97(8), P2–Cu1–N20 = 111.07(8), N10–Cu1–N20 = 80.97(12), P2– Cu1–P29 = 113.38(3), N10–Cu1–P29 = 115.10(8), N20–Cu1–P29 = 121.22(8)°.

Selected Theoretical bond parameters (B3LYP-D3//6-31G**/LANL2DZ):

Ground State (S_0): Cu1–P2 = 2.3149, Cu1–N10 = 2.1235, Cu1–N20 = 2.1156, Cu1–P29 = 2.3038 Å; P2–Cu1–N10 = 108.49, P2–Cu1–N20 = 118.29, N10–Cu1–N20 = 78.61, P2– Cu1–P29 = 113.34, N10–Cu1–P29 = 117.84, N20–Cu1–P29 = 115.77°.

First Triplet Excited State (T_1): Cu1–P2 = 2.391, Cu1–N10 = 1.985, Cu1–N20 = 2.008, Cu1–P29 = 2.413 Å; P2–Cu1–N10 = 129.61, P2–Cu1–N20 = 109.19, N10–Cu1–N20 = 83.04, P2– Cu1–P29 = 105.78, N10–Cu1–P29 = 98.12, N20–Cu1–P29 = 132.90°.

[Cu(POP)(6,6'-Me$_2$bpy)][PF$_6$]·2H$_2$O·0.5CH$_2$Cl$_2$.

$C_{48.5}H_{45}ClCuF_6N_2O_3P_3$, M = 1009.81, orange block, monoclinic, space group $P2_1/c$, a = 16.3230(8), b = 15.5884(9), c = 20.3378(11) Å, β = 105.944(3)°, U = 4975.9(3) Å^3, Z = 4, D_c = 1.348 Mg m^{-3}, μ(Cu-Kα) = 2.571 mm^{-1}, T = 123 K. Total 40330 reflections, 8670 unique, R_{int} = 0.084. Refinement of 8631 reflections (570 parameters) with $I>3\sigma(I)$ converged at final R_1 = 0.1341 (R_1 all data = 0.1342), wR_2 = 0.3231 (wR_2 all data = 0.3235), gof = 0.9898. CCDC 1009455.

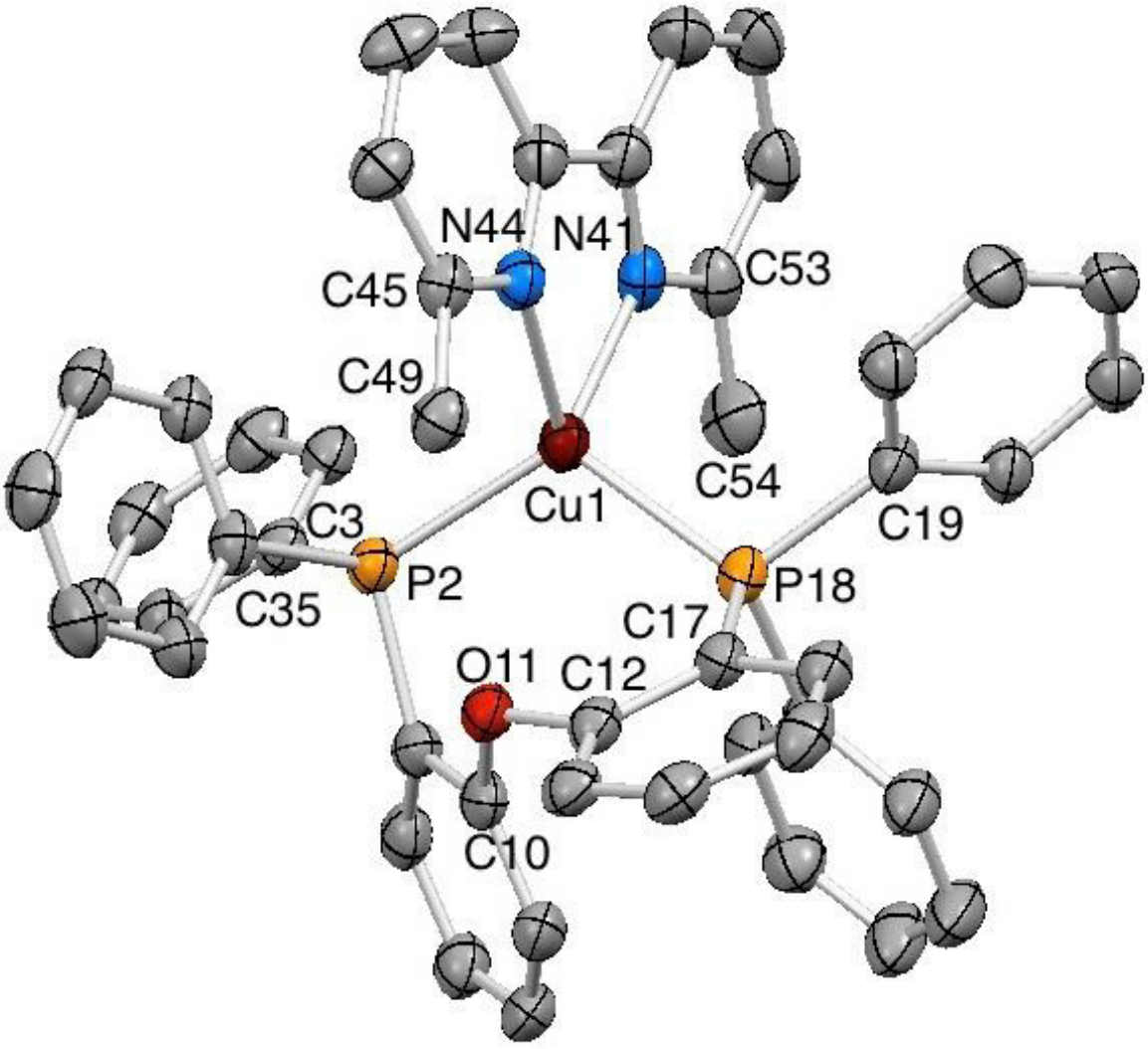

Structure of the [Cu(POP)(6,6'-Me$_2$bpy)]$^+$ cation in [Cu(POP)(6,6'-Me$_2$bpy)][PF$_6$] with ellipsoids plotted at the 40% probability level; H atoms omitted for clarity. Selected bond parameters: Cu1–P2 = 2.267(2), Cu1–P18 = 2.288(2), Cu1–N41 = 2.085(6), Cu1–N44 = 2.116(6), O11–C10 = 1.393(9), O11–C12 = 1.393(8) Å; P2–Cu1–P18 = 113.36(8), P2–Cu1–N41 = 125.98(17), P18–Cu1–N41 = 109.16(16), P2–Cu1–N44 = 111.51(16), P18–Cu1–N44 = 112.00(17), N41–Cu1–N44 = 80.2(2), C10–O11–C12 = 118.6(5)°.

[Cu(xantphos)(6,6'-Me$_2$bpy)][PF$_6$].

$C_{51}H_{44}CuF_6N_2OP_3$, M = 971.38, yellow block, triclinic, space group $P\bar{1}$, a = 11.3520(7), b = 14.0919(9), c = 14.8225(10) Å, α = 89.240(2), β = 68.865(2), γ = 88.481(2)°, U = 2210.88(15) Å^3, Z = 2, D_c = 1.459 Mg m^{-3}, μ(Cu-Kα) = 2.294 mm^{-1}, T = 123 K. Total 36576 reflections, 7980 unique, R_{int} = 0.030. Refinement of 7676 reflections (577 parameters) with $I > 2\sigma(I)$ converged at final R_1 = 0.0549 (R_1 all data = 0.0563), wR_2 = 0.1380 (wR_2 all data = 0.1386), gof = 0.8779. CCDC 1422373.

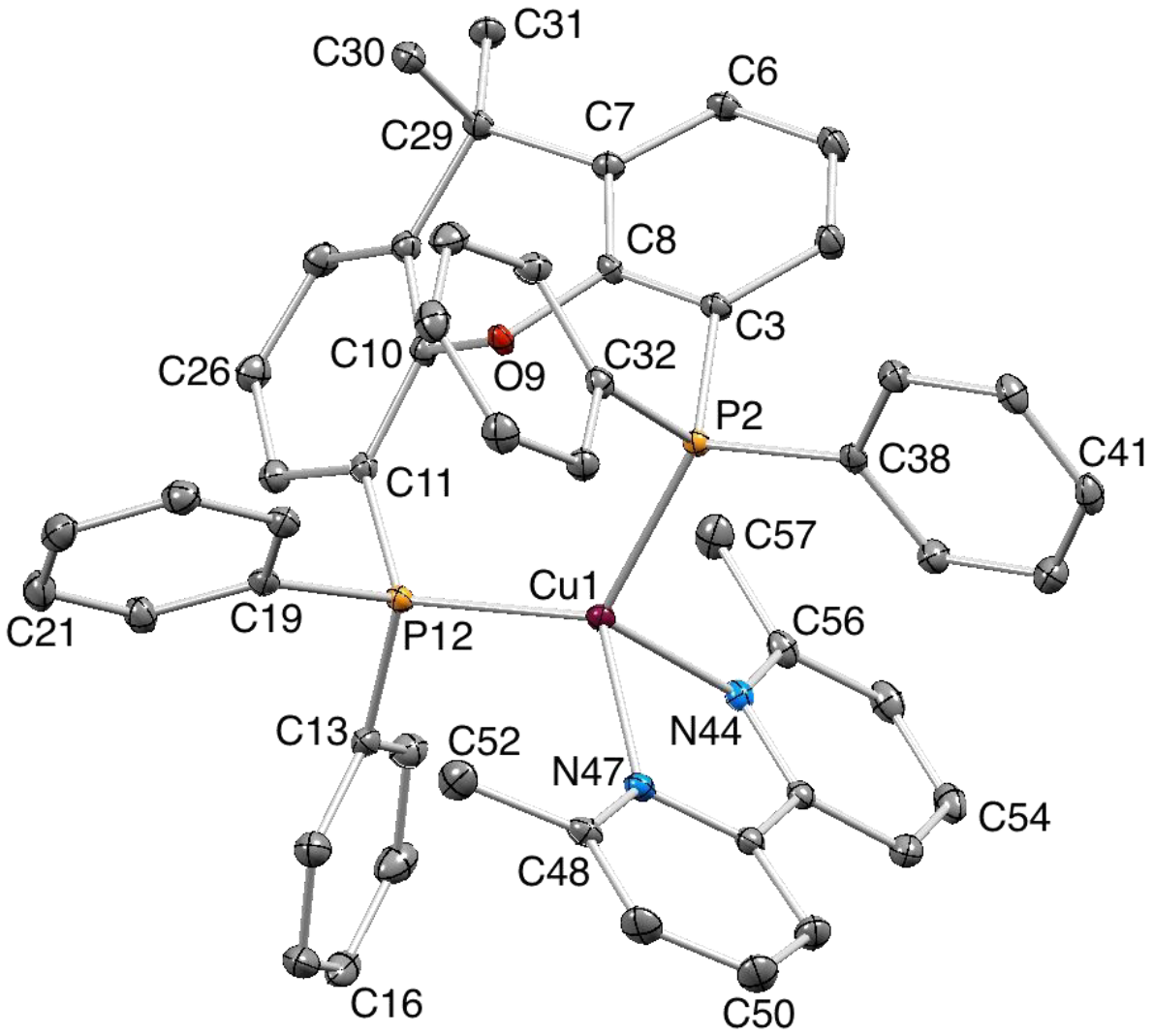

Structure of the [Cu(xantphos)(6,6'-Me$_2$bpy)]$^+$ cation in [Cu(xantphos)(6,6'-Me$_2$bpy)][PF$_6$] with ellipsoids plotted at 30% probability level; H atoms are omitted. Selected bond parameters: Cu1–P2 = 2.3068(7), Cu1–P12 = 2.2774(7), Cu1–N44 = 2.085(2), Cu1–N47 = 2.108(2) Å; P2–Cu1–P12 = 119.47(3), P2–Cu1–N44 = 105.00(6), P12–Cu1–N44 = 118.00(6), P2–Cu1–N47 = 112.36(6), P12–Cu1–N47 = 115.44(6)°, N44–Cu1–N47 = 79.66(9)°.

Selected Theoretical bond parameters (B3LYP-D3//6-31G**/LANL2DZ):

Ground State (S_0): Cu1–P2 = 2.3331, Cu1–P12 = 2.3309, Cu1–N44 = 2.1504, Cu1–N47 = 2.1427 Å; P2–Cu1–P12 = 113.15, P2–Cu1–N44 = 118.51, P12–Cu1–N44 = 112.46, P2–Cu1–N47 = 113.49, P12–Cu1–N47 = 116.75, N44–Cu1–N47 = 78.34°.

First Triplet Excited State(T_1): Cu1–P2 = 2.418, Cu1–P12 = 2.375, Cu1–N44 = 2.072, Cu1–N47 = 1.971 Å; P2–Cu1–P12 = 106.28, P2–Cu1–N44 = 110.35, P12–Cu1–N44 = 117.68, P2–Cu1–N47 = 94.23, P12–Cu1–N47 = 141.76, N44–Cu1–N47 = 82.92°.

[Cu(POP)(6-Etbpy)][PF_6]·Et_2O.

$C_{52}H_{50}CuF_6N_2O_2P_3$, M = 1005.44, yellow block, triclinic, space group $P\bar{1}$, a = 9.8765(10), b = 14.2651(15), c = 18.6704(19) Å, α = 103.932(3), β = 95.012(3), γ = 107.013(3)°, U = 2405.8(2) Å^3, Z = 2, D_c = 1.388 Mg m^{-3}, μ(Cu-Kα) = 2.141 mm^{-1}, T = 123 K. Total 31470 reflections, 8397 unique, R_{int} = 0.028. Refinement of 8323 reflections (595 parameters) with $I > 2\sigma(I)$ converged at final R_1 = 0.0534 (R_1 all data = 0.0537), wR_2 = 0.1356 (wR_2 all data = 0.1355), gof = 1.0230. CCDC 1422374.

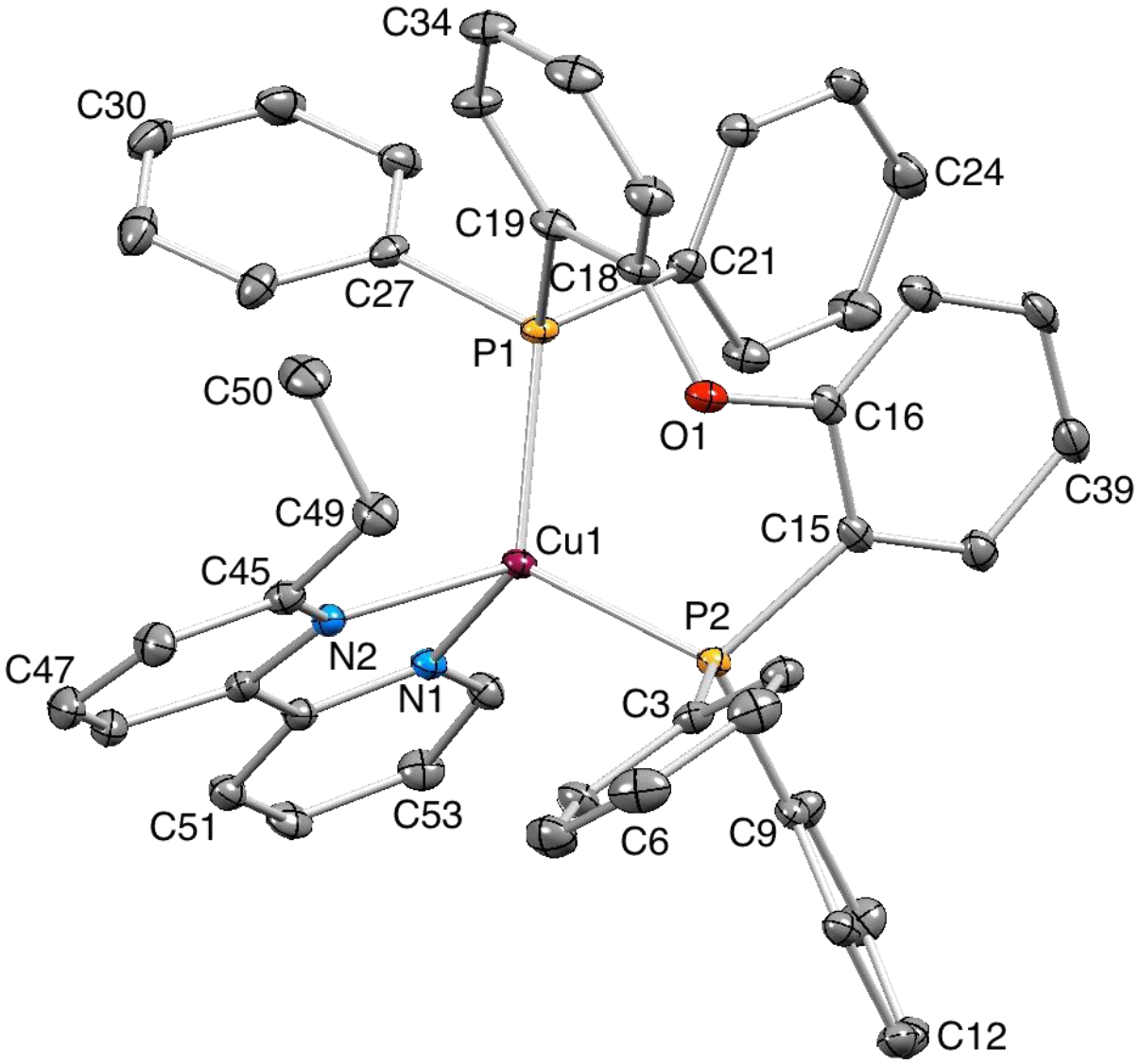

Structure of the [Cu(POP)(6-Etbpy)]$^+$ cation in [Cu(POP)(6-Etbpy)][PF_6]·Et_2O with ellipsoids plotted at 40% probability level; H atoms are omitted. Selected bond parameters: Cu1–P1 = 2.2752(7), Cu1–P2 = 2.2654(7), Cu1–N1 = 2.056(2), Cu1–N2 = 2.098(2) Å; P1–Cu1–P2 = 113.08(3), P1–Cu1–N1 = 113.61(6), P2–Cu1–N1 = 116.75(6), P1–Cu1–N2 = 112.48(6), P2–Cu1–N2 = 116.95(6), N1–Cu1–N2 = 80.11(8)°.

Selected Theoretical bond parameters (B3LYP-D3//6-31G**/LANL2DZ):

Ground State(S_0): Cu1–P1 = 2.3044, Cu1–P2 = 2.3049, Cu1–N1 = 2.1170, Cu1–N2 = 2.1308 Å; P1–Cu1–P2 = 113.04, P1–Cu1–N1 = 111.48, P2–Cu1–N1 = 120.72, P1–Cu1–N2 = 119.09, P2–Cu1–N2 =110.09, N1–Cu1–N2 =78.61°.

First Triplet Excited State(T_1): Cu1–P1 = 2.335, Cu1–P2 = 2.427, Cu1–N1 = 2.028, Cu1–N2 = 1.961 Å; P1–Cu1–P2 = 103.57, P1–Cu1–N1 = 104.09, P2–Cu1–N1 = 94.96, P1–Cu1–N2 = 152.01, P2–Cu1–N2 =122.71, N1–Cu1–N2 =82.46°.

[Cu(xantphos)(6-Etbpy)][PF_6]·CH_2Cl_2·$5H_2O$.

$C_{51}H_{49}CuF_6N_2O_{2.5}P_3$, M = 1083.33, yellow block, triclinic, space group $P\bar{1}$, a = 10.9607(7), b = 15.1290(10), c = 18.4236(13) Å, α = 110.648(4), β = 96.075(4), γ = 108.716(3)°, U = 2623.7(3) Å^3, Z = 2, D_c = 1.371 Mg m^{-3}, μ(Cu-Kα) = 2.926 mm^{-1}, T = 123 K. Total 32742 reflections, 9509 unique, R_{int} = 0.044. Refinement of 8432 reflections (622 parameters) with $I > 2\sigma(I)$ converged at final R_1 = 0.0694 (R_1 all data = 0.0756), wR_2 = 0.1860 (wR_2 all data = 0.1894), gof = 1.0230. CCDC 1429456.

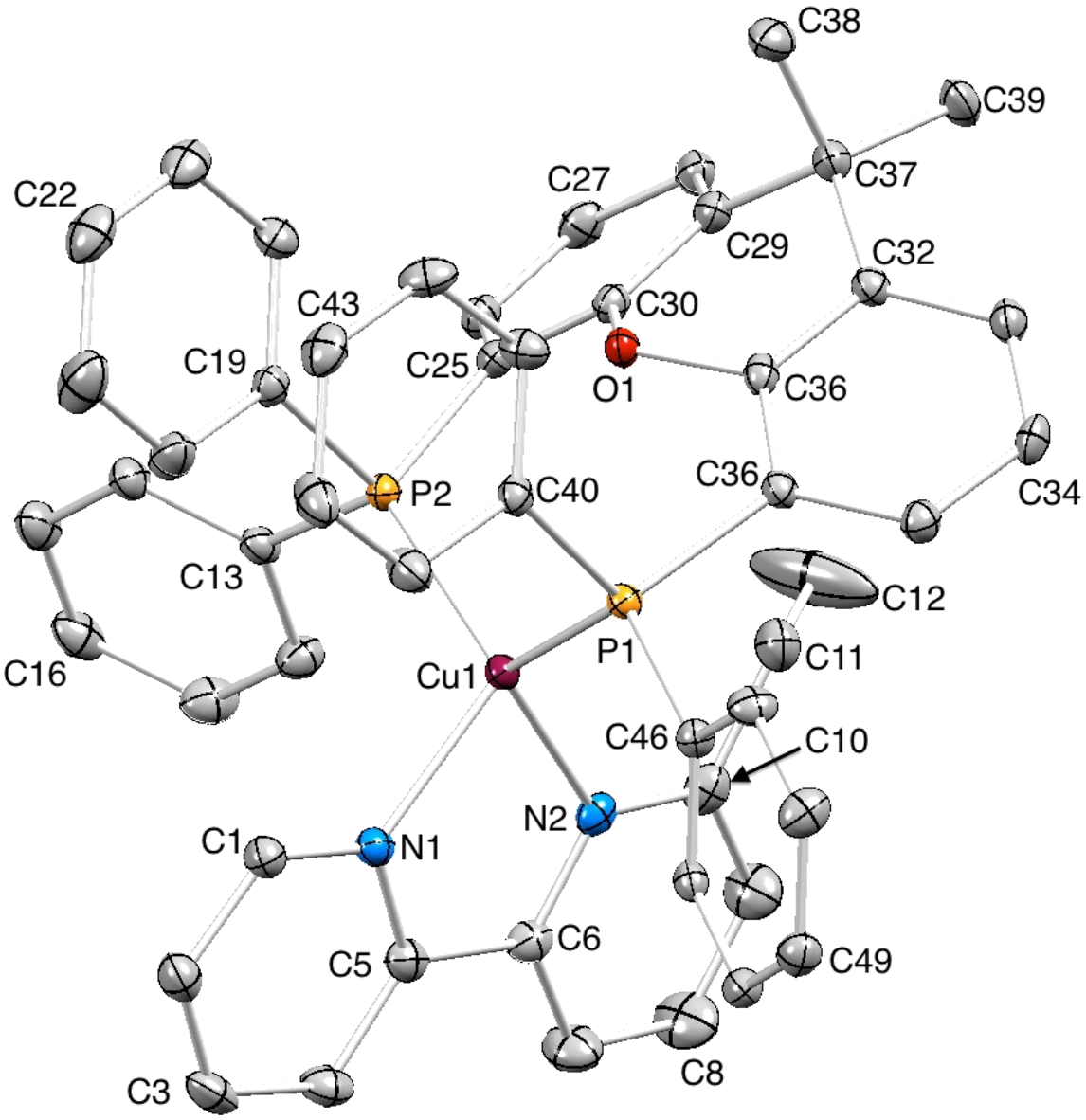

Structure of the [Cu(xantphos)(6-Etbpy)]$^+$ cation in [Cu(xantphos)(6-Etbpy)][PF_6]·CH_2Cl_2·$1.5H_2O$ with ellipsoids plotted at 40% probability level; H atoms are omitted. Selected bond parameters: Cu1–P2 = 2.2665(10), Cu1–P1 = 2.2548(10), Cu1–N2 = 2.080(3), Cu1–N1 = 2.056(3) Å; P2–Cu1–P1 = 113.33(4), P2–Cu1–N2 = 113.26(9), P1–Cu1–N2 = 119.59(8), P2–Cu1–N1 = 112.16(9), P1–Cu1–N1 = 113.96(9), N2–Cu1–N1 = 80.40(12)°.

Selected Theoretical bond parameters (B3LYP-D3//6-31G**/LANL2DZ):

Ground State(S_0): Cu1–P2 = 2.3099, Cu1–P1 = 2.3103, Cu1–N2 = 2.1209, Cu1–N1 = 2.1248 Å; P2–Cu1–P1 = 113.39, P2–Cu1–N2 = 120.75, P1–Cu1–N2 = 112.97, P2–Cu1–N1 = 110.10, P1–Cu1–N1 = 116.71, N2–Cu1–N1 = 78.58°.

First Triplet Excited State(T_1): Cu1–P2 = 2.393, Cu1–P1 = 2.392, Cu1–N2 = 2.004, Cu1–N1 = 1.989 Å; P2–Cu1–P1 = 106.01, P2–Cu1–N2 = 132.09, P1–Cu1–N2 = 109.13, P2–Cu1–N1 = 99.88, P1–Cu1–N1 = 128.33, N2–Cu1–N1 = 82.83°

[Cu(POP)(6-Phbpy)][PF_6]·Et_2O.

$C_{56}H_{50}CuF_6N_2O_2P_3$, M = 1053.49, yellow block, triclinic, space group $P\bar{1}$, a = 11.7097(7), b = 14.0940(8), c = 16.9221(10) Å, α = 110.418(2), β = 105.114(2), γ = 96.608(2)°, U = 2460.4(3) Å^3, Z = 2, D_c = 1.422 Mg m^{-3}, μ(Cu-Kα) = 2.123 mm^{-1}, T = 123 K. Total 31167 reflections, 8708 unique, R_{int} = 0.021. Refinement of 8536 reflections (631 parameters) with $I > 2\sigma(I)$ converged at final R_1 = 0.0421 (R_1 all data = 0.0425), wR_2 = 0.1093 (wR_2 all data = 0.1095), gof = 0.9770. CCDC 1422375.

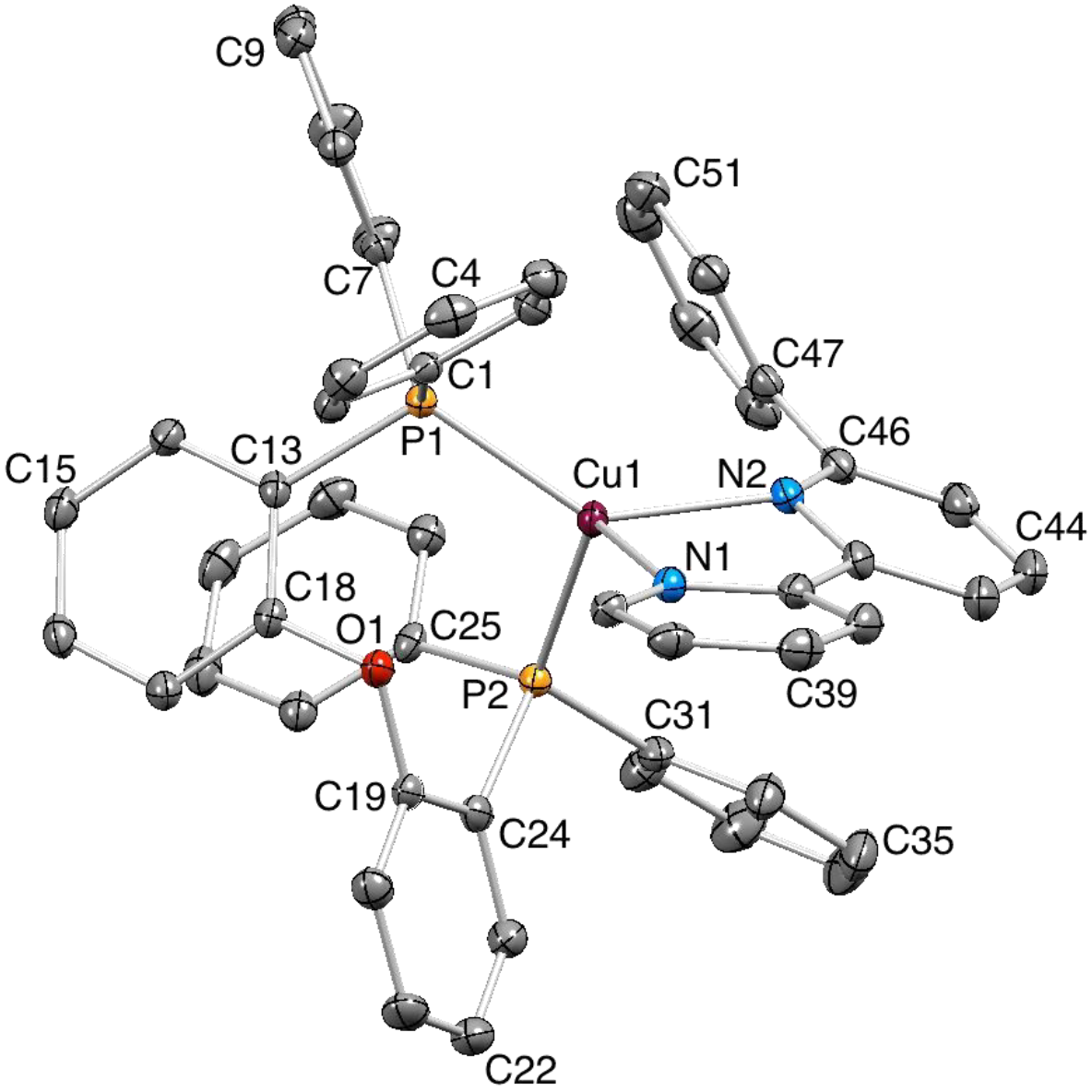

Fig. S11. Structure of the [Cu(POP)(6-Phbpy)]$^+$ cation in [Cu(POP)(6-Phbpy)][PF_6]·Et_2O with ellipsoids plotted at 40% probability level; H atoms are omitted. Selected bond parameters: Cu1–P2 = 2.2774(5), Cu1–P1 = 2.2707(5), Cu1–N1 = 2.1164(16), Cu1–N2 = 2.1129(16) Å; P2–Cu1–P1 = 109.407(19), P2–Cu1–N1 = 112.07(5), P1–Cu1–N1 = 107.78(5), P2–Cu1–N2 = 104.63(5), P1–Cu1–N2 = 139.15(5), N1–Cu1–N2 = 78.65(6)°.
Selected Theoretical bond parameters (B3LYP-D3//6-31G**/LANL2DZ):
Ground State(S_0): Cu1–P2 = 2.296, Cu1–P1 = 2.343, Cu1–N1 = 2.131, Cu1–N2 = 2.1154 Å; P2–Cu1–P1 = 113.85, P2–Cu1–N1 = 113.59, P1–Cu1–N1 = 101.38, P2–Cu1–N2 = 131.53, P1–Cu1–N2 = 108.97, N1–Cu1–N2 = 77.86°.
First Triplet Excited State(T_1): Cu1–P2 = 2.450, Cu1–P1 = 2.388, Cu1–N1 = 2.035, Cu1–N2 = 1.979 Å; P2–Cu1–P1 = 102.97, P2–Cu1–N1 = 122.95, P1–Cu1–N1 = 102.88, P2–Cu1–N2 = 97.34, P1–Cu1–N2 = 151.25, N1–Cu1–N2 = 82.27°

[Cu(xantphos)(6-Phbpy)][PF_6].

$C_{55}H_{44}CuF_6N_2OP_3$, M = 1019.42, yellow plate, monoclinic, space group $P2/n$, a = 10.1842(7), b = 29.746(2), c = 16.1630(12) Å, β = 98.762(3)°, U = 4839.3(6)Å^3, Z = 4, D_c = 1.399 Mg m^{-3}, μ(Cu-Kα) = 2.126 mm^{-1}, T = 123 K. Total 45877 reflections, 8964 unique, R_{int} = 0.053. Refinement of 8089 reflections (613 parameters) with $I > 2\sigma(I)$ converged at final R_1 = 0.0442 (R_1 all data = 0.0616), wR_2 = 0.0715 (wR_2 all data = 0.1159), gof = 1.0005. CCDC 1435492.

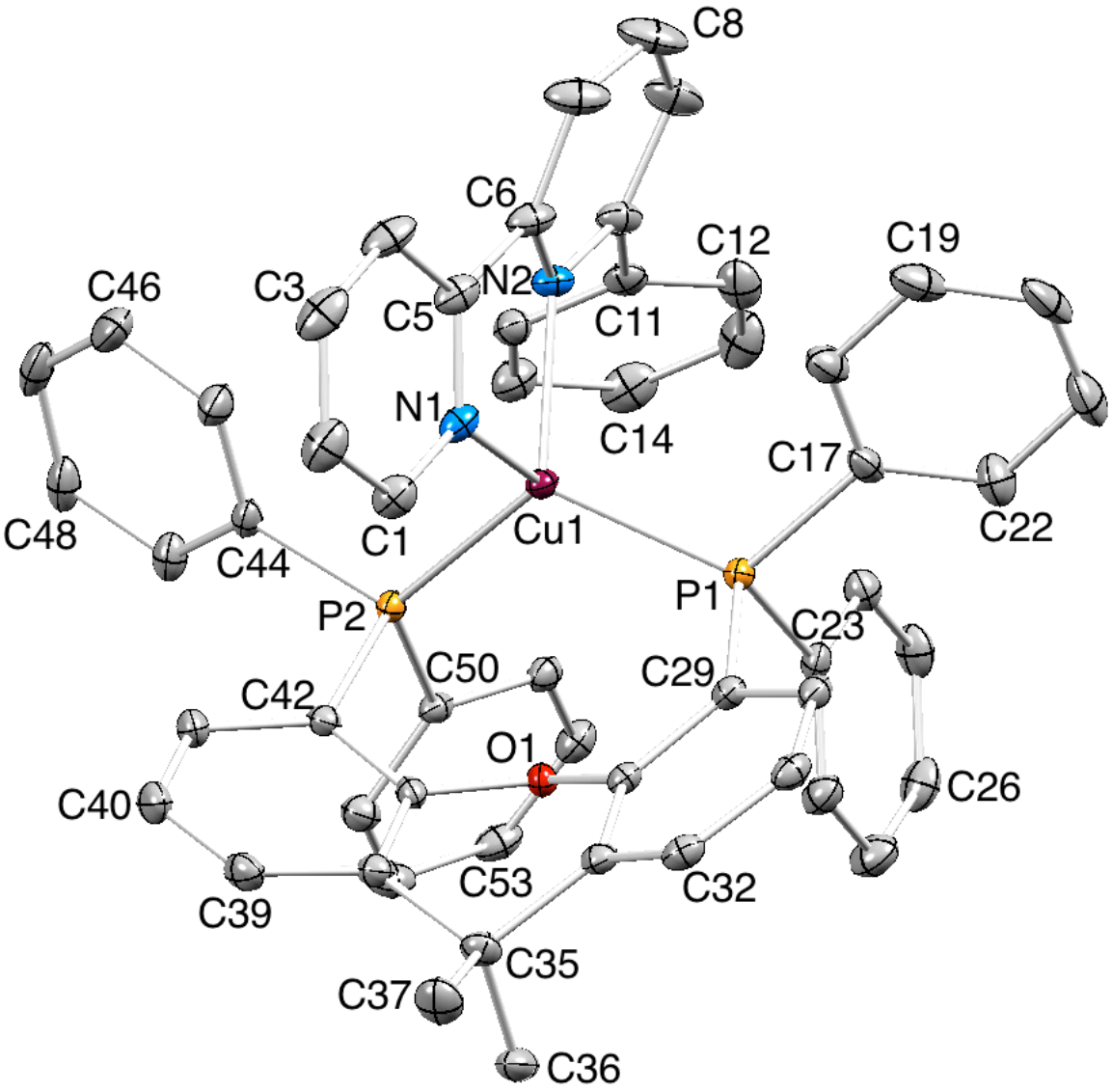

Structure of the [Cu(xantphos)(6-Phbpy)]$^+$ cation in [Cu(xantphos)(6-Phbpy)][PF_6] with ellipsoids plotted at 40% probability level; H atoms are omitted. Selected bond parameters: Cu1–P2 = 2.2497(11), Cu1–P1 = 2.2672(11), Cu1–N1 = 2.104(3), Cu1–N2 = 2.099(3) Å; P2–Cu1–P1 = 117.10(4), P2–Cu1–N1 = 105.87(10), P1–Cu1–N1 = 111.16(9), P2–Cu1–N2 = 123.69(9), P1–Cu1–N2 = 112.04(10), N1–Cu1–N2 = 79.24(13)°.

Selected Theoretical bond parameters (B3LYP-D3//6-31G**/LANL2DZ):

Ground State (S_0): Cu1–P2 = 2.3129, Cu1–P1 = 2.3101, Cu1–N1 = 2.1263, Cu1–N2 = 2.1839Å; P2– Cu1–P1 = 112.98, P2–Cu1–N1 = 132.78, P2-Cu1–N2 = 104.35, N1–Cu1–P1 = 107.53, N2–Cu1–P1 = 115.42, N1–Cu1-N2 = 78.08°.

First Triplet Excited State (T_1): Cu1–P2 = 2.3800, Cu1–P1 = 2.4354, Cu1–N1 = 1.9793, Cu1–N2 = 2.0456Å; P2–Cu1–P1 = 104.13, P2–Cu1–N1 = 151.28, P2-Cu1–N2 = 102.02, N1–Cu1–P1 = 96.57, N2–Cu1–P1 = 123.92, N1–Cu1-N2 = 81.99°.

[Cu(POP)(4,4'-tBu$_2$bpy)][PF6]·2CH$_2$Cl$_2$.

$C_{56}H_{56}Cl_4Cu_1F_6N_2O_1$, M = 1185.34, colourless plate, monoclinic, space group $P2_1/c$, a = 13.3408(5), b = 16.9615(7), c = 24.7382(10) Å, α = 90 β = 93.136(2)°, γ = 90 °, U = 5589.4(2)Å^3, Z = 4, D_c = 1.409 Mg m^{-3}, μ(Cu-Kα) = 3.634 mm^{-1}, T = 123 K. Total 51953 reflections, 10068 unique, R_{int} = 0.022. Refinement against F^2 of all 10066 reflections (658 parameters) converged at final R_1 = 0.0418, wR_2 = 0.1013, gof = 0.9358. CCDC XXXXXX.

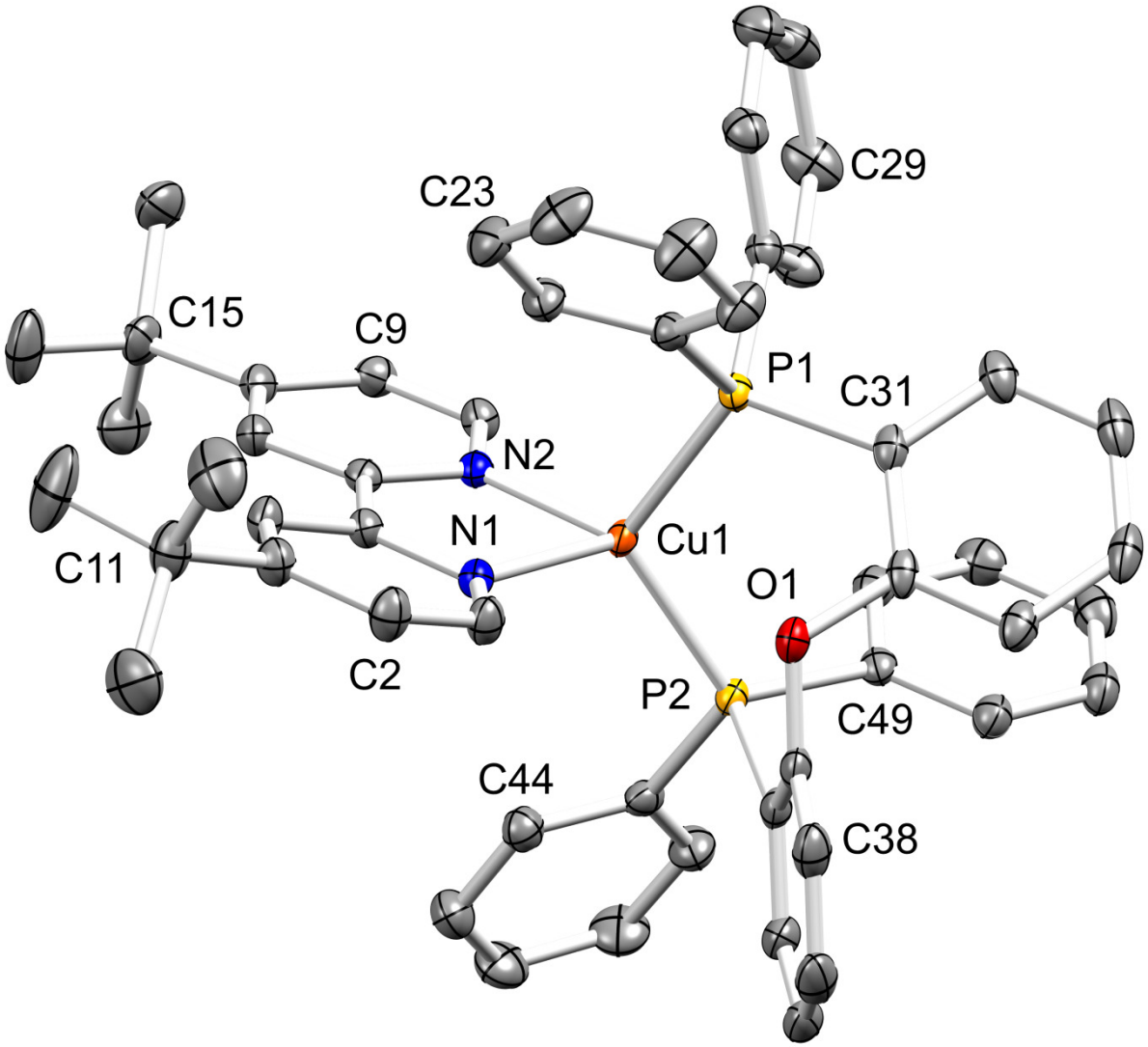

Structure of the [Cu(POP)(4,4'-tBu$_2$bpy)]$^+$ cation in [Cu(POP)(4,4'-tBu$_2$bpy)][PF$_6$]·2CH$_2$Cl$_2$ with ellipsoids plotted at 50% probability level; H atoms are omitted. Selected bond parameters: Cu1–P1 = 2.2385(5), Cu1–P2 = 2.2202(5), Cu1–N1 = 2.0682(16), Cu1–N2 = 2.0461(16) Å; P1–Cu1–P2 = 114.673(19), P1–Cu1–N1 = 105.39(5), P2–Cu1–N1 = 117.81(5), P1–Cu1–N2 = 114.41(4), P2–Cu1–N2 = 119.24(5), N1–Cu1–N2 = 79.97(6)°.

[Cu(POP)(5,5'-Me$_2$bpy)][PF$_6$].

$C_{48}H_{40}CuF_6N_2OP_3$, M = 931.31, yellow block, monoclinic, space group $P2_1/n$, a = 18.554(2), b = 11.4743(12), c = 22.167(2) Å, β = 113.880(4)°, U = 4315.1(8) Å^3, Z = 4, D_c = 1.433 Mg m^{-3}, μ(Cu-Kα) = 2.326 mm^{-1}, T = 123 K. Total 43751 reflections, 7916 unique, R_{int} = 0.031. Refinement of 7850 reflections (550 parameters) with $I > 2\sigma(I)$ converged at final R_1 = 0.0284 (R_1 all data = 0.0287), wR_2 = 0.0639 (wR_2 all data = 0.0640), gof = 0.9127. CCDC XXXXX.

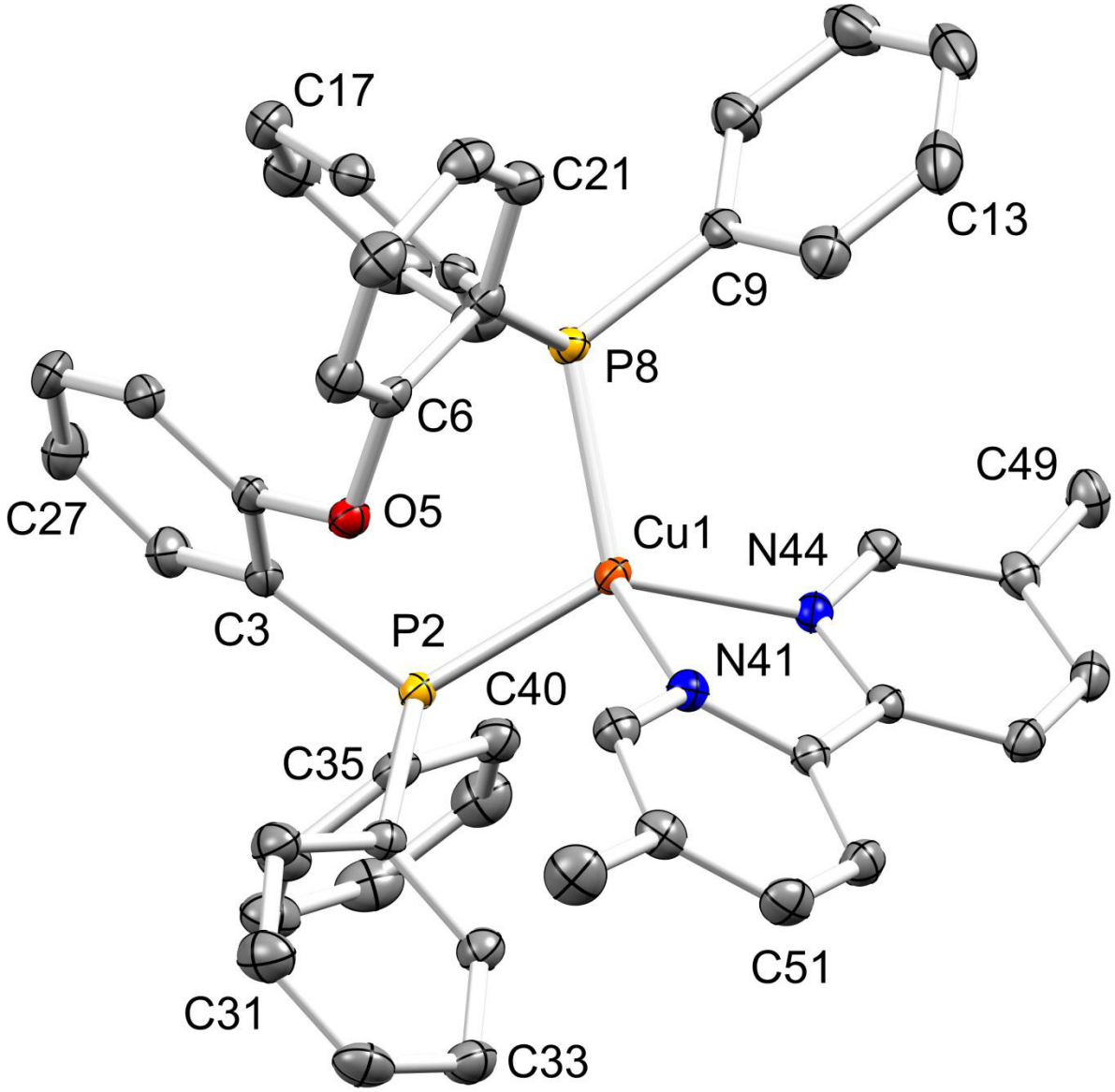

Structure of the [Cu(POP)(5,5'-Me$_2$bpy)]$^+$ cation in [Cu(POP)(5,5'-Me$_2$bpy)][PF$_6$] with ellipsoids plotted at 50% probability level; H atoms are omitted. Selected bond parameters: Cu1–P2 = 2.2535(4), Cu1–P8 = 2.2396(4), Cu1–N41 = 2.0820(11), Cu1–N44 = 2.0421(11) Å; P2–Cu1–P8 = 110.537(15), P2–Cu1–N41 = 104.10(4), P8–Cu1–N41 = 120.11(3), P2–Cu1–N44 = 127.20(3), P8–Cu1–N44 = 111.80(3), N41–Cu1–N44 = 80.17(5)°.

[Cu(POP)(6-Etphen)][PF_6].

$C_{50}H_{40}CuF_6N_2OP_3$, M = 955.33, yellow block, triclinic, space group $P\bar{1}$, a = 10.1640(8), b = 13.9335(11), c = 18.7219(14) Å, α = 102.552(2) β = 97.085(2), γ = 107.584(2)°, U = 2415.7(3) Å^3, Z = 2, D_c = 1.43 Mg m^{-3}, μ(Cu-Kα) = 3.133 mm^{-1}, T = 123 K. Total 32433 reflections, 8856 unique, R_{int} = 0.026. Refinement of 8704 reflections (568 parameters) with $I > 2\sigma(I)$ converged at final R_1 = 0.0340 (R_1 all data = 0.0344), wR_2 = 0.0808 (wR_2 all data = 0.0808), gof = 0.9218. CCDC XXXXX.

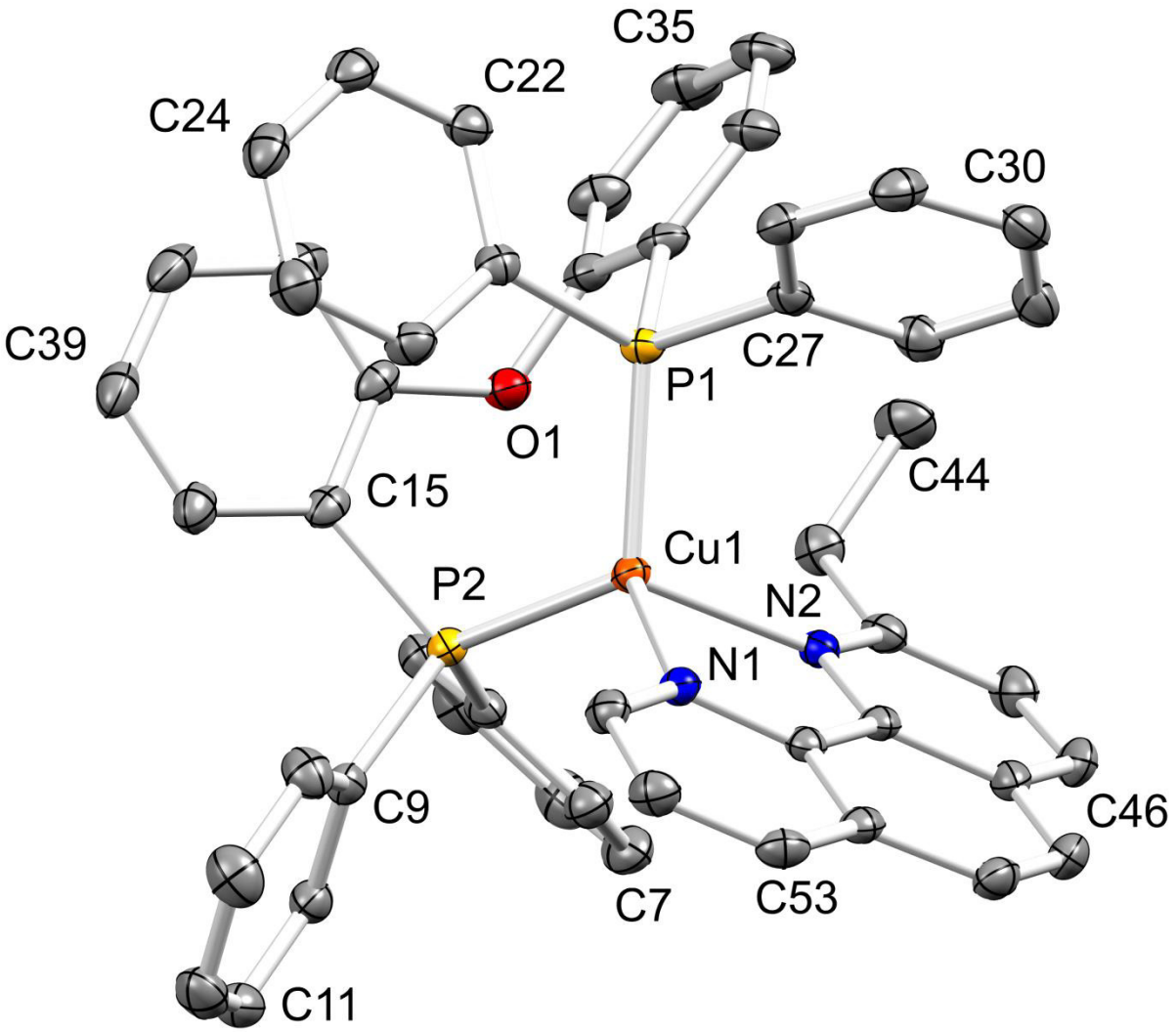

Structure of the [Cu(POP)(6-Etphen)]$^+$ cation in [Cu(POP)(6-Etphen)][PF_6] with ellipsoids plotted at 40% probability level; H atoms are omitted. Selected bond parameters: Cu1–P2 = 2.2488(5), Cu1–P1 = 2.2668(5), Cu1–N2 = 2.0924(13), Cu1–N1 = 2.0613(13) Å; P2–Cu1–P1 = 115.363(17), P2–Cu1–N2 = 116.46(4), P1–Cu1–N2 = 110.22(4), P2–Cu1–N1 = 115.23(4), P1–Cu1–N1 = 113.52(4), N2–Cu1–N1 = 81.59(5)°.

[Cu(xantphos)(6-Etphen)][PF_6].

$C_{53}H_{44}CuF_6N_2OP_3$, M = 995.40, yellow block, monoclinic, space group $P2_1/n$, a = 10.5631(8), b = 21.3906(16), c = 20.2696(15) Å, β = 93.185(3)°, U = 4572.9(6)Å^3, Z = 4, D_c = 1.446 Mg m^{-3}, μ(Cu-Kα) = 2.234 mm^{-1}, T = 123 K. Total 31841 reflections, 8090 unique, R_{int} = 0.029. Refinement of 7552 reflections (595 parameters) with $I > 2\sigma(I)$ converged at final R_1 = 0.0444 (R_1 all data = 0.0471), wR_2 = 0.1010 (wR_2 all data = 0.1019), gof = 0.8993. CCDC XXXXX.

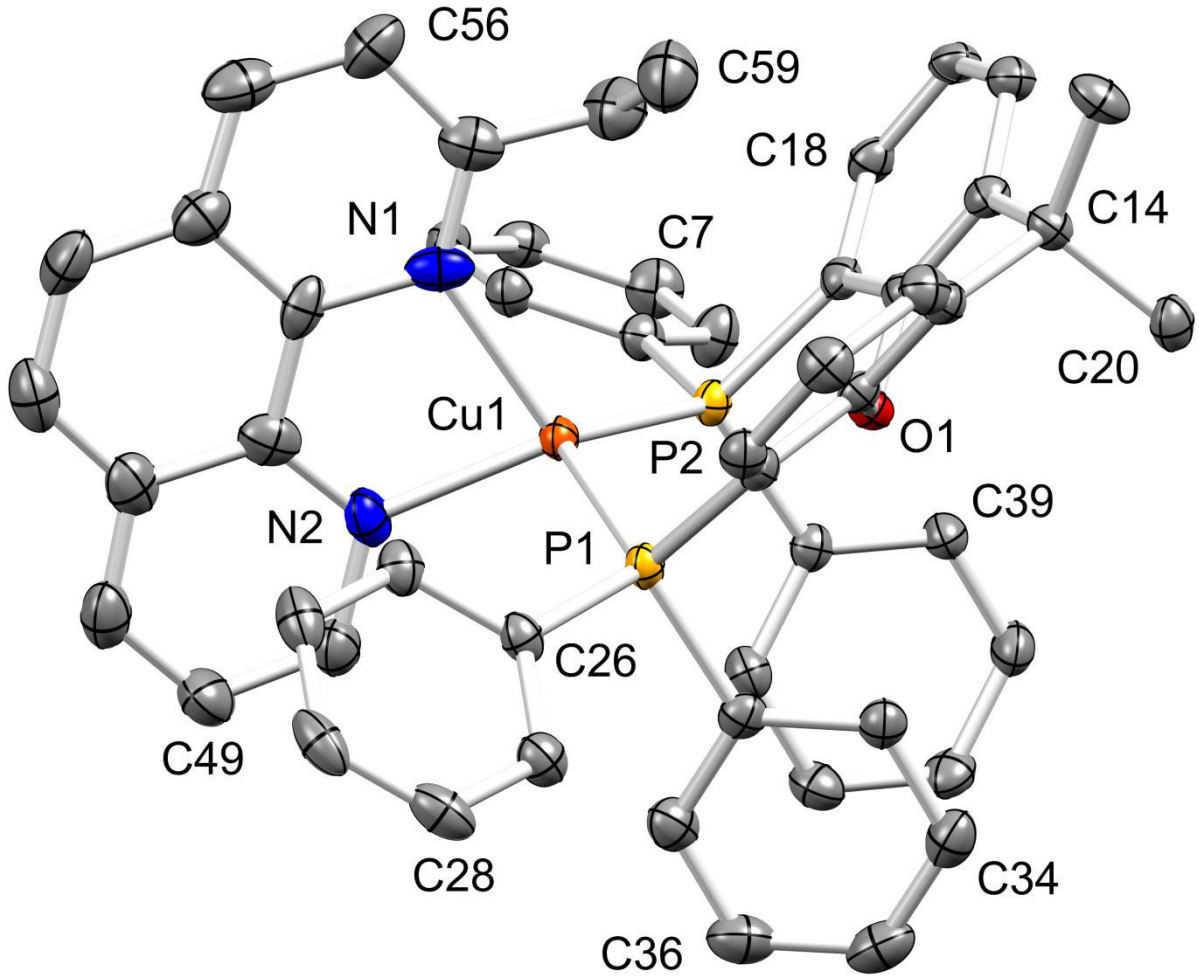

Structure of the [Cu(xantphos)(6-Etphen)]$^+$ cation in [Cu(xantphos)(6-Etphen)][PF_6] with ellipsoids plotted at 40% probability level; H atoms are omitted. Selected bond parameters: Cu1–P1 = 2.2915(6), Cu1–P2 = 2.2600(6), Cu1–N1 = 2.134(2), Cu1–N2 = 2.068(2) Å; P1–Cu1–P2 = 112.38(2), P1–Cu1–N1 = 115.60(6), P2–Cu1–N1 = 116.74(6), P1–Cu1–N2 = 103.92(6), P2–Cu1–N2 = 124.15(6), N1–Cu1–N2 = 80.39(9)°.

Acknowledgement for the alkyl chapter

We thank the European Research Council (Advanced Grant 267816 LiLo), Swiss National Science Foundation (Grant number 200020_144500), University of Basel, European Union 7th framework program LUMINET (TREASORES Grant 314068 and LUMINET Grant 316906), the Spanish Ministry of Economy and Competitiveness (MINECO) (MAT2011-24594 and CTQ2012-31914) and the Generalitat Valenciana (Prometeo/2012/053) for support. PD Dr Daniel Häussinger, Dr Roché Walliser, Thomas Müntener and Yann Baumgartner are thanked for help with low temperature NMR spectroscopic measurements.

References

1 R. D. Costa, D. Tordera, E. Ortí, H. J. Bolink, J. Schönle, S. Graber, C. E. Housecroft, E. C. Constable and J. A. Zampese, *J. Mater. Chem.* 2011, **21**, 16108.

2 G. J. Kubas, *Inorg. Synth*., 1979, **19**, 90.

3 M. Nishikawa, K. Nomoto, S. Kume and H. Nishihara, *Inorg. Chem.*, 2013, **52**, 369 and references therein.

4 V. Desvergnes-Breuil, V. Hebbe, C. Dietrich-Buchecker, J.-P. Sauvage and J. Lacour, *Inorg. Chem.*, 2003, **42**, 255; V. Hebbe-Viton, V. Desvergnes, J. J. Jodry, C. Dietrich-Buchecker, J.-P. Sauvage and J. Lacour, *Dalton Trans.*, 2006, 2058; I. Pianet and J.-M. Vincent, *Inorg. Chem.*, 2004, **43**, 2947.

5 See for example: G. Tárkányi, P. Király, G. Pálinkás and A. Deák, *Mag. Res. Chem.*, 2007, **45**, 917; A. Pintado-Alba, H. de la Riva, M. Nieuwhuyzen, D. Bautista, P. R. Raithby, H. A. Sparkes, S. J. Teat, J. M. López-de-Luzuriaga and M. C. Lagunas, *Dalton Trans.*, 2004, 3459.

6 S. Keller, F. Brunner, A. Prescimone, E. C. Constable and C. E. Housecroft, *Inorg. Chem. Comm*., 2015, **58**, 64 and references cited therein.

7 F. Brunner, S. Graber, Y. Baumgartner, D. Häussinger, A. Prescimone, E. C. Constable, C. E. Housecroft, *Dalton Trans.*, 2017, **46**, 6379.

8 See for example: N. Armaroli, G. Accorsi, G. Bergamini, P. Ceroni, M. Holler, O. Moudam, C. Duhayon, B. Delavaux-Nicot and J.-F. Nierengarten, *Inorg. Chim. Acta*, 2007, **360**, 1032; K. Saito, T. Arai, N. Takahashi, T. Tsukuda and T. Tsubomura, *Dalton Trans.* **2006**, 4444.

9 C. E. Housecroft, E. C. Constable, *Chem. Soc. Rev.*, 2015, **44**, 8386.

10 R. D. Costa, E. Ortí, H. J. Bolink, S. Graber, C. E. Housecroft, E. C. Constable, *Adv. Funct. Mater.* **2010**, *20*, 1511.

11 I. Andrés-Tomé, J. Fyson, F.B. Dias, A.P. Monkman, G. Iacobellis, P. Coppo, *Dalton Trans.*, 2012, **41**, 8669.

12 M. Tromp, A. J. Dent, J. Headspith, T. L. Easun, X.-Z. Sun, M. W. George, O. Mathon, G. Smolentsev, M. L. Hamilton and J. Evans, *J. Phys. Chem. B*, 2013, **117**, 7381.

13 N. Armaroli, G. Accorsi, F. Cardinali and A. Listorti, *Top. Curr. Chem.*, 2007, **280**, 69.

14 T. J. Penfold, S. Karlsson, G. Capano, F. A. Lima, J. Rittmann, M. Reinhard, M. H. Rittmann-Frank, O. Braem, E. Baranoff, R. Abela, I. Tavernelli, U. Rothlisberger, C. J. Milne and M. Chergui, *J. Phys. Chem. A*, 2013, **117**, 4591.

15 C. E. Housecroft and E. C. Constable, Chemistry: *An Introduction to Organic, Inorganic and Physical Chemistry*, Pearson Education Limited, Essex, England, **4**, 2010.

16 N. J. Turro, *Modern Molecular Photochemistry*, University Science Books, Sausalito, California, 1991.

17 N. A. Gothard, M.W. Mara, J. Huang, J.M. Szarko, B. Rolczynski, J. V. Lockard, L. X. Chen, *J. Phys Chem. A*, 2012, **116**, 1984.

18 X.-L. Chen, R. Yu, Q.-K. Zhang, L.-J. Zhou, X.-Y. Wu, Q. Zhang and C.-Z. Lu, *Chem. Mater*., 2013, **25**, 3910.

19 N. S. Murray, S. Keller, E. C. Constable, C. E. Housecroft, M. Neuburger and A. Prescimone, *Dalton Trans.*, 2015, **44**, 7626.

20 F. Brunner, L. Martínez-Sarti, S. Keller, A. Pertegás, A. Prescimone, E.C. Constable, H.J. Bolink and C.E. Housecroft, *Dalton Trans.*, 2016, **45**, 15180.

21 D. Tordera, S. Meier, M. Lenes, R. D. Costa, E. Ortí, W. Sarfert and H. J. Bolink, *Adv. Mater.*, 2012, **24**, 897.

22 M. Lenes, G. Garcia-Belmonte, D. Tordera, A. Pertegás, J. Bisquert and H. J. Bolink, *Adv. Funct. Mater.*, 2011, **21**, 1581.

23 S. van Reenen, P. Matyba, A. Dzwilewski, R. A. J. Janssen, L. Edman and M. Kemerink, *J. Am. Chem. Soc.*, 2010, **132**, 13776.

24 R. D. Costa, A. Pertegás, E. Ortí and H. J. Bolink, *Chem. Mater*., 2010, **22**, 1288.

25 D. Tordera, S. Meier, M. Lenes, R. D. Costa, E. Ortí, W. Sarfert and H. J. Bolink, *Adv. Mater.*, 2012, **24**, 897.

26 M. Lenes, G. Garcia-Belmonte, D. Tordera, A. Pertegás, J. Bisquert and H. J. Bolink, *Adv. Funct. Mater.*, 2011, **21**, 1581.

27 S. van Reenen, P. Matyba, A. Dzwilewski, R. A. J. Janssen, L. Edman and M. Kemerink, *J. Am. Chem. Soc.*, 2010, **132**, 13776.

28 M. Elie, S. Gaillard, J. L. Renaud, *Luminescent Cationic Copper(I) Complexes: Synthesis, Photophysical Properties and Application in Light-Emitting Electrochemical Cells* in *Light-Emitting Electrochemical Cells*, Springer International Publishing AG, Cham, Switzerland, 1st edn, 2017.

29 Q. Zhang, Q. Zhou, Y. Cheng, L. Wang, D. Ma, X. Jing, F. Wang, *Adv. Funct. Mater.*, 2006, **16**, 1203.

30 *Light-Emitting Electrochemical Cells*, ed. R. D. Costa, Springer International Publishing AG, Cham, Switzerland, 1st edn, 2017.

31 Y. Sekiguchi, Y. Kanuma, K. Omodera, K. Abe, M. Hayashi, S. Yamamoto, Assignee: Taisho Pharmaceutical Co., Ltd., Japan; Arena Pharmaceutical Inc., Jpn. Kokai Tokkyo Koho (2007), JP 2007291087 A 20071108.

32 Y.-Q. Fang, G. S. Hanan, *Synlett.*, 2003, **6**, 852.
33 M. D. Weber, M. Viciano-Chumillas, D. Armentano, Joan Cano, R. D. Costa, *Dalton Trans.*, 2017, **46**, 6312.
34 H.-C. Su, H.-F. Chen, Y.-C, Shen, C.-T. Liao and K.-T. Wong, *J. Mater. Chem.*, 2011, **21**, 9653.
35 A. B. Tamayo, S. Garon, T. Sajoto, P. I. Djurovich, I. M. Tsyba, R. Bau and M. E. Thompson, *Inorg. Chem.*, 2005, **44**, 8723.
36 Bruker Analytical X-ray Systems, Inc., 2006, APEX2, version 2 User Manual, M86-E01078, Madison, WI.
37 P. W. Betteridge, J. R. Carruthers, R. I. Cooper, K. Prout and D. J. Watkin, *J. Appl. Cryst*., 2003, **36**, 1487.
38 I. J. Bruno, J. C. Cole, P. R. Edgington, M. K. Kessler, C. F. Macrae, P. McCabe, J. Pearson, R. Taylor, *Acta Crystallogr., Sect. B*, 2002, **58**, 389.
39 C. F. Macrae, I. J. Bruno, J. A. Chisholm, P. R. Edgington, P. McCabe, E. Pidcock, L. Rodriguez-Monge, R. Taylor, J. van de Streek and P. A. Wood, *J. Appl. Cryst*., 2008, **41**, 466.
40 M. J. Frisch, G. W. Trucks, H. B. Schlegel, G. E. Scuseria, M. A. Robb, J. R. Cheeseman, G. Scalmani, V. Barone, B. Mennucci, G. A. Petersson, H. Nakatsuji, M. Caricato, X. Li, H. P. Hratchian, A. F. Izmaylov, J. Bloino, G. Zheng, J. L. Sonnenberg, M. Hada, M. Ehara, K. Toyota, R. Fukuda, J. Hasegawa, M. Ishida, T. Nakajima, Y. Honda, O. Kitao, H. Nakai, T. Vreven, J. A. Montgomery, Jr, J. E. Peralta, F. Ogliaro, M. Bearpark, J. J. Heyd, E. Brothers, K. N. Kudin, V. N. Staroverov, R. Kobayashi, J. Normand, K. Raghavachari, A. Rendell, J. C. Burant, S. S. Iyengar, J. Tomasi, M. Cossi, N. Rega, N. J. Millam, M. Klene, J. E. Knox, J. B. Cross, V. Bakken, C. Adamo, J. Jaramillo, R. Gomperts, R. E. Stratmann, O. Yazyev, A. J. Austin, R. Cammi, C. Pomelli, J. W. Ochterski, R. L. Martin, K. Morokuma, V. G. Zakrzewski, G. A. Voth, P. Salvador, J. J. Dannenberg, S. Dapprich, A. D. Daniels, O. Farkas, J. B. Foresman, J. V. Ortiz, J. Cioslowski and D. J. Fox, Gaussian 09, Revision D.01, Gaussian, Inc., Wallingford, CT, 2009.
41 C. Lee, W. Yang and R. G. Parr, *Phys. Rev. B: Condens. Matter. Mater. Phys*., 1988, **37**, 785.
42 A. D. Becke, *J. Chem. Phys.*, 1993, **98**, 5648.
43 M. M. Francl, W. J. Pietro, W. J. Hehre, J. S. Binkley, M. S. Gordon, D. J. DeFrees and J. A. Pople, *J. Chem. Phys.*,1982, **77**, 3654.
44 P. J. Hay and W. R. Wadt, *J. Chem. Phys.*, 1985, **82**, 299.
45 S. Grimme, J. Antony, S. Ehrlich and H. Krieg, *J. Chem. Phys.*, 2010, **132,** 154104.
46 S. Grimme, S. Ehrlich and L. Goerigk, *J. Comp. Chem*., 2011, **32,** 1456.
47 J. Tomasi and M. Persico, *Chem. Rev*., 1994, **94**, 2027.
48 C. S. Cramer and D. G. Truhlar, *Solvent Effects and Chemical Reactivity*, Kluwer, 1996, pp. 1–80.
49 J. Tomasi, B. Mennucci and R. Cammi, *Chem. Rev.*, 2005, **105**, 2999.
50 M. E. Casida, C. Jamorski, K. C. Casida and D. R. Salahub, *J. Chem. Phys*., 1998, **108**, 4439.
51 C. Jamorski, M. E. Casida and D. R. Salahub, *J. Chem. Phys.*,1996, **104**, 5134.
52 M. Petersilka, U. J. Gossmann and E. K. U. Gross, *Phys. Rev. Lett.,* 1996, **76**, 1212.
53 M. Shaul and Y. Cohen, *J. Org. Chem*., 1999, **64**, 9358.
54 P. J. Pijper, H. van der Goot, H. Timmernam and W. Th. Nauta, *Eur. J. Med. Chem.*, 1984, **19**, 399.
55 E. C. Constable, R. P. G. Henney, T. A. Leese and D. A. Tocher, *J. Chem. Soc., Dalton Trans*., 1990, 443.
56 L. Hintermann, L. Xiao and A. Labonne, *Angew. Chem. Int. Ed.*, 2008, **47**, 8246.
57 G. J. Kubas, *Inorg. Synth*., 1979, **19**, 90.

Chapter II. Luminescent copper(I) complexes with bisphosphanes and halogen-substituted 2,2'-bipyridine ligands

Summary

This chapter is a soon to be submitted paper[3] about the effects of chloro- and bromo-substitution in the 2,2'-bipyridine (bpy) ligand of [Cu(P^P)(bpy)][PF_6] complexes (P^P = bis(2-(diphenylphosphino)phenyl)ether (POP) or 4,5-bis(diphenylphosphino)-9,9-dimethylxanthene (xantphos)). The bpy ligands that were chosen for this study are 6,6'-dichloro-2,2'-bipyridine (6,6'-Cl_2bpy), 6,6'-dibromo-2,2'-bipyridine (6,6'-Br_2bpy) and 6-bromo-2,2'-bipyridine (6-Brbpy). The described six heteroleptic copper(I) complexes were characterized with the usual analytical, structural, photophysical and electrochemical methods. Single crystal X-ray diffraction yielded solid state structures for the complexes with 6,6'-Cl_2bpy and 6-Brbpy. For [Cu(POP)(6-Brbpy)][PF_6], high pressure single crystal X-ray experiments up to 4.5 GPa were successfully performed at the Diamond Light Source (Beamline I19). We have described in Chapter I that alkyl and aryl substituents at the bpy ligand in general have a positive effect on the emissive properties of the complexes, even more so when the substitution is in 6-position at the bipyridine. The motivation behind this project was to find out whether halogen atoms in the 6-position of the bpy unit would also be beneficial to the photophysical properties and device performance of LECs built with these emitters. In terms of steric properties, we expected the halogen atoms *ortho* to the coordinating nitrogen of the bpy to have a stabilizing effect on the tetrahedral complex geometry that is similar to that of alkyl groups. Considering the electronic properties, while alkyl groups are weakly electron donating (+*I*), halogen atoms can have a positive inductive effect on the *ortho* and *para* positions of a π system (the so-called $+I_\pi$ effect), in combination with a +*M* effect. We expected these two combined effects to have an influence on the orbital characteristics of the complex and as a result, on its photophysical properties. LECs with [Cu(POP)(6,6'-Cl_2bpy)][PF_6] respectively [Cu(xantphos)(6,6'-Cl_2bpy)][PF_6] as emitters were prepared by the team of Henk Bolink in Valencia and the device properties such as electroluminescence, efficiency, brightness and device lifetime are described in this chapter.

[3] S. Keller, A. Prescimone, H. Bolink, A. Pertegás, G. Longo, E. C. Constable and C. E. Housecroft, "Luminescent Cu(I) complexes with bisphosphanes and halogen-substituted 2,2'-bipyridine ligands, submission to Dalton Trans. planned for January 2018.

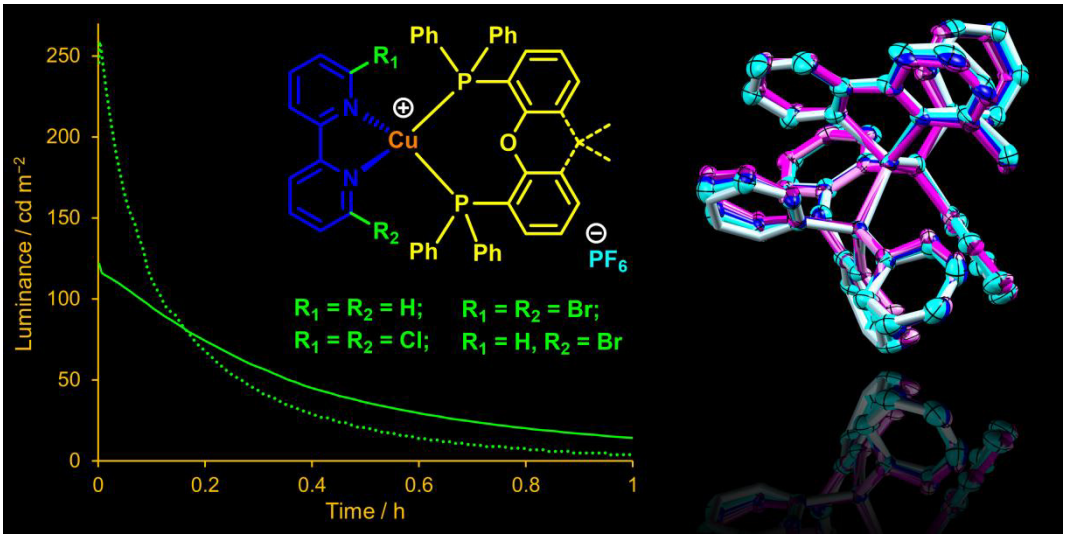

Contribution of Sarah Keller: Idea of the project and selection of ligands ❖ Synthesis of starting materials, ligands and complexes ❖ Analytical characterization (electrospray mass spectroscopy, NMR spectroscopy) ❖ Conduction of high pressure X-ray experiments ❖ Photophysical and electrochemical characterization ❖ Writing of the manuscript.

Dalton Trans.

ARTICLE

Luminescent copper(I) complexes with bisphosphanes and halogen-substituted 2,2'-bipyridine ligands

Cite this: DOI: 10.1039/xoxxoooooox

Sarah Keller,[a] Alessandro Prescimone,[a] Henk Bolink,[b] Antonio Pertegás,[b] Giulia Longo,[b] Edwin C. Constable[a] and Catherine E. Housecroft*[a]

Received ooth January 2012,
Accepted ooth January 2012

DOI: 10.1039/xoxxoooooox

www.rsc.org/

Heteroleptic [Cu(P^P)(N^N)][PF_6] complexes, where N^N is a halogen substituted 2,2'-bipyridine (bpy) and P^P is either bis(2-(diphenylphosphino)phenyl)ether (POP) or 4,5-bis(diphenylphosphino)-9,9-dimethylxanthene (xantphos) have been investigated. In order to stabilize the tetrahedral geometry of the copper(I) complexes, the steric demand of the bpy ligand was increased by employing a 6- or 6,6'-substitution pattern using halo-substituents. The six copper(I) complexes with either POP or xantphos and 6,6'-Cl_2-2,2'-bipyridine (6,6'-Cl_2bpy), 6-Br-2,2'-bipyridine (6-Brbpy) and 6,6'-Br_2-2,2'-bipyridine (6,6'-Br_2bpy) are orange emitters in the solid state and solution, and their photophysical and electrochemical properties were evaluated. The solid state structures for [Cu(POP)(6,6'-Cl_2bpy)][PF_6], [Cu(xantphos)(6,6'-Cl_2bpy)][PF_6]·CH_2Cl_2, [Cu(POP)(6-Brbpy)][PF_6] and [Cu(xantphos)(6-Brbpy)][PF_6]·0.7Et_2O obtained from single crystal X-ray diffraction are described including high-pressure experiments for [Cu(POP)(6-Brbpy)][PF_6]. Finally, [Cu(POP)(6,6'-Cl_2bpy)][PF_6] and [Cu(xantphos)(6,6'-Cl_2bpy)][PF_6], which show photoluminescence quantum yields of 15 and 17%, respectively, in the solid state, were tested as luminophores in light-emitting electrochemical cells (LECs). The devices exhibit orange electroluminescence and very short turn-on times (<5 to 12 seconds). Maximum luminance values of 121 and 259 cd m^{-2} (complex with POP respectively xantphos) are reached at an average current density of 100 A m^{-2} and the external quantum efficiencies come to 1.2% for both complexes.

Introduction

The development of light-emitting electrochemical cells (LECs) with ionic transition metal complexes (iTMCs) as emitters initially used ruthenium(II) complexes based upon $[Ru(bpy)_3]^{2+}$ (bpy = 2,2'-bipyridine) in the emissive layer.[1,2] However, a much broader spectrum of emission colours is achieved by using cyclometallated iridium(III) complexes of the type $[Ir(C^N)_2(N^N)]^+$, the archetype complex being $[Ir(ppy)_2(bpy)]^+$ (Hppy = 2-phenylpyridine).[3] While LECs and OLEDs (organic light emitting diodes) based on iridium-iTMCs remain an active area of research, attention has recently turned to the use of Cu-iTMCs.[3,4,5] In contrast to ruthenium and iridium, copper is Earth-abundant and thus leads to low-cost LECs. McMillin first demonstrated the potential for copper(I)-based emitters,[6,7] and the most studied families for LECs are $[Cu(N^N)(POP)]^+$ and $[Cu(N^N)(xantphos)]^+$ complexes (N^N is usually a derivative of bpy or 1,10-phenanthroline (phen), POP = bis(2-(diphenylphosphino)phenyl)ether, xantphos = 4,5-bis(diphenylphosphino)-9,9-dimethylxanthene).[8,9,10,11,12,1314,15,16]

In $[Cu(N^N)(POP)]^+$ and $[Cu(N^N)(xantphos)]^+$, the emission properties of the Cu-iTMCs can be altered by introducing substituents into the 6- and 6'-positions of bpy or 2- and 9-positions of phen.[6,9,10] Significant enhancement of LEC performance is observed with the introduction of simple alkyl groups (methyl or ethyl) at these positions.[10] Monomeric copper(I) complexes with halido ligands coordinating to the copper at as well as dimeric complexes with bridging halido ligands between the copper atoms show good emissive properties and thermally activated delayed fluorescence (TADF), and are promising materials for light-emitting devices.[17,18,19,20,21,22] We have previously investigated the effect of introducing peripheral halo-substituents into [Cu(P^P)(6,6'-Me_2-4,4'-Ph_2bpy)][PF_6] complexes and found that fluorine and chlorine substitution leads to improved properties of the complexes and the respective LECs.[16] However, the number of copper(I) complexes in the literature that have a halo-substituted N^N chelating ligand is surprisingly scarce. The homoleptic $[Cu(6,6'\text{-}Br_2bpy)_2][ClO_4]$[23] and heteroleptic $[Cu(6,6'\text{-}Br_2bpy)(bpy(Mes)_2)][BF_4]$[24] complexes are some of the rare examples with a halogen-bpy. Most of the reported compounds are copper complexes with halogen modified phenanthrolines,[25,26,27] with $[Cu(5\text{-}Cl\text{-}phen)(PPh_3)_2]^+$ and $[Cu(4,7\text{-}Cl_2\text{-}phen)(PPh_3)_2]^+$ being two of the few heteroleptic examples thereof that include phosphorus ligands.[28]

We now explore the effects of introducing chloro- or bromo-substituents into the bpy domain using 6- or 6,6'-substitution patterns on the [Cu(P^P)(bpy)][PF_6] complexes. We were curious to find out whether halogen atoms in the 6-position of the bpy unit would be as good in stabilizing the tetrahedral complex geometry and improving the photophysical properties and performance in LECs of the complexes as alkyl groups.[9,10] Alkyl groups are weakly electron donating (+*I*), and halogen atoms can have a positive inductive effect on the *ortho* and *para* positions of a π system (the so-called $+I_\pi$ effect) in combination with a +*M* effect.[29] We argue that these two combined effects should have an influence on the orbital characteristics of the complex, the HOMO–LUMO gap and therefore also the colour of the emission.

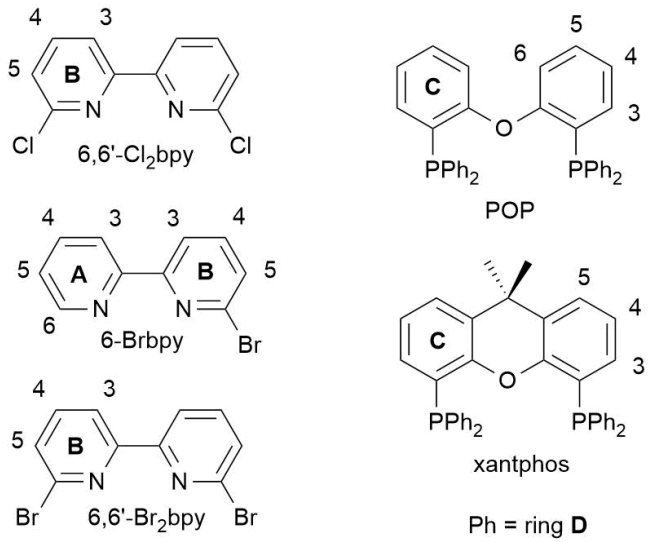

Scheme 1. Structures of ligands with ring and atom labels for NMR spectroscopic assignments.

Experimental

General. ^{1}H, ^{13}C and ^{31}P NMR spectra were recorded at room temperature using a Bruker Avance III-500 or III-400 NMR spectrometer. ^{1}H and ^{13}C NMR chemical shifts were referenced to residual solvent peaks with respect to δ(TMS) = 0 ppm and ^{31}P NMR chemical shifts with respect to δ(85% aqueous H_3PO_4) = 0 ppm. Solution absorption and emission spectra were measured using an Agilent 8453 spectrophotometer and a Shimadzu RF-5301PC spectrofluorometer, respectively. Electrospray ionization (ESI) mass spectra were recorded on a Bruker esquire 3000plus or Shimadzu LCMS-2020 instrument. Quantum yields for CH_2Cl_2 solution and powder samples were measured using a Hamamatsu absolute photoluminescence (PL) quantum yield spectrometer C11347 Quantaurus-QY. Emission lifetimes and powder emission spectra were measured with a Hamamatsu Compact Fluorescence lifetime Spectrometer C11367 Quantaurus-Tau, using an LED light source with λ_{exc} = 365 nm.

The compounds 6,6'-dichloro-2,2'-bipyridine (6,6'-Cl_2bpy),[30] and [$Cu(MeCN)_4$][PF_6][31] were prepared following literature methods and the NMR spectroscopic data matched those reported. POP was purchased from Acros, xantphos from Fluorochem, 6-bromo-2,2'-bipyridine (6-Brbpy) and 6,6'-dibromo-2,2'-bipyridine (6,6'-Br_2bpy) from TCI chemicals. All chemicals were used as received.

[Cu(POP)(6,6'-Cl_2bpy)][PF_6]. A colourless solution of [$Cu(MeCN)_4$][PF_6] (93 mg, 0.25 mmol) and POP (134 mg, 0.25 mmol) in CH_2Cl_2 (40 mL) was stirred for 2 h. Then 6,6'-Cl_2bpy (56 mg, 0.25 mmol) was added and the yellow solution was stirred for another 2 h. The solution was filtered and the solvent from the filtrate was removed in vacuo. The orange powder was redissolved in CH_2Cl_2 and layered with Et_2O. This gave [Cu(POP)(6,6'-Cl_2bpy)][PF_6] as orange crystals (208 mg, 0.21 mmol, 86%). ^{1}H NMR (500 MHz, CD_2Cl_2) δ / ppm 8.10 (dd, *J* = 7.9 Hz, 2H, H^{B3}), 7.98 (d, *J* = 7.9 Hz, 2H, H^{B4}), 7.41 (d, *J* = 7.9 Hz, 2H, H^{B5}), 7.32–7.25 (m, 6H, H^{C5+D4}), 7.16–7.08 (m, 20H, $H^{C3+C4+D2+D3}$), 6.86 (m, 2H, H^{C6}). ^{13}C NMR (126 MHz, CD_2Cl_2) δ / ppm 158.6 (s, C^{C1}), 152.6 (s, C^{B2}), 152.1 (s, C^{B6}), 141.8 (s, C^{B4}), 134.2 (s, C^{C3}), 133.7 (t, *J* = 8.5 Hz, C^{D2}), 132.6 (s, C^{C5}), 131.8 (t, *J* = 17.5 Hz, C^{D1}), 130.4 (s, C^{D4}), 129.1 (t, *J* = 5.3 Hz, C^{D3}), 127.7 (s, C^{B5}), 125.9 (t, *J* = 16.2 Hz, C^{C2}), 125.4 (s, C^{C4}), 121.9 (s, C^{B3}), 120.1 (s, C^{C6}). ^{31}P NMR (162 MHz, CD_2Cl_2) δ / ppm −12.3 (broad, FWHM = 180 Hz, POP), −144.5 (septet, J_{PF} = 710 Hz, $[PF_6]^-$). ESI MS: *m/z* 827.0 $[M–PF_6]^+$ (base peak, calc. 827.1). Found C 57.59, H 4.21, N 3.13; $C_{46}H_{34}Cl_2CuF_6N_2OP_3 \cdot Et_2O$ requires C 57.40, H 4.24, N 2.68.

[Cu(xantphos)(6,6'-Cl_2bpy)][PF_6]. A colourless solution of xantphos (145 mg, 0.25 mmol) and 6,6'-Cl_2bpy (56 mg, 0.25 mmol) in CH_2Cl_2 (20 mL) was added dropwise to a colourless solution of [$Cu(MeCN)_4$][PF_6] (93 mg, 0.25 mmol) in CH_2Cl_2 (20 mL). After stirring for 2h, the yellow solution was filtered and the solvent was removed in vacuo. The orange-yellow powder was redissolved in CH_2Cl_2 and layered with Et_2O. This gave [Cu(xantphos)(6,6'-Cl_2bpy)][PF_6] as yellow crystals in good yield (202 mg, 0.20 mmol, 80%). ^{1}H NMR (500 MHz, $(CD_3)_2CO$) δ / ppm 8.36 (d, *J* = 7.5 Hz, 2H, H^{B3}), 8.17 (t, *J* = 7.9 Hz, 2H, H^{B4}), 7.81 (dd, *J* = 7.8, 1.4 Hz, 2H, H^{C5}), 7.66 (d, *J* = 7.7 Hz, 2H, H^{B5}), 7.43–7.40 (m, 4H, H^{D4}), 7.29 (t, *J* = 7.7 Hz, 2H, H^{C4}), 7.25–7.20 (m, 16H, H^{D2+D3}), 7.00 (m, 2H, H^{C3}), 1.73 (s, 6H, $H^{xantphos\text{-}Me}$). ^{13}C NMR (126 MHz, $(CD_3)_2CO$) δ / ppm 156.0 (C^{C1}), 151.5 (C^{B2}), 142.7 (C^{B4}), 134.1 (t, *J* = 7.9 Hz, C^{D2}), 132.3 (t, *J* = 16.9 Hz, C^{D1}), 131.2 (C^{C3}), 131.0 (C^{D4}), 129.7 (t, *J* = 4.9 Hz, C^{D3}), 128.6 (C^{C5}), 128.0 (m, C^{C4+C2}), 122.7 (C^{B3}), 36.7 ($C^{xantphos\text{-}bridge}$), 29.0 ($C^{xantphos\text{-}Me}$). ^{31}P NMR (162 MHz, CD_2Cl_2) δ / ppm −11.9 (broad, FWHM = 150 Hz, xantphos), −144.5 (septet, J_{PF} = 710 Hz, $[PF_6]^-$). ESI MS: *m/z* 867.0 $[M–PF_6]^+$ (base peak, calc. 867.1). Found C 57.64, H 4.22, N 3.12; $C_{49}H_{38}Cl_2CuF_6N_2OP_3$ requires C 58.14, H 3.78, N 2.77.

[Cu(POP)(6-Brbpy)][PF_6]. A colourless solution of [$Cu(MeCN)_4$][PF_6] (93 mg, 0.25 mmol) and POP (134 mg, 0.25 mmol) in CH_2Cl_2 (40 mL) was stirred for 2 h. Then 6-Brbpy (59 mg, 0.25 mmol) was added and the yellow solution was stirred for another 2 h. The solution was filtered and the solvent was removed in vacuo. [Cu(POP)(6-Brbpy)][PF_6] was isolated as a yellow powder (226 mg, 0.23 mmol, 92%). ^{1}H NMR (500

MHz, CD_2Cl_2) δ /ppm 8.20 (d, J = 7.8 Hz, 2H, H^{A3+B3}), 8.01 – 7.98 (m, 1H, H^{A6}), 7.92 (td, J = 8.0, 1.6 Hz, 1H, H^{A4}), 7.83 (t, J = 7.9 Hz, 1H, H^{B4}), 7.52 (dd, J = 7.9, 0.6 Hz, 1H, H^{B5}), 7.49 – 7.46 (m, 4H, $H^{D2/D2'}$), 7.37 (t, J = 7.5 Hz, 2H, $H^{D4/D4'}$), 7.27 (t, J = 7.3 Hz, 4H, $H^{D3/D3'}$), 7.26 – 7.23 (m, 4H, $H^{C5+ D4/D4'}$), 7.08 (t, J = 7.8 Hz, 4H, $H^{D3/D3'}$), 7.03 (td, J = 7.7, 0.8 Hz, 2H, H^{C4}), 7.00 (m, 1H, H^{A5}), 6.95 (dtd, J = 8.2, 2.5, 1.0 Hz, 2H, H^{C6}), 6.90 (dtd, J = 7.8, 4.1, 1.6 Hz, 2H, H^{C3}), 6.80 – 6.76 (m, 4H, $H^{D2/D2'}$). ^{13}C NMR (126 MHz, CD_2Cl_2) δ /ppm 158.3 (t, J = 6.1 Hz, C^{C1}), 153.7 (C^{B2}), 151.4 (t, J = 2.3 Hz, C^{A2}), 149.6 (C^{A6}), 143.1 (C^{B6}), 141.0 (C^{B4}), 139.0 (C^{A4}), 135.1 (t, J = 8.5 Hz, $C^{D2/D2'}$), 134.6 (C^{C3}), 132.7 (t, J = 7.7 Hz, $C^{D2/D2'}$), 132.6 ($C^{C5+ D4/D4'}$), 131.5 (t, J = 18.1 Hz, $C^{D1/D1'}$), 131.1 ($C^{D4/D4'}$), 130.8 (C^{B5}), 130.6 (t, J = 16.2 Hz, $C^{D1/D1'}$), 129.3 (t, J = 5.2 Hz, $C^{D3/D3'}$), 129.1 (t, J = 4.9 Hz, $C^{D3/D3'}$), 126.5 (C^{A5}), 125.7 (t, J = 2.5 Hz, C^{C4}), 125.0 (t, J = 15.1 Hz, C^{C2}), 123.1 (C^{A3}), 121.7 (C^{B3}), 120.6 (t, J = 2.1 Hz, C^{C6}). ^{31}P NMR (162 MHz, CD_2Cl_2) δ / ppm −11.2 (broad, FWHM = 250 Hz, POP), −144.5 (septet, J_{PF} = 710 Hz, $[PF_6]^-$). ESI MS: *m/z* 837.4 $[M–PF_6]^+$ (base peak, calc. 837.1). Found C 55.99, H 3.77, N 3.06; $C_{46}H_{35}BrCuF_6N_2OP_3$ requires C 56.25, H 3.59, N 2.85.

[Cu(xantphos)(6-Brbpy)][PF$_6$]. A colourless solution of xantphos (145 mg, 0.25 mmol, 1.0 eq) and 6-Brbpy (59 mg, 0.25 mmol, 1.0 eq) in CH_2Cl_2 (20 mL) was added to a colourless solution of $[Cu(MeCN)_4][PF_6]$ (93 mg, 0.25 mmol, 1.0 eq) in CH_2Cl_2 (20 mL) and the resulting yellow solution was stirred for 2 h. The solvent was removed in vacuo and the yellow powder was redissolved in CH_2Cl_2 and layered with Et_2O. This gave $[Cu(xantphos)(6\text{-}Brbpy)][PF_6]$ as yellow crystals in good yield (244 mg, 0.24 mmol, 96 %). ^{1}H NMR (500 MHz, $(CD_3)_2CO$, 298 K) δ /ppm 8.56 (dd, J = 8.0, 0.5 Hz, 1H, H^{B3}), 8.50 (d, J = 8.2 Hz, 1H, H^{A3}), 8.38 (d, J = 4.3 Hz, 1H, H^{A6}), 8.15 (t, J = 7.9 Hz, 1H, H^{B4}), 8.12 (td, J = 7.8, 1.5 Hz, 1H, H^{A4}), 7.87 (dd, J = 7.9, 0.6 Hz, 1H, H^{B5}), 7.84 (dd, J = 7.8, 1.4 Hz, 2H, H^{C4}), 7.51 (ddd, J = 7.5, 5.1, 0.9 Hz, 1H, H^{A5}), 7.42 (t, J = 7.4 Hz, 2H, $H^{D4/D4'}$), 7.34 (t, J = 7.4 Hz, 2H, $H^{D4/D4'}$), 7.29 (m, 6H, $H^{C5+D3/D3'}$), 7.22 – 7.15 (m, 8H, $H^{D2/D2'+D3/D3'}$), 7.08 – 7.04 (m, 4H, $H^{D2/D2'}$), 6.78 – 6.74 (m, 2H, H^{C3}), 1.84 (s, 3H, $H^{xantphos\text{-}Me}$), 1.70 (s, 3H, $H^{xantphos\text{-}Me}$). ^{13}C NMR (126 MHz, $(CD_3)_2CO$, 298 K) δ /ppm 155.9 (C^{C1}), 153.9 (C^{B2}), 152.0 (C^{A2}), 149.8 (C^{A6}), 143.1 (C^{B6}), 142.2 (C^{B4}), 140.1 (C^{A4}), 134.6 (C^{C6}), 133.8 (t, J = 8.1 Hz, $C^{D2/D2'}$), 133.7 (t, J = 8.1 Hz, $C^{D2/D2'}$), 132.6 ($C^{D1/D1'}$), 132.3 ($C^{D1/D1'}$), 131.7 (C^{C3}), 131.5 (C^{B5}), 131.1 ($C^{D4/D4'}$), 130.9 ($C^{D4/D4'}$), 129.9 (t, J = 4.9 Hz, $C^{D3/D3'}$), 129.7 (t, J = 4.9 Hz, $C^{D3/D3'}$), 128.6 (C^{C4}), 127.6 (C^{A5}), 126.1 (t, J = 2.7 Hz, C^{C5}), 124.3 (C^{A3}), 122.6 (C^{B3}), 121.4 (t, J = 14.4 Hz, C^{C2}), 36.8 ($C^{xantphos\text{-}bridge}$), 30.1 ($C^{xantphos\text{-}Me}$), 27.3 ($C^{xantphos\text{-}Me}$). ^{31}P{^{1}H} NMR (202 MHz, $(CD_3)_2CO$, 298 K) δ/ppm −12.4 (broad, FWHM = 350 Hz, xantphos), −144.2 (septet, J_{PF} = 709 Hz, $[PF_6]^-$). ESI MS: *m/z* 877.3 $[M–PF_6]^+$ (base peak, calc. 877.1). Found C 57.50, H 4.03, N 3.05; $C_{49}H_{39}BrCuF_6N_2OP_3$ requires C 57.57, H 3.85, N 2.74.

[Cu(POP)(6,6'-Br$_2$bpy)][PF$_6$]. A colourless solution of $[Cu(MeCN)_4][PF_6]$ (56 mg, 0.15 mmol) and POP (81 mg, 0.15 mmol) in CH_2Cl_2 (40 mL) was stirred for 2 h. Then 6,6'-Br_2bpy (47 mg, 0.15 mmol) was added and the yellow solution was stirred for another 2 h. The solution was filtered and the solvent from the filtrate was removed in vacuo. [Cu(POP)(6,6'-Br_2bpy)][PF_6] was isolated as orange-yellow powder in good yield (93 mg, 0.09 mmol, 60 %). ^{1}H NMR (500 MHz, $(CD_3)_2CO$, 298 K) δ /ppm 8.44 (dd, J = 8.0, 0.8 Hz, 2H, H^{B3}), 8.08 (t, J = 7.9 Hz, 2H, H^{B4}), 7.83 (dd, J = 7.9, 0.6 Hz, 2H, H^{B5}), 7.44 (ddd, J = 8.2, 7.1, 2.0 Hz, 2H, H^{C5}), 7.37 – 7.33 (m, 4H, H^{D4}), 7.30 – 7.20 (m, 20H, $H^{D2+D3+C3+C4}$), 7.05 – 7.02 (m, 2H, HC^{C6}). ^{13}C NMR (126 MHz, $(CD_3)_2CO$, 298 K) δ /ppm 159.0 (t, J = 5.7 Hz, C^{C1}), 153.9 (C^{B2}), 143.2 (C^{B6}), 142.1 (C^{B4}), 134.6 (C^{C3}), 134.2 (t, J = 7.7 Hz, C^{D2}), 133.1 (C^{C5}), 132.6 (t, J = 17.2 Hz, C^{D1}), 132.2 (C^{B5}), 130.8 (C^{D4}), 129.5 (t, J = 4.6 Hz, C^{D3}), 126.3 (C^{C2}), 125.9 (t, J = 2.3 Hz, C^{C4}), 123.0 (C^{B3}), 120.7 (t, J = 1.8 Hz, C^{C6}). ^{31}P NMR (162 MHz, $(CD_3)_2CO$, 300 K) δ/ppm −13.6 (broad, FWHM = 155 Hz, POP), −144.2 (septet, J_{PF} = 707 Hz, $[PF_6]^-$). ESI MS: *m/z* 915.1 $[M–PF_6]^+$ (base peak, calc. 915.0). Found C 51.78, H 3.43, N 3.13; $C_{46}H_{34}Br_2CuF_6N_2OP_3$ requires C 52.07, H 3.23, N 2.64.

[Cu(xantphos)(6,6'-Br$_2$bpy)][PF$_6$]. A colourless solution of xantphos (145 mg, 0.25 mmol, 1.0 eq) and 6,6-Br_2bpy (78 mg, 0.25 mmol, 1.0 eq) in CH_2Cl_2 (20 mL) was added to a colourless solution of $[Cu(MeCN)_4][PF_6]$ (93 mg, 0.25 mmol, 1.0 eq) in CH_2Cl_2 (20 mL) and the resulting yellow solution was stirred for 2 h. The solvent was removed in vacuo and the yellow powder was redissolved in CH_2Cl_2 and layered with Et_2O. $[Cu(xantphos)(6,6'\text{-}Br_2bpy)][PF_6]$ was isolated as canary-yellow powder in excellent yield (260 mg, 0.24 mmol, 96 %). ^{1}H NMR (500 MHz, $(CD_3)_2CO$, 298 K) δ /ppm 8.31 (dd, J = 8.0, 0.8 Hz, 2H, H^{B3}), 8.03 (t, J = 7.9 Hz, 2H, H^{B4}), 7.80 (dd, J = 7.9, 0.8 Hz, 2H, H^{B5}), 7.79 (dd, J = 7.8, 1.4 Hz, 2H, H^{C5}), 7.43 (t, J = 7.3 Hz, 4H, H^{D4}), 7.33 – 7.29 (m, 8H, H^{D2}), 7.29 (d, J = 5.1 Hz, 2H, H^{C4}), 7.25 (t, J = 7.6 Hz, 8H, H^{D3}), 7.10 – 7.06 (m, 2H, H^{C3}), 1.71 (s, 6H, $H^{xantphos\text{-}Me}$). ^{13}C NMR (126 MHz, $(CD_3)_2CO$, 298 K) δ /ppm 155.9 (t, J = 6.4 Hz, C^{C1}), 153.4 (C^{B2}), 142.5 (C^{B6}), 142.1 (C^{B4}), 134.3 (t, J = 7.6 Hz, C^{D2}), 134.2 (t, J = 1.9 Hz, C^{C6}), 132.1 (t, J = 16.9 Hz, C^{D1}), 131.9 (C^{B5}), 131.2 (C^{C3}), 131.0 (C^{D4}), 129.6 (t, J = 4.6 Hz, C^{D3}), 128.6 (C^{C5}), 126.0 (t, J = 2.4 Hz, C^{C4}), 123.0 (C^{B3}), 36.7 ($C^{xantphos\text{-}bridge}$), 29.0 ($C^{xantphos\text{-}Me}$). ^{31}P NMR (162 MHz, $(CD_3)_2CO$, 300 K) δ/ppm −13.0 (broad, FWHM = 140 Hz, xantphos), −144.2 (septet, J_{PF} = 708 Hz, $[PF_6]^-$). ESI MS: *m/z* 955.2 $[M–PF_6]^+$ (base peak, calc. 955.0). Found C 53.38, H 3.92, N 2.63; $C_{49}H_{38}Br_2CuF_6N_2OP_3$ requires C 53.45, H 3.48, N 2.54.

Crystallography. Ambient pressure data were collected on a Bruker Kappa Apex2 diffractometer with data reduction, solution and refinement using the programs APEX[32] and CRYSTALS.[33] For $[Cu(xantphos)(6,6'\text{-}Cl_2bpy)][PF_6]\cdot CH_2Cl_2$, SQUEEZE[34] was used to treat the solvent region. 92 e^-/unit cell were found: that corresponds to 46 e^-/formula. This can be rationalised as one molecule of CH_2Cl_2 per formula unit. All the formulae have been modified to keep account for this result. Structural analysis was carried out using Mercury v. 3.7.[35,36] High-pressure single crystal experiments were carried out using a Merrill-Bassett diamond anvil cell[37] (half-opening angle 40°), equipped with Boehler-Almax diamonds with 600 µm culets

and a tungsten gasket.[38] Hexane was used as hydrostatic medium and a small ruby chip was loaded into the cell as the pressure calibrant with the ruby fluorescence used to measure the pressure.[39] Diffraction data were collected using synchrotron radiation of wavelength λ = 0.4859 Å at room temperature on a Newport IS4CCD (4 circle) diffractometer with a Pilatus 300K detector at Station I19 at the Diamond Light Source, Harwell Science and Innovation Campus. Integrations were carried out using the program CrysAlisPro[40] and absorption corrections with the program ABSPACK.[29] Refinements were carried out with CRYSTALS[23] using the ambient pressure structure as starting models.

[Cu(POP)(6,6'-Cl_2bpy)][PF_6].

$C_{46}H_{34}Cl_2CuF_6N_2OP_3$, M = 972.15, light orange block, monoclinic, space group $P2_1/c$, a = 10.4351(6), b = 18.8158(10), c = 22.3310(12) Å, β = 99.434(4)°, U = 4325.3(4) Å^3, Z = 4, D_c = 1.493 Mg m^{-3}, μ(Cu-Kα) = 3.457 mm^{-1}, T = 123 K. Total 48007 reflections, 7953 unique, R_{int} = 0.067. Refinement of 4914 reflections (673 parameters) with $I > 2\sigma(I)$ converged at final R_1 = 0.0642 (R_1 all data = 0.0990), wR_2 = 0.1610 (wR_2 all data = 0.1949), gof = 0.9366. CCDC 1535144.

[Cu(xantphos)(6,6'-Cl_2bpy)][PF_6]·CH_2Cl_2.

$C_{50}H_{40}Cl_4CuF_6N_2OP_3$, M = 1012.21, yellow block, triclinic, space group $P\bar{1}$, a = 11.2546(11), b = 14.3360(13), c = 18.0998(16) Å, α = 113.273(4), β = 100.571(4), γ = 90.543(4) °, U = 2626.3(4) Å^3, Z = 2, D_c = 1.39 Mg m^{-3}, μ(Cu-Kα) = 3.825mm^{-1}, T = 123 K. Total 32725 reflections, 9421 unique, R_{int} = 0.038. Refinement of 9049 reflections (883 parameters) with $I > 2\sigma(I)$ converged at final R_1 = 0.1077 (R_1 all data = 0.1098), wR_2 = 0.2742 (wR_2 all data = 0.2745), gof = 0.9428. CCDC 1535142.

[Cu(POP)(6-Brbpy)][PF_6].

$C_{46}H_{35}BrCuF_6N_2OP_3$, M = 982.16, yellow block, monoclinic, space group $P2_1/c$, a = 15.3402(6), b = 14.2344(5), c = 19.2659(7) Å, β = 90.9159(12)°, U = 4206.34(15) Å^3, Z = 4, D_c = 1.551 Mg m^{-3}, μ(Cu-Kα) = 3.491 mm^{-1}, T = 123 K. Total 35307 reflections, 7329 unique, R_{int} = 0.022. Refinement of 7293 reflections (541 parameters) with $I > 2\sigma(I)$ converged at final R_1 = 0.0281 (R_1 all data = 0.0282), wR_2 = 0.0673 (wR_2 all data = 0.0673), gof = 0.8936. CCDC 1535141.

For high pressure data and respective CCDC codes of this structure see Table S1†.

[Cu(xantphos)(6-Brbpy)][PF_6]·0.7Et_2O.

$C_{49}H_{39}BrCuF_6N_2OP_3$·0.7$C_4H_{10}O$ or $C_{51.80}H_{46}BrCuF_6N_2O_{1.70}P_3$, M = 1074.11, yellow block, triclinic, space group $P\bar{1}$, a = 11.0101(5), b = 15.0994(7), c = 18.1016(9) Å, α = 108.840(3), β = 98.138(3), γ = 109.910(3)°, U = 2568.6(2) Å^3, Z = 2, D_c = 1.389 Mg m^{-3}, μ(Cu-Kα) = 2.916 mm^{-1}, T = 123 K. Total 32455 reflections, 9339 unique, R_{int} = 0.035. Refinement of 8428 reflections (596 parameters) with $I > 2\sigma(I)$ converged at final R_1 = 0.1060 (R_1 all data = 0.1121), wR_2 = 0.2611 (wR_2 all data = 0.2626), gof = 1.0223. CCDC 1583875.

LEC fabrication. LECs were prepared on top of a patterned indium tin oxide (ITO, 15 Ω □$^{-1}$) coated glass substrates previously cleaned as follows: (a) 5 minutes sonication with soap, (b) 5 minutes sonication in deionized water, (c) 5 minutes sonication in isopropanol and (d) UV-O_3 lamp for 20 min. Prior to the deposition of the emitting layer, a layer of poly(3,4-ethylenedioxythiophene): poly(styrenesulfonate) (PEDOT:PSS) (CLEVIOS™ P VP AI 4083, aqueous dispersion, 1.3–1.7% solid content, Heraeus) was spin-coated on the glass substrate at 1000rpm, and following annealed at 150 ºC for 15 minutes. The so prepared PEDOT:PSS presented a thickness of 60nm, determined with an Ambios XP-1 profilometer. The active layer solution was prepared by dissolution in butan-2-one of the copper complex and the ionic liquid 1-ethyl-3-methylimidazolium hexafluoridophosphate [Emim][PF_6] (>98.5%, Sigma-Aldrich) in a molar ratio of 4:1. The solutions were filtered with 0.25 μm pore filter and immediately spin-coated on the substrate at 1500rpm for 60 seconds, creating an emitting layer of 110 nm. The devices were then transferred to an inert atmosphere glovebox (<0.1 ppm O_2 and H_2O, MBraun), where a layer (70 nm) of aluminium (the top electrode) was thermally evaporated onto the devices using an Edwards Auto500 evaporator integrated in the glovebox. The area of the device was 6.5 mm^2. The devices were not encapsulated and were characterized inside the glovebox at room temperature. The same emitting solution employed in the preparation of the devices was also deposited on a quartz substrate, subsequentially used for the evaluation of the photoluminescence quantum yield with a Hamamatsu absolute quantum yield C9920. The device lifetime was measured by applying a pulsed current (with 50% duty cycle) and monitoring the voltage and luminance versus time by a True Colour Sensor MAZeT (MTCSiCT Sensor) with a Botest OLT OLED Lifetime-Test System. The average current density is determined by multiplying the peak current density by the time-on time and dividing by the total cycle time. The average luminance is directly obtained by taking the average of the obtained photodiode results and correlating it to the value of a luminance meter. The current efficiency is obtained by dividing the average luminance by the average current density. The electroluminescent (EL) spectra were measured using an Avantes AvaSpec-2048 Fiber Optic Spectrometer during device lifetime measurement.

Results and discussion

Synthesis and characterization of [Cu(P^P)(N^N][PF_6] complexes

The [Cu(P^P)(N^N][PF_6] complexes were synthesized by addition of the ligands to a solution of [Cu(MeCN)$_4$][PF_6] in CH_2Cl_2. The reaction of POP with [Cu(MeCN)$_4$][PF_6] leads to 3-coordinate [Cu(POP)(MeCN)]$^+$ or [Cu(POP-*P,P′*)(POP-*P*)]$^+$, whereas xantphos reacts with [Cu(NCMe)$_4$]$^+$ to give [Cu(POP-*P,P′*)$_2$]$^+$.[41] For the complexes with POP, the synthetic procedure used the established sequential addition of the two ligands; the bpy ligand was added after a two hour stirring period of POP and [Cu(MeCN)$_4$][PF_6].[42] For the [Cu(xantphos)(N^N)][PF_6] complexes, a concerted addition of the two ligands was chosen. The compounds [Cu(POP/xantphos)(N^N)][PF_6] with N^N =

6,6'-Cl_2bpy, 6-Brbpy or 6,6'-Br_2bpy were isolated as yellow to orange solids in yields of 60 to 96%.

Structural characterization

X-ray quality crystals of [Cu(POP)(6,6'-Cl_2bpy)][PF_6], [Cu(xantphos)(6,6'-Cl_2bpy)][PF_6]·CH_2Cl_2, [Cu(POP)(6-Brbpy)][PF_6] and [Cu(xantphos)(6-Brbpy)][PF_6]·0.7Et_2O were obtained by diffusion of Et_2O into the solutions of the respective complex in CH_2Cl_2. ORTEP-style diagrams of the cations in the complexes are illustrated in Fig. 1–2 and Fig. S1†–S2† and important angles and bond distances are summarized in Table 1. The compounds [Cu(xantphos)(6,6'-Cl_2bpy)][PF_6]·CH_2Cl_2 and [Cu(xantphos)(6-Brbpy)][PF_6] crystallize in the triclinic space group *P*−1, whereas [Cu(POP)(6,6'-Cl_2bpy)][PF_6] and [Cu(POP)(6-Brbpy)][PF_6] both crsytallize in the monoclinic space group $P2_1/c$ Each copper(I) cation exhibits a distorted tetrahedral geometry, with the angles between the N^N and the P^P chelating ligands lying between ~80 and ~90°. For the cations with xantphos, the angles between the planes through the P–Cu–P and N–Cu–N units are close to the 90° of an ideal tetrahedral coordination geometry (89.5° for [Cu(xantphos)(6,6'-Cl_2bpy)]$^+$ and 87.0° for [Cu(xantphos)(6-Brbpy)]$^+$). These are also the cations in which the bpy ligand is twisted the least, with N–C–C–N torsions of ~1°. The Cu–P and Cu–N bond distances as well as the P–Cu–P chelating angles are unexceptional for all the complexes (Table 1).

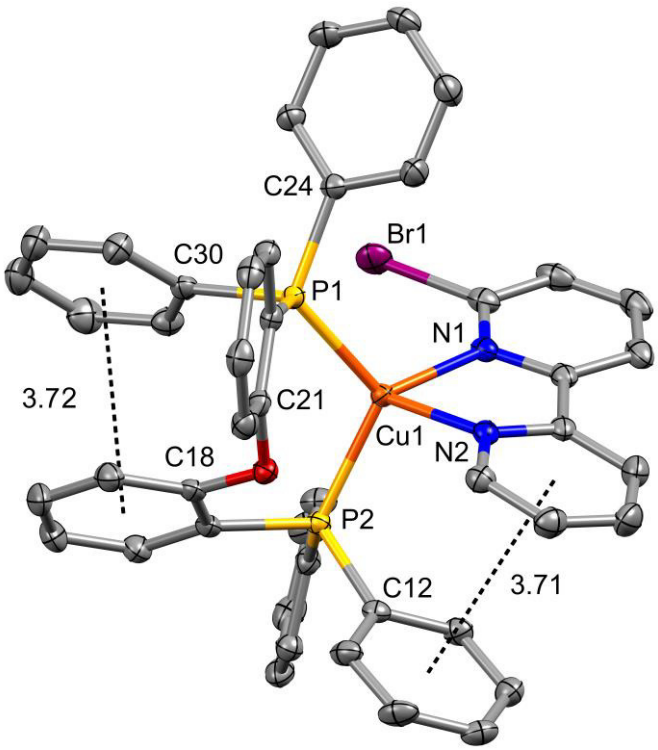

Fig. 1. Structure of the cation [Cu(POP)(6-Brbpy)]$^+$ in [Cu(POP)(6-Brbpy)][PF_6]. Ellipsoids plotted at 50% probability level, H atoms omitted, centroid···centroid distances = 3.72 Å respectively 3.71 Å.

In the structure of [Cu(POP)(6-Brbpy)][PF_6] (Fig. 1), two arene rings show π-stacking interactions within the parameters suggested by Janiak.[43] Although not perfectly aligned, the ring of the POP backbone that includes C18 and is attached to P2 and the phenyl ring at P1 that includes C30 show a centroid···centroid distance of 3.72 Å with the angle between the ring planes coming to 13.70°. A smaller angle of 9.75° was found for the phenyl ring with C12 at the phosphorus atom P2 and the pyridine ring with N2, with the centroid···centroid distance as short as 3.71 Å. The distance between the copper centre and the bromine atom comes to 3.5017(3) Å, which suggests little to no interaction between the two atoms. A relatively short distance of 2.577 Å between the oxygen of the phenyl ether and the hydrogen H531 at the carbon atom in ortho position to N2 was found. In the analogue cation with xantphos (Fig. 2) the phenyl rings with C17 at P1 and C38 at P2 exhibit π-stacking interactions with a centroid···centroid distance of 3.83 Å and the angle between the rings coming to 7.03°. The 6-Brbpy ligand is disordered over two orientations with occupancies of 0.8 and 0.2, with the bromine atom facing towards the bowl-shaped xanthene backbone in the preferred orientation.

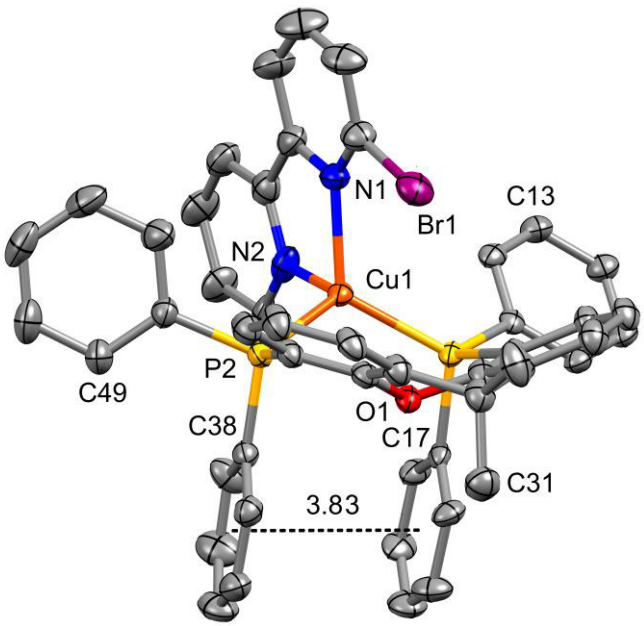

Fig. 2. Structure of the cation [Cu(xantphos)(6-Brbpy)]$^+$ in [Cu(xantphos)(6-Brbpy)][PF_6]·0.7Et_2O. Ellipsoids plotted at 50% probability level, H atoms omitted, centroid···centroid distance = 3.83 Å.

In the structures of [Cu(POP)(6,6'-Cl_2bpy)][PF_6] (Fig. S1†) and [Cu(xantphos)(6,6'-Cl_2bpy)][PF_6]·CH_2Cl_2 (Fig. S2†), the POP respectively xantphos ligand is disordered. The Cu–Cl distances are in the range 3.37 and 3.46 Å and are too far for bonding interactions, but in [Cu(xantphos)(6,6'-Cl_2bpy)][PF_6] there is a short contact of 2.444 Å between F5 of the [PF_6]$^-$ anion and H21 of the bpy ring with N1. The centroid···centroid distance of 4.0 Å between the phenyl rings at P1 with C23 and

Table 1. Comparison of structural parameters of the [Cu(P^P)(N^N)][PF_6] complexes.

Complex cation	Cu–P distance / Å	Cu–N distance / Å	P–Cu–P chelating angle / deg	N–Cu–N chelating angle / deg	Angle between P–Cu–P and N–Cu–N plane / deg	N–C–C–N torsion angle /deg
[Cu(POP)(6,6'-Cl_2bpy)]$^+$	Cu1–P1 = 2.2422(13); Cu1–P2 = 2.2751(14)	Cu1–N1 = 2.134(4); Cu1–N2 = 2.107(4)	117.19(5)	78.15(17)	85.98	15.8(7)
[Cu(xantphos)(6,6'-Cl_2bpy)]$^+$	Cu1–P1 = 2.2545(15); Cu1–P2 = 2.2875(15)	Cu1–N1 = 2.097(5); Cu1–N2 = 2.104(5)	114.74(6)	76.7(2)	89.49	1(1)
[Cu(POP)(6-Brbpy)]$^+$	Cu1–P1 = 2.2362(5); Cu1–P2 = 2.2628(5)	Cu1–N1 = 2.0858(14); Cu1–N2 = 2.0782(14)	114.280(18)	79.53(6)	81.96	9.6(2)
[Cu(xantphos)(6-Brbpy)]$^+$	Cu1–P1 = 2.2428(15); Cu1–P2 = 2.2615(17)	Cu1–N1 = 2.087(5); Cu1–N2 = 2.050(3)	113.90(6)	81.7(2)	87.01	0.8(9)

at P2 with C36 and the ring plane angle of 12.1° indicate π-stacking interaction for [Cu(xantphos)(6,6'-Cl_2bpy)]$^+$.

Structure of [Cu(POP)(6-Brbpy)][PF_6] under high pressure

The single crystal X-ray structures of [Cu(POP)(6-Brbpy)][PF_6] and [Cu(xantphos)(6-Brbpy)][PF_6] were investigated under conditions of increasing pressure in the hydrostatic environment of a diamond pressure cell. Unfortunately, data quality for [Cu(xantphos)(6-Brbpy)][PF_6] was too poor and therefore only the high pressure structure of [Cu(POP)(6-Brbpy)][PF_6] is described here. In addition to the structure under ambient conditions, data at 0.16, 1.3, 1.8, 3.5, 4.2 and 4.5 GPa were obtained and the overlaid structures of the [Cu(POP)(6-Brbpy)]$^+$ cations with increased pressure are illustrated in Fig. 3.

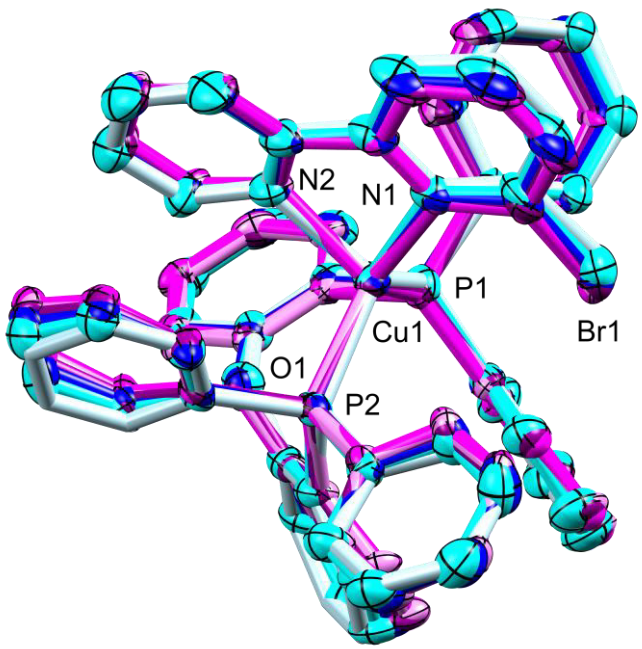

Fig. 3. Structure of [Cu(xantphos)(6-Brbpy)][PF_6] under increasing pressure (ambient to 4.5 GPa). Colour change from light blue to purple with increasing pressure. Ellipsoids plotted at 50% probability level, H atoms omitted.

On going from ambient pressure to 0.16 GPa, the cell dimensions *a, b, c* and *β* as well as the volume increase slightly. This is attributed to the lower temperature of the data collection at ambient pressure, which is 123 K, versus the measurements at increased pressure, which are performed at ambient temperature. With further increased pressure, the cell lengths *a, b* and *c* and the angle *β* decrease, the volume shrinks from 4274(3) Å^3 at 0.16 GPa to 3450.3(19) Å^3 at 4.5 GPa, which is around 81% of the original volume. A phase change was not observed; the structure remains monoclinic $P2_1/c$ with $Z = 4$. Also the bond lengths and angles of the copper(I) cation undergo only little change. The bond distances between copper and the coordinated atoms are shortened as a result of the higher pressure, but not drastically, for example Cu1–P1 changes from 2.250(6) Å at 0.16 GPa to 2.170(3) Å at 4.5 GPa and Cu1–N2 from 2.110(14) to 2.017(4) Å. The bromine atom also moves closer to the aromatic ring, with Br1–C1 decreasing from 1.881(17) to 1.824(3) Å. Interestingly, the ligands become more perpendicular with increased pressure, with the angle between the planes through P1–Cu1–P2 and N1–Cu1–N2 coming to 83.63° at 0.16 GPa and 86.09° at 4.5 GPa. This is related to slight changes in the angles between the nitrogen and the phosphorus atoms, where some angles become slightly wider or smaller, but all within a range of ±3°.

Photophysical properties

The solution absorption spectra of the complexes in CH_2Cl_2 (2.5×10^{-5} mol dm^{-3}) are illustrated in Fig. 3. In addition to high energy bands that are assigned to ligand-based transitions, the complexes show broad metal-to-ligand charge transfer (MLCT) bands in the range 350 to 470 nm; this is typical for [Cu(P^P)(bpy)][PF_6] complexes.[10,16] The maximum wavelengths λ_{max} of the MLCT bands depend on the bpy ligand for this series and are the same for POP and xantphos (see Fig. S3†). The MLCT bands for the complexes with the unsymmetrically substituted 6-Brbpy are the most blue-shifted, while the change from 6,6'-Br_2bpy to 6,6'-Cl_2bpy has little effect on λ_{max} of the MLCT bands.

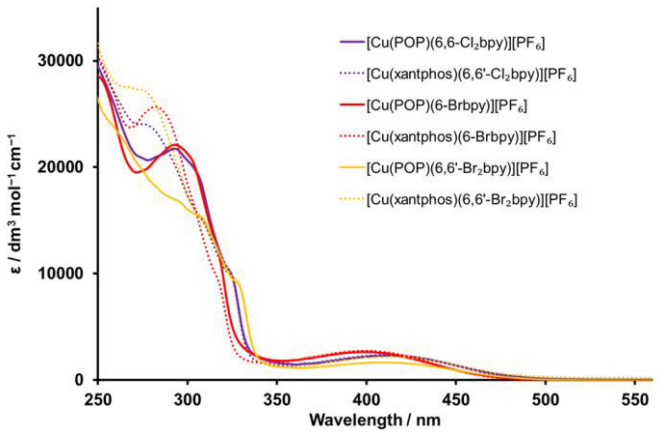

Fig. 3. Solution absorption spectra of the [Cu(P^P)(bpy)][PF_6] complexes (CH_2Cl_2, 2.5×10^{-5} mol dm^{-3}).

The emission spectra of the complexes in solution (CH_2Cl_2, 2.5×10^{-5} mol dm^{-3}) are illustrated in Fig. 4 and the photophysical properties are summarized in Table 3. The complexes are emissive in the orange to red region with λ_{em}^{max} = 600 and 650 nm and the bands are structured with two emission maxima. This has also been reported for related [Cu(P^P)(bpy)][PF_6] complexes.[9,10,16] As observed for the MLCT bands in the absorption spectra, the exchange of the P^P chelating ligand has little effect on the emission wavelength in solution. Halogen atoms extend the conjugated system to which they are attached and are known to withdraw σ electrons, but repel π electrons. In a conjugated π system, the electrons are only withdrawn from every other atom, and there is even a small increase in the electron density in the other atoms of the aromatic system. In a six electron ring systems, the atoms where the electron density is increased are therefore those in ortho and para position to the halogen-substituted carbon atom.[29] For halogens in the 6-position of pyridine or bpy, this means that the electron density at the nitrogen atom is slightly increased with respect to unsubstituted bpy, which should make them better σ donors and worse π acceptors. As a result, the LUMO should be destabilized, which increases the HOMO–LUMO gap and leads to a blueshift of the emission wavelength. Indeed, in solution a small hypsochromic shift of the emission was observed for the halogen-substituted complexes with respect to those with unsubstituted bpy (Table 3).

Within the series of complexes with halido-bpys, a bathochromic shift for the emission maxima of the complexes with 6-Brbpy with respect to the complexes with Br_2bpy and 6,6'-Cl_2bpy takes place (Fig.4). This might be due to superior stabilization of the tetrahedral complex geometry by bpy ligands that are symmetrically substituted in both 6-positions instead of only mono-substitution. However, all the complexes are weak emitters in solution, with the highest PLQY of 1.7% for a deaerated solution of [Cu(POP)(6,6'-Cl_2bpy)][PF_6] (reduction of the amount of dissolved O_2 by a 20 min gas flow of argon through the solution). Comparison with the respective PLQY of [Cu(xantphos)(6,6'-Me_2bpy)][PF_6] (10% upon deaeration) indicates that chloro (and even less bromo) substituents in the 6,6'-positions of the bpy ligand are not as efficient at enhancing the emissive properties of [Cu(P^P)(bpy)][PF_6] complexes as methyl groups. It is, however, not clear if this is due to a less effective stabilization of the tetrahedral complex geometry of the halo-bpys or because of additional or enhanced non-radiative pathways caused by the halogen substitution.

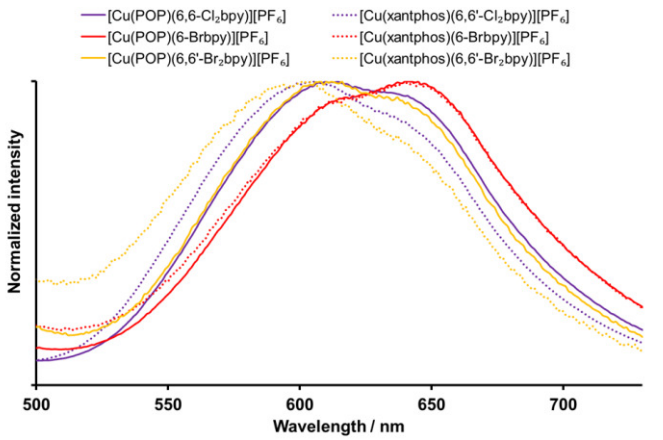

Fig. 4. Normalized solution emission spectra of [Cu(P^P)(bpy)][PF_6] complexes (CH_2Cl_2, 2.5×10^{-5} mol dm^{-3}). For λ_{exc} see Table 2.

In the solid state, the complexes [Cu(POP)(6,6'-Cl_2bpy)][PF_6], [Cu(xantphos)(6,6'-Cl_2bpy)][PF_6], [Cu(xantphos)(6-Brbpy)][PF_6] and [Cu(xantphos)(6,6'-Br_2bpy)][PF_6] show the highest PLQYs of this series. However, with 11 to 17%, the values are moderate in comparison with complexes that feature methyl groups in the 6,6'-positions at the bpy ligand (e.g. 37% for [Cu(xantphos)(6,6'-Me_2bpy)][PF_6]). The complexes are yellow to orange emitters in the solid state (Fig. 5), this blueshift on going from solution to powder is typically observed for these $[Cu(P^P)(N^N)]^+$ cations. The influence of the phosphane ligand on the photophysical properties in the solid state strongly depends on the bpy in this series. For the complexes with 6,6'-Cl_2bpy, the emission maxima are almost at the same wavelength for both the POP and xantphos complexes, and the PLQY values are the same order of magnitude. In the complexes with 6-Brbpy, the effects of the phosphane differ strongly; [Cu(xantphos)(6-Brbpy)][PF_6] emits at higher energy and also has a much higher PLQY (16.3%) than the respective complex with POP (3.9%). For the compounds with 6,6'-Br_2bpy, the emission maximum is strongly blue-shifted for the xantphos complex (544 nm vs. 596 nm for [Cu(POP)(6,6'-Br_2bpy)][PF_6]), but the PLQY values are in the same order of magnitude for both complexes.

Table 3. Emission maxima, photoluminescence quantum yields (PLQY) and lifetimes ($\tau_{1/2}$) for [Cu(P^P)(N^N)][PF_6] complexes.

Complex cation	CH_2Cl_2 solution[a]				Powder[b]		
	λ_{exc}/ nm	λ_{em}^{max} / nm	PLQY (non-deaerated / deaerated) / %	$\tau_{1/2}$ (non-(non-deaerated / deaerated) / ns	λ_{em}^{max} / nm	PLQY / %	$\tau_{1/2}$ / µs
[Cu(POP)(bpy)]$^+$	390	618, 649	0.4/0.5	43/46[b]	580	3.0	1.5
[Cu(xantphos)(bpy)]$^+$	390	620, 650	0.5/0.5[b]	75/104[b]	587	1.7	1.3
[Cu(POP)(6,6'-Cl_2bpy)]$^+$	400	611, 636	0.9/1.7[c]	218/372[c]	584	14.8	2.7
[Cu(xantphos)(6,6'-Cl_2bpy)]$^+$	400	605, 629	0.7/0.9[c]	115/138[c]	587	17.1	3.3
[Cu(POP)(6-Brbpy)]$^+$	400	618, 641	0.6/0.8[c]	159/239[c]	582	3.9	2.5
[Cu(xantphos)(6-Brbpy)]$^+$	400	617, 640	0.5/0.6[c]	155/217[c]	569	16.3	4.8
[Cu(POP)(6,6'-Br_2bpy)]$^+$	400	608, 636	0.6/0.8	90/107	596	6.3	2.6
[Cu(xantphos)(6,6'-Br_2bpy)]$^+$	400	601, 632	0.5/0.6[c]	38/38[c]	544	10.9	2.3

[a]Solution concentration = 2.5×10^{-5} mol dm^{-3}. [b]λ_{exc} = 365 nm. [c]λ_{exc} = 405 nm.

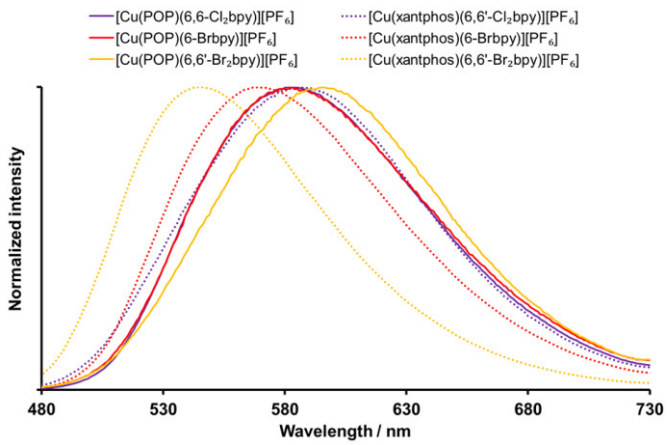

Fig. 5. Normalized emission spectra of solid [Cu(P^P)(N^N)][PF_6] complexes. For λ_{exc} see Table 2.

In the solid state emission spectra, only [Cu(xantphos)(6-Brbpy)][PF_6] and [Cu(xantphos)(6,6'-Br_2bpy)][PF_6] show a noteworthy blueshift compared to the complexes with naked bpy, as would have been expected from the halogen substitution. However, one also has to keep packing interactions in mind, which can have a considerable additional influence on solid state emission maxima that exceeds possible electronic effects of the attached halogen atoms.

Electrochemistry

The electrochemical behaviour of the heteroleptic complexes was investigated using cyclic voltammetry (CV) and the oxidation potentials $E_{1/2}^{ox}$ are summarized in Table 2. The oxidation potentials for the copper(I) complexes with halo-substituted bpy ligands are shifted to higher potential (+0.90 to +0.98 V) compared to complexes with unmodified bpy (+0.72 V for [Cu(POP)(bpy)][PF_6] and +0.76 V for [Cu(xantphos)(bpy)][PF_6]). The higher potentials required for the Cu^+/Cu^{2+} oxidation for these halo-substituted complexes are consistent with the electron withdrawing effects of the halo-groups. The oxidation processes are quasi-reversible and no reduction processes were visible for any of the complexes. In general, substituents in 6- or 6,6'-position should stabilize the tetrahedral complex geometry and hamper the Cu^+/Cu^{2+} oxidation process, thus the electrochemical oxidation potential should be at higher voltages, which is in agreement with our observation. Even higher voltages than for the alkyl substituted complexes [Cu(POP)(6-Mebpy)][PF_6][9] (+0.69 V) and [Cu(POP)(6,6'-Me_2bpy)][BF_4] (+0.82 V)[44] are required for the series with halido-bpys, which might be due to the stronger electron-donating effect of the halogens on the coordinating nitrogen. Halogen atoms next to the nitrogen at the bpy therefore have the combined effect of stabilizing the tetrahedral geometry and increasing the electron density at the nitrogen donor.

Table2. Cyclic voltammetric data for [Cu(P^P)(bpy)][PF_6] complexes referenced to internal Fc/Fc^+ = 0.V; CH_2Cl_2 (freshly distilled) solutions with [^{n}Bu_4N][PF_6] as supporting electrolyte and scan rate of 0.1 V s^{-1}. Processes are quasi-reversible.

Complex cation	$E_{1/2}^{ox}$ / V	($E_{pc} - E_{pa}$ / mV)
[Cu(POP)(bpy)]$^+$	+0.72	110
[Cu(xantphos)(bpy)]$^+$	+0.76	110
[Cu(POP)(6,6'-Cl_2bpy)]$^+$	+0.98	170
[Cu(xantphos)(6,6'-Cl_2bpy)]$^+$	+0.93	90
[Cu(POP)(6-Brbpy)]$^+$	+0.93	90
[Cu(xantphos)(6-Brbpy)]$^+$	+0.90	90
[Cu(POP)(6,6'-Br_2bpy)]$^+$	+0.97	120
[Cu(xantphos)(6,6'-Br_2bpy)]$^+$	+0.98	140

Device properties

The complexes [Cu(POP)(6,6'-Cl_2bpy)][PF_6] and [Cu(xantphos)(6,6'-Cl_2bpy)][PF_6] were tested in LEC devices, fabricated in a double layer architecture, by depositing a poly(3,4-ethylenedioxythiophene):poly(styrenesulfonate) (PEDOT:PSS) layer and the emissive layer sandwiched between indium tin oxide (ITO) and aluminium electrodes. The active layer contained the respective copper(I) complex mixed with the ionic liquid (IL) 1-ethyl-3-methylimidazolium hexafluoridophosphate [Emim][PF_6] with a molar ratio of 4:1 (Cu complex:IL). LECs were operated using a block-wave pulsed current of either 50 or 100 A m^{-2} (1 kHz and 50% duty cycle). Both [Cu(POP)(6,6'-Cl_2bpy)][PF_6] and

[Cu(xantphos)(6,6'-Cl_2bpy)][PF_6] show very similar yellow electroluminescence with maxima at 586 and 587 nm, respectively (Fig. 6). The electroluminescence is similar to the photoluminescence of thin films of the same composition as the active layer of the LEC (Fig. S4†), with λ_{em}^{max}= 581 nm for [Cu(POP)(6,6'-Cl_2bpy)][PF_6] and 589 nm for [Cu(xantphos)(6,6'-Cl_2bpy)][PF_6]. With 7.5% for the POP and 10.5% for the xantphos containing complex, the PLQYs of the complexes in the films are lower than in the powders, which can be attributed to the higher flexibility of complexes in the environment of the ionic liquid as opposed to the rigidity in powder.

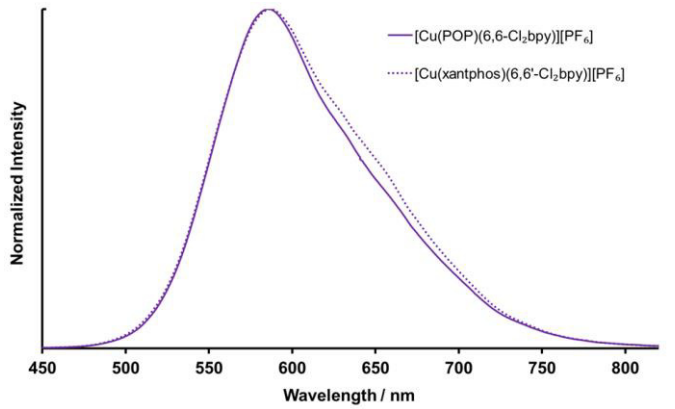

Fig. 6. Electroluminescence (EL) spectra for ITO/PEDOT:PSS/[Cu(P^P)(6,6'-Cl_2bpy)][PF_6]:[Emim][PF_6] 4:1/Al LECs operated at pulsed current (average density current 100 A m^{-2}, 1 kHz, 50% duty cycle, block wave).

The devices show very fast turn on times, acceptable luminance but relatively poor stability (Fig. 7, 8, S5†, S6† and Table 4). Especially the extremely short turn on times t_{on} are noteworthy, with only 12 seconds or less needed to reach the maximum luminance. For the [Cu(xantphos)(6,6'-Cl_2bpy)][PF_6] the maximum luminance values Lum_{max} are higher (140 and 259 cd m^{-2}) than for the respective complex with POP (64 and 121 cd m^{-2}), which is consistent with the higher PLQY values of the former. In comparison, the device with [Cu(xantphos)(6,6'-Me_2bpy)][PF_6] has a slightly higher Lum_{max} value and better efficiency (145 cd m^{-2} and 3.0 cd A^{-1}). However, this complex has a significantly higher PLQY in a thin film (21.8%) of the same setup as the active layer than the chloro-complexes (7.5 and 10.5%). Considering these thin film PLQY values together with an outcoupling factor of 20%, [Cu(POP)(6,6'-Cl_2bpy)][PF_6] and [Cu(xantphos)(6,6'-Cl_2bpy)][PF_6] have a theoretical maximum EQE of 1.5% and 2.0 %. The observed EQE values for the devices operated at 100 A m^{-2} are 1.2% for both complexes, which is equivalent to 80 respectively 60% of the respective theoretical maximum. With the thin film PLQYs in mind, the devices with the complexes with 6,6'-Cl_2bpy perform significantly better than with [Cu(xantphos)(6,6'-Me_2bpy)][PF_6]. In the complexes with 6,6'-Cl_2bpy, the lifetimes $t_{1/2}$ are longer for the POP analogue (35 and 17 vs. 11 and 5 hours). A similar trend, but with much better overall values, has been observed for complexes with 6-Etbpy, where the device with [Cu(xantphos)(6-Etbpy)][PF_6] gave the higher luminance, but shorter lifetime (77 cd m^{-2} and 51 hours) in comparison to [Cu(POP)(6-Etbpy)][PF_6] (53 cd m^{-2} and 82 hours).[10] For the device with [Cu(xantphos)(6,6'-Cl_2bpy)][PF_6], although the maximum luminance is comparable to that of [Cu(xantphos)(6,6'-Me_2bpy)][PF_6], the device lifetime is even shorter (11 min vs. 48 min, both at 50 A m^{-2}). These results illustrate again the previously observed trade-off between either a brightly shining or long-living device.[10]

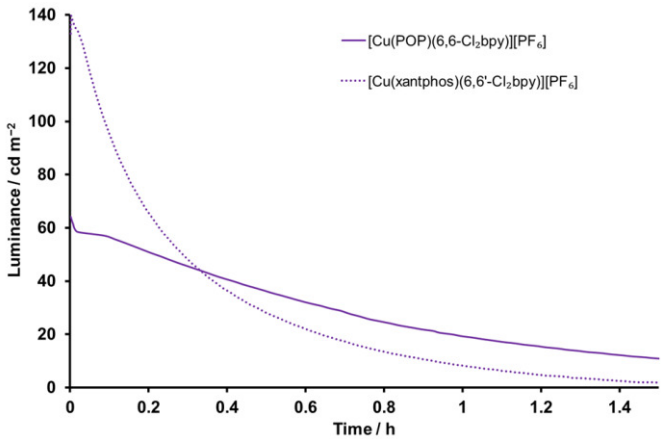

Fig. 7. Luminance versus time characteristics for ITO/PEDOT:PSS/[Cu(P^P)(6,6'-Cl_2bpy)][PF_6]:[Emim][PF_6] 4:1/Al LECs operated at pulsed current (average current density 50 A m^{-2}, 1 kHz, 50% duty cycle, block wave).

Although substitution of the bpy ligand with chloro-substituents in the 6,6'-positions is detrimental for the device lifetime, we have shown the positive effects on the turn-on time and efficiency of the devices.

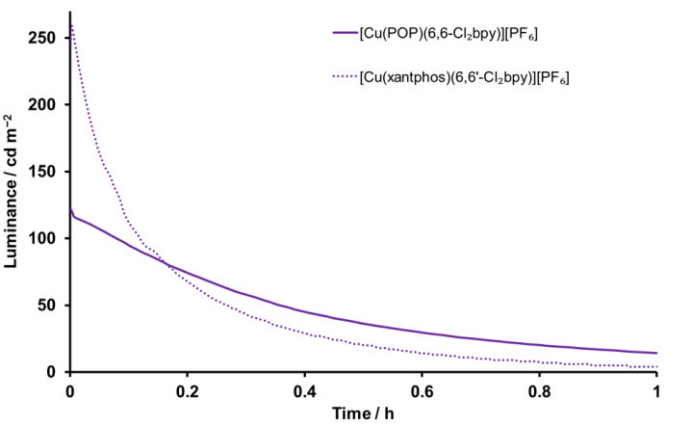

Fig. 8. Luminance versus time characteristics for ITO/PEDOT:PSS/[Cu(P^P)(6,6'-Cl_2bpy)][PF_6]:[Emim][PF_6] 4:1/Al LECs operated at pulsed current (average current density 100 A m^{-2}, 1 kHz, 50% duty cycle, block wave).

Table 4. Performance of ITO/PEDOT:PSS/[Cu(P^P)^N^N)][PF_6]:[Emim][PF_6] 4:1 molar ratio/Al LECs measured using a pulsed current driving (average current density 50 respectively 100 A m^{-2}, 1 kHz, 50% duty cycle, block wave).

Complex	Avg. current density / A m^{-2}	t_{on} [a] / s	Lum_0 [b] / cd m^{-2}	Lum_{max} [c] / cd m^{-2}	$t_{1/2}$ [d] / min	EQE_{max} [e] / %	PCE_{max} [f] / lm W^{-1}	$Efficacy_{max}$ / cd A^{-1}	λ_{EL}^{max} / nm
[Cu(POP)(6,6-Cl_2bpy)][PF_6]	50	<5	64	64	35	0.6	0.3	1.3	586
[Cu(POP)(6,6-Cl_2bpy)][PF_6]	100	<5	121	121	17	0.5	0.3	1.2	586
[Cu(xantphos)(6,6-Cl_2bpy)][PF_6]	50	12	133	140	11	1.2	0.7	2.8	587
[Cu(xantphos)(6,6-Cl_2bpy)][PF_6]	100	12	246	259	5	1.2	0.6	2.7	587

[a] Time to reach the maximum luminance. [b] Initial luminance. [c] Maximum luminance reached. [d] Time to reach one-half of the maximum luminance. [e] Maximum external quantum efficiency reached. [f] Maximum power conversion efficiency reached.

Conclusions

Six copper(I) complexes of the motif [Cu(P^P)(bpy)][PF_6] with chloro- and bromo-substituted bpy ligands were isolated.

Single crystal X-ray diffraction of solid state structures for [Cu(POP)(6,6'-Cl_2bpy)][PF_6], [Cu(xantphos)(6,6'-Cl_2bpy)][PF_6]·CH_2Cl_2, [Cu(POP)(6-Brbpy)][PF_6] and [Cu(xantphos)(6-Brbpy)][PF_6]·0.7Et_2O show that all the complexes are coordinated in a distorted tetrahedral geometry. High-pressure single crystal X-ray experiments for [Cu(POP)(6-Brbpy)][PF_6] reveal the high stability of the complex geometry under pressures up to 4.5 GPa.

Halogens substitution at a conjugated π system withdraw σ electrons from the atom they are attached to, however due to their repulsive effect on π electrons, the neighbouring and also every other atom in the system is subject to a small increase in the electron density.[29] As a result, the electron density at the nitrogen atom in 6-halo-substituted bpy is increased, which should make it a better σ donor and worse π acceptor. As a result the LUMO is destabilized and the complex emission blueshifted, which was observed in solution. Comparison of the solution PLQYs (1.7% and lower) with that of [Cu(xantphos)(6,6'-Me_2bpy)][PF_6] (10%)[10] shows that halogen atoms in the 6,6'-positions at the bpy ligand are not as efficient at enhancing the emissive properties of [Cu(P^P)(bpy)][PF_6] complexes as methyl groups, which might be due to additional radiative pathways offered by the halogens or a worse stabilization of the complex geometry. However, electrochemical measurements show that the oxidation process Cu^+/Cu^{2+} for the complexes with halo-substituents requires even higher voltages than for the alkyl substituted complexes [Cu(POP)(6-Mebpy)][PF_6][9] (+0.69 V) and [Cu(POP)(6,6'-Me_2bpy)][BF_4] (+0.82 V)[45]. Therefore the impairment of the emissive properties must be related to processes happening in the excited state rather than the ground state and the quenching is more likely due to the electronic nature of the halogens, and a less effective stabilization of the tetrahedral complex geometry does not seem to be the cause.

The LEC devices (50 A m^{-2} operation) of the complexes with 6,6'-Cl_2bpy have extraordinarily fast turn on times (<12 seconds), also compared to those of [Cu(POP)(6,6'-Me_2bpy)][PF_6] (23 min)[9] and [Cu(xantphos)(6,6'-Me_2bpy)][PF_6] (10 min).[10] Luminance values Lum_{max} are similar, with 140 cd m^{-2} for [Cu(xantphos)(6,6'-Cl_2bpy)][PF_6] vs. 145 cd m^{-2} for [Cu(xantphos)(6,6'-Me_2bpy)][PF_6]. This is especially noteworthy when the PLQY values of thin films (device style) are taken into account, which are significantly higher for [Cu(xantphos)(6,6'-Me_2bpy)][PF_6] (21.8%) than for the complexes with 6,6'-Cl_2bpy (7.5 and 10.5%, respectively). As a result, the devices perform at up to 60 respectively 80% of the theoretical EQE, which is very efficient. The only detrimental effect of the chlorine atoms lies in the device stability, but it is not clear how and why exactly the devices degrade, if this is due to complex oxidation, ligand dissociation or other processes in the cell.

For future studies, a combination of an unsymmetrically substituted bpy with a methyl or ethyl group on one side in 6-position and a chlorine atom next the nitrogen atom at the other ring might be interesting. Also the effect of chlorine atoms in the 4-positions at the bpy in combination with alkyl groups in 6-position might be worth investigating, to see if a combination of high luminance and short turn-on time with long device lifetime can be achieved.

Acknowledgements

We acknowledge the Swiss National Science Foundation (Grant number 162631) and the University of Basel for financial support. Furthermore we would like to thank Diamond Light Source for access to beamline I19 (MT12801) and especially Dr. Dave R. Allan. Y. Maximilian Klein is thanked for the effort to share the shift work at the Diamond Light Source.

Notes and references

[a]Department of Chemistry, University of Basel, BPR 1096, Mattenstrasse 24a, CH-4058 Basel, Switzerland; email: catherine.housecroft@unibas.ch
[b]Instituto de Ciencia Molecula, Universidad de Valencia, 46980 Paterna (Valencia), Spain

†Electronic Supplementary Information (ESI) available: CCDC 1535141–1535144, 1583875, 1584752–1584757. See DOI: 10.1039/b000000x/

1 H. Rudmann, S. Shimada and M. F. Rubner, *J. Am. Chem. Soc*., 2002, **124**, 4918.
2 C. M. Elliott, F. Pichot, C. J. Bloom and L. S. Rider, *J. Am. Chem. Soc*., 1998, **120**, 6781.
3 R. D. Costa, E. Ortí, H. J. Bolink, F. Monti, G. Accorsi and N. Armaroli, *Angew. Chem. Int. Ed.*, 2012, **51**, 8178.
4 F. Dumur, *Org. Electronics*, 2015, **21**, 27
5 M. Magni, P. Biagini, A. Colombo, C. Dragonetti, D. Roberto and A. Valore, *Coord. Chem. Rev.*, 2016, **322**, 69.
6 D. G. Cuttell, S.-M. Kuang, P. E. Fanwick, D. R. McMillin and R. A. Walton, *J. Am. Chem. Soc.*, 2002, **124**, 6.
7 S.-M. Kuang, D. G. Cuttell, D. R. McMillin, P. E. Fanwick and R. A. Walton, *Inorg. Chem.*, 2002, **41**, 3313.
8 R.D. Costa, D. Tordera, E. Ortí, H.J. Bolink, J. Schönle, S. Graber, C.E. Housecroft, E.C. Constable and J.A. Zampese, *J. Mater. Chem.* 2011, **21**, 16108.
9 S. Keller, E. C. Constable, C. E. Housecroft, M. Neuburger, A. Prescimone, G. Longo, A. Pertegás, M. Sessolo and H. J. Bolink, *Dalton Trans.*, 2014, **43**, 16593.
10 S. Keller, A. Pertegás, G. Longo, L. Martinez, J. Cerdá, J.M. Junquera-Hernández, A. Prescimone, E. C. Constable, C. E. Housecroft, E. Ortí and H. J. Bolink, *J. Mater. Chem. C*, 2016, **4**, 3857.
11 R. Czerwieniec and H. Yersin, *Inorg. Chem.*, 2015, **54**, 4322.
12 D. Asil, J. A. Foster, A. Patra, X. de Hatten, J. del Barrio, O. A. Scherman, J.R. Nitschke and R. H. Friend, *Angew. Chem. Int. Ed.*, 2014, **53**, 8388.
13 N. Armaroli, G. Accorsi, M. Holler, O. Moudam, J.-F. Nierengarten, Z. Zhou, R.T. Wegh and R. Welter, *Adv. Mater.*, 2006, **18**, 1313.
14 C. Bizzarri, C. Strabler, J. Prock, B. Trettenbrein, M. Ruggenthaler, C.-H. Yang, F. Polo, A. Iordache, P. Brüggeller and L. De Cola, *Inorg. Chem*., 2014, **53**, 10944.
15 M.D. Weber, C. Garino, G. Volpi, E. Casamassa, M. Milanesio, C. Barolo and R. D. Costa, *Dalton Trans.*, 2016, **45**, 8984.
16 F. Brunner, L. Martínez-Sarti, S. Keller, A. Pertegás, A. Prescimone, E.C. Constable, H.J. Bolink and C.E. Housecroft, *Dalton Trans.*, 2016, **45**, 15180.
17 R. Czerwieniec, M. J. Leitl, H. H.H. Homeier and H. Yersin, *Coord. Chem. Rev.*, 2016, **325**, 2.
18 D. Volz, D. M. Zink, T. Bocksrocker, J. Friedrichs, M. Nieger, T. Baumann, U. Lemmer and S. Bräse, *Chem. Mater.*, 2013, **25**, 3414.
19 D. Volz, Y. Chen, M. Wallesch, R. Liu, C. Fléchon, D. M. Zink, J. Friedrichs, H. Flügge, R. Steininger, J. Göttlicher, C. Heske, L. Weinhardt, S. Bräse, F. So and T. Baumann, *Adv. Mater.*, 2015, **27**, 2538.
20 M. J. Leitl, F.-R. Küchle, H. A. Mayer, L. Wesemann and H. Yersin, *J. Phys. Chem. A*, 2013, **117**, 11823.
21 H. Ohara, A. Kobayashia and M. Kato, *Dalton Trans.*, 2014, **43**, 17317.
22 A. Tsuboyama, K. Kuge, M. Furugori, S. Okada, M. Hoshino and K. Ueno, *Inorg. Chem.*, 2007, **46**, 1992.
23 M. D. Ward, S. M. Couchman and J. C. Jeffery, *Acta Cryst.*, 1998, **54**, 1820.
24 M. G. Fraser, H. van der Salm, S. A. Cameron, A. G. Blackman and K. C. Gordon, *Inorg. Chem.*, 2013, **52**, 2980.
25 M. Schmittel, C. Michel, S.-X. Liu, D. Schildbach and D. Fenske, *Eur. J. Inorg. Chem.*, 2001, 1155.
26 C. C. L. McCrory, X. Ottenwaelder, T. D. P. Stack and C. E. D. Chidsey, *J. Phys. Chem. A*, 2007, **111**, 12641.
27 C. J. Hawkins and D. D. Perrin, *J. Chem Soc.*, 1963, 2996.
28 D. J. Casadonte and D. R. McMillin, *J. Am. Chem. Soc.*, 1987, **109**, 331.
29 D. T. Clark, J. N. Murrell and J. M. Tedder, *J. Chem. Soc.*, 1963, 1250.
30 E. C. Constable and K. R. Seddon, *Tetrahedron*, 1983, **39**, 291.
31 G. J. Kubas, *Inorg. Synth*., 1979, **19**, 90.
32 Bruker Analytical X-ray Systems, Inc., 2006, APEX2, version 2 User Manual, M86-E01078, Madison, WI.
33 P. W. Betteridge, J. R. Carruthers, R. I. Cooper, K. Prout and D. J. Watkin, *J. Appl. Cryst*., 2003, **36**, 1487.
34 A. L. Spek, *Acta Cryst. C*, 2015, **71**, 9.
35 I. J. Bruno, J. C. Cole, P. R. Edgington, M. K. Kessler, C. F. Macrae, P. McCabe, J. Pearson and R. Taylor, *Acta Crystallogr., Sect. B*, 2002, **58**, 389.
36 C. F. Macrae, I. J. Bruno, J. A. Chisholm, P. R. Edgington, P. McCabe, E. Pidcock, L. Rodriguez-Monge, R. Taylor, J. van de Streek and P. A. Wood, *J. Appl. Cryst*., 2008, **41**, 466.

37 S. A. Moggach, D. R. Allan, S. Parsons and J. E. Warren, *J. Appl. Cryst.*, 2008, **41**, 249.
38 I. Kantor, V. Prakapenka, A. Kantor, P. Dera, A. Kurnosov, S. Sinogeikin, N. Dubrovinskaia and L. Dubrovinsky, *Rev. Sci. Instrum.,* 2012, **83**, 125102.
39 D. M. Adams, R. Appleby and S. K. Sharma, *J. Phys. E: Sci. Instrum.,* 1976, **9**, 1140.
40 CrysAlisPro 1.171.38.41k (Rigaku OD, 2015)
41 J. Yuasa, M. Dan and T. Kawai, *Dalton Trans.*, 2013, **42**, 16096.
42 R. D. Costa, D. Tordera, E. Ortí, H. J. Bolink, J. Schönle, S. Graber, C. E. Housecroft, E. C. Constable and J. A. Zampese, *J. Mater. Chem.,* 2011, **21**, 16108.
43 C. Janiak, *J. Chem. Soc*., *Dalton Trans*., 2000, 3885.
44 I. Andrés-Tomé, J. Fyson, F. Baiao Dias, A. P. Monkman, G. Iacobellis and P. Coppo, *Dalton Trans.*, 2012, **41**, 8669.
45 I. Andrés-Tomé, J. Fyson, F. Baiao Dias, A. P. Monkman, G. Iacobellis and P. Coppo, *Dalton Trans.*, 2012, **41**, 8669.

Electronic supplementary data to accompany

Luminescent Cu(I) complexes with bisphosphanes and halogen-substituted 2,2'-bipyridine ligands

Sarah Keller,[a] Alessandro Prescimone,[a] Henk Bolink,[b] Antonio Pertegás,[b] Giulia Longo,[b] Edwin C. Constable[a] and Catherine E. Housecroft*[a]

[a]Department of Chemistry, University of Basel, BPR 1096, Mattenstrasse 24a, CH-4058 Basel, Switzerland; email: catherine.housecroft@unibas.ch
[b]Instituto de Ciencia Molecula, Universidad de Valencia, 46980 Paterna (Valencia), Spain

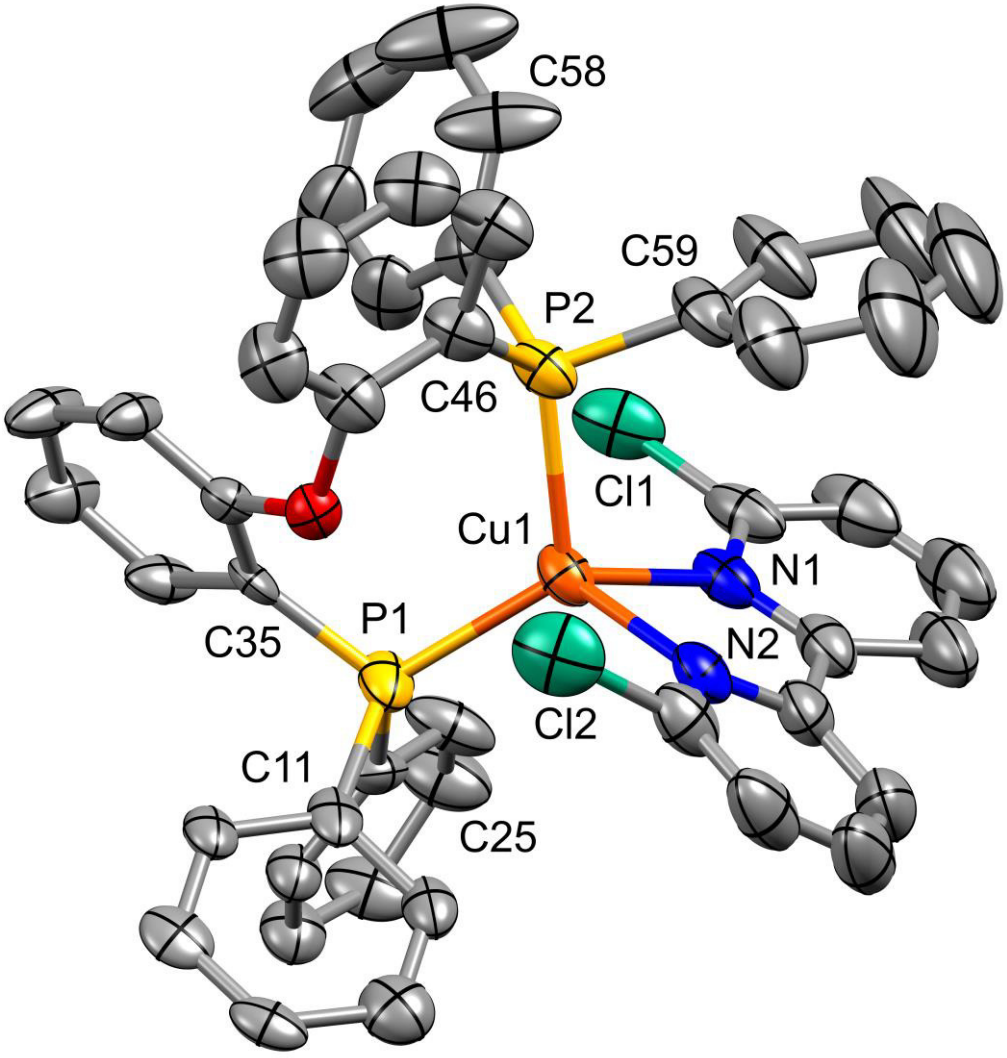

Fig. S1: Structure of the $[Cu(POP)(6,6\text{-}Cl_2bpy)]^+$ cation in $[Cu(POP)(6,6\text{-}Cl_2bpy)][PF_6]$. The POP ligand is heavily disordered (not shown), four disordered aromatic rings had to be refined as rigid bodies. Ellipsoids plotted at 50% probability level, H atoms omitted.

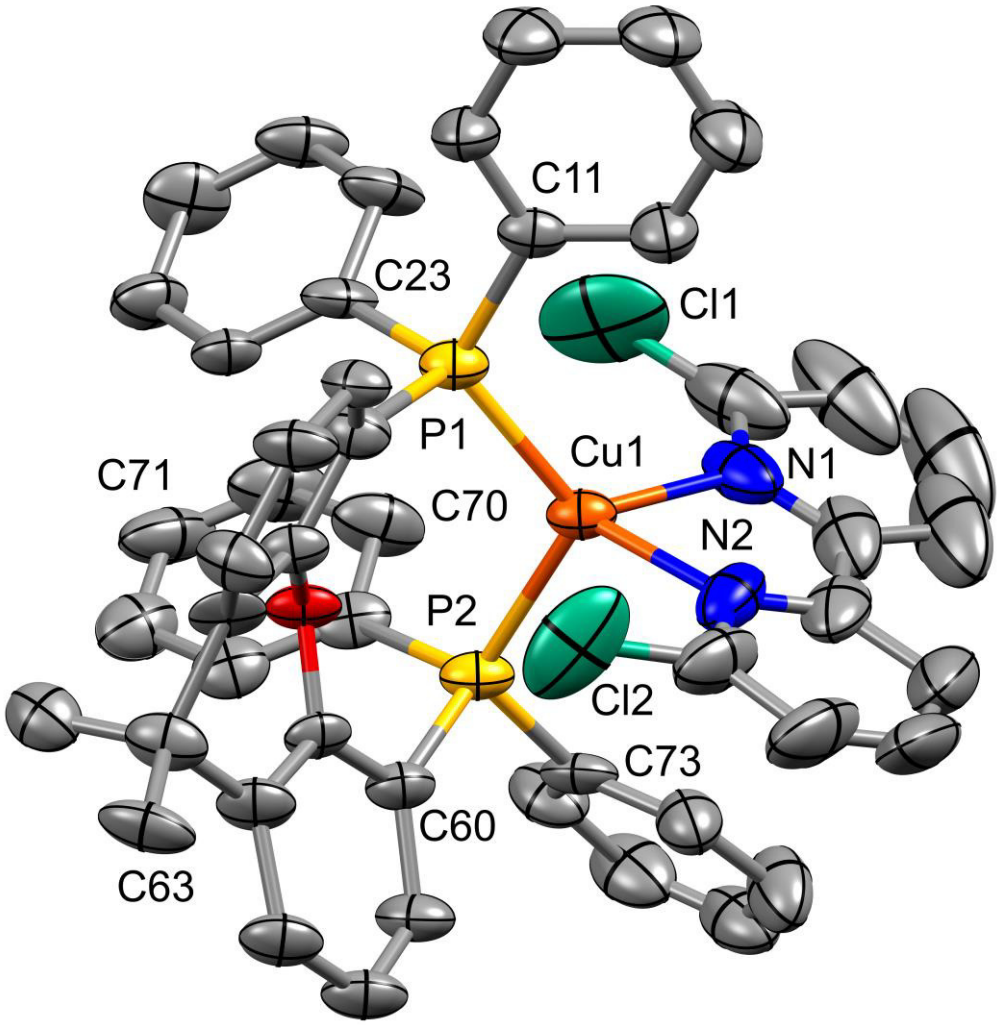

Fig. S2: Structure of the $[Cu(xantphos)(6,6\text{-}Cl_2bpy)]^+$ cation in $[Cu(xantphos)6,6\text{-}Cl_2bpy)][PF_6]$. The xantphos ligand is heavily disordered with the xanthene bowl in two different orientations (not shown). Ellipsoids plotted at 50% probability level, H atoms omitted.

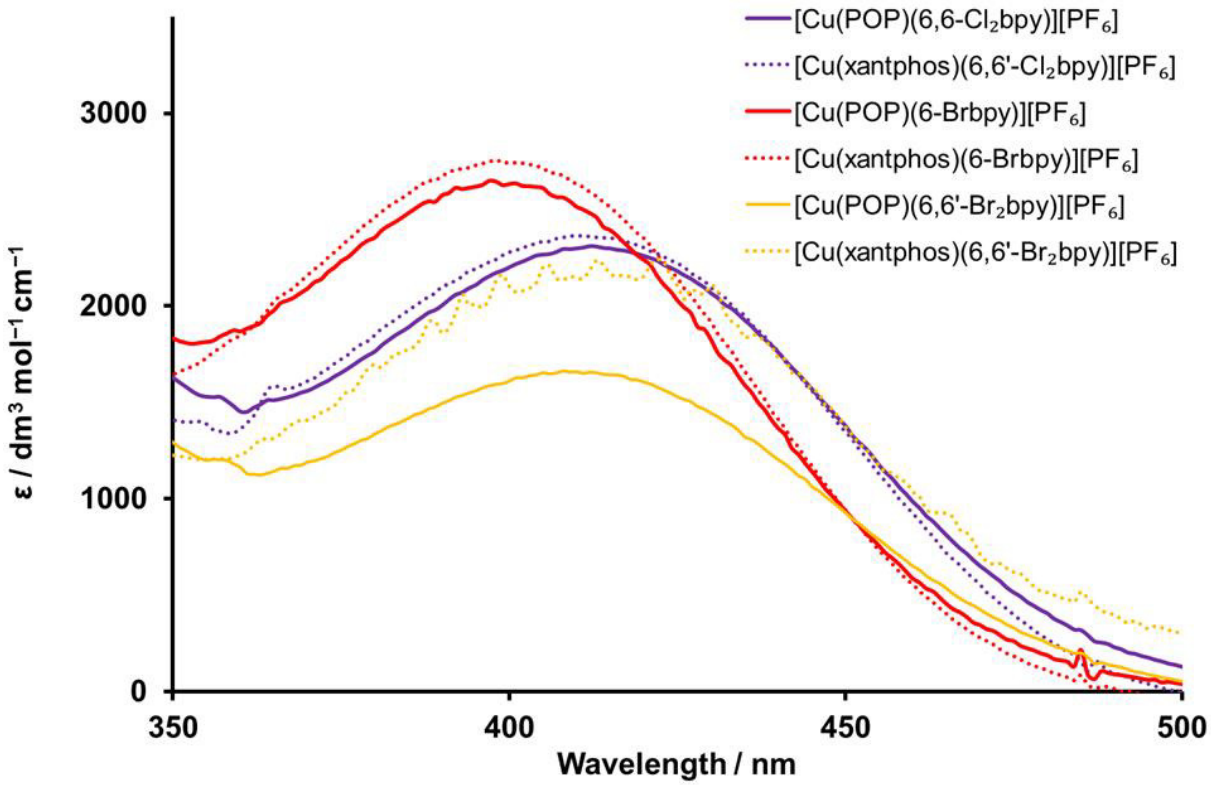

Fig. S3: Zoom into the MLCT area of the solution absorption spectra of the [Cu(P^P)(bpy)][PF_6] complexes (CH_2Cl_2, 2.5×10^{-5} mol dm^{-3}).

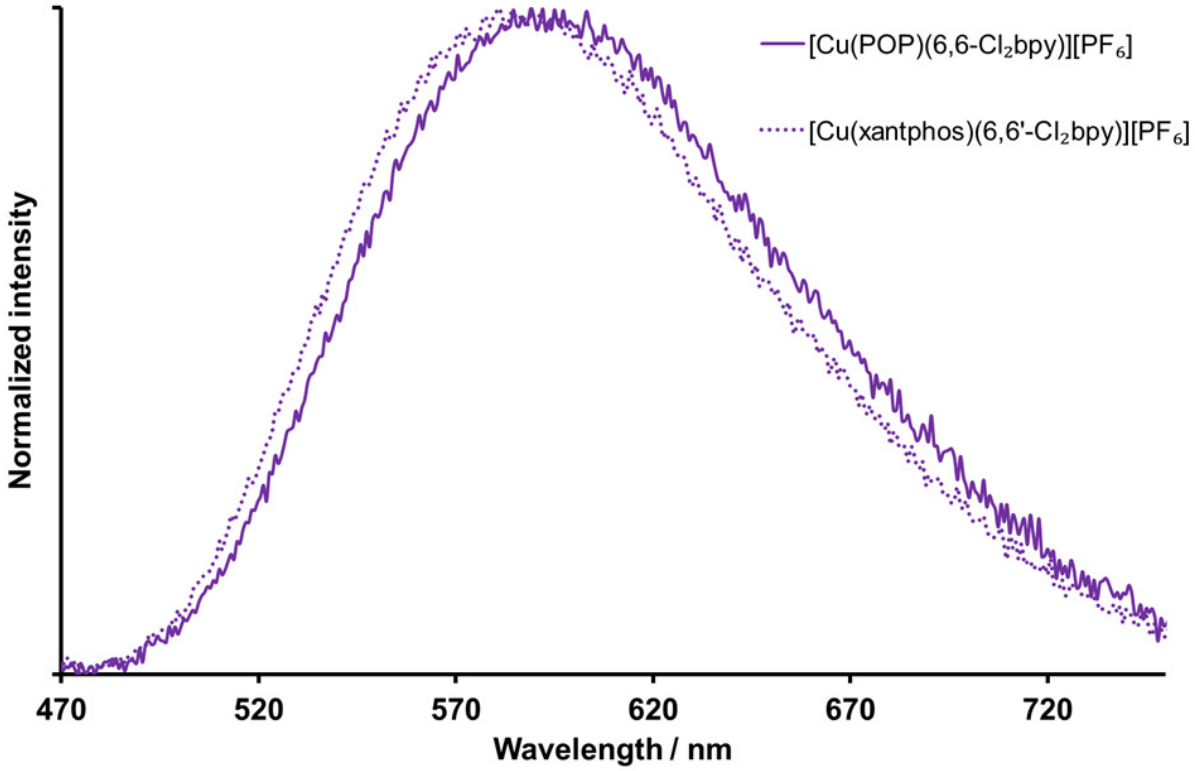

Fig. S4: Photoluminescence spectra of thin films composed of [Cu(P^P)(6,6'-Cl_2bpy)][PF_6]:[Emim][PF_6] at a 4:1 molar ratio (λ_{exc} = 360 nm).

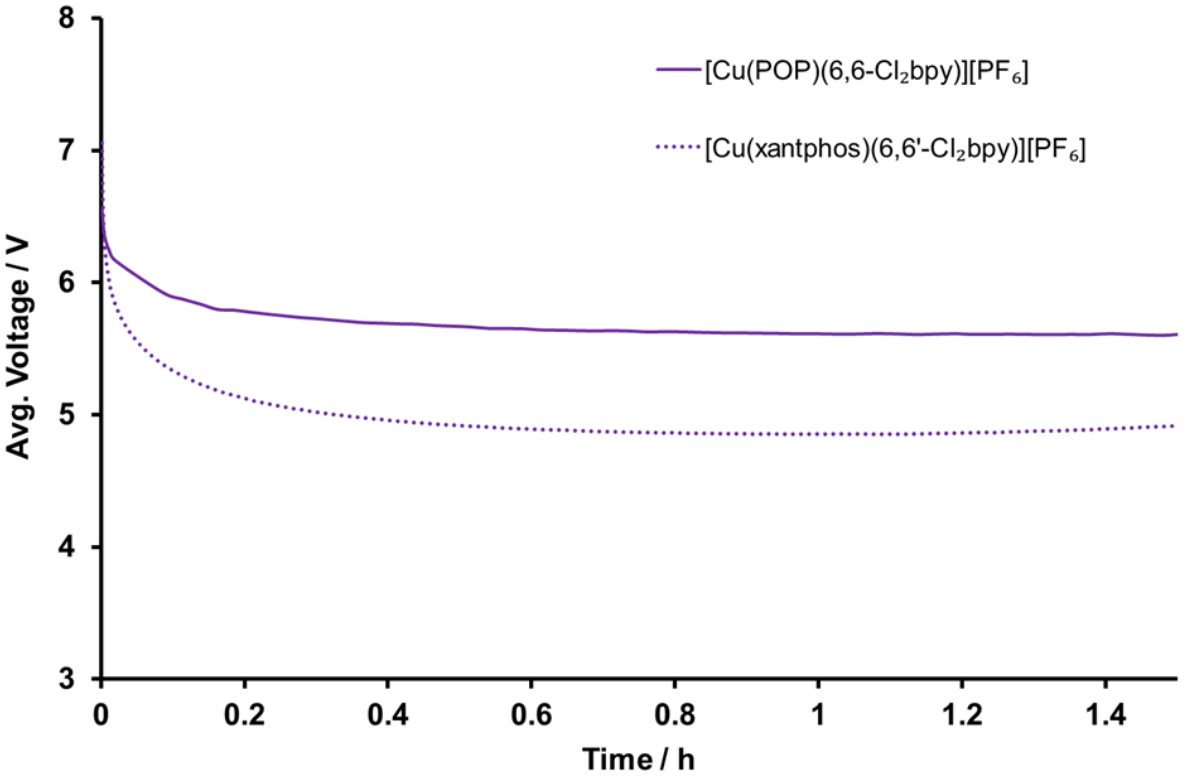

Fig. S5: Average Voltage versus time characteristics for ITO/PEDOT:PSS/[Cu(P^P)^N^N)][PF_6]:[Emim][PF_6] 4:1/Al LECs operated at pulsed current (average density current 50 A m^{-2}, 1 kHz, 50% duty cycle, block wave).

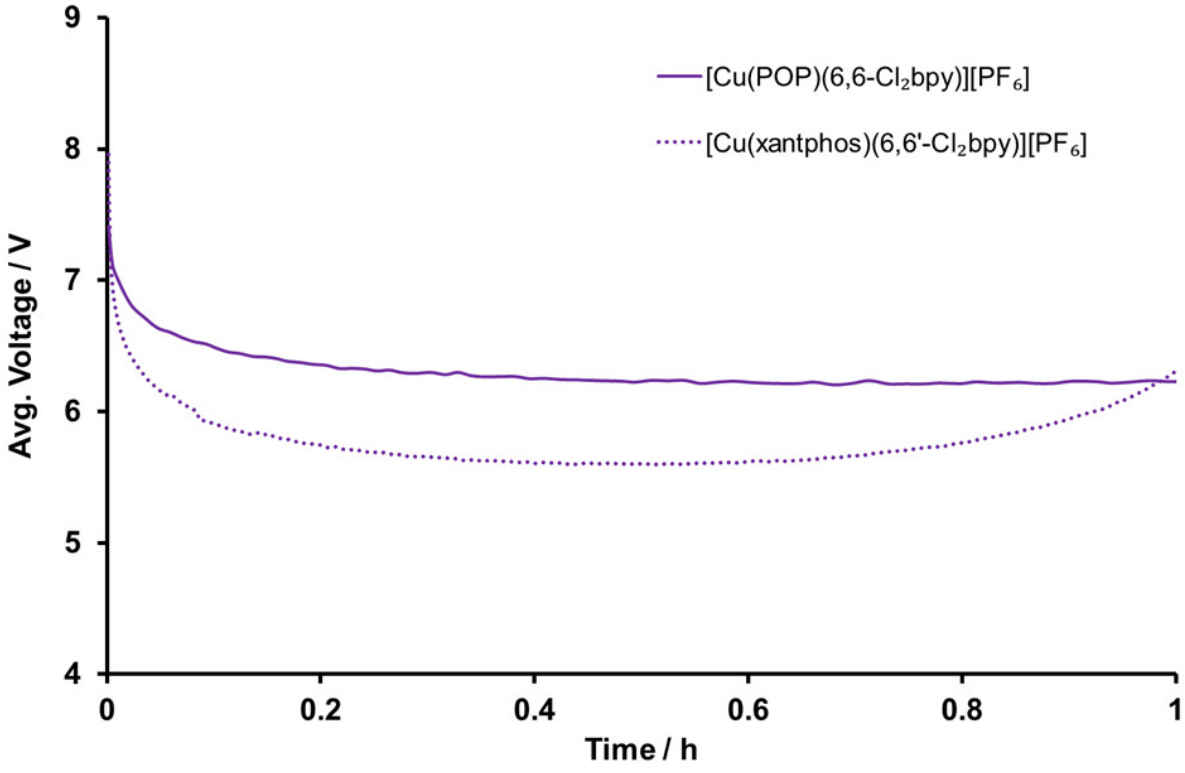

Fig. S6: Average Voltage versus time characteristics for ITO/PEDOT:PSS/[Cu(P^P)^N^N)][PF_6]:[Emim][PF_6] 4:1/Al LECs operated at pulsed current (average density current 100 A m^{-2}, 1 kHz, 50% duty cycle, block wave).

S1. Experimental details for ambient and high pressure single crystal X-ray diffraction of [Cu(POP)(6-Brbpy)][PF_6]

For all structures: $C_{46}H_{35}BrCuF_6N_2OP_3$, M_r = 982.16, monoclinic, $P2_1/c$, Z = 4.

	P_0	sk58_01	sk58_02	sk58_03
CCDC code	1535141	1584757	1584754	1584752
Crystal data				
Temperature (K)	123	293	293	293
Pressure (GPa)	ambient	0.16	1.30	1.80
a, *b*, *c* (Å)	15.3402 (6), 14.2344 (5), 19.2659 (7)	15.459 (10), 14.2430 (12), 19.413 (8)	15.123 (8), 13.6502 (10), 18.868 (7)	14.960 (8), 13.2757 (8), 18.724 (6)
β (°)	90.9159 (12)	90.03 (6)	91.32 (5)	92.23 (5)
V (Å^3)	4206.34 (15)	4274 (3)	3894 (2)	3716 (2)
D_x (Mg m^{-3})	1.551	1.526	1.675	1.755
Radiation type	Cu *K*α	Synchrotron, λ = 0.48590 Å	Synchrotron, λ = 0.48590 Å	Synchrotron, λ = 0.48590 Å
μ (mm^{-1})	3.49	1.62	1.78	1.87
Crystal size (mm)	0.12 × 0.10 × 0.08	0.04 × 0.02 × 0.02	0.04 × 0.02 × 0.02	0.04 × 0.02 × 0.02
Data collection				
Diffractometer	Bruker Kappa Apex2	Pilatus 300K	Pilatus 300K	Pilatus 300K
Radiation source	Cu *K*α	Diamond Light Source Beamline I19	Diamond Light Source Beamline I19	Diamond Light Source Beamline I19
Monochromator	Graphite	Double crystal Silicon 111	Double crystal Silicon 111	Double crystal Silicon 111
Absorption correction	Multi-scan *SADABS* (Siemens, 1996)	Multi-scan *CrysAlis PRO* 1.171.38.41 (Rigaku Oxford Diffraction, 2015) Empirical absorption correction using spherical harmonics, implemented in SCALE3 ABSPACK scaling algorithm.	Multi-scan *CrysAlis PRO* 1.171.38.41 (Rigaku Oxford Diffraction, 2015) Empirical absorption correction using spherical harmonics, implemented in SCALE3 ABSPACK scaling algorithm.	Multi-scan *CrysAlis PRO* 1.171.38.41 (Rigaku Oxford Diffraction, 2015) Empirical absorption correction using spherical harmonics, implemented in SCALE3 ABSPACK scaling algorithm.
T_{min}, T_{max}	0.65, 0.76	0.033, 1.000	0.079, 1.000	0.074, 1.000
No. of measured, independent and	35307, 7329, 7293	26697, 6179, 2242	24175, 5560, 2847	22897, 5151, 2851

observed [$I > 2.0\sigma(I)$] reflections				
R_{int}	0.022	0.157	0.119	0.115
$(\sin\theta/\lambda)_{max}$ (Å^{-1})	0.595	0.799	0.797	0.797
Refinement				
$R[F^2 > 2\sigma(F^2)]$, $wR(F^2)$, S	0.028, 0.067, 0.89	0.095, 0.364, 1.08	0.071, 0.238, 1.01	0.067, 0.102, 1.13
No. of reflections	7329	6128	5534	5126
No. of parameters	541	541	445	445
No. of restraints	0	584	584	598
H-atom treatment	H-atom parameters constrained	H-atom parameters constrained	H-atom parameters not refined	H-atom parameters not refined
$\Delta\rangle_{max}$, $\Delta\rangle_{min}$ (e Å^{-3})	0.88, -0.39	1.19, -1.46	0.73, -0.72	0.74, -0.96

	sk58_04	sk58_05	sk58_06
CCDC code	1584753	1584755	1584756
Crystal data			
Temperature (K)	293	293	293
Pressure (GPa)	3.50	4.20	4.50
a, b, c (Å)	14.765 (8), 12.9897 (9), 18.629 (6)	14.652 (7), 12.7677 (9), 18.624 (6)	14.622 (6), 12.6860 (8), 18.613 (6)
β (°)	92.14 (5)	91.96 (5)	92.10 (4)
V (Å^3)	3570 (2)	3482 (2)	3450.3 (19)
D_x (Mg m^{-3})	1.827	1.873	1.891
Radiation type	Synchrotron, λ = 0.48590 Å	Synchrotron, λ = 0.48590 Å	Synchrotron, λ = 0.48590 Å
μ (mm^{-1})	1.94	1.99	2.01
Crystal size (mm)	0.04 × 0.02 × 0.02	0.04 × 0.02 × 0.02	0.04 × 0.02 × 0.02
Data collection			
Diffractometer	Pilatus 300K	Pilatus 300K	Pilatus 300K
Radiation source	Diamond Light Source Beamline I19	Diamond Light Source Beamline I19	Diamond Light Source Beamline I19
Monochromator	Double crystal Silicon 111	Double crystal Silicon 111	Double crystal Silicon 111
Absorption correction	Multi-scan *CrysAlis PRO* 1.171.38.41 (Rigaku Oxford Diffraction, 2015) Empirical absorption correction using spherical harmonics, implemented in SCALE3 ABSPACK	Multi-scan *CrysAlis PRO* 1.171.38.41 (Rigaku Oxford Diffraction, 2015) Empirical absorption correction using spherical harmonics, implemented in SCALE3 ABSPACK	Multi-scan *CrysAlis PRO* 1.171.38.41 (Rigaku Oxford Diffraction, 2015) Empirical absorption correction using spherical harmonics, implemented in SCALE3 ABSPACK

	scaling algorithm.	scaling algorithm.	scaling algorithm.
T_{min}, T_{max}	0.3168, 1.000	0.169, 1.000	0.225, 1.000
No. of measured, independent and observed [$I > 2.0\sigma$ (I)] reflections	22406, 4883, 2802	19321, 4281, 2817	20918, 4800, 3064
R_{int}	0.106	0.094	0.103
$(\sin \theta/\lambda)_{max}$ (Å^{-1})	0.797	0.795	0.796
Refinement			
$R[F^2 > 2\sigma (F^2)]$, $wR(F^2)$, S	0.066, 0.092, 1.15	0.059, 0.088, 1.10	0.063, 0.097, 1.11
No. of reflections	4859	4276	4784
No. of parameters	445	445	415
No. of restraints	613	613	542
H-atom treatment	H-atom parameters not refined	H-atom parameters not refined	H-atom parameters not refined
$\Delta\rangle_{max}$, $\Delta\rangle_{min}$ (e Å^{-3})	0.88, -1.00	0.77, -0.72	0.97, -0.84

Computer programs: Apex2 (Bruker AXS, 2006), *CrysAlis PRO* 1.171.38.41k (Rigaku OD, 2015), *SUPERFLIP* (Palatinus & Chapuis, 2007), form ambient pressure structure), form 1.6 kbar structure), form 13 kbar structure), form 18 kbar structure), form 35 kbar structure), form 42 kbar structure), *CRYSTALS* (Betteridge *et al.*, 2003), *CAMERON* (Watkin *et al.*, 1996).

Chapter III. CF_3 substitution of [Cu(P^P)(bpy)][PF_6] complexes: Effects on photophysical properties and light-emitting electrochemical cell performance

Summary

In this paper,[4] we describe our results of CF_3-subsitution in the 2,2'-bipyridine (bpy) ligand in a series of [Cu(P^P)(bpy)][PF_6] complexes where P^P is either bis(2-(diphenylphosphino)phenyl)ether (POP) and 4,5-bis(diphenylphosphino)-9,9-dimethylxanthene (xantphos). The investigated bpys are 6,6'-$(CF_3)_2$-2,2'-bipyridine (6,6'-$(CF_3)_2$bpy), 6-CF_3-2,2'-bipyridine (6-CF_3bpy), 5,5'-$(CF_3)_2$-2,2'-bipyridine (5,5'-$(CF_3)_2$bpy), 4,4'-$(CF_3)_2$-2,2'-bipyridine (4,4'-$(CF_3)_2$bpy) and 6,6'-Me_2-4,4'-$(CF_3)_2$-2,2'-bipyridine (6,6'-Me_2-4,4'-$(CF_3)_2$bpy). Single-crystal X-ray diffraction yielded solid state structures of [Cu(xantphos)(bpy)][PF_6], [Cu(xantphos)(4,4'-$(CF_3)_2$bpy)][PF_6] [Cu(POP)(6-CF_3bpy)][PF_6]·1.3Et_2O·0.35H_2O, [Cu(xantphos)(6-CF_3bpy)][PF_6]·2Et_2O·1.5CH_2Cl_2, [Cu(POP)(4,4'-$(CF_3)_2$bpy)][PF_6]·0.5CH_2Cl_2 and [Cu(POP)(5,5'-$(CF_3)_2$bpy)][PF_6]·0.5Et_2O with each copper(I) centre in a distorted tetrahedral environment. The bpy ligands were selected with the intention to study the effect of CF_3 groups in different positions at the bpy on the stability of the complexes, their emissive properties and behaviour in light-emitting electrochemical cells (LECs). The compounds with CF_3-bpys are compared to the complexes with unsubstituted bpy, [Cu(POP)(bpy)][PF_6] and [Cu(xantphos)(bpy)][PF_6]. We were especially interested to find out whether CF_3 groups have a comparable beneficial influence on the complex properties as alkyl groups have (Chapter I) and compare these compounds with [Cu(xantphos)(6-Mebpy)][PF_6] and [Cu(xantphos)(6,6'-Me_2bpy)][PF_6].[2] The detailed study of the photophysical properties includes solution absorption spectroscopy, solution and solid state emission spectroscopy including PLQY and lifetime measurements, and in addition also low-temperature (77K) emission spectra and lifetimes were measured with the complexes in a frozen glass matrix of Me-THF. The thermally activated delayed fluorescence (TADF) behaviour of these compounds is discussed on the base of these experiments and the extensive DFT calculations performed by the group of Enrique Ortí in Valencia. The promising complexes [Cu(POP)(6-CF_3bpy)][PF_6], [Cu(xantphos)(6-CF_3bpy)][PF_6] and [Cu(xantphos)(6,6'-Me_2-4,4'-$(CF_3)_2$bpy)][PF_6] were incorporated into LECs by the team of Henk Bolink in Valencia and the devices were thoroughly characterized, in terms of electroluminescence, efficiency, brightness and device lifetime.

[4] S. Keller, F. Brunner, J. M. Junquera-Hernández, A. Pertegás, M.-G. La-Placa, A. Prescimone, E. C. Constable, H. J. Bolink, E. Ortí and C. E. Housecroft, "CF_3 substitution of [Cu(P^P)(bpy)][PF_6] complexes: Effects on photophysical properties and light-emitting electrochemical cell performance", *ChemPlusChem*, submitted 20.11.2017.

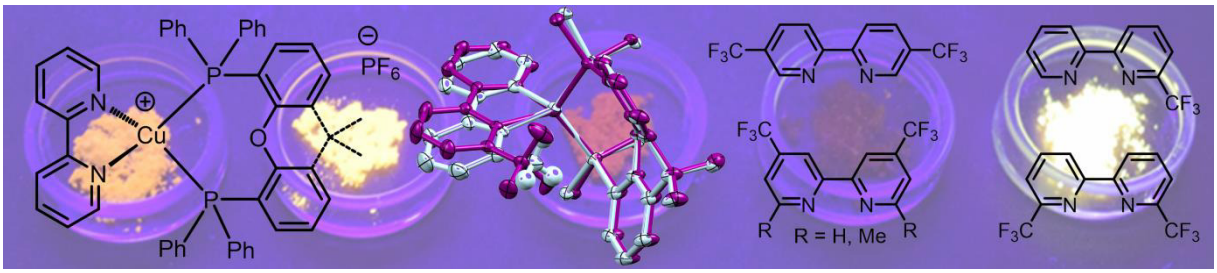

Contribution of Sarah Keller: Idea of the project and selection of ligands ❖ Synthesis of most complexes ❖ Analytical characterization (electrospray mass spectroscopy, NMR spectroscopy) ❖ Photophysical and electrochemical characterization ❖ Conduction and interpretation of low-temperature photophysics ❖ Writing of the manuscript, except paragraphs about DFT calculations and devices.

CF_3 Substitution of [Cu(P^P)(bpy)][PF_6] complexes: Effects on Photophysical Properties and Light-emitting Electrochemical Cell Performance

Sarah Keller,[a] Fabian Brunner,[a] José M. Junquera-Hernández,[b] Antonio Pertegás,[b] Maria-Grazia La-Placa,[b] Alessandro Prescimone,[a] Edwin C. Constable,[a] Henk J. Bolink,[b] Enrique Ortí*[b] and Catherine E. Housecroft*[a]

Abstract: We report [Cu(P^P)(N^N)][PF_6] complexes with P^P = bis(2-(diphenylphosphino)phenyl)ether (POP) or 4,5-bis(diphenylphosphino)-9,9-dimethylxanthene (xantphos), N^N = CF_3-substituted 2,2'-bipyridines (6,6'-$(CF_3)_2$bpy, 6-CF_3bpy, 5,5'-$(CF_3)_2$bpy, 4,4'-$(CF_3)_2$bpy, 6,6'-Me_2-4,4'-$(CF_3)_2$bpy). We present the effects of CF_3 substitution on structures, and electrochemical and photophysical properties. The HOMO–LUMO gap is tuned by the N^N ligand; the largest redshift in the MLCT band is for [Cu(P^P)(5,5'-$(CF_3)_2$bpy)][PF_6]. In solution, the compounds are weak yellow to red emitters. The emission properties depend on the substitution pattern but this cannot be explained by simple electronic arguments. For powders, [Cu(xantphos)(4,4'-$(CF_3)_2$bpy)][PF_6] has the highest PLQY (50.3%) with an emission lifetime of 12 μs. Compared to 298 K solution behaviour, excited state lifetimes lengthen in frozen Me-THF (77 K) indicating thermally activated delayed fluorescence (TADF). TD-DFT calculations show that the energy gap between the lowest-energy singlet and triplet excited states (0.12–0.20 eV) permits TADF. LECs with [Cu(POP)(6-CF_3bpy)][PF_6], [Cu(xantphos)(6-CF_3bpy)][PF_6] or [Cu(xantphos)(6,6'-Me_2-4,4'-$(CF_3)_2$bpy)][PF_6] emit yellow electroluminescence. A LEC with [Cu(xantphos)(6,6'-Me_2-4,4'-$(CF_3)_2$bpy)][PF_6] had the fastest turn-on time (8 min); the LEC with the longest lifetime ($t_{1/2}$ = 31 h) contained [Cu(xantphos)(6-CF_3bpy)][PF_6]; these LECs reached maximum luminances of 131 and 109 cd m^{-2}.

Introduction

The development of solid-state lighting based on the widely distributed organic light-emitting diodes (OLEDs) has had a massive impact on technology, especially for screens and displays.[1,2,3] Light-emitting electrochemical cells (LECs) are less well established, but are emerging devices which, like OLEDs, are based on the principle of electroluminescence. Compared to OLEDs, LECs are simpler in setup, more straight-forward in their processing and therefore also cheaper in production.[4] Whereas polymer-based or purely organic emitting materials are known for both LECs and OLEDs, the employment of transition metal complexes has certain advantages. Depending on the combination of different ligands and their substitution with functional groups, the properties of these metal complexes can be tuned in terms of emission colour, quantum yield and excited state lifetime.[5,6] For example, for $[Ir(ppy)_2(bpy)]^+$ (Hppy = 2-phenylpyridine, bpy = 2,2'-bipyridine) type complexes, different emission colours, photoluminescence quantum yields (PLQY) and device performances have been obtained upon modification of the cyclometallating Hppy or the ancillary bpy ligands.[5,6] Whereas iridium-based emitters can be extremely efficient,[7,8,9] their replacement by copper-based compounds has the advantage of higher abundance and therefore lower marked price of copper compared to iridium, which also translates to the costs of the devices.[10] Furthermore, many copper complexes are proven to exhibit thermally activated delayed fluorescence (TADF), a mechanism which allows the thermal population of the energetically higher singlet excited state from the triplet excited state. As a consequence, emission processes from all excited states are possible and in theory allow for quantum yields up to 100% to be reached.[11,12,13,14]

We have previously shown for [Cu(P^P)(bpy)][PF_6] complexes (where P^P = bis(2-diphenylphosphinophenyl)ether (POP) or 4,5-bis(diphenylphosphino)-9,9-dimethylxanthene (xantphos)), that the PLQY of the complex and the efficiency and lifetime in LEC devices are increased upon addition of methyl or ethyl groups in one or both 6-positions of the bpy ligand.[15,16] Costa *et al.*[17] systematically studied the effect of electron donating and electron withdrawing substituents at the 4-positions of bpy in [Cu(P^P)(bpy)][PF_6] complexes. The more negative the σ-Hammett parameter σ_p, which describes the σ-donation ability of a given substituent, the more enhanced is the performance of the LEC employing the respective compound, within a given series of complexes. We have demonstrated that the incorporation of

[a] S. Keller, F. Brunner, Dr. A. Prescimone, Prof. Dr. E.C. Constable, Prof. Dr. C.E. Housecroft
Department of Chemistry
University of Basel
BPR 1096, Mattenstrasse 24a, Basel 4058, Switzerland
E-mail: catherine.housecroft@unibas.ch
[b] Dr. J.M. Junquera, Dr. A. Pertegás, M.-G. La-Placa, Dr. H.J. Bolink, Prof. Dr. E. Ortí
Instituto de Ciencia Molecular,
Universidad de Valencia,
ES-45980 Paterna, Valencia, Spain
e-mail: enrique.orti@uv.es

Supporting information for this article is given via a link at the end of the document.((Please delete this text if not appropriate))

remote fluoro groups in [Cu(POP)(N^N)][PF_6] and [Cu(xantphos)(N^N)][PF_6], where N^N = 4,4'-bis(4-fluorophenyl)-6,6'-dimethyl-2,2'-bipyridine, leads to an enhancement of solid state and solution photophysical properties and is also beneficial to LEC performance.[18] This finding prompted us to investigate the potential positive effects that the introduction of CF_3 substituents may also have. Substitution with one or more trifluoromethyl groups is a common motif in coordination chemistry, especially for *N,N'*-chelating ligands incorporating pyrrole, pyrazole, triazole and tetrazole rings, as discussed for pyridyl azolates by Y. Chi *et al.*[19] Modification with CF_3 groups is often employed in luminescent materials containing Cu(I), Ir(III) and Pt(II) to Ru(II) and Os(II) complexes. However, CF_3-modified 2,2'-bipyridines are rarely mentioned in the literature, and copper complexes coordinated by a CF_3-substituted bpy are even more scarce.[20] The molar volume of a CF_3 group is significantly larger than for a methyl group and the steric effect is often comparable to that of an isopropyl group.[21] Furthermore, the electronic properties of methyl and CF_3 differ in that the former acts as a weak σ-donor whereas the latter has electron-withdrawing properties and therefore a more positive σ-Hammett parameter σ_p than alkyl groups.

Our aim in the present investigation was to prepare a series of copper(I) complexes of the type [Cu(POP)(bpy)][PF_6] and [Cu(xantphos)(bpy)][PF_6] with bpy ligands that are substituted with CF_3 groups in the 4-, 5- or 6-positions. The chemical structure of the POP, xantphos and bpy ligands used is given in Scheme 1. The electrochemical and photophysical properties of the new complexes are compared with those employing unsubstituted bpy as model compounds and with the Cu(I) complexes with alkyl-substituted bpy ligands,[16] and are interpreted with the help of density functional calculations. Those complexes with more promising photophysical properties are tested in LEC devices.

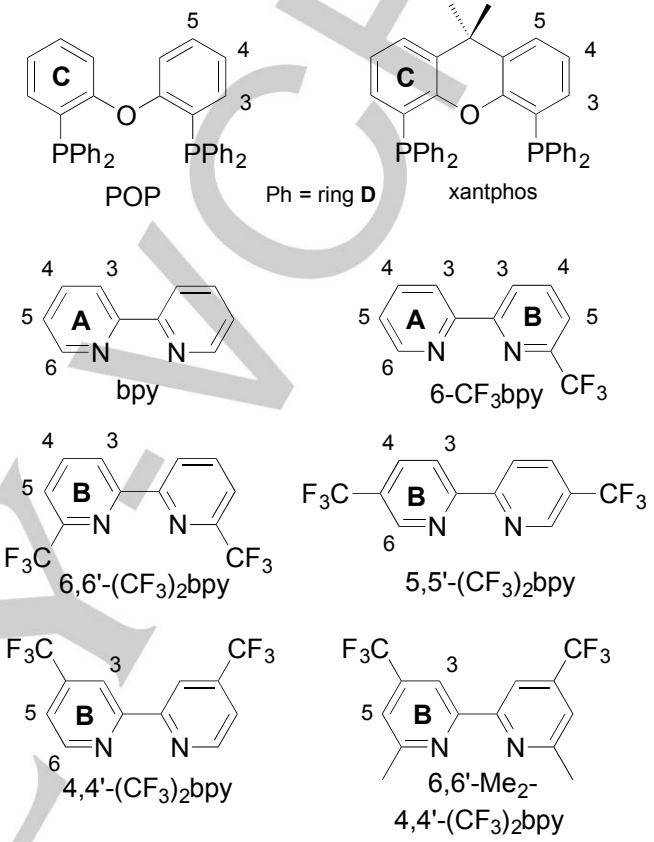

Scheme 1. Structures of ligands with ring and atom labels for NMR spectroscopic assignments.

Results and Discussion

Synthesis, stability and characterization of [Cu(P^P)(N^N][PF_6] complexes

The [Cu(P^P)(N^N)][PF_6] complexes with P^P = POP and xantphos and N^N = bpy, 6-CF_3bpy, 5,5'-$(CF_3)_2$bpy and 4,4'-$(CF_3)_2$bpy, as well as the [Cu(xantphos)(6-Mebpy)][PF_6], [Cu(xantphos)(6,6'-Me_2bpy)][PF_6] and [Cu(xantphos)(6,6'-Me_2-4,4'-$(CF_3)_2$bpy)][PF_6] complexes (see Scheme 1 for ligands), were synthesized following the standard procedures[15,16,22] and were isolated as bright yellow to orange solids with yields of 52 to 96%. The formation of heteroleptic [Cu(P^P)(bpy)][PF_6] complexes was confirmed by one- and two-dimensional NMR spectroscopic techniques (^{1}H, ^{31}P, ^{19}F, ^{13}C, COSY, NOESY, HMQC, HMBC), which allowed for the unambiguous assignment of all signals. On the NMR spectroscopic timescale, the spectra of the compounds dissolved in acetone-d_6 are in accordance with C_{2v} symmetry for the complex cations containing symmetrically substituted bpy ligands.[16] The base peaks in the electrospray mass spectra match the respective $[Cu(P^P)(N^N)]^+$ cations, with isotope patterns agreeing with the calculated ones. Elemental analysis was performed to confirm the purity of the bulk compounds.

Because of the constraints of the xanthene unit, the xantphos ligand is less sterically demanding than POP. As a consequence, the addition of the POP to $[Cu(MeCN)_4]^+$ leads to $[Cu(POP)(MeCN)]^+$ or $[Cu(POP\text{-}P,P')(POP\text{-}\kappa^1P)]^+$. On the other hand, xantphos reacts with $[Cu(MeCN)_4]^+$ to give $[Cu(xantphos\text{-}\kappa^2P)_2]^+$.[23] This difference in behaviour leads to varying approaches to the preparation of [Cu(POP)(N^N)][PF_6] and [Cu(xantphos)(N^N][PF_6]. Whereas for complexes with POP, the bpy ligand was added after an initial reaction of POP and [Cu(MeCN)$_4$][PF_6] in CH_2Cl_2 (sequential addition),[15,16] for complexes with xantphos, a mixture of both the bisphosphane and the N^N ligand was added to the solution of [Cu(MeCN)$_4$][PF_6] to avoid formation of $[Cu(xantphos)_2]^+$ and facilitate the formation of heteroleptic $[Cu(xantphos)(bpy)]^+$.[16]

Substitution at the 6,6'-positions of the bpy ligand has a significant effect on both the photophysics and the stability of the $[Cu(P^P)(bpy)]^+$ complexes. Substituents in 6,6'-positions shield the copper(I) centre from solvent attack and

therefore reduce quenching by avoiding the so-called "solvent-related excited-state relaxations".[12,26] In general, large sterically demanding ligands in copper(I) complexes prevent a geometrical rearrangement of the tetrahedral cation towards more flattened structures upon excitation and thus help elongating excited state lifetimes. This structural effect was studied in detail for $[Cu(phen)_2]^+$ complexes.[24,25,26] However, if the substituents in the 6,6'-positions are too large or electronically repulsive, the exclusive formation of heteroleptic $[Cu(P\text{^}P)(N\text{^}N)]^+$ is not achievable and, instead, mixtures of homoleptic $[Cu(N\text{^}N)_2]^+$ and $[Cu(xantphos)_2]^+$ are obtained. This phenomenon has also been observed for complexes with phenanthrolines of different steric demand in the 2,9-positions together with a series of P^P chelating ligands.[27] Interestingly, substituents in the 4,4'-positions of the bpy ligand also appear to have an influence on the ligand redistribution (Scheme 2). For 6,6'-Me_2bpy, with 1.0 equivalents of xantphos and 1.2 equivalents of POP, respectively, an exclusive formation of the heteroleptic $[Cu(P\text{^}P)(bpy)]^+$ complexes was achieved (removal of excess P^P chelating ligand by subsequent layer crystallization (CH_2Cl_2/Et_2O).[16] In the case of 6,6'-Me_2-4,4'-$(CF_3)_2$bpy pure heteroleptic [Cu(xantphos)(6,6'-Me_2-4,4'-$(CF_3)_2$bpy)][PF_6] was obtained with 1.2 equivalents of xantphos (and following recrystallization to remove excess xantphos). However, the analogous reaction with POP leads to a mixture of free 6,6'-Me_2-4,4'-$(CF_3)_2$bpy and $[Cu(POP)_2][PF_6]$ with heteroleptic [Cu(POP)(6,6'-Me_2-4,4'-$(CF_3)_2$bpy)][PF_6], which we were not able to isolate without the side products and was therefore not characterized further (see Figure S1–S3 for NMR spectra).

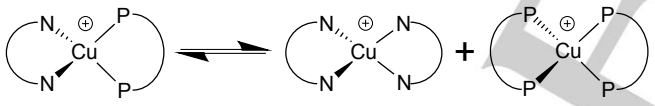

Scheme 2. Ligand redistribution results in an equilibrium between heteroleptic and homoleptic cations.

The sensitivity of the ligand redistribution equilibrium (Scheme 2) towards substituents in the 6,6'-positions of the bpy ligand was again corroborated by the unsuccessful attempts to isolate $[Cu(P\text{^}P)(6,6'\text{-}(CF_3)_2bpy)][PF_6]$ complexes. NMR spectra of the crude product of the reaction of $[Cu(MeCN)_4][PF_6]$ with POP (1.0 as well as 1.1 equivalents) in CH_2Cl_2 and subsequent addition of 6,6'-$(CF_3)_2$bpy identify the material as a mixture of $[Cu(POP)_2][PF_6]$, $[Cu(POP)(MeCN)_2][PF_6]$ and $[Cu(6,6'\text{-}(CF_3)_2bpy)_2][PF_6]$.[28] In the mass spectrum, the base peak at *m/z* 601.2 was assigned to $[Cu(POP)]^+$, and no peak envelope arising from $[Cu(POP)(6,6'\text{-}(CF_3)_2bpy)]^+$ was detected.

The attempted synthesis of [Cu(xantphos)(6,6'-$(CF_3)_2$bpy)][PF_6] from $[Cu(MeCN)_4][PF_6]$, 6,6'-$(CF_3)_2$bpy and xantphos (1.0 as well as 1.2 equivalents) in CH_2Cl_2 yielded a pale orange solid upon solvent removal. NMR spectroscopic data for the crude product showed a mixture of $[Cu(xantphos)(MeCN)_2]^+$ and $[Cu(6,6'\text{-}(CF_3)_2bpy)_2][PF_6]$.[28] In the electrospray mass spectrum, peak envelopes at *m/z* 641.3 and 1219.7 were assigned to $[Cu(xantphos)]^+$ and $[Cu(xantphos)_2]^+$, but no ion attributed to $[Cu(xantphos)(6,6'\text{-}(CF_3)_2bpy)]^+$ was observed. Layer recrystallization (CH_2Cl_2/Et_2O) of the crude material led to a mixture of colourless (dominant) and orange crystals, which could be manually separated. While the orange crystals were identified as homoleptic $[Cu(6,6'\text{-}(CF_3)_2bpy)_2][PF_6]$,[28] analysis of the colourless crystals showed the formation of a one-dimensional coordination polymer $[\{Cu(xantphos)(\mu\text{-}PO_2F_2)\}_n]$, with the copper centres linked by μ-PO_2F_2 units which stem from partial hydrolysis of the $[PF_6]^-$ anion.[29]

Closer inspection of the spatial properties of the CF_3 group helps us to understand why the formation of the heteroleptic $[Cu(P\text{^}P)(6,6'\text{-}(CF_3)_2bpy)][PF_6]$ complexes was not successful. Whereas the calculated van der Waals radius for a methyl group lies between 1.715 and 2.230 Å, the reported values for a CF_3 group are between 2.107 and 2.743 Å.[30] Although the van der Waals radius is a reasonable parameter to compare, it is only an intrinsic property. In order to determine the steric effect, which is an extrinsic phenomenon, coulombic interactions between all the atoms or groups involved in the interaction have to be taken into consideration. A number of different approaches to analyse the steric effect of typical substituents show that a CF_3 group is comparable with an isopropyl group.[21,31] Considering that two ethyl groups in the 6,6'-positions at the bpy are already too sterically demanding to allow the exclusive formation of heteroleptic $[Cu(P\text{^}P)(6,6'\text{-}Et_2bpy)]^+$ cations, the steric requirements of two CF_3 groups are way beyond what these type of heteroleptic $[Cu(P\text{^}P)(bpy)][PF_6]$ complexes can offer.

In the case of unsubstituted bipyridine, $[Cu(POP)(bpy)][PF_6]$ was previously synthesized and characterized.[43] In contrast, $[Cu(xantphos)(bpy)]^+$ has only been reported as the $[BF_4]^-$ salt.[22] We decided that $[Cu(POP)(bpy)][PF_6]$ and $[Cu(xantphos)(bpy)][PF_6]$ would serve well as reference complexes to compare the effects of attaching CF_3 and methyl groups in different positions in the bpy ligand. $[Cu(xantphos)(6,6'\text{-}Me_2bpy)][PF_6]$ and [Cu(xantphos)(6-Mebpy)][PF_6] were investigated in an earlier study[16] and are included here for comparative purposes.

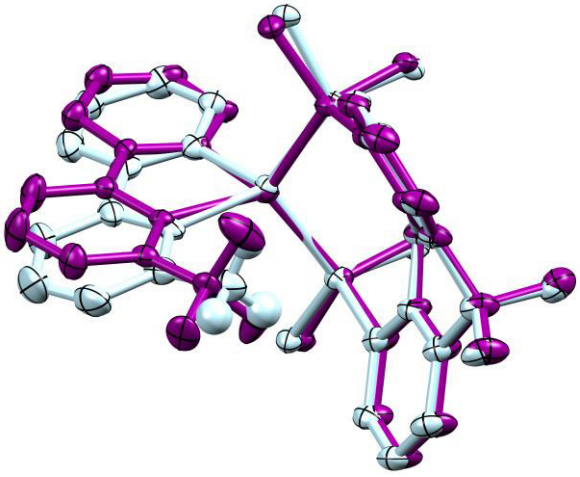

Figure 1. Overlay of the molecular structures of [Cu(xantphos)(6-Mebpy)]$^+$ (light blue) and the major conformation of [Cu(xantphos)(6-CF_3bpy)]$^+$ (purple) with ellipsoids plotted at 50% probability level. Only the ipso-C atoms of the PPh_2 phenyl rings are shown and H atoms are omitted, with exception of the methyl group at the bipyridine to allow for a better comparison with the CF_3 group. The Cu atoms, pairs of corresponding N atoms and corresponding P atoms were overlaid.

Structural characterization

X-ray quality crystals of [Cu(xantphos)(bpy)][PF_6], [Cu(POP)(6-CF_3bpy)][PF_6]·1.3Et_2O·0.35H_2O, [Cu(xantphos)(6-CF_3bpy)][PF_6]·2Et_2O·1.5CH_2Cl_2, [Cu(POP)(4,4'-$(CF_3)_2$bpy)][PF_6]·0.5CH_2Cl_2, [Cu(xantphos)(4,4'-$(CF_3)_2$bpy)][PF_6] and [Cu(POP)(5,5'-$(CF_3)_2$bpy)][PF_6]·0.5Et_2O were grown by layering Et_2O over CH_2Cl_2 solutions of the compounds. ORTEP-style diagrams of the cations in the complexes are illustrated in Figure S4-S9 in the Supporting Information. We compare these structures to those published for [Cu(POP)(bpy)][PF_6]·$CHCl_3$,[43] [Cu(xantphos)(6-Mebpy)][PF_6]·CH_2Cl_2·0.4Et_2O and [Cu(xantphos)(6,6'-Me_2bpy)][PF_6].[16] Most of the complexes crystallize in the triclinic space group *P*−1, with the exception of [Cu(xantphos)(bpy)][PF_6] and [Cu(POP)(bpy)][PF_6]·$CHCl_3$ (both monoclinic $P2_1/n$) and [Cu(POP)(5,5'-$(CF_3)_2$bpy)][PF_6]·0.5Et_2O (monoclinic $P2_1/c$). The Cu–P and Cu–N bond distances show little variation and are found to be within 2.2159(11) and 2.2841(10) Å, and between 2.014(2) and 2.1523(19) Å, respectively. Whereas the N–Cu–N angles in all of the complexes stay very close to 80° (79.25(9) – 80.97(12)°), the P–Cu–P chelating angles range from 111.87(3) to 119.47(3)° for the complexes with POP and from 113.38(3) to 122.58(4)° for those with xantphos. In the case of the unsymmetrical [Cu(xantphos)(6-CF_3bpy)]$^+$ cation, the 6-CF_3bipy ligand is disordered over two orientations with occupancies of 0.75 (CF_3 group facing towards the xanthene "bowl") and 0.25 (CF_3 away from the xanthene "bowl"), respectively. The major conformation is identical to the one reported for the [Cu(xantphos)(6-Mebpy)]$^+$ cation.[16] In Table 1, the dihedral angle between the planes through N–Cu–N and P–Cu–P illustrates the distortion from the orthogonal coordination of the two ligands. Whereas [Cu(xantphos)(bpy)]$^+$ and [Cu(POP)(6-CF_3bpy)]$^+$ show the largest distortion (79.63 and 79.03°, respectively), the cations where the angle comes closest to 90° are [Cu(POP)(bpy)]$^+$ (88.52°) and [Cu(xantphos)(6-Mebpy)]$^+$ (87.92°). It appears that the dihedral angle is predominantly influenced by packing effects since no clear trend within the series of bpy ligands or upon exchange of POP and xantphos could be identified. The dihedral N–C–C–N angle defining the interring rotation of the bpy ligands varies from no torsion at all (0(1)°) for [Cu(POP)(4,4'-$(CF_3)_2$bpy)]$^+$ to a significant torsion of 20.5(2)° for [Cu(xantphos)(bpy)]$^+$. It is worth pointing out that the parameters for [Cu(xantphos)(6-CF_3bpy)]$^+$ are very close to those of [Cu(xantphos)(6-Mebpy)]$^+$, which is also illustrated in the structure overlay of the two cations in Figure 1.

Table 1. Comparison of structural parameters of the [Cu(P^P)(N^N)]$^+$ cations

Complex cation	P–Cu–P chelating angle / deg	N–Cu–N chelating angle / deg	Angle between P–Cu–P and N–Cu–N planes / deg	N–C–C–N torsion angle /deg
[Cu(POP)(bpy)]$^+$ [a]	119.47(3)	79.66(7)	88.52	–2.8(3)
[Cu(xantphos)(bpy)]$^+$	113.816(14)	79.32(5)	79.63	20.5(2)
[Cu(POP)(6-CF_3bpy)]$^+$	115.68(3)	80.35(10)	79.03	–18.3(4)
[Cu(xantphos)(6-CF_3bpy)]$^+$	113.55(3)	79.93(9)	86.61	0.6(4)
[Cu(POP)(5,5'-$(CF_3)_2$bpy)]$^+$	111.87(3)	79.25(9)	83.54	6.2(3)
[Cu(POP)(4,4'-$(CF_3)_2$bpy)]$^+$	113.02(5)	79.7(2)	85.83	0(1)
[Cu(xantphos)(4,4'-$(CF_3)_2$bpy)]$^+$	122.58(4)	79.63(13)	84.63	–17.2(5)
[Cu(xantphos)(6-Mebpy)]$^+$ [a]	113.38(3)	80.97(12)	87.92	1.7(5)
[Cu(xantphos)(6,6'-Me_2bpy)]$^+$ [a]	119.47(3)	79.66(9)	85.48	6.7(3)

[a] Published data for [Cu(POP)(bpy)][PF_6]·$CHCl_3$,[43] [Cu(xantphos)(6-Mebpy)][PF_6]·CH_2Cl_2·0.4Et_2O and [Cu(xantphos)(6,6'-Me_2bpy)][PF_6].[16]

Electrochemistry

Cyclic voltammetry was used to characterize the redox properties of the copper(I) cations (Table 2), and a representative cyclic voltammogram of [Cu(POP)(4,4'-$(CF_3)_2$bpy)][PF_6] is illustrated in Figure S10 in the Supporting Information. The lowest oxidation potential $E_{1/2}^{ox}$ (vs. Fc^+/Fc), which corresponds to a Cu^+/Cu^{2+} process, was observed at +0.72 and +0.76 V for the reference complexes [Cu(POP)(bpy)][PF_6] and [Cu(xantphos)(bpy)][PF_6], respectively. The substituted complexes present $E_{1/2}^{ox}$ values between +0.85 and +0.96 V, the highest value corresponding to [Cu(xantphos)(6,6'-Me_2-4,4'-$(CF_3)_2$bpy)][PF_6]. In comparison to the other complexes, which have potential separations (E_{pc} –

E_{pa}) between 100 and 180 mV, a significantly larger separation of 280 mV was recorded for [Cu(xantphos)(6,6'-Me_2-4,4'-$(CF_3)_2$bpy)][PF_6]. All complexes show a second oxidation peak at around +1.2 V which corresponds to an oxidation of the phosphane ligand (Figure S10). The second reduction peak at around +0.1 V is connected to this overoxidation; it is not visible when the scan is recorded only up to +1.0 V and only the first oxidation is covered. The complexes with CF_3-modified bpy ligands show reduction processes in addition to the typical oxidation process, which is in contrast to similar complexes with unsubstituted or alkyl-substituted bpy ligands. For the complexes with two CF_3 groups at the bipyridine, this reduction is located around –1.6 V, whereas for the complexes with mono-substituted 6-CF_3bpy this value is cathodically shifted being around –1.9 V.

Table 2. Cyclic voltammetric data for [Cu(N^N)(P^P)][PF_6] complexes referenced to internal Fc/Fc^+ = 0.V; CH_2Cl_2 (freshly distilled) solutions with [^{n}Bu_4N][PF_6] as supporting electrolyte and scan rate of 0.1 V s^{-1}. Processes are quasi-reversible.

Complex cation	$E_{1/2}^{ox}$ / V ($E_{pc} - E_{pa}$ / mV)	$E_{1/2}^{red}$ / V	ΔE /V
[Cu(POP)(bpy)]$^+$	+0.72 (110)	–	–
[Cu(xantphos)(bpy)]$^+$	+0.76 (110)	–	–
[Cu(POP)(6-CF_3bpy)]$^+$	+0.90 (170)	–1.94	2.84
[Cu(xantphos)(6-CF_3bpy)]$^+$	+0.92 (100)	–1.89	2.81
[Cu(POP)(5,5'-$(CF_3)_2$bpy)]$^+$	+0.89 (150)	–1.59	2.48
[Cu(xantphos)(5,5'-$(CF_3)_2$bpy)]$^+$	+0.94 (180)	–1.55	2.49
[Cu(POP)(4,4'-$(CF_3)_2$bpy)]$^+$	+0.88 (110)	–1.66	2.54
[Cu(xantphos)(4,4'-$(CF_3)_2$bpy)]$^+$	+0.92 (140)	–1.62	2.54
[Cu(xantphos)(6,6'-Me_2-4,4'-$(CF_3)_2$bpy)]$^+$	+0.96 (280)	–1.67	2.63
[Cu(xantphos)(6-Mebpy)]$^+$	+0.85 (100)	–	–
[Cu(xantphos)(6,6'Me_2bpy)]$^+$	+0.90 (150)	–	–

Ground state theoretical calculations

The geometry of all the [Cu(N^N)(P^P)]$^+$ cations in their ground electronic state S_0 was optimized at the DFT B3LYP/(6-31**G+LANL2DZ) level without imposing any symmetry restriction. Table S1 in the Supporting Information summarizes the values calculated for selected structural parameters. Calculations satisfactorily reproduce the distorted-tetrahedral configuration defined by the P^P and N^N ligands around the metal centre. The Cu−P bond lengths range from 2.368 to 2.433 Å, and the Cu−N bond lengths are between 2.152 and 2.276 Å, slightly overestimating (~0.1 Å) the reported X-ray values (Table 1). The N−Cu−N and P−Cu−P chelating angles present values between 75.38 and 77.26º and between 113.71 and 116.89º, respectively, and slightly underestimate the X-ray values. The angle between the planes through N–Cu–N and P–Cu–P illustrating the distortion from the orthogonal coordination of the two ligands is in a range between 85 and 90º, which is slightly narrower than that observed experimentally. It should be stressed that the theoretical geometries correspond to minimum-energy structures optimized in solution and do not take into account the packing forces acting in the solid state. These forces tend to reduce the coordination distances and to increase the chelating angles.

Figure 2 sketches the evolution of the energy calculated for the highest-occupied (HOMO) and lowest-unoccupied molecular orbital (LUMO) along the series of complexes studied. The topology of the molecular orbitals does not vary significantly along the series, so only the contour plots for the reference complexes [Cu(xantphos)(bpy)]$^+$ and [Cu(POP)(bpy)]$^+$ are shown in Figure 2. As previously found for this type of complexes,[16,43] the HOMO appears mainly centred on the metal with a small contribution from the phosphorus atoms, whereas the LUMO spreads over the bpy ligand. The energy of the HOMO slightly changes along both series being between –6.03 and –6.19 eV. This small change is an expected result, because the HOMO is centred on a region of the complex that remains structurally unchanged along the series, and is consistent with the small variation observed in the oxidation potentials of the substituted complexes (0.85–0.96 V). The attachment of CF_3 groups in 4,4'- and 5,5'-positions of the bpy causes a small stabilization of the HOMO (~0.1 eV) in good agreement with the higher oxidation potentials measured experimentally for these complexes (Table 2). Substitution of POP by xantphos also leads to a small stabilization of the HOMO (~0.05 eV) in accord with the slightly more positive oxidation potentials recorded for the xantphos derivatives.

As shown in Figure 2, the energy of the LUMO features larger changes because the attachment of electron-withdrawing CF_3 groups to the bpy ligand, where the LUMO is located, provokes the stabilization of this orbital. The addition of a single CF_3 group stabilizes the LUMO by around 0.2 eV, whereas the introduction of a second group causes an additional stabilization of 0.3 eV. The effect is slightly larger (0.07eV) when substitution is made in 5,5'-positions compared with 4,4'-positions. The introduction of electron-donor methyl groups in [Cu(xantphos)(N^N)]$^+$ is the contrary, inducing a small destabilization of the LUMO of 0.04 eV upon introduction of the first Me in passing from [Cu(xantphos)(bpy)]$^+$ to [Cu(xantphos)(6-Mebpy)]$^+$, and of 0.12 eV after introducing the second group in [Cu(xantphos)(6,6'-Me_2bpy)]$^+$. In the complex cation [Cu(xantphos)(6,6'-Me_2-4,4'-$(CF_3)_2$bpy)]$^+$, where both CF_3 and Me groups are added, the effects sum up and the LUMO appears 0.12 eV higher in energy than that of [Cu(xantphos)(4,4'-$(CF_3)_2$bpy)]$^+$. The trends predicted for the energy of the LUMO perfectly explain the reduction

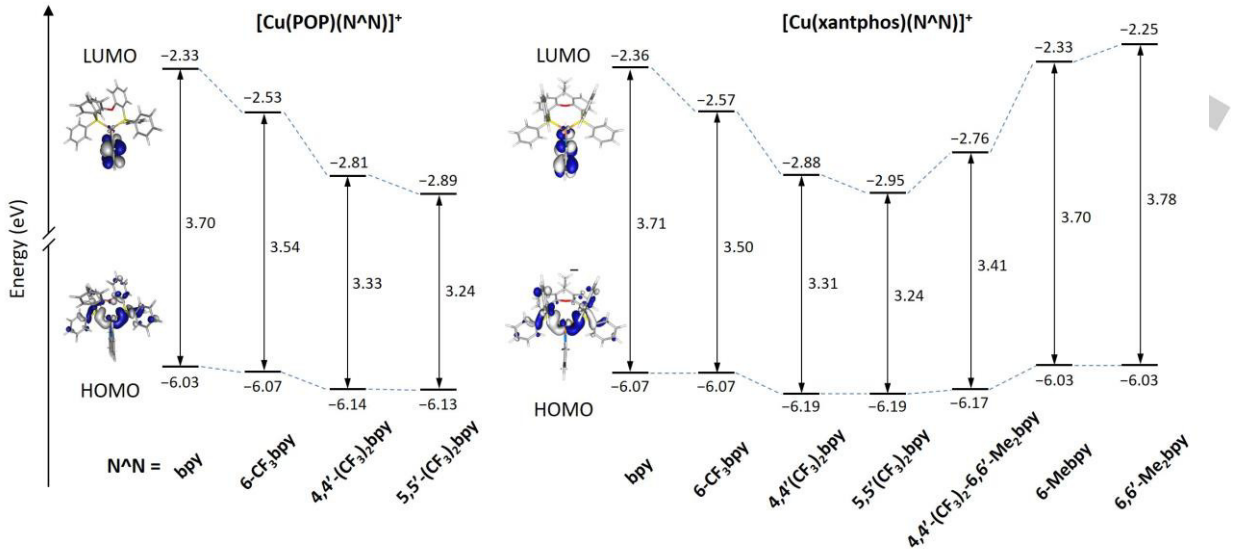

Figure 2. Energy diagram showing the energies calculated for the HOMO and LUMO of $[Cu(POP)(N^N)]^+$ and $[Cu(xantphos)(N^N)]^+$ complexes. The HOMO−LUMO energy gap is also quoted. Isovalue contour plots (±0.03 a.u.) are shown for the HOMO and LUMO of the reference complexes (N^N = bpy)

potentials discussed above for complexes including CF_3 groups (Table 2). In summary, complexes incorporating the 6-CF_3bpy ligand present a more negative potential than complexes bearing two CF_3 groups, and, within the latter, complexes substituted in 4,4'-positions show less negative potentials (by 0.07 V) than complexes substituted in 5,5'-positions due to the LUMO stabilization (0.07 eV) in passing from 4,4'- to 5,5'-substituted derivatives.

The smallest HOMO−LUMO energy gap (3.24 eV) is obtained for $[Cu(POP)(5,5'\text{-}(CF_3)_2bpy)]^+$ and $[Cu(xantphos)(5,5'\text{-}(CF_3)_2bpy)]^+$, followed by those calculated for $[Cu(xantphos)(4,4'\text{-}(CF_3)_2bpy)]^+$ (3.31 eV), $[Cu(POP)(4,4'\text{-}(CF_3)_2bpy)]^+$ (3.33 eV) and $[Cu(xantphos)(6,6'\text{-}Me_2\text{-}4,4'\text{-}(CF_3)_2bpy)]^+$ (3.41 eV). Complexes $[Cu(xantphos)(6\text{-}CF_3bpy)]^+$ and $[Cu(POP)(6\text{-}CF_3bpy)]^+$ with a single CF_3 group feature intermediate gap values of 3.50 and 3.54 eV, respectively, and the widest gaps correspond to unsubstituted or Me-substituted complexes with values in the 3.70–3.78 eV range (Figure 2). These trends correctly reproduce the relative order of the electrochemical gaps inferred from redox potentials (Table 1).

The HOMO−LUMO gap can be used, in a first approach, to predict the relative energy of the lowest-energy singlet (S_1) and triplet (T_1) electronic excited states, usually described by the HOMO→LUMO excitation in this type of complexes. On this basis, unsubstituted and Me-substituted complexes will be the ones featuring S_1 and T_1 at higher energies and bluer absorption/emission wavelengths. These wavelengths will shift to the red as CF_3 groups are added, the maximum shift being expected for complexes bearing the 5,5'-$(CF_3)_2$bpy ligand which show the lowest HOMO−LUMO gap. However, it has to be considered that, although this energy ordering may be correct at the ground state optimum geometries (Franck-Condon region), geometry relaxation of the excited state cannot be ignored when dealing with emission processes as discussed below.

Photophysical properties and excited states

The UV-Vis absorption spectra of CH_2Cl_2 solutions of the $[Cu(P^P)(bpy)][PF_6]$ complexes show, in addition to ligand-centred bands around 280 nm, very broad bands in the region between 350 and 480 nm, that are assigned to MLCT transitions (Figure 3, Table 3 and Figure S11). For a given bpy, the MLCT absorption bands of the respective complexes with POP and xantphos are very similar in both the value of λ_{max} and the shape of the band. This suggests that the energy difference between the HOMO and the LUMO is mainly determined by the *N,N'*-chelating ligand in accord with the DFT results discussed above. Since the HOMO is fully located on the {Cu(P^P)} domain and is similar for all the complexes, we can directly observe the effect of the substitution pattern in the bpy ligand on the HOMO−LUMO gap from the MLCT maxima. Because of the similarity of the absorption spectra between the respective

pairs of POP and xantphos complexes, we focus only on the series of xantphos complexes and compare this group to [Cu(xantphos)(bpy)][PF_6] with unsubstituted bpy as the model compound. All of the complexes with one or more CF_3 groups at the bpy show a redshift with respect to [Cu(xantphos)(bpy)][PF_6], corroborating the energy lowering of the LUMO and the smaller HOMO–LUMO gap predicted theoretically. The largest redshift of 400 meV (54 nm) is observed for [Cu(xantphos)(5,5'-$(CF_3)_2$bpy)][PF_6] and the smallest comes to 153 meV (19 nm) for [Cu(xantphos)(6-CF_3bpy)][PF_6] (see also Table S2), in perfect agreement with the HOMO−LUMO gaps calculated for these complexes. Substitution of the bpy ligand with one or two methyl groups in the 6-positions results in a blueshift of 17 and 69 meV (2 and 8 nm) for the respective complex, in accord with the destabilization of the LUMO and the increase of the HOMO–LUMO distance.

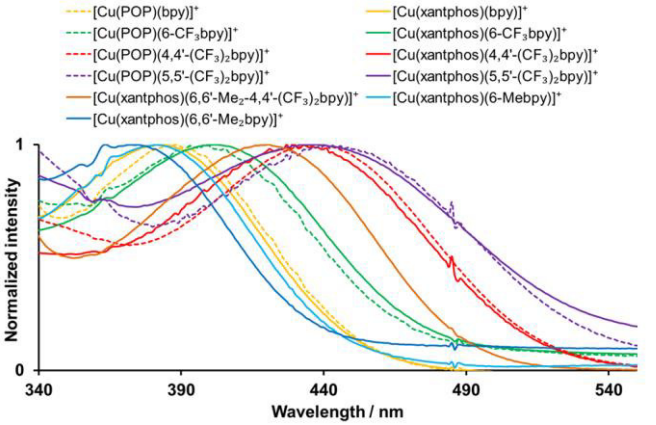

Figure 3. Expansion of the lowest-energy MLCT region of the normalized solution absorption spectra of the [Cu(P^P)(N^N)][PF_6] complexes (CH_2Cl_2, 2.5 × 10^{-5} mol dm^{-3}). For the full spectrum see Figure S10, and for a comparison of the maxima, see Table S2.

To gain a deeper insight into the nature of the electronic excited states giving rise to the absorption spectra, singlet (S_n) and triplet (T_n) excited states were calculated for all the complexes using the time dependent DFT (TD-DFT) approach. Table 4 summarizes the vertical excitation energies computed for the lowest-energy singlet (S_1) and triplet (T_1) states at the optimized geometry of S_0. For all the complexes, both S_1 and T_1 result from the HOMO→LUMO monoexcitation with a contribution always exceeding 90%. This supports the MLCT

Table 3. Absorption and emission maxima, photoluminescence quantum yields (PLQY) and lifetimes ($\tau_{1/2}$) for [Cu(P^P)(N^N)][PF_6] complexes.

Complex cation	CH_2Cl_2 solution[a]					Powder[b]			Me-THF at 77 K	
	UV-Vis MLCT λ^{max} / nm	λ_{exc} / nm	λ_{em}^{max} / nm	PLQY (non-deaerated / deaerated) / %	$\tau_{1/2}$ (non-deaerated / deaerated) / ns	λ_{em}^{max} / nm	PLQY / %	$\tau_{1/2}$ / µs	λ_{em}^{max} / nm	$\tau_{1/2}$ / µs
[Cu(POP)(bpy)]+ [e]	388	388	618, 649[a]	0.4/0.5	43/46	581[c]	3.0[c]	1.5[c]	610	16
[Cu(xantphos)(bpy)]+	383	390	620, 650[a]	0.5/0.5	75/104	587[c]	1.7[c]	1.3[c]	613	11
[Cu(POP)(6-CF_3bpy)]+	399	380	618, 646[a]	0.7/0.7	95/119	575[c]	6.2[c]	2.9[c]	610	45
[Cu(xantphos)(6-CF_3bpy)]+	402	380	622, 647[a]	0.6/0.6	84/99	581[c]	11.1[c]	2.9[c]	595	31
[Cu(POP)(5,5'-$(CF_3)_2$bpy)]+	441	-	-	-/-	-/-	648	0.5[d]	0.185[d]	656	––
[Cu(xantphos)(5,5'-$(CF_3)_2$bpy)]+	437	-	-	-/-	-/-	647	0.5[d]	0.251[d]	646	––
[Cu(POP)(4,4'-$(CF_3)_2$bpy)]+	436	430	667, 697[b] (very weak)	-/-	-/-	664[d]	0.5[d]	0.096[d]	650	3
[Cu(xantphos)(4,4'-$(CF_3)_2$bpy)]+	433	430	667, 705[b] (very weak)	-/-	-/-	632[d]	0.9[d]	0.579[d]	652	5
[Cu(xantphos)(6,6'-Me_2-4,4'-$(CF_3)_2$bpy)]+	421	400	612, 637[a]	0.5/0.5	39/39	517[c]	50.3[c]	12[c]	604	42
[Cu(xantphos)(6-Mebpy)]+	381	379	605, 635[a]	1.0/1.8	27/78	547[c]	33.8	9.6[c]	567	46
[Cu(xantphos)(6,6'-Me_2bpy)]+	375	379	606, 635[a]	1.6/10.0	451/3406	539[c]	37.3[c]	11.4[c]	551	88

[a]Solution concentration = 2.5 × 10^{-5} mol dm^{-3}. [b]Solution concentration = 5.0 × 10^{-5} mol dm^{-3}. [c]λ_{exc} = 365 nm. [d]λ_{xc} = 405 nm. Deaeration was by flow of argon. [e][Cu(POP)(bpy)][PF_6] was prepared according to the literature (ref. 43) but measurements were made for the present work.

character of the S_1 and T_1 states since the HOMO→LUMO excitation implies an electron transfer from the {Cu(P^P)} environment to the bpy ligand (see Figure 2). The oscillator strength (*f*) calculated for the electronic transition to the S_1 state lies between 0.06 and 0.13 (Table 4), the next singlet excited state with *f* values higher than 0.01 being around 0.9 eV above S_1. Excited states with high oscillator strengths (~0.40), centred on the ligands, are found around 285 nm (~4.35 eV) in good agreement with the intense bands observed in this region in the absorption spectrum. These results identify the S_1 state as responsible of the low-energy absorption band observed in the spectra in the 350–500 nm region (Figures 3 and S11). The vertical excitation energies calculated for S_1 (Table 4) are in good agreement with the absorption maxima correctly reproducing the experimental trends (Table 3). Complexes with Me substituents feature S_1 energies blue shifted with respect to the reference complexes, whereas S_1 states of complexes with one or two CF_3 groups appears gradually shifted to the red. The lowest excitation energy is predicted for [Cu(POP)(5,5'-$(CF_3)_2$bpy)]$^+$ (2.65 eV, 468 nm) and [Cu(xantphos)(5,5'-$(CF_3)_2$bpy)]$^+$ (2.66 eV, 467 nm) in very good agreement with experimental λ^{max} values (441 and 437 nm, respectively). The [Cu(xantphos)(6,6'-Me_2-4,4'-$(CF_3)_2$bpy)]$^+$ complex presents an excitation energy (2.80 eV, 442 nm) lower than the [Cu(xantphos)(4,4'-$(CF_3)_2$bpy)]$^+$ complex (2.71 eV, 457 nm) due to the presence of methyl groups. The energy ordering of the S_1 states also agrees with that expected from the MO analysis and the electrochemical gaps, and corroborates that light absorption, which takes place around the ground state optimal geometry, can be explained based on electronic factors without considering the flattening effects that the HOMO→LUMO excitation has on the molecular geometry of the excited states as explained below. The T_1 states are computed 0.16–0.20 eV below S_1 (Table 4) and the vertical excitation energies to T_1 follow the same trends discussed above for S_1.

Table 4. Vertical excitation energies (*E*) calculated at the TD-DFT B3LYP/(6-31G**+LANL2DZ) level for the lowest singlet (S_1) and triplet (T_1) excited states of complexes [Cu(N^N)(P^P)]$^+$ in CH_2Cl_2 solution. S_0→S_1 oscillator strengths (*f*) are given within parentheses.

Complex cation	S_1	T_1
	E (eV/nm) (*f*)	*E* (eV)
[Cu(POP)(bpy)]$^+$	3.089 / 401 (0.08)	2.906
[Cu(xantphos)(bpy)]$^+$	3.085 / 402 (0.09)	2.893
[Cu(POP)(6-CF_3bpy)]$^+$	2.930 / 423 (0.06)	2.772
[Cu(xantphos)(6-CF_3bpy)]$^+$	2.874 / 431 (0.07)	2.704
[Cu(POP)(5,5'-$(CF_3)_2$bpy)]$^+$	2.647 / 468 (0.06)	2.484
[Cu(xantphos)(5,5'-$(CF_3)_2$bpy)]$^+$	2.655 / 467 (0.07)	2.483
[Cu(POP)(4,4'-$(CF_3)_2$bpy)]$^+$	2.739 / 453 (0.09)	2.531
[Cu(xantphos)(4,4'-$(CF_3)_2$bpy)]$^+$	2.713 / 457 (0.13)	2.512
[Cu(xantphos)(6,6'-$Me_2$4,4'-$(CF_3)_2$-bpy)]$^+$	2.802 / 442 (0.11)	2.639
[Cu(xantphos)(6-Mebpy)]$^+$	3.088 / 402 (0.09)	2.896
[Cu(xantphos)(6,6'-Me_2bpy)]$^+$	3.145 / 394 (0.06)	2.985

Figure 4 illustrates the normalized solution emission spectra of the [Cu(P^P)(bpy)][PF_6] complexes in CH_2Cl_2 upon excitation in the region of their respective MLCT band; values of λ_{em}^{max} are presented in Table 3. Due to their poor emissive behaviour, the spectra of the complexes with 4,4'-$(CF_3)_2$bpy are not included in Figure 3. The complexes with 5,5'-$(CF_3)_2$bpy were non-emissive in solution. With emission maxima between 605 and 705 nm, the complexes are yellow to red emitters in solution. The bands are structured with two maxima, and as in the absorption spectra, the emission bands are only slightly affected by a change from POP to xantphos for a given N^N ligand. In contrast to the absorption spectra where a redshift was observed, the emission of complexes with 6-CF_3bpy remains almost unchanged with respect to the unsubstituted complexes and that of complex with 6,6'-Me_2-4,4'-$(CF_3)_2$bpy is slightly blueshifted. The largest blueshift is recorded for the complexes with 6-Mebpy and 6,6'-Me_2bpy.

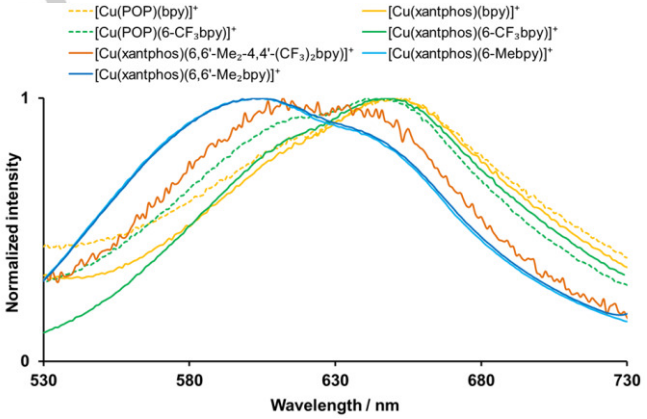

Figure 4. Solution emission spectra of [Cu(P^P)(N^N)][PF_6] complexes (CH_2Cl_2, 2.5 × 10^{-5} mol dm^{-3}). For λ_{exc} see Table 3.

The solid-state (powder) emission spectra for all complexes are shown in Figure 5. The only complexes where the emission is redshifted with respect to the spectra of the complexes with unsubstituted bpy are those with 5,5'-$(CF_3)_2$bpy and 4,4'-$(CF_3)_2$bpy. The redshift is more pronounced for the complexes with POP, being 83 nm for [Cu(POP)(4,4'-$(CF_3)_2$bpy)][PF_6] and 67 nm for [Cu(POP)(5,5'-$(CF_3)_2$bpy)][PF_6] (Table 3). The emission maxima of [Cu(POP)(6-CF_3bpy)][PF_6] and [Cu(xantphos)(6-CF_3bpy)][PF_6] both are shifted 6 nm to shorter wavelengths. In contrast to the solution emission spectra, where complexes with 6-Mebpy and 6,6'-Me_2bpy exhibit the largest shift to shorter wavelengths, the complex with the most blueshifted (70 nm) solid state emission is [Cu(xantphos)(6,6'-Me_2-4,4'-$(CF_3)_2$bpy)][PF_6].

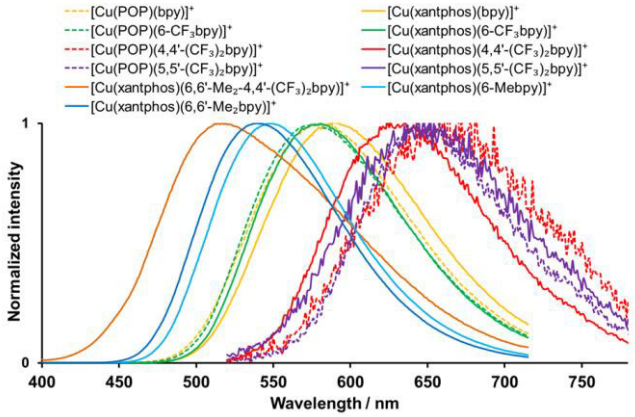

Figure 5. Normalized powder emission spectra of [Cu(P^P)(N^N)][PF_6] complexes. For λ_{exc} see Table 3.

In order to visualize the solid state emission, photographs of the powder samples of [Cu(xantphos)(N^N)][PF_6] under normal and under UV light (λ_{exc} = 365 nm) are shown in Figure 6. Solid [Cu(xantphos)(5,5'-$(CF_3)_2$bpy)][PF_6] appears nearly non-emissive, (consistent with the low solid-state PLQY, Table 3). Overall, the photophysical properties of both POP and xantphos complexes with 5,5'-$(CF_3)_2$bpy are impaired with respect to their respective reference complexes with naked bpy, and we have to conclude that a modification with CF_3 groups in this position is not beneficial for emissive applications. With PLQY = 0.9%, the weak red emission of solid [Cu(xantphos)(4,4'-$(CF_3)_2$bpy)][PF_6] is just visible by eye (Figure 6). However, even for a red emitter this value is too low to qualify this complex as luminophore, and as a result the 4,4'-substitution of the bpy ligand with CF_3 groups appears detrimental. In contrast, [Cu(POP)(6-CF_3bpy)][PF_6] and [Cu(xantphos)(6-CF_3bpy)][PF_6] have increased PLQY and lifetime values, both in solution and in powder, when compared to their respective reference complexes [Cu(POP)(bpy)][PF_6] and [Cu(xantphos)(bpy)][PF_6]. Whereas the powder PLQY is only doubled for [Cu(POP)(6-CF_3bpy)][PF_6] (6.2% in comparison to 3.0% for the model compound), the value is more than six times higher for [Cu(xantphos)(6-CF_3bpy)][PF_6] (11.1% versus 1.7%). Although the CF_3 group in the 6-position of the bpy appears to be beneficial for the photophysical properties, it is less efficient than a methyl group in this position (PLQY 9.5% for [Cu(POP)(6-Mebpy)][PF_6],[15] and 33.8% for [Cu(xantphos)(6-Mebpy)][PF_6]).[16]

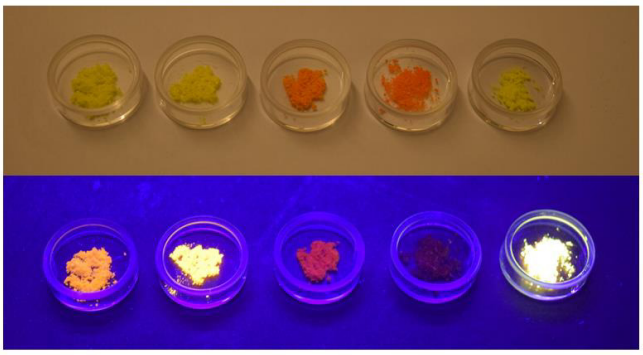

Figure 6. Powder samples of [Cu(xantphos)(N^N)][PF_6] complexes under normal light (top) and under UV light (λ_{exc} = 365 nm, bottom). From left to right: [Cu(xantphos)(bpy)][PF_6], [Cu(xantphos)(6-CF_3bpy)][PF_6], [Cu(xantphos)(4,4'-$(CF_3)_2$bpy)][PF_6], [Cu(xantphos)(5,5'-$(CF_3)_2$bpy)][PF_6] and [Cu(xantphos)(6,6'-Me_2-4,4'-$(CF_3)_2$bpy][PF_6].

The highest powder PLQY was measured for [Cu(xantphos)(6,6'-Me_2-4,4'-$(CF_3)_2$bpy)][PF_6] (PLQY = 50.3%). Due to this high quantum yield, the emission in the photograph in Figure 6 appears to be almost white, whereas according to the CIE coordinates (0.449, 0.532, see also Figure S12), the colour of the emitted light is between the green and the yellow region. For all the complexes, the emission maxima are blueshifted on going from solution to solid state, which has been observed in earlier studies of similar compounds.[16] In general, the emissive properties of the complexes are enhanced in solid state compared to solution. The only complex with a noteworthy quantum yield in solution is [Cu(xantphos)(6,6'-Me_2bpy)][PF_6] with 1.6 versus 10.0% for non-deaerated and deaerated solutions. The higher solution quantum yield is usually attributed to the steric protection of the copper(I) centre by the methyl groups attached to the bpy, which also help to avoid tetrahedron flattening. It is therefore surprising that the PLQY of [Cu(xantphos)(6,6'-Me_2-4,4'-$(CF_3)_2$bpy)][PF_6] in solution (0.5%, Table 3) is two orders of magnitude lower than in powder (50.3%) and also significantly lower than the PLQY of [Cu(xantphos)(6,6'-Me_2bpy)][PF_6]. It appears that although the methyl groups should retain a beneficial effect, this is cancelled out in solution by the CF_3 groups in 4,4'-positions, which seem to offer additional non-radiative pathways in solution and thus quench the excited state. The effect on the photophysical properties of substitution with CF_3 groups in the 4,4'-positions of the bpy is therefore rather ambiguous. Whereas in solution the CF_3 groups lead to a weakening and redshift of the emission, in solid state the emission is only redshifted and less intense for [Cu(POP)(4,4'-$(CF_3)_2$bpy)][PF_6] and [Cu(xantphos)(4,4'-$(CF_3)_2$bpy)][PF_6], but for [Cu(xantphos)(6,6'-Me_2-4,4'-$(CF_3)_2$bpy)][PF_6] it is blueshifted and increased even in comparison to [Cu(xantphos)(6,6'-Me_2bpy)][PF_6].

In order to probe the emission processes further, low temperature lifetime and emission spectra of the complexes were recorded. Solutions of the compounds in Me-THF form a glass at 77 K and this approximates to the situation in the solid state. The emission spectra of the complexes with xantphos (with the exception of [Cu(xantphos)(5,5'-$(CF_3)_2$bpy)][PF_6], see above) are illustrated in Figure 7 and the maxima and lifetime values are summarized in Table 3 and compared to the room temperature values of the powder (Table S4).

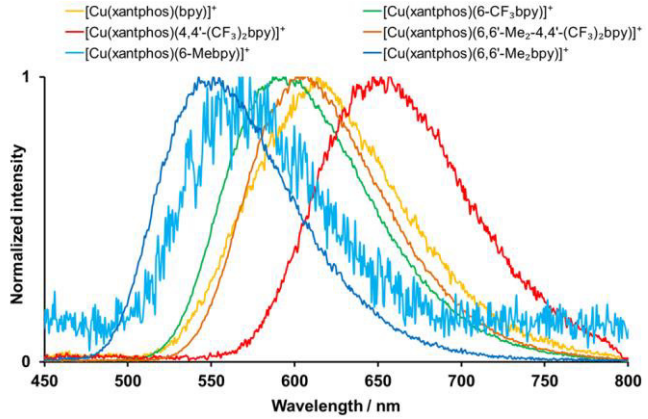

Figure 7. Normalized emission spectra of [Cu(P^P)(N^N)][PF_6] complexes in Me-THF at 77 K, λ_{exc} = 410 nm.

The excited state lifetimes are found to be lengthened for all the complexes, which indicates that they are, as confirmed for similar compounds, TADF emitters.[11, 32, 33] TADF describes the emission from the singlet excited state S_1 which has been (re)populated from the long-lived triplet excited state T_1 by making use of the available thermal energy k_BT. This process is favourable for the application of a molecule as an emitter for two reasons. First, the repopulation of the singlet excited state allows the harvesting of, in theory, 100% of all photons, which equals a PLQY of 100%, respectively all excitons when the situation in the electroluminescent device is considered. Second, TADF processes lead to a shortening of the excited state lifetime. Phosphorescence from T_1 can be a very slow process in comparison to fluorescence from S_1 and is therefore not ideal when it comes to the application of the molecule in light-emitting devices.

At 77 K, TADF is reduced or even completely impeded, depending on the energy gap between T_1 and S_1. As a consequence, the contribution of the slower phosphorescence to the emission is increased, which can be directly evidenced by the significant elogation of the lifetime. This is up to 88 µs for [Cu(xantphos)(6,6'-Me_2bpy)][PF_6], which is an almost eight-fold increase with respect to powder at room temperature (11.4 µs). For [Cu(xantphos)(6,6'-Me_2-4,4'-$(CF_3)_2$bpy)][PF_6], which has a powder lifetime (12.0 µs) similar to [Cu(xantphos)(6,6'-Me_2bpy)][PF_6], the lifetime at 77 K is only less than four-fold increased to 42 µs (Table S4). This could be either due to a shorter phosphorescence lifetime or a smaller energy gap between the triplet and singlet excited states. This energy gap can also be inferred by comparing the powder emission maxima at room temperature and the emission in the frozen Me-THF glass at 77 K. As with lower temperature the proportion of triplet emission increases, the emission maxima should normally be moved to longer wavelengths. This is the case for all the complexes reported here, except for [Cu(xantphos)(5,5'-$(CF_3)_2$bpy)][PF_6], where the emission maximum is basically unchanged, and [Cu(POP)(4,4'-$(CF_3)_2$bpy)][PF_6], with a blueshift of 14 nm (40 meV). The redshift for the other complexes indicates that at room temperature, the majority of the emission stems from the singlet state. The largest redshift is observed for [Cu(xantphos)(6,6'-Me_2-4,4'-$(CF_3)_2$bpy)][PF_6] (345 meV, 87 nm).

To understand the emission processes more thoroughly, the effects of geometry relaxation on the lowest-energy S_1 and T_1 states were investigated theoretically. The geometries of the T_1 states were first optimized at the spin-unrestricted UB3LYP level and they feature relevant differences with respect to those calculated for the ground state S_0. As explained above, T_1 originates in the HOMO→LUMO excitation and implies a charge transfer from a *d* orbital of the Cu atom to a molecular orbital centred on the bpy moiety of the complexes. The metal centre is hence partially oxidized and tends to adopt a squared-planar coordination sphere, typical of four-fold coordinated d^9 copper complexes, instead of the tetrahedral coordination preferred by d^{10} copper complexes. This tendency is clearly illustrated by the angle formed by the N–Cu–N and P–Cu–P planes that changes from values close to 90° in S_0, typical of a tetrahedral coordination in which both ligands are orthogonal, to values as low as 58° in T_1 (Table S1). The presence of substituents in 6,6'-positions hinders the bending of the bpy moiety and limits the flattening distortion of the tetrahedron in T_1. Thus, complexes with one of those positions substituted by a Me or a CF_3 present an angle between the planes through N–Cu–N and P–Cu–P between 70.3 and 71.4°, which is significantly larger than for complexes with no substituent in the 6,6'-positions (~50°). The complexes [Cu(xantphos)(6,6'-Me_2bpy)]$^+$ and [Cu(xantphos)(6,6'-Me_2-4,4'-$(CF_3)_2$bpy]$^+$ with both positions substituted by Me groups present even less flattened structures with angles of 74.3 and 74.4°, respectively (Table S1).

The flattening of the complex structure is accompanied by a large stabilization of the T_1 state that, for complexes with no substituent in 6,6'-positions of the bpy, amounts to 0.8–0.9 eV with respect to the energies at the equilibrium geometry of S_0. This relaxation energy decreases to ~0.6 eV for [Cu(xantphos)(6,6'-Me_2bpy)]$^+$ and [Cu(xantphos)(6,6'-Me_2-4,4'-$(CF_3)_2$bpy)]$^+$ due to the hindering effect of the Me groups that limits the geometrical relaxation. Therefore, the energy position of the T_1 state relative to S_0 not only depends on the electron-donating or electron-withdrawing character of the substituent groups but also on the positions on the ligands where they are introduced due to the purely structural effects they induce. This justifies the fact that the emission maxima recorded for the family of complexes studied does not follow the trends observed for absorption (see above), and also explains that the TD-DFT energies computed for T_1 (Table 4) do not

reproduce the experimental trends observed in the emission spectra because they are based only on electronic considerations (they are calculated at the geometry of S_0) with no geometry relaxation. When the emission energies from T_1 are determined as the vertical energy difference between the T_1 and S_0 states at the T_1 relaxed geometry, they fully support the experimental trends observed at 77 K where TADF is suppressed and emission mainly results from phosphorescence from T_1. $[Cu(POP)(bpy)]^+$, $[Cu(xantphos)(bpy)]^+$ and $[Cu(POP)(6\text{-}CF_3bpy)]^+$ are calculated to emit at very similar wavelengths (730, 737 and 735 nm, respectively) whereas the emission of $[Cu(xantphos)(6\text{-}CF_3bpy)]^+$ is blueshifted (691 nm) and that of complexes with 4,4'- and 5,5'-$(CF_3)_2$bpy is redshifted (1.34–1.41 eV, 920–875 nm). Complex $[Cu(xantphos)(6,6'\text{-}Me_2\text{4,4'-}(CF_3)_2bpy)]^+$, whose absorption wavelength and S_1 energy were shifted to the red with respect to $[Cu(xantphos)(bpy)]^+$, features a T_1 energy (1.80 eV, 688 nm) and a emission maximum at 77 K (2.05 eV, 604 nm) bluer than the reference complex (1.68 and 2.01 eV, respectively). The theoretical values underestimate the experimental emission energies (Table 3) because they are calculated at the fully relaxed geometry of T_1 whereas this relaxation is expected to be severely restricted in the glass at 77 K. As a conclusion, the emission energies of $[Cu(P\text{^}P)(bpy)]^+$ complexes with substituents at 6,6'-positions of the bpy do not correspond to those expected from electronic considerations (MO analysis or electrochemical and optical absorption gaps) because 6,6'-substitution hinders the tetrahedron flattening associated to T_1 relaxation and limits its stabilization. The T_1 state therefore stays at higher energies than in complexes with no substituent at 6,6'-positions, thus leading to a bluer emission than expected.

Finally, the S_1 and T_1 states were fully optimized using the TD-DFT approach to evaluate the adiabatic energy difference ($\Delta E(S_1 - T_1)$) between these states at their respective minimum-energy geometries. It should be mentioned that the complexes in the S_1 state undergo flattening distortions of the tetrahedral structure similar to those discussed above for T_1 because both states originate in the HOMO→LUMO excitation. The values of $\Delta E(S_1 - T_1)$ were computed for a set of representative complexe cations ($[Cu(POP)(bpy)]^+$, $[Cu(xantphos)(bpy)]^+$, $[Cu(POP)(4,4'\text{-}(CF_3)_2bpy)]^+$, $[Cu(xantphos)(4,4'\text{-}(CF_3)_2bpy)]^+$ and $[Cu(xantphos)(6,6'\text{-}Me_2\text{-}4,4'\text{-}(CF_3)_2bpy)]^+$) and in all cases are found in the 0.12–0.20 eV range. These values are significantly lower than the 0.37 eV (3000 cm^{-1}) proposed by Yersin and coworkers.[12,34] to allow the population of S_1 from T_1 at room temperature and, therefore, contribution from S_1 to the emission by TADF should be expected at room temperature. The ΔE values calculated for the reference complexes $[Cu(POP)(bpy)]^+$ and $[Cu(xantphos)(bpy)]^+$ are 0.177 and 0.185 eV, respectively, slightly above the ideal value of 0.12 eV for TADF being exploited in electroluminescent devices, but still in the range of other Cu complexes for which TADF has been reported previously. The inclusion of CF_3 groups in the 4,4'-positions has little effect on ΔE that slightly increases for $[Cu(POP)(4,4'\text{-}(CF_3)_2bpy)]^+$ (0.189 eV) and $[Cu(xantphos)(4,4'\text{-}(CF_3)_2bpy)]^+$ (0.197 eV). However, the addition of Me groups in 6,6'-positions favours a decrease in ΔE, and the value of 0.110 eV computed for $[Cu(xantphos)(6,6'\text{-}Me_2\text{-}4,4'\text{-}(CF_3)_2bpy)]^+$ points to this complex as the one expected to feature TADF at lower temperatures.

Electroluminescent devices

Light-emitting electrochemical cells (LECs) were fabricated with complexes $[Cu(POP)(6\text{-}CF_3bpy)][PF_6]$, $[Cu(xantphos)(6\text{-}CF_3bpy)][PF_6]$ and $[Cu(xantphos)(6,6'\text{-}Me_2\text{-}4,4'\text{-}(CF_3)_2bpy)][PF_6]$ because only these CF_3-substituted complexes show significant PLQY values in powder (6.2, 11.1 and 50.3%, respectively, Table 3). The LECs were fabricated in a double layer architecture, by depositing a poly(3,4-ethylenedioxythiophene):poly(styrenesulfonate) (PEDOT:PSS) layer and the emissive layer sandwiched between indium tin oxide (ITO) and aluminium electrodes. The active layer contained the copper(I) complex mixed with the ionic liquid (IL) 1-ethyl-3-methylimidazolium hexafluoridophosphate [Emim][PF_6] at a 4:1 (Cu complex:IL) molar ratio. The IL was added to shorten the turn-on time of the LEC by increasing the

Table 5. Performance of ITO/PEDOT:PSS/$[Cu(P\text{^}P)\text{^}N\text{^}N)][PF_6]$:[Emim][$PF_6$] 4:1 molar ratio/Al LECs measured using a pulsed current driving (average current density 100 A m^{-2}, 1 kHz, 50% duty cycle, block wave).

Complex	t_{on} [a] / min	Lum_0 [b] /cd m^{-2}	Lum_{max} [c] /cd m^{-2}	$t_{1/2}$ [d] / h	EQE_{max} [e] / %	PCE_{max} [f] /lm W^{-1}	$Efficacy_{max}$ / cd A^{-1}	λ_{EL}^{max} / nm
$[Cu(POP)(6\text{-}CF_3bpy)][PF_6]$	22	39	65	8.5	0.4	0.2	0.7	595
$[Cu(xantphos)(6\text{-}CF_3bpy)][PF_6]$	137	5	109	31.0	0.5	0.4	1.1	589
$[Cu(xantphos)(6,6'\text{-}Me_2\text{-}4,4'\text{-}(CF_3)_2bpy)][PF_6]$	8	59	131	2.0	0.6	0.4	1.3	593

[a] Time to reach the maximum luminance. [b] Initial luminance. [c] Maximum luminance reached. [d] Time to reach one-half of the maximum luminance. [e] Maximum external quantum efficiency reached. [f] Maximum power conversion efficiency reached.

concentration of ionic species and thereby the ionic mobility in the light-emitting layer.[35,36] To enhance the device response and lifetime, LECs were operated using a block-wave pulsed current of 100 A m^{-2} (1 kHz and 50% duty). The LEC characteristics are summarized in Table 5 and the luminance and average voltage versus time plots are depicted in Figure 8 and S13, respectively.

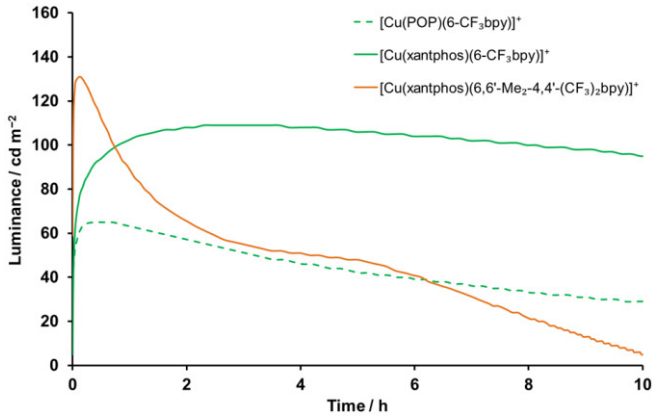

Figure 8. Luminance versus time characteristics for ITO/PEDOT:PSS/[Cu(P^P)^N^N)][PF_6]:[Emim][PF_6] 4:1/Al LECs operated at pulsed current (average current density 100 A m^{-2}, 1 kHz, 50% duty cycle, block wave).

All three LECs have orange electroluminescence (Figure S14) with maximum emission in the 589–595 nm range and a shoulder around 650 nm similar to that observed for the spectra in solution (Figure 4). The emission maxima are slightly blue-shifted with respect to the photoluminescence spectra recorded for the active thin film (Cu complex:IL at a 4:1 molar ratio) with maxima in the 596–606 nm range (Figure S15). It should be noted that the PLQY significantly decreases in passing from powder to the active thin film composition for both [Cu(POP)(6-CF_3bpy)][PF_6] (PLQY = 4%), [Cu(xantphos)(6-CF_3bpy)][PF_6] (5%) and especially for [Cu(xantphos)(6,6'-Me_2-4,4'-$(CF_3)_2$bpy)][PF_6] (16%). This decrease in PLQY has been observed for Cu-based emitters and is related to the different environment surrounding the complex.[16,18] In thin amorphous films, the structural rearrangement of the complex upon excitation is less hindered than in powder which leads to poorer emissive properties. The presence of the CF_3 group results in a slight red-shift of the electroluminescence when comparing to the analogous complexes substituted with methyl groups [Cu(POP)(6-Mebpy)][PF_6] (λ_{EL}^{max} = 574 nm)[15] and [Cu(xantphos)(6-Mebpy)][PF_6] (λ_{EL}^{max} = 583 nm).[16]

Once biased, the electrical resistance of the device is reduced due to the presence of ions in agreement with the operational mechanism established for LECs.[37] Hence, the luminance is initially low and rises up gradually (Figure 8). The time needed to achieve the maximum luminance (t_{on}) is an indicator of the device response, and the operational lifetime ($t_{1/2}$) is usually defined as the time to reach one-half of the maximum luminance. The LEC containing [Cu(xantphos)(6,6'-Me_2-4,4'-$(CF_3)_2$bpy)][PF_6] has the shortest t_{on} (8 min) and $t_{1/2}$ (2h). When the active material is [Cu(POP)(6-CF_3bpy)][PF_6] or [Cu(xantphos)(6-CF_3bpy)][PF_6], the device response is slower with t_{on} values of 22 and 137 min, respectively. Following this trend, the respective LEC lifetimes are 8.5 and 31 hours when using these two complexes (Table 5). These values indicate a clear link between the t_{on} and $t_{1/2}$; the faster the t_{on} the shorter is $t_{1/2}$. On the one hand, the LEC with [Cu(xantphos)(6-CF_3bpy)][PF_6] (with shorter t_{on} and $t_{1/2}$) rapidly reaches its minimum voltage (~4.8 V) which then increases over time (see Figure S13). This voltage profile is indicative of a fast ionic mobility at the beginning of operation. However, over time, charge transport is hindered as evidenced by an increasing resistance during operation. On the other hand, the LEC with [Cu(xantphos)(6-CF_3bpy)][PF_6] shows a voltage profile which decreases over time during device operation.The luminance as well as the efficacy of the LECs are in agreement with the trend obtained for the PLQY in thin film. [Cu(xantphos)(6,6'-Me_2-4,4'-$(CF_3)_2$bpy)][PF_6] with a PLQY of 16% achieves a maximum luminance of 131 cd m^{-2} and a maximum efficacy of 1.3 cd A^{-1}). [Cu(POP)(6-CF_3bpy)][PF_6] with a PLQY of 4% achieves 65 cd m^{-2} and 0.7 cd A^{-1} in the LEC. However, the LEC using [Cu(xantphos)(6-CF_3bpy)][PF_6], with a PLQY of 5% in thin film similar to [Cu(POP)(6-CF_3bpy)][PF_6], exhibits a higher performance with a luminance (109 cd m^{-2}) and a efficacy (1.1 cd A^{-1}) similar to [Cu(xantphos)(6,6'-Me_2-4,4'-$(CF_3)_2$bpy)][PF_6]. Considering the PLQY values in thin film and a typical outcoupling of 20%, the theoretical maximum external quantum efficiency (EQE_{max}) predicted for LECs with [Cu(xantphos)(6-CF_3bpy)][PF_6] and [Cu(xantphos)(6,6'-Me_2-4,4'-$(CF_3)_2$bpy)][PF6] when all injected electrons and holes combine is 1 and 3.2%, respectively, whereas the experimental values are 0.5 and 0.6% (Table 5). The smaller difference found between the theoretical and the experimental value for the LEC with [Cu(xantphos)(6-CF_3bpy)][PF_6] indicates a lower exciton-quenching, which is probably related with a better balance between electrons and holes in the device.[38] With this in mind, together, the time-dependence characteristics and the voltage profile indicate that the characteristics of the LEC with [Cu(xantphos)(6-CF_3bpy)][PF_6] are limited by permanent degradation while with [Cu(xantphos)(6-CF_3bpy)][PF_6] the doping-induced quenching is the main decay factor.

Similar complexes with xanthphos, [Cu(xantphos)(6-Mebpy)][PF_6] and [Cu(xantphos)(6,6'-Me_2bpy)][PF_6], have been previously characterized with the same composition and architecture in LECs but operated with a lower pulsed current (50 A m^{-2}).[16] Compared with [Cu(xantphos)(6-CF_3bpy)][PF_6], substitution of the CF_3 group by a Me group leads to a LEC device with a slightly shorter t_{on} (102 min) but also a reduced $t_{1/2}$

(15 h). The attachment of the second methyl group (6,6'-Me_2bpy) reduces the response time (10 min) but also the lifetime $t_{1/2}$ (0.8 h) of the LEC. Further substitution with CF_3 groups in the 4,4'-positions (6,6'-Me_2-4,4'-$(CF_3)_2$bpy) has benefits on the time-dependence characteristics of the LEC because both the t_{on} (8 min) and $t_{1/2}$ (2 h) are improved with respect to [Cu(xantphos)(6,6'-Me_2bpy)][PF_6], even if the device is operated at higher current densities (100 A m^{-2} vs. 50 A m^{-2}). However, the presence of CF_3 groups is detrimental for both the luminance and the efficiency of the device, which are less for the LEC with [Cu(xantphos)(6,6'-Me_2bpy-4,4'-$(CF_3)_2$)][PF_6] (131 cd m^{-2} and 1.3 cd A^{-1}, respectively) than with [Cu(xantphos)(6,6'-Me_2bpy)][PF_6] (145 cd m^{-2} and 3.0 cd A^{-1}).[16] This negative effect is due to the lower PLQY of the CF_3-substituted emitters in the active films.

Conclusions

We have investigated a series of heteroleptic [Cu(POP)(N^N)][PF_6] and [Cu(xantphos)(N^N)][PF_6] complexes in which the N^N ligand is a bpy substituted with CF_3 groups in either the 6-, 5- or 4-positions. The effects of incorporating both methyl and trifluoromethyl into the bpy domain on the structural, electrochemical and photophysical properties of the complexes have been studied. The single crystal structures of [Cu(xantphos)(bpy)][PF_6], [Cu(xantphos)(4,4'-$(CF_3)_2$bpy)][PF_6] [Cu(POP)(6-CF_3bpy)][PF_6]·1.3Et_2O·0.35H_2O, [Cu(xantphos)(6-CF_3bpy)][PF_6]·2Et_2O·1.5CH_2Cl_2, [Cu(POP)(4,4'-$(CF_3)_2$bpy)][PF_6]·0.5CH_2Cl_2 and [Cu(POP)(5,5'-$(CF_3)_2$bpy)][PF_6]·0.5Et_2O have been determined; each copper(I) centre is in a distorted tetrahedral environment.

Introducing the CF_3 groups pushes the value of $E_{1/2}^{ox}$ for the Cu^+/Cu^{2+} process to higher potentials (+0.85 to +0.96 V) with respect to [Cu(POP)(bpy)]$^+$ and [Cu(xantphos)(bpy)]$^+$, and the observed trends in $E_{1/2}^{ox}$ are consistent with results of DFT calculations. The HOMO–LUMO separation is significantly altered by the nature of the N^N ligand, with the largest redshift in the MLCT band being for [Cu(P^P)(5,5'-$(CF_3)_2$bpy)]$^+$; this observation is corroborated by DFT calculations. In solution, the compounds are weak yellow to red emitters, but the emission is enhanced on going to the solid state. Powdered [Cu(xantphos)(4,4'-$(CF_3)_2$bpy)][PF_6] (λ_{em}^{max} = 517 nm) exhibits the highest PLQY (50.3%). The emission properties strongly depend on the substitution pattern and cannot be explained by simple electronic considerations due to the flattening of the tetrahedral structure experienced by the complex upon excitation. Compared to solution behaviour at 298 K, excited state lifetimes lengthen for all complexes in frozen Me-THF (77 K), which is indicative of TADF. TD-DFT calculations reveal that $\Delta E(S_1 - T_1)$ lies in the range 0.12–0.20 eV, which is a small enough energy to allow TADF.

LECs were fabricated with [Cu(POP)(6-CF_3bpy)][PF_6], [Cu(xantphos)(6-CF_3bpy)][PF_6] or [Cu(xantphos)(6,6'-Me_2-4,4'-$(CF_3)_2$bpy)][PF_6] in the emissive layer. All showed yellow electroluminescence (λ_{em}^{max} = 589–595 nm). The LEC with [Cu(xantphos)(6,6'-Me_2-4,4'-$(CF_3)_2$bpy)][PF_6] had the fastest turn-on time (8 min), whereas the longest lived LEC ($t_{1/2}$ = 31 h) contained [Cu(xantphos)(6-CF_3bpy)][PF_6]; these LECs reached maximum luminances of 131 and 109 cd m^{-2} respectively. Although the device with [Cu(xantphos)(6-CF_3bpy)][PF_6] was operated at higher current density (100 A m^{-2} vs. 50 A m^{-2}), its lifetime $t_{1/2}$ is more than twice as long as for the device with the respective [Cu(xantphos)(6-Mebpy)][PF_6] complex (31 vs. 15 h). However, compared to LECs with CF_3-free bpy-based [Cu(POP)(N^N)]$^+$ or [Cu(xantphos)(N^N)]$^+$ complexes, those incorporating CF_3 groups performed less well; CF_3 substituents are detrimental to both the luminance and the efficiency of the LEC.

Acknowledgements

Financial support from the Swiss National Science Foundation (Grant number 162631), the University of Basel, the MINECO of Spain (CTQ2015-71154-P and Unidad de Excelencia María de Maeztu MDM-2015-0538), the Generalitat Valenciana (PROMETEO/2016/ 135) and European FEDER funds (CTQ2015-71154-P) is acknowledged. Prof. Dr. Oliver S. Wenger and Dr. Christopher Bryan Larsen are thanked for use of their LP920-KS instrument from Edinburgh Instruments, including Quantel Brilliant b Nd:YAG laser and iCCD camera from Andor, for low-temperature emission and lifetime measurements.

Keywords: copper • 2,2'-bipyridine • chelating bis(phosphane) • trifluoromethyl • light-emitting electrochemical cell

1 N. T. Kalyani, H. Swart, S. J. Dhoble, *Principles and Applications of Organic Light Emitting Diodes (OLEDs)*, Woodhead Publishing, Duxford, United Kingdom, **2017**.

2 Yi-Lu Chang, *Efficient Organic Light Emitting-Diodes (OLEDs)*, CRC Press Taylor&Francis group, Boca Raton, Florida, **2016**.

3 H. Yersin, *Highly Efficient OLEDs with Phosphorescent Materials*, Wiley-VCH Verlag GmbH & Co. KGaA, Weinheim, Germany, **2008**.

4 H. Rudmann, S. Shimada, M. F. Rubner, *J. Am. Chem. Soc.* **2002**, *124*, 4918-4921.

5 R.D. Costa, E. Ortí, H.J. Bolink, F. Monti, G. Accorsi, N. Armaroli, *Angew. Chem. Int. Ed.* **2012**, *51*, 8178-8211.

6 C. E. Housecroft, E.C. Constable, *Coord. Chem. Rev.* **2017**, *350*, 155-177.

7 H. J. Bolink, E. Coronado, R. D. Costa, N. Lardiés, E. Ortí, *Inorg. Chem.* **2008**, *47*, 9149-9151.

8 R. D. Costa, E. Ortí, H. J. Bolink, S. Graber, C. E. Housecroft, E. C. Constable, *Adv. Funct. Mater.* **2010**, *20*, 1511-1520.

9 K. J. Suhr, L. D. Bastatas, Y. Shen, L. A. Mitchell, B. J. Holliday, J. D. Slinker, *ACS Appl. Mater. Interfaces* **2016**, *8*, 8888-8892.

10 See for example: C. E. Housecroft and E. C. Constable, *Chem. Soc. Rev.* **2015**, *44*, 8386-8398.

11 R. Czerwieniec, H. Yersin, *Inorg. Chem.* **2015**, *54*, 4322-4327.

12 R. Czerwieniec, M. J. Leitl, H. H. H. Homeier, H. Yersin, *Coord. Chem. Rev.* **2016**, *325*, 2-28.

13 L. Bergmann, G. J. Hedley, T. Baumann, S. Bräse, I. D.W. Samuel, *Sci. Adv.* **2016**, *2*, e1500889.

14. M. Osawa, M. Hashimoto, I. Kawata, M. Hoshino, *Dalton Trans.* **2017**, *46*, 12446-12455.

15 S. Keller, E. C. Constable, C. E. Housecroft, M. Neuburger, A. Prescimone, G. Longo, A. Pertegás, M. Sessolo, H. J. Bolink, *Dalton Trans.* **2014**, *43*, 16593-16596.

16 S. Keller, A. Pertegás, G. Longo, L. Martinez, J. Cerdá, J. M. Junquera-Hernández, A. Prescimone, E. C. Constable, C. E. Housecroft, E. Ortí, H. J. Bolink, *J. Mater. Chem. C.* **2016**, *4*, 3857-3871.

17 M. D. Weber, M. Viciano-Chumillas, D. Armentano, J. Cano, R. D. Costa, *Dalton Trans.* **2017**, *46*, 6312-6323.

18 F. Brunner, L. Martínez-Sarti, S. Keller, A. Pertegás, A. Prescimone, E. C. Constable, H. J. Bolink, C. E. Housecroft, *Dalton Trans.* **2016**, *45*, 15180-15192.

19 Y. Chi, B. Tong, P.-T. Chou, *Coord. Chem. Rev.* **2014**, *281*, 1-25.

20 F. Brunner, Y. M. Klein, S. Keller, C. D. Morris, A. Prescimone, E. C. Constable, C. E. Housecroft, *RSC Adv.* **2015**, *5*, 58694-58703.

21 D. O'Hagana, H. S. Rzepa, *Chem. Commun.* **1997**, 645-652 and references therein.

22 I. Andrés-Tomé, J. Fyson, F.B. Dias, A.P. Monkman, G. Iacobellis, P. Coppo, *Dalton Trans.* **2012**, *41*, 8669-8674.

23 J. Yuasa, M. Dan, T. Kawai, *Dalton Trans.* **2013**, *42*, 16096-16101.

24 M. W. Mara, K. A. Fransted, L. X. Chen, *Coord. Chem. Rev.* **2015**, *282-283*, 2-18.

25 M. Tromp, A. J. Dent, J. Headspith, T. L. Easun, X.-Z. Sun, M. W. George, O. Mathon, G. Smolentsev, M. L. Hamilton, J. Evans, *J. Phys. Chem. B* **2013**, *117*, 7381-7387.

26 T. J. Penfold, S. Karlsson, G. Capano, F. A. Lima, J. Rittmann, M. Reinhard, M. H. Rittmann-Frank, O. Braem, E. Baranoff, R. Abela, I. Tavernelli, U. Rothlisberger, C. J. Milne, M. Chergui, J. *Phys. Chem. A* **2013**, *117*, 4591-4601.

27 A. Kaeser, M. Mohankumar, J. Mohanraj, F. Monti, M.Holler, J.-J.Cid, O. Moudam, I.Nierengarten, L. Karmazin-Brelot, C. Duhayon, B. Delavaux-Nicot, N. Armaroli, J.-F. Nierengarten, *Inorg. Chem.* **2013**, *52*, 12140-12151.

28 F. Brunner, Y. M. Klein, S. Keller, C. D. Morris, A. Prescimone, E. C. Constable, C. E. Housecroft, *RSC Adv.* **2015**, *5*, 58694-58703.

29 S. Keller, F. Brunner, A. Prescimone, E. C. Constable, C. E. Housecroft, *Inorg. Chem. Comm.* **2015**, *58*, 64-66.

30 M. Charton, *J. Am. Chem. Soc.* **1969**, *91*, 615-618.

31 K. Uneyama, *Organofluorine Chemistry*, Blackwell Publishing, Oxford, UK, **2006**.

32 M. Y. Wong, E. Zysman-Colman in *Light-Emitting Electrochemical Cells*, ed. R. D. Costa, Springer International Publishing AG, Cham, Switzerland, **2017**, pp. 237-266.

33 M. Elie, S. Gaillard, J.-L. Renaud, in *Light-Emitting Electrochemical Cells*, ed. R. D. Costa, Springer International Publishing AG, Cham, Switzerland, **2017**, pp. 287-327.

34 M. J. Leitl, V. A. Krylova, P. I. Djurovich, M. E. Thompson, H. Yersin, *J. Am. Chem. Soc.* **2014**, *136*, 16032-16038.

35 S. T. Parker, J. D. Slinker, M. S. Lowry, M. P. Cox, S. Bernhard, G. G. Malliaras, *Chem. Mater.* **2005,** *17,* 3187-3190.

36 R. D. Costa, A. Pertegás, E. Ortí, H. J. Bolink, *Chem. Mater.* **2010**, *22*, 1288-1290.

37 S. van Reenen, P. Matyba, A. Dzwilewski, R. A. J. Janssen, L. Edman, M. Kemerink, *J. Am. Chem. Soc.*, **2010**, *132*, 13776-13781.

38 H.-C. Su, J.-H. Hsu, *Dalton Trans.* **2015**, *44*, 8330-8345.

FULL PAPER

Text for Table of Contents

Sarah Keller, Fabian Brunner, José M. Junquera-Hernández, Antonio Pertegás, Maria-Grazia La-Placa, Alessandro Prescimone, Edwin C. Constable, Henk J. Bolink, Enrique Ortí* and Catherine E. Housecroft*

Page No. – Page No.

CF_3 Substitution of [Cu(P^P)(bpy)][PF_6] Complexes: Effects on Photophysical Properties and Light-emitting Electrochemical Cell Performance

[a] S. Keller, F. Brunner, Dr. A. Prescimone, Prof. Dr. E.C. Constable, Prof. Dr. C.E. Housecroft
Department of Chemistry
University of Basel
BPR 1096, Mattenstrasse 24a, Basel 4058, Switzerland
E-mail: catherine.housecroft@unibas.ch

[b] Dr. J.M. Junquera-Hernández, Dr. A. Pertegás, M.-G. La-Placa, Dr. H.J. Bolink, Prof. Dr. E. Ortí
Instituto de Ciencia Molecular,
Universidad de Valencia,
ES-45980 Paterna, Valencia, Spain
e-mail: enrique.orti@uv.es

Supporting information for this article is given via a link at the end of the document.

CF_3 Substitution of [Cu(P^P)(bpy)][PF_6] Complexes: Effects on Photophysical Properties and Light-Emitting Electrochemical Cell Performance

Sarah Keller,[a] Fabian Brunner,[a] José M. Junquera-Hernández,[b] Antonio Pertegás,[b] Maria-Grazia La-Placa,[b] Alessandro Prescimone,[a] Edwin C. Constable,[a] Henk J. Bolink,[b] Enrique Ortí*[b] and Catherine E. Housecroft*[a]

[a] Department of Chemistry, University of Basel, Mattenstrasse 24a, BPR 1096, CH-4058 Basel, Switzerland; e-mail: catherine.housecroft@unibas.ch

[b] Instituto de Ciencia Molecula, Universidad de Valencia, 46980 Paterna (Valencia), Spain; e-mail: enrique.orti@uv.es

Experimental Section

General. ^{1}H, ^{13}C and ^{31}P NMR spectra were recorded at room temperature using a Bruker Avance III-600, III-500 or III-400 NMR spectrometer. ^{1}H and ^{13}C NMR chemical shifts were referenced to residual solvent peaks with respect to δ(TMS) = 0 ppm, ^{19}F NMR chemical shifts with respect to an external reference of $CFCl_3$ (δ = 0 ppm) and ^{31}P NMR chemical shifts with respect to δ(85% aqueous H_3PO_4) = 0 ppm. Solution absorption and emission spectra were measured using an Agilent 8453 spectrophotometer and a Shimadzu RF-5301PC spectrofluorometer, respectively. Electrospray ionization (ESI) mass spectra were recorded on a Bruker esquire 3000plus instrument or Shimadzu LCMS-2020 instrument. Quantum yields for CH_2Cl_2 solution and powder samples were measured using a Hamamatsu absolute photoluminescence (PL) quantum yield spectrometer C11347 Quantaurus-QY. Emission lifetimes and powder emission spectra were measured with a Hamamatsu Compact Fluorescence lifetime Spectrometer C11367 Quantaurus-Tau, using an LED light source with λ_{exc} = 365 nm. Low temperature emission and lifetime experiments were performed using an LP920-KS instrument from Edinburgh Instruments. 410 nm excitation was obtained from pulsed third-harmonic radiation from a Quantel Brilliant b Nd:YAG laser equipped with a Rainbow optical parameter oscillator (OPO). The laser pulse duration was ~10 ns and the pulse frequency 10 Hz, with a typical pulse energy of 7 mJ. Detection of the spectra occurred on an iCCD camera from Andor. Single-wavelength kinetics were recorded using a photomultiplier tube. Photoluminescence

measurements on thin film were performed on samples with the same composition than the emissive layer of LECs. Each complex was mixed with the ionic liquid (IL) 1-ethyl-3-methylimidazolium hexafluoridophosphate ([Emim][PF_6]) in a 4-to-1 molar ratio. This mixture was spin-coated on pre-cleaned quartz substrates and quantum yields and emission spectra were recorded using a Hamamatsu absolute quantum yield C9920.

The compounds 4,4'-$(CF_3)_2$-2,2'-bipyridine (4,4'-$(CF_3)_2$bpy),[1] 6,6'-dimethyl-4,4'-$(CF_3)_2$-2,2'-bipyridine (6,6'-Me_2-4,4'-$(CF_3)_2$bpy),[2] 6-Me-2,2'-bipyridine (6-Mebpy)[3], [$Cu(MeCN)_4$][PF_6][4] and [Cu(POP)(bpy)][PF_6][5] were prepared following literature methods and the NMR spectroscopic data matched those reported. POP was purchased from Acros, xantphos from Fluorochem, 6,6'-dimethyl-2,2'-bipyridine (6,6'-Me_2bpy) from Angene and 5,5'-$(CF_3)_2$-2,2'-bipyridine (5,5'-$(CF_3)_2$bpy) from TCI chemicals. All other chemicals were used as received.

6-CF_3-2,2'-bipyridine (6-CF_3bpy).

2-Chloro-6-(trifluoromethyl)pyridine (423 mg, 2.32 mmol, 1.0 eq) and $Pd(PPh_3)_4$ (135 mg, 0.11 mmol, 0.05 eq) were added to a 10−20 mL microwave tube. The tube was then evacuated and refilled with nitrogen three times. Dry THF (5 mL) and a solution of 2-pyridylzinc bromide (0.5 M in THF, 7 mL, 3.50 mmol, 1.5 eq) were added, the tube was sealed and put into the microwave reactor at 110 °C for 2 h. The reaction mixture was poured into a separation flask, sat. aqueous $NaHCO_3$ was added and the mixture was extracted with CH_2Cl_2 (3 x 50 mL). The combined organic layers were washed with water (2 x 100 mL) and dried over $MgSO_4$. The solvent was removed and the brown crude material was redissolved in CH_2Cl_2 and filtered over silica. The solvent was removed to give 6-(trifluoromethyl)-2,2'-bipyridine (318 mg, 1.42 mmol, 61%) as a white solid. The product contained minor impurities but was used for further reactions. ^{1}H NMR (400 MHz, CD_2Cl_2, 298 K) *δ*/ppm 8.69 (ddd, *J* = 4.7, 1.8, 0.9 Hz, 1H, H^{A6}), 8.65 (dt, *J* = 8.0, 0.8 Hz, 1H, H^{B3}), 8.48 (dt, *J* = 8.0, 1.1 Hz, 1H, H^{A3}), 8.02 (td, *J* = 7.8, 0.7 Hz, 1H, H^{B4}), 7.87 (td, *J* = 7.8, 1.8 Hz, 1H, H^{A4}), 7.71 (dd, *J* = 7.8, 1.0 Hz, 1H, H^{B5}), 7.38 (ddd, *J* = 7.5, 4.8, 1.2 Hz, 1H, H^{A5}). ^{13}C NMR (126 MHz, CD_2Cl_2, 298 K) *δ*/ppm 156.7 (C^{B2}), 154.8 (C^{A2}), 149.3 (C^{A6}), 148.0 (q, *J* = 35 Hz, C^{B6}), 138.4 (C^{B4}), 137.3 (C^{A4}), 124.6 (C^{A5}), 123.6 (C^{B3}), 121.7 (unresolved q, *J* = 270 Hz, C^{CF3}), 120.3 (q, *J* = 2.9 Hz, C^{B6}). ^{19}F NMR (376 MHz, CD_2Cl_2, 300K) *δ*/ppm −68.4 (s, CF_3). ESI MS: *m/z* 225.1 $[M–PF_6]^+$ (base peak, calc. 224.0).

[Cu(xantphos)(bpy)][PF_6].

The compounds xantphos (145 mg, 0.25 mmol, 1.0 eq) and bpy (39 mg, 0.25 mmol, 1.0 eq), 1.0 eq) were dissolved in CH_2Cl_2 (20 mL). The colourless solution was added to a colourless solution of [$Cu(MeCN)_4$][PF_6] (93 mg, 0.25 mmol, 1.0 eq) in CH_2Cl_2 (20 mL) and the now yellow solution was stirred for 2 h. The solvent was removed *in vacuo* and the

yellow powder was redissolved in CH_2Cl_2 and layered with Et_2O. This gave [Cu(xantphos)(bpy)][PF_6] as yellow crystals in good yield (225 mg, 0.24 mmol, 96%). ^{1}H NMR (500 MHz, $(CD_3)_2CO$, 298 K) *δ*/ppm 8.64 (d, *J* = 8.2 Hz, 2H, H^{B3}), 8.35 – 8.33 (m, 2H, H^{B6}), 8.17 (td, *J* = 7.9, 1.6 Hz, 2H, H^{B4}), 7.87 (dd, *J* = 7.8, 1.4 Hz, 2H, H^{C5}), 7.47 (ddd, *J* = 7.6, 5.1, 1.0 Hz, 2H, H^{B5}), 7.34 (t, *J* = 7.5 Hz, 4H, H^{D4}), 7.28 (t, *J* = 7.7 Hz, 2H, H^{C4}), 7.20 (t, J = 7.8 Hz, 8H, H^{D3}), 7.06 – 7.02 (m, 8H, H^{D2}), 6.60 (dtd, *J* = 7.7, 3.9, 1.4 Hz, 2H, H^{C3}), 1.80 (s, 6H, $H^{xantphos\text{-}Me}$). ^{13}C NMR (126 MHz, $(CD_3)_2CO$, 298 K) *δ*/ppm 155.7 (t, *J* = 6.5 Hz, C^{C1}), 152.8 (t, *J* = 2.4 Hz, C^{B2}), 150.1 (C^{B6}), 140.0 (C^{B4}), 135.1 (t, *J* = 1.8 Hz, C^{C6}), 133.7 (t, *J* = 8.2 Hz, C^{D2}), 132.4 (t, *J* = 17.4 Hz, C^{D1}), 131.9 (C^{C3}), 130.9 (C^{D4}), 129.7 (t, *J* = 5.0 Hz, C^{D3}), 128.6 (C^{C5}), 127.3 (C^{B5}), 126.2 (t, *J* = 2.6 Hz, C^{C4}), 123.8 (C^{B3}), 120.6 (t, *J* = 13.8 Hz, C^{C2}), 37.0 ($C^{xantphos\text{-}bridge}$), 28.4 ($C^{xantphos\text{-}Me}$). ^{31}P{^{1}H} NMR (202 MHz, $(CD_3)_2CO$, 298 K) *δ*/ppm −12.7 (broad, FWHM = 345 Hz, xantphos), −144.2 (septet, J_{PF} = 708 Hz, $[PF_6]^-$). ESI MS: *m/z* 797.4 $[M–PF_6]^+$ (base peak, calc. 797.2). Found C 62.11, H 4.44, N 3.37; [Cu(xantphos)(bpy)][PF_6] requires C 62.39, H 4.27, N 2.97.

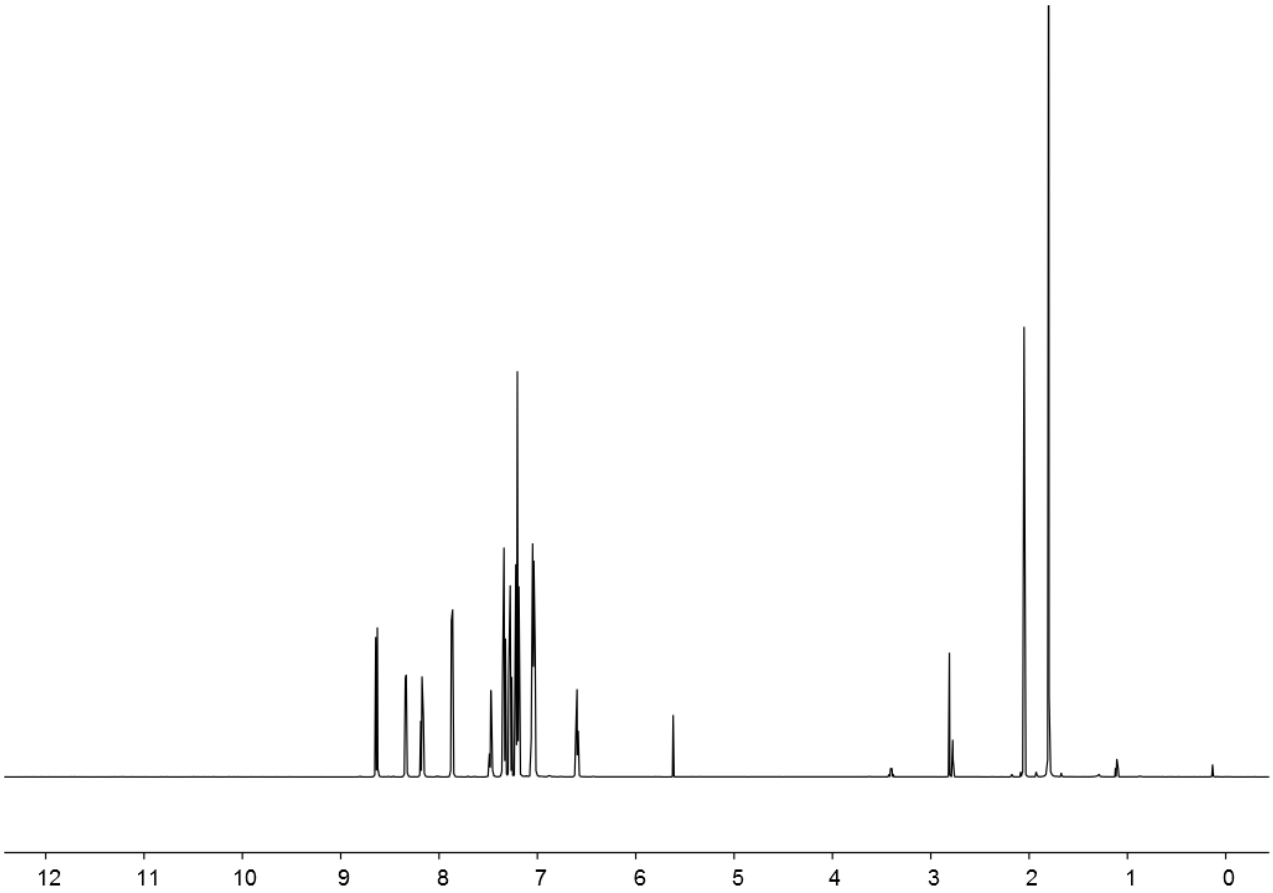

^{1}H NMR spectrum (400 MHz, $(CD_3)_2CO$) of [Cu(xantphos)(bpy)][PF_6]. Chemical shifts are in *δ*/ pm.

[Cu(xantphos)(6,6'-Me_2-4,4'-$(CF_3)_2$bpy)][PF_6]. A colourless solution of xantphos (174 mg, 0.30 mmol, 1.2 eq) and 6,6'-Me_2-4,4'-$(CF_3)_2$bpy (80 mg, 0.25 mmol, 1.0 eq) in CH_2Cl_2 (15

mL) was added dropwise to a colourless solution of $[Cu(MeCN)_4][PF_6]$ (93 mg, 0.25 mmol, 1.0 eq) in CH_2Cl_2 (15 mL). After stirring for 2h, the yellow solution was filtered and the solvent was removed in vacuo. The yellow powder was redissolved in CH_2Cl_2 and layered with Et_2O. This gave [Cu(xantphos)(6,6'-Me_2-4,4'-$(CF_3)_2$bpy)][PF_6] as yellow crystals in good yield (172 mg, 0.16 mmol, 64%). ^{1}H NMR (500 MHz, $(CD_3)_2CO$, 298 K) *δ*/ppm 8.66 (broad signal, FWHM = 3.6 Hz, 2H, H^{B3}), 7.87 (dd, *J* = 7.8, 1.4 Hz, 2H, H^{C5}), 7.81 (broad signal, FWHM = 3.4 Hz, 2H, H^{B5}), 7.47 – 7.43 (m, 4H, H^{D4}), 7.35 (t, *J* = 7.7 Hz, 2H, H^{C4}), 7.28 – 7.22 (m, 8H, H^{D3}), 7.24 – 7.19 (m, 8H, H^{D2}), 7.10 – 7.07 (m, 2H, H^{C3}), 2.34 (s, 6H, bpy-Me), 1.77 (s, 6H, $H^{xantphos\text{-}Me}$). ^{13}C NMR (126 MHz, $(CD_3)_2CO$, 298 K) *δ*/ppm 161.4 (C^{B6}), 155.6 (t, *J* = 6.5 Hz, C^{C1}), 153.3 (C^{B2}), 140.8 (q, *J* = 34.4 Hz, C^{B4}), 134.8 (t, *J* = 1.7 Hz, C^{C6}), 134.0 (t, *J* = 7.6 Hz, C^{D2}), 132.0 (t, *J* = 16.8 Hz, C^{D1}), 131.3 (C^{C3}), 131.2 (C^{D4}), 129.9 (t, *J* = 4.6 Hz, C^{D3}), 129.1 (C^{C5}), 126.5 (t, *J* = 2.2 Hz, C^{C4}), 123.5 (q, *J* = 270 Hz, C^{CF3}), 123.4 (q, *J* = 3.3 Hz, C^{B5}), 122.0 (t, *J* = 13.5 Hz, C^{C2}), 117.9 (q, *J* = 3.2 Hz, C^{B3}), 36.8 (t, *J* = 1.3 Hz, $C^{xantphos\text{-}bridge}$), 28.9 ($C^{xantphos\text{-}Me}$), 27.3 ($C^{bpy\text{-}Me}$). ^{19}F NMR (376 MHz, $(CD_3)_2CO$, 300K) *δ*/ ppm −65.2 (s, CF_3). ^{31}P NMR (162 MHz, $(CD_3)_2CO$, 296 K) *δ*/ppm −12.9 (broad, FWHM = 145 Hz, xantphos), −144.5 (septet, J_{PF} = 710 Hz, $[PF_6]^-$). ESI MS: *m/z* 961.0 $[M–PF_6]^+$ (base peak, calc. 961.2). Found C 56.77, H 4.30, N 2.62; [Cu(xantphos)(6,6'-Me_2-4,4'-$(CF_3)_2$bpy)][PF_6]·H_2O requires C 56.57, H 3.94, N 2.49.

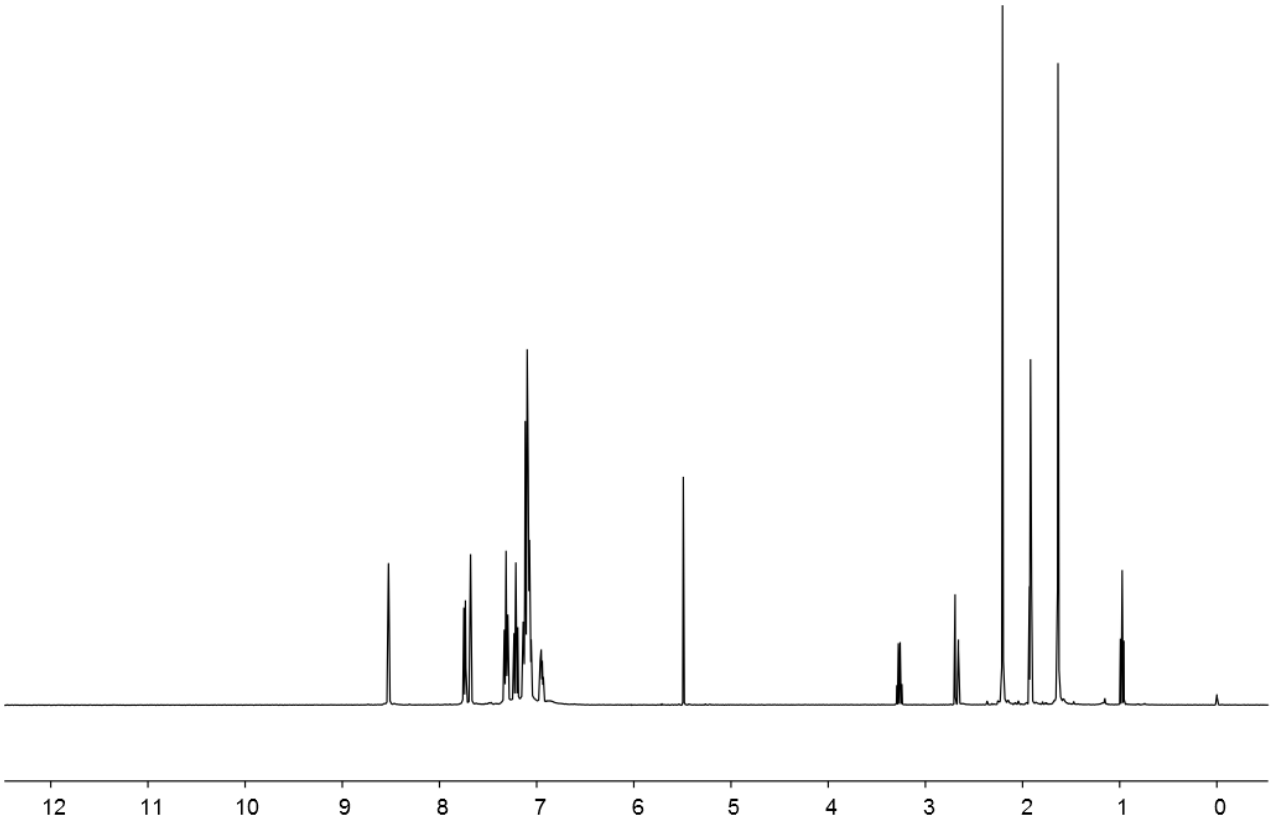

^{1}H NMR spectrum (400 MHz, $(CD_3)_2CO$) of [Cu(xantphos)(6,6'-Me_2-4,4'-$(CF_3)_2$bpy)][PF_6]. Chemical shifts are in *δ*/ pm.

[Cu(POP)(4,4'-$(CF_3)_2$bpy)][PF_6].

A colourless solution of POP (135 mg, 0.25 mmol, 1.0 eq) and [$Cu(MeCN)_4$][PF_6] (93 mg, 0.25 mmol, 1.0 eq) in CH_2Cl_2 (30 mL) was stirred for 2h. 4,4'-$(CF_3)_2$bpy (73 mg, 0.25 mmol, 1.0 eq) was added and the solution turned orange. After stirring for 2h, the solution was filtered and the solvent was removed in vacuo. The orange powder was redissolved in CH_2Cl_2 and layered with Et_2O. This gave [Cu(POP)(4,4'-$(CF_3)_2$bpy)][PF_6] as orange crystals in good yield (174 mg, 0.17 mmol, 68%). ^{1}H NMR (500 MHz, $(CD_3)_2CO$, 298 K) *δ*/ppm 9.17 (broad, FWHM = 3.7 Hz, 2H, H^{B3}), 8.97 (d, *J* = 5.4 Hz, 2H, H^{B6}), 7.84 – 7.82 (m, 2H, H^{B5}), 7.46 (ddd, *J* = 8.2, 7.5, 1.6 Hz, 2H, H^{C5}), 7.38 (t, *J* = 7.4 Hz, 4H, H^{D4}), 7.27 (t, *J* = 7.7 Hz, 8H, H^{D3}), 7.25 – 7.22 (m, 2H, H^{C6}), 7.18 – 7.14 (m, 8H, H^{D2}), 7.12 (td, *J* = 7.6, 0.8 Hz, 2H, H^{C4}), 6.81 (dtd, *J* = 7.9, 4.3, 1.6 Hz, 2H, H^{C3}). ^{13}C NMR (126 MHz, $(CD_3)_2CO$, 298 K) *δ*/ppm 159.2 (t, *J* = 6.0 Hz, C^{C1}), 153.4 (t, *J* = 2.0 Hz, C^{B2}), 151.9 (C^{B6}), 140.5 (q, *J* = 34.6 Hz, C^{B4}), 135.1 (C^{C3}), 134.0 (t, *J* = 8.1 Hz, C^{D2}), 133.4 (C^{C5}), 131.4 (t, *J* = 17.8 Hz, C^{D1}), 131.2 (C^{D4}), 129.8 (t, *J* = 4.9 Hz, C^{D3}), 126.3 (t, *J* = 2.2 Hz, C^{C4}), 124.2 (t, *J* = 15.5 Hz, C^{C2}), 123.5 (q, *J* = 270 Hz, C^{CF3}) 123.3 (q, *J* = 3.2 Hz, C^{B5}), 121.6 (C^{C6}), 120.8 (q, *J* = 3.2 Hz, C^{B3}). ^{19}F NMR (376 MHz, $(CD_3)_2CO$, 300K) *δ*/ppm −65.1 (s, CF_3), −72.6 (d, J_{PF} = 708 Hz, $[PF_6]^-$). ^{31}P NMR (162 MHz, $(CD_3)_2CO$, 300 K) *δ*/ppm −10.7 (broad, FWHM = 185 Hz, POP), −144.2 (septet, J_{PF} = 708 Hz, $[PF_6]^-$). ESI MS: *m/z* 893.3 $[M–PF_6]^+$ (base peak, calc. 893.1). Found C 55.35, H 3.58, N 2.98; [Cu(POP)(4,4'-$(CF_3)_2$bpy)][PF_6] requires C 55.47, H 3.30, N 2.70.

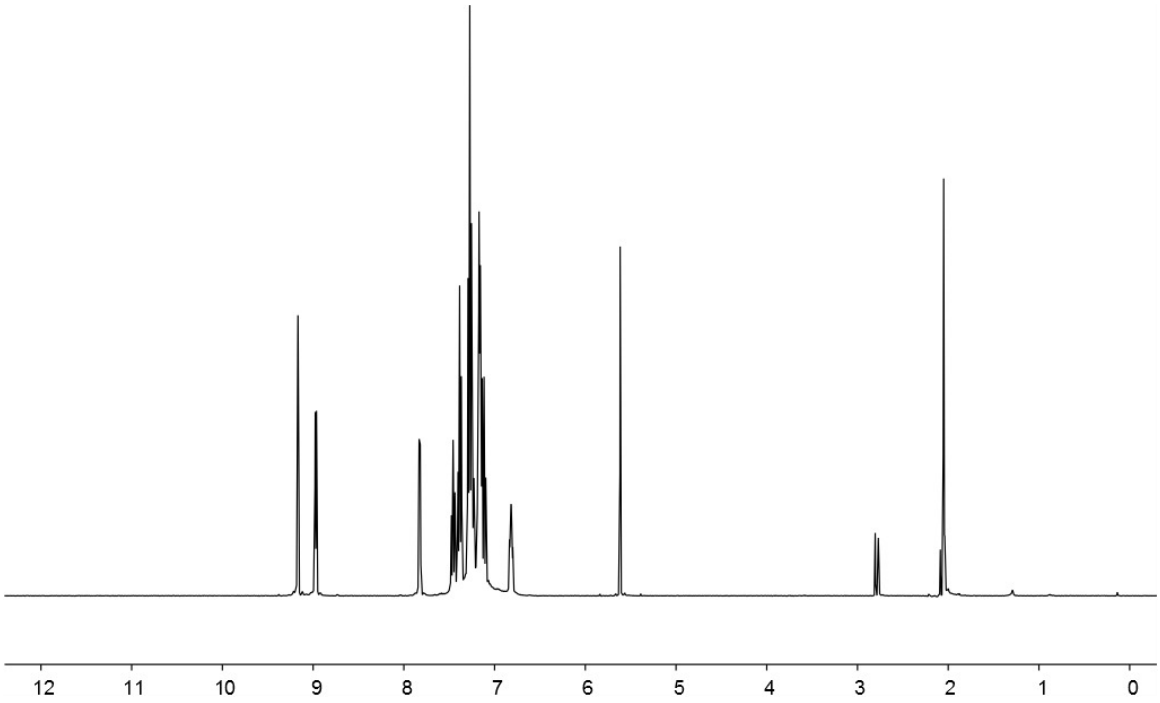

^{1}H NMR spectrum (400 MHz, $(CD_3)_2CO$) of [Cu(POP)(4,4'-$(CF_3)_2$bpy)][PF_6]. Chemical shifts are in *δ*/ pm.

[Cu(xantphos)(4,4'-$(CF_3)_2$bpy)][PF_6].

A colourless solution of xantphos (145 mg, 0.25 mmol, 1.0 eq) and 4,4'-$(CF_3)_2$bpy (73 mg, 0.25 mmol, 1.0 eq) in CH_2Cl_2 (15 mL) was added dropwise to a colourless solution of [$Cu(MeCN)_4$][PF_6] (93 mg, 0.25 mmol, 1.0 eq) in CH_2Cl_2 (15 mL). The resulting solution turns dark red. After stirring for 2h, the now orange solution was filtered and the solvent was removed in vacuo. The orange powder was redissolved in CH_2Cl_2 and layered with Et_2O. This gave [Cu(xantphos)(4,4'-$(CF_3)_2$bpy)][PF_6] as orange crystals in good yield (203 mg, 0.19 mmol, 76%). ^{1}H NMR (500 MHz, $(CD_3)_2CO$, 298 K) *δ*/ppm 9.14 (broad signal, FWHM = 3.9 Hz, 2H, H^{B3}), 8.67 (d, *J* = 5.3 Hz, 2H, H^{B6}), 7.91 – 7.89 (m, 2H, H^{C5}), 7.90 (d, *J* = 6.4 Hz, 2H, H^{B5}), 7.37 (t, J = 7.5 Hz, 4H, H^{D4}), 7.31 (t, *J* = 7.7 Hz, 2H, H^{C4}), 7.22 (t, *J* = 7.7 Hz, 8H, H^{D3}), 7.10 – 7.06 (m, 8H, H^{D2}), 6.72 (dtd, *J* = 7.7, 4.2, 1.4 Hz, 2H, H^{C3}). ^{13}C NMR (126 MHz, $(CD_3)_2CO$, 298 K) *δ*/ppm 155.6 (t, *J* = 6.3 Hz, C^{C1}), 153.1 (C^{B2}), 151.5 (C^{B6}), 140.7 (q, *J* = 34.4 Hz, C^{B4}), 135.0 (t, *J* = 1.7 Hz, C^{C6}), 133.7 (t, *J* = 7.9 Hz, C^{D2}), 132.1 (C^{C3}), 131.9 (t, *J* = 17.8 Hz, C^{D1}), 131.1 (C^{D4}), 129.9 (t, *J* = 4.8 Hz, C^{D3}), 129.1 (C^{C5}), 126.3 (t, *J* = 2.4 Hz, C^{C4}), 123.8 (q, *J* = 3.2 Hz, C^{B5}), 123.4 (q, *J* = 273 Hz, C^{CF3}), 121.0 (q, *J* = 3.3 Hz, C^{B3}), 120.0 (t, *J* = 14.6 Hz, C^{C2}), 36.9 ($C^{xantphos\text{-}bridge}$), 28.6 ($C^{xantphos\text{-}Me}$). ^{19}F NMR (376 MHz, $(CD_3)_2CO$, 300K) *δ*/ppm −65.2 (s, CF_3), −72.6 (d, J_{PF} = 708 Hz, $[PF_6]^-$). ^{31}P NMR (162 MHz, $(CD_3)_2CO$, 300 K) *δ*/ppm −12.0 (broad, FWHM = 155 Hz, xantphos), −144.2 (septet, J_{PF} = 708 Hz, $[PF_6]^-$). ESI MS: *m/z* 933.3 $[M–PF_6]^+$ (base peak, calc. 933.2). Found C 55.01, H 3.62, N 2.79; [Cu(xantphos)(4,4'-$(CF_3)_2$bpy)][PF_6]·$2H_2O$ requires C 54.92, H 3.80, N 2.51.

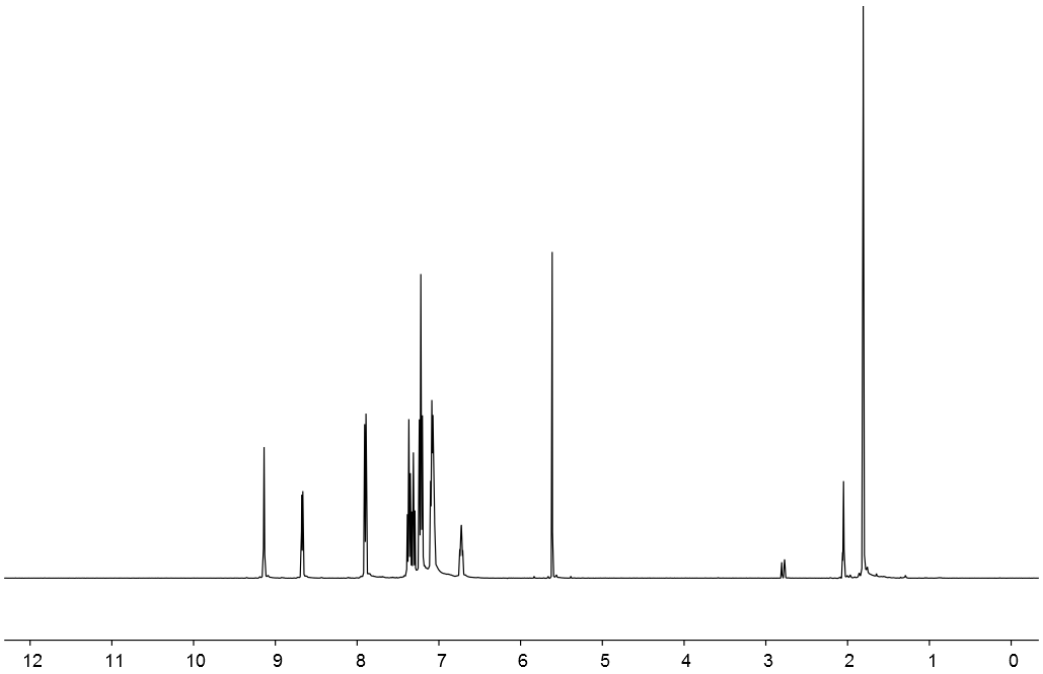

^{1}H NMR spectrum (400 MHz, $(CD_3)_2CO$) of [Cu(xantphos)(4,4'-$(CF_3)_2$bpy)][PF_6]. Chemical shifts are in *δ*/ pm.

[Cu(POP)(5,5'-$(CF_3)_2$bpy)][PF_6].

A colourless solution of POP (135 mg, 0.25 mmol, 1.0 eq) and [$Cu(MeCN)_4$][PF_6] (93 mg, 0.25 mmol, 1.0 eq) in CH_2Cl_2 (30 mL) was stirred for 2h. 5,5'-$(CF_3)_2$bpy (73 mg, 0.25 mmol, 1.0 eq) was added and the solution turned orange. After stirring for 2h, the solution was filtered and the solvent was removed in vacuo. The orange powder was redissolved in CH_2Cl_2 and layered with Et_2O. This gave [Cu(POP)(5,5'-$(CF_3)_2$bpy)][PF_6] as orange crystals in good yield (192 mg, 0.18 mmol, 72%). ^{1}H NMR (500 MHz, $(CD_3)_2CO$, 298 K) *δ*/ppm 8.96 (d, *J* = 8.2 Hz, 2H, H^{B3}), 8.95 (s, 2H, H^{B6}), 8.55 (dd, *J* = 8.2, 1.8 Hz, 2H, H^{B4}), 7.44 (ddd, *J* = 8.2, 7.5, 1.7 Hz, 2H, H^{C5}), 7.38 (t, *J* = 7.7 Hz, 4H, H^{D4}), 7.26 (t, *J* = 7.8 Hz, 8H, H^{D3}), 7.22 – 7.17 (m, 10H, H^{D2+C6}), 7.11 (td, *J* = 7.6, 0.9 Hz, 2H, H^{C4}), 6.83 (dtd, *J* = 7.9, 4.3, 1.6 Hz, 2H, H^{C3}). ^{13}C NMR (126 MHz, $(CD_3)_2CO$, 298 K) *δ*/ppm 158.9 (t, *J* = 6.1 Hz, C^{C1}), 154.7 (C^{B2}), 147.3 (m, C^{B6}), 137.1 (m, C^{B4}), 135.0 (C^{C3}), 134.2 (t, *J* = 8.2 Hz, C^{D2}), 133.4 (C^{C5}), 131.20 (C^{D4}), 131.15 (t, *J* = 17.8 Hz, C^{D1}), 129.8 (t, *J* = 4.9 Hz, C^{D3}), 129.4 (q, *J* = 34.3 Hz, C^{B5}), 126.4 (q, *J* = 2.2 Hz, C^{C4}), 125.2 (C^{B3}), 124.4 (t, *J* = 15.6 Hz, C^{C2}), 123.6 (q, *J* = 273.0 Hz, CF_3), 121.5 (t, *J* = 1.8 Hz, C^{C6}). ^{19}F NMR (376 MHz, $(CD_3)_2CO$, 300K) *δ*/ppm −63.3 (s, CF_3), −72.6 (d, J_{PF} = 708 Hz, $[PF_6]^-$). ^{31}P NMR (162 MHz, $(CD_3)_2CO$, 300 K) *δ*/ppm −10.3 (broad, FWHM = 203 Hz, POP), −144.2 (septet, J_{PF} = 708 Hz, $[PF_6]^-$). ESI MS: *m/z* 893.3 $[M–PF_6]^+$ (base peak, calc. 893.1). Found C 54.61, H 3.80, N 2.93; [Cu(POP)(5,5'-$(CF_3)_2$bpy)][PF_6]·H_2O requires C 54.53, H 3.43, N 2.65.

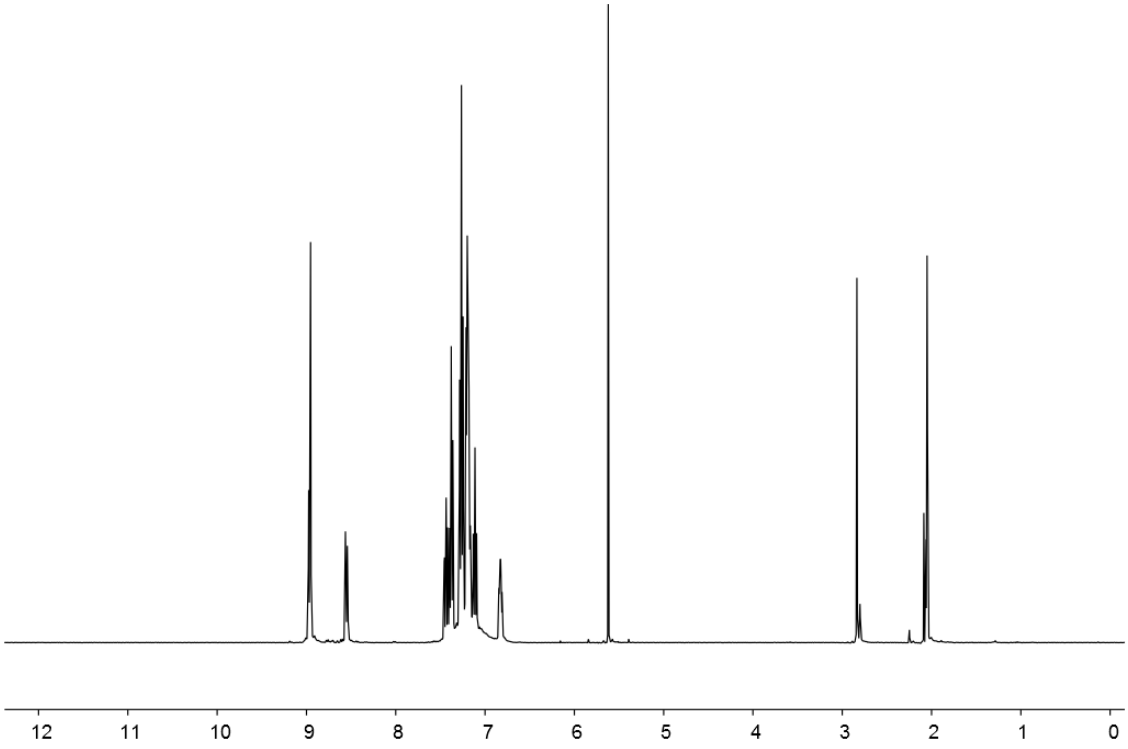

^{1}H NMR spectrum (400 MHz, $(CD_3)_2CO$) of [Cu(POP)(5,5'-$(CF_3)_2$bpy)][PF_6]. Chemical shifts are in *δ*/ pm.

[Cu(xantphos)(5,5'-$(CF_3)_2$bpy)][PF_6].

A colourless solution of xantphos (145 mg, 0.25 mmol, 1.0 eq) and 5,5'-$(CF_3)_2$bpy (73 mg, 0.25 mmol, 1.0 eq) in CH_2Cl_2 (15 mL) was added dropwise to a colourless solution of [Cu(MeCN)$_4$][PF_6] (93 mg, 0.25 mmol, 1.0 eq) in CH_2Cl_2 (15 mL). The resulting solution turns dark red. After stirring for 2h, the now orange solution was filtered and the solvent was removed in vacuo. The orange powder was redissolved in CH_2Cl_2 and layered with Et_2O. This gave [Cu(xantphos)(5,5'-$(CF_3)_2$bpy)][PF_6] as orange crystals in good yield (244 mg, 0.23 mmol, 92%). ^{1}H NMR (500 MHz, $(CD_3)_2CO$, 298 K) *δ*/ppm 8.96 (d, *J* = 8.3 Hz, 2H, H^{B3}), 8.57 (d, *J* = 8.1 Hz, 2H, H^{B4}), 8.48 (broad signal, FWHM = 8.4 Hz, 2H, H^{B6}), 7.91 (dd, *J* = 7.9, 1.4 Hz, 2H, H^{C5}), 7.36 (t, *J* = 7.4 Hz, 4H, H^{D4}), 7.30 (t, *J* = 7.7 Hz, 2H, H^{C4}), 7.22 (t, *J* = 7.8 Hz, 8H, H^{D3}), 7.10 – 7.06 (m, 8H, H^{D2}), 6.66 (ddd, *J* = 7.7, 5.5, 2.3 Hz, 2H, H^{C3}), 1.82 (s, 6H, $H^{xantphos\text{-}Me}$). ^{13}C NMR (126 MHz, $(CD_3)_2CO$, 298 K) *δ*/ppm 155.7 (t, *J* = 6.2 Hz, C^{C1}), 154.6 (C^{B2}), 146.9 (q, *J* = 4.1 Hz, C^{B6}), 137.4 (m, C^{B4}), 135.1 (t, *J* = 1.6 Hz, C^{C6}), 133.8 (t, *J* = 8.0 Hz, C^{D2}), 132.0 (C^{C3}), 131.6 (t, *J* = 17.9 Hz, C^{D1}), 131.1 (C^{D4}), 129.8 (t, *J* = 4.9 Hz, C^{D3}), 129.4 (q, *J* = 33.2 Hz, C^{B5}), 128.8 (C^{C5}), 126.4 (t, *J* = 2.4 Hz, C^{C4}), 125.6 (m, C^{B3}), 124.5, 123.5 (q, *J* = 270 Hz, C^{CF3}), 120.1 (t, *J* = 14.5 Hz, C^{C2}), 37.0 (t, *J* = 1.4 Hz, $C^{xantphos\text{-}bridge}$), 28.2 ($C^{xantphos\text{-}Me}$). ^{19}F NMR (376 MHz, $(CD_3)_2CO$, 300K) *δ*/ppm −63.2 (s, CF_3), −72.5 (d, J_{PF} = 708 Hz, [PF_6]$^-$). ^{31}P NMR (162 MHz, $(CD_3)_2CO$, 300 K) *δ*/ppm −11.0 (broad, FWHM = 165 Hz, xantphos), −144.2 (septet, J_{PF} = 708 Hz, [PF_6]$^-$). ESI MS: *m/z* 933.4 [M–PF_6]$^+$ (base peak, calc. 933.2). Found C 54.11, H 3.76, N 2.68; [Cu(xantphos)(5,5'-$(CF_3)_2$bpy)][PF_6]·3H_2O requires C 54.05, H 3.91, N 2.47.

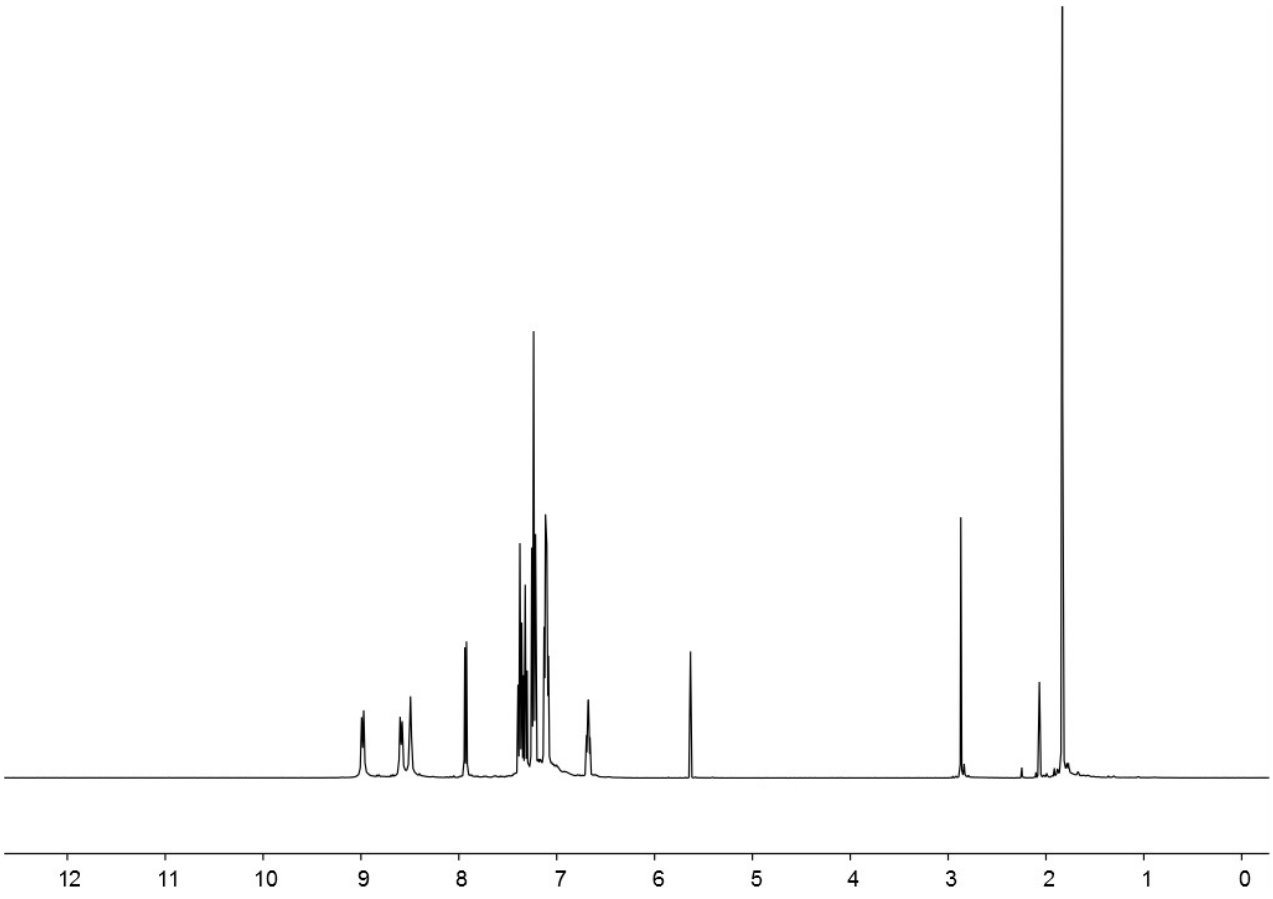

^{1}H NMR spectrum (400 MHz, $(CD_3)_2CO$) of [Cu(xantphos)(5,5'-$(CF_3)_2$bpy)][PF_6]. Chemical shifts are in *δ*/ pm.

[Cu(POP)(6-CF_3bpy)][PF_6].

A colourless solution of POP (148 mg, 0.27 mmol, 1.1 eq) and [$Cu(MeCN)_4$][PF_6] (93 mg, 0.25 mmol, 1.0 eq) in CH_2Cl_2 (30 mL) was stirred for 1.5h. 6-CF_3bpy (56 mg, 0.25 mmol, 1.0 eq) was added and the solution turned yellow. After stirring for 1h, the solution was filtered and the solvent was removed in vacuo. The yellow solid was redissolved in CH_2Cl_2 and layered with Et_2O. This gave [Cu(POP)(6-CF_3bpy)][PF_6] as yellow crystals in good yield (239 mg, 0.24 mmol, 96%). ^{1}H NMR (500 MHz, $(CD_3)_2CO$, 298 K) *δ*/ppm 8.85 (d, *J* = 8.2 Hz, 1H, H^{B3}), 8.65 (d, *J* = 8.2 Hz, 1H, H^{A3}), 8.45 (t, *J* = 8.0 Hz, 1H, H^{B4}), 8.27 (d, *J* = 4.3 Hz, 1H, H^{A6}), 8.13 (td, *J* = 7.8, 1.7 Hz, 1H, H^{A4}), 8.00 (dd, *J* = 7.8, 0.9 Hz, 1H, H^{B5}), 7.49 – 7.11 (overlapping m, 16H, H^{D2+D3}), 7.43 – 7.48 (overlapping ddd, *J* = 8.2, 7.4, 1.7 Hz, 2H, H^{C5}), 7.28 – 7.24 (overlapping m , 1H, H^{A5}), 7.18 – 7.12 (m, 4H, H^{C4+C6}), 6.99 – 6.73 (overlapping m, 4H, H^{D4}), 6.94 – 6.89 (overlapping m, 2H, H^{C3}). ^{13}C NMR (126 MHz, $(CD_3)_2CO$, 298 K) *δ*/ppm 157.6 (C^{C1}), 154.2 (C^{B2}), 151.1 (C^{A2}), 149.2 (C^{A6}), 146.8 (C^{B6}), 140.9 (C^{B4}), 139.0 (C^{A4}), 134.0 (C^{C3}), 132.3 (C^{C5}), 130.2 (C^{D3}), 128.7 (t, *J* = 5.0 Hz, C^{D2}), 126.4 (C^{B3}), 126.3 (C^{A5}), 125.2 (t, *J* = 2.5 Hz, C^{C4}), 124.8 (C^{C2}), 123.6 (C^{A3}), 123.3 (C^{B5}),

120.0 (C^{C6}). ^{19}F NMR (235 MHz, $(CD_3)_2CO$, 300K) δ/ppm −66.3 s, CF_3), −72.6 (d, J_{PF} = 707 Hz, $[PF_6]^-$). ^{31}P NMR (162 MHz, $(CD_3)_2CO$, 300 K) δ/ppm −12.6 (broad, FWHM = 270 Hz, POP), −144.2 (septet, J_{PF} = 708 Hz, $[PF_6]^-$). ESI MS: *m/z* 825.5 $[M–PF_6]^+$ (base peak, calc. 825.2). Found C 57.90, H 3.87, N 3.24; [Cu(POP)(6-CF_3bpy)][PF_6] requires C 58.12, H 3.63, N 2.88.

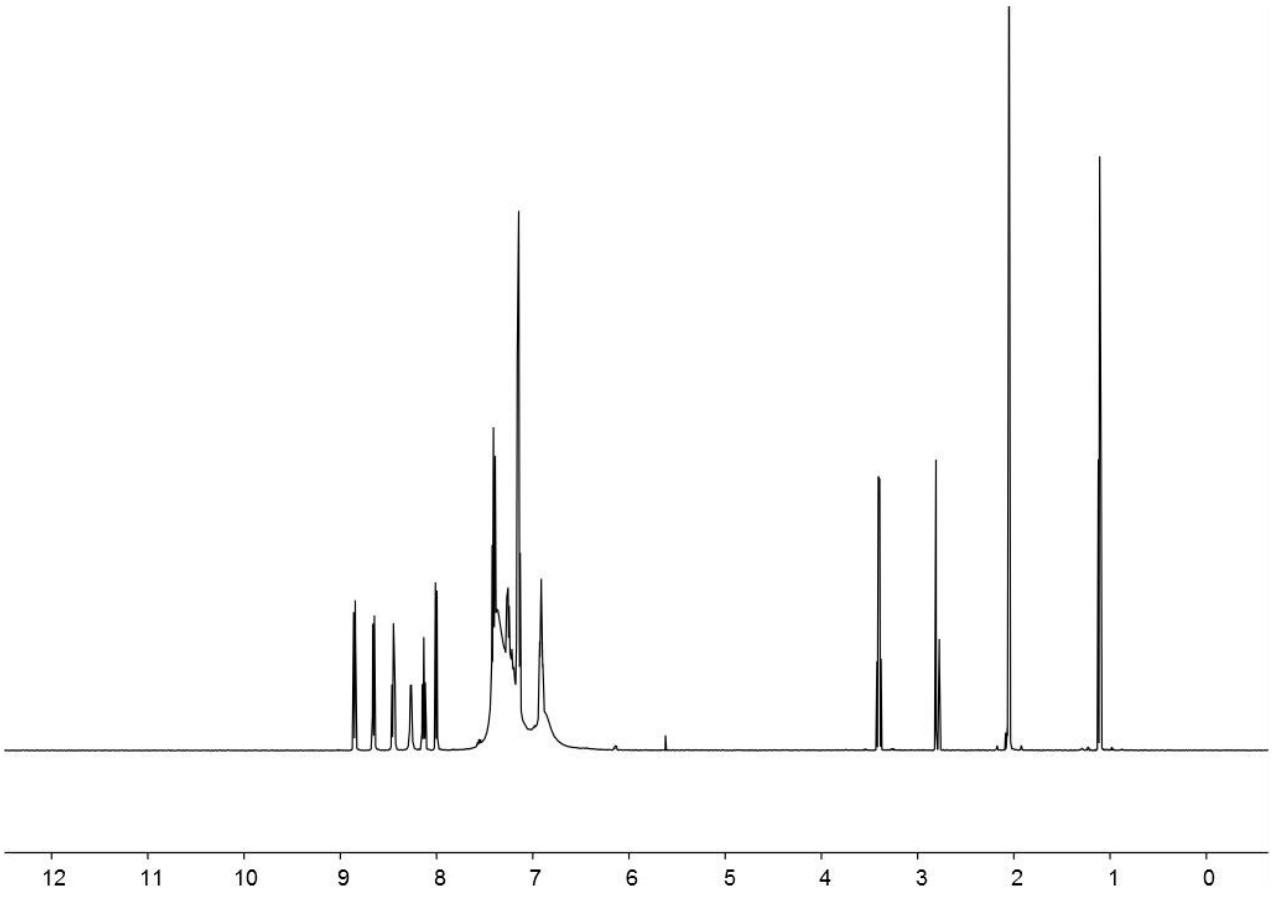

^1H NMR spectrum (400 MHz, $(CD_3)_2CO$) of [Cu(POP)(6-CF_3bpy)][PF_6]. Chemical shifts are in δ/ pm.

[Cu(xantphos)(6-CF_3bpy)][PF_6].

A colourless solution of xantphos (145 mg, 0.25 mmol, 1.0 eq) and 6-CF_3bpy (56 mg, 0.25 mmol, 1.0 eq) in CH_2Cl_2 (15 mL) was added dropwise to a colourless solution of [Cu($MeCN)_4$][PF_6] (93 mg, 0.25 mmol, 1.0 eq) in CH_2Cl_2 (15 mL). The resulting solution turns orange, then yellow. After stirring for 2h, solution was filtered and the solvent was removed in vacuo. The bright yellow powder was redissolved in CH_2Cl_2 and layered with Et_2O. This gave [Cu(xantphos)(6-CF_3bpy)][PF_6] as yellow crystals in moderate yield (136 mg, 0.13 mmol, 52%). ^1H NMR (500 MHz, $(CD_3)_2CO$, 298 K) δ/ppm 8.77 (d, J = 8.2 Hz, 1H, H^{B3}), 8.60 (d, J = 8.1 Hz, 1H, H^{A3}), 8.49 (t, J = 8.0 Hz, 1H, H^{B4}), 8.15 (td, J = 7.8, 1.6 Hz, 1H, H^{A4}), 8.12 (d, J = 8.0 Hz, 1H, H^{B5}), 7.98 (broad s, 1H, H^{A6}), 7.86 (dd, J = 7.8, 1.4

Hz, 2H, H^{C5}), 7.44 – 7.40 (overlapping m, 1H, H^{A5}), 7.36 (t, *J* = 7.6 Hz, 4H, H^{D4}), 7.28 (t, *J* = 7.7 Hz, 2H, H^{C4}), 7.23 (m, 8H, H^{D3}), 7.08 (broad m, 8H, H^{D2}), 6.79 (m, 2H, H^{C3}), 1.87 – 1.70 (overlapping m, 6H, $H^{Me/Me'}$). ^{13}C NMR (126 MHz, $(CD_3)_2CO$, 298 K) *δ*/ppm 155.5 (t, *J* = 6.4 Hz, C^{C1}), 154.6 (C^{B2}), 151.9 (C^{A2}), 149.4 (C^{A6}), 147.5 (C^{B6}), 142.0 (C^{B4}), 140.2 (C^{A4}), 134.6 (t, *J* = 1.8 Hz, C^{C6}), 133.85 (t, *J* = 8.1 Hz, C^{D2}), 132.5 (C^{D1}), 131.6 (C^{C3}), 131.0 (C^{D4}), 129.8 (C^{D3}), 128.7 (C^{C5}), 127.6 (C^{A5}), 127.23 (C^{B3}), 126.1 (t, *J* = 2.6 Hz, C^{C4}), 124.8 (C^{A3}), 124.4 (C^{B5}), 120.9 (t, *J* = 14.3 Hz, C^{C2}), 36.8 (C^{a}), 28.9 ($C^{Me/Me'}$), 28.5 ($C^{Me/Me'}$). ^{19}F NMR (276 MHz, $(CD_3)_2CO$, 300K) *δ*/ppm −67.3 s, CF_3), −72.6 (d, J_{PF} = 708 Hz, $[PF_6]^-$). ^{31}P NMR (162 MHz, $(CD_3)_2CO$, 300 K) *δ*/ppm −12.2 (broad, FWHM = 220 Hz, POP), −144.3 (septet, J_{PF} = 708 Hz, $[PF_6]^-$). ESI MS: *m/z* 865.5 $[M–PF_6]^+$ (base peak, calc. 865.2). Found C 59.30, H 4.00, N 3.04; [Cu(xantphos)(6-CF_3bpy)][PF_6] requires C 59.38, H 3.89, N 2.77.

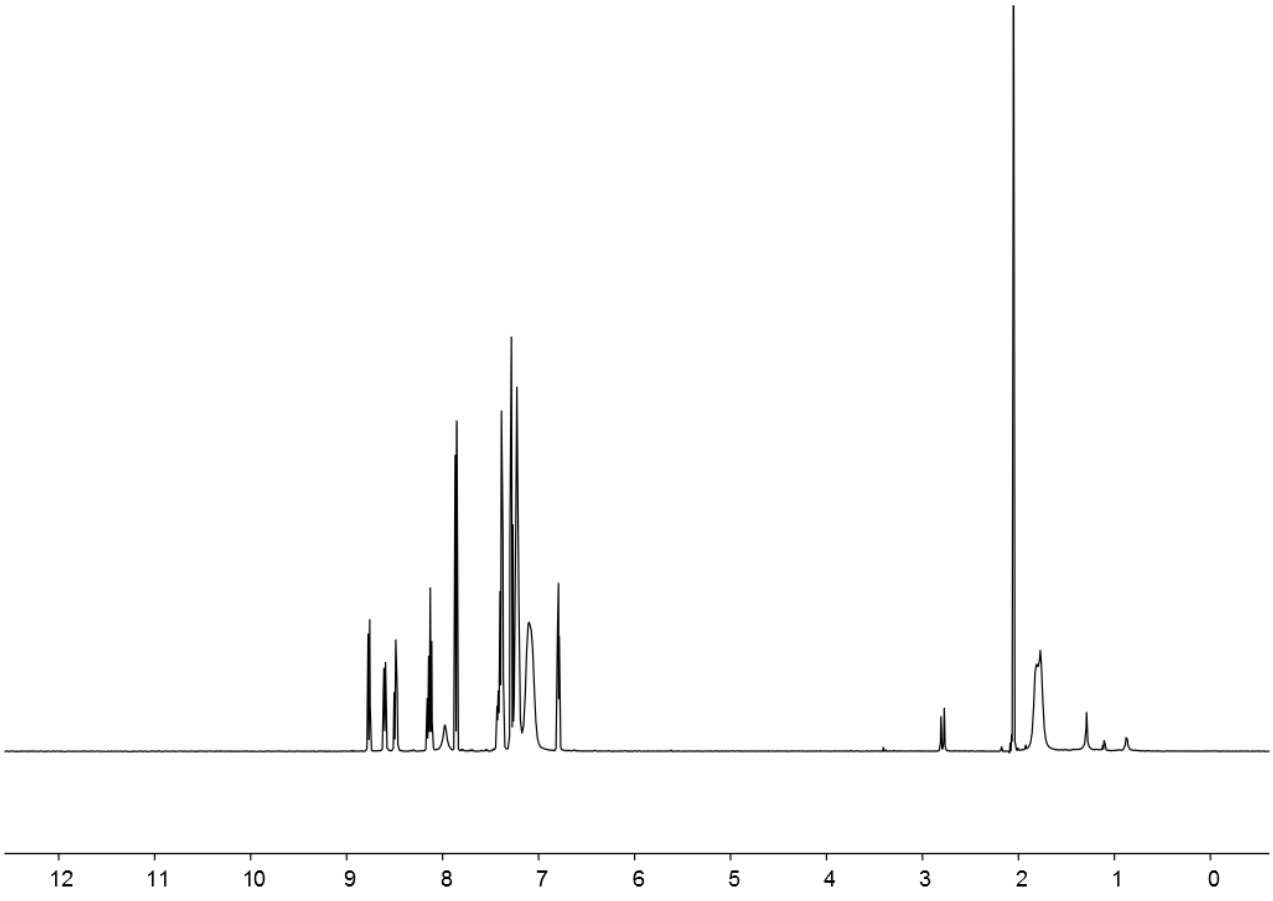

^{1}H NMR spectrum (400 MHz, $(CD_3)_2CO$) of [Cu(xantphos)(6-CF_3bpy)][PF_6]. Chemical shifts are in *δ*/ pm.

Crystallography. Single crystal data were collected on a STOE StadiVari diffractometer equipped with a Pilatus300K detector and with a Metaljet D2 source or a Bruker APEX-II diffractometer; data reduction, solution and refinement used the programs STOE X-AREA, STOE X-RED, APEX2, SuperFlip and CRYSTALS respectively.[6,7,8] Structural analysis was carried out using Mercury v. 3.7.[9,10]

[Cu(xantphos)(bpy)][PF$_6$]. $C_{49}H_{40}CuF_6N_2OP_3$, M = 943.32, yellow block, monoclinic, space group $P2_1/n$, a = 10.4166(10), b = 21.747(2), c = 19.1754(18) Å, β = 95.873(3)º, U = 4320.9(7) Å^3, Z = 4, D_c = 1.450 Mg m^{-3}, μ(Cu-Kα) = 2.331 mm^{-1}, T = 123 K. Total 27920 reflections, 7723 unique, R_{int} = 0.028. Refinement of 7596 reflections (559 parameters) with I >2σ(I) converged at final R_1 = 0.0302 (R_1 all data = 0.0306), wR_2 = 0.0753 (wR_2 all data = 0.0753), gof = 1.0277. CCDC 1581158.

[Cu(POP)(6-CF$_3$bpy)][PF$_6$]·1.3Et$_2$O·0.35H$_2$O. $C_{52.20}H_{48.70}CuF_9N_2O_{2.65}P_3$, M = 1073.92, yellow plate, triclinic, space group $P-1$, a = 12.6148(12), b = 14.9099(14), c = 16.1666(16) Å, α = 67.949(3), β = 72.032(3), γ = 85.037(3)º, U = 2679.4(5) Å^3, Z = 2, D_c = 1.331 Mg m^{-3}, μ(Cu-Kα) = 2.050 mm^{-1}, T = 123 K. Total 28983 reflections, 9323 unique, R_{int} = 0.026. Refinement of 9183 reflections (612 parameters) with I >2σ(I) converged at final R_1 = 0.0639 (R_1 all data = 0.0644), wR_2 = 0.1675 (wR_2 all data = 0.1679), gof = 0.9790. CCDC 1581154.

[Cu(xantphos)(6-CF$_3$bpy)][PF$_6$]·2Et$_2$O·1.5CH$_2$Cl$_2$. $C_{54.75}H_{50.50}Cl_{1.50}CuF_9N_2O_2P_3$, M = 1149.14, light orange block, triclinic, space group $P-1$, a = 11.0046(10), b = 15.2198(14), c = 18.3954(17) Å, α = 109.966(3), β = 96.715(4), γ = 109.663(3)º, U = 2631.8(4) Å^3, Z = 2, D_c = 1.450 Mg m^{-3}, μ(Cu-Kα) = 2.801 mm^{-1}, T = 123 K. Total 46919 reflections, 9253 unique, R_{int} = 0.026. Refinement of 9175 reflections (763 parameters) with I >2σ(I) converged at final R_1 = 0.0678 (R_1 all data = 0.0680), wR_2 = 0.1666 (wR_2 all data = 0.1666), gof = 0.9748. CCDC 1581155.

[Cu(POP)(4,4'-(CF$_3$)$_2$bpy)][PF$_6$]·0.5CH$_2$Cl$_2$. $C_{48.50}H_{35}ClCuF_{12}N_2OP_3$, M = 1081.72, yellow block, triclinic, space group $P-1$, a = 10.6772(5), b = 12.0684(6), c = 19.9763(8) Å, α = 85.488(4), β = 75.246(3), γ = 75.767(4)º, U = 2412.4(2) Å^3, Z = 2, D_c = 1.489 Mg m^{-3}, μ(Ga-Kα) = 3.89 mm^{-1}, T = 123 K. Total 32869 reflections, 9391 unique, R_{int} = 0.068. Refinement of 7495 reflections (631 parameters) with I >2σ(I) converged at final R_1 = 0.1388 (R_1 all data = 0.1530), wR_2 = 0.3094 (wR_2 all data = 0.3439), gof = 0.9382. CCDC 1581156.

[Cu(xantphos)(4,4'-(CF$_3$)$_2$bpy)][PF$_6$]. $C_{51}H_{38}CuF_{12}N_2OP_3$, M = 1079.32, yellow plate, triclinic, space group $P-1$, a = 11.4273(10), b = 13.1246(11), c = 17.1646(15) Å, α = 86.333(4), β = 72.361(3), γ = 73.413(4)º, U = 2350.5(4) Å^3, Z = 2, D_c = 1.525 Mg m^{-3}, μ(Cu-Kα) = 2.412 mm^{-1}, T = 123 K. Total 26603 reflections, 8065 unique, R_{int} = 0.047. Refinement of 7011 reflections (631 parameters) with I >2σ(I) converged at final R_1 =

0.0822 (R_1 all data = 0.0897), wR_2 = 0.2022 (wR_2 all data = 0.2051), gof = 1.1303. CCDC 1581157.

[Cu(POP)(5,5'-$(CF_3)_2$bpy)][PF_6]·0.5Et_2O. $C_{50}H_{39}CuF_{12}N_2O_{1.5}P_3$, M = 1076.32, light orange block, monoclinic, space group $P2_1/c$, a = 22.6472(17), b = 22.0637(15), c = 18.8935(13) Å, β = 94.420(3)º, U = 9412.7(12) Å^3, Z = 8, D_c = 1.519 Mg m^{-3}, μ(Cu-Kα) = 2.415 mm^{-1}, T = 123 K. Total 65314 reflections, 16314 unique, R_{int} = 0.027. Refinement of 14862 reflections (1245 parameters) with I >2σ(I) converged at final R_1 = 0.0529 (R_1 all data = 0.0565), wR_2 = 0.1399 (wR_2 all data = 0.1416), gof = 0.9395. CCDC 1581159.

Computational details. DFT calculations were performed for a group of eleven [Cu(P^P)(N^N)]$^+$ cations ((P^P) = POP, (N^N) = bpy, 6-CF_3bpy, 4,4'-$(CF_3)_2$bpy and 5,5'-$(CF_3)_2$bpy; (P^P) = xantphos, (N^N) = bpy, 6-CF_3bpy, 6-Mebpy, 4,4'-$(CF_3)_2$bpy, 5,5'-$(CF_3)_2$bpy, 6,6'-Me_2-4,4'-$(CF_3)_2$bpy and 6,6'-Me_2bpy) using the D.01 revision of the Gaussian 09 program package.[11] The Becke's three-parameter B3LYP exchange-correlation functional[12,13] was used together with the 6-31G** basis set for C, H, F, N and O,[14] and the "double-ζ" quality LANL2DZ basis set for the Cu atom.[15] Relativistic effects were accounted for by means of an effective core potential (ECP), which was used to replace the inner core electrons of Cu. The geometries of all the complexes in their singlet ground electronic state (S_0) were fully optimized without imposing any symmetry restriction. The geometry of the lowest-energy triplet excited state (T_1) was also optimized for all complexes at the spin-unrestricted UB3LYP level using a spin multiplicity of three. The lowest-lying excited states of each complex, both singlet and triplet, were computed at the minimum-energy geometry optimized for S_0 using the time-dependent DFT (TD-DFT) approach.[16,17,18] All the calculations were performed in the presence of the solvent (CH_2Cl_2). Solvent effects were considered within the self-consistent reaction field (SCRF) theory using the polarized continuum model (PCM) approach.[19,20,21] Phosphorescent emission energies were estimated as the vertical energy difference between T_1 and S_0 at the optimized minimum-energy geometry of T_1. The calculation of the energy of S_0 at the T_1 geometry was performed as an equilibrium single-point calculation with respect to the solvent reaction field/solute electronic density polarization process. The S_1 and T_1 states of a representative set of complexes were also optimized using the TD-DFT approach.

LEC fabrication. All materials were used as received. Poly(3,4-ethylenedioxythiophene):polystyrene sulfonate (PEDOT:PSS Clevios P VP AI 4083) was purchased from Heraeus. The ionic liquid (IL) 1-ethyl-3-methylimidazolium hexafluoridophosphate > 97% ([Emim][PF_6]) were purchased from Sigma Aldrich. The

photolithography-patterned indium tin oxide (ITO) glass substrates were purchased from Naranjo Substrates (www.naranjosubstrates.com).

LECs were prepared as follows. The substrates were subsequently cleaned with soap, deionized water, and isopropanol in an ultrasonic bath for 5 minutes each, followed by 20 minutes of UV-ozone treatment. Onto the clean ITO substrates, the PEDOT:PSS ink was filtered with a 0.45 μm pore size filter yielding to 80 nm thick film. The PEDOT:PSS layer was dried at 150 ºC for 15 minutes. On top of it, a 120 nm thick film of the emissive layer (complex:IL in a 4-to-1 molar ratio) was deposited from dichloromethane solution, which was filtered using 0.22μm pore filter. After the emissive layer coating, the samples were transferred to a glove box (MBraun, O_2 < 0.1 ppm, H_2O < 0.1 ppm) and a 70 nm thick film of aluminum was deposited as top electrode contact using a shadow mask. The active area in all devices is 6.5 mm^2.

LEC characterization. LECs were tested by applying a pulsed current and by monitoring the voltage and the luminance with a True Colour Sensor (MTCSiCT Sensor, MAZeT GimbH) using a Lifetime Test System (Botest OLT OLED Lifetime-Test System, Botest System GmbH). The pulsed current consisted of a block wave at 1 kHz frequency with a duty cycle of 50%. The peak current density of the pulse was 200 A m^{-2} and the average current density was 100 A m^{-2}. Electroluminescence spectra were recorded using an Avantes fibre optics photo-spectrometer. All devices were tested without encapsulation and were characterized inside the glove-box at room temperature.

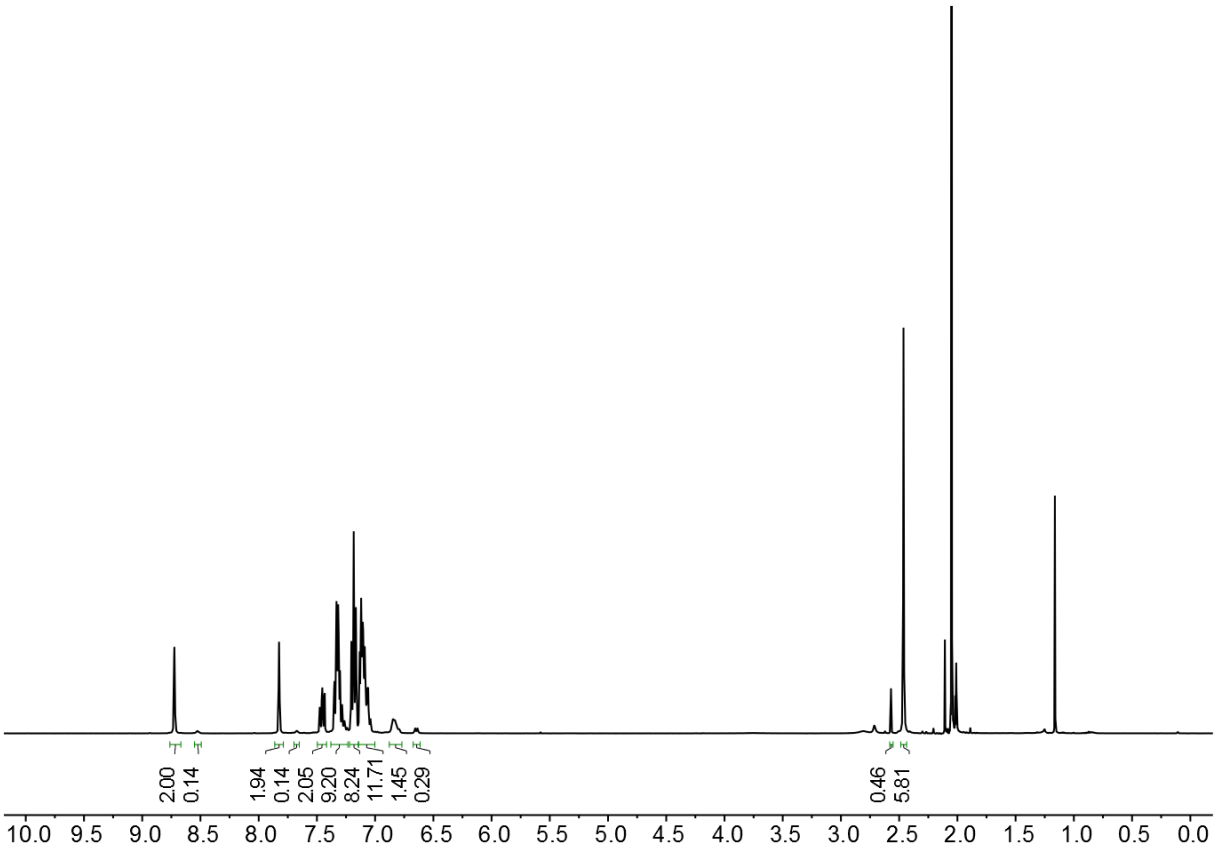

Figure S1. ^{1}H NMR spectrum (400 MHz, $(CD_3)_2CO$) of a 1 : 1.2 : 1 mixture of $[Cu(MeCN)_4][PF_6]$, POP and 6,6'-Me_2-4,4'-$(CF_3)_2$bpy. Chemical shifts are in δ/ pm.

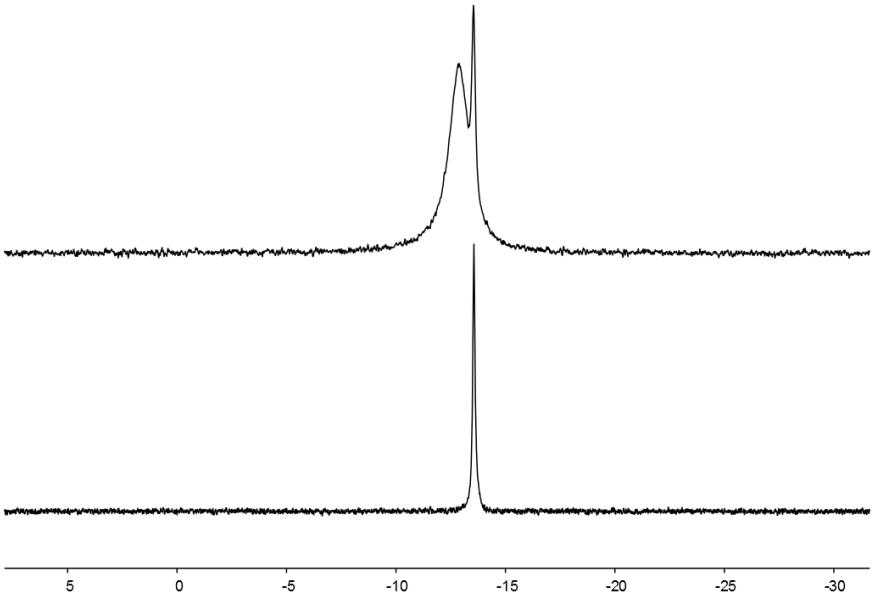

Figure S2. Part of the ^{31}P NMR spectrum (162 MHz, $(CD_3)_2CO$) of a 1:1.2:1 mixture of $[Cu(MeCN)_4][PF_6]$, POP and 6,6'-Me_2-4,4'-$(CF_3)_2$bpy (top) and ^{31}P NMR spectrum (162 MHz, $(CD_3)_2CO$) of $[Cu(POP)_2][PF_6]$ (bottom). Chemical shifts are in δ/ pm.

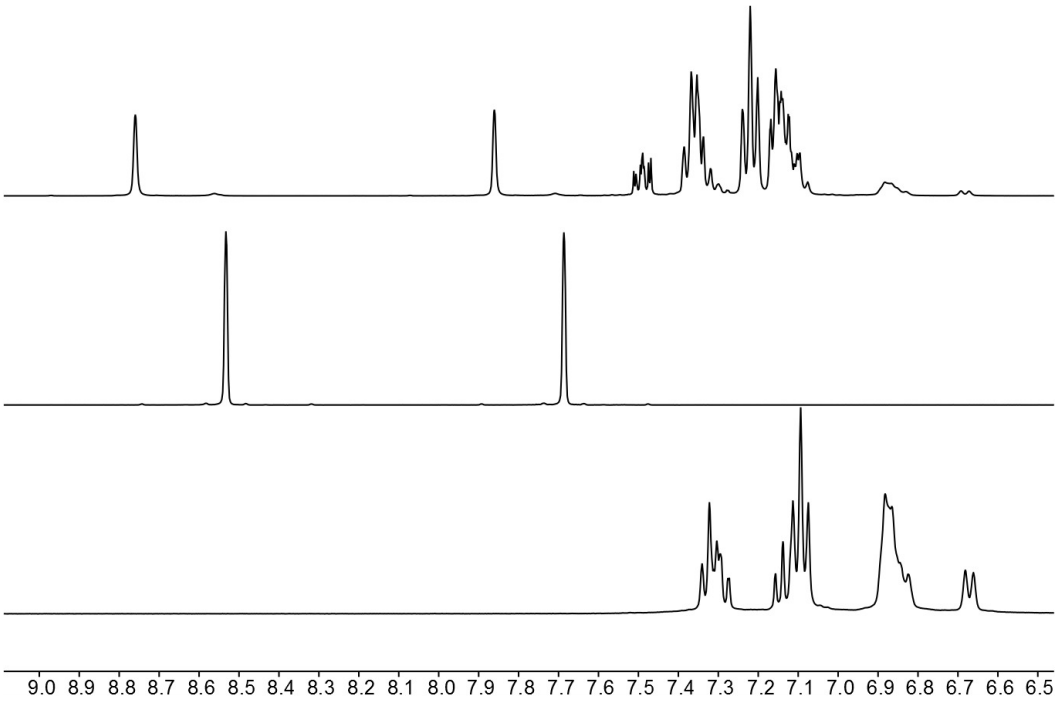

Figure S3. ^{1}H NMR spectra (400 MHz, $(CD_3)_2CO$) of a 1:1.2:1 mixture of $[Cu(MeCN)_4][PF_6]$, POP and 6,6'-Me_2-4,4'-$(CF_3)_2$bpy (top), free 6,6'-Me_2-4,4'-$(CF_3)_2$bpy (middle) and $[Cu(POP)_2][PF_6]$ (bottom).

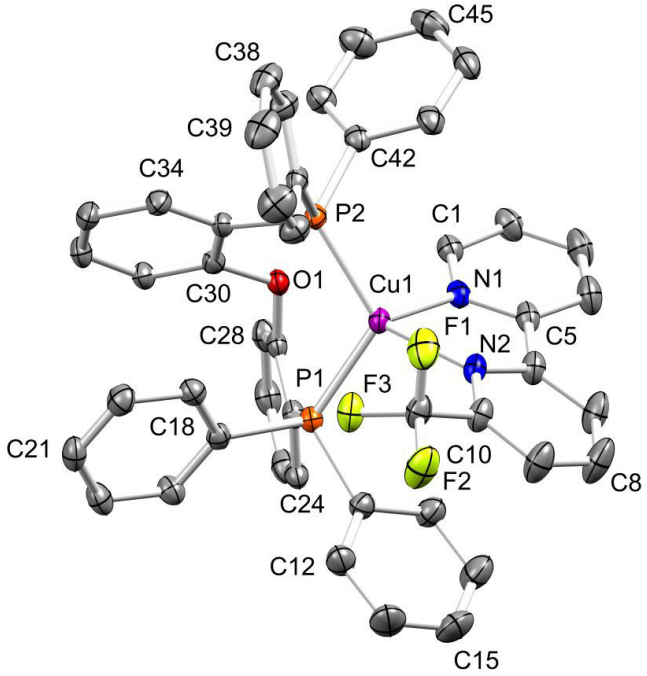

Figure S4. Structure of the $[Cu(POP)(6\text{-}CF_3bpy)]^+$ cation in $[Cu(POP)(6\text{-}CF_3bpy)][PF_6]\cdot 1.3Et_2O\cdot 0.35H_2O$ with ellipsoids plotted at 50% probability level; H atoms are omitted. Selected bond parameters: Cu1–P1 = 2.2679(8), Cu1–P2 = 2.2307(8), Cu1–N1 = 2.079(2), Cu1–N2 = 2.134(2) Å; P1–Cu1–P2 = 115.68(3), P1–Cu1–N1 = 110.29(7), P2–Cu1–N1 = 106.16(7), P1–Cu1–N2 = 104.16(7), P2–Cu1–N2 = 133.19(7), N1–Cu1–N2 = 80.35(10)°.

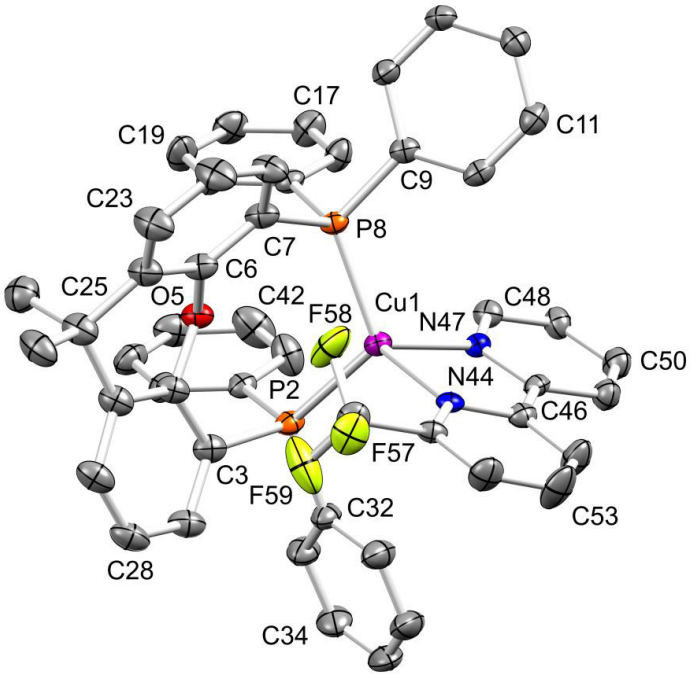

Figure S5. Structure of the $[Cu(xantphos)(6\text{-}CF_3bpy)]^+$ cation in $[Cu(xantphos)(6\text{-}CF_3bpy)][PF_6]\cdot 2Et_2O\cdot 1.5CH_2Cl_2$ with ellipsoids plotted at 50% probability level; H atoms are omitted. Selected bond parameters: Cu1–P2 = 2.2710(9), Cu1–P8 = 2.2655(9), Cu1–N47 = 2.014(2), Cu1–N44 = 2.1523(19) Å; P2–Cu1–P8 = 113.55(3), P2–Cu1–N47 = 111.46(8), P8–Cu1–N47 = 112.06(8), P2–Cu1–N44 = 112.47(8), P8–Cu1–N44 = 122.56(8), N47–Cu1–N44 = 79.93(9)°.

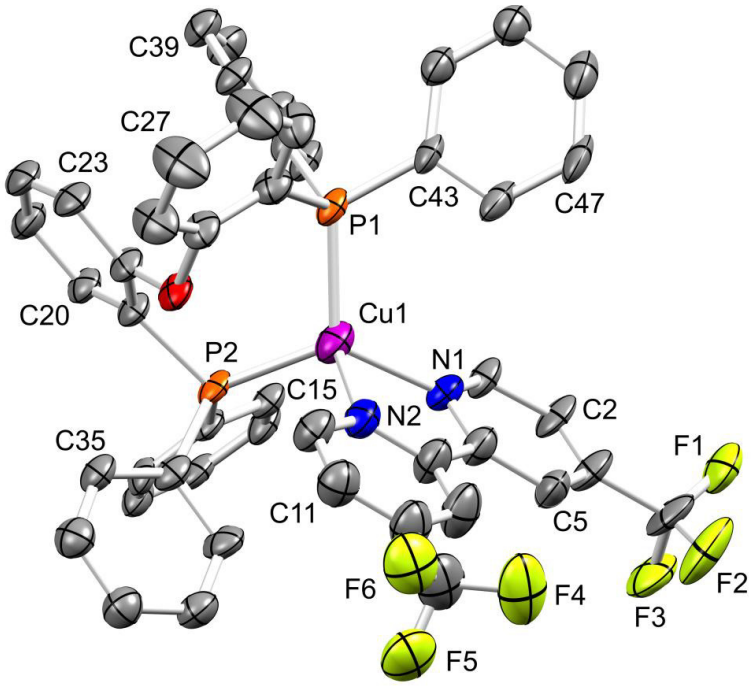

Figure S6. Structure of the $[Cu(POP)(4,4'\text{-}(CF_3)_2bpy)]^+$ cation in $[Cu(POP)(4,4'\text{-}(CF_3)_2bpy)][PF_6]\cdot 0.5CH_2Cl_2$ with ellipsoids plotted at 30% probability level; H atoms are omitted. Selected bond parameters: Cu1–P2 = 2.2566(16), Cu1–P1 = 2.2477(15), Cu1–N2 = 2.084(6), Cu1–N1 = 2.057(5) Å; P2–Cu1–P1 = 113.02(5), P2–Cu1–N2 = 106.79(17), P1–Cu1–N2 = 113.76(16), P2–Cu1–N1 = 119.99(15), P1–Cu1–N1 = 117.99(15), N2–Cu1–N1 = 79.7(2)°.

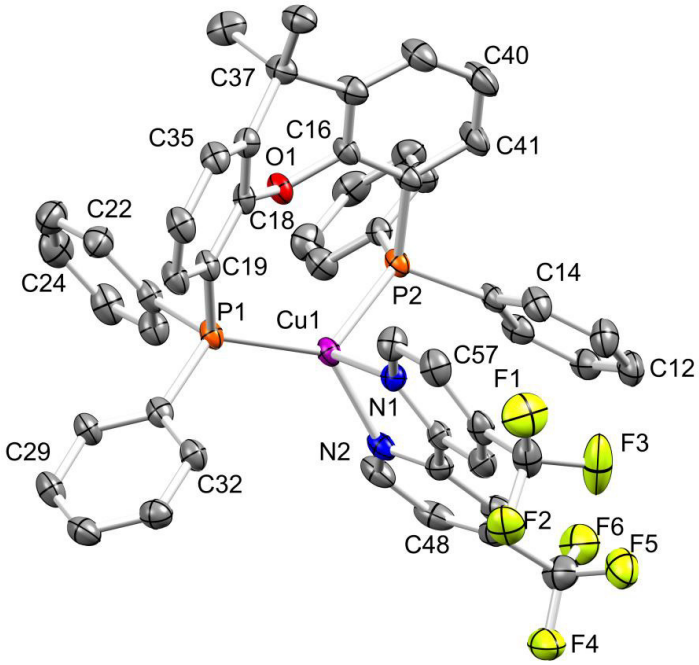

Figure S7. Structure of the $[Cu(xantphos)(4,4'\text{-}(CF_3)_2bpy)]^+$ cation in $[Cu(xantphos)(4,4'\text{-}(CF_3)_2bpy)][PF_6]$ with ellipsoids plotted at 50% probability level; H atoms are omitted. Selected bond parameters: Cu1–P2 = 2.2841(10), Cu1–P1 = 2.2159(11), Cu1–N2 = 2.062(3), Cu1–N1 = 2.083(3) Å; P2–Cu1–P1 = 122.58(4), P2–Cu1–N2 = 100.17(9), P1–Cu1–N2 = 130.08(9), P2–Cu1–N1 = 102.65(9), P1–Cu1–N1 = 111.04(9), N2–Cu1–N1 = 79.63(13)°.

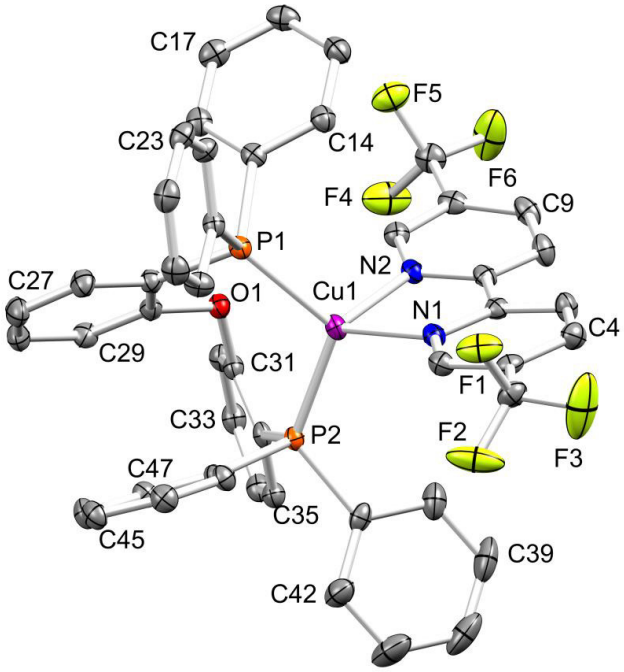

Figure S8. Structure of the $[Cu(POP)(5,5'\text{-}(CF_3)_2bpy)]^+$ cation in $[Cu(POP)(5,5'\text{-}(CF_3)_2bpy)][PF_6]\cdot 0.5Et_2O$ with ellipsoids plotted at 50% probability level; second disordered cation in the unit cell and H atoms are omitted. Selected bond parameters: Cu1–P1 = 2.2523(8), Cu1–P2 = 2.2604(8), Cu1–N1 = 2.078(2), Cu1–N2 = 2.076(2) Å; P1–Cu1–P2 = 111.87(3), P1–Cu1–N1 = 124.27(7), P2–Cu1–N1 = 114.18(7), P1–Cu1–N2 = 108.33(7), P2–Cu1–N2 = 114.26(6), N1–Cu1–N2 = 79.25(9)°.

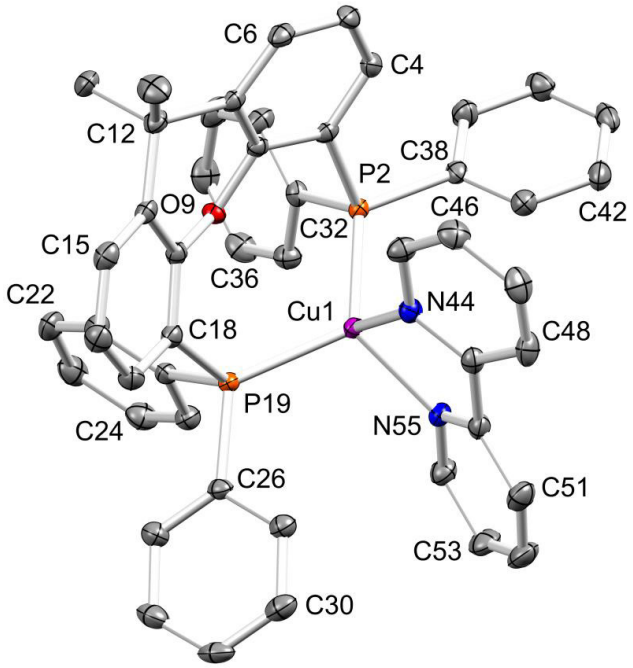

Figure S9. Structure of the $[Cu(xantphos)(bpy)]^+$ cation in $[Cu(xantphos)(bpy)[PF_6]$ with ellipsoids plotted at 50% probability level; H atoms are omitted. Selected bond parameters: Cu1–P2 = 2.2539(4), Cu1–P19 = 2.2830(4), Cu1–N44 = 2.1210(12), Cu1–N55 = 2.0583(12) Å; P2–Cu1–P19 = 113.816(14), P2–Cu1–N44 = 105.59(3), P19–Cu1–N44 = 116.58(3), P2–Cu–N55 = 125.38(3), P19–Cu1–N55 = 111.24(3), N44–Cu1–N55 = 79.32(5)°.

Table S1. Selected structural parameters calculated at the B3LYP/(6-31G**+LANL2DZ) level in CH_2Cl_2 solution for the $[Cu(P^P)(N^N)]^+$ complexes in their electronic ground state S_0. The angle formed by the P–Cu–P and N–Cu–N planes (last column) is reported for both the S_0 and T_1 (within parentheses) states at their respective optimized geometries.

Complex	Cu–P bond length (Å)	Cu–N bond length (Å)	P–Cu–P chelating angle (°)	N–Cu–N chelating angle (°)	P–Cu–P/N–Cu–N angle (°)
$[Cu(POP)(bpy)]^+$	2.380; 2.380	2.159; 2.161	115.51	77.10	88.79 (58.03)
$[Cu(xantphos)(bpy)]^+$	2.376; 2.382	2.166; 2.155	115.92	77.10	88.88 (58.34)
$[Cu(POP)(6\text{-}CF_3bpy)]^+$	2.428; 2.393	2.276; 2.159	116.59	75.38	85.07 (71.43)
$[Cu(xantphos)(6\text{-}CF_3bpy)]^+$	2.404; 2.392	2.260; 2.152	115.63	75.80	88.52 (70.67)
$[Cu(POP)(5,5'\text{-}(CF_3)_2bpy)]^+$	2.372; 2.378	2.164; 2.172	115.93	76.49	85.33 (57.94)
$[Cu(xantphos)(5,5'\text{-}(CF_3)_2bpy)]^+$	2.379; 2.376	2.183; 2.157	116.89	76.25	88.87 (57.95)
$[Cu(POP)(4,4'\text{-}(CF_3)_2bpy)]^+$	2.368; 2.383	2.162; 2.167	115.94	76.82	85.59 (57.93)
$[Cu(xantphos)(4,4'\text{-}(CF_3)_2bpy)]^+$	2.380; 2.381	2.177; 2.155	116.65	76.65	89.13 (58.71)
$[Cu(xantphos)(6,6'\text{-}Me_2\text{-}4,4'\text{-}(CF_3)_2bpy)]^+$	2.429; 2.421	2.206; 2.202	114.68	76.68	89.56 (74.26)
$[Cu(xantphos)(6\text{-}Mebpy)]^+$	2.397; 2.400	2.178; 2.153	113.92	77.26	88.98 (70.31)
$[Cu(xantphos)(6,6'\text{-}Me_2bpy)]^+$	2.433; 2.425	2.195; 2.197	113.71	77.16	88.99 (74.43)

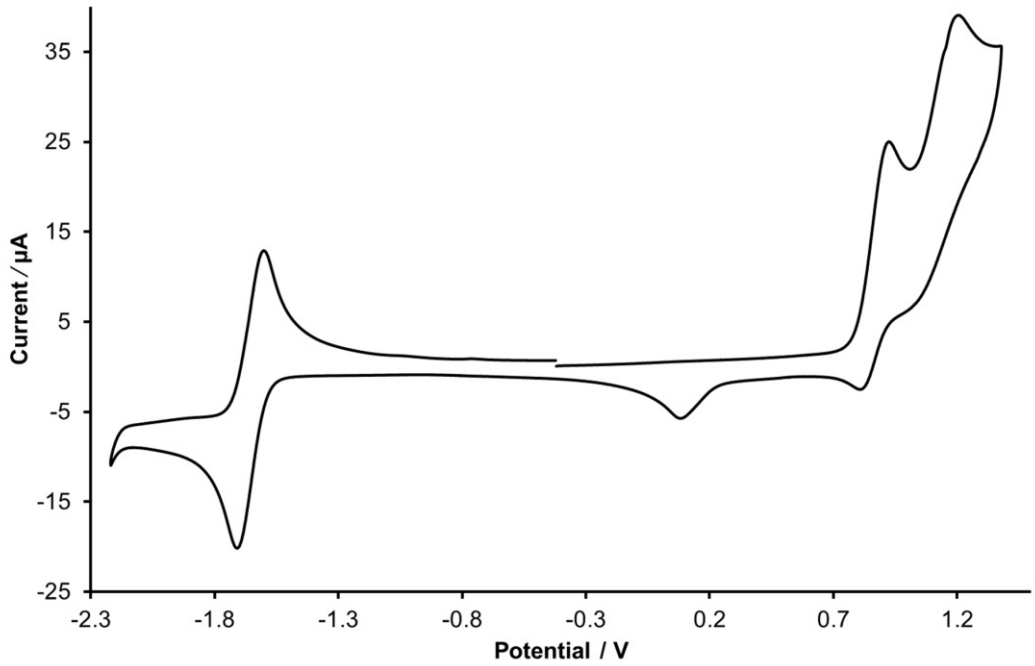

Figure S10. Cyclic voltammogram of a CH_2Cl_2 solution of [Cu(POP)(4,4'-$(CF_3)_2$bpy)][PF_6] (vs. Fc^+/Fc, [*n*Bu_4N][PF_6] supporting electrolyte, scan rate = 0.1 V s^{-1}).

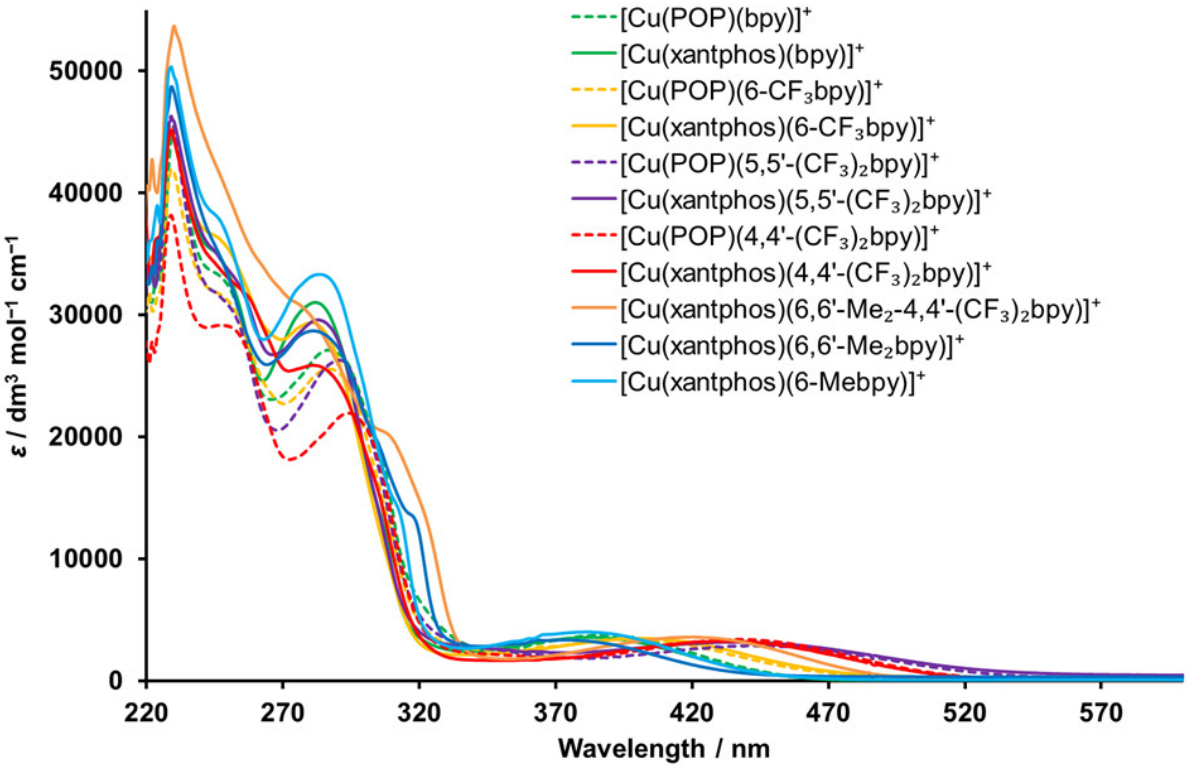

Figure S11. Solution absorption spectra of the [Cu(P^P)(N^N)][PF_6] complexes (CH_2Cl_2, 2.5 × 10^{-5} mol dm^{-3}).

Table S2. Comparison of the MLCT maxima of the absorption spectra of [Cu(xantphos)(N^N)][PF_6] complexes with respect to [Cu(xantphos)(bpy)][PF_6] (CH_2Cl_2, 2.5×10^{-5} mol dm^{-3}).

	UV-Vis MLCT λ_{max} / nm	Δ / nm	Δ / cm^{-1}	Δ / meV
[Cu(xantphos)(bpy)][PF_6]	383	0	0	0
[Cu(xantphos)(6-CF_3bpy)][PF_6]	402	19	1234	153
[Cu(xantphos)(5,5'-$(CF_3)_2$bpy)][PF_6]	437	54	3226	400
[Cu(xantphos)(4,4'-$(CF_3)_2$bpy)][PF_6]	433	50	3015	374
[Cu(xantphos)(6,6'-Me_2-4,4'-$(CF_3)_2$bpy)][PF_6]	421	38	2357	292
[Cu(xantphos)(6-Mebpy)][PF_6]	381	-2	-137	-17
[Cu(xantphos)(6,6'-Me_2bpy)][PF_6]	375	-8	-557	-69

Table S3. Comparison of the maxima of the powder emission spectra of [Cu(P^P)(N^N)][PF_6] complexes with respect to [Cu(xantphos)(bpy)][PF_6] and [Cu(POP)(bpy)][PF_6], respectively.

	Powder emission λ_{max} / nm	Δ / nm	Δ / cm^{-1}	Δ / meV
[Cu(POP)(bpy)][PF_6]	581	0	0	0
[Cu(xantphos)(bpy)][PF_6]	587	0	0	0
[Cu(POP)(6-CF_3bpy)][PF_6]	575	-6	-180	-22
[Cu(xantphos)(6-CF_3bpy)][PF_6]	581	-6	-176	-22
[Cu(POP)(5,5'-$(CF_3)_2$bpy)][PF_6]	648	67	1780	221
[Cu(xantphos)(5,5'-$(CF_3)_2$bpy)][PF_6]	647	60	1580	196
[Cu(POP)(4,4'-$(CF_3)_2$bpy)][PF_6]	664	83	2151	267
[Cu(xantphos)(4,4'-$(CF_3)_2$bpy)][PF_6]	632	45	1213	150
[Cu(xantphos)(6,6'-Me_2-4,4'-$(CF_3)_2$bpy)][PF_6]	517	-70	-2307	-286
[Cu(xantphos)(6-Mebpy)][PF_6]	547	-40	-1246	-154
[Cu(xantphos)(6,6'-Me_2bpy)][PF_6]	539	-48	-1517	-188

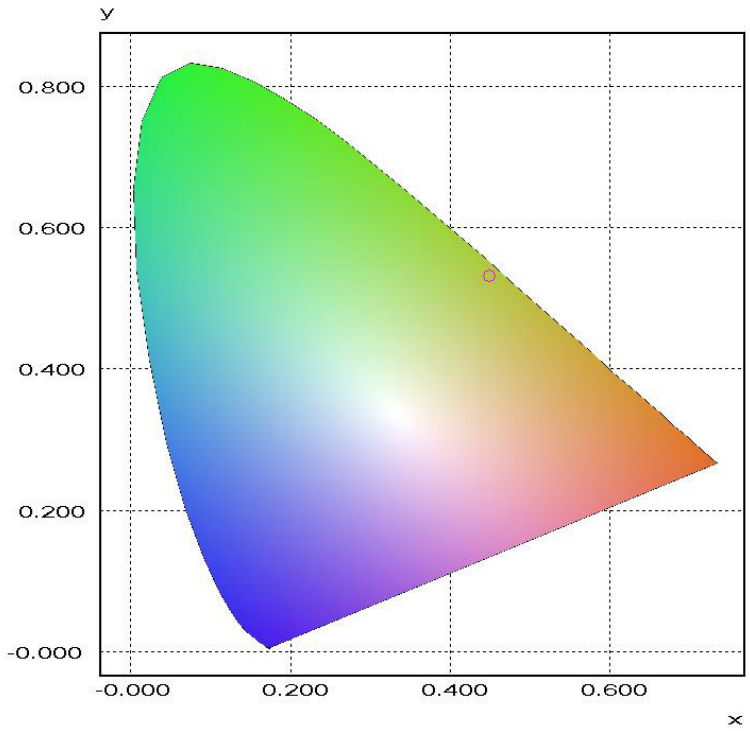

Figure S12. CIE coordinates of solid [Cu(xantphos)(6,6'-Me_2-4,4'-$(CF_3)_2$bpy)][PF_6], λ_{exc} = 365 nm.

Table S4. Emission maxima and lifetime values of frozen solutions of the complexes in Me-THF at 77 K.

	λ_{em}^{max} / nm		Energy difference[a]			Lifetime /µs		
Complex	77 K Me-THF	Powder	Δ / nm	Δ / cm^{-1}	Δ / meV	77 K Me-THF	Powder	Factor increase[a]
[Cu(POP)(bpy)][PF_6]	610	581	29	818	101	16	1.5	10.7
[Cu(xantphos)(bpy)][PF_6]	613	587	26	723	90	11	1.3	8.5
[Cu(POP)(6-CF_3bpy)][PF_6]	610	575	35	998	124	45	2.9	15.5
[Cu(xantphos)(6-CF_3bpy)][PF_6]	595	581	14	405	50	31	2.9	10.7
[Cu(POP)(5,5'-$(CF_3)_2$bpy)][PF_6]	656	648	8	188	23	––	0.185	––
[Cu(xantphos)(5,5'-$(CF_3)_2$bpy)][PF_6]	646	647	−1	−24	−3	––	0.251	––
[Cu(POP)(4,4'-$(CF_3)_2$bpy)][PF_6]	650	664	−14	−324	−40	3	0.096	31.3
[Cu(xantphos)(4,4'-$(CF_3)_2$bpy)][PF_6]	652	632	20	485	60	5	0.579	8.6
[Cu(xantphos)(6,6'-Me_2-4,4'-$(CF_3)_2$bpy)][PF_6]	604	517	87	2786	345	42	12	3.5
[Cu(xantphos)(6-Mebpy)][PF_6]	567	547	20	645	80	46	9.6	4.8
[Cu(xantphos)(6,6'-Me_2bpy)][PF_6]	551	539	12	404	50	88	11.4	7.7

[a]Comparison between powder emission at 298 K and emission in frozen glass (77 K).

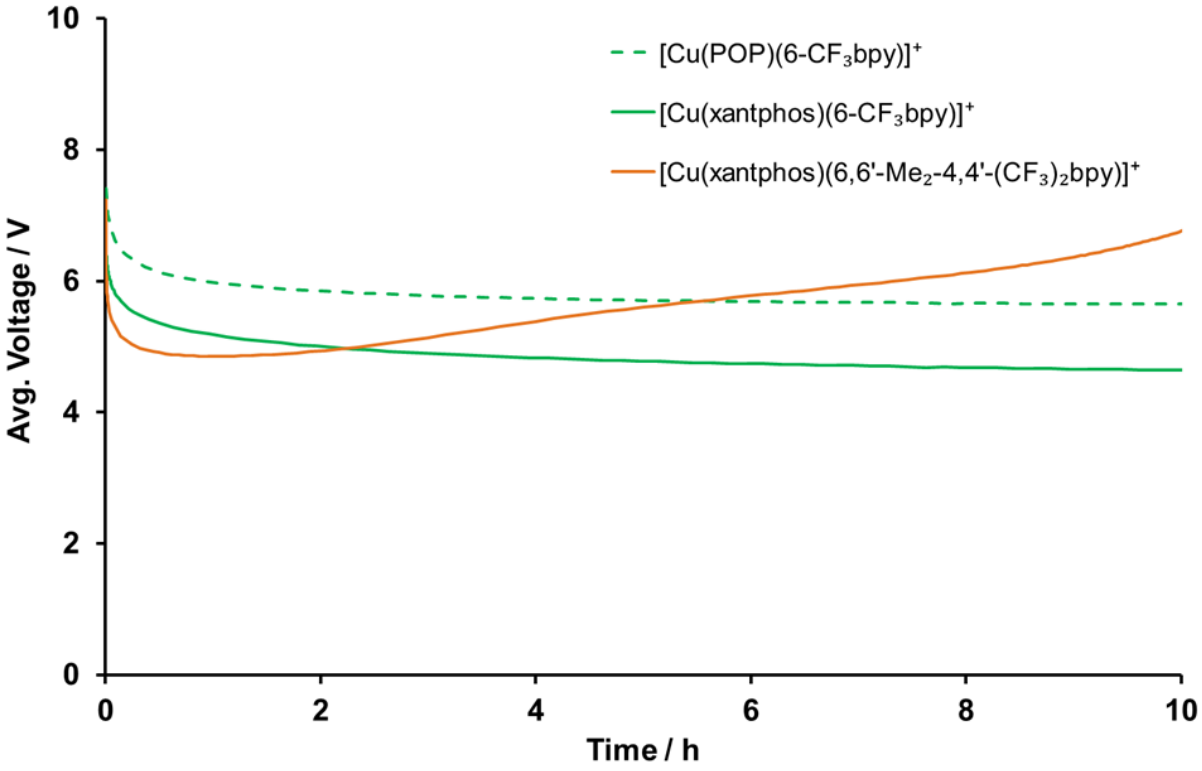

Figure S13. Average voltage versus time characteristics for ITO/PEDOT:PSS/[Cu(P^P)^N^N)][PF_6]:[Emim][PF_6] 4:1/Al LECs operated at pulsed current (average density current 100 A m^{-2}, 1 kHz, 50% duty cycle, block wave).

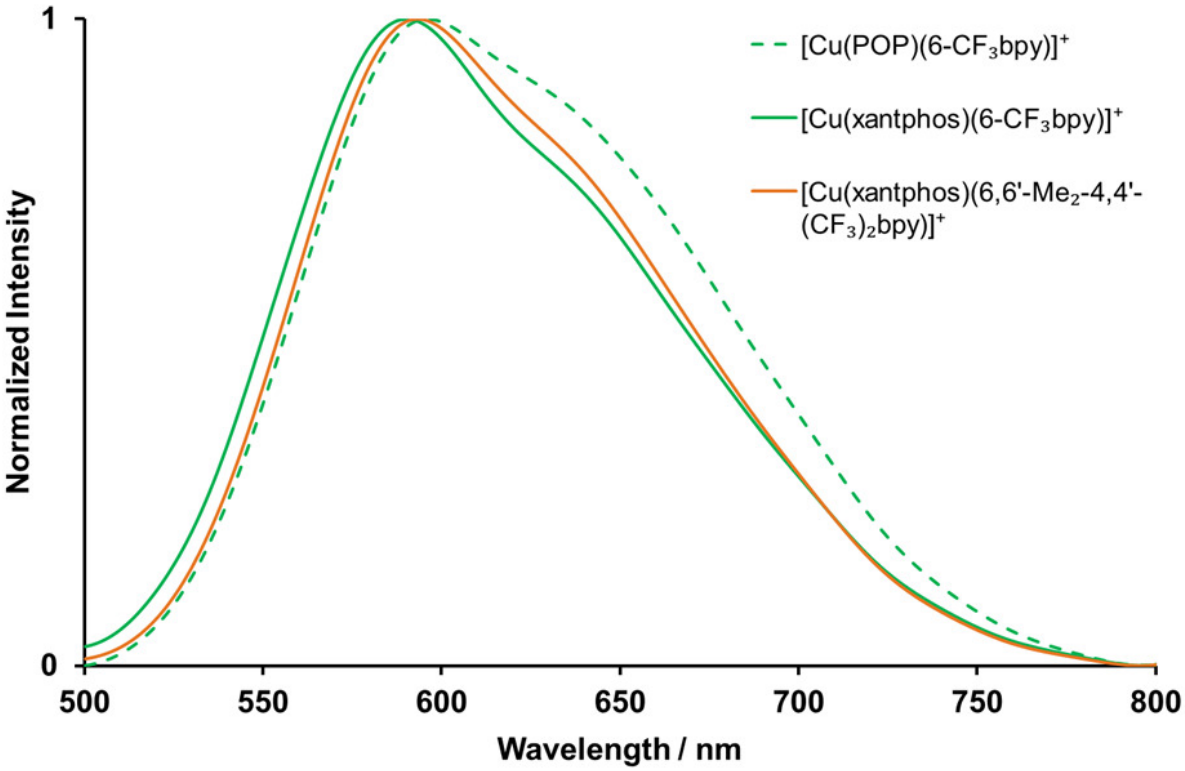

Figure S14. Electroluminescence (EL) spectra for ITO/PEDOT:PSS/[Cu(P^P)^N^N)][PF_6]:[Emim][PF_6] 4:1/Al LECs operated at pulsed current (average density current 100 A m^{-2}, 1 kHz, 50% duty cycle, block wave).

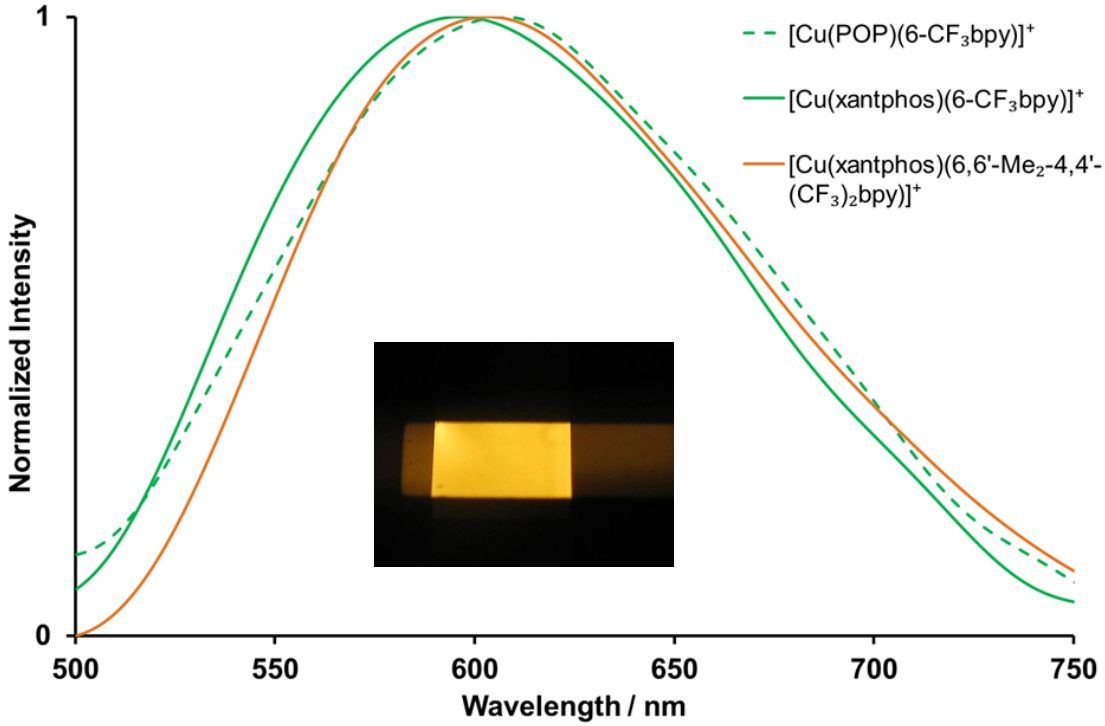

Figure S15. Photoluminescence spectra of thin films composed of [Cu(P^P)^N^N)][PF_6]:[Emim][PF_6] at a 4:1 molar ratio (λ_{exc} = 360 nm). Inset: A photograph of the LEC with [Cu(xantphos)(6 -CF_3bpy)][PF_6].

References

1 R. M. O'Donnell, R. N. Sampaio, G. Li, P. G. Johansson, C. L. Ward, G. J. Meyer, *J. Am. Chem. Soc.* **2016**, *138*, 3891-3903.

2 T. Güden-Silber, K. Klein, M. Seitz, *Dalton Trans.* **2013**, *42*, 13882-13888.

3 M. Shaul, Y. Cohen, *J. Org. Chem.* 1999, **64**, 9358-9364.

4 G. J. Kubas, *Inorg. Synth*. **1979**, *19*, 90-92.

5 R. D. Costa, D. Tordera, E. Ortí, H. J. Bolink, J. Schönle, S. Graber, C. E. Housecroft, E. C. Constable, J. A. Zampese, *J. Mater. Chem.* 2011, **21**, 16108-16118.

6 Stoe & Cie (2011). X-area Software, Stoe & Cie (1996). XRED V1.08.

7 L. Palatinus and G. Chapuis, *J. Appl. Cryst*., 2007, **40**, 786-790.

8 P.W. Betteridge, J.R. Carruthers, R.I. Cooper, K. Prout and D.J. Watkin, *J. Appl. Cryst*., 2003, **36**, 1487-1487.

9 I. J. Bruno, J. C. Cole, P. R. Edgington, M. K. Kessler, C. F. Macrae, P. McCabe, J. Pearson, R. Taylor, *Acta Crystallogr., Sect. B* **2002**, *58*, 389-397.

10 C. F. Macrae, I. J. Bruno, J. A. Chisholm, P. R. Edgington, P. McCabe, E. Pidcock, L. Rodriguez-Monge, R. Taylor, J. van de Streek and P. A. Wood, *J. Appl. Cryst*. **2008**, *41*, 466-470.

11 Gaussian 09, Revision D.01, M. J. Frisch, G. W. Trucks, H. B. Schlegel, G. E. Scuseria, M. A. Robb, J. R. Cheeseman, G. Scalmani, V. Barone, B. Mennucci, G. A. Petersson, H. Nakatsuji, M. Caricato, X. Li, H. P. Hratchian, A. F. Izmaylov, J. Bloino, G. Zheng, J. L. Sonnenberg, M. Hada, M. Ehara, K. Toyota, R. Fukuda, J. Hasegawa, M. Ishida, T. Nakajima, Y. Honda, O. Kitao, H. Nakai, T. Vreven, J. A. Montgomery Jr., J. E. Peralta, F. Ogliaro, M. Bearpark, J. J. Heyd, E. Brothers, K. N. Kudin, V. N. Staroverov, R. Kobayashi, J. Normand, K. Raghavachari, A. Rendell, J. C. Burant, S. S. Iyengar, J. Tomasi, M. Cossi, N. Rega, J. M. Millam, M. Klene, J. E. Knox, J. B. Cross, V. Bakken, C. Adamo, J. Jaramillo, R. Gomperts, R. E. Stratmann, O. Yazyev, A. J. Austin, R. Cammi, C. Pomelli, J. Ochterski, R. L. Martin, K. Morokuma, V. G. Zakrzewski, G. A. Voth, P. Salvador, J. J. Dannenberg, S. Dapprich, A. D. Daniels, Ö. Farkas, J. B. Foresman, J. V. Ortiz, J. Cioslowski, D. J. Fox, Gaussian, Inc., Wallingford CT, **2009**.

12 C. Lee, W. Yang, R.G. Parr, *Phys. Rev. B* **1988**, *37*, 785-789.

13 A. D. Becke, *J. Chem. Phys.* **1993**, *98*, 5648-5652.

14 M. M. Francl, W. J. Pietro, W. J. Hehre, J. S. Binkley, M. S. Gordon, D. J. DeFrees, J. A. Pople, *J. Chem. Phys.* **1982**, *77*, 3654-3665.

15 P. J. Hay, W. R. Wadt, *J. Chem. Phys.* **1985**, *82*, 299-310.

16 M. Petersilka, U. J. Gossmann, E. K. U. Gross, *Phys. Rev. Lett.* **1996**, *76*, 1212-1215.

17 C. Jamorski, M. E. Casida, D. R. Salahub, *J. Chem. Phys.* **1996**, *104*, 5134-5147.

18 M. E. Casida, C. Jamorski, K. C. Casida, D. R. Salahub, *J. Chem. Phys.* **1998**, *108*, 4439-4449.

19 J. Tomasi, M. Persico, *Chem. Rev.* **1994**, *94*, 2027-2094.

20 C. J. Cramer, D. G. Truhlar, In Solvent Effects and Chemical Reactivity. O. Tapia, J. Bertrán, (Eds.), Kluwer, **1996**, pp. 1–80.

21 J. Tomasi, B. Mennucci, R. Cammi, *Chem. Rev.* **2005**, *105*, 2999-3094.

Chapter IV. Hexafluoridophosphate partial hydrolysis leading to the one-dimensional coordination polymer [{Cu(xantphos)(μ-PO_2F_2)}$_n$]

Summary

This paper[5] describes the fortuitous formation of an inorganic copper(I) coordination polymer. In the scope of the project with CF_3 substituted 2,2'-bipyridines as the N^N chelating ligand in [Cu(P^P)(N^N)][PF_6] complexes, with P^P being the usual bis(2-(diphenylphosphino)phenyl)ether (POP) or 4,5-bis(diphenylphosphino)-9,9-dimethylxanthene (xantphos), 6,6'-$(CF_3)_2$bpy was one of the ligands that we wanted investigate for these complexes. However, we found that two CF_3 groups in 6-positions at the bpy are two repulsive for an exclusive formation of the heteroleptic complexes. Recrystallization of the crude material of the reaction of [Cu(MeCN)$_4$][PF_6] with xantphos and 6,6'-$(CF_3)_2$bpy yielded colourless crystals. Unexpectedly, single crystal X-ray diffraction identified them as copper(I) centres coordinated by a chelating xantphos molecule and bridged by {PO_2F_2} units, thus forming infinite chains. The partial hydrolysis of the $[PF_6]^-$ anion to $[PO_2F_2]^-$ is also nicely visible as a triplet in the ^{31}P NMR spectrum, with J_{PF} = 962 Hz, of the dissolved crystals of [{Cu(xantphos)(μ-PO_2F_2)}$_n$].

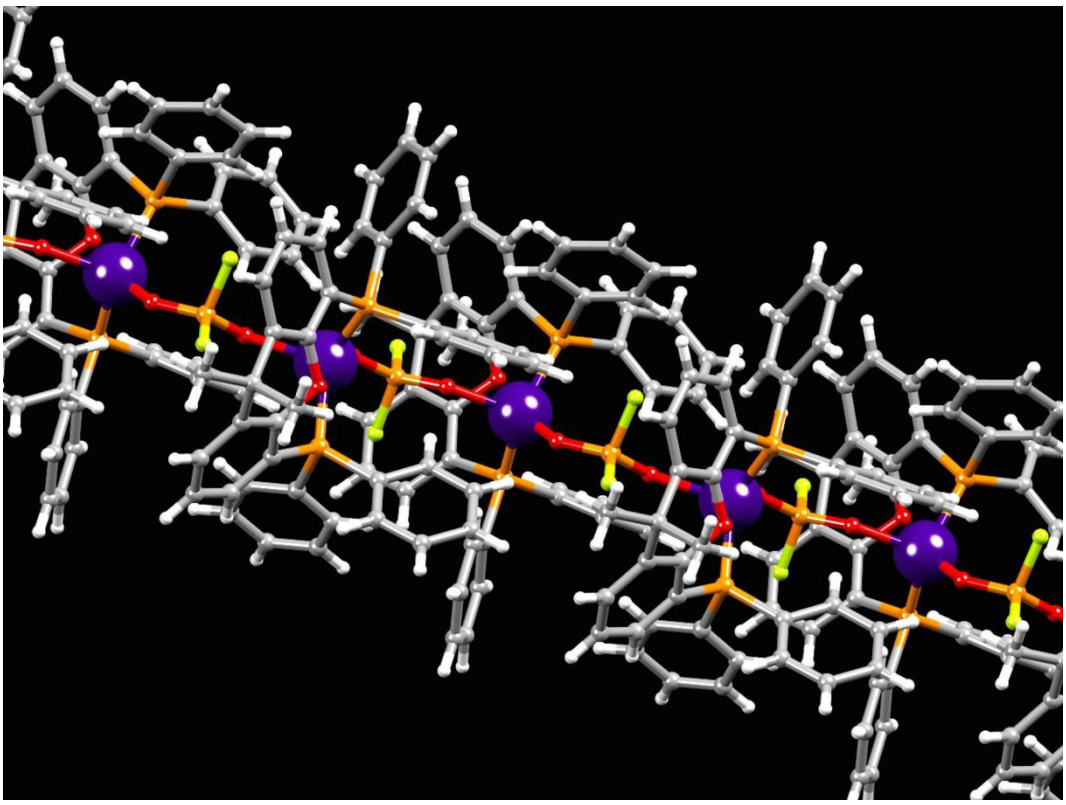

Contribution of Sarah Keller: Idea of the project with CF_3-substituted bpys that lead to this discovery ❖ Analytical characterization (electrospray mass spectroscopy, NMR spectroscopy) ❖ Writing of the manuscript.

Inorganic Chemistry Communications 58 (2015) 64–66

Contents lists available at ScienceDirect

Inorganic Chemistry Communications

journal homepage: www.elsevier.com/locate/inoche

Hexafluoridophosphate partial hydrolysis leading to the one-dimensional coordination polymer [{Cu(xantphos)(μ-PO_2F_2)}$_n$]

Sarah Keller, Fabian Brunner, Alessandro Prescimone, Edwin C. Constable, Catherine E. Housecroft *

Department of Chemistry, University of Basel, Spitalstrasse 51, CH 4056 Basel, Switzerland

ARTICLE INFO

Article history:
Received 28 April 2015
Received in revised form 25 May 2015
Accepted 3 June 2015
Available online 7 June 2015

Keywords:
Coordination polymer
Copper(I)
Hexafluoridophosphate hydrolysis
Crystal structure
P^P chelate
μ-PO_2F_2 units

ABSTRACT

The one-dimensional coordination polymer [{Cu(xantphos)(μ-PO_2F_2)}$_n$] (xantphos = 4,5-bis(diphenylphosphino)-9,9-dimethylxanthene) is reported, the first extended structure in which copper(I) centres are linked by μ-PO_2F_2 units.

The hexafluoridophosphate, $[PF_6]^-$, counterion is a ubiquitous choice in preparative inorganic chemistry due to a broad range of favourable properties including its weak coordination and straightforward handling. This counterion has become well-established in materials with applications including ionic liquids and batteries [1–3]. Nonetheless, hydrolysis of $[PF_6]^-$ is not unprecedented [4] and can lead to unexpected complexes containing $[PO_2F_2]^-$ or $[PO_3F]^{2-}$ groups [5–9]. Hydrolysis is catalysed by certain metal salts [10] and has also been observed under electrolytic conditions [11]. We report here the fortuitous formation of a one-dimensional coordination polymer consisting of chains of {Cu(μ-O_2PF_2)} units.

The attempted synthesis of [Cu(xantphos)(6,6′-$(CF_3)_2$bpy)][PF_6] (xantphos = 4,5-bis(diphenylphosphino)-9,9-dimethylxanthene) from equimolar amounts of [$Cu(MeCN)_4$][PF_6], xantphos and 6,6′-bis(trifluoromethyl)-2,2′-bipyridine (6,6′-$(CF_3)_2$bpy) following procedures used for related complexes [12,13] yielded a slightly orange solid, in contrast to the intense yellow or orange which is characteristic of [Cu(xantphos)(N^N)][PF_6] complexes (N^N = derivative of bpy) [13]. Crystal growth by layering yielded colourless crystals as the dominant product, in addition to some orange crystals. Parallel studies identified the orange crystals as [Cu(6,6′-$(CF_3)_2$bpy)$_2$][PF_6] [14]. The failure to obtain [Cu(xantphos)(6,6′-$(CF_3)_2$bpy)][PF_6] is probably related to the electronic and steric factors of the two CF_3 groups combined with the bulky xantphos ligand. The related complex [Cu(POP)(6,6′-Me_2bpy)][PF_6] (POP = bis(2-diphenylphosphinophenyl)ether, 6,6′-Me_2bpy = 6,6′-dimethyl-2,2′-bipyridine) can be isolated [12], and the increased demands of CF_3 versus CH_3 are consistent with the larger Tolman cone angle of $P(CF_3)_3$ (137°) versus PMe_3 (118°) [15]. Single crystal X-ray diffraction revealed the colourless crystals to be the one-dimensional coordination polymer [{Cu(xantphos)(μ-PO_2F_2)}$_n$]. The NMR spectroscopic data were consistent with the presence of $[PO_2F_2]^-$ rather than $[PF_6]^-$. The solvent from the crystallization tube was carefully removed, and the orange crystals manually separated from the colourless crystals. The latter were washed with Et_2O, dried in air and dissolved in CD_2Cl_2. Signals in the ^{1}H NMR spectrum [16] are consistent with the {Cu(xantphos)} unit. The ^{19}F NMR spectrum shows a broad doublet at δ –82.6 ppm (J_{PF} = 964 Hz) characteristic of $[PO_2F_2]^-$ [4]. In the ^{31}P NMR spectrum (Fig. 1) there is a coincidental overlap of a singlet arising from the {Cu(xantphos)} unit (δ −16.81 ppm) and the middle of the triplet assigned to the $[PO_2F_2]^-$ ion (δ −16.98 ppm, J_{PF} = 962 Hz). The electrospray mass spectrum (positive mode) showed a peak envelope at m/z 641.4 arising from $[Cu(xantphos)]^+$; although the $[PO_2F_2]^-$ anion was not observed in the negative mode, the spectrum showed a peak at m/z 63 assigned to $[PO_2]^-$ which is a characteristic fragment [17,18].

The coordination polymer [{Cu(xantphos)(μ-PO_2F_2)}$_n$] crystallizes in the monoclinic space group $P2_1/c$ [19]; the structure of the repeat unit is shown in Fig. 2 and part of one polymer chain in Fig. 3. The copper atom is in a distorted tetrahedral environment, bonded by the two P atoms of the xantphos ligand and two O atoms of different μ-O_2PF_2 groups. The PF_2 unit of the bridging {PO_2F_2} group is disordered and has been modelled over two sites with fractional occupancies of 70 and 30%. Both orientations were constrained to be tetrahedral; only the major

* Corresponding author.
E-mail address: catherine.housecroft@unibas.ch (C.E. Housecroft).

http://dx.doi.org/10.1016/j.inoche.2015.06.002
1387-7003/

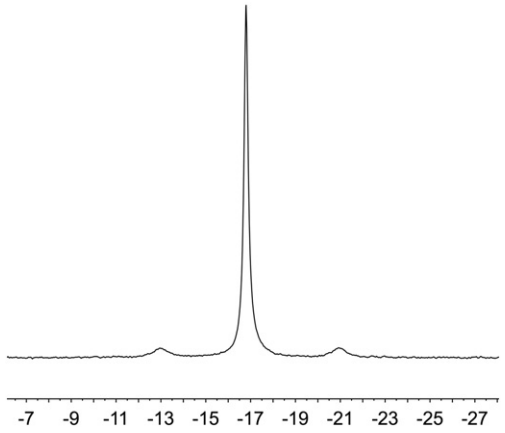

Fig. 1. 243 MHz ^{31}P NMR spectrum of a CD_2Cl_2 solution of dissolved crystals of [{Cu(xantphos)(μ-PO_2F_2)}$_n$] showing overlapping singlet and triplet (J_{PF} = 962 Hz). Chemical shifts in δ/ppm.

orientation is discussed below. Although the ability of $[PO_2F_2]^-$ to function as a bridging ligand is known (25 hits in a search of the Cambridge Structural Database, version 5.36 with February 2015 updates [20] using Conquest version 1.1.7 [21]), [{Cu(xantphos)(μ-PO_2F_2)}$_n$] is the first reported coordination polymer in which {PO_2F_2} connects copper(I) centres. In the Cu(xantphos) unit, the Cu–P distances and P–Cu–P bond angle are in accord with literature values [20]. Although xantphos is a relatively rigid ligand compared to POP (Scheme 1), the fused ring domain in xantphos (Scheme 1) undergoes a conformational change associated with the sp^3 carbon of the CMe_2 unit (C17–C19–C23 = 106.9(3)°). The C–O–C angle of 114.2(2)° coupled with the C–O bond distances of 1.387(4) and 1.397(4) Å are consistent with some π-localization across the C–O–C unit. In free xantphos, the corresponding

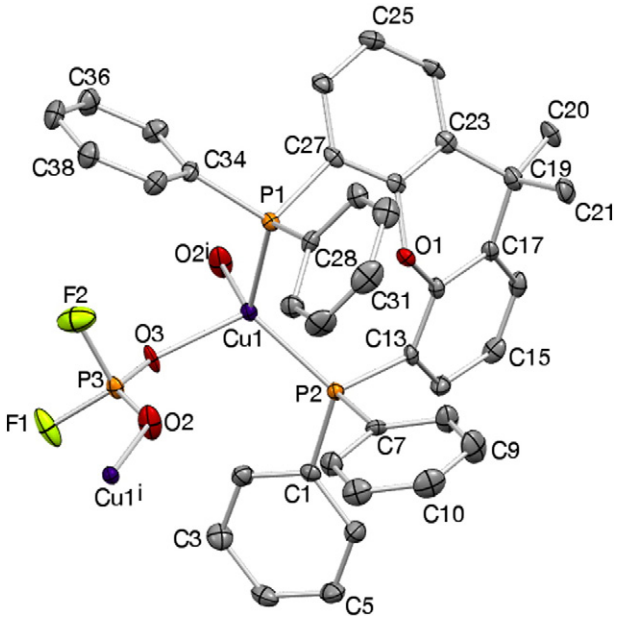

Fig. 2. The repeat unit (including atoms defining polymer connectivity) in [{Cu(xantphos)(μ-PO_2F_2)}$_n$]; H atoms omitted and ellipsoids plotted at 40% probability. Symmetry codes: i = 1 − *x*, $^1/_2$ + *y*, $^3/_2$ − *z*. Selected bond parameters: Cu1–O2i = 2.167(2), Cu1–O3 = 2.063(2), Cu1–P1 = 2.2434(10), Cu1–P2 = 2.2299(9), O3–P3 = 1.450(4), O2–P3 = 1.407(5), F2–P3 = 1.617(3), F1–P3 = 1.547(5) Å; O2i–Cu1–P1 = 105.55(8), O2i–Cu1–P2 = 110.04(8), P1–Cu1–P2 = 117.64(4), O2i–Cu1–O3 = 97.83(8), P1–Cu1–O3 = 110.92(7), P2–Cu1–O3 = 112.76(8), F2–P3–F1 = 98.4(3), F2–P3–O3 = 104.8(2), F1–P3–O3 = 108.9(3), F2–P3–O2 = 105.0(3), F1–P3–O2 = 112.6(3), O3–P3–O2 = 123.7(3)°.

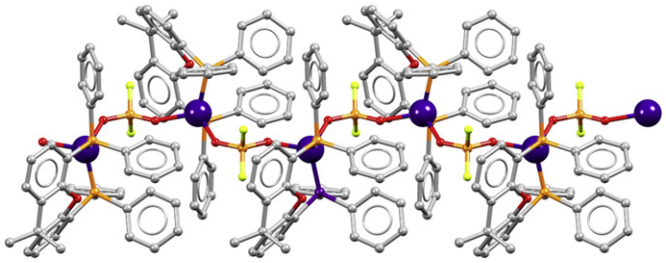

Fig. 3. Part of one polymer chain in [{Cu(xantphos)(μ-PO_2F_2)}$_n$] viewed down the c-axis; the chain follows the *b*-axis.

angle is 117.4° [22]. Despite the π-contribution, the heterocyclic ring tends to adopt a boat conformation (survey of 173 structures containing xantphos in the CSD, version 5.36 with February 2015 updates [20]); the conformation is variable and is affected if the O atom is involved in coordination [23]. In [{Cu(xantphos)(μ-PO_2F_2)}$_n$], the angle between the planes containing atoms C18, O1 and C28 and atoms C17, C18, C23 and C28 is 31.9° and that between the planes containing atoms C17, C18, C23 and C28 and C17, C19 and C23 is 32.3°. The corresponding internal angles of the boat in free xantphos are 20.8° and 24.34°.

The one-dimensional polymer chain is propagated by a screw axis running parallel to the crystallographic *b*-axis, and the Cu···Cu separation of adjacent copper atoms in a chain is 5.9590(9) Å. The copper atoms and connecting O–P–O motifs in a chain are essentially coplanar (deviation from a least squares plane through these atoms < 0.14 Å), and the O atom of the xantphos ligand also lies in this plane. Polymer chains are related by a glide plane with a distance between the planes containing the Cu(μ-O–P–O) units of 9.3214(5) Å. The chains are packed closely together with no solvent-accessible voids; interactions between adjacent chains are dominated by H···H contacts.

Given the general application of $[PF_6]^-$ as a counterion in our work over many years, particularly in the isolation of [Cu(N^N)(POP)][PF_6] [24] and [Cu(N^N)(POP)][PF_6] complexes (N^N = bpy derivatives) [12,25], the hydrolysis of $[PF_6]^-$ to $[PO_2F_2]^-$ was unexpected. We attribute it to a combination of adventitious water and to the catalytic action of copper(I), possibly in the presence of the xantphos ligand.

Acknowledgements

We acknowledge the Swiss National Science Foundation, the University of Basel and the European Research Council (Advanced Grant 267816 LiLo) for financial support.

Appendix A. Supplementary material

CCDC 1053233 contains the supplementary crystallographic data for this paper. These data can be obtained free of charge via www.ccdc.cam.ac.uk/conts/retrieving.html (or from the Cambridge Crystallographic Data Centre, 12 Union Road, Cambridge CB2 1EZ, UK; fax: (+44) 1223-336-033; or e-mail: deposit@ccdc.cam.ac.uk). Supplementary data associated with this article can be found, in the online version, at http://dx.doi.org/10.1016/j.inoche.2015.06.002.

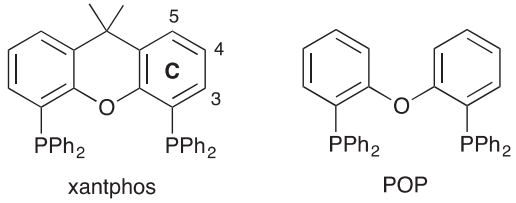

Scheme 1. Structures of xantphos and POP. Ring labelling in xantphos is for NMR assignments; Ph ring = D.

References

[1] R.D. Costa, E. Ortí, H.J. Bolink, F. Monti, G. Accorsi, N. Armaroli, Angew. Chem. Int. Ed. 51 (2012) 8178.
[2] J.P. Hallett, T. Welton, Chem. Rev. 111 (2011) 3508.
[3] J.B. Goodenough, Y. Kim, Chem. Mater. 22 (2010) 587.
[4] R. Fernández-Galán, B.R. Manzano, A. Otero, M. Lanfranchi, M.A. Pellinghelli, Inorg. Chem. 22 (1994) 2309.
[5] M. Albrecht, K. Hübler, W. Kaim, Z. Anorg. Allg. Chem. 626 (2000) 1033.
[6] N.P. Deifel, K.T. Holman, C.L. Cahill, Chem. Commun. (2008) 6037.
[7] N.R. Brooks, A.J. Blake, N.R. Champness, J.W. Cunningham, P. Hubberstey, M. Schröder, Cryst. Growth Des. 1 (2001) 395.
[8] D. Dermitzaki, C.P. Raptopoulou, V. Psycharis, A. Escuer, S.P. Perlepes, T.C. Stamatatos, Dalton Trans. 43 (2014) 14520.
[9] T.T. da Cunha, F. Pointillart, B. Le Guennic, C.L.M. Pereira, S. Golhen, O. Cador, L. Ouahab, Inorg. Chem. 52 (2013) 9711.
[10] D. Wiedmann, E. Świętek, W. Macyk, A. Grohmann, Z. Anorg. Allg. Chem. 639 (2013) 1483 (and refs. therein.).
[11] A.J. Tasiopoulos, N.C. Harden, K.A. Abboud, G. Christou, Polyhedron 22 (2003) 133.
[12] S. Keller, E.C. Constable, C.E. Housecroft, M. Neuburger, A. Prescimone, G. Longo, A. Pertegás, M. Sessolo, H.J. Bolink, Dalton Trans. 43 (2014) 16593 (and references therein.).
[13] I. Andrés-Tomé, J. Fyson, F.B. Dias, A.P. Monkman, G. Iacobellis, P. Coppo, Dalton Trans. 41 (2012) 8669.
[14] F. Brunner, Y. M. Klein, S. Keller, C. D. Morris, A. Prescimone, E. C. Constable, C. E. Housecroft, 2015, submitted.
[15] C.A. Tolman, Chem. Rev. 77 (1977) 313.
[16] A solution of xantphos (145 mg, 0.25 mmol) and 6,6′-$(CF_3)_2$bpy (73 mg, 0.25 mmol) in CH_2Cl_2 (20 ml) was added to a solution of $[Cu(MeCN)_4][PF_6]$ (93 mg, 0.25 mmol) in CH_2Cl_2 (20 ml). The resulting pale yellow solution was stirred for 2 h, and then solvent was removed in vacuo. The yellow residue was redissolved in CH_2Cl_2 (4 ml), transferred to a layer tube and layered with Et_2O. After one day, colourless crystals mixed with a minor component of orange crystals were obtained. The colourless crystals were collected and analysed. ^{1}H NMR (600 MHz, CD_2Cl_2, 298 K) δ/ppm 7.61 (dd, J = 7.6, 1.5 Hz, 2H, H^{C5}), 7.43–7.29 (m, 12H, H^{D3+D4}), 7.24 (m, 8H, H^{D2}), 7.16 (t, J = 7.7 Hz, 2H, H^{C4}), 6.64 (m, 2H, H^{C3}), 1.67 (s, 6H, H^{Me}). ^{19}F NMR (565 MHz, CD_2Cl_2, 298 K) δ/ppm –82.6 (broad d, J_{PF} = 964 Hz). ^{31}P NMR (243 MHz, CD_2Cl_2, 298 K) δ/ppm −16.98 (t, J_{PF} = 962 Hz, PF_2), −16.81 (br, xantphos). ESI MS positive mode: m/z 641.4 $[M–PO_2F_2]^+$ (base peak, calc. 641.1); ESI MS negative mode: m/z 62.5 (base peak, calc. 63.0, $[PO_2]^-$). Found C 63.18, H 4.59, N 0.53; $C_{39}H_{32}CuF_2O_3P_3 \cdot {}^1/_3$MeCN requires C 62.95, H 4.40, N 0.62%.
[17] V. Kraft, M. Grützke, W. Weber, M. Winter, S. Nowak, J. Chromatogr. A 1354 (2014) 92.
[18] M. Wachsmann, K.G. Heumann, Int. J. Mass Spectrom. Ion Process. 108 (1991) 75.
[19] $C_{39}H_{32}CuF_2O_3P_3$, M = 743.14, colourless block, monoclinic, space group $P2_1/c$, a = 12.4347(15), b = 10.8870(13), c = 25.682(3) Å, β = 100.220(3)°, U = 3421.6(7) Å^3, Z = 4, Dc = 1.443 Mg m^{-3}, μ(Cu-Kα) = 2.636 mm^{-1}, T = 123 K. Total 27,376 reflections, 5965 unique, R_{int} = 0.032. Refinement of 5913 reflections (460 parameters) with $I > 2\sigma(I)$ converged at final R_1 = 0.0737 (R_1 all data = 0.0737), wR_2 = 0.1888 (wR_2 all data = 0.1888), gof = 0.9956.
[20] F.H. Allen, Acta Crystallogr. B 58 (2002) 380.
[21] I.J. Bruno, J.C. Cole, P.R. Edgington, M. Kessler, C.F. Macrae, P. McCabe, J. Pearson, R. Taylor, Acta Crystallogr. B (58) (2002) 389.
[22] S. Hillebrand, J. Bruckmann, C. Kruger, M.W. Haenel, Tetrahedron Lett. 36 (1995) 75.
[23] (See for example:). D. Fujino, H. Yorimitsu, A. Osuka, J. Am. Chem. Soc. 136 (2014) 6255.
[24] S.Y. Brauchli, F.J. Malzner, E.C. Constable, C.E. Housecroft, RSC Avd. 4 (2014) 62728 (and refs. therein.).
[25] R.D. Costa, D. Tordera, E. Ortí, H.J. Bolink, J. Schönle, S. Graber, C.E. Housecroft, E.C. Constable, J.A. Zampese, J. Mater. Chem. 21 (2011) 16108.

Chapter V. Copper(I) and silver(I) complexes of 9,9-dimethyl-4,5-bis(di-*tert*-butylphosphino)xanthene: photophysical properties and structural perturbation under pressure

Summary

The idea behind this paper[6] was to investigate a bisphosphane ligand in [Cu(P^P)(N^N)][PF_6] complexes that is sterically more demanding than our "standard" ligands bis(2-(diphenylphosphino)phenyl)ether (POP) and 4,5-bis(diphenylphosphino)-9,9-dimethylxanthene (xantphos). In addition to the increased steric crowing at the phosphorus atoms in 4,5-bis(di-*tert*-butylphosphino)xanthene (*t*Bu-xantphos), the *tert*-butyl groups also lead to a different electronic situation, because of their electron-donating +*I* effect. As N^N chelating ligands, 2,2'-bipyridine (bpy), 6-Mebpy, 6-Brbpy and 4,4'-*t*Bu_2-bpy were investigated, which lead to the formation of heteroleptic copper(I) complexes for all ligands except 6-Brbpy. In this case, single crystal X-ray diffraction gave a [Cu(*t*Bu-xantphos)]$^+$ cation and the NMR spectroscopic analysis showed that the 6-Brbpy was not coordinated to the metal. For comparative reasons, also [Ag(*t*Bu-xantphos)(bpy)][PF_6] was synthesized. The complexes were non-emissive in solution and only weakly emissive in solid state, which we attributed to vibrational quenching by the many C–H bonds of the *tert*-butyl groups at the phosphorus atoms. The crystal structures of [Cu(*t*Bu-xantphos)(bpy)][PF_6] and [Ag(*t*Bu-xantphos)(bpy)][PF_6] were investigated under increasing pressure in a diamond pressure cell at the beamline I19 at the synchrotron Diamond Light Source.

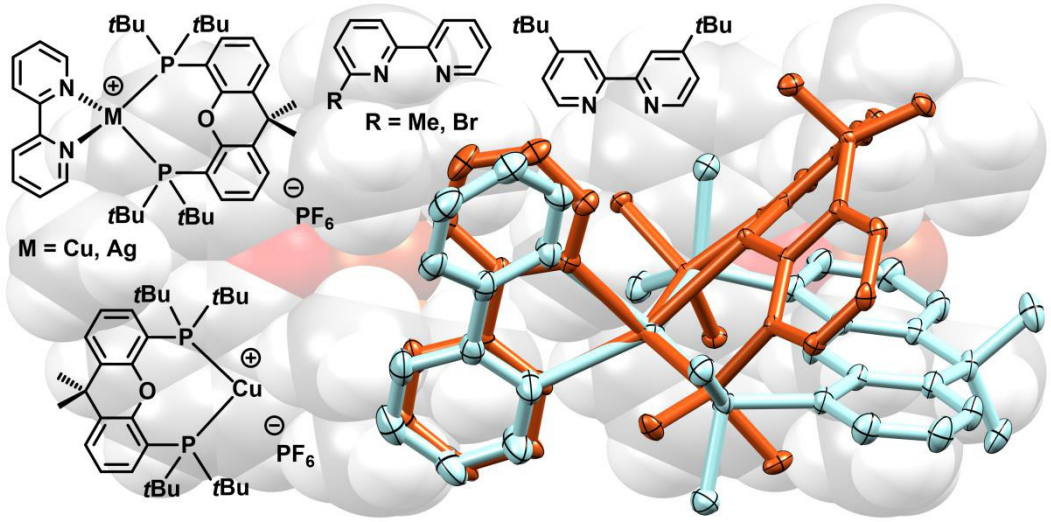

Contribution of Sarah Keller: Idea of the project and selection of ligands ❖ Synthesis of starting materials, ligands and complexes ❖ Analytical characterization (electrospray mass spectroscopy, NMR spectroscopy) ❖ Conduction of high pressure X-ray experiments ❖ Photophysical and electrochemical characterization ❖ Writing of the manuscript.

Photochem & Photobiol. Sciences

ARTICLE

Copper(I) and silver(I) complexes of 9,9-dimethyl-4,5-bis(di-*tert*-butylphosphino)xanthene: photophysical properties and structural perturbation under pressure

Cite this: DOI: 10.1039/x0xx00000x

Received 00th January 2012,
Accepted 00th January 2012

DOI: 10.1039/x0xx00000x

www.rsc.org/

Sarah Keller,[a] Alessandro Prescimone,[a] Edwin C. Constable[a] and Catherine E. Housecroft*[a]

The heteroleptic complexes [Cu(*t*Bu-xantphos)(bpy)][PF_6] and [Ag(*t*Bu-xantphos)(bpy)][PF_6], where *t*Bu-xantphos = 9,9-dimethyl-4,5-bis(di-*tert*-butylphosphino)xanthene and bpy = 2,2'-bipyridine have been synthesized and their photophysical properties investigated. Single crystal X-ray diffraction of the compounds under ambient and increased pressure allows insights into pressure-induced structural perturbation. For the copper(I) complexes, the effects of changing the N^N ligand from bpy to 6-methyl-2,2'-bipyridine (6-Mebpy), 6-bromo-2,2'-bipyridine (6-Brbpy), and 4,4'-di(*tert*-butyl)-2,2'-bipyridine (4,4'-*t*Bu_2bpy) were also investigated.

Introduction

Luminescent devices include light-emitting diodes (LEDs), organic light-emitting diodes (OLEDs) and light-emitting electrochemical cells (LECs) and are part of the solid state lighting (SSL) technology. The latter is increasingly replacing traditional lighting systems and has revolutionized screen technology for, for example, smartphones, computers and televisions.[1,2,3,4] The emissive materials for LECs and OLEDs can be polymers, molecular organics or ionic transition metal complexes (iTMCs).[5] For iTMC devices, copper(I) based compounds have increasingly gained interest due to the high Earth-abundance of copper and its low cost, and the fact that both the singlet and the triplet excited states can be harvested via thermally activated delayed fluorescence (TADF).[6,7] Complexes where the copper centre is coordinated by a combination of a P^P chelating ligand (e.g. bis(2-(diphenylphosphino)phenyl)ether (POP) or 4,5-bis(diphenylphosphino)-9,9-dimethylxanthene (xantphos)) and an N^N ligand such as 2,2'-bipyridines (bpy) or phenanthrolines with varying substituents, are a particularly interesting class of emitters for LECs[8] and OLEDs.[9] They often exhibit high photoluminescence quantum yields (PLQY) of up to 70% in the solid state and, when used as emitters in LECs, luminance values of 145 cd m^{-2} and device lifetimes of ~80 hours have been achieved.[10,11] When it comes to the design of the copper complexes, the stabilization of the tetrahedral geometry plays a crucial role in avoiding quenching processes and increasing the PLQYs and excited state lifetimes.[12] Substituents in the 6-positions of the bpy, for example alkyl or CF_3 groups, prevent the tetrahedron from flattening, make the structure more rigid and improve the emissive properties of the complex.[11,13,14]

We have been interested in the effect of a change in the steric and electronic properties of the chelating bisphosphane and decided to investigate the potential of 9,9-dimethyl-4,5-bis(di-*tert*-butylphosphino)xanthene (*t*Bu-xantphos) as the chelating phosphane. The disadvantage of alkyl phosphanes, as opposed to aryl phosphanes, is that they are prone to oxidation to phosphane oxides. However, we hoped that the sterically hindered *t*Bu_2P groups would not only shield the copper centre and stabilize the tetrahedral geometry, but would in addition decrease the tendency for phosphane oxidation.

The ligand *t*Bu-xantphos is often used for catalysis in combination with different metals, for example in the copper-catalysed alkylboration of alkenes.[15] However, there are very few cases in which metal complexes containing *t*Bu-xantphos have been isolated and characterized. Examples are the rhodium complex [(*t*Bu-xantphos)RhCl] and its hydride, [(*t*Bu-xantphos)RhH_2Cl].[16] For group 11, no complexes with copper or silver and *t*Bu-xantphos have been described although the complex [(*t*Bu-xantphos}AuCl] has been successfully used as a catalyst to transform C−F to C−X bonds (X = O, S, N).[17]

It has previously been established that silver complexes with the motif $[Ag(P^P)(N^N)]^+$ show reasonable emissive properties and promising results in LECs[18] and recently a silver complex with excellent TADF properties and PLQY of 100% was reported,[19] which motivated us to investigate the analogous Ag^+ complex with *t*Bu-xantphos and bpy.

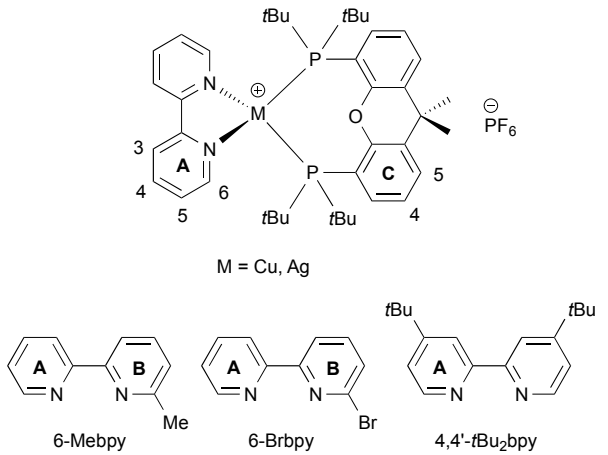

Scheme 1. Structure of the N^N ligands and complexes with ring labels for NMR spectroscopic assignments.

Experimental

General. ^{1}H, ^{13}C and ^{31}P NMR spectra were recorded at room temperature using a Bruker Avance III-600, III-500 or III-400 NMR spectrometer. ^{1}H and ^{13}C NMR chemical shifts were referenced to residual solvent peaks with respect to δ(TMS) = 0 ppm and ^{31}P NMR chemical shifts with respect to δ(85% aqueous H_3PO_4) = 0 ppm. Solution absorption and emission spectra were measured using an Agilent 8453 spectrophotometer and a Shimadzu RF-5301PC spectrofluorometer, respectively. Electrospray ionization (ESI) mass spectra were recorded on a Shimadzu LCMS-2020 instrument. Quantum yields for CH_2Cl_2 solution and powder samples were measured using a Hamamatsu absolute photoluminescence (PL) quantum yield spectrometer C11347 Quantaurus-QY. Emission lifetimes and powder emission spectra were measured with a Hamamatsu Compact Fluorescence lifetime Spectrometer C11367 Quantaurus-Tau, using an LED light source with λ_{exc} = 365 nm.

[Cu(MeCN)$_4$][PF$_6$][20] and 6-Mebpy[21] were prepared following literature methods, *t*Bu-xantphos was purchased from Strem chemicals, bpy from Apollo Scientific, 6-Brbpy from TCI, 4,4'-*t*Bu$_2$bpy from Sigma-Aldrich and Ag[PF$_6$] from Fluorochem. All chemicals were used as received.

[Cu(*t*Bu-xantphos)(bpy)][PF$_6$].

Under nitrogen, a solution of *t*Bu-xantphos (75 mg, 0.15 mmol, 1.0 eq) in dry CH_2Cl_2 (10 ml) was added to a solution of [Cu(MeCN)$_4$][PF$_6$] (56 mg, 0.15 mmol, 1.0 eq) in dry CH_2Cl_2 (5 ml). The colourless solution was stirred for 2 h. A solution of bpy (23 mg, 0.15 mmol, 1.0 eq) in dry CH_2Cl_2 (5 ml) was added to the mixture and the resulting yellow solution was stirred for two hours. All volatiles were removed in vacuo and the residue was washed with hexane to yield [Cu(*t*Bu-xantphos)(bpy)]PF$_6$] (69 mg, 0.08 mmol, 53 %) as yellow powder. ^{1}H NMR (500 MHz, CD_2Cl_2, 298 K) δ/ppm 8.72 (d, J = 4.3 Hz, 2H, H^{A6}), 8.40 (dt, J = 8.0, 0.9 Hz, 2H, H^{A3}), 7.89 (td, J = 7.8, 1.8 Hz, 2H, H^{A4}), 7.73 (dd, J = 7.8, 1.4 Hz, 2H, H^{C5}), 7.71 – 7.65 (m, 2H, H^{C3}), 7.369 (t, J = 7.7 Hz, 2H, H^{A5}), 7.366 (dd, J = 7.5, 1.1 Hz, 2H, H^{C4}), 1.67 (s, 6H, H$^{xantphos-Me}$), 1.34 – 1.29 (m, 36H, H^{tBu}). ^{13}C NMR (126 MHz, CD_2Cl_2, 298 K) δ/ppm 155.5 (C^{A2}), 154.3 (t, J = 5.6 Hz, C^{C1}), 149.9 (C^{A6}), 137.9 (C^{A4}), 133.6 (t, J = 1.8 Hz, C^{C6}), 133.3 (C^{C3}), 129.7 (C^{C5}), 125.2 (C^{C4}), 124.9 (C^{A5}), 121.9(C^{A3}), 118.3 (t, J = 11.5 Hz, C^{C2}), 36.2 (C$^{xantphos-bridge}$), 35.6 (t, J = 7.3 Hz, C$^{tBu-quat}$), 31.0 (t, J = 4.4 Hz, C^{tBu}), 30.3 (C$^{xantphos-Me}$). ^{31}P{^{1}H} NMR (202 MHz, CD_2Cl_2, 298 K) δ/ppm 20.6 (broad, FWHM = 110 Hz), −144.5 (sept, J_{PF} = 710 Hz, [PF$_6$]$^-$). ESI MS: m/z 561.1 [Cu(*t*Bu-xantphos)]$^+$ (base peak, calc. 561.3, base peak for [Cu(*t*Bu-xantphos)(bpy)]$^+$, calc. 717.3). Found C 56.73, H 6.68, N 3.41; $C_{41}H_{56}CuF_6N_2OP_3$ requires C 57.04, H 6.54, N 3.24%.

[Cu(*t*Bu-xantphos)(6-Mebpy)][PF$_6$].

Under nitrogen, a solution of *t*Bu-xantphos (75 mg, 0.15 mmol, 1.0 eq) in dry CH_2Cl_2 (10 ml) was added to a solution of [Cu(MeCN)$_4$][PF$_6$] (56 mg, 0.15 mmol, 1.0 eq) in dry CH_2Cl_2 (5 ml). The colourless solution was stirred for 2 h. A solution of 6-Mebpy (26 mg, 0.15 mmol, 1.0 eq) in dry CH_2Cl_2 (5 ml) was added to the mixture and the resulting yellow solution was stirred for two hours. All volatiles were removed in vacuo and the residue was washed with hexane to yield [Cu(xant-*t*Bu-phos)(6-Mebpy)]PF$_6$] (78 mg, 0.09 mmol, 60 %) as yellow solid. ^{1}H NMR (500 MHz, CD_2Cl_2, 298 K) δ/ppm 8.64 (d, J = 4.1 Hz, 1H, H^{A6}), 8.43 (dt, J = 8.0, 0.9 Hz, 1H, H^{A3}), 8.21 (d, J = 7.8 Hz, 1H, H^{B3}), 7.81 (td, J = 7.8, 1.8 Hz, 1H, H^{A4}), 7.75 (dd, J = 7.8, 1.4 Hz, 2H, H^{C5}), 7.73 – 7.69 (m, 1H, H^{B4}), 7.69 – 7.66 (m, 2H, H^{C3}), 7.39 (t, J = 7.8 Hz, 2H, H^{C4}), 7.30 (ddd, J = 7.4, 4.8, 1.0 Hz, 1H, H^{A5}), 7.19 (d, J = 7.6 Hz, 1H, H^{B5}), 2.61 (s, 3H, H^{Me}), 1.66 (s, 6H, H$^{xantphos-Me}$), 1.42 – 1.39 (m, 36H, H^{tBu}). ^{13}C NMR (126 MHz, CD_2Cl_2, 298 K) δ/ppm 158.5 (C^{B6}), 156.8 (C^{A2}), 155.8 (C^{B2}), 154.0 (t, J = 5.6 Hz, C^{C1}), 149.6 (C^{A6}), 137.5 (C^{B4}), 137.3 (C^{A4}), 133.5 (t, J = 2.0 Hz, C^{C6}), 133.3 (C^{C3}), 130.1 (C^{C5}), 125.3 (t, J = 2.5 Hz, C^{C4}), 124.1 (C^{A5}), 123.8 (C^{B5}), 121.4 (C^{A3}), 118.4 (C^{B3}), 117.6 (t, J = 13.5 Hz, C^{C2}), 36.2 (t, J = 1.1 Hz, C$^{xantphos-bridge}$), 35.5 (t, J = 8.4 Hz, C$^{tBu-quat}$), 30.9 (t, J = 4.3 Hz, C^{tBu}), 30.5 (C$^{xantphos-Me}$), 25.0 (C^{Me}). ^{31}P{^{1}H} NMR (202 MHz, CD_2Cl_2, 298 K) δ/ppm 22.1 (broad, FWHM = 63 Hz), −144.5 (sept, J_{PF} = 710 Hz, [PF$_6$]$^-$). ESI MS: *m/z* 561.4 [Cu(*t*Bu-xantphos)]$^+$ (base peak, calc. 561.3, base peak for [Cu(*t*Bu-xantphos)(6-Mebpy)]$^+$, calc. 731.3). Found C 59.72, H 7.28, N 2.90; $C_{42}H_{58}CuF_6N_2OP_3{\cdot}C_6H_{14}$ requires C 59.83, H 7.53, N 2.91%.

[Cu(*t*Bu-xantphos)][PF$_6$].

In an attempt to prepare [Cu(*t*Bu-xantphos)(6-Brbpy)][PF$_6$], [Cu(*t*Bu-xantphos)][PF$_6$] was isolated. Under nitrogen, a solution of *t*Bu-xantphos (75 mg, 0.15 mmol, 1.0 eq) in dry CH_2Cl_2 (10 ml) was added to a solution of [Cu(MeCN)$_4$][PF$_6$] (56 mg, 0.15 mmol, 1.0 eq) in dry CH_2Cl_2 (5 ml). The colourless solution was stirred for 2 h. A solution of 6-Brbpy (35 mg, 0.15 mmol, 1.0 eq) in dry CH_2Cl_2 (5 ml) was added to the mixture and the resulting yellow solution was stirred for two hours. All volatiles were removed in vacuo and the residue was washed with hexane to yield a pale orange solid (82 mg) which was identified as a mixture of [Cu(*t*Bu-xantphos)][PF$_6$] and 6-Brbpy. The ^{1}H and ^{13}C NMR resonances assigned to free 6-Brbpy matched those reported.[22] [Cu(*t*Bu-xantphos)][PF$_6$]: ^{1}H

NMR (500 MHz, CD_2Cl_2, 298 K) δ/ppm 7.74 (dd, J = 7.8, 1.3 Hz, 2H, H^{C5}), 7.69–7.66 (m, 2H, H^{C3}), 7.38 (t, J = 7.8 Hz, 2H, H^{C4}), 1.65 (s, 6H, $H^{xantphos\text{-}Me}$), 1.42 – 1.39 (m, 36H, H^{tBu}). ^{13}C NMR (126 MHz, CD_2Cl_2, 298 K) δ/ppm 154.1 (t, J_{PC} = 5.6 Hz, C^{C1}), 133.7 (t, J_{PC} = 2.0 Hz, C^{C6}), 133.3 (C^{C3}), 130.0 (C^{C5}), 125.3 (t, J_{PC} = 2.5 Hz, C^{C4}), 117.5 (t, J_{PC} = 13.6 Hz, C^{C2}), 36.2 ($C^{xantphos\text{-}Me}$), 35.4 (t, J = 8.4 Hz, $C^{tBu\text{-}quat}$), 30.8 (t, J = 4.3 Hz, C^{tBu}), 30.2 ($C^{xantphos\text{-}Me}$). $^{31}P\{^1H\}$ NMR (202 MHz, CD_2Cl_2, 298 K) δ/ppm 21.7 (broad, FWHM = 57 Hz), −144.5 (sept, J_{PF} = 710 Hz, $[PF_6]^-$). ESI MS: *m/z* 561.3 [Cu(*t*Bu-xantphos)]$^+$ (base peak, calc. 561.3). Insufficient pure material for elemental analysis.

[Cu(*t*Bu-xantphos)(4,4'-*t*Bu$_2$bpy)][PF$_6$].

Under nitrogen, a solution of *t*Bu-xantphos (75 mg, 0.15 mmol, 1.0 eq) in dry CH_2Cl_2 (10 ml) was added to a solution of $[Cu(MeCN)_4][PF_6]$ (56 mg, 0.15 mmol, 1.0 eq) in dry CH_2Cl_2 (5 ml). The colourless solution was stirred for 2 h. A solution of 4,4'-*t*Bu$_2$bpy (40 mg, 0.15 mmol, 1.0 eq) in dry CH_2Cl_2 (5 ml) was added to the mixture and the resulting yellow solution was stirred for two hours. All volatiles were removed in vacuo and the residue was washed with hexane to yield [Cu(*t*Bu-xantphos)(4,4'-*t*Bu$_2$bpy)]PF_6] (116 mg, 0.12 mmol, 80 %) as yellow solid. ^1H NMR (500 MHz, CD_2Cl_2, 298 K) δ/ppm 8.66 (broad signal, FWHM = 16.6 Hz, 2H, H^{A6}), 8.34 (broad signal, FWHM = 9.2 Hz, 2H, H^{A3}), 7.71 (dd, J = 7.7, 1.3 Hz, 2H, H^{C5}), 7.70 – 7.67 (m, 2H, H^{C3}), 7.42 – 7.39 (m, 2H, H^{A5}), 7.34 (t, J = 7.7 Hz, 2H, H^{C4}), 1.68 (s, 6H, $H^{xantphos\text{-}Me}$), 1.40 (s, 18H, $H^{bpy\,tBu}$), 1.26 – 1.23 (m, consisting of two singlets and a broad signal in the middle, 36H, $H^{P\,tBu}$). ^{13}C NMR (126 MHz, CD_2Cl_2, 298 K) δ/ppm 162.6 (C^{A4}), 155.0 (m, C^{A2+C1}), 149.9 (C^{A6}), 133.9 (C^{C6}), 133.3 (C^{C3}), 129.0 (C^{C5}), 124.8 (C^{C4}), 122.4 (m, C^{A5}), 119.0 (m, C^{A3+C2}), 36.3 ($C^{xantphos\text{-}bridge}$), 35.6 (t, J = 6.0 Hz, $C^{tBu\text{-}quat}$), 31.0 (t, J = 4.5 Hz, C^{tBu}), 30.8 ($C^{bpy\,tBu}$), 29.7 ($C^{xantphos\text{-}Me}$). $^{31}P\{^1H\}$ NMR (202 MHz, CD_2Cl_2, 298 K) δ/ppm 17.7 (broad, FWHM = 180 Hz), −144.5 (sept, J_{PF} = 710 Hz, $[PF_6]^-$). ESI MS: *m/z* 561.4 [Cu(*t*Bu-xantphos)]$^+$ (base peak, calc. 561.3, base peak for [Cu(*t*Bu-xantphos)(4,4'-*t*Bu$_2$bpy)]$^+$, calc. 829). Found C 59.65, H 7.74, N 3.06; $C_{49}H_{72}CuF_6N_2OP_3{\cdot}H_2O$ requires C 59.23, H 7.51, N 2.82%.

[Ag(*t*Bu-xantphos)(bpy)][PF$_6$].

Under nitrogen, a solution of *t*Bu-xantphos (75 mg, 0.15 mmol, 1.0 eq) in dry CH_2Cl_2 (10 ml) was added to a solution of $AgPF_6$ (38 mg, 0.15 mmol, 1.0 eq) in dry CH_2Cl_2 (5 ml). The colourless solution was stirred for 2 h. A solution of bpy (23 mg, 0.15 mmol, 1.0 eq) in dry CH_2Cl_2 (5 ml) was added to the mixture and the resulting yellow solution was stirred for two hours. All volatiles were removed in vacuo to yield [Ag(*t*Bu-xantphos)(bpy)][PF_6] (99 mg, 0.11 mmol, 73 %) as colourless powder. Small impurities of free *t*Bu-xantphos.

^1H NMR (500 MHz, CD_2Cl_2, 298 K) δ/ppm 8.70 (ddd, J = 4.8, 1.8, 0.9 Hz, 2H, H^{A6}), 8.35 (dt, J = 8.0, 1.0 Hz, 2H, H^{A3}), 7.90 (ddd, J = 8.0, 7.6, 1.8 Hz, 2H, H^{A4}), 7.70 – 7.68 (m, 4H, H^{C3+C5}), 7.39 (ddd, J = 7.5, 4.8, 1.2 Hz, 2H, H^{A5}), 7.31 (t, J = 7.7 Hz, 2H, H^{C4}), 1.63 (s, 6H, $H^{xantphos\text{-}Me}$), 1.33 – 1.29 (m, consisting of two singlets and a broad signal in the middle, 36H, H^{tBu}). ^{13}C NMR (126 MHz, CD_2Cl_2, 298 K) δ/ppm 155.7 (C^{A2}), 155.1 (t, J = 5.8 Hz, C^{C1}), 150.2 (C^{A6}), 138.1 (C^{A4}), 133.8 (m, C^{C5+C6}), 129.1 (C^{C3}), 124.8 (C^{A5}), 124.2 (m, C^{C4}), 122.2 (C^{A3}), 118.4 (td, J = 7.9, 3.1 Hz, C^{C2}), 36.0 (m, $C^{xantphos\text{-}bridge}$), 35.6 (m, $C^{tBu\text{-}quat}$), 31.0 (td, J = 5.3, 0.9 Hz, C^{tBu}), 30.0 ($C^{xantphos\text{-}Me}$). $^{31}P\{^1H\}$ NMR (202 MHz, CD_2Cl_2, 298 K) δ/ppm 28.0 (d, $J_{31P-109Ag}$ = 519 Hz), 28.0 (d, $J_{31P-107Ag}$ = 444 Hz), 10.5 (*t*Bu-xantphos, 7%), −144.5 (sept, J_{PF} = 710 Hz, $[PF_6]^-$). ESI MS: *m/z* 605.4 [Ag(*t*Bu-xantphos)]$^+$ (base peak, calc. 605.2, base peak for [Ag(*t*Bu-xantphos)(bpy)]$^+$, calc. 761.3). Found: C 54.43, H 6.36, N 3.21; $C_{41}H_{56}AgF_6N_2OP_3$ requires C 54.25, H 6.22, N 3.09%.

Crystallography. Ambient pressure data were collected on a Bruker Kappa Apex2 diffractometer with data reduction, solution and refinement using the programs APEX[23] and CRYSTALS.[24] Structural analysis was carried out using Mercury v. 3.9.[25,26] High-pressure single crystal experiments were carried out using a Merrill-Bassett diamond anvil cell[27] (half-opening angle 40°), equipped with Boehler-Almax diamonds with 600 μm culets and a tungsten gasket.[28] Hexane was used as hydrostatic medium and a small ruby chip was loaded into the cell as the pressure calibrant with the ruby fluorescence used to measure the pressure.[29] Diffraction data were collected using synchrotron radiation of wavelength λ = 0.4859 Å at room temperature on a Newport IS4CCD (4 circle) diffractometer with a Pilatus 300K detector at Station I19 at the Diamond Light Source, Harwell Science and Innovation Campus. Integrations were carried out using the program CrysAlisPro[30] and absorption corrections with the program ABSPACK.[29] Refinements were carried out with CRYSTALS[23] using the ambient pressure structure as starting models.

[Cu(*t*Bu-xantphos)(bpy)][PF$_6$].

$C_{41}H_{56}CuF_6N_2OP_3$, M = 863.36, yellow block, monoclinic, space group P $2_1/c$, a = 12.2247(10), b = 15.0283(12), c = 22.5879(19) Å, β = 98.452(3)°, U = 4104.7(6) Å^3, Z = 4, D_c = 1.397 Mg m^{-3}, μ(Cu-Kα) = 2.385 mm^{-1}, T = 123 K. Total 88540 reflections, 7254 unique, R_{int} = 0.033. Refinement of 7132 reflections (655 parameters) with I >2σ(I) converged at final R_1 = 0.0331 (R_1 all data = 0.0334), wR_2 = 0.0337 (wR_2 all data = 0.0345), gof = 1.0796. CCDC 1583820.

For high pressure data and respective CCDC codes see Table S1†.

[Cu(*t*Bu-xantphos)][PF$_6$]·H$_2$O.

$C_{31}H_{52}CuF_6O_3P_3$, M = 743.21, yellow plate, orthorhombic, space group *I2mm*, a = 10.6543(8), b = 11.1834(14), c = 15.7615(11) Å, U = 1878.0(3) Å^3, Z = 2, D_c = 1.314 Mg m^{-3}, μ(Cu-Kα) = 2.538 mm^{-1}, T = 123 K. Total 3944 reflections, 1711 unique, R_{int} = 0.034. Refinement of 1698 reflections (126 parameters) with I >2σ(I) converged at final R_1 = 0.1497 (R_1 all data = 0.1505), wR_2 = 0.1635 (wR_2 all data = 0.1639), gof = 1.1082. CCDC 1583821.

[Ag(*t*Bu-xantphos)(bpy)][PF$_6$].

$C_{41}H_{56}AgF_6N_2OP_3$, M = 907.68, colourless block, triclinic, space group P−1, a = 12.3873(9), b = 12.5363(9), c = 15.3282(12) Å, α = 104.142(3), β = 109.108(2), γ = 103.339(2)°; U = 2051.8(3) Å^3, Z = 2, D_c = 1.469 Mg m^{-3}, μ(Cu-Kα) = 5.576 mm^{-1}, T = 123 K. Total 26703 reflections,

7397 unique, R_{int} = 0.027. Refinement of 7256 reflections (523 parameters) with $I > 2\sigma(I)$ converged at final R_1 = 0.0383 (R_1 all data = 0.0387), wR_2 = 0.0779 (wR_2 all data = 0.0779), gof = 0.8973. CCDC 1583822.
For high pressure data and respective CCDC codes see Table S2†.

Results and discussion

Synthesis and characterization of [Cu(*t*Bu-xantphos)(bpy)][PF_6] complexes and [Ag(*t*Bu-xantphos)(bpy)][PF_6]

The syntheses of the [Cu(*t*Bu-xantphos)(N^N)][PF_6] complexes with N^N = bpy, 6-Mebpy and 4,4'-(*t*Bu)$_2$bpy, as well as [Ag(*t*Bu-xantphos)(bpy)][PF_6] were carried out following the standard procedures for [Cu(POP)(N^N)][PF_6] complexes.[14,15,31] An analogous reaction was carried out between [Cu(MeCN)$_4$][PF_6], *t*Bu-xantphos and 6-Brbpy, but, as described below, this reaction failed to produce the desired heteroleptic complex. Since alkyl phosphanes are prone to oxidation (although dialkylbiarylphosphanes were found to be air stable[32]), inert conditions (N_2 atmosphere, dry and degassed solvents) were applied during the reaction as a precaution. The solid products were air stable and were isolated in yields of 53 to 80%. The base peaks in the electrospray mass spectra were assigned to [Cu(*t*Bu-xantphos)]$^+$ for all the copper complexes, or to [Ag(*t*Bu-xantphos)]$^+$. Mass peaks arising from the heteroleptic [Cu(*t*Bu-xantphos)(N^N)]$^+$ cations or [Ag(*t*Bu-xantphos)(bpy)]$^+$ were not detected. Elemental analysis was performed to confirm the purity of the bulk compounds [Cu(*t*Bu-xantphos)(bpy)][PF_6], [Cu(*t*Bu-xantphos)(6-Mebpy)][PF_6], [Cu(*t*Bu-xantphos)(4,4'-*t*Bu$_2$bpy)][PF_6] and [Ag(*t*Bu-xantphos)(bpy)][PF_6]. Unambiguous confirmation of the formation of the heteroleptic complexes came from NMR spectroscopic measurements.

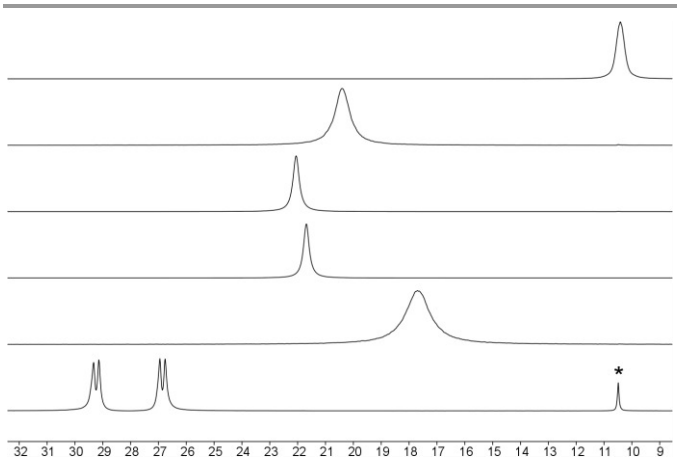

Fig. 1. Parts of the $^{31}P\{^1H\}$ NMR spectra (202 MHz, 298 K) of CD_2Cl_2 solutions of *t*Bu-xantphos (top), [Cu(*t*Bu-xantphos)(bpy)][PF_6], [Cu(*t*Bu-xantphos)(6-Mebpy)][PF_6], [Cu(*t*Bu-xantphos)][PF_6] with 6-Brbpy, [Cu(*t*Bu-xantphos)(4,4'-*t*Bu$_2$bpy)][PF_6] and [Ag(*t*Bu-xantphos)(bpy)][PF_6] (bottom, signal labelled with an asterisk indicates free *t*Bu-xantphos ligand).

The compounds were analysed by 1- and 2-dimensional NMR spectroscopic techniques (^{1}H, ^{31}P, ^{13}C, COSY, NOESY, HMQC, HMBC), which allowed the unambiguous assignment of all signals. The ^{31}P NMR spectra showed broad signals for the copper complexes and a set of two doublets for [Ag(*t*Bu-xantphos)(bpy)][PF_6] (Fig. 1) in addition to the septet at δ −144.5 ppm arising from [PF_6]$^-$ (not shown).

The NOESY spectra provide an invaluable tool for the confirmation that heteroleptic [Cu(*t*Bu-xantphos)(bpy)][PF_6] species (as opposed to a mixture of homoleptic species or free ligands) are present in solution. Cross peaks between the signal of the *t*Bu groups of *t*Bu-xantphos and proton H^{A6} of bpy (see Scheme 1 for atom labelling) as well as between *t*Bu and the Me group of 6-Mebpy demonstrate a through-space interaction between the two ligands coordinated to the same metal atom. This confirms the formation of [Cu(*t*Bu-xantphos)(bpy)][PF_6], [Ag(*t*Bu-xantphos)(bpy)][PF_6], [Cu(*t*Bu-xantphos)(4,4'-*t*Bu$_2$bpy)][PF_6] and [Cu(*t*Bu-xantphos)(6-Mebpy)][PF_6] (Fig. 2 and Fig. S1† to Fig. S9†). For the product of the attempted preparation of [Cu(*t*Bu-xantphos)(6-Brbpy)][PF_6], no cross peaks between H^{A6} and *t*Bu were observed (Fig. S10† and S11†). In this case, the steric hindrance of the *tert*-butyl groups coupled with the size of the bromo substituent prevented coordination of the 6-Brbpy to copper(I). This is further supported by the fact that the signals in the ^{1}H NMR spectrum which were assigned to 6-Brbpy in the complex solution coincide exactly with the signals of a sample of free 6-Brbpy (see Fig. S12†). Furthermore, crystallization of the product obtained from this synthesis yielded single crystals of [Cu(*t*Bu-xantphos)][PF_6] (see crystallography section).

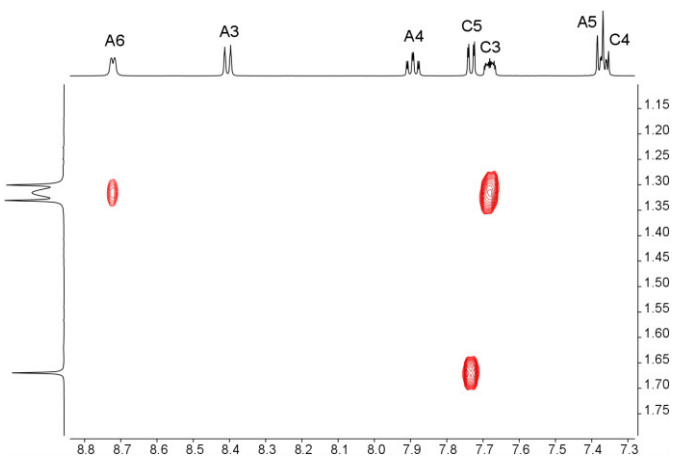

Fig. 2. Part of the NOESY spectrum of [Cu(*t*Bu-xantphos)(bpy)][PF_6] in CD_2Cl_2 at 298 K, 500 MHz. The NOESY cross peak between the *t*Bu signal at δ 1.31 ppm and the H^{A6} signal at δ 8.72 ppm is clearly visible.

Electrochemistry

The electrochemical behaviour of the heteroleptic complexes was investigated using cyclic voltammetry (CV), with the voltammogram for [Cu(*t*Bu-xantphos)(bpy)][PF_6] illustrated in Fig. 3 as an example. The oxidation potentials $E_{1/2}^{ox}$ (see Table 1) for [Cu(*t*Bu-xantphos)(bpy)][PF_6] (+0.70 V) and [Cu(*t*Bu-xantphos)(4,4'-*t*Bu$_2$bpy)][PF_6] (+0.62 V) are at lower potentials

than for [Cu(xantphos)(bpy)][PF_6] (+0.76 V). This indicates that Cu^+/Cu^{2+} oxidation is easier for the complexes with *t*Bu-xantphos than xantphos. This is consistent with the stronger electron-donating character of the *tert*-butyl groups at the phosphorus atoms in *t*Bu-xantphos versus the phenyl groups in xantphos. The differences of 270 mV for [Cu(*t*Bu-xantphos)(bpy)][PF_6] and 370 mV for [Cu(*t*Bu-xantphos)(4,4'-tBu$_2$bpy)][PF_6] between the anodic and cathodic peaks demonstrate the irreversibility or pseudo-reversibility of the oxidation processes. The second oxidation peak as illustrated for [Cu(*t*Bu-xantphos)(bpy)][PF_6] in Fig. 3, was found for all the complexes and is attributed to oxidation of the phosphane ligand. Reduction processes for the compounds were poorly resolved.

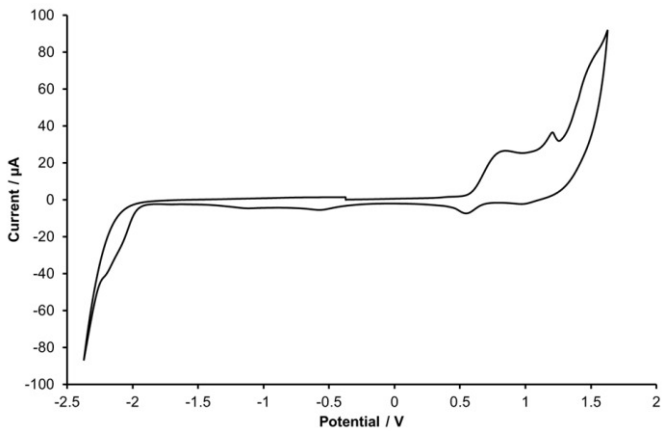

Fig. 3. Cyclic voltammogram of a CH_2Cl_2 solution of [Cu(*t*Bu-xantphos)(bpy)][PF_6] (vs. Fc^+/Fc, [nBu$_4$N][PF_6] supporting electrolyte, scan rate = 0.1 V s^{-1}).

Table 1. Cyclic voltammetric data for [Cu(*t*Bu-xantphos)(bpy)][PF_6] complexes and [Ag(*t*Bu-xantphos)(bpy)][PF_6] referenced to internal Fc/Fc^+ = 0.V; CH_2Cl_2 (freshly distilled) solutions with [^{n}Bu$_4$N][PF_6] as supporting electrolyte and scan rate of 0.1 V s^{-1}. Processes are quasi-reversible unless otherwise stated (ir = irreversible).

Complex cation	$E_{1/2}^{ox}$ / V	($E_{pc} - E_{pa}$ / mV)
[Cu(*t*Bu-xantphos)(bpy)]$^+$	+0.70	270
[Cu(xantphos)(bpy)]$^+$	+0.76	110
[Cu(*t*Bu-xantphos)(6-Mebpy)]$^+$	Only red. peak at +0.57 visible	ir
[Cu(*t*Bu-xantphos)(4,4'-tBu$_2$bpy)]$^+$	+0.62	370
[Ag(*t*Bu-xantphos)(bpy)]$^+$	+0.87	90
*t*Bu-xantphos	Ox1: Only ox. peak at +0.46 visible; Ox2: +0.96	Ox2: 330

For [Ag(*t*Bu-xantphos)(bpy)]$^+$, the oxidation potential of +0.87 V is of a similar order of magnitude as is reported for neutral silver complexes with POP and CF_3-functionalized 2-pyridyl pyrrolides (+0.74 V and +0.76 V vs. Fc^+/Fc, irreversible).[33] For [Ag(dppb)$_2$][PF_6] (where dppb = 1,2-bis-(diphenylphosphino)benzene), $E_{1/2}^{ox}$ value of +0.48 V *vs* Fc^+/Fc with a peak separation of 80 mV was reported (in MeCN)[34] and CV measurements of [Ag(dppb)$_2$][BF_4] in CH_2Cl_2 gave an oxidation potential of +0.99 V (SCE, quasi-reversible).[35] In contrast to the oxidation of the copper complexes, which are metal centred processes of the type Cu^+/Cu^{2+}, the oxidation processes of silver(I) compounds are usually ligand centred.

Photophysical properties

Each of the solution absorption spectra of the heteroleptic copper complexes and [Ag(*t*Bu-xantphos)(bpy)][PF_6] exhibits the most intense band around 230 nm, followed by a second band at ~280 nm with shoulders (see Fig. 4). In contrast to analogous copper(I) complexes with xantphos or POP, the broad band typically around 360 to 440 nm, which is assigned to MLCT transitions,[11] is missing. Rather than the typical yellow colour of [Cu(POP)(N^N][PF_6] or [Cu(xantphos)(N^N][PF_6] complexes, solutions of [Cu(*t*Bu-xantphos)(N^N][PF_6] compounds (1.0×10^{-4} mol dm^{-3}) appear colourless by eye. For [Ag(P^P)(N^N)]$^+$ complexes the absence of an MLCT band in the visible area is the norm[18,30] rather than the exception.[19] In the solid state, however, the copper(I) complexes exhibit colours from bright yellow to orange and the significantly more concentrated solutions (0.02 mol dm^{-3}) used for NMR spectroscopic measurements are yellow.

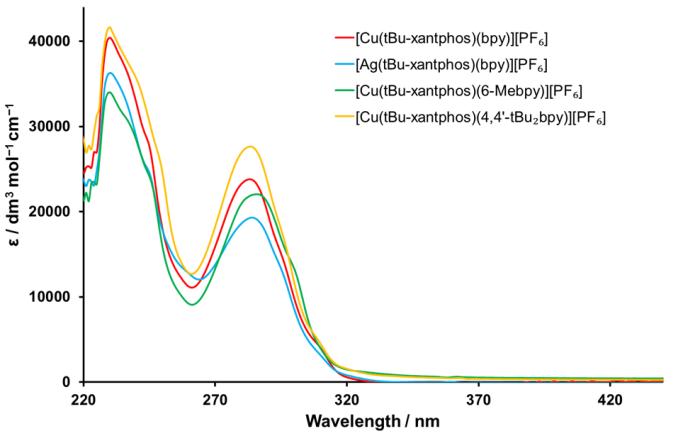

Fig. 4. Solution absorption spectra of the [Cu(*t*Bu-xantphos)(bpy)][PF_6] complexes and [Ag(*t*Bu-xantphos)(bpy)][PF_6] (CH_2Cl_2, 2.5×10^{-5} mol dm^{-3}).

None of the complexes shows a detectable emission in CH_2Cl_2 solutions (both non-deaerated and deaerated). Even in the solid state, where the complexes are in a rigid environment and solution related quenching processes do not occur, the emissions are very weak for all the complexes in this series. The PLQY values are below 1% for the copper(I) complexes with *t*Bu-xantphos and 2.5% for [Ag(*t*Bu-xantphos)(bpy)][PF_6] (Table 2). The emission spectra are illustrated in Fig. S13† and Fig. 5 (normalized), with the emission maxima listed in Table 2. Comparison of the non-normalized spectra in Fig. S13† underlines how weakly emissive the copper(I) complexes are with respect to [Ag(*t*Bu-xantphos)(bpy)][PF_6], whereas in Fig. 6 the normalization of the spectra illustrates the shift of the emission maxima. The most blue-shifted emission is exhibited by [Ag(*t*Bu-xantphos)(bpy)][PF_6]; the emission spectrum shows two maxima at 447 and 470 nm. The emission is most likely ligand-centred for the silver complex. For the copper(I)

complexes, the emission maxima move to shorter wavelengths on going from bpy to 6-Mebpy to 4,4'-tBu$_2$bpy.

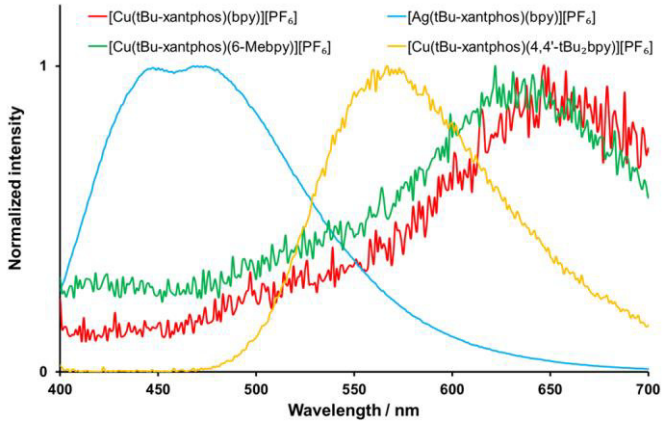

Fig. 5. Normalized emission spectra of the [Cu(tBu-xantphos)(bpy)][PF$_6$] complexes in solid state.

Discussion of vibrational quenching

In order to be a promising candidate as an emissive material in LECs or OLEDs, the iTMC needs to exhibit high PLQY values, which in turn means that non-radiative decay pathways should be minimized. A successful strategy to enhance the photophysical properties of copper(I) complexes is by stabilizing the tetrahedral geometry of the copper(I) centre, typically by introducing sterically demanding substituents which disfavours flattening of the coordination sphere in the excited state. Considering the steric crowding of four *tert*-butyl groups (see crystallography section), this was achieved in the case of [Cu(tBu-xantphos)(bpy)][PF$_6$], so there has to be another origin for the almost complete quenching of the emission even in the solid state, that is related to the *tert*-butyl groups. A vague recommendation for the design of emitting complexes to refrain from the incorporation of CH_2- and CH_3-groups in order to avoid vibrational quenching was found in the literature.[36] The C–H stretching modes are some of the highest frequency vibrations, with C_{sp2}–H vibrations between 3100 and 3010 cm^{-1} and C_{sp3}–H vibrations between 2950 and 2850 cm^{-1}.[37] The more vibrations that are present and the higher the energy of these vibrations, the easier it is to match an electronic gap with vibrational energy.[38] Although the C–H vibrations on the phenyl rings in xantphos are higher in energy than those of the *tert*-butyl groups in tBu-xantphos, the number of C–H bonds in the former are fewer than the latter (20 H in four phenyl substituents versus 36 H in four tBu substituents). We have observed that *tert*-butyl groups introduced into the 4,4'-positions of the bpy ligand in [Cu(xantphos/POP)(4,4'-tBu$_2$bpy)]$^+$ do not lead to such a quenching effect,[39] and therefore we conclude that the closeness to the copper centre plays an important role in the quenching mechanism. One way to study the vibrational quenching is by making use of the isotopic effect. It has been shown that replacement of hydrogen atoms with deuterium in organic molecules leads to a reduction in vibrational quenching and enhancement of luminance;[33] a similar effect has been observed for some lanthanoid metal complexes.[40,41] The isotopic effect of the exchange of ^{12}C for ^{13}C has also been studied for the fullerenes C_{60} and C_{70}.[42] However, to the best of our knowledge, vibrational quenching effects in copper(I) complexes have not previously been described.

Table 2. Emission maxima and photoluminescence quantum yields (PLQY) for the [Cu(tBu-xantphos)(N^N)][PF$_6$] complexes and [Ag(tBu-xantphos)(bpy)][PF$_6$] in solid state (λ_{exc} = 365 nm).

Complex cation	λ_{em}^{max} / nm (powder)	PLQY / % (powder)
[Cu(tBu-xantphos)(bpy)]$^+$	647	0.4
[Cu(xantphos)(bpy)]$^+$	587	1.7
[Cu(tBu-xantphos)(6-Mebpy)]$^+$	622	0.4
[Cu(tBu-xantphos) (4,4'-tBu$_2$bpy)]$^+$	567	0.4
[Ag(tBu-xantphos)(bpy)]$^+$	447, 470	2.5

Steric and electronic properties of xantphos vs. tBu-xantphos

Replacing substituents in phosphanes involves a change in both electronic and steric effects. A detailed study of steric effects of phosphorus ligands was published in 1977 by Tolman.[43] The Tolman cone angle Θ between the most outer atoms of a ligand and the metal centre is since then a ubiquitous parameter for assessing steric demand. A comparison of the cone angles of PPh_3 (145°) and $PPhtBu_2$ (170°)[44] indicates the significantly increased steric demand of the ligands tBu-xantphos vs. xantphos. For complexes with chelating bisphosphanes the bite angle P–M–P is usually given as the main characteristic element. However, the two angles are correlated in that a chelating ligand with a wide bite angle also leads to a large cone angle, and *vice versa.* A useful parameter to compare chelating ligands independent from the coordinated metal is defined as the natural bite angle which describes the chelating angle as only determined by the backbone of the ligand.[45] Calculations using molecular mechanics show that the preferred bite angle of the phosphane ligand is also larger for tBu-xantphos (140°) than for xantphos (108°).[46] In theory, an increase of these angles should lead to a decreased *s* character of the lone pair at the phosphorus. This is an example of how the electronic and steric effects are interlinked. While phenyl groups exhibit an inductive *–I* effect together with a positive *+M* effect, the *+I* properties of the *tert*-butyl groups of tBu-xantphos should also lead to an increased electron density at the phosphorus atom.

Structural characterization of the complexes

Single crystal X-ray diffraction quality crystals were obtained by layer crystallization, by slow diffusion of Et_2O into CH_2Cl_2 solutions of the complexes. The single crystal structures of the tBu-xantphos[47] and xantphos ligands[48] have been reported.

Structures at ambient pressure

[Cu(*t*Bu-xantphos)(bpy)][PF_6] crystallized in the monoclinic space group $P2_1/c$, and the structure of the cation is illustrated in Fig. 6. Unexpectedly, the copper(I) atom is five-coordinate with the *t*Bu-xantphos ligands showing κ^3 binding from the phosphorus atoms and, in addition, from the oxygen donor of the xanthene unit with a short Cu–O distance of 2.6699(11) Å. Although these type of bisphosphanes with phenylether backbones are usually found in a bidentate chelating mode (κ^2), due to the ability of the oxygen to coordinate, similar geometries as in complexes with traditional PCP or PNP pincer ligands have been reported.[49] Both the Cu–P distances (Cu1–P2 = 2.3522(5) Å; Cu1–P1 = 2.3283(4) Å) as well as the Cu–N distances (Cu1–N2 = 2.1725(14) Å; Cu1–N1 = 2.1366(14) Å) are longer than in [Cu(xantphos)(bpy)][PF_6] (see Table 3). The central ring of the xanthene unit is in the boat conformation, as also found in the structure of [Cu(xantphos)(bpy)][PF_6].[14] Comparison of the fold angles, which are the angles between the mean planes that contain the outer aromatic rings of the xanthene backbone, gives values of 39.08° for [Cu(*t*Bu-xantphos)(bpy)][PF_6] and 32.40° for [Cu(xantphos)(bpy)][PF_6], thus revealing that the xanthene backbone is even less flattened in the former structure than in the latter. The P–Cu–P chelating angle in [Cu(*t*Bu-xantphos)(bpy)][PF_6] (129.297(17)°) is significantly larger than in [Cu(xantphos)(bpy)][PF_6] (113.816(14)°), a trend which is in agreement with the aforementioned preferred bite angles (140° for *t*Bu-xantphos and 108° for xantphos).[41] With an ionic radius R_i of 0.60 Å (coordination number CN = 4), Cu^+ is relatively small in comparison to other metal cations (e.g. Ag^+, R_i = 1.00 Å for CN = 4),[50] which is reflected in short bond distances. In order to stay within an efficient bonding distance, but also allow the bpy to coordinate to the copper centre, the folding of the xanthene backbone is required. Due to the steric crowding of the *tert*-butyl groups at the phosphorus atoms, the boat ring of the xanthene unit is folded towards the copper atom, thus allowing the oxygen to approach closely to the copper centre. Another noteworthy feature is the position of the bpy ligand which is strongly tilted to the side and almost completely located above the xanthene backbone. The distance between the hydrogen H441 next to the nitrogen N1 of the bpy to atom O1 of the *t*Bu-xantphos ligand is 2.45(2) Å and this is consistent with a weak hydrogen-bonded interaction. However, while contributing to the tilting of the bpy, it is unlikely to be the driving force behind it.[51]

The structure of the cation in [Ag(*t*Bu-xantphos)(bpy)][PF_6], which crystallized in the triclinic space group $P\bar{1}$, is illustrated in Fig. 7 and an overlay with the structure of the copper analogue is shown in Fig. 8. The silver centre is coordinated in a distorted tetrahedral geometry, but not as distorted as the copper centre in the analogue structure, with the angle between the *t*Bu-xantphos ligand and the bpy coming to 82.44°. As expected due to the larger atomic radius of silver, the Ag–P distances as well as the Ag–N distances are longer than in the respective copper cation (see Table 3). One of the most noticeable difference to the copper analogue is the almost flat geometry of the xanthene unit in [Ag(*t*Bu-xantphos)(bpy)][PF_6] (fold angle 5.89°). Furthermore, there is no bond from the oxygen of *t*Bu-xantphos to the silver centre, with the distance d(Ag–O) being 3.035(2) Å. While the P–Ag–P bite angle of 128.27(2)° is very close to the P–Cu–P bite angle, the longer Ag–P bonds allow for a flatter geometry of the xanthene backbone.

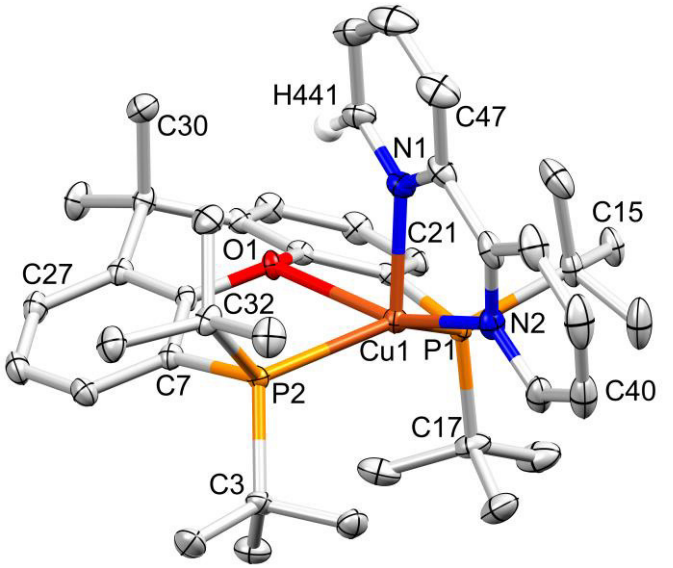

Fig. 6. Structure of the [Cu(*t*Bu-xantphos)(bpy)]$^+$ cation in [Cu(*t*Bu-xantphos)(bpy)][PF_6]. Ellipsoids plotted at 50% probability level, positions of H atoms refined, H atoms omitted except for H441 to show proximity to O1 (2.45(2) Å).

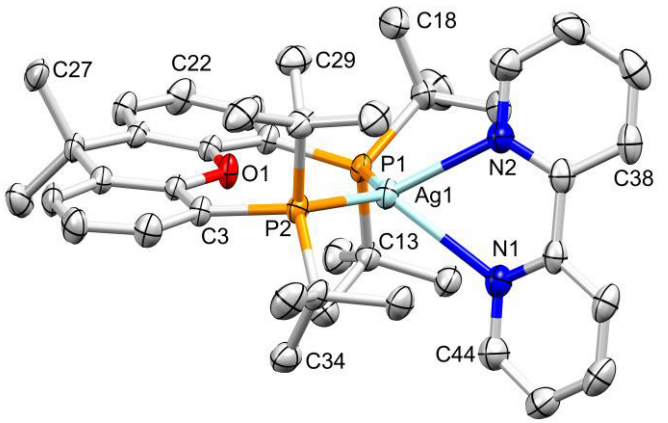

Fig. 7. Structure of the [Ag(*t*Bu-xantphos)(bpy)]$^+$ cation in [Ag(*t*Bu-xantphos)(bpy)][PF_6]. Ellipsoids plotted at 50% probability level, H atoms omitted.

The silver analogue also differs from the [Cu(*t*Bu-xantphos)(bpy)]$^+$ cation in terms of chelation by the bpy ligand. In contrast to the tilted coordination, the bpy in [Ag(*t*Bu-xantphos)(bpy)]$^+$ is almost perfectly opposite of the xanthene unit and by eye one might almost expect a mirror plane through the cation that cuts the bipyridine in half.

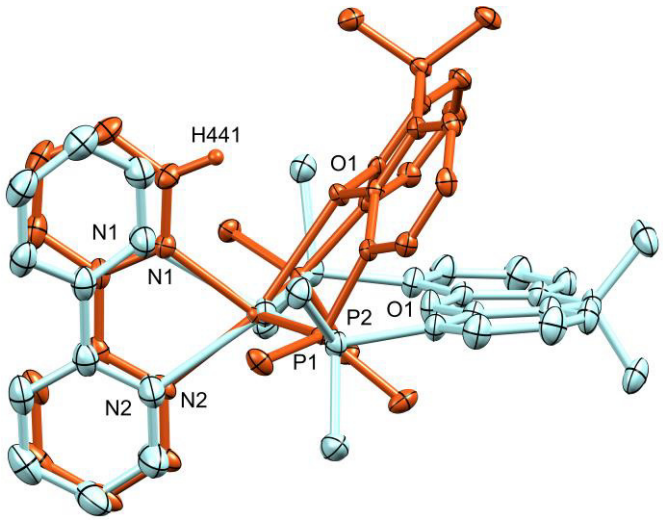

Fo 8. Overlay of the crystal structures of the cations [Cu(*t*Bu-xantphos)(bpy)]$^+$ (dark orange) and [Ag(*t*Bu-xantphos)(bpy)]$^+$ (silver blue) with ellipsoids plotted at 50% probability level. Only the *ipso*-C atoms of the $PtBu_2$ groups are shown and H atoms are omitted. The metallic centres of the cations were overlaid.

Crystallization setups of the mixture obtained from the reaction of $[Cu(MeCN)_4][PF_6]$, *t*Bu-xantphos and 6-Brbpy yielded crystals of [Cu(*t*Bu-xantphos)][PF_6]·H_2O. The compound crystallizes in the orthorhombic space group *I2mm*. The copper atom is coordinated by one *t*Bu-xantphos ligand through two phosphorus atoms and the oxygen atom, no close contacts to the $[PF_6]^-$ anion or solvent molecules were observed. To our knowledge, this is one of the few structures where a copper(I) cation is only coordinated from one side by a chelating bisphosphane ligand. Other examples feature a P^N^P ligand with also either a *tert*-butyl or isobutyl group at the phosphorus atoms.[52,53]

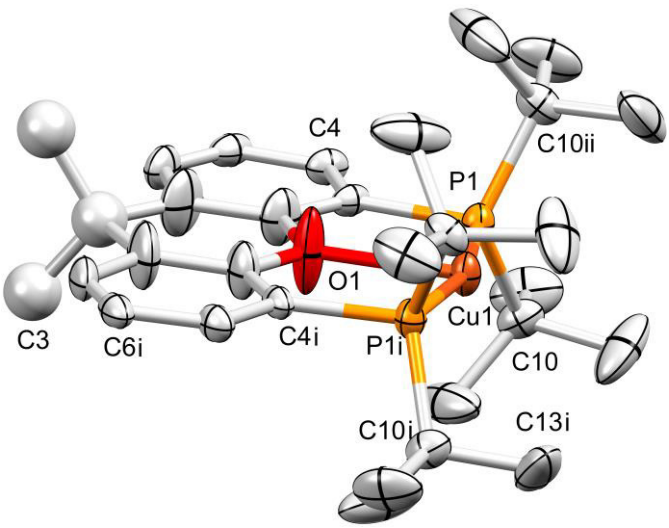

Fig. 8. Structure of the [Cu(*t*Bu-xantphos)(bpy)]$^+$ cation in [Cu(*t*Bu-xantphos)(bpy)][PF_6]·H_2O. Ellipsoids plotted at 50% probability level, H atoms omitted. Symmetry generated atoms: i = x, y, 1−z, ii = x, 1−y, z. The CMe_2 group was refined isotropically (see text).

Although the electron donating +*I* effect of the *tert*-butyl groups bonded to the phosphorus atoms might be expected to facilitate an oxidation to Cu(II), we observed that, even after weeks in non-deaerated solvents (CH_2Cl_2/Et_2O), no colour change was observed in the solid material of the crystallisation setup. This might be explainable by the packing in solid state: In the spacefill model of two [Cu(*t*Bu-xantphos)(bpy)]$^+$ cations in Fig. 9 the packing shows that the methyl groups of the xanthene unit of the next cation almost fill the open "pocket" between the *tert*-butyl groups and therefore hinders the access to the copper centre, thus stabilizing the oxidation state +I.

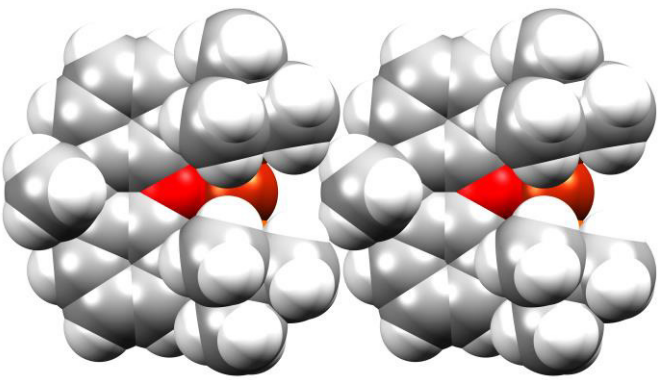

Fig. 9. Spacefill structure of the [Cu(*t*Bu-xantphos)(bpy)]$^+$ cation in [Cu(*t*Bu-xantphos)(bpy)][PF_6]·H_2O.

The middle ring of the xanthene unit has a flat geometry, but the bridging CMe_2 carbon atom C9 and O1 possess a high thermal motion that might suggest some orientational disorder. C9 lies on the two mirror planes making it very difficult to investigate whether the disorder is real of just high libration. An attempt to model the possible disorder was made but did not lead to a reasonable solution. For this reason the CMe_2 group was refined isotropically. The [Cu(*t*Bu-xantphos)]$^+$ cation is symmetry generated by a mirror plane through Cu1, O1 and the CMe_2 unit of the xanthene backbone. Another mirror plane goes through Cu1, the phosphorus atoms and the xanthene unit, which results in a perfect *mer*-κ^3 coordination of the *t*Bu-xantphos ligand. The Cu–P bonds (2.208(3) Å) are shorter than in [Cu(*t*Bu-xantphos)(bpy)]$^+$ and [Cu(xantphos)(bpy)]$^+$ and the same is true for the Cu–O bond (2.253(14) Å).

Structures at high pressure

The effect of increased pressure on the structures of [Cu(*t*Bu-xantphos)(bpy)][PF_6] and [Ag(*t*Bu-xantphos)(bpy)][PF_6] was studied by single crystal X-ray diffraction of crystals of the compounds in a diamond pressure cell. In order to assure that the pressure on the crystal is equivalent from all sides, hydrostatic conditions in the pressure cell were generated by flooding the cell with hexane. The change of the crystal parameters of [Cu(*t*Bu-xantphos)(bpy)][PF_6] was studied from 0.3 to 3.3 GPa. However the observed changes are only marginal (see Fig. 10 and Table S1†). The angle β increases with pressure from 98.56(2)° for 0.3 GPa to 99.44(3)° for 3.3 GPa. As expected, the lengths of the cell axes become shorter

with increasing pressure, which is also reflected in the shrinking cell volume from 4064(3) $Å^3$ at 0.3 GPa to 3623(3) $Å^3$ at 2.3 GPa, which represents a reduced volume of 89%. In the last step, however, where the pressure is quite dramatically increased from 2.3 to 3.3 GPa, a phase change takes place. This results in a doubling of the cell axis *a* from 11.787(8) Å to 23.191(18) Å with a concomitant doubling of *Z* from 4 to 8.

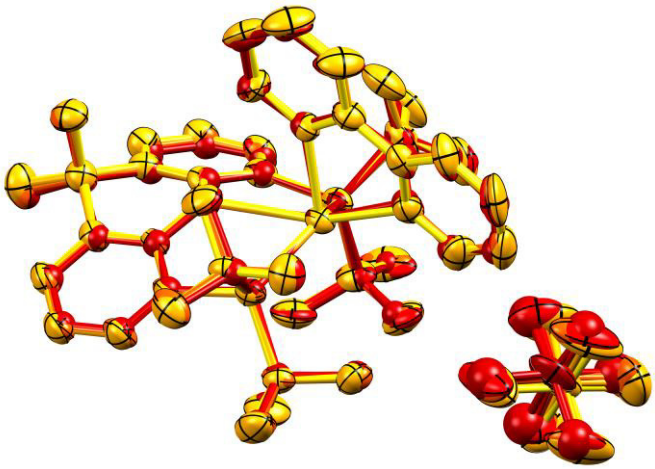

Fig. 10. Crystal structure of [Cu(*t*Bu-xantphos)(bpy)][PF_6] upon increasing the pressure from ambient (yellow) to 2.3 GPa (dark red). Ellipsoids plotted at 50% probability level, H atoms omitted.

In the case of [Ag(*t*Bu-xantphos)(bpy)][PF_6], the pressure study goes from 1.0 GPa to 4.5 GPa, but without the structure undergoing any phase change. As in the respective copper(I) complex, all cell axes decrease with augmented pressure, here resulting in a reduced cell volume of 91% (see Table S2†). As the overlay in Fig. 11 shows, only minor changes in the structure take place.

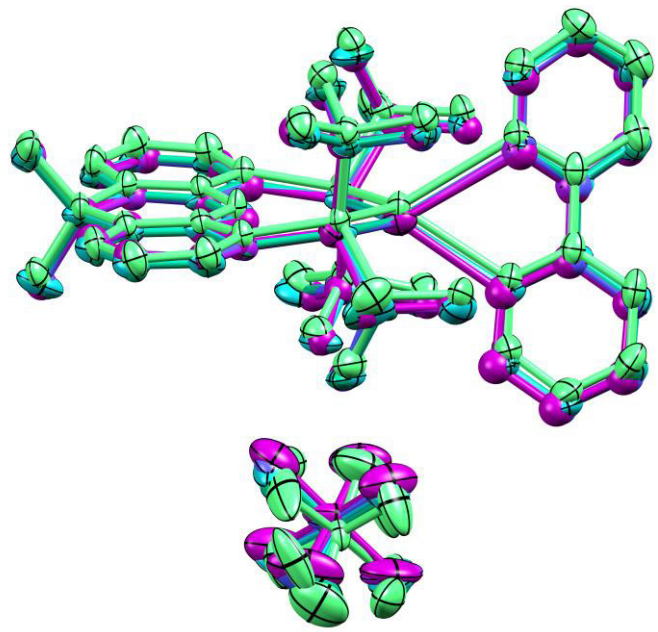

Fig. 11. Crystal structure of [Ag(*t*Bu-xantphos)(bpy)][PF_6] upon increasing the pressure from ambient (green) to 4.5 GPa (purple). Ellipsoids plotted at 50% probability level, H atoms omitted.

For both structures, the high pressure study confirmed the rigidity of the packing as well as the stability of the ligand coordination.

Conclusions

A series of [Cu(*t*Bu-xantphos)(N^N)][PF_6] complexes with N^N = bpy, 6-Mebpy and 4,4'-tBu$_2$bpy as well as [Ag(*t*Bu-xantphos)(bpy)][PF_6] was synthesized. The solid state structures of [Cu(*t*Bu-xantphos)(bpy)][PF_6] and [Ag(*t*Bu-xantphos)(bpy)][PF_6] were investigated at ambient and high pressure (up to 3.3 GPa) using single crystal X-ray diffraction experiments. The structures underwent little change upon increased pressure. Attempts to synthesize [Cu(*t*Bu-xantphos)(6-Brbpy)][PF_6] yielded [Cu(*t*Bu-xantphos)][PF_6] which was structurally characterized. While in [Ag(*t*Bu-xantphos)(bpy)][PF_6], the *t*Bu-xantphos ligand is only coordinated via the phosphorus atoms, in the structures with copper(I) the ligand adopts a *P,O,P'*-pincer type coordination. The photophysical properties of the compounds with *t*Bu-xantphos contrast with those of the corresponding xantphos containing complexes. The poorer emissive properties of the former are mainly attributed to the *tert*-butyl groups inducing vibrational C–H quenching of the emission. This prompts a future a study of the isotope effect upon exchange of hydrogen for deuterium in alkyl groups at various positions on the ligands and the resulting influence on the photochemistry of the complexes.

Acknowledgements

We acknowledge the Swiss National Science Foundation (Grant number 162631) and the University of Basel for financial support. Furthermore we would like to thank Diamond Light Source for access to beamline I19 (MT15176) and especially Dr. Dave R. Allan. Y. Maximilian Klein and Dr. Andrea Pannwitz are thanked for their efforts to share the shift work at the Diamond Light Source.

Notes and references

[a]Department of Chemistry, University of Basel, BPR 1096, Mattenstrasse 24a, CH-4058 Basel, Switzerland; email: catherine.housecroft@unibas.ch

†Electronic Supplementary Information (ESI) available: CCDC 1583820–1583822, 1583828–1583828, 1583832–1583835, 1583842–1583845. See DOI: 10.1039/b000000x/

1 A. Kitai, *Materials for Solid State Lighting and Displays*, John Wiley & Sons, West Sussex, United Kingdom, 2017.

2 N. Thejokalyani, S. J. Dhoble, *Renewable Sustainable Energy Rev.*, 2014, **32**, 448.

3 A. De Almeida, B. Santos, B. Paolo, M. Quicheron, *Renewable Sustainable Energy Rev.*, 2014, **34**, 30.

4 S. Tang, L. Edman, Top. Curr. Chem. (Z), 2016, **374**, 1.

5 E. Fresta, R. D. Costa, *J. Mater. Chem. C*, 2017, **5**, 5643.

6 See for example: C. E. Housecroft and E. C. Constable, *Chem. Soc. Rev.*, 2015, **44**, 8386.

7 R. Czerwieniec, M. J. Leitl, H. H.H. Homeier, H. Yersin, *Coord. Chem. Rev.*, 2016, **325**, 2.

8 M. Elie, S. Gaillard, J.-L. Renaud, in *Light-Emitting Electrochemical Cells*, ed. R. D. Costa, Springer International Publishing AG, Cham, Switzerland, 1st edn, 2017, pp. 287–327.

9 Q. Zhang, T. Komino, S. Huang, S. Matsunami, K. Goushi, and C. Adachi, *Adv. Funct. Mater.*, 2012, **22**, 2327.

10 F. Brunner, L. Martínez-Sarti, S. Keller, A. Pertegás, A. Prescimone, E. C. Constable, H. J. Bolink and C. E. Housecroft, *Dalton Trans.*, 2016, **45**, 15180.

11 S. Keller, A. Pertegás, G. Longo, L. Martinez, J. Cerdá, J. M. Junquera-Hernández, A. Prescimone, E. C. Constable, C. E. Housecroft, E. Ortí, H. J. Bolink, *J. Mater. Chem. C.*, 2016, **4**, 3857.

12 M. W. Mara, K. A. Fransted, L. X. Chen, *Coord. Chem. Rev.*, 2015, **2**, 282.

13 C. L. Linfoot, M. J. Leitl, P. Richardson, A. F. Rausch, O. Chepelin, F. J. White, H. Yersin and N. Robertson, *Inorg. Chem.*, 2014, **53**, 10854.

14 S. Keller, F. Brunner, J.M. Junquera, A. Pertegás, M.-G. La-Placa, A. Prescimone, E.C. Constable, H.J. Bolink, E. Ortí and C.E. Housecroft, *ChemPlusChem*, 2017 submitted cplu.201700501.

15 W. Su, T.-J. Gong, X. Lu, M.-Y. Xu, C.-G. Yu, Z.-Y. Xu, H.-Z, Yu, B. Xiao, Y. Fu, *Angew. Chem. Int. Ed.*, 2015, **54**, 12957.

16 M. C. Haibach, D. Y. Wang, T. J. Emge, K. Krogh-Jespersen, A. S. Goldman, *Chem. Sci.*, 2013, **4**, 3683.

17 J.-Y. Hu, J. Zhang, G.-X. Wang, H.-L. Sun, J.-L. Zhang, *Inorg. Chem.*, 2016, **55**, 2274.

18 O. Moudam, A. C. Tsipis, S. Kommanaboyina, P. N. Horton, S. J. Coles, *RSC Adv.*, 2015, **5**, 95047.

19 M. Z. Shafikov, A. F. Suleymanova, R. Czerwieniec, H. Yersin, *Chem. Mater.*, 2017, **29**, 1708.

20 G. J. Kubas, *Inorg. Synth.*, 1979, **19**, 90.

21 M. Shaul and Y. Cohen, *J. Org. Chem.*, 1999, **64**, 9358.

22 G. S. Hanan, U. S. Schubert, D. Volkmer, E. Rivière, J.-M. Lehn, N. Kyritsakas and J. Fischer, *Can. J. Chem.*, 1997, **75**, 169.

23 Bruker Analytical X-ray Systems, Inc., 2006, APEX2, version 2 User Manual, M86-E01078, Madison, WI.

24 P. W. Betteridge, J. R. Carruthers, R. I. Cooper, K. Prout and D. J. Watkin, *J. Appl. Cryst.*, 2003, **36**, 1487.

25 I. J. Bruno, J. C. Cole, P. R. Edgington, M. K. Kessler, C. F. Macrae, P. McCabe, J. Pearson, R. Taylor, *Acta Crystallogr., Sect. B*, 2002, **58**, 389.

26 C. F. Macrae, I. J. Bruno, J. A. Chisholm, P. R. Edgington, P. McCabe, E. Pidcock, L. Rodriguez-Monge, R. Taylor, J. van de Streek and P. A. Wood, *J. Appl. Cryst.*, 2008, **41**, 466.

27 S. A. Moggach, D. R. Allan, S. Parsons, J. E. Warren, Journal of Applied Crystallography 2008, 41, 249.

28 I. Kantor, V. Prakapenka, A. Kantor, P. Dera, A. Kurnosov, S. Sinogeikin, N. Dubrovinskaia, L. Dubrovinsky, *Review of Scientific Instruments* **2012**, *83*, 125102.

29 D. M. Adams, R. Appleby, S. K. Sharma, *J. Phys. E: Sci. Instrum.* **1976**, *9*, 1140.

30 CrysAlisPro 1.171.38.41k (Rigaku OD, 2015)

31 I. Andrés-Tomé, J. Fyson, F.B. Dias, A.P. Monkman, G. Iacobellis, P. Coppo, *Dalton Trans.*, 2012, **41**, 8669.

32 T. E. Barder, S. L. Buchwald, *J. Am. Chem. Soc.*, 2007, **129**, 5096.

33 C.-W. Hsu, C.-C. Lin, M.-W. Chung, Y. Chi, G.-H. Lee, P.-T. Chou, C.-H. Chang and P.-Y. Chen, *J. Am. Chem. Soc.*, 2011, **133**, 12085.

34 S. Igawa, M. Hashimoto, I. Kawata, M. Hoshino and M. Osawa, *Inorg. Chem.*, 2012, **51**, 5805.

35 A. Kaeser, O. Moudam, G. Accorsi, I. Séguy, J. Navarro, A. Belbakra, C. Duhayon, N. Armaroli, B. Delavaux-Nicot and J.-F. Nierengarten, *Eur. J. Inorg. Chem.*, 2014, **8**, 1345.

36 L. Bergmann, D. M. Zink, S. Bräse, T. Baumann, D. Volz, in *Photoluminescent Materials and Electroluminescent Devices*, ed. N. Armaroli, H. J. Bolink, *Top. Curr. Chem. Z*, 2016, **374**, 201.

37 C. E. Housecroft and E. C. Constable, Chemistry: *An Introduction to Organic, Inorganic and Physical Chemistry*, Pearson Education Limited, Essex, England, **4**, 2010.

38 N. J. Turro, *Modern Molecular Photochemistry*, University Science Books, Sausalito, California, 1991.

39 S. Keller, E. C. Constable and C. E. Housecroft, unpublished results (thesis).

40 C. Doffek, N. Alzakhem, C. Bischof, J. Wahsner, T. Güden-Silber, J. Lügger, C. Platas-Iglesias and M. Seitz, *J. Am. Chem. Soc.*, **2012**, 134, 16413.

41 I. Hemmilä, V.-M. Mukkala, and H. Takalo, *J. Fluoresc.*, 1995, **5**, 159.
42 C. Baleizão and M. N. Berberan-Santos, *ChemPhysChem.*, 2011, **12**, 1247.
43 C. A. Tolman, *Chem. Rev.*, 1977, **77**, 313.
44 J. A. Bilbrey, A. H. Kazez, J. Locklin and W. D. Allen, *J. Comput. Chem.*, 2013, **34**, 1189.
45 C. P. Casey and G. T. Whiteker, *Isr. J. Chem.*, 1990, **30**, 299.
46 M.-N. Birkholz, Z. Freixa and P. W. N. M. van Leeuwen, *Chem. Soc. Rev.*, 2009, **38**, 1099.
47 C. Mispelaere-Canivet, J.-F. Spindler, S. Perrio, P. Beslin, *Tetrahedron*, 2005, **61**, 5253.
48 S. Hillebrand, J. Bruckmann, C. Krüger, M. W. Haenel, *Tetrahedron Lett.*, 1995, **36**, 75.
49 G. M. Adams, A. S. Weller, *Coord. Chem. Rev.*, 2017, http://dx.doi.org/10.1016/j.ccr.2017.08.004.
50 "Ionic radii in crystals", in *CRC Handbook of Chemistry and Physics*, Internet Version 2005, David R. Lide, ed., <http://www.hbcpnetbase.com>, CRC Press, Boca Raton, FL, 2005.
51 T. Steiner, *Angew. Chem. Int. Ed.*, 2002, **41**, 48.
52 J. I. van der Vlugt, E. A. Pidko, D. Vogt, M. Lutz and A. L. Spek, *Inorg. Chem.*, 2009, **48**, 7513.
53 S. B. Harkins N. P. Mankad, A. J. M. Miller, R. K. Szilagyi, and J. C. Peters, *J. Am. Chem. Soc.*, 2008, **130**, 3478.

Electronic supplementary data to accompany

Photophysics and high pressure X-ray crystallography of Cu(I) and Ag(I) complexes with 9,9-dimethyl-4,5-bis(di-*tert*-butylphosphino)xanthene

Sarah Keller,[a] Alessandro Prescimone,[a] Edwin C. Constable[a] and Catherine E. Housecroft*[a]

[a]Department of Chemistry, University of Basel, BPR 1096, Mattenstrasse 24a, CH-4058 Basel, Switzerland; email: catherine.housecroft@unibas.ch

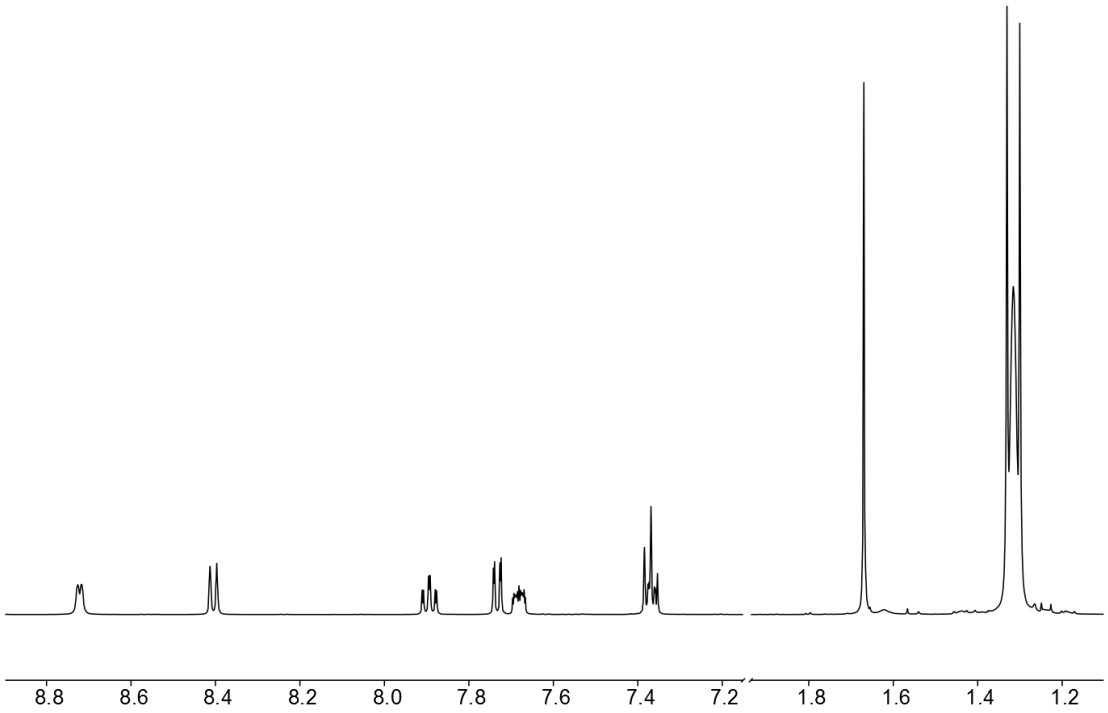

Fig. S1: ^{1}H NMR spectrum (cutout) of [Cu(*t*Bu-xantphos)(bpy)][PF_6] in CD_2Cl_2 at 298 K, 500 MHz.

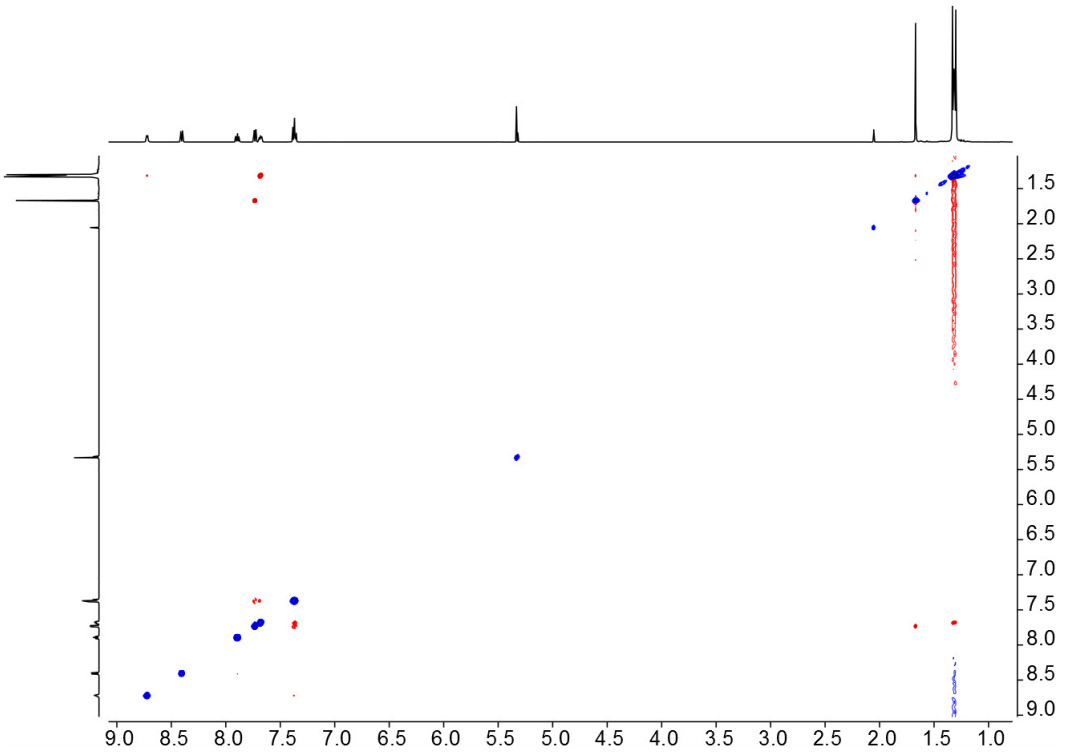

Fig. S2: NOESY spectrum of [Cu(*t*Bu-xantphos)(bpy)][PF_6] in CD_2Cl_2 at 298 K, 500 MHz. The NOESY cross peak between the *t*Bu signal of *t*Bu-xantphos at δ 1.31 ppm and the H^{A6} signal at δ 8.72 ppm is clearly visible.

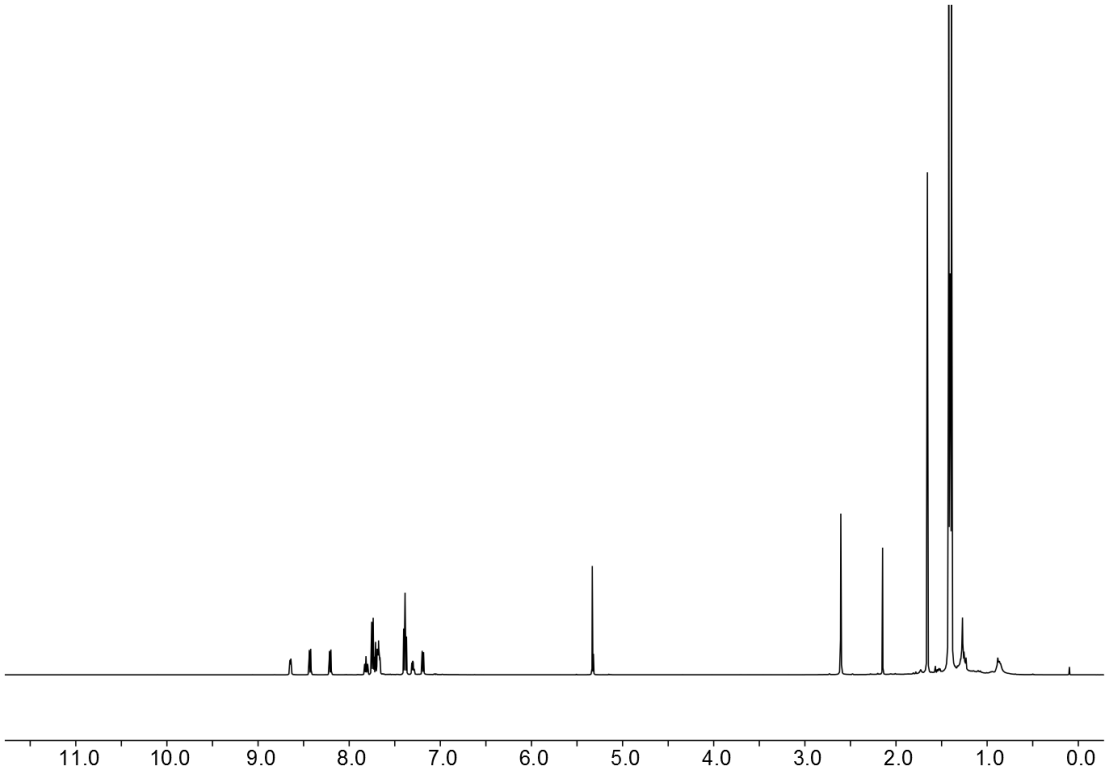

Fig. S3: ^{1}H NMR spectrum of [Cu(*t*Bu-xantphos)(6-Mebpy)][PF_6] in CD_2Cl_2 at 298 K, 500 MHz.

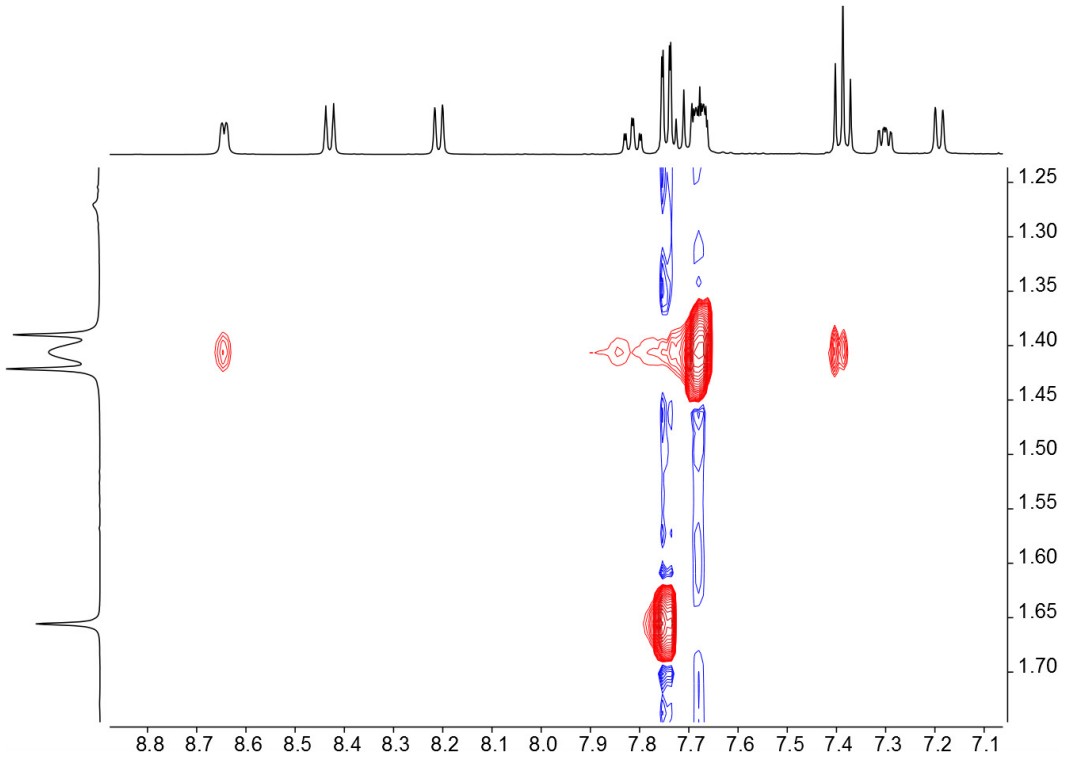

Fig. S4: NOESY spectrum (cutout) of [Cu(*t*Bu-xantphos)(6-Mebpy)][PF_6] in CD_2Cl_2 at 298 K, 500 MHz. The NOESY cross peak between the *t*Bu signal of *t*Bu-xantphos at δ 1.40 ppm and the H^{A6} signal at δ 8.64 ppm is clearly visible.

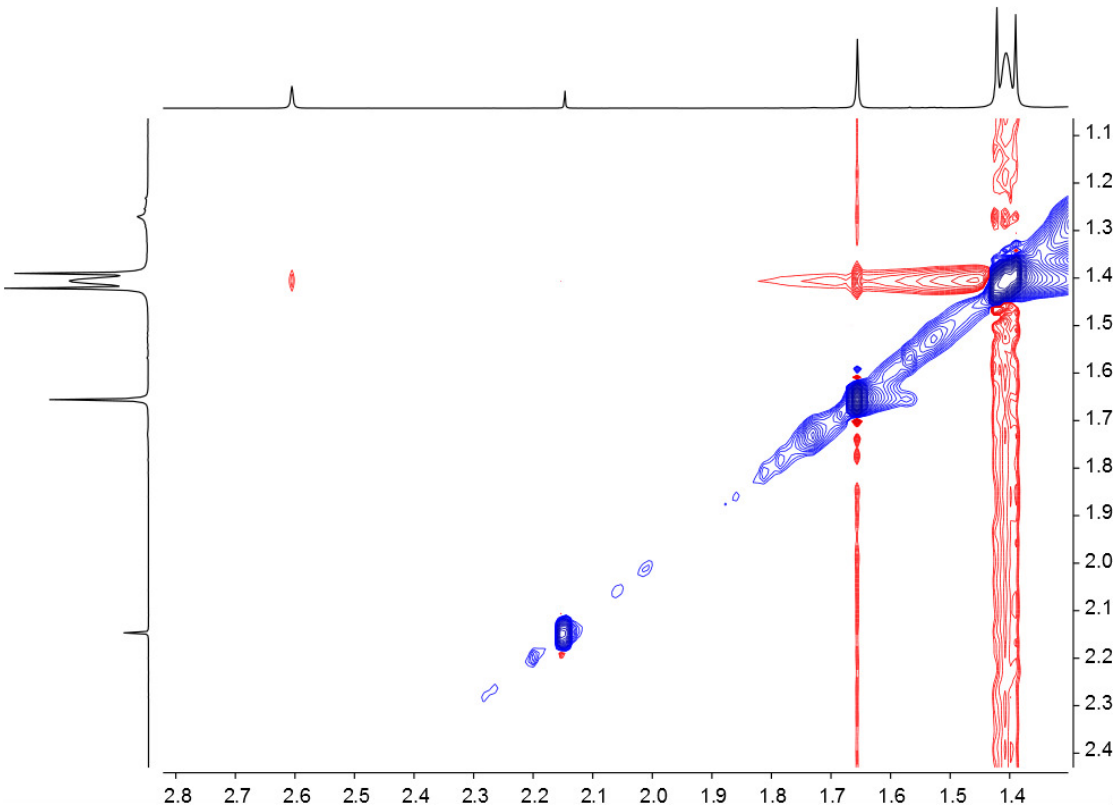

Fig. S5: NOESY spectrum (cutout) of [Cu(*t*Bu-xantphos)(6-Mebpy)][PF_6] in CD_2Cl_2 at 298 K, 500 MHz. The NOESY cross peak between the *t*Bu signal of *t*Bu-xantphos at δ 1.40 ppm and the Me signal of 6-Mebpy at δ 2.61 ppm is clearly visible.

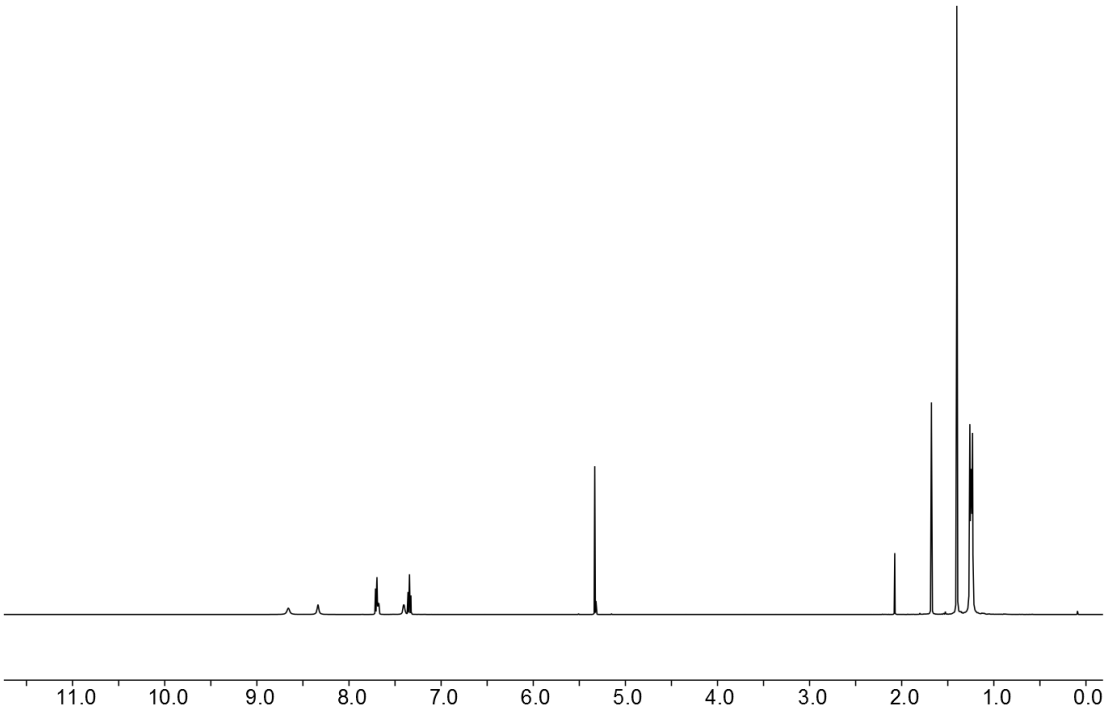

Fig. S6: ^{1}H NMR spectrum of [Cu(*t*Bu-xantphos)(4,4'-*t*Bu$_2$bpy)][PF$_6$] in CD_2Cl_2 at 298 K, 500 MHz.

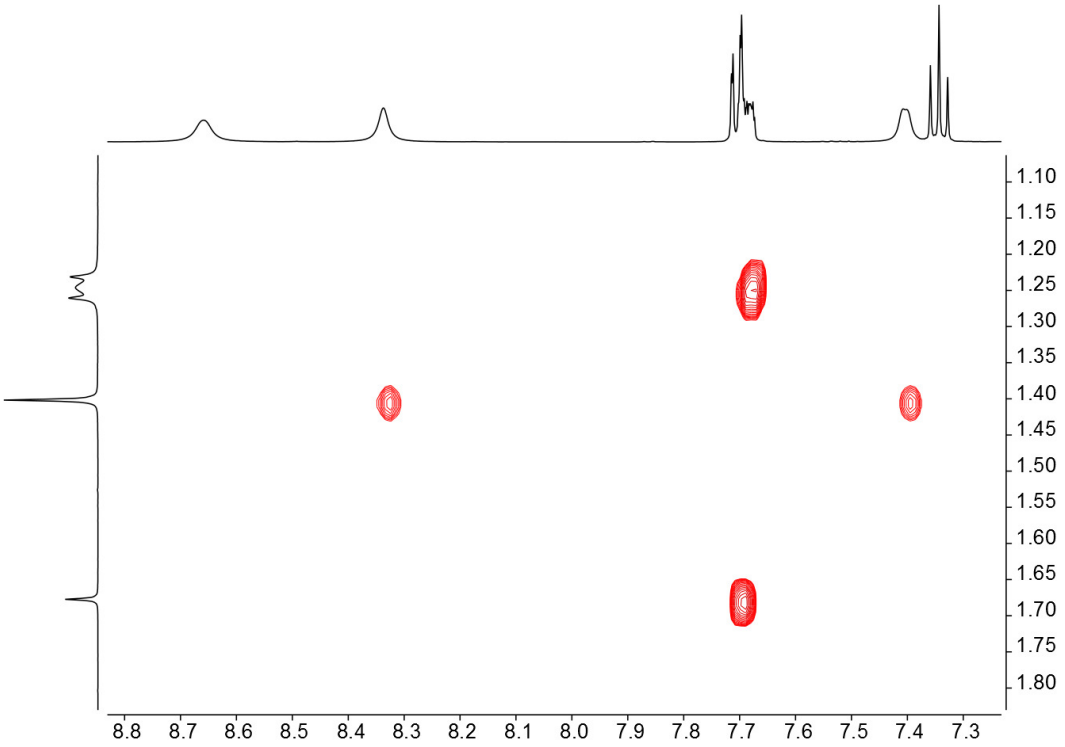

Fig. S7: NOESY spectrum (cutout) of [Cu(*t*Bu-xantphos)(4,4'-*t*Bu$_2$bpy)][PF$_6$] in CD_2Cl_2 at 298 K, 500 MHz. The NOESY cross peak between the *t*Bu signal of *t*Bu-xantphos at δ 1.25 ppm and the H^{A6} signal at δ 8.66 ppm is clearly visible.

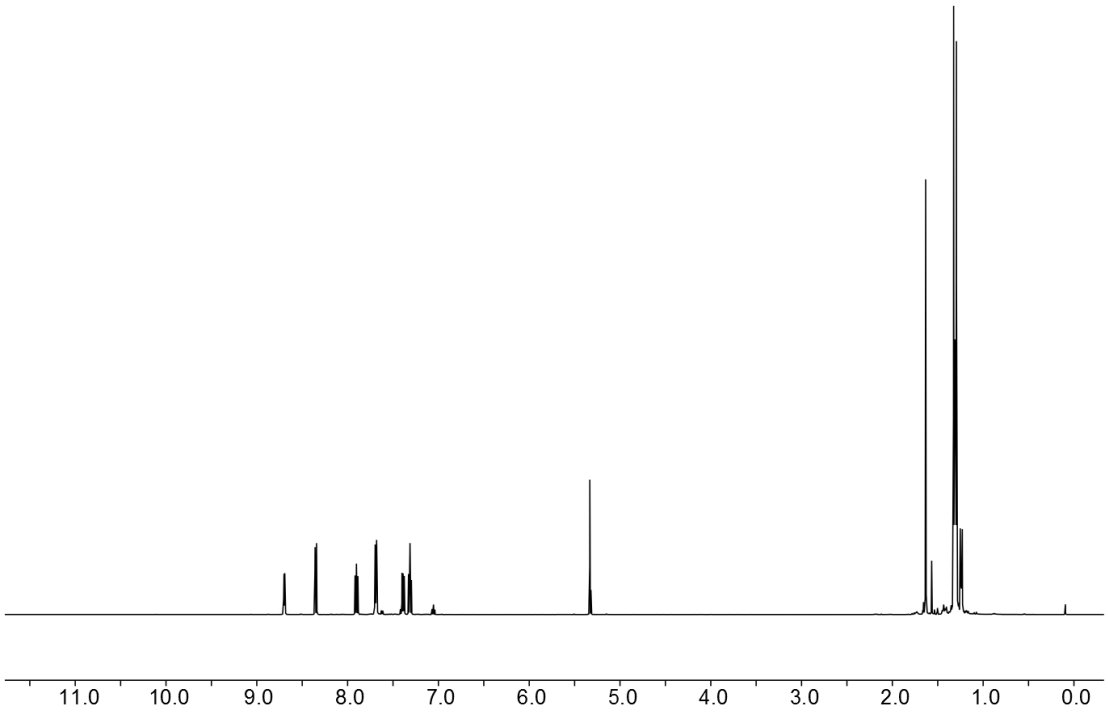

Fig. S8: ^{1}H NMR spectrum of [Ag(*t*Bu-xantphos)(bpy)][PF_6] in CD_2Cl_2 at 298 K, 500 MHz.

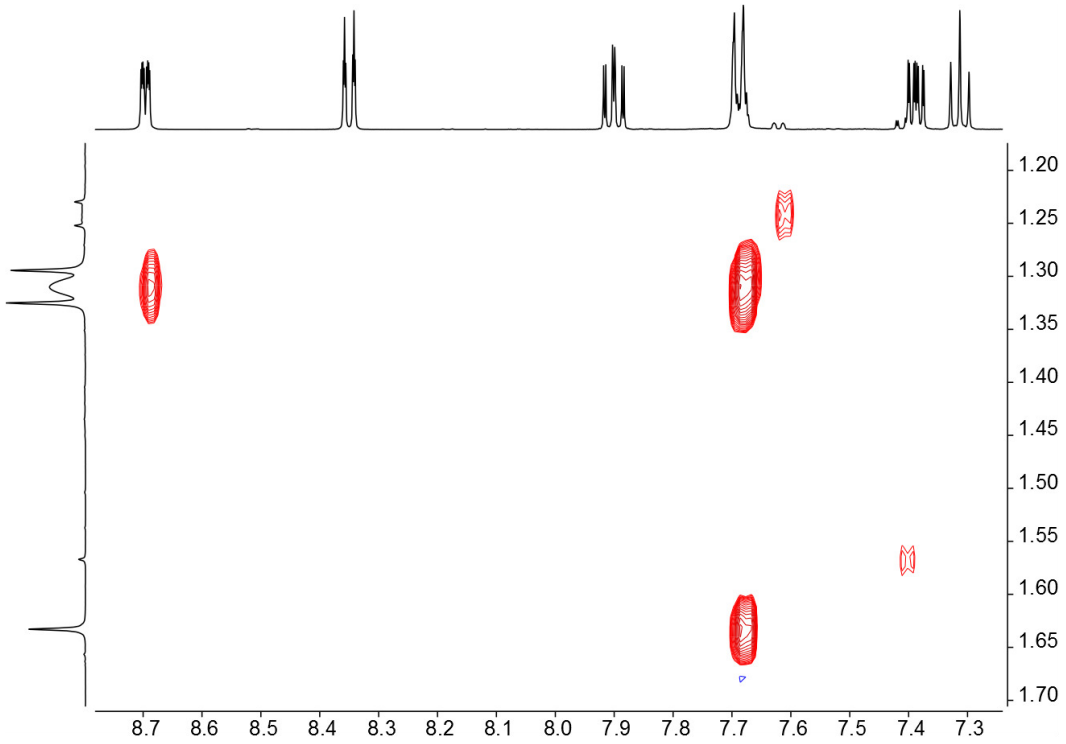

Fig. S9: NOESY spectrum (cutout) of [Ag(*t*Bu-xantphos)(bpy)][PF_6] in CD_2Cl_2 at 298 K, 500 MHz. The NOESY cross peak between the *t*Bu signal of *t*Bu-xantphos at δ 1.31 ppm and the H^{A6} signal at δ 8.70 ppm is clearly visible.

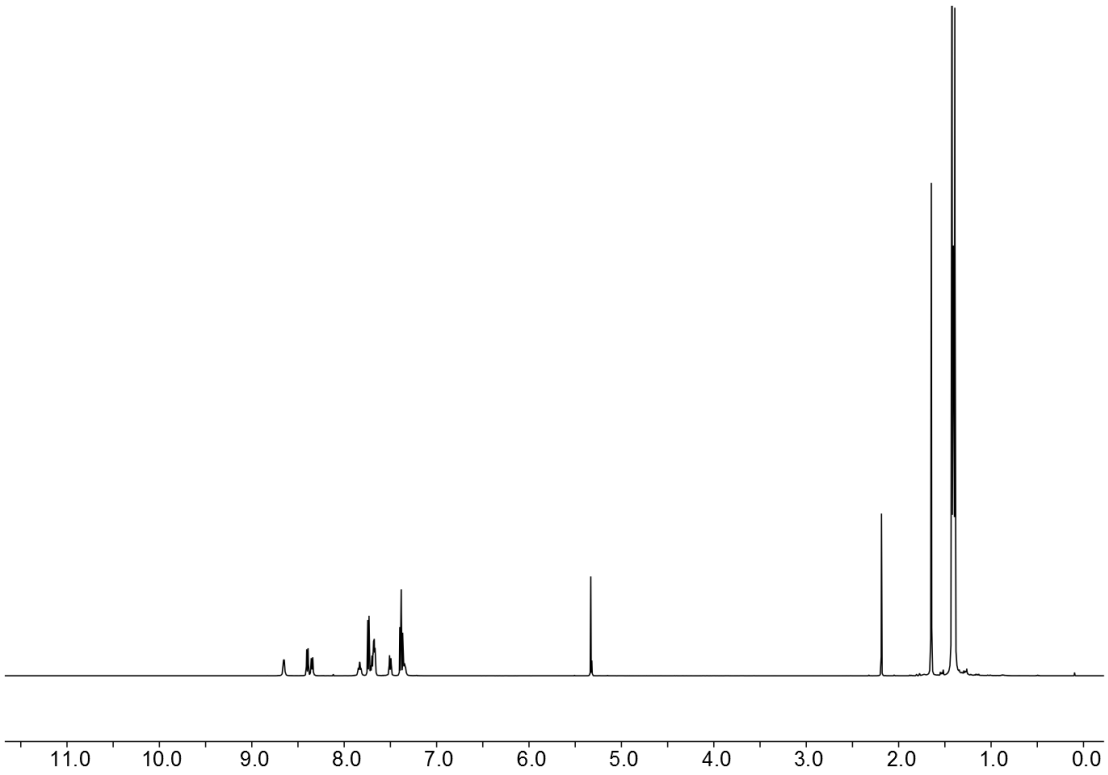

Fig. S10: ^{1}H NMR spectra of the residue of the attempted preparation of [Cu(*t*Bu-xantphos)(6-Brbpy)][PF_6] in CD_2Cl_2 at 298 K, 500 MHz.

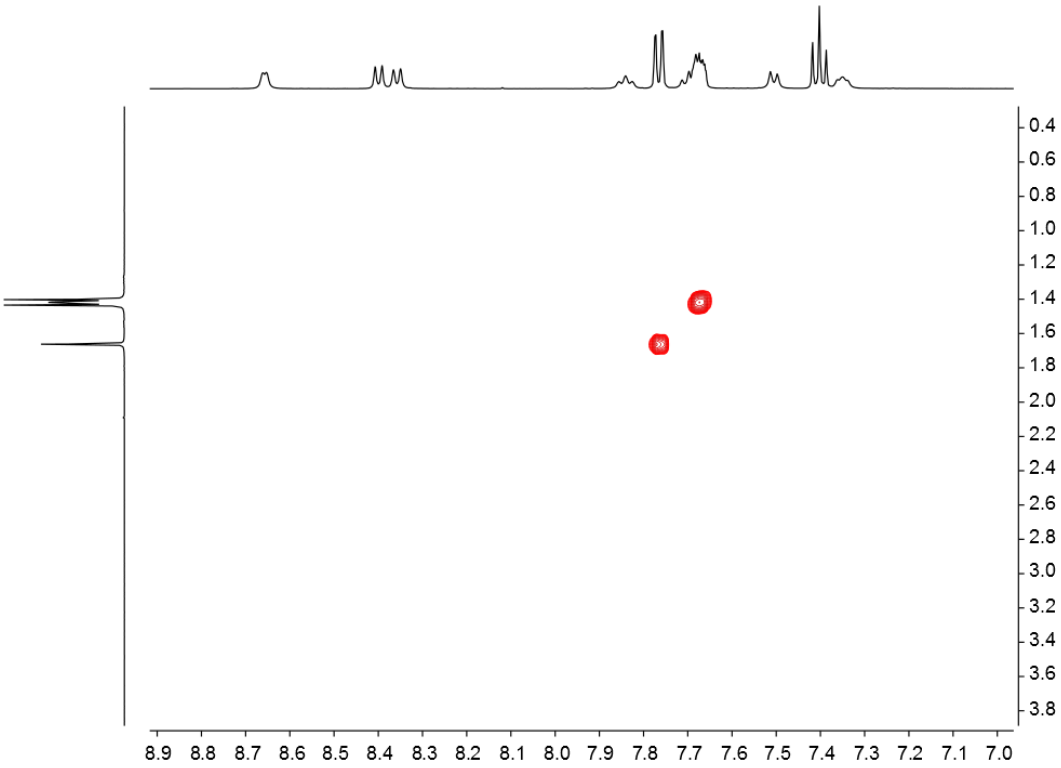

Fig. S11: NOESY spectrum (cutout) of the attempted preparation of [Cu(*t*Bu-xantphos)(6-Brbpy)][PF_6] in CD_2Cl_2 at 298 K, 500 MHz. The absence of a NOESY cross peak between the *t*Bu signal of *t*Bu-xantphos at δ 1.40 ppm and the H^{A6} signal at δ 8.64 ppm is clearly visible.

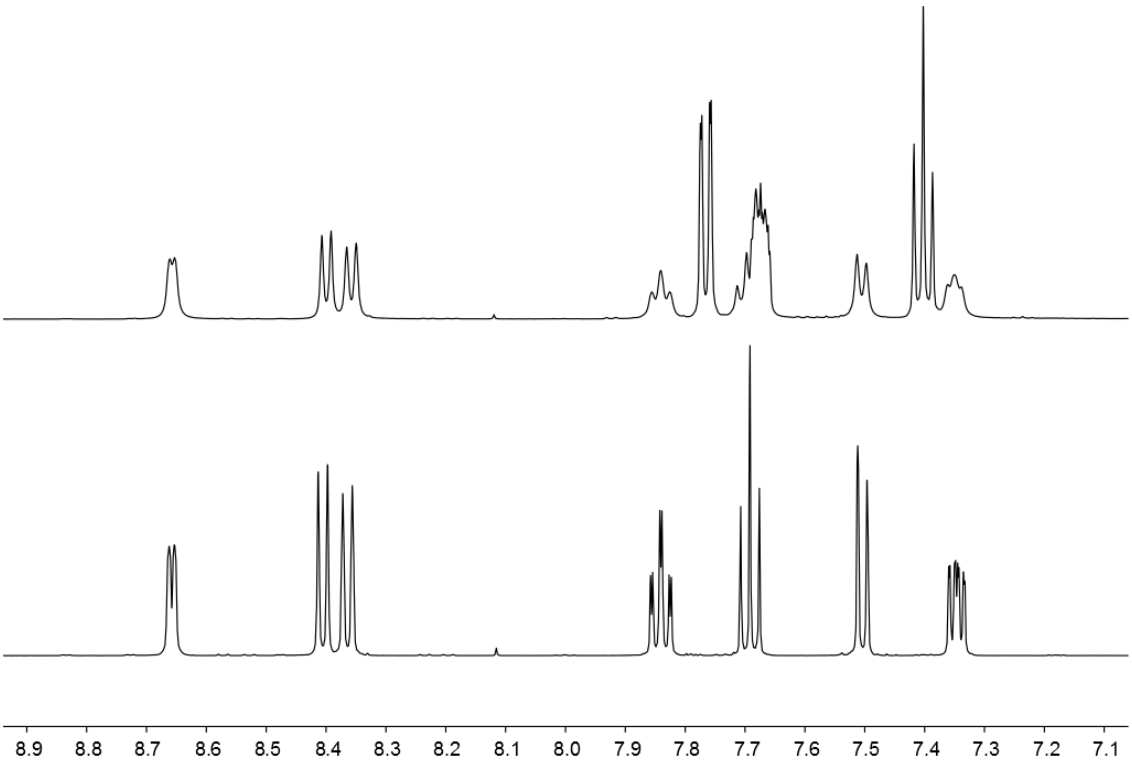

Fig. S12: ^{1}H NMR spectra (cutout) of the residue of the attempted preparation of [Cu(*t*Bu-xantphos)(6-Brbpy)][PF_6] (top) and of free 6-Brbpy (bottom) in CD_2Cl_2 at 298 K, 500 MHz.

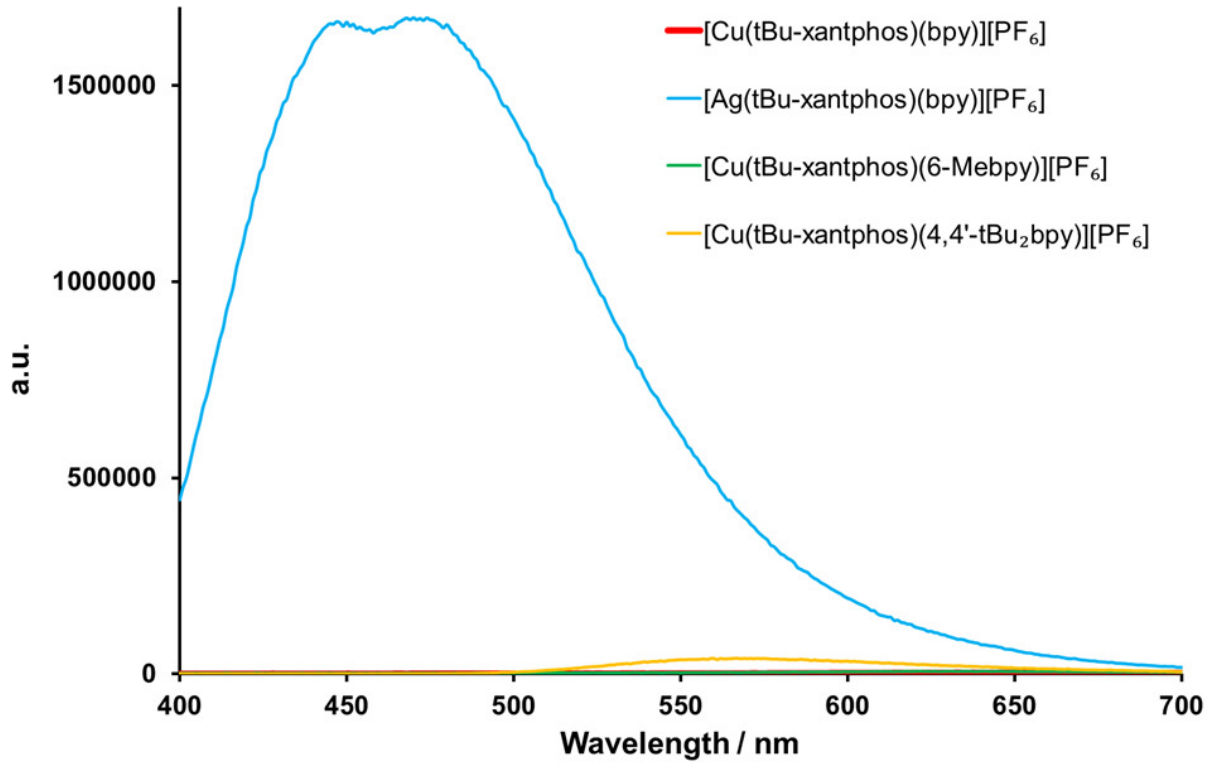

Fig. S13: Emission spectra of the [Cu(*t*Bu-xantphos)(bpy)][PF_6] complexes and [Ag(*t*Bu-xantphos)(bpy)][PF_6] in solid state.

Table S1. Experimental details for ambient and high pressure single crystal X-ray diffraction of [Cu(*t*Bu-xantphos)(bpy)][PF_6]

For all structures: $C_{41}H_{56}CuF_6N_2OP_3$, M_r = 863.36, monoclinic, $P2_1/c$.

Crystal data				
CCDC code	1583820	1583828	1583832	1583834
Temperature (K)	123	293	293	293
Pressure (GPa)	ambient	0.3	0.7	1.2
a, *b*, *c* (Å)	12.2247 (10), 15.0283 (12), 22.5879 (19)	12.187 (8), 15.0361 (10), 22.427 (2)	11.962 (9), 14.7798 (9), 22.070 (2)	11.892 (8), 14.6820 (8), 21.9164 (18)
β (°)	98.452 (3)	98.56 (2)	98.83 (2)	98.94 (2)
V (Å^3)	4104.7 (6)	4064 (3)	3856 (3)	3780 (2)
Z	4	4	4	4
F(000)	1808	1808	1808	1808
Radiation type	Cu *K*α	Synchrotron, λ = 0.48590 Å	Synchrotron, λ = 0.48590 Å	Synchrotron, λ = 0.48590 Å
μ (mm^{-1})	2.38	0.72	0.76	0.77
Crystal size (mm)	0.14 × 0.12 × 0.10	0.05 × 0.05 × 0.04	0.05 × 0.05 × 0.04	0.05 × 0.05 × 0.04
Data collection				
Diffractometer	Bruker Kappa Apex2	Pilatus 300K	Pilatus 300K	Pilatus 300K
Radiation source	Cu *K*α	Diamond Light Source Beamline I19	Diamond Light Source Beamline I19	Diamond Light Source Beamline I19
Monochromator	Graphite	Double crystal Silicon 111	Double crystal Silicon 111	Double crystal Silicon 111
Absorption correction	Multi-scan *SADABS* (Siemens, 1996)	Multi-scan *CrysAlis PRO* 1.171.38.41k (Rigaku Oxford Diffraction, 2015) Empirical absorption correction using spherical harmonics, implemented in SCALE3 ABSPACK scaling algorithm.	Multi-scan *CrysAlis PRO* 1.171.38.41k (Rigaku Oxford Diffraction, 2015) Empirical absorption correction using spherical harmonics, implemented in SCALE3 ABSPACK scaling algorithm.	Multi-scan *CrysAlis PRO* 1.171.38.41k (Rigaku Oxford Diffraction, 2015) Empirical absorption correction using spherical harmonics, implemented in SCALE3 ABSPACK scaling algorithm.
T_{min}, T_{max}	0.68, 0.79	0.377, 1.000	0.377, 1.000	0.418, 1.000
No. of measured, independent and observed [$I > 2.0\sigma(I)$]	88540, 7254, 7132	16222, 3446, 2263	15253, 2965, 2091	15269, 2899, 2007

reflections				
R_{int}	0.033	0.104	0.100	0.095
$(\sin \theta/\lambda)_{max}$ (Å^{-1})	0.596	0.625	0.625	0.625
Refinement				
$R[F^2 > 2\sigma(F^2)]$, $wR(F^2)$, S	0.033, 0.034, 1.08	0.076, 0.121, 1.11	0.078, 0.114, 1.18	0.083, 0.129, 1.15
No. of reflections	7062	3442	2963	2899
No. of parameters	655	439	439	439
No. of restraints	0	552	552	552
H-atom treatment	Only H-atom coordinates refined	H atoms treated by a mixture of independent and constrained refinement	H atoms treated by a mixture of independent and constrained refinement	H atoms treated by a mixture of independent and constrained refinement
$\Delta\rangle_{max}$, $\Delta\rangle_{min}$ (e Å^{-3})	0.98, -0.49	0.74, -0.67	0.62, -0.67	0.79, -0.67

Crystal data		
CCDC code	1583842	1583844
Temperature (K)	293	293
Pressure (GPa)	2.3	3.3
a, b, c (Å)	11.787 (8), 14.4808 (8), 21.5025 (19)	23.191 (18), 14.3350 (9), 21.247 (2)
β (°)	99.22 (2)	99.44 (3)
V (Å^3)	3623 (3)	6968 (5)
Z	4	8
F(000)	1808	3616
Radiation type	Synchrotron, λ = 0.48590 Å	Synchrotron, λ = 0.48590 Å
μ (mm^{-1})	0.81	0.84
Crystal size (mm)	0.05 × 0.05 × 0.04	0.05 × 0.05 × 0.04
Data collection		
Diffractometer	Pilatus 300K	Pilatus 300K
Radiation source	Diamond Light Source Beamline I19	Diamond Light Source Beamline I19
Monochromator	Double crystal Silicon 111	Double crystal Silicon 111
Absorption correction	Multi-scan *CrysAlis PRO* 1.171.38.46 (Rigaku Oxford Diffraction, 2015) Empirical absorption correction using spherical harmonics, implemented in SCALE3 ABSPACK scaling algorithm.	Multi-scan *CrysAlis PRO* 1.171.38.46 (Rigaku Oxford Diffraction, 2015) Empirical absorption correction using spherical harmonics, implemented in SCALE3 ABSPACK scaling algorithm.
T_{min}, T_{max}	0.230, 1.000	0.113, 1.000
No. of measured,	15236, 2787, 1690	29125, 5365, 2263

independent and observed [$I > 2.0\sigma(I)$] reflections		
R_{int}	0.136	0.202
$(\sin\theta/\lambda)_{max}$ (Å^{-1})	0.625	0.625
Refinement		
$R[F^2 > 2\sigma(F^2)]$, $wR(F^2)$, S	0.172, 0.432, 1.11	0.127, 0.143, 1.15
No. of reflections	2782	3934
No. of parameters	194	467
No. of restraints	210	484
H-atom treatment	H atoms treated by a mixture of independent and constrained refinement	H atoms treated by a mixture of independent and constrained refinement
$\Delta\rangle_{max}$, $\Delta\rangle_{min}$ (e Å^{-3})	1.78, -1.57	1.05, -0.96

Computer programs: Apex2 (Bruker AXS, 2006), *CrysAlis PRO* 1.171.38.41k (Rigaku OD, 2015), *SUPERFLIP* (Palatinus & Chapuis, 2007), form ambient pressure structure), form ambient pressure structure, form 3kbar structure, form 12kbar structure, *CRYSTALS* (Betteridge *et al.*, 2003), *CAMERON* (Watkin *et al.*, 1996).

Table 2. Experimental details for ambient and high pressure single crystal X-ray diffraction of [Ag(*t*Bu-xantphos)(bpy)][PF_6]

For all structures: $C_{41}H_{56}AgF_6N_2OP_3$, M_r = 907.68, triclinic, $P\bar{1}$, Z = 2, $F(000)$ = 940.

	SK170_123K	SK170_1	SK170_2	SK170_3
Crystal data				
CCDC code	1583822	1583829	1583833	1583835
Temperature (K)	123	293	293	293
Pressure (GPa)	ambient	1.0	1.7	2.5
a, b, c (Å)	12.3873 (9), 12.5363 (9), 15.3282 (12)	12.0890 (14), 12.3457 (16), 14.6171 (14)	11.9737 (11), 12.2317 (13), 14.4143 (6)	11.8753 (14), 12.1267 (16), 14.2710 (9)
α, β, γ (°)	104.142 (3), 109.108 (2), 103.339 (2)	104.131 (12), 108.001 (11), 104.296 (11)	103.770 (6), 108.026 (6), 104.548 (8)	103.601 (9), 108.062 (8), 104.620 (11)
V (Å^3)	2051.8 (3)	1885.1 (5)	1825.2 (3)	1777.5 (4)
D_x (Mg m^{-3})	1.469	1.599	1.652	1.696
Radiation type	Cu $K\alpha$	Synchrotron, λ = 0.48590 Å	Synchrotron, λ = 0.48590 Å	Synchrotron, λ = 0.48590 Å

μ (mm^{-1})	5.58	0.73	0.75	0.77
Crystal size (mm)	0.09 × 0.08 × 0.06	0.09 × 0.08 × 0.06	0.09 × 0.08 × 0.06	0.09 × 0.08 × 0.06
Data collection				
Diffractometer	Bruker Kappa Apex2	Pilatus 300K	Pilatus 300K	Pilatus 300K
Radiation source	Cu *K*α	Diamond Light Source Beamline I19	Diamond Light Source Beamline I19	Diamond Light Source Beamline I19
Monochromator	Graphite	Double crystal Silicon 111	Double crystal Silicon 111	Double crystal Silicon 111
Scan method	ϕ & ω scans	ω rotation with 0.4 degree frames'_diffrn_detector_area_resol_mean scans	ω rotation with 0.4 degree frames'_diffrn_detector_area_resol_mean scans	ω rotation with 0.4 degree frames'_diffrn_detector_area_resol_mean scans
Absorption correction	Multi-scan *SADABS* (Siemens, 1996)	Multi-scan *CrysAlis PRO* 1.171.38.41k (Rigaku Oxford Diffraction, 2015) Empirical absorption correction using spherical harmonics, implemented in SCALE3 ABSPACK scaling algorithm.	Multi-scan *CrysAlis PRO* 1.171.38.46 (Rigaku Oxford Diffraction, 2015) Empirical absorption correction using spherical harmonics, implemented in SCALE3 ABSPACK scaling algorithm.	Multi-scan *CrysAlis PRO* 1.171.38.46 (Rigaku Oxford Diffraction, 2015) Empirical absorption correction using spherical harmonics, implemented in SCALE3 ABSPACK scaling algorithm.
T_{min}, T_{max}	0.54, 0.72	0.707, 1.000	0.563, 1.000	0.330, 1.000
No. of measured, independent and observed [$I > 2.0\sigma(I)$] reflections	26703, 7397, 7256	7006, 2524, 1990	7820, 2499, 1972	7386, 2415, 1633
R_{int}	0.027	0.050	0.045	0.074
$(\sin\theta/\lambda)_{max}$ ($Å^{-1}$)	0.610	0.625	0.625	0.625
Refinement				
$R[F^2 > 2\sigma(F^2)]$, $wR(F^2)$, S	0.038, 0.078, 0.90	0.058, 0.086, 0.96	0.059, 0.107, 0.96	0.118, 0.126, 1.17
No. of reflections	7336	2495	2468	2375
No. of parameters	523	439	439	229
No. of restraints	100	544	544	250
H-atom treatment	H-atom parameters constrained	H atoms treated by a mixture of independent and constrained refinement	H atoms treated by a mixture of independent and constrained refinement	H atoms treated by a mixture of independent and constrained refinement

$\Delta\rangle_{max}$, $\Delta\rangle_{min}$ (e Å^{-3})	1.29, -0.74	0.42, -0.34	0.49, -0.44	1.01, -0.99

Crystal data		
CCDC code	1583843	1583845
Temperature (K)	293	293
Pressure (GPa)	4.0	4.5
a, *b*, *c* (Å)	11.7672 (15), 12.0577 (15), 14.1541 (12)	11.704 (2), 12.033 (2), 14.1045 (16)
α, β, γ (°)	103.490 (11), 108.215 (10), 104.502 (11)	103.362 (15), 108.356 (15), 104.447 (15)
V (Å^3)	1737.6 (4)	1719.0 (6)
D_x (Mg m^{-3})	1.735	1.754
Radiation type	Synchrotron, λ = 0.48590 Å	Synchrotron, λ = 0.48590 Å
μ (mm^{-1})	0.79	0.80
Crystal size (mm)	0.09 × 0.08 × 0.06	0.09 × 0.08 × 0.06
Data collection		
Diffractometer	Pilatus 300K	Pilatus 300K
Radiation source	Diamond Light Source Beamline I19	Diamond Light Source Beamline I19
Monochromator	Double crystal Silicon 111	Double crystal Silicon 111
Scan method	ω rotation with 0.4 degree frames'_diffrn_detector_area_resol _mean scans	ω rotation with 0.4 degree frames'_diffrn_detector_area_resol _mean scans
Absorption correction	Multi-scan *CrysAlis PRO*, Agilent Technologies, Version 1.171.37.33 (release 27-03-2014 CrysAlis171 .NET) (compiled Mar 27 2014,17:12:48) Empirical absorption correction using spherical harmonics, implemented in SCALE3 ABSPACK scaling algorithm.	Multi-scan *CrysAlis PRO* 1.171.38.46 (Rigaku Oxford Diffraction, 2015) Empirical absorption correction using spherical harmonics, implemented in SCALE3 ABSPACK scaling algorithm.
T_{min}, T_{max}	0.413, 1.000	0.909, 1.000
No. of measured, independent and observed [$I > 2.0\sigma(I)$] reflections	7233, 2360, 1537	7131, 2347, 1267
R_{int}	0.089	0.082
(sin θ/λ)$_{max}$ (Å^{-1})	0.625	0.625
Refinement		
$R[F^2 > 2\sigma(F^2)]$, $wR(F^2)$, S	0.147, 0.238, 0.99	0.142, 0.224, 1.15
No. of reflections	2295	2247

No. of parameters	219	219
No. of restraints	238	238
H-atom treatment	H atoms treated by a mixture of independent and constrained refinement	H atoms treated by a mixture of independent and constrained refinement
$\Delta\rangle_{max}$, $\Delta\rangle_{min}$ (e Å^{-3})	1.26, -1.02	1.50, -1.54

Computer programs: Apex2 (Bruker AXS, 2006), *CrysAlis PRO* 1.171.38.41k (Rigaku OD, 2015), *SUPERFLIP* (Palatinus & Chapuis, 2007), form ambient pressure structure), form 10kbar structure), form 17kbar structure), form 25kbar structure), *CRYSTALS* (Betteridge *et al.*, 2003), *CAMERON* (Watkin *et al.*, 1996).

Chapter VI. Self-Assembly of heteroleptic dinuclear silver(I) complexes bridged by bis-(diphenylphosphino)ethyne

Summary

The idea behind this project, that ultimately lead to this paper,[7] was to study the self-assembling behaviour of $Ag[PF_6]$ with either 0.5 or one equivalent of the bridging ligand bis(diphenylphosphino)ethyne (dppa) together with a chelating N^N ligand (N^N = 6,6'-dimethyl-2,2'-bipyridine (6,6'-Me_2bpy) or 2,2':6',2''-terpyridine (tpy)). All obtained species consist of dinuclear cations $[Ag_2(dppa)_n(N^N)_2]^{2+}$ (n = 1, 2) and were analysed in solution using NMR spectroscopic methods at low and room temperatures (^{1}H, ^{1}H{^{31}P}, COSY, NOESY, ^{13}C, HMQC and HMBC). In addition to these standard methods, also ^{31}P{^{1}H} and ^{31}P-^{109}Ag HSQC spectroscopic measurements were performed and give deeper insights into the dynamic processes in solution as well as a correlation between the number of coordinating phosphorus atoms at the silver centres and the coupling constants $^1J_{31P\text{-}109Ag}$ and $^1J_{109Ag\text{-}31P}$. Single crystal X-ray diffraction yielded two pseudo-polymorphic structures for the doubly-bridged $[Ag_2(dppa)_2(tpy)_2][PF_6]_2$, with the tpy ligand either in bidentate or tridentate coordination, and one for the singly-bridged $[Ag_2(dppa)(6,6'\text{-}Me_2bpy)_2][PF_6]_2$.

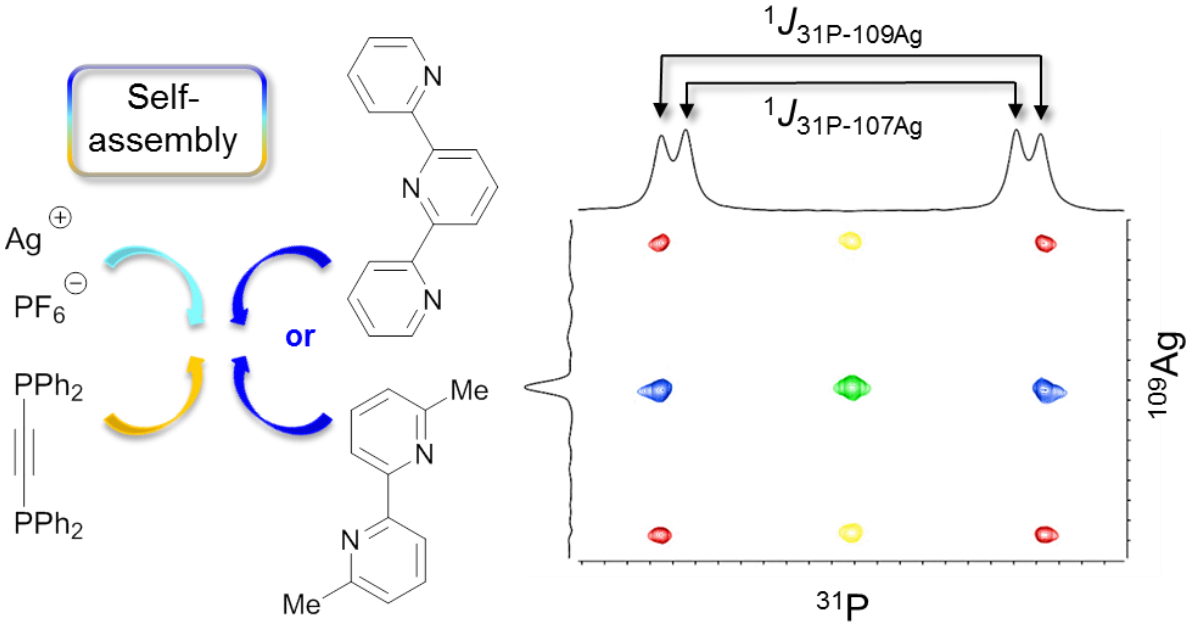

Contribution of Sarah Keller: Idea of the project and selection of ligands ❖ Synthesis of complexes ❖ Analytical characterization (electrospray mass spectroscopy, NMR spectroscopy, part of the single crystal X-ray diffraction) ❖ Writing of the manuscript.

Dalton Transactions

PAPER

View Article Online
View Journal

Cite this: DOI: 10.1039/c7dt03923a

Self-assembly of heteroleptic dinuclear silver(I) complexes bridged by bis(diphenylphosphino) ethyne†

Sarah Keller,[a] Timothy N. Camenzind,‡[a] Johannes Abraham,[b] Alessandro Prescimone,[a] Daniel Häussinger,[b] Edwin C. Constable[a] and Catherine E. Housecroft*[a]

Received 18th October 2017,
Accepted 13th December 2017

DOI: 10.1039/c7dt03923a

rsc.li/dalton

We present a study of the self-assembling behaviour in solution of $Ag[PF_6]$ with one equivalent of an N^N ligand (N^N = 6,6′-dimethyl-2,2′-bipyridine (6,6′-Me_2bpy) or 2,2′:6′,2″-terpyridine (tpy)), together with either 0.5 or one equivalent of the bridging ligand bis(diphenylphosphino)ethyne (dppa). Each product contains a dinuclear cation, with one or two dppa ligands bridging the two Ag^+ centres; 6,6′-Me_2bpy and tpy, respectively, act as chelating ligands. The compounds have been analysed in solution using NMR spectroscopic methods (^{1}H, ^{1}H{^{31}P}, COSY, NOESY, ^{13}C, HMQC and HMBC), including room and low temperature measurements. ^{31}P{^{1}H} NMR spectra recorded at different temperatures allow a deeper insight into the dynamic equilibrium processes. In addition, solution ^{31}P–^{109}Ag HSQC spectroscopic measurements were performed and show, *inter alia*, the ratio of the splitting in the F1 dimension and the $^1J_{^{31}P-^{109}Ag}$ coupling constant in the fully coupled HSQC. Single crystal X-ray diffraction yielded two pseudo-polymorphic structures for the doubly-bridged $[Ag_2(dppa)_2(tpy)_2][PF_6]_2$ and one for the singly-bridged $[Ag_2(dppa)(6,6'\text{-}Me_2bpy)_2][PF_6]_2$.

Introduction

Copper(I) complexes are emerging from fundamental research into applications such as dye-sensitized solar cells and light-emitting devices.[1,2] For the latter, complexes of the type $[Cu(N^N)(POP)]^+$ and $[Cu(N^N)(xantphos)]^+$ are particularly under investigation with N^N usually being a derivative of 2,2′-bipyridine (bpy) or 1,10-phenanthroline (phen), POP = bis(2-(diphenylphosphino)phenyl)ether, xantphos = 4,5-bis (diphenylphosphino)-9,9-dimethylxanthene.[3–11]

Despite the lower abundance and higher price of silver compared to copper, silver(I) complexes are also gaining attention. Heteroleptic silver(I) complexes with N^N and P^P-chelating ligands exhibit promising emissive properties[12] including thermally activated delayed fluorescence (TADF)[13] and have recently been applied as luminophores in light-emitting electrochemical cells[14] and also as UV-absorbing luminescent down-shifters for organic solar cells.[15] With its rigid alkyne backbone, bis(diphenylphosphino)ethyne (dppa, Scheme 1) is a typical bridging ligand. Complexes with a range of metals have been reported, for example with Pt, Pd, Ni, Mo Ru, Cu or Re.[16] While the phosphane ligand typically acts as σ-donor through phosphorus, there are few examples where dppa exhibits side-on coordination *via* the alkyne bridge.[17,18] For copper, a few dinuclear complexes with a combination of brid-

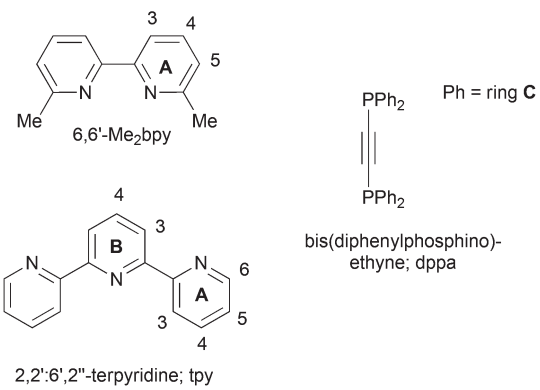

Scheme 1 Structures of applied ligands with ring and atom labels for NMR spectroscopic assignments.

[a]Department of Chemistry, University of Basel, BPR 1096, Mattenstrasse 24a, CH-4058 Basel, Switzerland. E-mail: catherine.housecroft@unibas.ch
[b]Department of Chemistry, University of Basel, St Johanns-Ring 19, CH-4056 Basel, Switzerland

†Electronic supplementary information (ESI) available: Fig. S1–S14: additional NMR spectra. CCDC 1580157–1580159. For ESI and crystallographic data in CIF or other electronic format see DOI: 10.1039/c7dt03923a

‡Current address: Department of Physics, University of Basel, Klingelbergstrasse 82, CH-4056 Basel, Switzerland.

ging dppa and N^N chelating ligands are already known, for example $[Cu_2(dppa)_2(N^N)_2]^{2+}$ cations where N^N is a substituted bpy,[19] a substituted phen,[20] di-2-pyridyl ketone[21] or 2,4,6-tris(2-pyridyl)-1,3,5-triazine.[22] For silver(I), complex cations with N^N chelating ligands and bridging phosphanes other than dppa are known, some of them exhibiting luminescent properties[23] or being subject to self-assembly into coordination polymers[24] or networks.[25] While analogous $[Ag_2(dppa)_n(N^N)_2]^{2+}$ cations (n = 1–3) are not, to our knowledge, known, dinuclear complexes with one, two or three dppa bridges between the silver(I) cations, but without additional ligands have been investigated by James *et al.*[26] The characterization of silver(I) phosphane complexes is greatly aided by the use of NMR spectroscopy including heteronuclear low temperature NMR spectroscopy and ^{31}P–^{109}Ag HSQC experiments, which provide invaluable insights when it comes to the characterization of these coordination compounds and their dynamic processes in solution. In order to apply these HSQC NMR techniques, a measurable spin–spin coupling between the abundant nucleus (in this case ^{31}P) and ^{109}Ag is required. A tendency for fast ligand exchange in solution, which results in the removal of the indirect coupling between ^{109}Ag and the other nucleus, can be avoided by using low measurement temperatures.[27] Inspiring examples for ^{109}Ag NMR studies of complexes in solution have been published by Berners-Price *et al.*[28] who studied monomeric, dimeric and trimeric silver(I) complexes with the 1,2-bis(di-2-pyridylphosphino)ethane ligand and Pregosin *et al.*[29] who investigated the coordination of $Ag(CF_3SO_3)$ by a chiral ferrocenylphosphine ligand.

Experimental

General

^1H, ^{13}C and ^{31}P NMR spectra were recorded using a Bruker Avance III-600, III-500 or III-400 NMR spectrometer and direct observe BBFO (600 and 400 MHz) or indirect detection BBI probes (500 MHz). All probes were equipped with self-shielded *z*-gradients. The $^{31}P\{^1H\}$–^{109}Ag HSQC spectra were recorded on a triple resonance $^1H/^{31}P$/low-gamma nucleus indirect TBI probe tuned to 600.132, 242.937 and 27.927 MHz (^1H, ^{31}P and ^{109}Ag). The 90° pulse length was 12.5 μs for ^{31}P and 45 μs for ^{109}Ag and the sweep widths 25 and 300 ppm respectively. The experiment was acquired with a modified phase-sensitive HSCQ sequence using 2k (128) data points in the F2 (F1) dimension resulting in an acquisition time of 166 ms (7.6 ms) following a hypercomplex States-TPPI scheme. Suitable ^1J coupling constants were converted to $\frac{1}{4}J$ delays in both INEPT periods. While WALTZ-16 proton decoupling was always applied, the HSQC was recorded with or without GARP ^{109}Ag decoupling during $t2$ and with or without a 180° ^{31}P refocusing pulse during $t1$ evolution, thus yielding a set of four HSQC spectra: J-coupling in F1 and F2 (four cross peaks), only in F1 (two cross peaks), only in F2 (two cross peaks) and fully decoupled (one cross peak). Typical experiment times were between 15 min and 1 h. ^1H and ^{13}C NMR chemical shifts were referenced to residual solvent peaks with respect to δ(TMS) = 0 ppm and ^{31}P NMR chemical shifts with respect to δ(85% aqueous H_3PO_4) = 0 ppm. ^{109}Ag chemical shifts were referenced to a solution of $AgNO_3$ (9.1 M) and $Fe(NO_3)_3$ (0.24 M) in D_2O (−47 ppm).[30] The sample temperature in the low temperature NMR experiments was calibrated using a 4% MeOH in CD_3OD sample. The ^{31}P and $^{31}P\{^1H\}$ NMR spectra were referenced to the signal of $[PF_6]^-$ with δ(septet) = −144.234 ppm where possible. Coalescence temperatures T_c were estimated by interpolation of the line widths of ^{31}P resonances and free activation enthalpies were obtained from T_c using the Eyring equation. Electrospray ionization (ESI) mass spectra were recorded on a Bruker esquire 3000plus. 2,2′:6′,2″-Terpyridine was either purchased from TCI chemicals or prepared following literature methods with the NMR spectroscopic data matching those reported.[31] $Ag[PF_6]$ and 6,6′-dimethyl-2,2′-bipyridine (6,6′-Me_2bpy) were purchased from Fluorochem and Angene respectively, and dppa from Acros Organics. All commercial chemicals were used as received.

$[Ag_2(dppa)_2(6,6'\text{-}Me_2bpy)_2][PF_6]_2$

A solution of dppa (49 mg, 0.125 mmol, 2.0 eq.) and 6,6′-Me_2bpy (23 mg, 0.125 mmol, 2.0 eq.) in CH_2Cl_2 (20 ml) was added to a solution of $Ag[PF_6]$ (32 mg, 0.125 mmol, 2.0 eq.) in CH_2Cl_2 (20 mL). The colourless solution was stirred for 2 h, filtered and the filtrate evaporated to dryness. The solid residue was redissolved in CH_2Cl_2 (2 mL) and layered with Et_2O. This yielded colourless crystals which were identified as $[Ag_2(dppa)_2(6,6'\text{-}Me_2bpy)_2][PF_6]_2$ (98 mg, 0.059 mmol, 94%). ^1H NMR (500 MHz, $(CD_3)_2CO$, 298 K) δ/ppm 8.38 (d, J = 8.0 Hz, 4H, H^{A3}), 8.11 (t, J = 7.8 Hz, 4H, H^{A4}), 7.62–7.52 (m, 24H, H^{C2+C4}), 7.47 (d, J = 7.6 Hz, 4H, H^{A5}), 7.42–7.36 (m, 16H, H^{C3}), 2.33 (s, 12H, H^{Me}). ^{13}C NMR (126 MHz, $(CD_3)_2CO$, 298 K) δ/ppm 159.2 (C^{A6}), 153.2 (C^{A2}), 140.9 (C^{A4}), 133.0 (d, J_{PC} = 18 Hz, C^{C2}), 132.5 (C^{C4}), 130.8 (half of d, $J \approx 20$ Hz, C^{C1}), 130.7 (d, J_{PC} = 10 Hz, C^{C3}), 126.5 (C^{A5}), 121.7 (C^{A3}), 27.5 (C^{Me}). ^{31}P NMR (162 MHz, $(CD_3)_2CO$, 295 K) δ/ppm −22.9 (broad, FWHM = 57 Hz). NMR (208 K): ^1H NMR (600 MHz, $(CD_3)_2CO$, 208 K) δ/ppm 8.52 (d, J = 7.8 Hz, 4H, H^{A3}), 8.18 (t, J = 7.7 Hz, 4H, H^{A4}), 7.61–7.54 (m, 24H, H^{C2+C4}), 7.49 (d, J = 7.6 Hz, 4H, H^{A5}), 7.37 (t, J = 7.4 Hz, 16H, H^{C3}), 2.16 (s, 12H, H^{Me}). $^{31}P\{^1H\}$ NMR (243 MHz, $(CD_3)_2CO$, 208 K) δ/ppm −21.5 (d, $^1J_{^{31}P-^{109}Ag}$ = 406.6 Hz, $[Ag_2(dppa)_2(6,6'\text{-}Me_2bpy)_2]^{2+}$), −22.9 (d, $^1J_{^{31}P-^{107}Ag}$ = 352.6 Hz, $[Ag_2(dppa)_2(6,6'\text{-}Me_2bpy)_2]^{2+}$). ESI MS: m/z 685.05 $[Ag(dppa)(6,6'\text{-}Me_2bpy)]^+$ (base peak, calc. 685.11). Found: C, 54.60; H, 4.23; N, 3.75; $C_{76}H_{64}Ag_2F_{12}N_4P_6$ requires C, 54.89; H, 3.88; N, 3.37%.

$[Ag_2(dppa)_2(tpy)_2][PF_6]_2$

A solution of dppa (39 mg, 0.097 mmol, 2.0 eq.) and tpy (23 mg, 0.097 mmol, 2.0 eq.) in CH_2Cl_2 (50 ml) was added to a solution of $Ag[PF_6]$ (25 mg, 0.097 mmol, 2.0 eq.) in CH_2Cl_2 (30 mL). The pale yellow solution was stirred for 2 h, filtered and the filtrate evaporated to dryness. This yielded a pale yellow solid which was identified as $[Ag_2(dppa)_2(tpy)_2][PF_6]_2$ (82 mg, 0.047 mmol, 94%). ^1H NMR (500 MHz, $(CD_3)_2CO$, 298 K) δ/

ppm 8.55 (d, J = 7.9 Hz, 4H, H^{B3}), 8.44 (d, J = 8.0 Hz, 4H, H^{A3}), 8.39 (t, J = 7.8 Hz, 2H, H^{B4}), 8.17 (broad signal, 4H, H^{A6}), 7.98 (td, J = 7.8, 1.7 Hz, 4H, H^{A4}), 7.48 (m, 16H, H^{C2}), 7.45 (m, 8H, H^{C4}), 7.26 (t, J = 7.7 Hz, 16H, H^{C3}), 7.01 (broad signal, 4H, H^{A5}). ^{13}C NMR (126 MHz, $(CD_3)_2CO$, 298 K) δ/ppm 154.2 (C^{B2}), 153.5 (C^{A2}), 150.8 (C^{A6}), 141.3 (C^{B4}), 139.6 (C^{A4}), 133.0 (d, J = 18.0 Hz, C^{C2}), 132.0 (C^{C4}), 131.6 (d, J = 26.9 Hz, C^{C1}), 130.4 (d, J = 9.7 Hz, C^{C3}), 126.0 (C^{A5}), 124.2 ($C^{B3/A3}$), 124.1 ($C^{B3/A3}$). ^{31}P{^{1}H} NMR (162 MHz, $(CD_3)_2CO$, 296 K) δ/ppm −22.9 (broad, FWHM = 110 Hz). NMR (208 K): ^{1}H NMR (600 MHz, $(CD_3)_2CO$, 208 K) δ/ppm 8.65 (d, J = 7.9 Hz, 4H, H^{B3}), 8.51–8.47 (m, 6H, H^{A3+B4}), 8.02–7.98 (m, 8H, H^{A4+A6}), 7.49 (q, J = 6.6 Hz, 16H, H^{C2}), 7.45 (t, J = 7.4 Hz, 8H, H^{C4}), 7.26 (t, J = 7.5 Hz, 16H, H^{C3}), 6.88–6.84 (m, 4H, H^{A5}). ^{31}P{^{1}H} NMR (243 MHz, $(CD_3)_2CO$, 208 K) δ/ppm −23.0 (d, $^1J_{^{31}P-^{109}Ag}$ = 410.6 Hz, $[Ag_2(dppa)_2(tpy)_2]^{2+}$), −23.0 (d, $^1J_{^{31}P-^{107}Ag}$ = 355.7 Hz, $[Ag_2(dppa)_2(tpy)_2]^{2+}$). ESI MS: m/z 734.00 $[Ag(dppa)(tpy)]^+$ (base peak, calc. 734.10). Found: C, 55.92; H, 3.87; N, 4.90; $C_{82}H_{62}Ag_2F_{12}N_6P_6$ requires C, 55.93; H, 3.55; N, 4.77%.

$[Ag_2(dppa)(6,6'\text{-}Me_2bpy)_2][PF_6]_2$

A solution of dppa (19.5 mg, 0.05 mmol, 1.0 eq.) and 6,6′-Me_2bpy (18.4 mg, 0.10 mmol, 2.0 eq.) in CH_2Cl_2 (15 ml) was added to a solution of $Ag[PF_6]$ (25.3 mg, 0.10 mmol, 2.0 eq.) in CH_2Cl_2 (15 mL). The colourless solution was stirred for 2 h and all volatiles were removed *in vacuo*. This yielded a colourless powder (49 mg, 0.039 mmol, 78%) which was identified as $[Ag_2(dppa)(6,6'\text{-}Me_2bpy)_2][PF_6]_2$. ^{1}H NMR (500 MHz, $(CD_3)_2CO$, 298 K) δ/ppm 8.40 (d, J = 8.0 Hz, 4H, H^{A3}), 8.13 (t, J = 7.8 Hz, 4H, H^{A4}), 8.01–7.95 (m, 8H, H^{C2}), 7.69–7.65 (m, 4H, H^{C4}), 7.63–7.58 (m, 12H, H^{A5+C3}), 2.66 (s, 12H, CH_3). ^{13}C NMR (126 MHz, $(CD_3)_2CO$, 295 K) δ/ppm 159.3 (C^{A6}), 152.4 (C^{A2}), 141.2 (C^{A4}), 133.8 (d, J = 18.2 Hz, C^{C2}), 133.0 (d, J = 2.1 Hz, C^{C4}), 131.6 (d, J = 11.2 Hz, C^{C1}), 130.8 (d, J = 11.6 Hz, C^{C3}), 126.6 (C^{A5}), 121.1 (C^{A3}), 104.1 (dd, J = 49.3, 4.4 Hz, C^{ethyne}), 27.6 (CH_3). ^{31}P NMR (162 MHz, $(CD_3)_2CO$, 295 K) δ/ppm −16.5 (broad FWHM = 60 Hz). NMR (208 K): ^{31}P{^{1}H} NMR (243 MHz, $(CD_3)_2CO$, 208 K) δ/ppm −16.1 (d, $^1J_{^{31}P-^{109}Ag}$ = 714.6 Hz, $[Ag_2(dppa)(6,6'\text{-}Me_2bpy)_2]^{2+}$), −16.1 (d, $^1J_{^{31}P-^{109}Ag}$ = 619.1 Hz, $[Ag_2(dppa)(6,6'\text{-}Me_2bpy)_2]^{2+}$), −16.4 (d, $^1J_{^{31}P-^{107}Ag}$ = 711.1 Hz, $[Ag_2(dppa)(6,6'\text{-}Me_2bpy)_2]^{2+}$, second conformer), −16.4 (d, $^1J_{^{31}P-^{109}Ag}$ = 615.5 Hz, $[Ag_2(dppa)(6,6'\text{-}Me_2bpy)_2]^{2+}$, second conformer).

$[Ag_2(dppa)(tpy)_2][PF_6]_2$

$AgPF_6$ (12.6 mg, 0.05 mmol, 2.0 eq.), dppa (9.9 mg, 0.025 mmol, 3.0 eq.) and terpy (11.5 mg, 0.05 mmol, 2.0 eq.) were placed in a round bottom flask. Acetone-d_6 (4 ml) was added and the solution was stirred for 2 h. NMR spectra were recorded and the signals assigned where possible. Identified species in solution are $[Ag_2(dppa)(tpy)_2][PF_6]_2$ and $[Ag_2(dppa)_2(tpy)_2][PF_6]_2$ plus unidentified side products. Room temperature NMR: ^{1}H NMR (500 MHz, $(CD_3)_2CO$, 298 K) δ/ppm 8.53 (d, J = 7.9 Hz, 4H, H^{B3}), 8.44 (dt, J = 8.1, 0.8 Hz, H^{A3}), 8.38 (t, J = 7.9 Hz, 2H, H^{B4}), 8.38–8.34 (broad signal, FWHM = 13 Hz, 4H, H^{A6}), 8.00 (td, J = 7.8 Hz, 4H, H^{A4}), 7.70–7.59 (broad signal, FWHM = 25 Hz, 8H, H^{C2}), 7.53 (t, J = 7.3 Hz, 4H, H^{C4}), 7.39 (t, J = 6.8 Hz, 8H, H^{C3}), 7.26 (broad signal, FWHM = 18 Hz, 4H, H^{A5}). ^{13}C NMR (126 MHz, $(CD_3)_2CO$, 298 K) δ/ppm 153.7, 153.1, 151.3 (C^{A6}), 141.5 (C^{B4}), 139.8 (C^{A4}), 133.3 (d, J = 20.6 Hz, C^{C2}), 132.4 (C^{C4}), 130.5 (d, J = 10.9 Hz, C^{C3}), 126.3 (C^{A5}), 124.2 (C^{B3}), 124.0 (C^{A3}). ^{31}P{^{1}H} NMR (162 MHz, $(CD_3)_2CO$, 296 K) δ/ppm −21.4 (broad, FWHM = 140 Hz). Low temperature NMR (208 K): ^{31}P{^{1}H} NMR (243 MHz, $(CD_3)_2CO$, 208 K) δ/ppm −20.6 (d, $^1J_{^{31}P-^{109}Ag}$ = 657.8 Hz, $[Ag_2(dppa)(tpy)_2]^{2+}$), −20.6 (d, $^1J_{^{31}P-^{107}Ag}$ = 572.8 Hz, $[Ag_2(dppa)(tpy)_2]^{2+}$), −23.0 (d, $^1J_{^{31}P-^{109}Ag}$ = 410.4 Hz, $[Ag_2(dppa)_2(tpy)_2]^{2+}$), −23.0 (d, $^1J_{^{31}P-^{107}Ag}$ = 355.8 Hz, $[Ag_2(dppa)_2(tpy)_2]^{2+}$).

Crystallography

Data were collected on a Bruker Kappa Apex2 diffractometer with data reduction, solution and refinement using the programs APEX[32] and CRYSTALS.[33] Structural analysis was carried out using Mercury v. 3.7.[34,35]

$[Ag_2(dppa)(6,6'\text{-}Me_2bpy)_2][PF_6]_2\cdot Et_2O$

$C_{53}H_{50}Ag_2F_{12}N_4O_1P_4$, M = 1326.61, colourless block, triclinic, space group $P\bar{1}$, a = 11.4217(7), b = 15.4399(10), c = 16.5048(10) Å, α = 90.991(2), β = 107.581(2), γ = 101.888(2)°, U = 2705.3(3) Å^3, Z = 2, D_c = 1.628 Mg m^{-3}, μ(Cu-Kα) = 7.666 mm^{-1}, T = 123 K. Total 20 062 reflections, 9500 unique, R_{int} = 0.021. Refinement of 9089 reflections (685 parameters) with $I > 2\sigma(I)$ converged at final R_1 = 0.0350 (R_1 all data = 0.0366), wR_2 = 0.0806 (wR_2 all data = 0.0810), gof = 0.9224. CCDC 1580157.†

$[Ag_2(dppa)_2(tpy)_2][PF_6]_2\cdot 2(CD_3)_2CO$ (pseudo-polymorph 1)

$C_{88}H_{74}Ag_2F_{12}N_6O_2P_6$, M = 1877.15, colourless block, triclinic, space group $P\bar{1}$, a = 12.1355(10), b = 12.5994(10), c = 14.8038 (12) Å, α = 95.415(3), β = 112.162(3), γ = 93.696(3)°, U = 2074.6 (3) Å^3, Z = 1, D_c = 1.502 Mg m^{-3}, μ(Cu-Kα) = 5.556 mm^{-1}, T = 123 K. Total 20 395 reflections, 7245 unique, R_{int} = 0.033. Refinement of 6529 reflections (523 parameters) with $I > 2\sigma(I)$ converged at final R_1 = 0.0258 (R_1 all data = 0.0291), wR_2 = 0.0283 (wR_2 all data = 0.0316), gof = 1.0823. CCDC 1580158.†

$[Ag_2(dppa)_2(tpy)_2][PF_6]_2\cdot CH_2Cl_2$ (pseudo-polymorph 2)

$C_{83}H_{64}Ag_2Cl_2F_{12}N_6P_6$, M = 1845.93, yellow block, monoclinic, space group $P2_1/c$, a = 23.7942(10), b = 30.1578(13), c = 44.766 (2) Å, α = 90, β = 95.386(2), γ = 90°, U = 31 981(2) Å^3, Z = 16, D_c = 1.533 Mg m^{-3}, μ(Cu-Kα) = 6.338 mm^{-1}, T = 123 K. Total 226 517 reflections, 59 009 unique, R_{int} = 0.045. Refinement of 52 995 reflections (4015 parameters) with $I > 2\sigma(I)$ converged at final R_1 = 0.0614 (R_1 all data = 0.0699), wR_2 = 0.1030 (wR_2 all data = 0.1046), gof = 0.8961. CCDC 1580159.†

Results and discussion

Synthesis and NMR spectroscopic characterization

The Ag^+ cation is known to accommodate a wider range of coordination numbers (two to six) than Cu^+, which prefers to adopt a tetrahedral coordination geometry. Previously reported

dinuclear species containing copper(I) and bridging dppa combined with an N^N chelating ligand feature a doubly-bridged $\{Cu_2(dppa)_2\}$ motif.[19–22] For an initial investigation of the reaction of Ag^+ with dppa and N^N ligands, we chose a combination of one chelating and one bridging ligand per Ag^+.

Reaction of $Ag[PF_6]$, 6,6′-Me_2bpy and dppa in a 1 : 1 : 1 ratio resulted in the isolation of a colourless crystalline solid. Preliminary structural data from single-crystal X-ray diffraction confirmed the doubly-bridged dimeric structure of $[Ag_2(dppa)_2(6,6'\text{-}Me_2bpy)_2][PF_6]_2$ (Scheme 2). Elemental analysis was consistent with $\{[Ag(dppa)(6,6'\text{-}Me_2bpy)][PF_6]\}_n$ and in the positive mode electrospray (ESI) mass spectrum, the base peak at m/z 685.05 arose from $[Ag(dppa)(6,6'\text{-}Me_2bpy)]^+$. No higher mass peaks were observed.

Solid $[Ag_2(dppa)_2(6,6'\text{-}Me_2bpy)_2][PF_6]_2$ was dissolved in acetone-d_6 and the room temperature ^{1}H NMR solution spectrum showed one set of signals, with the integrals consistent with a 1 : 1 ratio of 6,6′-Me_2bpy : dppa. An indicator for the formation of the $[Ag_2(dppa)_2(6,6'\text{-}Me_2bpy)_2]^{2+}$ cation was a cross peak in the NOESY spectrum between the methyl groups of 6,6′-Me_2bpy and the H^{C2} protons of the phenyl rings of dppa (Fig. S1 and S2,† see Scheme 2 for atom labelling). On lowering the temperature from 298 to 208 K, no additional signals appeared in the ^{1}H NMR spectrum although some shifting of resonances including that of the H^{Me} protons in 6,6′-Me_2bpy was observed (Fig. S3†). The solution $^{31}P\{^1H\}$ NMR spectrum at 298 K showed a septet for $[PF_6]^-$ and a signal at δ −21.1 ppm (FWHM = 38 Hz) arising from dppa. Upon cooling the sample from 298 to 208 K, the ^{31}P NMR resonance split into two doublets centred at δ −21.5 ppm (Fig. 1). The latter result from coupling to ^{109}Ag and ^{107}Ag, with coupling constants of 407 Hz ($^1J_{^{31}P-^{109}Ag}$) and 353 Hz ($^1J_{^{31}P-^{107}Ag}$), respectively (Fig. 2).

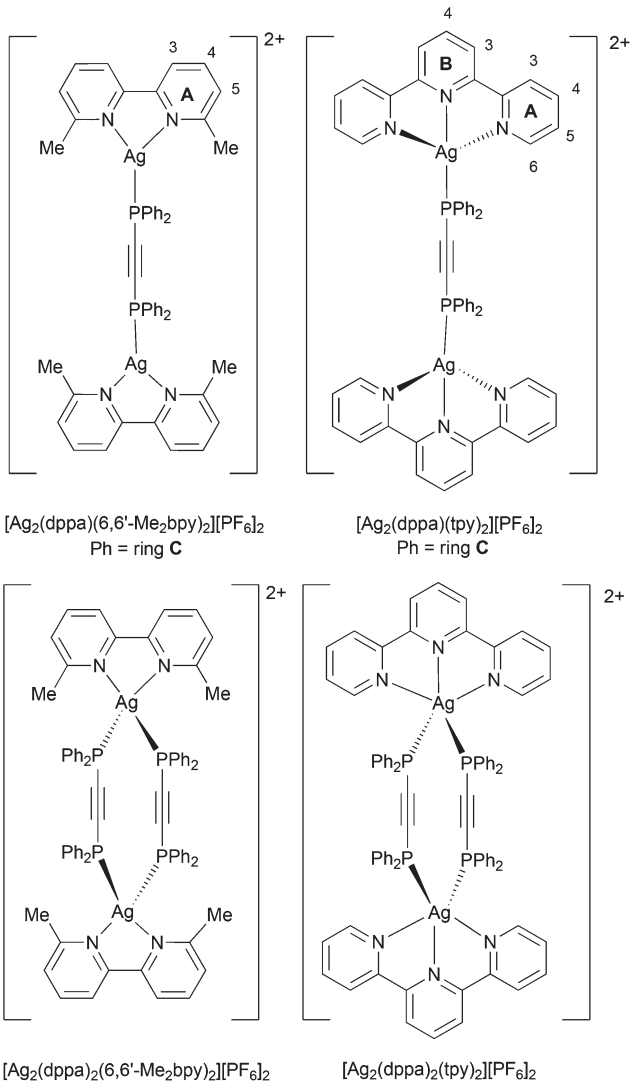

Scheme 2 Structures of dinuclear complexes with one and two dppa bridges; ring and atom labels for NMR spectroscopic assignments.

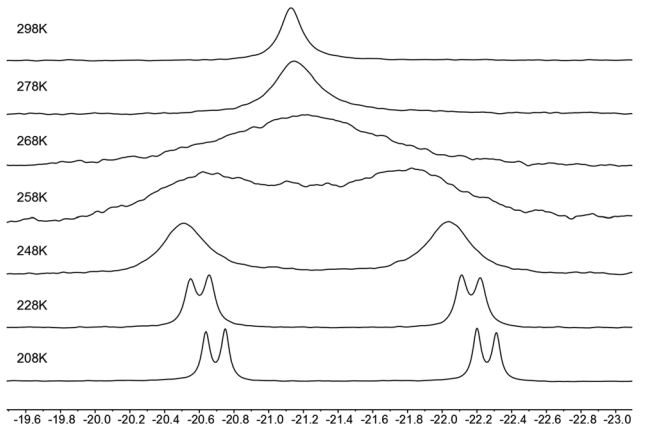

Fig. 1 Variable temperature (243 MHz) $^{31}P\{^1H\}$ NMR spectra of $[Ag_2(dppa)_2(6,6'\text{-}Me_2bpy)_2][PF_6]_2$ in $(CD_3)_2CO$.

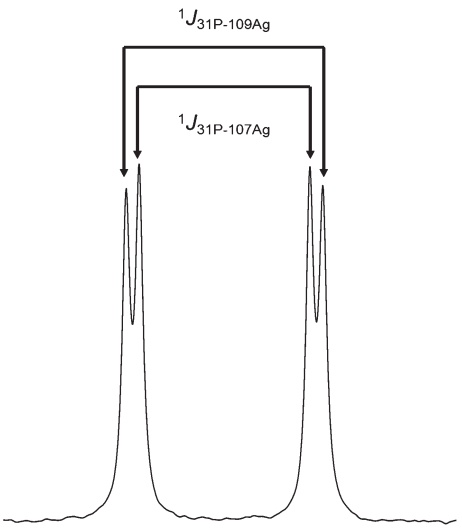

Fig. 2 Illustration of the two doublets and the two coupling constants $^1J_{^{31}P-^{109}Ag}$ and $^1J_{^{31}P-^{107}Ag}$ in the 243 MHz $^{31}P\{^1H\}$ NMR spectrum of $[Ag_2(dppa)_2(6,6'\text{-}Me_2bpy)_2][PF_6]_2$ in $(CD_3)_2CO$ at 208 K.

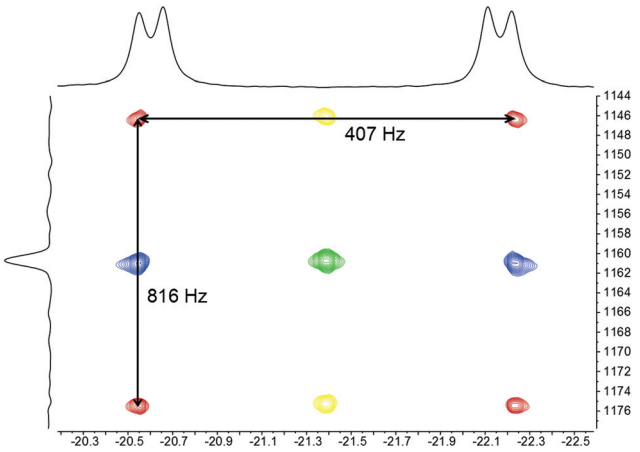

Fig. 3 $^{31}P\{^{1}H\}$–^{109}Ag HSQC spectrum of $[Ag_2(dppa)_2(6,6'\text{-}Me_2bpy)_2][PF_6]_2$ in $(CD_3)_2CO$ at 228 K. Cross peaks without decoupling are coloured in red, with $\{^{31}P\}$ decoupling in blue, with $\{^{109}Ag\}$ decoupling in yellow, and with both $\{^{31}P\}$ and $\{^{109}Ag\}$ decoupling green.

The $^{31}P\{^{1}H\}$–^{109}Ag HSQC spectrum was recorded at 228 K and is shown in Fig. 3. The $^{109}Ag\{^{31}P\}$ NMR projection is plotted in the vertical dimension (F1) and the $^{31}P\{^{1}H\}$ NMR spectrum in the horizontal dimension (F2). Depending on the additional decoupling (none, $\{^{31}P\}$, $\{^{109}Ag\}$, or both $\{^{31}P\}$ and $\{^{109}Ag\}$), a different number of cross peaks results. The chemical shift of the ^{109}Ag NMR signal is at δ 1161 ppm with a splitting of 816 Hz in the F1 dimension (^{109}Ag) and a coupling constant of 407 Hz in the F2 (^{31}P) dimension. While for a heteronuclear two-spin AX spin system, the distances between the cross peaks in the fully or partially coupled spectra are always equal to the $^{1}J(AX)$ coupling constant in F1 and F2, it can be shown elegantly by the product operator formalism, that for a heteronuclear three-spin AX_2 spin system (I_{1z}, I_{2z}, S_{3z}; $^{1}J_{13} = {}^{1}J_{23}$) the modulation of the pure in-phase terms at the end of the HSQC sequence before the final t_2 evolution can be written as:[36]

$$\cos(2J_{13}\pi t_1)\cos(\Omega_3 t_1)(I_{1x} + I_{2x})$$

which is equivalent to:

$$\frac{1}{2}(\cos((\Omega_3 \ \pm \ 2J_{13}\pi)t_1)(I_{1x} + I_{2x})$$

This explains the spacing of the two resonances in F1 by two times the coupling constant $^{1}J_{^{31}P-^{109}Ag}$. It is, therefore, of additional analytical value to record the $^{31}P\{^{1}H\}$–^{109}Ag HSQC spectrum without decoupling in F2 and F1, as the doubling of the splitting constant in F1 unambiguously discriminates between an AX and an AX_2 spin system and allows, in combination with the ^{109}Ag chemical shift and the range of the $^{1}J_{^{31}P-^{109}Ag}$ coupling constant, a detailed description of the number of bridging ligands in solution. The doubling of the splitting constants as a result of two attached phosphorus atoms at one silver centre has also been reported by Pregosin *et al.*[29] From this part of the investigation, we were able to conclude that the $[Ag_2(dppa)_2(6,6'\text{-}Me_2bpy)_2]^{2+}$ complex remains intact in solution and does not undergo any ligand redistributions.

Following from the investigation of the assembly process involving a 1 : 1 : 1 mixture of $Ag[PF_6]$, 6,6′-Me_2bpy and dppa, we turned our attention to a 1 : 1 : 1 combination of $Ag[PF_6]$, tpy and dppa. X-ray quality crystals were grown by layering Et_2O over a concentrated solution of the compound in CH_2Cl_2 and a second set of crystals grew in an NMR sample of the compound in acetone-d_6 after few days. The structures of two pseudo-polymorphs of $[Ag_2(dppa)_2(tpy)_2][PF_6]_2$ (differing in solvate) are described later. Elemental analysis for the bulk material was in agreement with $\{[Ag(dppa)(tpy)][PF_6]\}_n$ and the dominant peak envelope in the electrospray mass spectrum (positive mode) at m/z 734.0 corresponded to $[Ag(dppa)(tpy)]^+$.

Solid $[Ag_2(dppa)_2(tpy)_2][PF_6]_2$ was dissolved in acetone-d_6 and the solution room temperature ^{1}H NMR spectrum was recorded. The relative integrals of the signals were in accord with a 1 : 1 ratio of tpy : dppa, and with one environment for each ligand. As in the reaction with 6,6′-Me_2bpy, the NOESY spectrum provided valuable information (Fig. S4 and S5†). At 208 K, a NOESY cross peak between the H^{A6} proton at tpy and the phenyl H^{C2} protons of dppa was consistent with the Ag^+ ion being bound to both ligands. This, along with confirmation of the 1 : 1 : 1 ratio of $Ag[PF_6]$, tpy and dppa was consistent with the presence of a dimer in solution. No additional signals appeared in the ^{1}H NMR spectrum on cooling from 298 to 208 K. The shifts of the signals for the dppa protons were little affected on cooling and the signals of the tpy protons H^{A3}, H^{A4}, H^{B3} and H^{B4} were shifted to higher frequency. In contrast, the signals for H^{A5} and H^{A6} shifted towards lower frequency (Fig. S6†). The spectroscopic signature for the tpy was consistent with either a tridentate bonding mode, or a bidentate mode undergoing fast exchange between two equivalent sites.[37] The symmetry of the tpy unit is maintained on the NMR timescale on going from 298 to 208 K, but the coordination mode of the tpy ligand in solution remains ambiguous. The chelating nature of tpy in the solid-state structure of $[Ag_2(dppa)_2(tpy)_2]^{2+}$ is discussed later.

In addition to the septet for $[PF_6]^-$, a signal at δ −22.9 ppm (FWHM = 110 Hz) was observed in the room temperature ^{31}P NMR spectrum. Cooling from 298 to 208 K leads to a splitting of this signal into two doublets centred at δ −23.0 ppm with coupling constants of 411 Hz ($^{1}J_{^{31}P-^{109}Ag}$) and 356 Hz ($^{1}J_{^{31}P-^{107}Ag}$), respectively (Fig. 4). The $^{31}P\{^{1}H\}$–^{109}Ag spectrum was recorded at 208 K and is illustrated in Fig. S7.† Both the shift of the ^{109}Ag signal (δ 1154 ppm) and the coupling constants in the F2 and F1 dimensions ($^{1}J_{^{31}P-^{109}Ag}$ and $^{1}J_{^{109}Ag-^{31}P}$, with $^{1}J_{^{109}Ag-^{31}P}$ being doubled again), are very similar: 411 and 840 Hz respectively for $[Ag_2(dppa)_2(tpy)_2]^{2+}$ and 407 and 816 Hz respectively for $[Ag_2(dppa)_2(6,6'\text{-}Me_2bpy)_2]^{2+}$ (Table 1). This is consistent with similar structures. The data are in agreement with the retention of $[Ag_2(dppa)_2(tpy)_2]^{2+}$ in solution.

Previous reports[21,26] confirm that $[Ag_2(dppa)(dppf)_2]^{2+}$ (dppf = 1,1′-bis(diphenylphosphino)ferrocene) and $[Ag_2(dppa)]^{2+}$ both contain single dppa bridges between two Ag(I) centres. We therefore decided to try to force a singly bridged mode by

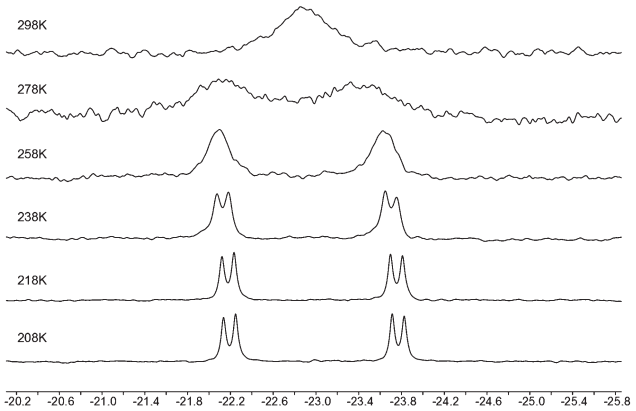

Fig. 4 Variable temperature 243 MHz $^{31}P\{^1H\}$ NMR spectra of $[Ag_2(dppa)_2(tpy)_2][PF_6]_2$ in $(CD_3)_2CO$.

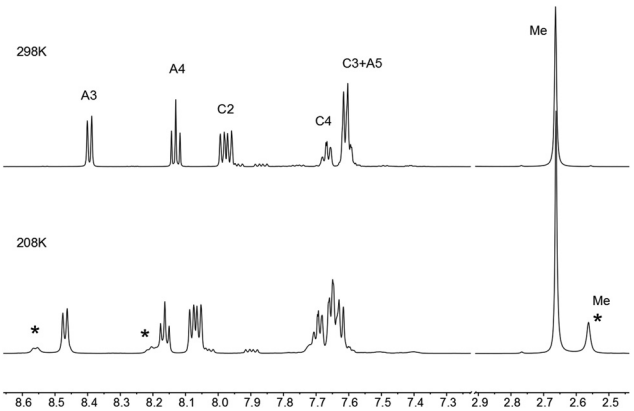

Fig. 5 Part of the ^1H NMR spectra of $[Ag_2(dppa)(6,6'\text{-}Me_2bpy)_2][PF_6]_2$ in $(CD_3)_2CO$ at 298 K, 500 MHz (top) and 208 K, 600 MHz (bottom), where a subspectrum is visible. Signals marked with an asterisk indicate the second conformer resolved at low temperature. For the full spectrum see Fig. S10.†

reducing the amount of dppa in the self-assembly process from 1.0 to 0.5 eq. with respect to $Ag[PF_6]$. We were curious to see whether the silver cation would be satisfied with threefold coordination or whether it would prefer additional donors, for example by making use of all three N-donors of the tpy ligand.

Reaction of $Ag[PF_6]$, 6,6′-Me_2bpy and dppa in a 2 : 2 : 1 ratio yielded a colourless solid. Single crystals were grown from a CH_2Cl_2 solution of the product layered with Et_2O, and X-ray diffraction confirmed the formation of $[Ag_2(dppa)(6,6'\text{-}Me_2bpy)_2][PF_6]_2$ (see later). The ^1H NMR spectrum of a solution of the isolated product in acetone-d_6 (298 K) was consistent with coordinated 6,6′-Me_2bpy and dppa ligands in a 2 : 1 ratio. A cross-peak in the NOESY spectrum between the methyl groups of 6,6′-Me_2bpy and the H^{C2} protons of the phenyl rings of dppa (Fig. S8 and S9†) confirmed the presence of an $\{AgN_2P\}$ coordination sphere, indicating the formation of $[Ag_2(dppa)(6,6'\text{-}Me_2bpy)_2]^{2+}$. On decreasing the temperature from 298 to 208 K, a subspectrum appeared in the ^1H NMR spectrum (Fig. 5, bottom and Fig. S10†) including an additional methyl signal at δ 2.55 ppm. The relative integrals of signals for the major and minor species showed the latter to comprise approximately 20% of the sample. In the ^{31}P NMR spectrum at 298 K, a septet from $[PF_6]^-$ was observed along with a broadened signal (FWHM = 60 Hz) at δ −16.5 ppm from dppa. Upon cooling (Fig. 6), the typical set of two doublets was resolved, centred at δ −16.1 ppm (Table 1), and at 208 K, a second set of doublets centred at δ −16.4 ppm ($^1J_{^{31}P-^{109}Ag}$ = 711 Hz) was observed. The data suggested that the minor species possessed similar structural properties to the dominant compound. An EXSY cross peak between the two methyl signals (major and minor) in the 208 K NOESY spectrum (Fig. S9,† δ 2.66 and 2.20 ppm), gave strong evidence that the subspectrum

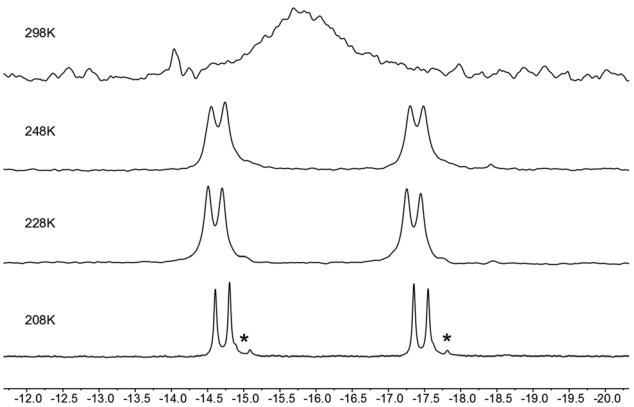

Fig. 6 Variable temperature 243 MHz $^{31}P\{^1H\}$ NMR spectra of $[Ag_2(dppa)(6,6'\text{-}Me_2bpy)_2][PF_6]_2$ in acetone-d_6. Signals marked with an asterisk indicate the smaller doublet assigned to the second conformer resolved at lower temperature.

Table 1 Overview of NMR chemical shifts and coupling constants (208 K)

Cation	$[Ag_2(dppa)(6,6'\text{-}Me_2bpy)_2]^{2+}$	$[Ag_2(dppa)(tpy)_2]^{2+}$	$[Ag_2(dppa)_2(6,6'\text{-}Me_2bpy)_2]^{2+}$	$[Ag_2(dppa)_2(tpy)_2]^{2+}$
N^N	6,6′-Me_2bpy	tpy	6,6′-Me_2bpy	tpy
Number of dppa bridges	1	1	2	2
δ (^{109}Ag)/ppm	735	765	1161	1154
δ (^{31}P)/ppm	−16.1	−20.6	−21.5	−23.0
$^1J_{^{31}P-^{109}Ag}$/Hz	715	658	407	411
Splitting F1/Hz	716	666	816	840
$T_{coalesc}$/K	286 (3)	278 (2)	262 (2)	287 (3)
$\Delta G^{\ddagger}$/kJ mol^{-1}	52.3 (5)	51.7 (4)	51.0 (4)	48.9 (5)

belonged not to a compositionally different species, but rather to a second conformer. A possible explanation is that at 208 K, the rotation of the alkyne bridge is slow with respect to the NMR spectroscopic time scale and that different conformers are resolved in the spectrum. The possible conformers are further discussed later.

In the $^{31}P\{^{1}H\}$–^{109}Ag HSQC spectrum (Fig. 7), the ^{109}Ag signal is centred at δ 735 ppm, resulting in a considerable shift of 426 ppm in comparison to the signal of $[Ag_2(dppa)_2(6,6'\text{-}Me_2bpy)_2][PF_6]_2$ (δ 1161 ppm). Two other significant differences are observed regarding the splitting patterns. The value of $^{1}J_{^{31}P-^{109}Ag}$ = 715 Hz for singly-bridged $[Ag_2(dppa)(6,6'\text{-}Me_2bpy)_2]^{2+}$ is significantly larger than $^{1}J_{^{31}P-^{109}Ag}$ = 407 Hz for doubly-bridged $[Ag_2(dppa)_2(6,6'\text{-}Me_2bpy)_2]^{2+}$. This is in accordance with James *et al.* who have reported that coupling constants decreased from 767 Hz for singly-bridged $[Ag_2(dppa)]^{2+}$ to 505 Hz in the doubly-bridged $[Ag_2(dppa)_2]^{2+}$ and to 377 Hz for the triply-bridged $[Ag_2(dppa)_3]^{2+}$.[26,38]

The second difference concerns the coupling of the silver nucleus to ^{31}P. In contrast to the doubly-bridged $[Ag_2(dppa)_2(6,6'\text{-}Me_2bpy)_2]^{2+}$ and $[Ag_2(dppa)_2(tpy)_2]^{2+}$, where the F1 splitting roughly doubles $^{1}J_{^{31}P-^{109}Ag}$, the two coupling constants are almost identical for the singly-bridged $[Ag_2(dppa)(6,6'\text{-}Me_2bpy)_2]^{2+}$ (715 Hz for $^{1}J_{^{31}P-^{109}Ag}$ and 716 Hz for the splitting in F1).

We next investigated the effects of changing the 6,6′-Me_2bpy ligand for tpy. An acetone-d_6 solution of $Ag[PF_6]$, tpy and dppa in a 2 : 2 : 1 ratio was stirred for 2 hours, concentrated and analysed by NMR spectroscopy. For this reaction, no crystalline product was isolated, and the investigation focused on speciation in the reaction mixture. While the signals for H^{B3}, H^{B4}, H^{A3} and H^{A4} were well resolved at 298 K, those for H^{A5} and H^{A6} as well as the signals of the C-ring protons were broadened (Fig. S13†). A cross peak in the NOESY spectrum (298 K), (Fig. S11†) showed the proximity of the H^{A6} and H^{C2} protons and indicated that Ag^{+} was coordinated by both tpy and dppa (Fig. S13†). The dppa ligand gave rise to a broad signal (δ −21.4 ppm, FWHM = 140 Hz) in ^{31}P NMR spectrum at 298 K. Upon cooling, this signal split into two sets of doublets with an integral ratio of 2 : 1 (Fig. 8). The smaller set of doublets centred at δ −20.6 ppm had a value of $^{1}J_{^{31}P-^{109}Ag}$ = 658 Hz. This is smaller than, but in the same range as, the coupling constant in $[Ag_2(dppa)(6,6'\text{-}Me_2bpy)_2]^{2+}$ (Table 1). The larger set of doublets was centred at δ −23.0 ppm with $^{1}J_{^{31}P-^{109}Ag}$ = 410 Hz. These values indicated the formation of the doubly-bridged $[Ag_2(dppa)_2(tpy)_2]^{2+}$, which was further confirmed by looking at the ^{1}H NMR and $^{31}P\{^{1}H\}$–^{109}Ag HSQC spectra at 208 K. The low temperature ^{1}H NMR spectrum showed nine relatively sharp signals (Fig. 9, top, Fig. S12 and S13,† bottom). However, the signals were located at different shifts than at room temperature, and in addition eight broad signals were visible. Compared with the low temperature ^{1}H NMR spectrum of the doubly-bridged $[Ag_2(dppa)_2(tpy)_2]^{2+}$ cation (Fig. 9), the sharp signals are con-

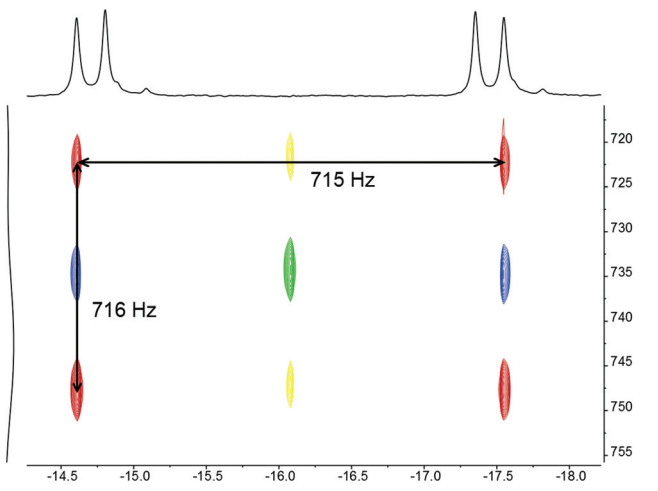

Fig. 7 $^{31}P\{^{1}H\}$–^{109}Ag HSQC spectrum of $[Ag_2(dppa)(6,6'\text{-}Me_2bpy)_2][PF_6]_2$ in $(CD_3)_2CO$ at 208 K. Cross peaks without decoupling are coloured in red, with $\{^{31}P\}$ decoupling in blue, with $\{^{109}Ag\}$ decoupling in yellow and with both $\{^{31}P\}$ and $\{^{109}Ag\}$ decoupling green.

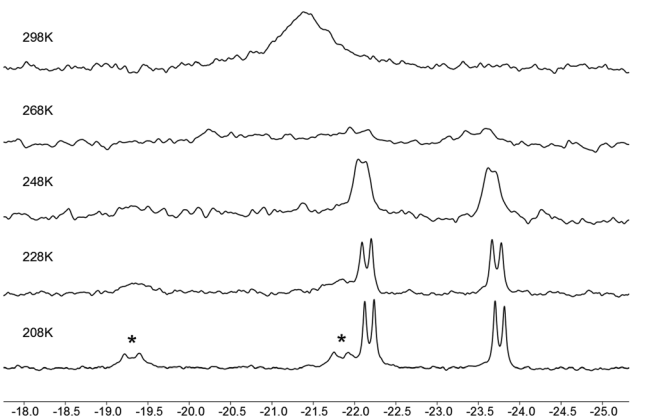

Fig. 8 Variable temperature 243 MHz $^{31}P\{^{1}H\}$ NMR spectra of a 2 : 2 : 1 mixture of $Ag[PF_6]$, tpy and dppa in acetone-d_6. Signals marked with an asterisk indicate the lower intensity resonance assigned to the mono-bridged $[Ag_2(dppa)(tpy)_2]^{2+}$ species resolved at lower temperature.

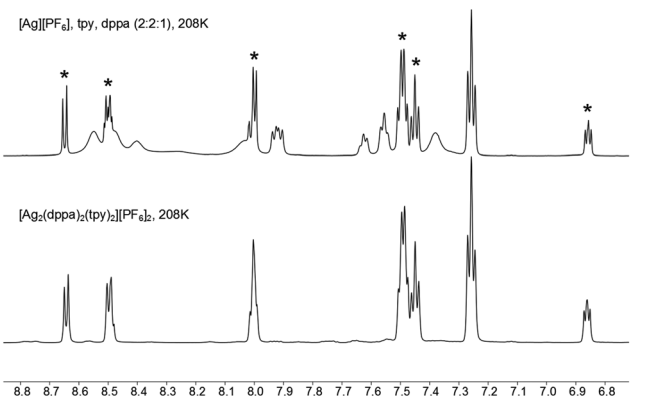

Fig. 9 ^{1}H NMR spectra of a 2 : 2 : 1 mixture of $[Ag][PF_6]$, tpy and dppa in $(CD_3)_2CO$ at 208 K, 600 MHz (top) and of $[Ag_2(dppa)_2(tpy)_2][PF_6]_2$ in $(CD_3)_2CO$ at 298 K, 500 MHz (bottom). Signals in the top spectrum that are in agreement with $[Ag_2(dppa)_2(tpy)_2][PF_6]_2$ are marked with an asterisk.

sistent with the signals for $[Ag_2(dppa)_2(tpy)_2]^{2+}$, both in shift and multiplicity, thus confirming the proposal that the dominant species in solution is the doubly-bridged cation.

Some of the remaining signals should then belong to a singly-bridged species. While the set of doublets in the $^{31}P\{^1H\}$ NMR spectrum (Fig. 8, 208 K) is shifted to lower frequency with respect to $[Ag_2(dppa)(6,6'\text{-}Me_2bpy)_2][PF_6]_2$ (δ −20.6 ppm *versus* δ −16.1 ppm), the coupling constants are sufficiently similar to indicate a singly-bridged $[Ag_2(dppa)(tpy)_2]^{2+}$ cation. This is further supported by the $^{31}P\{^1H\}$–^{109}Ag HSQC spectrum (Fig. S14†). With a chemical shift of δ 765 ppm, the ^{109}Ag NMR signal is close to that of the singly-bridged $[Ag_2(dppa)(6,6'\text{-}Me_2bpy)_2]^{2+}$ cation. Furthermore, the coupling constant in the F1 dimension, $^1J_{^{109}Ag-^{31}P}$ = 666 Hz deviates only slightly from the one observed in F2, $^1J_{^{31}P-^{109}Ag}$ (658 Hz), which is in the same order of magnitude and in contrast to the doubly-bridged cations, where the splitting pattern in F1 was doubled with respect to $^1J_{^{31}P-^{109}Ag}$. Therefore, we conclude that the minor product of the 2 : 2 : 1 mixture of $Ag[PF_6]$, 6,6′-Me_2bpy and dppa in acetone-d_6 at 208 K is the singly-bridged $[Ag_2(dppa)(tpy)_2][PF_6]_2$, which undergoes rapid exchange with the doubly-bridged cation at higher temperature.

Crystal structure of $[Ag_2(dppa)(6,6'\text{-}Me_2bpy)_2][PF_6]_2\cdot Et_2O$

Colourless crystals were grown by layer diffusion of Et_2O into a CH_2Cl_2 solution of $[Ag_2(dppa)(6,6'\text{-}Me_2bpy)_2][PF_6]_2$. The compound crystallizes in the space group $P\bar{1}$ and the asymmetric unit contains one complex cation, two $[PF_6]^-$ anions and one Et_2O molecule. The complex (Fig. 10) consists of two Ag^+ cations which are each chelated by a 6,6′-Me_2bpy ligand with Ag–N distances between 2.249(2) and 2.302(2) Å and bridged by one dppa molecule, with relatively short Ag–P distances of 2.3475(6) and 2.3390(7) Å.

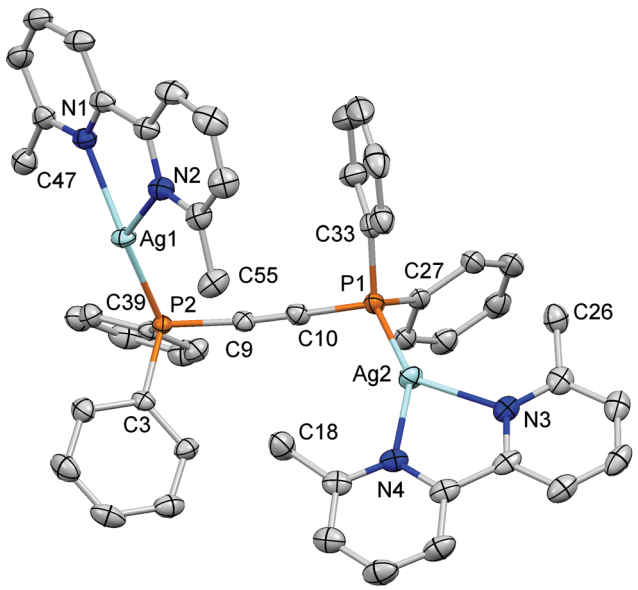

Fig. 10 Structure of $[Ag_2(dppa)(6,6'\text{-}Me_2bpy)_2][PF_6]_2\cdot Et_2O$; H atoms and solvent molecules omitted for clarity. Ellipsoids are plotted at 50% probability level. Selected bond parameters are listed in Table 2.

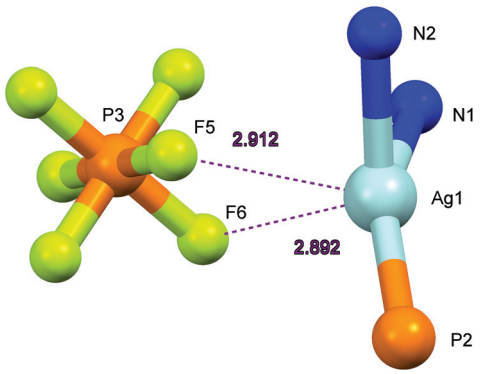

Fig. 11 Coordination geometry around Ag1, showing the coordinated nitrogen atoms of the bipyridine, one phosphorus atom of dppa and the close contacts to F5 and F6 of one $[PF_6]^-$ anion.

Each silver centre is coordinated in a trigonal planar geometry, each by two nitrogen atoms and one phosphorus atom (Fig. 10). Atoms N1, N2 and P2 form the trigonal plane around Ag1, with interligand bond angles of P2–Ag1–N1 = 150.29(6)°, P2–Ag1–N2 = 129.72(6)° and N1–Ag1–N2 = 73.25(9)°. The three angles sum up to approximately 353°; the small deviation from 360° fits well with the displacement of the silver cation from the trigonal plane (*ca.* 0.30 Å). This could be due to Ag1 exhibiting short contacts to F5 (2.912(2) Å) and F6 (2.892(2) Å) of the $[PF_6]^-$ anion (Fig. 11), which is accommodated in a pocket. Taking F5 and F6 into consideration, Ag1 is quasi 5-coordinate. For Ag2, the respective angles are P1–Ag2–N3 = 135.41(7)°, P1–Ag2–N4 = 150.53(7)° and N3–Ag2–N4 = 73.63(9)°, summing to 359.57(13)° and displacing Ag2 almost in the plane of P1, N3 and N4 (distance *ca.* 0.08 Å). This is in good agreement with the geometry around the Cu^+ cations in $[Cu_2(dppa)(dppf)_2]^{2+}$, where the angles sum up to 360° and the displacement of the Cu^+ cation is 0.02 Å.[21]

Fig. 12 shows a view down the dppa bond and shows an eclipsed conformation. One phenyl group of P2 (containing

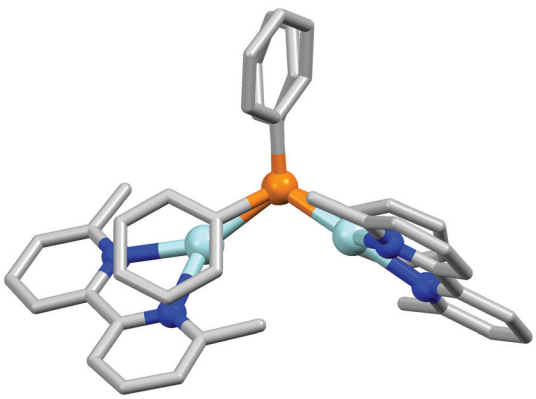

Fig. 12 Looking down the dppa bond from P1 to P2 shows the eclipsed structure with one dppa phenyl group on top of the phenyl group attached to the other phosphorus atom and the bipyridines on top of the respective opposite phenyl ring.

C39) is on top of the phenyl group of P1 containing C27 and the each of the 6,6′-Me_2bpy ligand lies over a phenyl group of the opposite phosphane. The angles involving the coordinated dppa ligands are Ag1–P2–C9 = 105.74(9)° and Ag2–P1–C10 = 116.15(9)° and the Ag–P–P–Ag torsion angle is found to be 108.14(3)°. Due to the low energy barrier for the rotation of the ethyne bond and phosphorus–C_{ethyne} bonds, a number of different conformers are possible (Scheme 3). Although the pyridine ring with N2 and the phenyl ring containing C33 appear roughly placed on top of each other, the displacement of 24.2° of the ring planes and the centroid–centroid distance of about 4.23 Å make π–π interactions rather inefficient and they can therefore be disregarded as a possible driving force to favour this particular conformer in the solid state.[39] When it comes to solutions, the presence of two conformers in acetone-d_6 was confirmed by NMR spectroscopy (see NMR section). It was not possible to assign the solution species to particular conformers, nor to say whether the dominant solution species agrees with the solid-state structure. Starting with the geometry from the crystal structure, structures of the six conformers on Scheme 3 were optimized at a molecular mechanics (MMFF) level[40] and were found to have very similar energies. This is probably not surprising, given the spatial separation of the Ag atoms and phenyl groups across the P–C≡C–P unit. For the optimizations, the N–Ag–N and N–Ag–P bond angles were constrained to 74 and 143°, respectively, to maintain a trigonal planar geometry at silver.

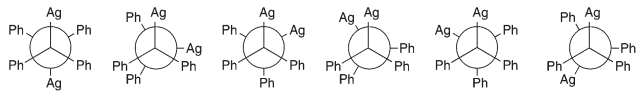

Scheme 3 Newman projections (along the P–C≡C–P vector) showing possible conformers of $[Ag_2(dppa)(6,6'\text{-}Me_2bpy)_2]^{2+}$. Only the positions of the Ag atoms and Ph groups in the *gauche* and *anti*-conformers are shown. The second (from left) conformer corresponds to the solid-state structure.

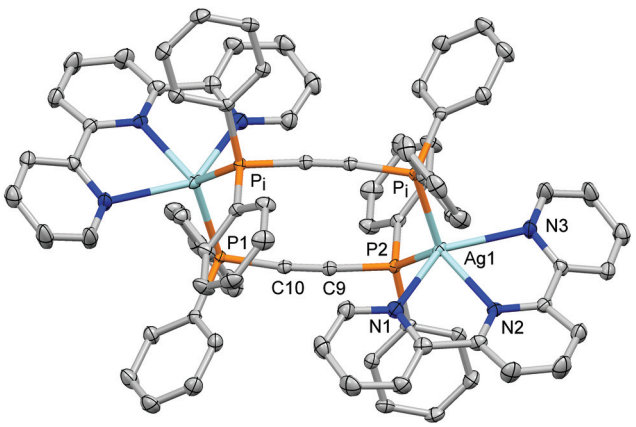

Fig. 13 Structure of $[Ag_2(dppa)_2(tpy)_2][PF_6]_2{\cdot}2Et_2O$; H atoms and solvent molecules omitted for clarity. Ellipsoids are plotted at 50% probability level. Selected bond parameters are listed in Table 2.

Crystal structure of $[Ag_2(dppa)_2(tpy)_2][PF_6]_2{\cdot}2(CH_3)_2CO$ (pseudo-polymorph 1)

Single crystals of $[Ag_2(dppa)_2(tpy)_2][PF_6]_2{\cdot}2(CH_3)_2CO$ were obtained from a stored NMR tube containing a sample of the compound in acetone-d_6. The compound crystallizes in the triclinic space group $P\bar{1}$. The asymmetric unit contains half a dimer, one $[PF_6]^-$ anion and one acetone molecule per asymmetric unit; the second half of the dimer is symmetry generated by inversion (Fig. 13). All nitrogen atoms of the tpy are attached to the silver cations, with Ag–N distances of

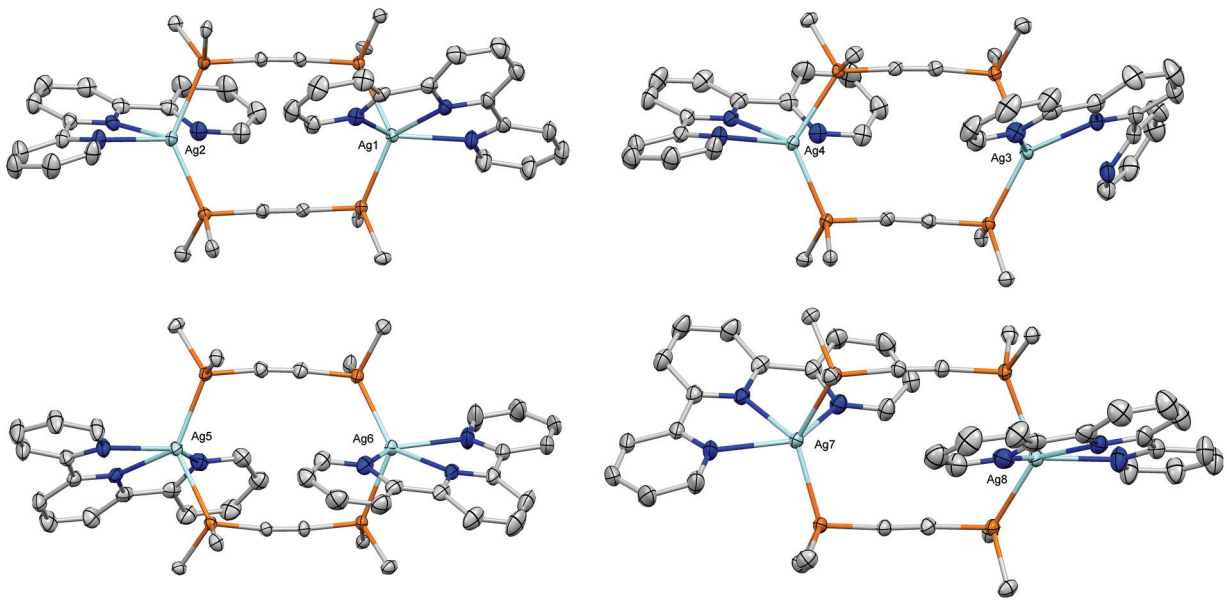

Fig. 14 Structure of $[Ag_2(dppa)_2(tpy)_2][PF_6]_2{\cdot}CH_2Cl_2$; H atoms and solvent molecules omitted for clarity. Ellipsoids are plotted at 50% probability level. Selected bond parameters are listed in Table 2.

Table 2 Comparison of structural parameters for the silver(I) coordination compounds

Compound	$[Ag_2(dppa)(6,6'\text{-}Me_2bpy)_2]$	$[Ag_2(dppa)_2(tpy)_2]\cdot 2(CH_3)_2CO$ pseudo-polymorph 1	$[Ag_2(dppa)_2(tpy)_2]\cdot 2CH_2Cl_2$ pseudo-polymorph 2			
			a Ag1Ag2	b Ag3Ag4	c Ag5Ag6	d Ag7Ag8
Number of Ag/unit cell	2	1	8	8	8	8
N^N chelating ligand	6,6′-Me_2bpy	tpy	tpy	tpy	tpy	tpy
Number of dppa bridges	1	2	2	2	2	2
Number of attached *N*/number of available *N*	4/4	6/6	5/6	4/6	6/6	6/6
Denticity	Both bidentate	Both tridentate	One bidentate (Ag2), one tridentate (Ag1)	Both bidentate	Both tridentate	Both tridentate
Ag–P distances	Ag1–P2 = 2.3475(6); Ag2–P1 = 2.3390(7)	Ag1–P1(2_766) = 2.4608(5); Ag1–P2 = 2.4228(5)	Ag1–P2 = 2.4120(9); Ag1–P4 = 2.4892(9); Ag2–P1 = 2.4341(9); Ag2–P3 = 2.4620(9)	Ag3–P5 = 2.3984(9); Ag3–P8 = 2.4997(9); Ag4–P6 = 2.4086(9); Ag4–P7 = 2.4545(9)	Ag5–P9 = 2.4792(9); Ag5–P12 = 2.4166(9); Ag6–P10 = 2.4760(9); Ag6–P11 = 2.4279(10)	Ag7–P13 = 2.4600(9); Ag7–P16 = 2.4127(9); Ag8–P14 = 2.4830(10); Ag8–P15 = 2.4257(10)
Ag–N distances	Ag1–N1 = 2.278(2); Ag1–N2 = 2.302(2); Ag2–N3 = 2.285(2); Ag2–N4 = 2.249(2)	Ag1–N1 = 2.5179 (18); Ag1–N2 = 2.3934(17); Ag1–N3 = 2.5100(18)	Ag1–N1 = 2.481(3); Ag1–N2 = 2.410(3); Ag1–N3 = 2.503(3); Ag2–N4 = 2.389(3); Ag2–N5 = 2.432(3); Ag2– N6 = 2.726(3)[a]	Ag3–N7 = 2.430(3); Ag3–N8 = 2.355(3); Ag3–N9 = 2.762(3)[a]; Ag4–N10 = 2.423(3); Ag4–N11 = 2.377(3); Ag4–N12 = 2.727(3)[a]	Ag5–N13 = 2.580(3); Ag5–N14 = 2.401(3); Ag5–N15 = 2.475(3); Ag6–N16 = 2.542(3); Ag6–N17 = 2.430(3); Ag6–N18 = 2.478(4)	Ag7–N19 = 2.462(3); Ag7–N20 = 2.394(3); Ag7–N21 = 2.533(3); Ag8–N22 = 2.553(4); Ag8–N23 = 2.431(3); Ag8–N24 = 2.454(4)
Dihedral angle Ag–P–P–Ag	108.14(3)	44.24(3)	28.94(4); −36.47(4)	24.91(5); −44.43(4)	40.80(4); −40.86(4)	29.79(5); −45.26(4)
Torsion angle P–C–C–P	21(4)	22(3)	−176(2); −31(7)	105(5); or 18(7)	27(5); 63(6)	−102(5); −39(8)
Tilting angle Ag–P–C	Ag1–P2–C9 = 105.74 (9); Ag2–P1–C10 = 116.15(9)	Ag1–P2–C9 = 114.29(7); C10–P1–Ag1(2_766) = 110.65(7)	Ag1–P4–C15 = 112.9(1); Ag1–P2–C3 = 111.0(1); Ag2–P3–C14 = 113.3(1); Ag2–P1–C4 = 109.7(1)	Ag3–P8–C103 = 110.3(1); Ag3–P5–C97 = 109.4(1); Ag4–P7–C102 = 117.4(1); Ag4–P6–C98 = 111.0(1)	Ag5–P12–C197 = 109.5(1); Ag5–P9–C191 = 113.7(1); Ag6–P11–C196 = 114.1(1); Ag6–P10–C192 = 111.6(1)	Ag8–P14–C286 = 112.4(1); Ag8–P15–C290 = 114.3(1); Ag7–P16–C291 = 108.0(1); Ag7–P13–C285 = 113.9(1)
Torsion angles N–C–C–N	−5.2(4); −1.7(4)	−12.1(3); 24.5(3)	19.8(5); −12.4(5); 23.1(5); 7.9(5) (to nonbonding N)	18.7(5); 20.0(5) (to nonbonding N); −6.4(5); −30.9(5) (to nonbonding N)	−16.7(6); 5.9(5); −9.4(5); −17.8(5)	10.3(6); 3.5(6); 22.2(5); −0.4(5)
Biting angles N–Ag–N	73.26(8); 73.64(9)	67.37(6); 68.11(6)	67.9(1); 67.1(1); 69.8(1); 63.8(1) (to nonbonding N)	69.7(1); 65.2(1) (to nonbonding N); 69.4(1); 65.5(1) (to nonbonding N)	66.1(1); 68.7(1); 67.6(1); 66.2(1)	68.0(1); 66.1(1); 66.6(1); 68.7(1)

[a] These long contacts are considered as non-bonded separations.

2.3934(17) Å for the middle nitrogen and 2.5100(18) and 2.5179(18) for the outer nitrogen atoms. With C9–C9 distances (or C10–C10 distances, respectively) of 4.113(3) Å, the dppa bridges are relatively close to each other. The dppa bridges are slightly bent inwards (distance P1–P2 = 4.1480(9) Å) and the Ag–P distances of 2.4608(5) and 2.4228(5) Å are slightly longer than in the singly-bridged $[Ag_2(dppa)(6,6'\text{-}Me_2bpy)_2]^{2+}$ cation.

If we focus on the bonds between the outer nitrogen atoms of the tpy ligand and the phosphorus atoms of the two dppa bridges towards the silver cation, the coordination geometry could be described as distorted tetrahedral (as was expected) with the following angles: P_i–Ag1–P2 = 116.286(18)°, P_i–Ag1–N3 = 100.15(5)°, P2–Ag1–N3 = 111.47(5)°, N3–Ag1–N1 = 134.71° and P1–Ag1–N1 = 96.00°. There are no close contacts between cations and anions or solvent molecules and also the packing shows no interactions such as for example stacking.

Crystal structure of $[Ag_2(dppa)_2(tpy)_2][PF_6]_2\cdot CH_2Cl_2$ (pseudo-polymorph 2)

Large single crystals of $[Ag_2(dppa)_2(tpy)_2][PF_6]_2\cdot CH_2Cl_2$ were grown by slow diffusion of Et_2O into a concentrated solution of the compound in CH_2Cl_2. The unit cell is monoclinic $P2_1/c$. In the unit cell, four crystallographically independent $[Ag_2(dppa)_2(tpy)_2]^{2+}$ cations are present (Fig. 14) and show the potential for tpy to act as a hypodentate ligand,[41] with bi-and tridentate coordinated tpy ligands coexisting in the same structure. Fig. 14 shows the structures of the four independent dications and Table 2 gives an overview of the important bond parameters, compared to the above discussed structure of $[Ag_2(dppa)_2(tpy)_2][PF_6]_2\cdot 2Et_2O$ and to $[Ag_2(dppa)(6,6'\text{-}Me_2bpy)_2][PF_6]_2\cdot Et_2O$. In the dications containing Ag5 and Ag6 or Ag7 and Ag8, all tpy ligands are tridentate. The dimer with Ag1 and Ag2 can be regarded as an intermediate, with one tpy coordinating through all three nitrogen atoms and the other tpy only with two. In the $[Ag_2(dppa)_2(tpy)_2]^{2+}$ cation with Ag3 and Ag4, both tpy ligands are bidentate and each has one non-coordinated nitrogen. While the bonded nitrogen atoms in this pseudo-polymorph have distances between ~2.36 and 2.58 Å, the distances that are considered non-bonding are longer (between around 2.73 and 2.76 Å). The same phenomenon of tpy in both a bidentate and tridentate coordination mode in the same crystal structure was found for $[Cu(tpy)(POP)]^+$ where one copper cation is tetra-coordinated and the other penta-coordinated. With Cu–N distances of around 2.1, 2.2 and 2.6 Å for the penta-coordinated cation and *ca.* 2.1, 2.1 and 3.1 Å for the tetra-coordinated cation, the bond distance between the bonded nitrogen atoms and the copper is significantly longer than for the unattached nitrogen, part a consequence of the third pyridine ring being oriented with the nitrogen facing away from the metal centre.[37]

Conclusions

Four silver complexes containing heteroleptic dications have been synthesized and characterized. Depending on the number of available bisphosphane bridges and the type of chelating nitrogen donor ligand, the coordination modes of the silver cations range from tricoordinate to pentacoordinate and underline the versatility of silver(I) as well as the unpredictability of the outcome of the self-assembly processes. Detailed ^{109}Ag–^{31}P HMQC measurements point out correlations between the number of coordinated phosphorus atoms at the silver and the $^1J_{^{31}P-^{109}Ag}$ *versus* the $^1J_{^{109}Ag-^{31}P}$ coupling constants as well as the chemical shift δ in the ^{109}Ag NMR spectra, which provides a useful tool for the characterization of similar compounds. The crystal structure of the singly-bridged $[Ag_2(dppa)(6,6'\text{-}Me_2bpy)_2]^{2+}$ cation shows an unexpected eclipsed conformation of the 2,2′-bipyridine and the phenyl rings of dppa and finally, a combination of bi- and tridentate for 2,2′:6′,2″-terpyridine ligands are found in different $[Ag_2(dppa)_2(tpy)_2]^{2+}$ cations and confirm the ability of 2,2′:6′,2″-terpyridine to exhibit hypodentate coordination.

Conflicts of interest

There are no conflicts to declare.

Acknowledgements

We thank the Swiss National Science Foundation (grant number 200020_162631) and the University of Basel for support. We are grateful to Thomas Müntener for helpful discussions on the product operator description of AX_2 spin systems and Felix Raps and Nathalia Münch for assistance with low temperature NMR spectra (both University of Basel).

Notes and references

1 D. G. Cuttell, S.-M. Kuang, P. E. Fanwick, D. R. McMillin and R. A. Walton, *J. Am. Chem. Soc.*, 2002, **124**, 6.
2 S.-M. Kuang, D. G. Cuttell, D. R. McMillin, P. E. Fanwick and R. A. Walton, *Inorg. Chem.*, 2002, **41**, 3313.
3 R. D. Costa, D. Tordera, E. Ortí, H. J. Bolink, J. Schönle, S. Graber, C. E. Housecroft, E. C. Constable and J. A. Zampese, *J. Mater. Chem.*, 2011, **21**, 16108.
4 S. Keller, E. C. Constable, C. E. Housecroft, M. Neuburger, A. Prescimone, G. Longo, A. Pertegás, M. Sessolo and H. J. Bolink, *Dalton Trans.*, 2014, **43**, 16593.
5 S. Keller, A. Pertegás, G. Longo, L. Martinez, J. Cerdá, J. M. Junquera-Hernández, A. Prescimone, E. C. Constable, C. E. Housecroft, E. Ortí and H. J. Bolink, *J. Mater. Chem. C*, 2016, **4**, 3857.
6 R. Czerwieniec and H. Yersin, *Inorg. Chem.*, 2015, **54**, 4322.
7 D. Asil, J. A. Foster, A. Patra, X. de Hatten, J. del Barrio, O. A. Scherman, J. R. Nitschke and R. H. Friend, *Angew. Chem., Int. Ed.*, 2014, **53**, 8388.
8 N. Armaroli, G. Accorsi, M. Holler, O. Moudam, J.-F. Nierengarten, Z. Zhou, R. T. Wegh and R. Welter, *Adv. Mater.*, 2006, **18**, 1313.

9 C. Bizzarri, C. Strabler, J. Prock, B. Trettenbrein, M. Ruggenthaler, C.-H. Yang, F. Polo, A. Iordache, P. Brüggeller and L. De Cola, *Inorg. Chem.*, 2014, **53**, 10944.
10 M. D. Weber, C. Garino, G. Volpi, E. Casamassa, M. Milanesio, C. Barolo and R. D. Costa, *Dalton Trans.*, 2016, **45**, 8984.
11 F. Brunner, L. Martínez-Sarti, S. Keller, A. Pertegás, A. Prescimone, E. C. Constable, H. J. Bolink and C. E. Housecroft, *Dalton Trans.*, 2016, **45**, 15180.
12 S. Durini, G. A. Ardizzoia, B. Therrien and S. Brenna, *New J. Chem.*, 2017, **41**, 3006.
13 M. Z. Shafikov, A. F. Suleymanova, R. Czerwieniec and H. Yersin, *Chem. Mater.*, 2017, **29**, 1708.
14 O. Moudam, A. C. Tsipis, S. Kommanaboyina, P. N. Horton and S. J. Coles, *RSC Adv.*, 2015, **5**, 95047.
15 O. Moudam, N. Bristow, S.-W. Chang, M. Horieb and J. Kettle, *RSC Adv.*, 2015, **5**, 12397.
16 W. Weymiens, J. C. Slootweg and K. Lammertsma, in *Phosphorus Compounds. Advanced Tools in Catalysis and Material Sciences*, ed. M. Peruzzini and L. Gonsalvi, Springer International Publishing AG, Dordrecht, Netherlands, 1st edn, 2011, vol. 37, pp. 21–55.
17 A. K. Powell and M. J. Went, *J. Chem. Soc., Dalton Trans.*, 1992, 439.
18 M. Haehnel, S. Hansen, K. Schubert, P. Arndt, A. Spannenberg, H. Jiao and U. Rosenthal, *J. Am. Chem. Soc.*, 2013, **135**, 17556.
19 A. Fazal, B. El Ali, L. Ouahab and M. Fettouhi, *Polyhedron*, 2013, **49**, 7.
20 A. Fazal, A. Al-Dawsari, B. El Ali, L. Ouahab and M. Fettouhi, *J. Coord. Chem.*, 2014, **67**(14), 2357.
21 Y.-C. Liu, C.-I. Li, W.-Y. Yeh, G.-H. Lee and S.-M. Peng, *Inorg. Chim. Acta*, 2006, **359**, 2361.
22 H.-W. Xu, L.-X. Zhang, Y.-H. Li and H.-F. Wang, *Synth. React. Inorg., Met.-Org., Nano-Met. Chem.*, 2011, **41**, 743.
23 A. Kaeser, B. Delavaux-Nicot, C. Duhayon, Y. Coppel and J.-F. Nierengarten, *Inorg. Chem.*, 2013, **52**, 14343.
24 E. Lozano, M. Nieuwenhuyzen and S. L. James, *Chem. – Eur. J.*, 2001, **7**(12), 2644.
25 M.-C. Brandys and R. J. Puddephatt, *J. Am. Chem. Soc.*, 2002, **124**, 3946.
26 S. L. James, E. Lozano and M. Nieuwenhuyzen, *Chem. Commun.*, 2000, 617.
27 G. H. Penner and X. Liu, *Prog. Nucl. Magn. Reson. Spectrosc.*, 2006, **49**, 151.
28 S. J. Berners-Price, R. J. Bowen, P. J. Harvey, P. C. Healy and G. A. Koutsantonis, *J. Chem. Soc., Dalton Trans.*, 1998, 1743.
29 F. Lianza, A. Macchioni, P. Pregosin and H. Ruegger, *Inorg. Chem.*, 1994, **33**, 4999.
30 C.-W. Burges, R. Koschmieder, W. Sahm and A. Schwenk, *Z. Naturforsch., A: Phys., Phys. Chem., Kosmophys.*, 1973, **28**, 1753.
31 D. L. Jameson and L. E. Guise, *Tetrahedron Lett.*, 1991, **32**, 1999.
32 *APEX2, version 2 User Manual, M86-E01078*, Bruker Analytical X-ray Systems, Inc., Madison, WI, 2006.
33 P. W. Betteridge, J. R. Carruthers, R. I. Cooper, K. Prout and D. J. Watkin, *J. Appl. Crystallogr.*, 2003, **36**, 1487.
34 I. J. Bruno, J. C. Cole, P. R. Edgington, M. K. Kessler, C. F. Macrae, P. McCabe, J. Pearson and R. Taylor, *Acta Crystallogr., Sect. B: Struct. Sci.*, 2002, **58**, 389.
35 C. F. Macrae, I. J. Bruno, J. A. Chisholm, P. R. Edgington, P. McCabe, E. Pidcock, L. Rodriguez-Monge, R. Taylor, J. van de Streek and P. A. Wood, *J. Appl. Crystallogr.*, 2008, **41**, 466.
36 POMA, v. 2.0; P. Güntert, N. Schaefer, G. Otting and K. Wüthrich, *J. Magn. Reson., Ser. A*, 1993, **101**, 103.
37 N. S. Murray, S. Keller, E. C. Constable, C. E. Housecroft, M. Neuburger and A. Prescimone, *Dalton Trans.*, 2015, **44**, 7626.
38 S. M. Socol and J. G. Verkade, *Inorg. Chem.*, 1984, **23**, 3487.
39 C. Janiak, *J. Chem. Soc., Dalton Trans.*, 2000, 3885.
40 *Spartan '16, v. 2.0.5*, Wavefunction Inc.
41 E. C. Constable and C. E. Housecroft, *Coord. Chem. Rev.*, 2017, **350**, 84.

Electronic supplementary data to accompany

Self-Assembly of heteroleptic dinuclear silver(I) complexes bridged by bis(diphenylphosphino)-acetylene

Sarah Keller,[a] Timothy N. Camenzind,[a,b] Johannes Abraham,[c] Alessandro Prescimone,[a] Daniel Häussinger,[c] Edwin C. Constable[a] and Catherine E. Housecroft*[a]

[a]Department of Chemistry, University of Basel, BPR 1096, Mattenstrasse 24a, CH-4058 Basel, Switzerland; email: catherine.housecroft@unibas.ch
[b]Current address: Department of Physics, University of Basel, Klingelbergstrasse 82, CH-4056 Basel, Switzerland
[c]Department of Chemistry, University of Basel, St. Johanns-Ring 19, CH-4056 Basel, Switzerland

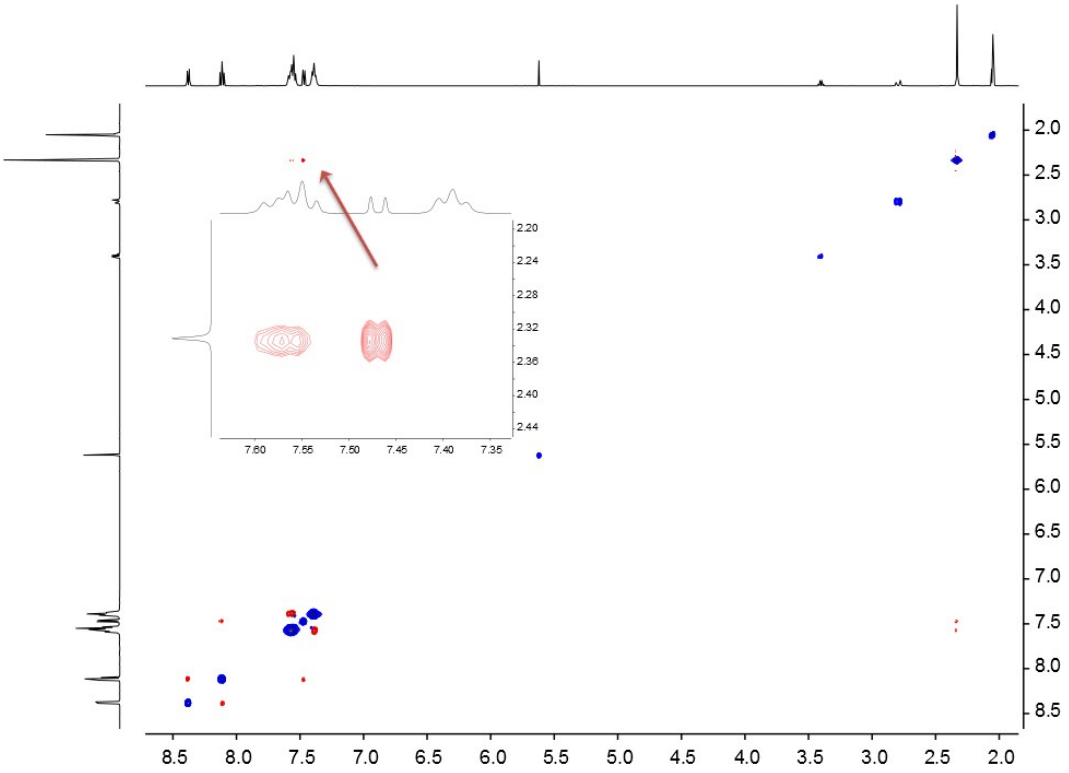

Fig. S1: NOESY spectrum of $[Ag_2(dppa)_2(6,6'\text{-}Me_2bpy)_2][PF_6]_2$ in $(CD_3)_2CO$ at 298 K, 500 MHz. The NOESY cross peaks between the Me signal at δ 2.33 ppm and the H^{C2+C4} signal at δ 7.57 ppm are clearly visible.

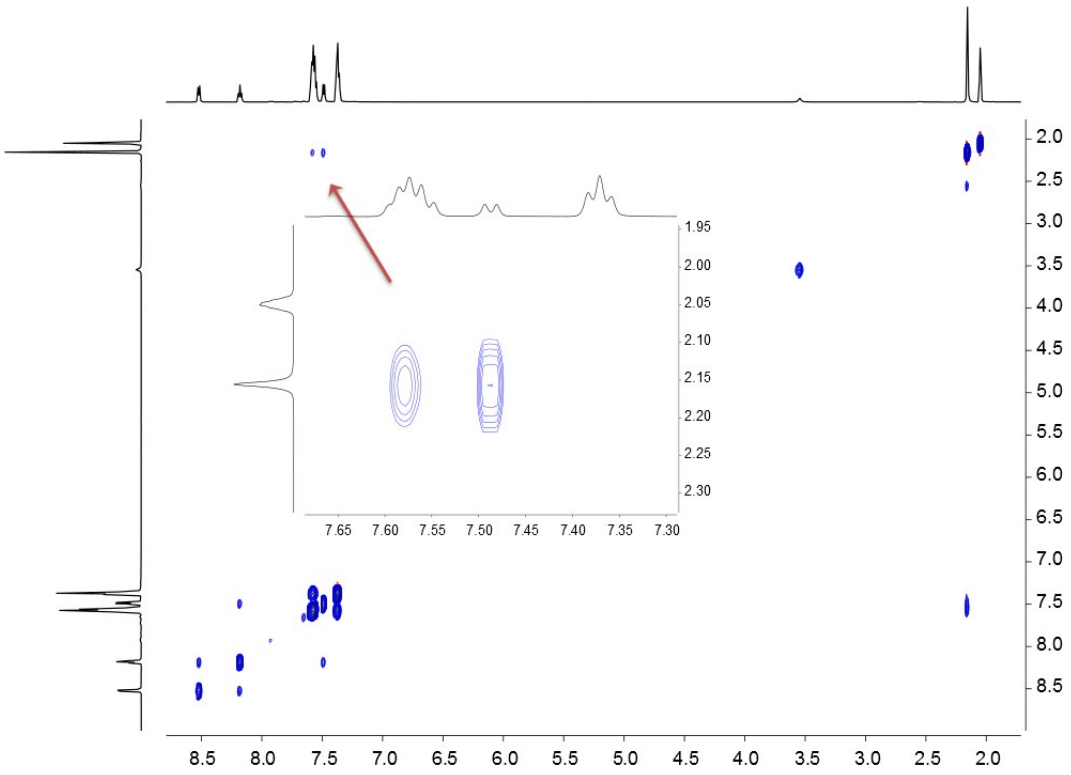

Fig. S2: NOESY spectrum of $[Ag_2(dppa)_2(6,6'\text{-}Me_2bpy)_2][PF_6]_2$ in $(CD_3)_2CO$ at 208 K, 600 MHz. The NOESY cross peaks between the Me signal at δ 2.16 ppm and the H^{C2+C4} signal at δ 7.58 ppm are clearly visible.

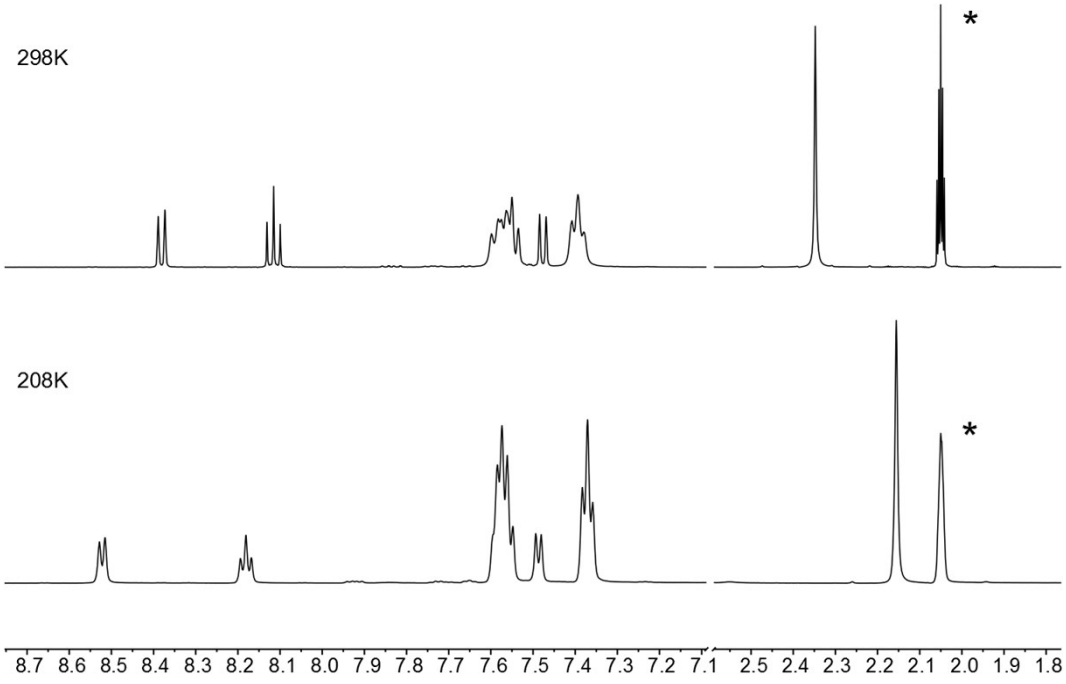

Fig. S3: ^1H NMR spectra of $[Ag_2(dppa)_2(6,6'\text{-}Me_2bpy)_2][PF_6]_2$ in $(CD_3)_2CO$ at 298 K, 500 MHz (top) and 208 K, 600 MHz (bottom). Signals marked with an asterisk indicate residual CD_3CD_2HCO.

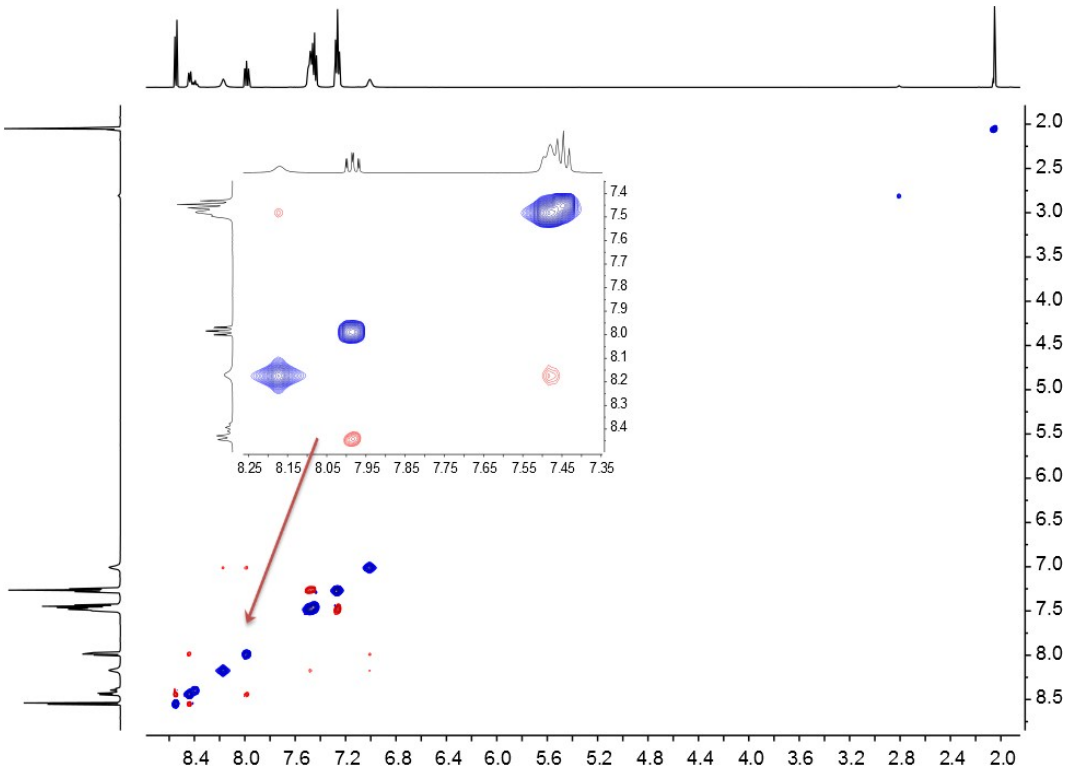

Fig. S4: NOESY spectrum of $[Ag_2(dppa)_2(tpy)_2][PF_6]_2$ in $(CD_3)_2CO$ at 298 K, 500 MHz. The NOESY cross peaks between the H^{A6} signal at δ 8.17 ppm and the H^{C2} signal at δ 7.48 ppm are sufficiently visible.

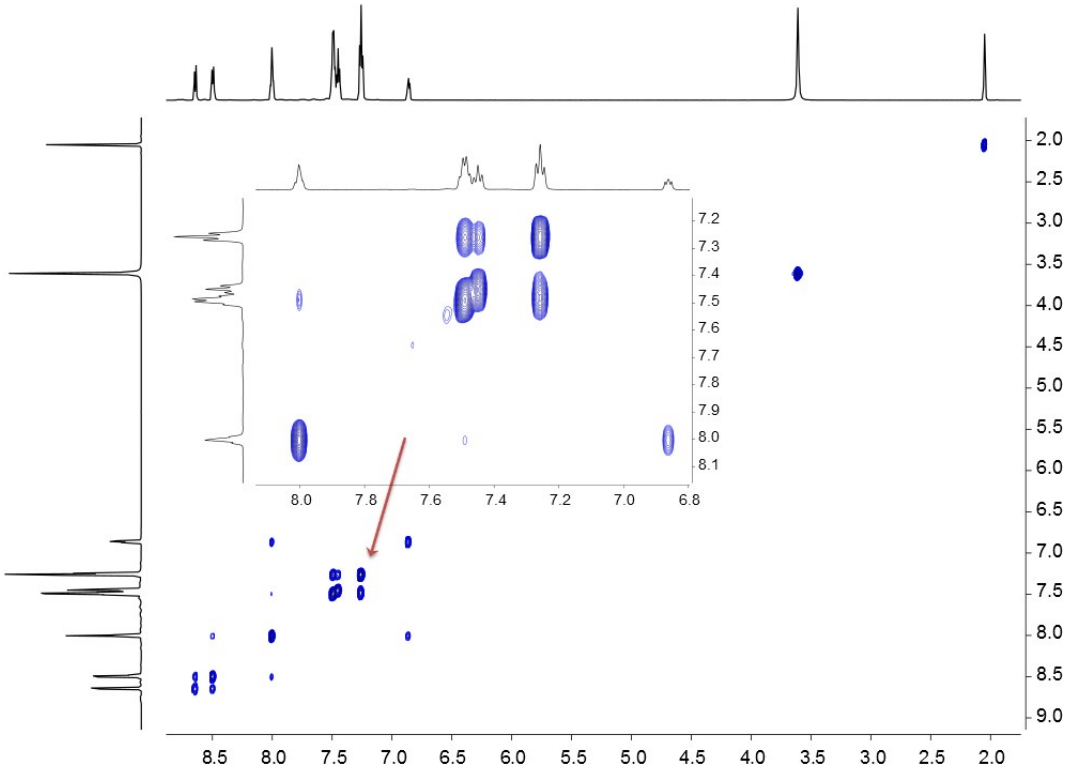

Fig. S5: NOESY spectrum of $[Ag_2(dppa)_2(tpy)_2][PF_6]_2$ in $(CD_3)_2CO$ at 208 K, 600 MHz. The NOESY cross peaks between the H^{A6} signal at δ 8.00 ppm and the H^{C2} signal at δ 7.49 ppm are sufficiently visible.

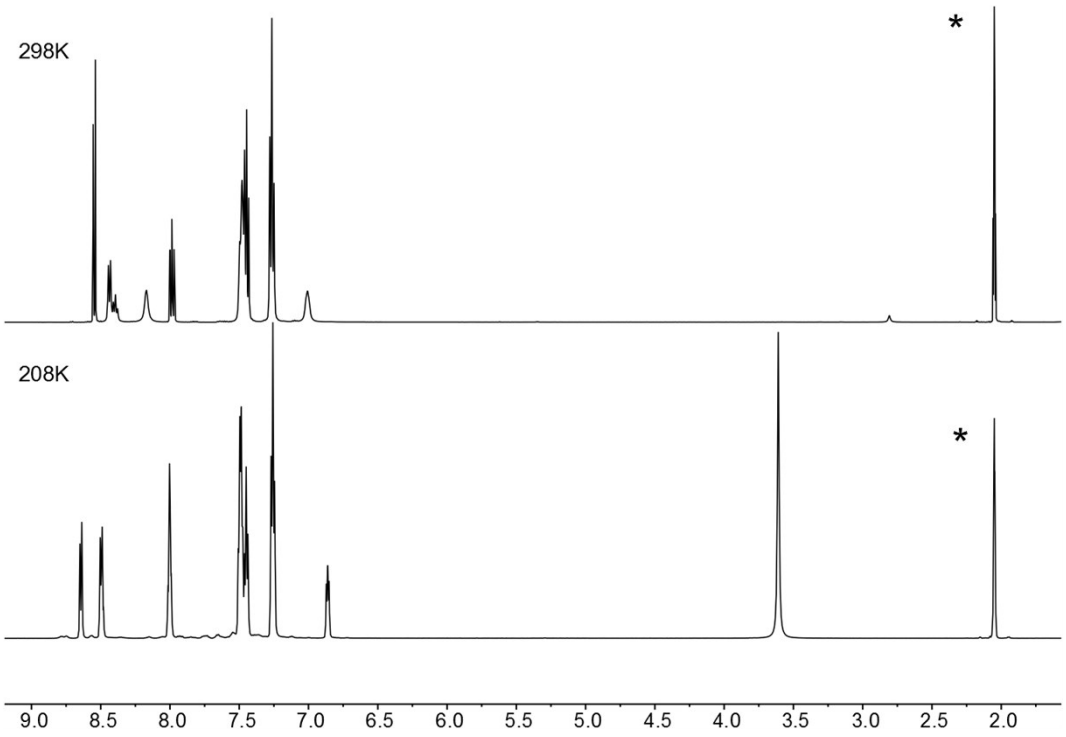

Fig. S6: ^{1}H NMR spectra of $[Ag_2(dppa)_2(tpy)_2][PF_6]_2$ in $(CD_3)_2CO$ at 298 K, 500 MHz (top) and 208 K, 600 MHz (bottom). Signals marked with an asterisk indicate residual CD_3CD_2HCO.

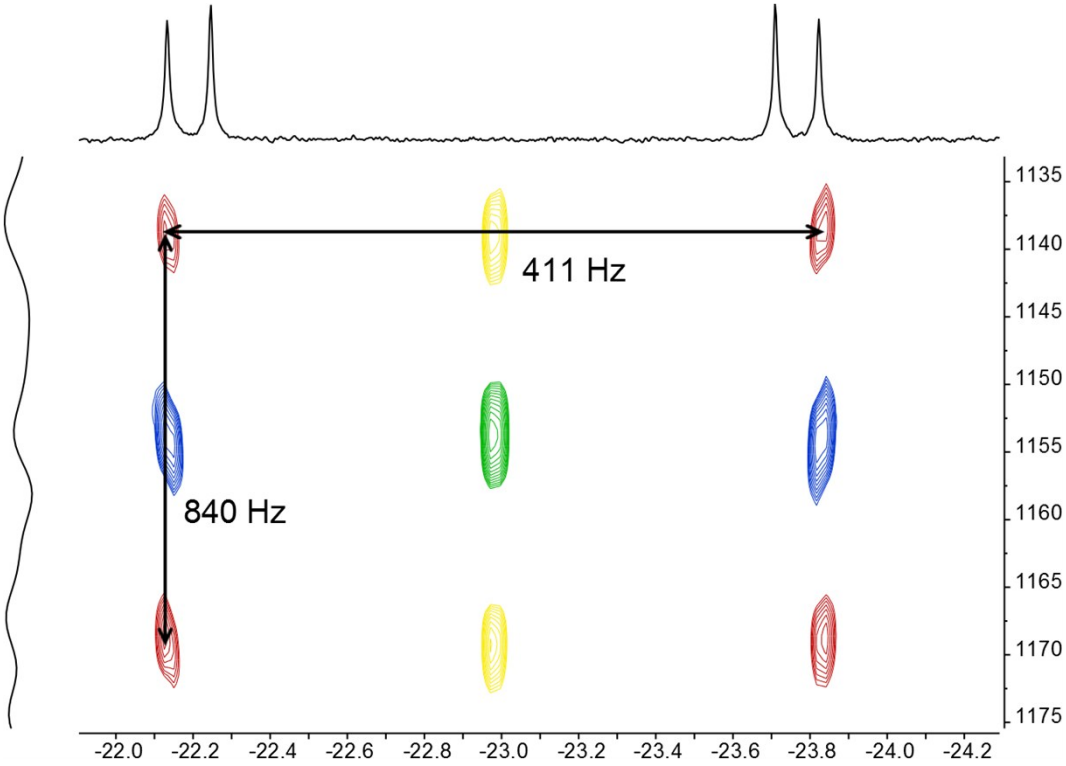

Fig. S7: $^{31}P\{^{1}H\}$-^{109}Ag HSQC spectrum of $[Ag_2(dppa)_2(tpy)_2][PF_6]_2$ in $(CD_3)_2CO$ at 208 K, 14.1 T. Cross peaks without decoupling are coloured in red, with $\{^{31}P\}$ decoupling in blue, with $\{^{109}Ag\}$ decoupling in yellow and with both $\{^{31}P\}$ and $\{^{109}Ag\}$ decoupling green.

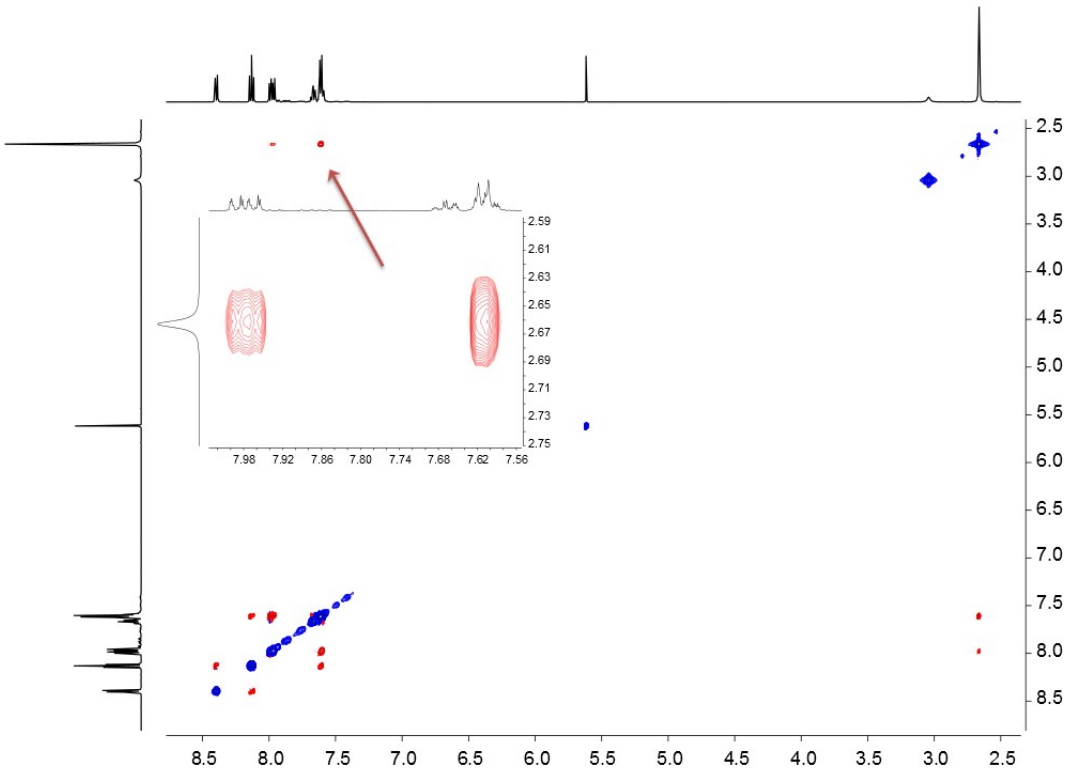

Fig. S8: NOESY spectrum of $[Ag_2(dppa)(6,6'\text{-}Me_2bpy)_2][PF_6]_2$ in $(CD_3)_2CO$ at 298 K, 500 MHz. The NOESY cross peaks between the Me signal at δ 2.66 ppm and the H^{C2} signal at δ 7.98 ppm are clearly visible.

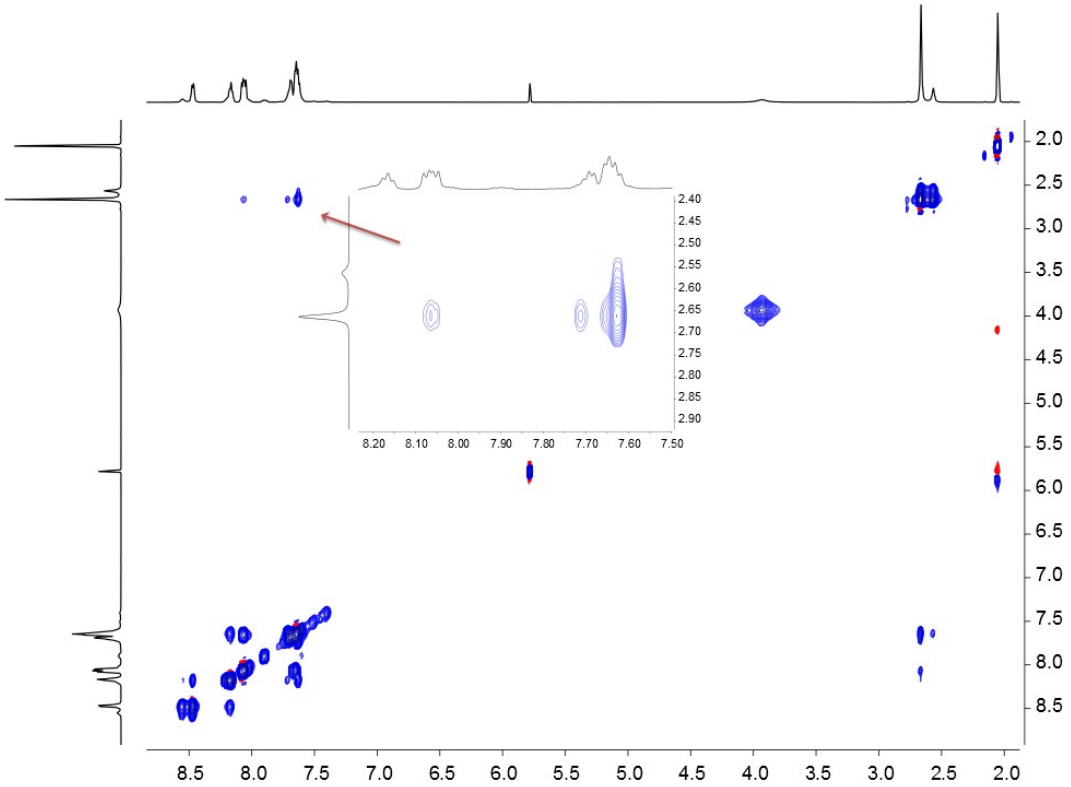

Fig. S9: NOESY spectrum of $[Ag_2(dppa)(6,6'\text{-}Me_2bpy)_2][PF_6]_2$ in $(CD_3)_2CO$ at 208 K, 600 MHz. The NOESY cross peaks between the Me signal at δ 2.66 ppm and the H^{C2} signal at δ 8.06 ppm are clearly

visible. Also we see an exchange between the main Me signal at δ 2.66 ppm and the additional Me signal at δ 2.56 ppm.

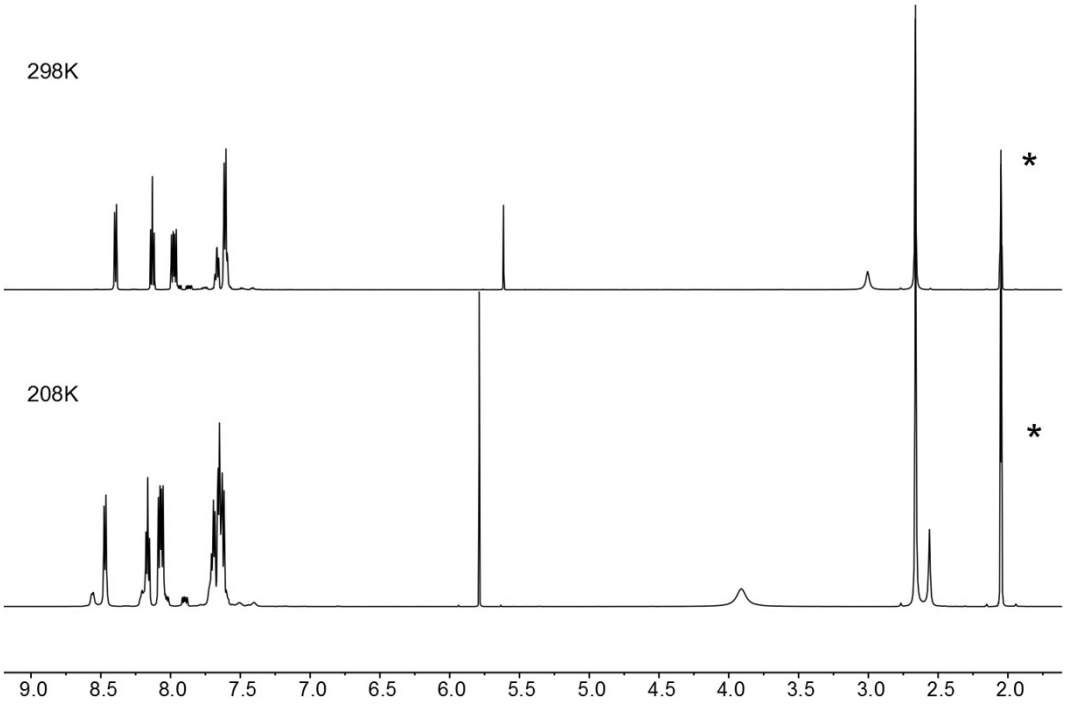

Fig. S10: ^{1}H NMR spectra of $[Ag_2(dppa)(6,6'\text{-}Me_2bpy)_2][PF_6]_2$ in $(CD_3)_2CO$ at 298 K, 500 MHz (top) and 208 K, 600 MHz (bottom). Signals marked with an asterisk indicate residual CD_3CD_2HCO.

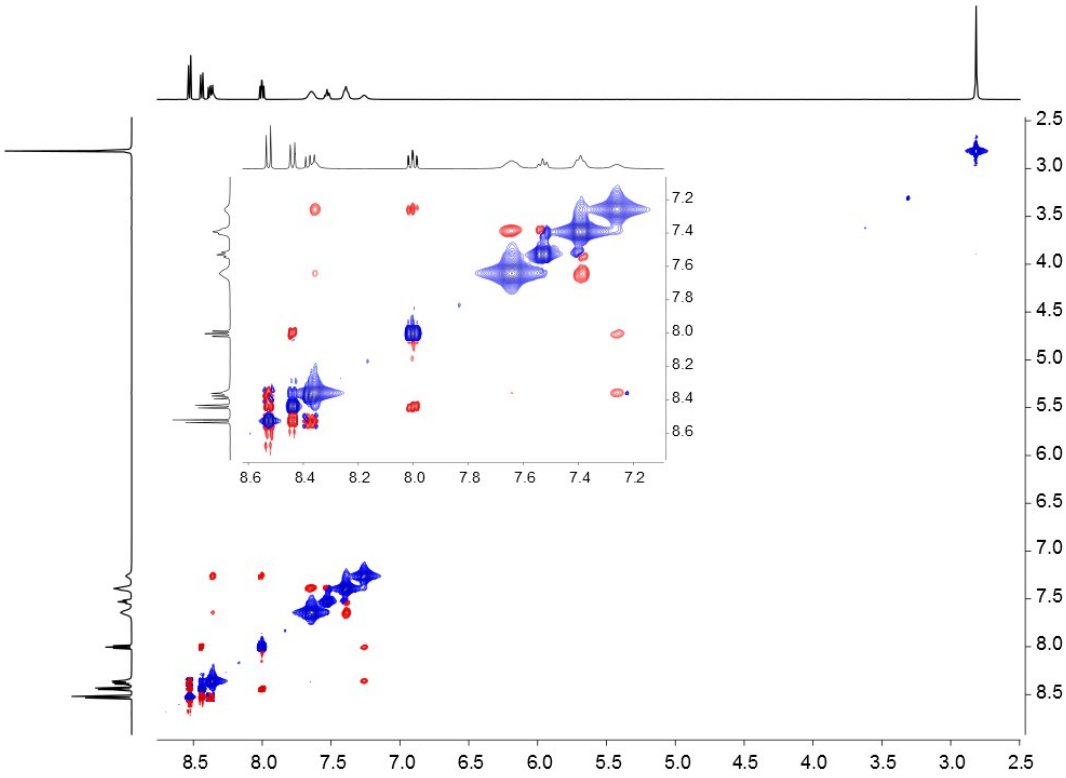

Fig. S11: NOESY spectrum of a 2:2:1 mixture of $[Ag][PF_6]$, tpy and dppa in $(CD_3)_2CO$ at 298 K, 500 MHz. The NOESY cross peaks between the H^{A6} signal at δ 8.36 ppm and the H^{C2} signal at δ 7.65 ppm are clearly visible.

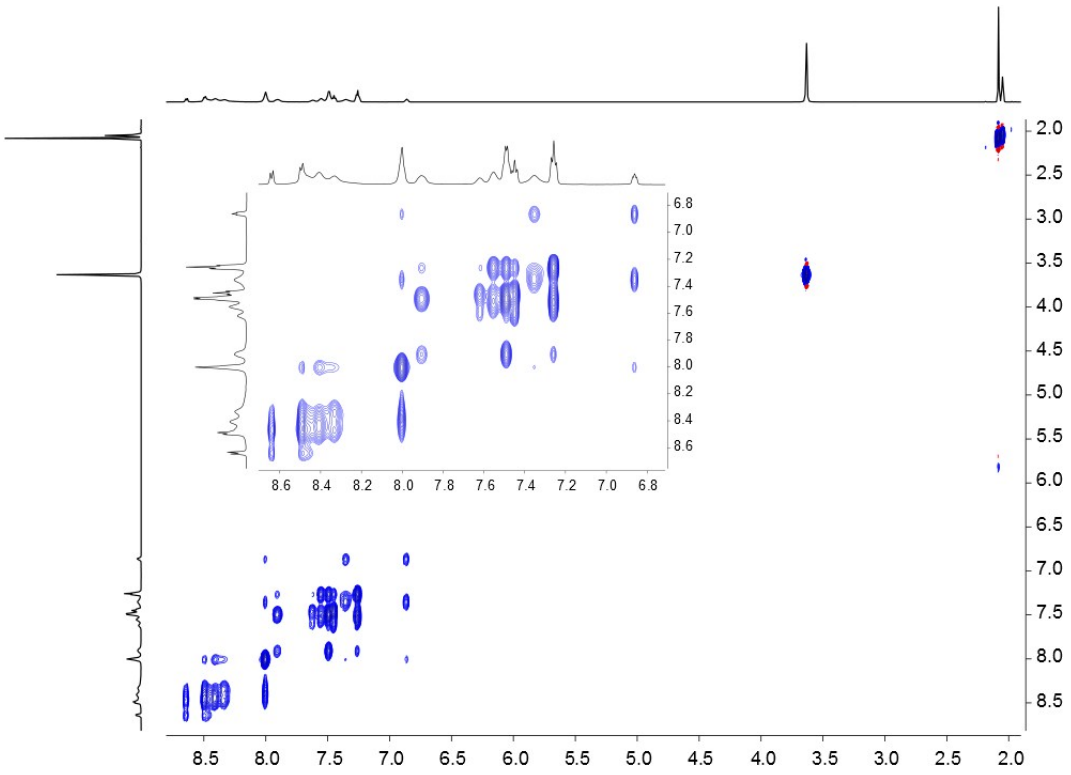

Fig. S12: NOESY spectrum of a 2:2:1 mixture of [Ag][PF_6], tpy and dppa in $(CD_3)_2CO$ at 208 K, 600 MHz.

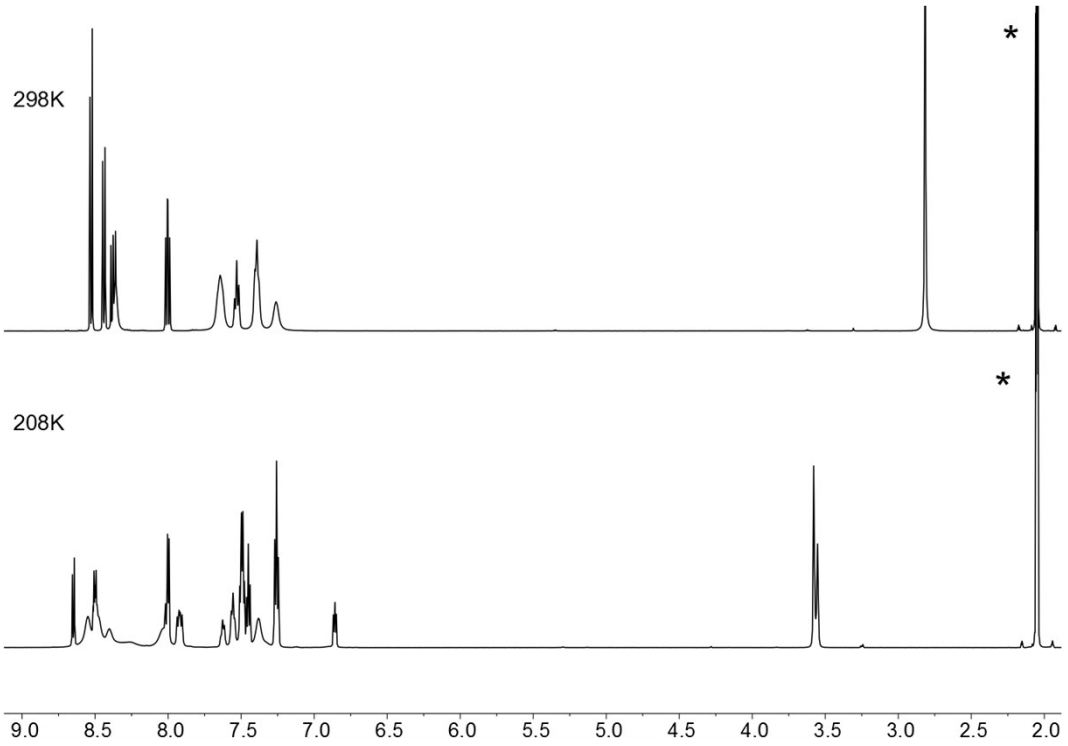

Fig. S13: ^{1}H NMR spectra of a 2:2:1 mixture of [Ag][PF_6], tpy and dppa in $(CD_3)_2CO$ at 298 K, 500 MHz (top) and 208 K, 600 MHz (bottom). Signals marked with an asterisk indicate residual CD_3CD_2HCO.

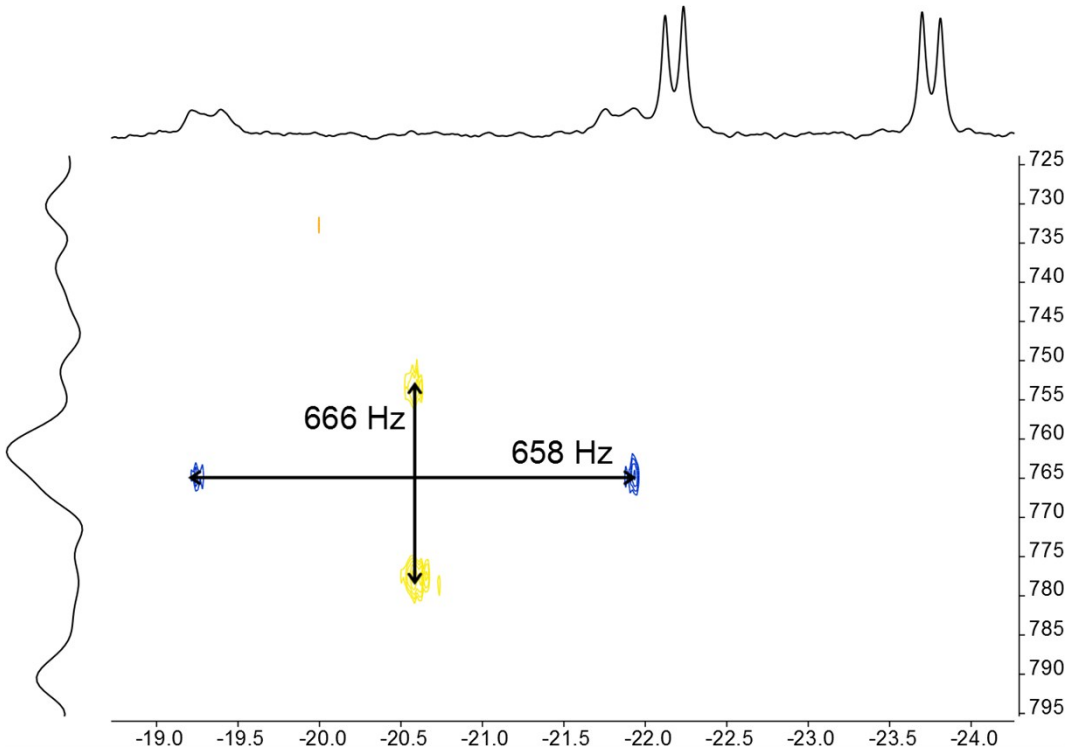

Fig. S14: $^{31}P\{^{1}H\}$-^{109}Ag HSQC spectrum of a 2:2:1 mixture of $Ag[PF_6]$, tpy and dppa in $(CD_3)_2CO$ at 208 K, 14.1 T. Cross peaks with $\{^{31}P\}$ decoupling are coloured in blue and with $\{^{109}Ag\}$ decoupling in yellow. The spectra without decoupling and with both $\{^{31}P\}$ and $\{^{109}Ag\}$ decoupling are not shown due to weak signal to noise ratio.

Acknowledgement

First of all I would like to thank Catherine and Ed, I seriously couldn't have wished for better supervisors! Your support of my sometimes good and sometimes up-in-the-cloud ideas, that you gave me the chance to explore, learn and grow along the way and were always ready to help, especially when I felt that I got stuck, and encouraged me when I was unsatisfied with my work. Catherine, I am extremely grateful for all your efforts in proofreading the papers and thesis, especially in the very stressful phase right now before the thesis submission. Thanks to you both for teaching me the skills needed in academia and also in life in general and thank you for believing in me.
My sincere acknowledgement goes to Professor Jean-François Nierengarten for agreeing to be the co-examiner for my thesis. Many thanks for all your effort and time to read and grade this thesis and coming down to Basel for the exam.
Furthermore I would like to thank all the members of the Constable/Housecroft research group that I worked with, from September 2013 to now and ongoing. I was very warmly welcomed into the group, included and my colleagues were extremely helpful to help me settle in and for example get used to instruments that I hadn't used before. I am truly grateful for the very pleasant environment and good times, both in the everyday lab and office life as well as at conferences that we visited together. In no particular order my thanks go to Annika Büttner, Angelo Lanzilotto, Maximilian Klein, Frederik Malzner, Thomas Müntener, Alexandra Wiesler, Nathalie Marinakis, Cedric Wobill, Fabian Brunner, Mariia Karpacheva, Isaak Nohara, Dr. Alessandro Prescimone, Dr. Davood Zare, Dr. Gabriel Schneider-Joerg, Dr. Marketa Smidkova, Dr. Jennifer Zampese, Liselotte Siegfried, Daniel Ris, Emanuel Kohler, Dr. Ewald Schönhofer, Dr. Nik Hostettler, Dr. Sven Brauchli, Dr. Colin Martin, Dr. Niamh Murray, Dr. Jonas Schönle, Dr. Srboljub Vujovic, Tatjana Kosmalski, Dr. Steffen Müller, Felix Brunner, Dr. Collin Morris, Dr. Roché Walliser, Dr. Biljana Bozic-Weber, Dr. Sebastian Fürer, Dr. Andreas Bünzli, Murat Alkan-Zambada, Dr. Cathrin Ertl, Dr. Markus Willgert, Dr. Alexander Stephens.

My special thanks go to the following people.
Nathalie Marinakis, thanks for being the best lab mate that one could wish for! For the countless scientific, career related and personal discussions, sharing happiness and joy and helping each other on the way. You are a huge contribution to how much I actually enjoyed and still enjoy the time in this lab. Thank you for having become such a wonderful friend.
Fabian Brunner, thank you for being the absolute dream Wahlpraktikum student, Master's student and coworker! It was and still is an absolute pleasure to work with you, share the research topic with you, attend conferences together with you or just joke around or discuss with you. I'm very glad to call you a friend and you definitely improve the mood in the lab.
Maximilian Klein, thank you for your relaxed and energetic way of being, making me laugh hundreds of times and being a great lab mate, conference pal and diving buddy! Also thanks for rocking the synchrotron three times with me and not only being a colleague, but also a friend to me. Also thanks for all the scientific exchange and the ligand sharing.
Alessandro Prescimone, thanks for so many crystal structures your patience to teach me and let me play with the diffractometer, the most pleasant lunch shoppings, the great times at the synchrotron and on the boat and being a great colleague and friend!
Angelo Lanzilotto, thanks for photophysical advice, being a great co-worker and conference buddy, your great and stupid jokes, funny times and our Napoli adventure!
Markus Neuburger, thank you for all your efforts teaching me picking and measuring crystals, solving the structures and explaining a lot about crystallography to me. Also thanks for the great lecture and all the structures.
Daniel Häussinger, thank you very much for all your effort and dedication with the silver project! Your patience and help with everything NMR related made a huge difference in many of my projects, it was a pleasure to work with you and I'm looking forward to investigate more about the mysterious silver together.
Andrea Pannwitz, thank you for the great two times at the synchrotron and especially the most enjoyable time there at the nightshifts together with you! Thanks for talking me into giving a presentation at the PCC seminar and I am extremely grateful for all your advice concerning postdoc applications.
Christopher Larsen, thanks for helping me with low-temperature lifetime and emission measurements, great scientific exchange and good times together at three conferences!
Laura Büldt, thanks for the great collaboration around copper and your help with the low-temperature lifetime.
Alexandra Wiesler, thanks for being a very nice and uncomplicated co-worker and great time at the conference in Greece and together on the boat.

Murat Alkan, thank you for doing an excellent job as a Wahlpraktikum student and Master student, your dedication to the project, eagerness to learn and not-funny (but funny) jokes.
Bernhard Jung for always being there when help and advice was needed concerning anything even only remotely related to IT, thanks for being so helpful and nice!
Jonas Schönle, thank you for letting me inherit some of your ligands and help me finding my way and learn the instruments at the beginning of my PhD.
Collin Morris for some ligands, scientific advice and a good time in the lab and in Singapore.
Cathrin Ertl, thanks for the good scientific exchange, helping me to settle in and nice lunchbreaks.
Steffen Müller, thank you for a few ligands, synthetic advice and a good time in the lab and the lunch breaks.
Niamh Murray, Emmanuel Kohler, Tatjana Kowslowski, Chantal Ekanem, Nathalie Marinakis for the relaxed and quiet atmosphere in the old office in the Spitalstrasse.
For good times in the Praktikum I'd like to thank my fellow assistants Max Klein, Nathalie Marinakis, Martin Kuss-Petermann, Miriam Schreier, Jaicy Vallapurackal, Annika Büttner, Roger Walliser and Frederik Malzner.
Furthermore I'd like to thank Beatrice Erismann, for doing a great job concerning bureaucratic and organizational issues. We are lucky to have you!
Also a big thank you to Bernhard Jung for his excellent support with IT and computer related issues, poster printing and much more!
The whole Werkstatt team for their great effort in maintaining and repairing instruments and making sure that the building doesn't fall apart. Special thanks also to Markus Ast, always having a friendly chat on the hallway, and Markus Hauri for being extra helpful and nice.

The people outside of the University of Basel that have my sincere acknowledgement:
Thanks also to Helmut Teichmann from Hamamatsu for not only the great customer service, but also for introducing me to potentially interesting people regarding my career.
My thanks also go to my former supervisors in Freiburg, Prof. Ingo Krossing and Alex Higelin, thank you for giving me so much on the way during my studies and thanks for igniting the fascination for research in me.
Thanks also to Chris Brown for the insightful discussions and some help with editing.
I'd also like to acknowledge the Reisefond of the Ressort Nachwuchsförderung Basel for enabling me to attend this many conferences.
Mama and Papa, it is impossible to find words to express how thankful I am to have you! Thank you for your love, for teaching me how to go my own way, believing in me, supporting me and always being there for me. Thank you, without you I wouldn't be who and where I am.
Thanks also to my wonderful family, my grandmother Hilde, my grandfather Hansjörg, my aunt Heike and my other grandmother Lisbeth. Also Dirk, Ingrid, Olga and Magnus. Thanks for being such a great family and always believing and supporting your little "Einstein".
My wonderful and amazing friends outside the lab, especially Reh, Kitty, Anna, Carina, Chrissi, Rouven, Philipp, Reike, Bernd, Flo, Frieda, Jochen, Jonas, Lisa, Doro, Pascal, Elora, Jasmin, Samuel, Christoph, Jan, Johnny, Lisa, Fabian, Chrigi, Dane, Thomas, Alex, Marion,. Thank you for the great times together, for being part of my life and letting me be part of yours. And thanks for all your understanding and support in the last few months of the thesis!
And last, but also first of all, my love Chris. Life is a million times more beautiful and enjoyable with you! I'm very grateful to have you at my side for so many years already and hopefully for many many more to come. Thank you for being there, all your support and understanding, always but especially in the last months, for your love and for just being you.

Image of a pair of interacting galaxies called Arp 273, “Rose of galaxies”. Picture of the ESO 455-23 globular cluster Terzan 1, Distance: 300 million light years, Constellation: Andromeda. Photo credit: NASA, ESA and the Hubble Heritage Team (STScI/AURA). Picture used with permission from ESA/Hubble. https://www.spacetelescope.org/images/heic1107a/ (17.11.2017)

Summary and Outlook

Summary of the PhD project

Heteroleptic copper(I) complexes with three different bisphosphanes (POP, xantphos and *t*Bu-xantphos) and broad selection of N^N chelating ligands, mostly 2,2'-bipyridines (bpys), were synthesized within the scope of this project (Chapters I, II, III and V). The employed bpy ligands are substituted with alky, aryl, CF_3 or halogen atoms in various positions and were, if not commercially available at a reasonable price, synthesized by different methods including homo- and heterocouplings (e.g. Neghishi) or alkylation and arylation with organolithium reagents or alkylmagnesium chlorides. All of the reported complexes were characterized by a range of analytical techniques. For all the complexes, structure and purity were confirmed using electrospray ionization (ESI) mass spectra and elemental analysis in addition to one-dimensional ^{1}H, ^{13}C ^{31}P or $^{31}P\{^{1}H\}$ as well as two-dimensional COSY, NOESY, HMQC and HMBC methods. $^{31}P\{^{1}H\}$ NMR spectra give important information about the exclusive formation of the heteroleptic complex or the presence of homoleptic side products. ^{31}P–^{1}H HMBC and low temperature NMR experiments were performed in order to study the conformational changes of [Cu(xantphos)(6-Phbpy)][PF_6] in solution (Chapter I).[2] In the series of complexes with CF_3-substituted bpys, ^{19}F NMR spectra were also recorded (Chapter III).[3]

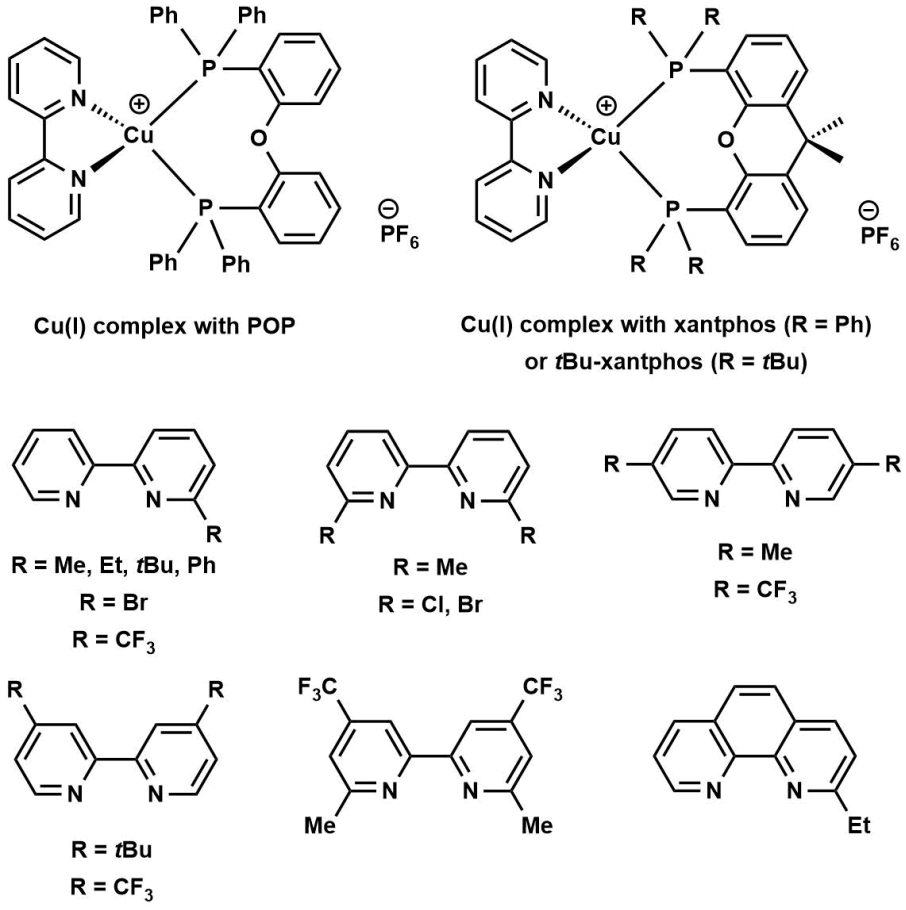

Scheme 1. Overview over copper(I) complexes and the employed ligands.

Single crystals were obtained for most of the complexes and analysed by single crystal X-ray diffraction. The crystals usually diffract very nicely so that good data was obtained and the structures could be solved and refined for publication. In all heteroleptic complexes, the copper centre is coordinated in a distorted tetrahedral geometry. Systematic effects of the different substitutions at the bpy on the complex geometry were not found, it appears that the complex geometry in solid state is largely influenced by packing effects. For some of the complexes with unsymmetrical bpy ligands, for example 6-Mebpy and 6-Brbpy, two orientations of the bpy with different occupancies were found in the crystal structures. The behaviour of the solid state structures of the complexes under increased pressure were conducted at the Diamond Light Source, beamline I19. For three structures[3],[6] (two

examples illustrated in Fig. 3), these studies gave data of satisfactory quality and we found that few changes take place under pressure. The high pressure study confirmed the rigidity of the packing as well as the robust nature of the ligand coordination.

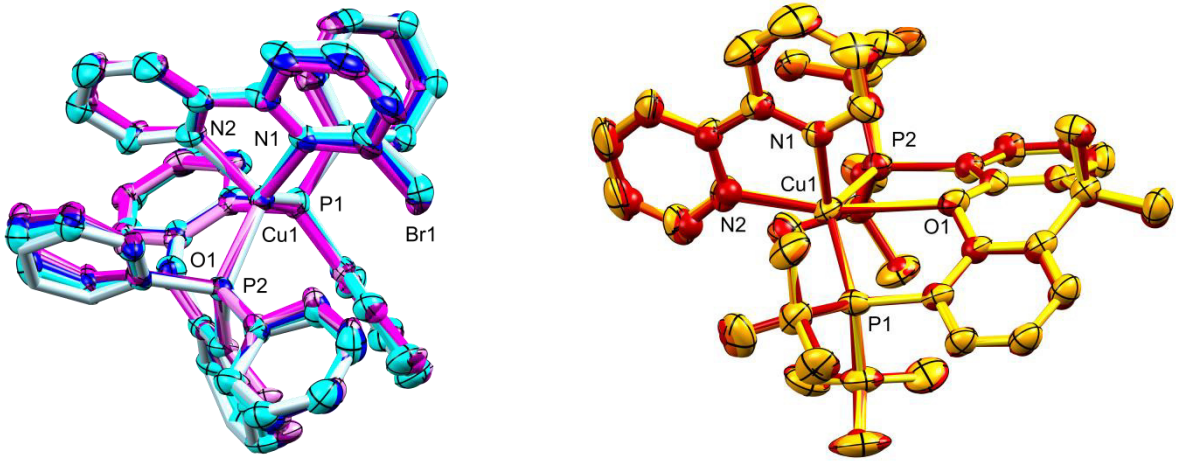

Fig. 1. Left: Structure of the cation in [Cu(xantphos)(6-Brbpy)][PF_6] under increasing pressure (ambient to 4.5 GPa). Colour change from light blue to purple with increasing pressure. Chapter II;[3] right: structure of the cation in [Cu(*t*Bu-xantphos)(bpy)][PF_6] upon increasing the pressure from ambient (yellow) to 2.3 GPa (dark red). Chapter V.[6] Ellipsoids plotted at 50% probability level, H atoms omitted.

Solution absorption and emission spectra of all heteroleptic copper(I) complexes were recorded. The complexes with POP and xantphos show broad bands in the area of 340 and 430 nm that are assigned to MLCT transitions. Alkyl substituents on the bpy usually lead to a blueshift of the MLCT band with respect to the complexes with unsubstituted bpy, whereas halogen atoms, phenyl and CF_3 groups lead to a redshift. It was surprising to find that these bands are missing for the complexes with *t*Bu-xantphos, the difference is illustrated by a comparison of the solution absorption spectra of [Cu(xantphos)(N^N)][PF_6] complexes (Chapter I) and those with *t*Bu-xantphos (Chapter V)[6] in Figure 2. The latter are also extremely poor emitters in solution and solid state, which we attribute to quenching mechanisms induced by the high-energy stretching vibrations of the many C–H bonds of the *tert*-butyl groups in *t*Bu-xantphos that are close to the copper centre. These type of copper(I) (and the related silver(I)) complexes are therefore not suited for application as emitters and we focused again on POP and xantphos as bisphosphane ligands for the complex design.

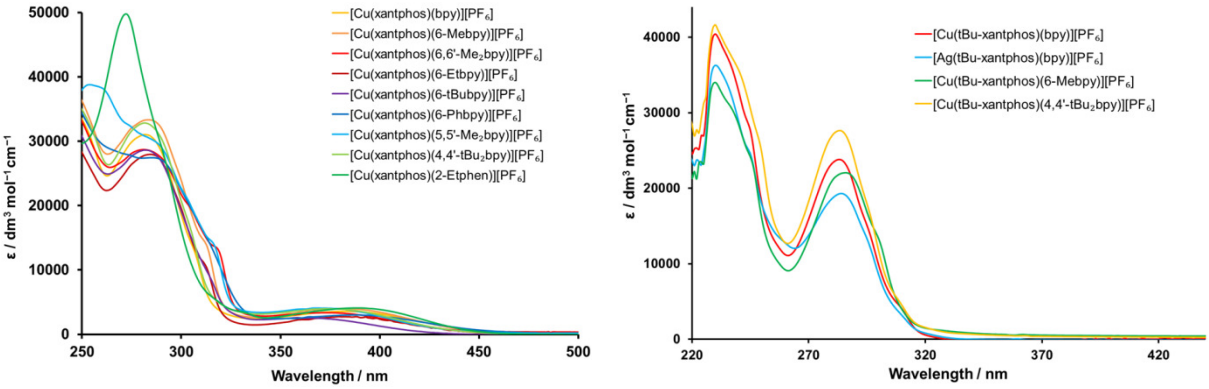

Fig. 2. Left: Solution absorption spectra of the [Cu(xantphos)(N^N)][PF_6] complexes (CH_2Cl_2, 2.5×10^{-5} mol dm^{-3}). Chapter I;[1],[2] right: Solution absorption spectra of the [Cu(*t*Bu-xantphos)(bpy)][PF_6] complexes and [Ag(*t*Bu-xantphos)(bpy)][PF_6] (CH_2Cl_2, 2.5×10^{-5} mol dm^{-3}). Chapter V.[6]

The complexes with POP and xantphos are yellow to red emitters in solution and powder, with λ_{em}^{max} values between 564 nm ([Cu(POP)(6,6'-Me_2bpy)][PF_6])[1] and 705 nm ([Cu(xantphos)(4,4'-$(CF_3)_2$bpy)][PF_6])[3] in solution, and ranging from 535 nm ([Cu(POP)(6,6'-Me_2bpy)][PF_6])[1] to 664 nm ([Cu(POP)(4,4'-$(CF_3)_2$bpy)][PF_6])[3] in solid state. In solution, most of the complexes exhibit poor PLQY values around 1%, which can in some cases be improved

upon deaeration by a 20 min gas flow of argon through the complex solution. In powder, the highest PLQY values were obtained for the complexes with methyl groups in both 6-positions at the bpy, 43% for [Cu(POP)(6,6'-Me_2bpy)][PF_6],[1] 37% for [Cu(xantphos)(6,6'-Me_2bpy)][PF_6][2] and 50% for [Cu(xantphos)(6,6'-Me_2-4,4'-$(CF_3)_2$bpy)][PF_6]. Substitution at the bpy with alkyl, aryl, CF_3 groups or halogen atoms has a positive effect on the PLQY with respect to the complexes with unsubstituted bpy in all cases but for [Cu(POP)(6-*t*Bubpy)][PF_6] and all complexes with 4,4'-$(CF_3)_2$bpy and 5,5'-$(CF_3)_2$bpy, where the powder PLQY was 1% for the former and even lower for the latter. The extent to which emissive properties of the complexes can vary upon different substitution is illustrated in Figure 3.

Fig. 3. Powder samples of [Cu(xantphos)(N^N)][PF_6] complexes under normal light (top) and under UV light (λ_{exc} = 365 nm, bottom). From left to right: [Cu(xantphos)(bpy)][PF_6], [Cu(xantphos)(6-CF_3bpy)][PF_6], [Cu(xantphos)(4,4'-$(CF_3)_2$bpy)][PF_6], [Cu(xantphos)(5,5'-$(CF_3)_2$bpy)][PF_6] and [Cu(xantphos)(6,6'-Me_2-4,4'-$(CF_3)_2$bpy][PF_6].

Light-emitting cells were prepared for the complexes with acceptable PLQY values or in cases where we wanted to compare the effect of a certain substituent. For all of the devices that were successfully tested in the scope of this project, the electroluminescence is yellow to orange. We found that a high PLQY of the complex in powder usually gives also high luminance values (Lum_{max}). The most efficient device was fabricated with [Cu(POP)(6,6'-Me_2bpy)][PF_6] with an efficacy of 5.2 cd A^{-1} and Lum_{max} of 53 cd m^{-2} (operation at 10 A m^{-2}),[1] the brightest device incorporated [Cu(POP)(2-Etphen)][PF_6], with an efficacy of 4.3 cd A^{-1} and Lum_{max} of 430 cd m^{-2} (operation at 100 A m^{-2}). Unfortunately, the device lifetimes $t_{1/2}$ of these LECs were not optimal, they only reached 1.5 and 4.8 hours, respectively. Extremely fast turn-on times t_{on} of 12 seconds or shorter were realized by the employment of [Cu(P^P)(6,6'-Cl_2bpy)][PF_6] complexes in the devices. The brightness of these devices was acceptable, with Lum_{max} values between 64 and 259 cd m^{-2} and the EQEs reaching up to 80% of the theoretical maximum. However, again the device lifetimes were disappointing and did not exceed 0.6 hours.[3] Devices with [Cu(P^P)(6-Etbpy)][PF_6] complexes in the active layer gave the best device lifetimes (at acceptable luminance values), with $t_{1/2}$ of 82 hours and 53 cd m^{-2} for the complex with POP and 51 hours and 77 cd m^{-2} for the one with xantphos, respectively.[2] While we have successfully optimized the luminance, turn-on time and lifetime in different devices, the combined optimization of all three parameters is our goal for future emitters and devices.

In two cases, attempts to synthesize the heteroleptic complexes yielded unexpected structures that were missing the bipyridine ligand as a result of the steric hindrance of the phosphane and/or the employed bpy. [Cu(*t*Bu-xantphos)]$^+$ (a complex cation with only the chelating bisphosphane *t*Bu-xantphos as ligand and no further substituents at the metal) was obtained in an attempt to synthesize [Cu(*t*Bu-xantphos)(6-Brbpy)][PF_6] (Chapter V).[6] In an attempt to synthesize [Cu(xantphos)(6,6'-$(CF_3)_2$bpy)][PF_6], partial hydrolysis of the [PF_6]$^-$ anion to [PO_2F_2]$^-$ took place upon single crystal growth. An inorganic coordination polymer [{Cu(xantphos)(μ-PO_2F_2)}$_n$] was obtained, with each copper(I) being coordinated by one chelating xantphos molecule and connected to the next copper atom by bridging {PO_2F_2} units. This structure was interesting enough to deserve a short communication and its own chapter (Chapter IV).[5]

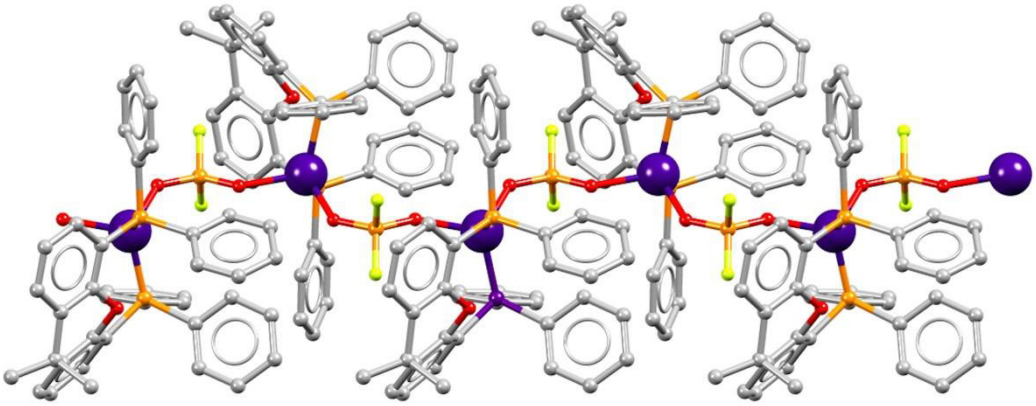

Fig. 4. Part of one polymer chain in [{Cu(xantphos)(μ-PO_2F_2)}$_n$] viewed down the *c*-axis; the chain follows the *b*-axis. Chapter IV.[5]

One of the side projects of the PhD project involved the self-assembling properties of heteroleptic silver(I) complexes (Chapter VI).[7] The dinuclear silver(I) complexes are all bridged by one or two bis(diphenylphosphino)ethane (dppa) molecules and each silver centre is coordinated either by a chelating 6,6'-Me_2bpy or a chelating terpyridine, which was found either in bidentate or tridentate coordination in the solid state. The complexes were studied in detail via one- and two-dimensional NMR spectroscopic methods, and especially $^{31}P\{^1H\}$-^{109}Ag HSQC spectra were found to be extremely insightful for the structure determination in solution. While for the singly-bridged $[Ag_2(dppa)(N\text{^}N)_2]^{2+}$ cations, the coupling constant $^1J_{31P\text{-}109Ag}$ is equivalent for the splitting of the cross peaks in the F1 dimension, for the doubly-bridged $[Ag_2(dppa)_2(N\text{^}N)_2]^{2+}$ species the splitting accounts to twice of the value of the coupling constant $^1J_{31P\text{-}109Ag}$. The $^{31}P\{^1H\}$-^{109}Ag HSQC spectrum is therefore an elegant method to the evaluate the structure of silver phosphane complexes.

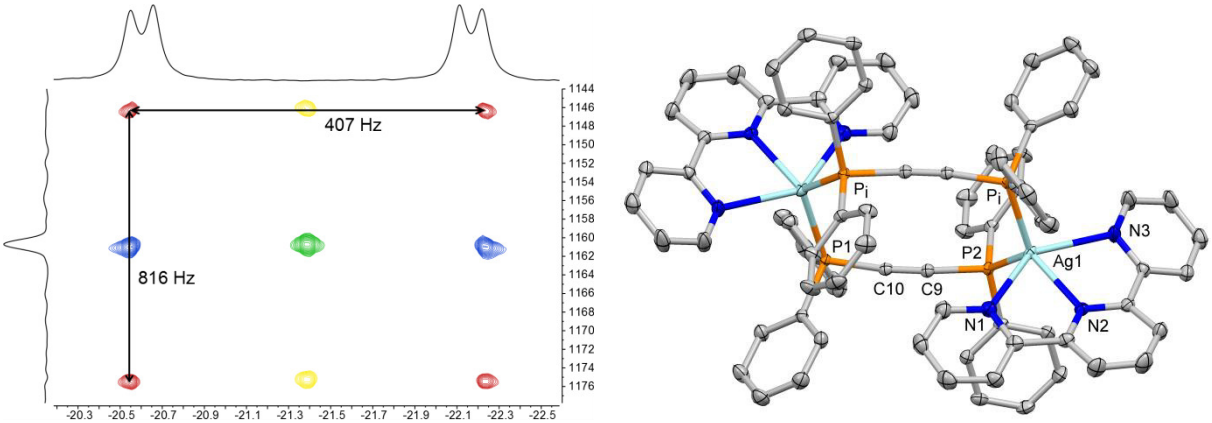

Fig. 5. Left: $^{31}P\{^1H\}$-^{109}Ag HSQC spectrum of a 1:1:1 mixture of Ag[PF_6], 6,6'-Me_2bpy and dppa in $(CD_3)_2CO$ at 228 K. Cross peaks without decoupling are coloured in red, with {^{31}P} decoupling in blue, with {^{109}Ag} decoupling in yellow, and with both {^{31}P} and {^{109}Ag} decoupling green; right: Structure of $[Ag_2(dppa)_2(tpy)_2][PF_6]_2 \cdot 2Et_2O$; H atoms and solvent molecules omitted for clarity. Ellipsoids are plotted at 50% probability level. Chapter VI.[7]

This PhD project has given valuable insights into the photophysical properties of heteroleptic copper(I) complexes and the effect of different substituents on the performance of light-emitting electrochemical cells. The results of these studies are already used to design the next generation of emissive copper(I) complexes in our lab. Although the number of parameters that have an influence on the device performance is enormous, and the best choice of ligand combination is not always straightforward, we have succeeded in this project in gaining invaluable insights into the design of highly emissive and stable Cu(I) complexes and display their use in efficient LECs. We now have a greater understanding of the effects of different chelating ligands on the photophysical properties, and in turn were able to increase the PLQY and systematically tune the emission colour of the complexes towards the red and blue. The lifetime of the LECs has been extended several times, from less than 8 to 82 hours, and very short turn-on times of the devices were achieved, showing the great potential of copper(I) complexes to become the state-of-the-art emitters for LECs. Two more PhD students are working on the development of copper(I) emitters in our lab, and

with our joint efforts the next generation of luminophores will be even brighter and give longer-living devices. Future work will also include further optimization of the device lifetimes and efficiencies, as these remain obstacles before commercial availability of copper-based LECs is realized. In addition to the main topic, side projects such as about the inorganic coordination polymer or the dimeric silver species gave interesting insights into the versatile coordinative behaviour of the coinage metals. In addition, they allowed us to follow our interest in coordination chemistry, show that investigation should not only go into depth but also into width, and familiarized us with additional techniques, such as ^{31}P–^{109}Ag NMR spectroscopy.

Perspective of LECs and copper(I) emitters

Solid state lighting in general is a very versatile technique, both for applications in displays and screens as well as in lamps for illumination. LEDs have been on the market for some time already, and OLEDs also are established now and have proven their outstanding properties. Regarding the prospect of copper(I) compounds as emitter material, the fact that copper-based luminophores are already employed in commercially available OLEDs shows the high potential of these materials. The German company Cynora, which was founded as start-up in 2003, develops TADF emitters, both organic materials and inorganic copper(I) complexes, for OLED applications.[1] In September 2017 the investment of the leading technology companies Samsung and LG into Cynora became public. They hope to improve materials for applications in AMOLED (Active Matrix OLED) displays and especially to obtain more efficient blue emitters, one of the main fields that Cynora has specialized in.[2] This illustrates the interest of the industry in new compounds and systems for lighting, including copper-based materials. Very often, for copper compounds sublimation is not a possibility as it destroys the complexes, however good results were obtained by co-depositing the starting material (usually copper iodide) and the ligands together.[3] OLEDs with high luminance and EQE values were obtained by solution processing of bis-halide bridged copper(I) complexes, as for example for complex 1 (Scheme 2), with Lum_{max} of 10000 cd m^{-2} (operation at 10 V) and an EQE of 23%, to our knowledge the highest EQE reported so far for an OLED with a solution processed Cu(I) based emissive layer.[4] Concerning OLEDs that incorporate copper(I) complexes of the general $[Cu(P\text{^}P)(N\text{^}N)]^+$ structure, the device with complex 2 (Scheme 2) yielded an EQE of 15% with a maximum luminance Lum_{max} of 3272 cd m^{-2},[5] whereas devices with complex 3a or 3b gave Lum_{max} values of 6563 and 5579 cd m^{-2} with EQEs of 5.8 and 7.4%, respectively.[6] By employing a negatively charged ligand, neutral copper(I) compounds can be obtained, which show good properties as emitters in OLEDs, for example complexes 4a-c with EQEs of 12, 16 and 18% (Scheme 2).[7]

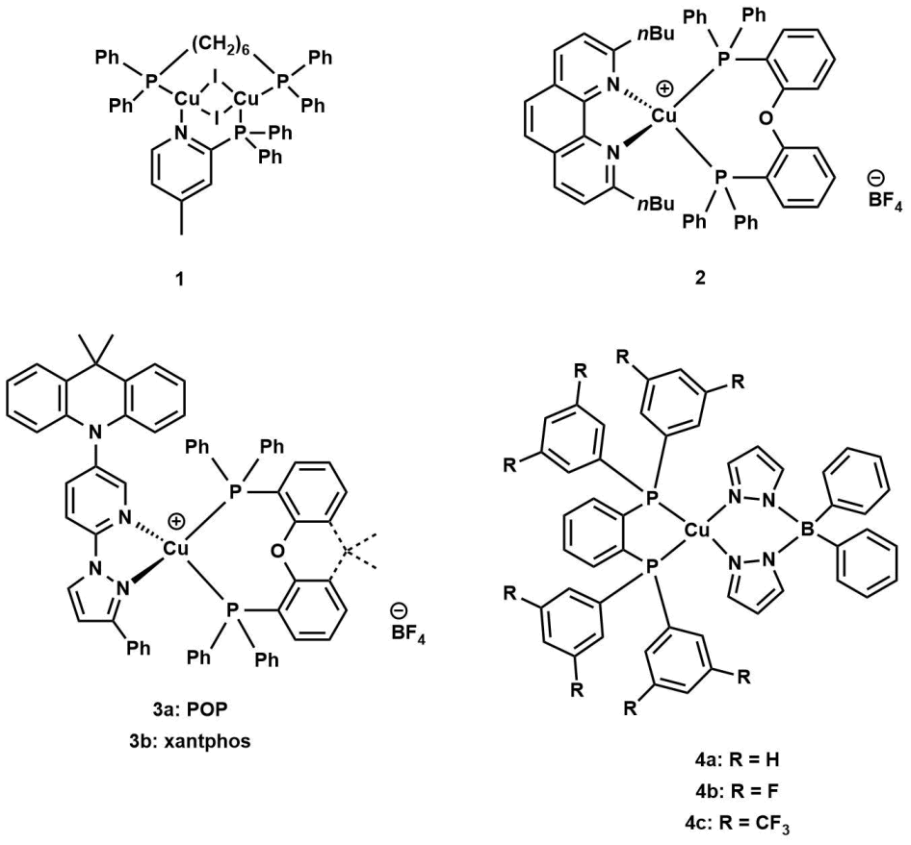

Scheme 2. Structures of copper(I) complexes that are efficient emitters in OLEDs.[4,5,6,7]

In order for a device to be applicable for illumination, the emitted light should, ideally, be white. White electroluminescence was realized for example with the copper iodide cluster $[DBFDP]_2Cu_4I_4$ with DBFDP being 2,9-di(diphenylphosphine)-dibenzofuran. The spin-coated OLED featured dual emission characteristics, leading to white EL with CIE 1931 coordinates of (0.37, 0.45) and maximum luminance Lum_{max} up to 1500 cd m^{-2}.[8] As these promising examples show, the future of OLEDs with copper-based emitters indeed looks bright and it is likely that these sustainable materials will replace iridium based compounds in the next couple of years.

However, when it comes to the future of light-emitting electrochemical cells as a competing technique to OLEDs, the outlook for the future is less clear. On one hand, there are all the advantages of LECs in comparison to OLEDs: The simple setup, energy-saving solution processing, relative stability towards air and as a result of these factors, fabrication costs one order of magnitude lower have been calculated.[9] LECs have also been shown to be very versatile when it comes to the style of the device, for example flexible devices have successfully been tested[10] and even weavable fibre-shaped LECs that could eventually be employed in light-emitting textiles.[11] Also light-emitting electrochemical cells with white-light emission have been realised.[12] But on the other hand there are still two major obstacles to overcome: The efficiency and especially the lifetime and stability of LECs, at least those based on copper(I). LECs with device lifetimes $t_{1/2}$ over 6000 hours and EQEs up to 2% were achieved for example with red-emitting iridium complexes,[13] but such long lifetimes are the exception. However, to be fair, research concerning LECs is not as established as that for OLEDs and there is, in general, less research activity about the former. In other words the development of LECs is several years behind that of OLEDs. For example, it is not yet resolved what exactly causes the degradation of the devices. In polymer LECs it has been shown that dark spots form upon long-term testing. It was postulated that these are spots of heavy doping as a result of chemical changes that happen at the cathode/polymer interface,[14] but whether this is the same mechanism that leads to the degradation of iTMC LECs remains obscure. Also while our collaborators in Valencia[15] do an excellent job in terms of device fabrication, the necessary manpower to play with the device parameters and make extended efforts to further optimize the LECs is simply missing. With more groups focussing especially on the elongation of the device lifetimes and the analysis of the degradation processes, the design of the LECs and would be facilitated. Also other options to improve the efficiency of LECs should be considered more, for example it has been shown that more of the light that is trapped in the substrate layer can be outcoupled by employing high-refractive index substrates and scattering layers into the device.[16] In the last twenty years the foundation stone was laid for the different types of LECs and the devices today are promising enough to encourage further research. Even if OLEDs will stay superior to LECs, a coexistence of the two technologies is well imaginable, with different types of devices tailored for the desired application and depending on the costs of the final product. It is our hope that the development of sustainable and energy-efficient lighting technology and the respective emitter compounds will be further pursued in the future and that possible investors and politicians recognize the importance and support the advancement of these systems. As a scientist, it is a pleasure to work on such a successful flagship project at the interface between fundamental research and applied science and to try and bring us closer to a World illuminated with sustainable lighting.

Impressions of past and future illumination[17]

References

1 https://www.cynora.com/de/home/ (12.11.2017)
2 https://www.notebookcheck.com/OLED-LG-und-Samsung-investieren-25-Millionen-Euro-in-Cynora.249910.0.html (12.11.2017)
3 C. Bizzarri, E. Spuling, D. M. Knoll, D. Volz and S. Bräse, *Coord. Chem. Rev.*, 2017, doi: /10.1016/j.ccr.2017.09.011.
4 D. Volz, Y. Chen, M. Wallesch, R. Liu, C. Fléchon, D.M. Zink, J. Friedrichs, H. Flügge, R. Steininger, J. Göttlicher, C. Heske, L. Weinhardt, S. Bräse, F. So and T. Baumann, *Adv. Mat.*, 2015, **27**, 2538.
5 Q. Zhang, T. Komino, S. Huang, S. Matsunami, K. Goushi and C. Adachi, *Adv. Funct. Mater.*, 2012, **22**, 2327.
6 D. Liang, X.-L. Chen, J.-Z. Liao, J.-Y. Hu, J.-H. Jia and C.-Z. Lu, *Inorg. Chem.*, 2016, **55**, 7467.
7 S. Igawa, M. Hashimoto, I. Kawata, M. Yashima, M. Hoshino and M. Osawa, *J. Mater. C*, 2013, **1**, 542.
8 M. Xie, C. Han, J. Zhang, G. Xie and Hui Xu, *Chem. Mater.*, 2017, **29**, 6606.
9 A. Sandström and L. Edman, *Energy Technol.*, 2015, **3**, 329
10 L. Martínez-Sarti, A. Pertegás, M. Monrabal-Capilla, E. Gilshteyn, I. Varjos, E. I. Kauppinen, A. G. Nasibulin, M. Sessolo and H. J. Bolink, *Organic Electronics*, 2016, **30**, 36.
11 Z. Zhang, K. Guo, Y. Li, X. Li, G. Guan, H. Li, Y. Luo, F. Zhao, Q. Zhang, B. Wei, Q. Pei and H. Peng, *Nature Photonics*, 2015, **9**, 233.
12 H.-C. Su and C.-Y. Cheng, *Isr. J. Chem.*, 2014, **54**, 855.
13 C. D. Ertl, C. Momblona, A. Pertegás, J. M. Junquera-Hernández, M.-G. La-Placa, A. Prescimone, E. Ortí, C. E. Housecroft, E. C. Constable and H. J. Bolink, *J. Am. Chem. Soc.*, 2017, **139**, 3237.
14 F. AlTal and J. Gao, *Organic Electronics*, 2015, **18**, 1.
15 Thanks to H. J. Bolink and E. Ortí including their group members, Instituto de Ciencia Molecular (ICMol), Universidad de Valencia.
16 Y.-F. Jang, T.-C. Lin, J.-Y. Guo, C.-M. F. Chiang, M.-L. Wu, H.-Y. Shen, T.-C. Chen, Z.-P. Yang, Y.-J. Lee, H.-C. Su, C.-H. Chang, S.-W. Liu, *Organic Electronics*, 2017, **51**, 149.
17 Creative Commons Zero (CC0) license and therefore free for personal and even commercial use. Picture taken from pexels.com or pixabay.com.

„Man muss noch Chaos in sich haben, um einen tanzenden Stern gebären zu können.“ – Friedrich Nietzsche in „Also sprach Zarathustra“

Picture of the ESO 455-23 globular cluster Terzan 1, Distance: 20000 light years, Constellation: Scorpius. Photo credit: NASA & ESA, Acknowledgement: Judy Schmidt (geckzilla.com). Picture used with permission from ESA/Hubble. https://www.spacetelescope.org/images/potw1550a/ (18.11.2017)